IMPLEMENTING OPERATIONAL OCEAN MONITORING AND FORECASTING SYSTEMS

EDITORS: ENRIQUE ALVAREZ FANJUL, STEFANIA CILIBERTI, AND PIERRE BAHUREL
GOOS/ETOOFS SECRETARIAT: DENIS CHANG SENG

unesco
Intergovernmental
Oceanographic
Commission

The Global Ocean Observing System
G OOS

MERCATOR OCEAN
INTERNATIONAL

5. Circulation modelling

1.
Introduction

CHAPTER AUTHOR

Enrique Álvarez Fanjul

1. Introduction

1.1.
Scope and purpose of this publication

It is difficult to overestimate the importance of the ocean for mankind and animal life on our planet. Covering 70% of the Earth's surface, the ocean is the world's largest source of oxygen and absorbs 50 times more carbon dioxide than the atmosphere. Climate is regulated by the ocean heat transport, making our world a habitable place.

For human beings, the ocean is also a source of food, economic resources, travel, and leisure activities. Fish accounts for about 17% of the animal protein consumed globally (FAO, 2020). The economic activities associated with the ocean are many and of crucial importance. For example, the FAO estimates that 59.6 million people in the world are engaged in fisheries activities. Only in the European Union, it is estimated that the blue sector employs almost three and a half million workers. World commerce heavily depends on marine transportation; approximately 50 thousand ships trade internationally, representing 80-90% of world trade (Schnurr and Walker, 2019). About 40% of the world population lives along coasts, which are now endangered by the sea level rise due to climate change and are of paramount importance for economic activity.

These facts and figures highlight that ocean forecasting is considered as a vital activity. The first scientific successful ocean forecasting method was developed during the second world war to facilitate the landings of the US Navy. Swell forecasts were produced by analyzing wind speeds and fetch extension. The first modern approaches, based on the use of numerical models (Pinardi et al., 2017), were developed during the 1950s with the establishment of the basics of storm surge forecasting (Hansen, 1956). Other relevant advances, including first 3-dimensional simulations, took place during the 1960s. Good examples of these achievements can be found on estuarine (Shubinski et al., 1965) and general circulation modeling (McWilliams, 1966).

Since those early successes, thanks to an ever-increasing computing capacity, ocean forecast techniques have evolved to what is today a complex body of codes, data and technologies able to deal with the non-linear and chaotic nature of ocean processes. Today, the scientific modeling community is committed to improve the reliability of the forecasts, mainly advancing on three leading edge areas: data assimilation, coupled forecasting and ensemble modeling.

Advances in computer power have played a relevant key in the progress of the discipline. Figure 1.1 shows the dramatic increase in supercomputing power during the last decades, from the first transistor-based machines to the present day petascale computing.
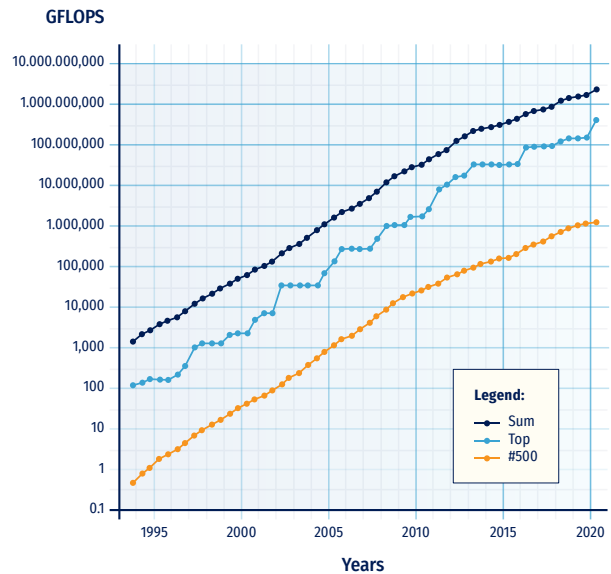
Figure 1.1. Supercomputers performance evolution, based on data from www.top500.org site. The logarithmic y-axis shows performance in GFLOPS. Dark blue line: combined performance of 500 largest supercomputers ("Sum"); Light blue line: fastest supercomputer ("Top"); Orange line: supercomputer in 500th place ("#500") (adapted from 🔗¹).

The following example illustrates the evolution of ocean forecasting over the last three decades. Figure 1.2 shows the output of two numerical simulations over the same area executed by the same team. The figure on the left was the result of a 1991 state-of-the-art 3D-baroclinic simulation covering the Ria de Vigo. It was the first simulation of this kind in that area, an estuary in the northwest of Spain. The right plot in Figure 1.2 shows a screenshot of the Portus system (Álvarez Fanjul et al., 2018) in the same geographical domain, as generated by an operational system running 3 decades later

The differences between both simulations, summarized in Table 1.1, are striking and demonstrate the great evolution that has taken place in the discipline.

The ocean forecasting discipline includes much more than the execution of the numerical models. There are several steps to transform the data produced into accessible and usable information. The downstream activities to produce tailored ser-

1. https://en.wikipedia.org/wiki/History_of_supercomputing

	1991 Ria de Vigo simulation	2021 Portus Operational system
Type of simulation	R&D offline simulation	Fully operational simulation integrated into a service, operated 24/7
Spatial resolution	800 meters	40 meters
Input	Climatological wind, rivers and boundary conditions	Operational, daily update, wind, rivers and boundary conditions
Execution time	Several hours of simulation per day	Minutes of simulation per day
Storage	Magnetic tape	Solid State Disk
Output	Mechanical plotter	Internet, available immediately at global level
Downstream applications	No	Several downstream applications (alert systems, oils spill, etc.)

Table 1.1. State-of-the-art of ocean forecast systems in 1991 and 2021.

vices and to serve all kinds of final users are more and more frequent and relevant. This creates a network of scientists, public institutions, private companies, and final users that today is driving the modeling community in a virtuous loop driven by the needs of the users.

The main objective of this guide is to promote the development of new marine forecasting systems around the globe along with the improvement of the existing ones, compiling and making available valuable information to the professionals in charge of developing these services. In writing the
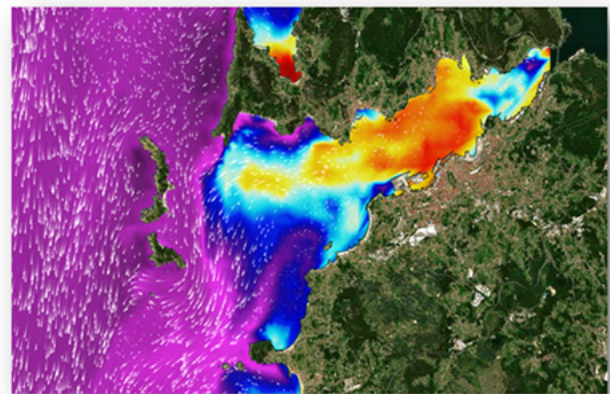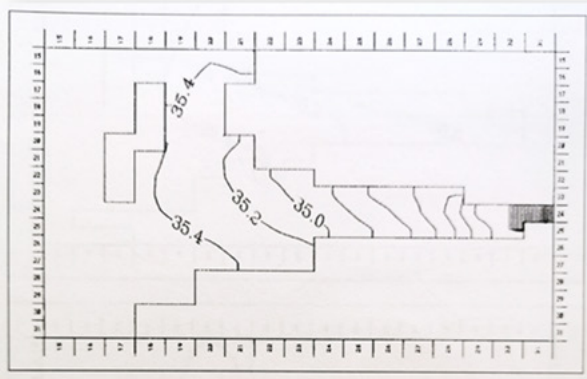
Figure 1.2. The Ria de Vigo estuarine system as seen by a 1991 simulation (on the left) and the 2021 Portus operational forecasting system (on the right, from 🔗²).

2. https://portus.puertos.es/index.html?locale=en#/

various chapters, the authors assumed that the reader has a general knowledge on ocean science but little or no background in ocean modeling. The present book intends to provide an overview of the entire value chain of an Operational Ocean Monitoring and Forecasting System (OOFS), explaining its basis. This guide will also focus, although to a lesser extent, into the more recent technical advances in the sector.

This publication, after the present introductory chapter, has the following structure:

• **Chapter 2**: Motivation and international context of ocean forecasting. This chapter describes the activities of the Expert Team on Operational Ocean Forecasting Systems (ETOOFS) and its connections with the World Meteorological Organization (WMO) and the Joint Technical Commission for Oceanography and Marine Meteorology (JCOMM). Special focus is made on Copernicus Marine Service and other well-established initiatives. Recent advances in open data policy are introduced, such as the Inspire Open Data Directive. The socio-economic impact of ocean forecasting is described by three pillars: applications, climate and ocean health.

• **Chapter 3**: Definition of ocean forecasting systems: temporal and spatial scales solved by marine modeling systems. This section includes a description of the various temporal and spatial scales involved in ocean modeling, explaining the differences between products derived from large time scales runs (such as re-analysis and scenarios) and forecasting services. It also deals with the significant variations found in the physics and numerical schemes associated with the different spatial scales (global, regional and coastal). This matter is further deepened for each variable in chapters 5 to 9.

• **Chapter 4**: Architecture of ocean monitoring and forecasting systems. It contains a general description of the common aspects to all ocean forecasting systems. It explains the basics related to system architecture (inputs, execution, outputs, etc.), quality control and products. The content of this section works as a template to the topics that will be developed in chapters from 5 to 9.

• **Chapters 5 to 9:** Detailed description of ocean forecasting systems, depending on the variable treated (chapter 5 for Circulation modeling, 6 for Sea-ice, 7 for Sea level and Storm surge modeling, 8 for Wave modeling, 9 for Biogeochemical modeling). The purpose of these chapters is to make understandable, even for non-expert readers, all theoretical and practical basis to properly set-up a forecasting system for a given variable. These chapters provide the physical background on the discipline.

• **Chapter 10**: Coupled prediction: integrated atmosphere–wave–ocean forecasting. In this chapter it is explained the importance of considering the processes described in previous chapters in an integrated way.

• **Chapter 11**: Downstream applications: from data to products. This chapter deals with the way the output data from models are transformed into tailored information for the end user. Examples are made for: web pages and other dissemination mechanisms, oil spill forecasting, alert systems, search and rescue, navigation aid, and fisheries

• **Chapter 12:** Challenges and future perspectives in ocean prediction. Future development and expectations in the field of ocean forecasting are described in the final chapter.

There is no claim of having included in a single monograph all the knowledge and beauty of ocean modeling. This guide hopes to be a guideline and inspiration to professionals all around the globe, stimulating the reader to research deeper knowledge on this vast field. If this objective is achieved, this publication is expected to foster the generation of valuable information that will be used in decision making processes and, therefore, to advocate a wiser and more sustainable relation with our always generous ocean.

1.2.
References

Álvarez Fanjul, E., Sotillo, M.G., Perez Gomez, B., Valdecasas, M.G., Perez Rubio, S., Lorente, P., Dapena, A.R., Martinez Marco, I., Luna, Y., Padorno, E., Santos Atienza, I., Hernandez, G.D., Lopez Lara, J., Medina, R., Grifoll, M., Espino, M., Mestres, M., Cerralbo, P., Sanchez Arcilla, A. (2018.) Operational oceanography at the service of the ports. In "New Frontiers in Operational Oceanography", E. Chassignet, A. Pascual, J. Tintoré, and J. Verron, Eds., *GODAE OceanView,* 729-736, doi:10.17125/gov2018.ch27.

FAO (2020). The State of World Fisheries and Aquaculture 2020. Sustainability in action. Rome, https://doi.org/10.4060/ca9229en

Hansen, W. (1956). Theorie zur Errechnung des Wasserstandes und der StrÖmungen in Randmeeren nebst Anwendungen. *Tellus,* 8:3, 287-300, https://doi.org/10.3402/tellusa.v8i3.9023

McWilliams, J., C. (1966). Modeling the Oceanic General Circulation. *Annual Review of Fluid Mechanics,* 28:1, 215-248.

Pinardi, N., Cavaleri, L., Coppini, G., De Mey, P., Fratianni, C., Huthnance, J., Lermusiaux, P.F.J., Navarra, A., Preller, R., Tibaldi, S. (2017). From weather to ocean predictions: an historical viewpoint. *Journal of Marine Research,* 75 (3), 103-159, https://doi.org/10.1357/002224017821836789

Schnurr, Riley E.J., and Walker, T.R. (2019). Marine Transportation and Energy Use. Reference Module in Earth Systems and Environmental Sciences, ISBN 9780124095489, https://doi.org/10.1016/B978-0-12-409548-9.09270-8

Shubinski, R.P., McCarty, J.C., and Lindorf, M.R. (1965). Computer Simulation of Estuarial Networks. *Journal of the Hydraulics Division ASCE,* 92(3), https://doi.org/10.1061/JYCEAJ.0001470

2.
Motivation and international context of ocean forecasting

CHAPTER AUTHORS

Pierre Bahurel and Enrique Alvarez Fanjul

2. Motivation and international context of ocean forecasting

Ocean forecasting took its modern form at the turn of the century, when marine experts on in situ observations, satellite observations, numerical modelling and data assimilation decided to move together towards an integrated approach. Since then, operational oceanography has evolved incredibly fast, fostering communities' engagement, bringing innovations to operations, and structuring new information services for users.

International cooperation was immediately adopted as a natural framework for the development of ocean forecasting, and this is still today an indispensable driving force pulling forward local and national initiatives across continents.

The Global Ocean Data Assimilation Experiment (GODAE), kicked off in 1997 (Bell et al, 2010), played a leading role catalysing the initial steps of this revolution by engaging stakeholders worldwide to build "a global system of observations, communications, modelling and assimilation, that will de-

liver regular, comprehensive information on the state of the oceans, in a way that will promote and engender wide utility and availability of this resource for maximum benefit to the community". Most of today's ocean forecasting centres were born to respond to this international call and are directly built on principles and methods designed in this framework.

GODAE has indeed established the foundation of an international cooperation for ocean forecasting and one of its first outcomes was to build the scientific and technical "common" required to develop and operate advanced ocean forecasting systems, promoting a cooperation based on openness and inclusiveness, and driven by constant innovation. This worldwide activity is benefitting ocean knowledge and is providing useful tools for decision making actions towards a more sustainable ocean. These motivations and principles are still framing and inspiring today our international cooperation for ocean forecasting.

2.1.

International cooperation for a sustainable ocean

Operational Ocean Forecasting Systems (OOFS) are amongst the main and more powerful tools to build the bridge between marine science and society needs, with a consistent and state-of-the-art digital depiction of the ocean environmental state. It took less than two decades to OOFS to emerge from science, gain realism and operational maturity, and convince users of their value; and this is not by chance if international cooperation was identified from the very first day as a key condition for success, being today the natural playground for the development of the OOFS capacity.

Given its importance in the socio-economic and environmental context, outlined in chapter 1, the role of OOFS is gaining relevance with time, both locally through expert services, and globally through international coordinated actions. This importance is being additionally reinforced by the increasing quality of the forecast services and the international cooperation in data exchange and creation of standards, vital tools for ocean forecasting.

The three pillars of the Global Ocean Observing System strategy (GOOS, 2020) can help to briefly describe this relevance. These are applications, climate, and ocean health:

- **Applications (blue economy):** Ocean forecasting is gaining worldwide relevance in creating applied solutions for final users to contribute to a virtuous blue economy. Both public institutions and private companies are taking active steps to implement the so-called "value chain", that transforms ocean observation into information to be employed by end user applications. This is invigorating economic activities, creating jobs, and providing solutions for environmental problems. Chapter 11 provides detailed insight on this particular and presents several relevant applications. Other outstanding set of examples can be found at 🔗 1.

- **Climate:** Climate change is threatening our ocean and, very particularly, our coasts. For example, sea level rise will produce an increase of coastal erosion and inundation events. And the earth climate cannot be explained without a fair understanding of the ocean climate. The study of climate change scenarios with numerical models is our best tool to assess the hazards, one of the key elements of risk analyses, together with vulnerability and exposure. Ocean global reanalyses produced by ocean forecasting centres as reference simulations

---

1. https://marine.copernicus.eu/services/use-cases

for the past decades are key elements in this domain. These simulations, together with scenario projections, allow us to create climate change impact studies that are the main source of information to design mitigation and adaptation strategies. On shorter time scales, dynamic risk reduction activities are vital for maintaining activities in a changing environment. In this sense, the OOFS will become even more relevant, as the number of extreme events increases. Examples of the ocean climate monitoring by OOFS can be found here, with indicators (🔗 2) and annual expert reports on the ocean climate (🔗 3): they are amongst the first OOFS products used by policy makers.

• **Ocean health:** Human activity is impacting ocean health, increasing its temperature and its acidification. This problem is having very visible and dramatic consequences, such as coral bleaching, increments of harmful algal blooms, migration of species and jellyfish proliferation. Ocean forecasting is a key tool to understand the internal dynamics of these processes and, therefore, provide solutions based on knowledge. Additionally, OOFS are providing vital information for strategic action areas to improve sustainability for future generations; food, energy, tourism transport, energy, and seabed mining, as described by the high-level panel for a sustainable ocean economy (🔗 4). All these activities are benefiting from the accurate forecasts that our present-day systems are providing.

The ocean dynamics is of course not limited by our national boundaries, so international cooperation is necessary when dealing with ocean forecasting. But the other reason for imposing international cooperation to ocean forecasting centres, as a mandatory framework for action, is the need to build a strong community voice supporting the policy effort towards a sustainable ocean. With the Ocean relevance increasingly present on international political agendas (see the UN Agenda 2030, the EU Green Deal, and many other initiatives), knowledge derived from OOFS is today essential, and the only way to achieve this is by action on a global framework. Even when OOFS implementation and ocean applications are local, they contribute to a global challenge. On the local scale they bridge the gap between ocean observations and applications and are active players of a prosperous Blue Economy. But their impact is global, by supporting assessment studies and contributing to an improved local sustainability policy that impacts, at the end, the global ocean.

Due to the previous reasons, the international structuration of the OOFS community is an essential condition for a sustainable development of the ocean. Ocean Forecasting is now a recognized player of international ocean governance fora such as the UN ocean initiatives where ocean policies are discussed. Remarkably, ocean forecasting has been identified by the UN as a key contributor for its 14th sustainable development goal "life below water".

2.2.
International cooperation to build our "common"

All ocean forecasting systems have in common their dependence on reliable ocean observations and state-of-the-art ocean modelling components, together with the human expertise and operational processes to design, develop and operate such systems. Marine services based on OOFS are consequently critically dependent on the considerable investments required to develop upstream research for capacity building and large infrastructures such as satellites, marine observation networks and super-computers. Such

massive investments are not affordable at the scale of one entity or one nation, and international cooperation is the only framework able to ensure a sustainable effort in this matter and build this indispensable framework for the OOFS worldwide community.

The "butterfly diagram" (Figure 2.1) illustrates the position of ocean forecasting in the overall value chain, bridging ocean observations with end-users (Bahurel et al., 2010). Ocean forecasting is present on the two steps signed with gears on the figure. On one hand, at the so-called "core services", where its mission consists in integrating the richness and variety of ocean observations to build a state-of-the-art description of the ocean environment, multi-variable, consistent in space and time, reliable, and immediately action-

2. https://marine.copernicus.eu/access-data/ocean-monitoring-indicators

3. https://marine.copernicus.eu/access-data/ocean-state-report

4. https://www.oceanpanel.org/
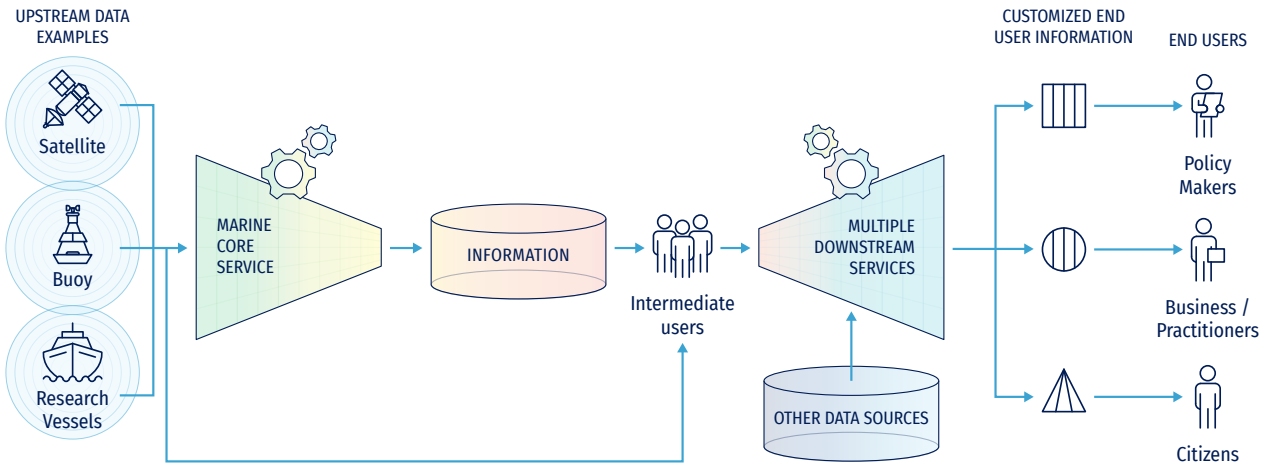
Figure 2.1. From observation to end user services: the ocean value chain.

able by expert services in their own fields of expertise. On a second step, intermediate users can use this freely available description to enrich the data via model downscaling and, finally, generate tailored information and indicators for decision making. This is done via a large variety of downstream services, such as storm surge forecast warning systems or water quality monitoring services.

The left wing of this butterfly (Marine Core Service) also illustrates the OOFS 'common' – i.e., the assets developed through international cooperation and shared by the OOFS community as a common good – that the GODAE initiative has invented two decades ago, and that international cooperation has developed through different channels.

This OOFS 'common' includes:

• **Data:** Ocean observations measured from space by satellites, and in situ by vessels and autonomous networks as well as different forcings or coupling with atmosphere and river run-off required to run OOFS systems. International cooperation has not only organised and simplified the access to these data worldwide, but also has strengthened the voice of the OOFS community for a sustained observation effort.

• **Tools:** Operational tools used to generate a reliable 4-dimensional description of the ocean environment and operate ocean forecasting systems include models, data assimilation systems and product generation software. Full-fledge integrated systems and their parameterization are specific to their purpose, location, and operating team but they are composed of individual bricks (e.g., NEMO -Nucleus for European Modelling of the Ocean- modelling tool) that are frequently shared to feed the OOFS common.

• **Standards:** data sharing or product validation are driven by expert processes and standards to reach efficiency to interoperability. One of the best examples is the adoption of common data formats to facilitate exchanges. The international community work started with GODAE in the field of product validation with the definition of common protocols ("metrics") now widely adopted by OOF centres worldwide.

• **Products:** together with input data entering OOFS, the output products generated by these systems (ocean forecasts, ocean simulations, ocean indicators, …) are widely shared to feed a common set, facilitating intercomparison and individual systems improvements.

• **Know-how:** the outcomes of research undertaken by scientists in the OOFS fields are of course a key asset for the community worldwide, and the scientific community has proposed in this matter fruitful models of cooperation; this common knowledge has been extending its scope with the development of OOFS through the sharing of best practices in the domain of system operations, market development and user uptake.

This is at the heart of international cooperation and its content is in constant evolution. It reveals the strength and the dynamism of the OOFS community: we are prepared to see in the coming years a bloom of innovation to support OOFS development in the coastal zones, marine biodiversity, polar areas, climate adaptation, all integrated in the new paradigm offered by digital twinning.

2.3.

International cooperation to foster openness and inclusiveness

The principle of openness – free and open sharing of data, exchange of knowledge, interdisciplinary cooperation – and the unwavering ambition to generate at every moment the best possible information to improve our knowledge on the ocean and contribute to a sustainable development are fundamentals in this approach. This principle is a cornerstone of international cooperation and has been a key factor of success of the development of ocean forecasting.

One of the most structuring elements has been the adoption of open & free data policy amongst our community. As previously mentioned, data sharing is a vital need to have a predicted ocean. The Resolution 40 of the World Meteorological Organization related to the exchange of meteorological data was the first model identified by weather oceanographers. Afterwards, the scope has been extended by several international initiatives developed to promote data exchange and systems interoperability at a wider scale, facilitating interdisciplinary approaches. For example, the INSPIRE Directive aims to create a European Union spatial data infrastructure for the purposes of EU environmental policies and activities which may have an impact on the environment (🔗 5).

This European Spatial Data Infrastructure is enabling the sharing of environmental spatial information among public sector organisations, facilitating its public access across Europe, and assisting in policymaking across boundaries. Beyond its simplicity for implementation (open sharing means less energy spent in control and more in value creation), openness is a key condition for inclusiveness. Being inclusive is identified as particularly important in the field of modern oceanography where stakeholders, motivations and situations are particularly diverse and rich. The Copernicus Marine service in Europe has shown the strength of a state-of-the-art operational service implemented by hundreds of experts and teams, distributed throughout Europe, coming from public and private sectors, from operational and research organisations, from different countries, from diverse cultures and relations to the ocean. Openness facilitates inclusiveness and enables diversity, bringing together the best skills and fostering capacity building. This principle of inclusiveness is particularly important to successfully manage the seamless integration of coastal centres in the OOFS framework, where – here again – the first priority will be to build a worldwide capacity open and benefitting to all.

2.4.

International frameworks to support OOFS development

Amongst the United Nations framework, the Intergovernmental Oceanographic Commission (IOC) of UNESCO is critically instrumental to build the world ocean 'basic infrastructure', i.e., observations, data management, and forecasting. Within IOC, the Global Ocean Observing System (GOOS) program is a key element of this community effort, and a powerful instrument to structure expert cooperation in the different related thematic areas (e.g., from physics to biology) and the different regions through the GOOS Regional Alliances. In this frame, the Expert Team on Operational Ocean Forecasting Systems (see below) is fully devoted to ocean forecasting. The IOC International Oceanographic Data and information Exchange (IODE)

program complements this effort, with special focus on the setting of ocean data information system.

Beyond IOC-UNESCO, the other GOOS sponsors – World Meteorological Organization (WMO), UN Environment Program (UNEP) and the International Science Council (ISC) – are all active players in this area. WMO offers a solid model of organisation, set for weather forecasting, where the management of basic infrastructures on one hand – see for instance the WMO Global Data Processing and Forecasting System (GDPFS) that coordinates Member capacities to prepare and make meteorological analyses and forecast products – and the management of weather services on the other, can inspire the world ocean community and propose immediate hooks to develop ocean/weather synergies, as it is already

5. https://inspire.ec.europa.eu/

the case for observations. The marine component of Global Environment Monitoring System (GEMS Ocean) of UNEP is another example where ocean prediction information is identified as a key source of information. As an illustration, we can observe how the World Environment Situation Room – which is an environmental dashboard operated by UNEP for its Member States – includes in its Ocean/ SDG14 section operational ocean prediction products.

It is in this framework where the ETOOFS (Expert Team on Operational Ocean Forecasting Systems) action takes place: hosted by IOC and co-sponsored as GOOS by IOC, WMO, UNEP and ISC, this body brings together experts representing each continent, highly motivated to share and improve their experience and skills to help developing countries build their national centres for operational oceanography. ETOOFS enables worldwide use of timely and reliable ocean forecasts for applications in national security, environmental protection, and the maritime economy. It is a vital operational link between observing networks and marine services.

Amongst others, the following ETOOFS activities are to be highlighted:

- Manage and maintain guide, scope and requirement documents for countries providing ocean forecasting services.

- Manage and maintain an overview of active operational ocean forecasting systems.

- Manage and promote the adoption of an international standard to support interoperability and common formatting of ocean forecast products and services.

- Guide and initiate actions contributing to improving operational ocean prediction system efficiency, fidelity and service quality.

- Promote and facilitate support for, and development of, operational and forecasting systems and their adoption in the wider community.

- Provide advice on operational ocean forecasting systems related matters and prepare submissions on the requirements of operational ocean forecasting systems operated by countries to other international groups.

Multilateral initiatives such as the G7 Future of Seas and Ocean Initiative (🔗 6) or the Blue Planet component of the international GEO (Group on Earth Observations) program (🔗 7) are other relevant frameworks where the value of OOFS is

progressively recognized and further developed. We observe for instance how the priorities set by the G7 FSOI (Future of the Seas and Oceans Initiative) on digital oceanography (amongst others) and by GEO Blue Planet on marine applications are dependent on ocean prediction.

It is also important to mention the tremendous contribution of large organisations such as the European Commission in Europe, which, in the frame of its space program Copernicus, has created and supports a unique Copernicus Marine forecasting service (Le Traon et al., 2017) organisation (🔗 8). This European-made service follows the international cooperation principles presented above, with a global impact as the first driver, and was the key to design, build and operate a "core" service following common good principles, and to implement a full open data policy and an inclusive service organisation across Europe. The link with the other continents – America, Asia, Australia, Africa – is at the heart of Copernicus Marine. Similarly, we can observe how the African Union has encouraged structuring initiatives for a prosperous Blue Economy across the African continent with IOC, with GEO and other programs where ocean forecasting is instrumental. The workshop organised by ETOOFS in the preparation phase of the present guide has shown a remarkable demand on all continents for a reinforced community approach and OOFS capacity development worldwide.

OceanPredict (🔗 9), which descends directly from the initial GODAE initiative, is the best international framework to develop science & technology initiatives in the field of ocean forecasting. At a scientific level, the modelling community is indeed self-organised thanks to it. This is a team dedicated to work with the Global Ocean Observing System (GOOS) and associated groups to co-design and co-develop the ocean observing and forecasting system of the future, with the aim of delivering the essential information needed for safety, wellbeing, and prosperity. OceanPredict is a vigorous and strong international coordination mechanism to build the ocean prediction capacity of the future. This will be achieved thanks to the improvement of the science, capacity, efficacy, use, and impact of ocean prediction systems, contributing to a seamless ocean information value-chain, from observations to end users, for economic and societal benefit.

Finally, the launch by IOC-UNESCO of a "UN Decade of Ocean Science for Sustainable Development" is an excellent opportunity to do more, reinforce international cooperation and enrich our community and knowledge in the field of ocean prediction. The relevance of ocean forecasting systems will be even larger in the future, with more reliable

---

and interoperable services, able to serve a wider range of final users. In this process, the activities of the UN Decade of Ocean Science will be of paramount importance (UNESCO-IOC, 2021). Under the vision "the science we need for the ocean we want", the Ocean Decade will implement transformative ocean science solutions for sustainable development. The following outcomes describe "the Ocean We Want, which is the aim and final target of this initiative:

- A clean ocean where sources of pollution are identified and reduced or removed.

- A healthy and resilient ocean where marine ecosystems are understood, protected, restored and managed.

- A productive ocean supporting sustainable food supply and a sustainable ocean economy.

- A predicted ocean where society understands and can respond to changing ocean conditions.

- A safe ocean where life and livelihoods are protected from ocean-related hazards.

- An accessible ocean with open and equitable access to data, information, technology, and innovation.

- An inspiring and engaging ocean where society understands and values the ocean in relation to human wellbeing and sustainable development.

As a part of the Decade activities, Mercator Ocean International will implement a Decade Collaborative Center for Ocean Prediction (OceanPrediction DCC). This initiative will provide: i) a global forum to focus and optimise the efforts of individual Decade programmes on achieving the collective goals of the Decade, ii) a communication and collaboration hub that brings together Decade programmes with ocean prediction activities, institutes, and organisations outside of the Decade, and iii) the global technical and organisational structure required to establish a pilot for a Global Ocean Data Processing, Modelling, and Forecasting System building on the innovations generated by Decade programmes – such as CoastPredict, Foresea or DITTO (Digital Twins of the Ocean) to name a few – and other national, regional, international and intergovernmental partners.

2.5.
An international community of Operational Ocean Forecasting Systems ready for the next steps

The OceanPredict website describes a first series of ocean forecasting systems, projects and centres, illustrating the worldwide dynamism of this scientific and operational domain: they are BlueLink in Australia, Concepts in Canada, ECCO, Hycom and NCEP in the United States, ECMWF and the Met Office in the United Kingdom, INCOIS in India, Mercator Ocean International in France, CMCC (Centro Euro Mediterraneo sui Cambiamenti Climatici) in Italy, MOVE/MRI in Japan, NMEFC (National Marine Environmental Forecasting Center) in China, REMO in Brazil and the NERSC (Nansen Environmental and Remote Sensing Center) in Norway: they have in common their global and basin-scale geographical extensions and also their international visibility. But how many other OOFS could we map all over the world? What about SAMOA (Sistemas de Apoyo Meteorológico y Oceanográfico de las Autoridades Portuarias) in Spain (Alvarez Fanjul et al., 2018)? How many of them are in the Pacific or along the African coast? In the Mediterranean only, and for the currents only, we can find 32 different forecasting systems according to the Mon-

GOOS webpage (🔗 [10]): they can be local, they can have different purposes, missions or maturities but they are exemplary of the richness and readiness of the OOFS community worldwide. It is time for us all to structure further this talented community and make it visible. The new international momentum offered by the UN Decade of Ocean Science on one hand and the technological breaks proposed by the integration of digital twinning is a real chance. Ocean prediction centres are ready for a new step in this digital oceanography, and they are well prepared: committed for a sustainable ocean, for a state-of-the-art common set of assets nourished by all and benefitting to all, and for an open and inclusive approach.

---

10. http://www.mongoos.eu/

2.6.
References

Alvarez Fanjul, E., Sotillo Garcia, M., Perez, B., Garcia Valdecasas, J.M., Perez Rubio, S., Lorente, P., Dapena, A.R., Martinez, M., Luna, Y., Padorno, E., Santos Atienza, I., Diaz Hernandez, G., Lara, J.L., Medina, R., Grifoll, M., Espino, M., Mestres, M., Cerralbo, P., Sanchez Arcilla, A. (2018). Operational oceanography at the service of the ports. In: "New Frontiers in Operational Oceanography", E. Chassignet, A. Pascual, J. Tintoré, and J. Verron, Eds., GODAE Oceanview, 729-736, doi:10.17125/gov2018.ch27

Bahurel, P., Adragna, F., Bell, M., Jacq, F., Johannessen, J., Le Traon, P.-Y., Pinardi, N., She, J. (2010). Ocean Monitoring and Forecasting Core Services, the European MyOcean Example. Proceedings of OceanObs'09: Sustained Ocean Observations and Information for Society, doi:10.5270/OceanObs09.pp.02

Bell, M., Lefebvre, M., Le Traon, P.-Y., Smith, N., Wilmer-Becker, K. (2009). GODAE: The global ocean data assimilation experiment. Oceanography, 22(3), 14-21, https://doi.org/10.5670/oceanog.2009.62

GOOS. (2020). A Roadmap for the Implementation of the Global Ocean Observing System 2030 Strategy. IOC, Paris, GOOS Report No. 249.

Le Traon et al. (2017). The Copernicus marine environmental monitoring service: main scientific achievements and future prospects. Special Issue Mercator Océan International #56. Available at: https://marine.copernicus.eu/it/node/594

UNESCO-IOC (2021). The United Nations Decade of Ocean Science for Sustainable Development (2021-2030) Implementation Plan. UNESCO, Paris (IOC Ocean Decade Series, 20).

3.
Definition of ocean forecasting systems: temporal and spatial scales solved by marine modeling systems

CHAPTER COORDINATOR

Enrique Alvarez Fanjul

CHAPTER AUTHORS *(in alphabetical order)*

Marcos Garcia Sotillo and John Wilkin

3. Definition of ocean forecasting systems: temporal and spatial scales solved by marine modeling systems

3.1.
Operational oceanography and ocean forecasting services: definition and main purpose

Operational Oceanography is defined as the set of activities for the generation of products and services providing information on the marine and coastal environment. OO is designed to meet different societal, economical, scientific and other user needs. As defined by the EuroGOOS, there are two main pillars in OO services: i) the monitoring element, which focuses on the systematic and long-term routine measurements of oceans and atmosphere, and their rapid interpretation and dissemination; and ii) the prediction component, which uses ocean models to generate a variety of products that may be nowcasts (the most accurate description of the present ocean state provided by the analyses), forecasts (the future condition of the ocean for as far ahead as possible) or hindcasts (the most complete description of past states, provided by reanalysis).

Understanding the physical behavior of ocean and coastal areas provides an important guidance to manage issues related to anthropic impacts and resource exploitation activities. A wide variety of operational ocean models have been and are currently used to tackle different issues and to support various service purposes. These different types of ocean model applications, specific for each problem to be solved, are based on different computer codes and parameterizations. They resolve a range of spatial and temporal scales (with different model resolutions) using a miscellany of data sources (as forcing initial and boundary conditions) and can rely or not on data assimilation methods to integrate observations (Schiller et al., 2018).

Wind, waves and sea-level traditionally were the most important met-ocean parameters for maritime activities due to their implications for marine safety and impacts on operations and navigation conditions. Therefore, these parameters have been the most extensively monitored and forecasted since earlier times and their forecasting has frequently been the responsibility of meteorological services. The traditionally strong connection between waves and weather prediction is reinforced by the direct interaction between waves and winds, which makes the waves a special case with specific models coupled only with atmospheric models (see Chapter 10), resulting in a separated development of ocean and wave models. Nevertheless, in the last decade the gap between ocean and wave models is diminishing and they are being progressively integrated in more comprehensive operational ocean coupled systems (in some cases also coupling with the atmosphere).

The sea level is the other key variable that counts with a long tradition in operational services based on specific models.

Sea level prediction services have supported very different human activities, mostly related to navigation in shallow waters being harbors, estuaries and other coastal areas impacted by tides and appreciably sub-tidal variability. Sea level forecasting of storm surge is a key element in coastal flooding warning systems. Originally, only astronomical tidal predictions were used in the sea level forecasting but progressively this approach was augmented by the use of storm surge models, which are based on single-layer homogeneous density barotropic ocean models but include also very detailed bathymetries with astronomical tidal forcing and a meteorological residual contribution (see Chapter 7). Currently, storm surge forecasting is also benefiting from the sea surface height products delivered by the available high-resolution 3D global and regional baroclinic models operated by different ocean forecasting services (Pérez et al., 2012).

A recent overview of the current European capacity in terms of operational modeling of marine and coastal systems (Capet et al., 2020) provides a comprehensive panorama of what are the essential ocean variables and phenomena of most interest in relation to their relevance for regional environmental issues and their impact on different economic sectors. An interesting output from the survey performed to underpin this study reveals that nowadays a vast majority of the identified OO forecast services operate hydrodynamic models (see info on them in Chapter 5), with waves and biogeochemical models (see Chapters 8 and 9) also represented but to a lesser extent. Other specific models, such as for particle drift prediction and sea ice (see Chapter 6), are scarcer in the operational landscape. The study also reveals how currents, salinity, temperature, and sea surface height are resolved for almost all operational models. Instead, basic variables of biogeochemistry (e.g., oxygen, nutrients, phyto- and zooplankton biomasses, suspended, and organic matter) are much less represented in the ocean forecasting services. To date, marine safety, oil spills and sea level monitoring appear as the phenomena mostly addressed by European operational models (with more than 40 implementations). Storm surges, water quality, and eutrophication are well-considered at present (~ 15-25 implementations) and will benefit from an extended coverage in the coming years (~ +30-50 % within 5 years). Finally, it must be pointed out that harmful algal blooms, shoreline/bathymetry changes, and ocean acidification receive some attention but remain limited in their coverage.

Biogeochemical models have a greater complexity, as they involve many more state variables, parameters, uncertain

processes, interactions and drivers, which means that they may not have yet reached the level of maturity required for accurate simulations and useful outputs; for these reasons their adoption in operational applications is presently limited. This also applies to the use of data assimilation in coastal operational application or sea ice coupled models, even though in the past decade substantial efforts have been dedicated to developing and improving comprehensive global and regional operational forecasting services. An example is the case of the service delivered by the marine component of the Copernicus Program of the European Union (Coperni-

cus Marine Service, 2021a) which provides free, regular and systematic information on the state of the Blue (physical including waves), White (sea ice) and Green (biogeochemical) ocean at global and regional scales, on the basis of model applications with the appropriate complexity suitable for operational forecasting. Finally, it is to be noted that sustained availability of global and regional scale core products, such as the ones delivered by Copernicus Marine Service, has fostered the development of specific "downstream" services devoted to coastal forecasting, favoring synergies between different existing services (Sotillo et al., 2021).

3.2.
Essential ocean variables covered by marine monitoring and forecasting systems

Numerical ocean models generate as output a substantial number of variables and volume of data. The variety of variables dealt by such models depends on the type of model applied, the processes included, and the systems involved (for example, ocean models can be coupled to atmospheric and surface wave models, as well as to sea ice models or biogeochemical ones). On the monitoring side, the ability to measure the ocean with new technologies and techniques (related to both remote-sensed and in-situ device observations) has been continuously enhanced since the 1980s as well, resulting in an extended range of ocean variables to deal with.

This wide variety in terms of variables used to monitor and model the ocean is reflected by the CF metadata conventions ([1]). These conventions are intended to be used with climate and forecast data derived from atmosphere, surface and ocean models, and from comparable observational datasets, and are designed to facilitate the processing and sharing of data files via widely used formats (e.g. NetCDF and ZARR) and web services (e.g. THREDDS and ERDDAP); their use is supported by a wide range of software. The CF Standard Names Table ([2]) is a living document that is continuously expanded following requests for new variables. In its version 77, dated 19 January 2021, there were 579 standard names that match a query for the strings "seawater" or "ocean". This number gives an idea of the broad panorama existing in terms of ocean climate and forecast variables.

Due to this great breadth and differentiation of ocean variables, the need arose to agree on some common key variables to monitor the ocean. In the late 1990s, in part motivated by requirements to support activities and negotiations in the framework of the UNFCCC and the IPCC, emerged the concept of ECVs. An ECV is a physical, chemical or biological variable (or a group of linked variables) that critically contributes to the characterization of Earth's climate. Furthermore, the ECV datasets progressively became also widely used in the context of mitigation and adaptation measures, as well as to assess risks and enable attribution of climate events to underlie causes. This is the fundamental importance of ECVs and the reason for which climate services focus resources to monitor and forecast these minimal sets of "key variables". Currently, there are 54 identified ECVs (GCOS, 2021). Global expert panels, coordinated by GCOS, are responsible for maintaining updated definitions of the ECVs required to systematically observe the Earth's changing climate. The ECV specification sheets are intended to be observation platform agnostic, not focusing on what any given existing or novel observational technology can deliver, but on the ultimate resolution and accuracy that the full network of coordinated systems can achieve to meet user requirements.

The WMO defines the following ECVs specifically focused on the ocean (WMO, 2021):

- 12 related to physics: Ocean Surface Heat Flux, Sea Ice (including Concentration, Extent/Edge, Thickness and Drift), Sea Level (Global Mean and Regional), Sea State (Wave Height), Surface Stress, Temperature, Salinity and Currents for both Sea Surface and Subsurface;

1. http://cfconventions.org/latest.html
2. http://cfconventions.org/standard-names
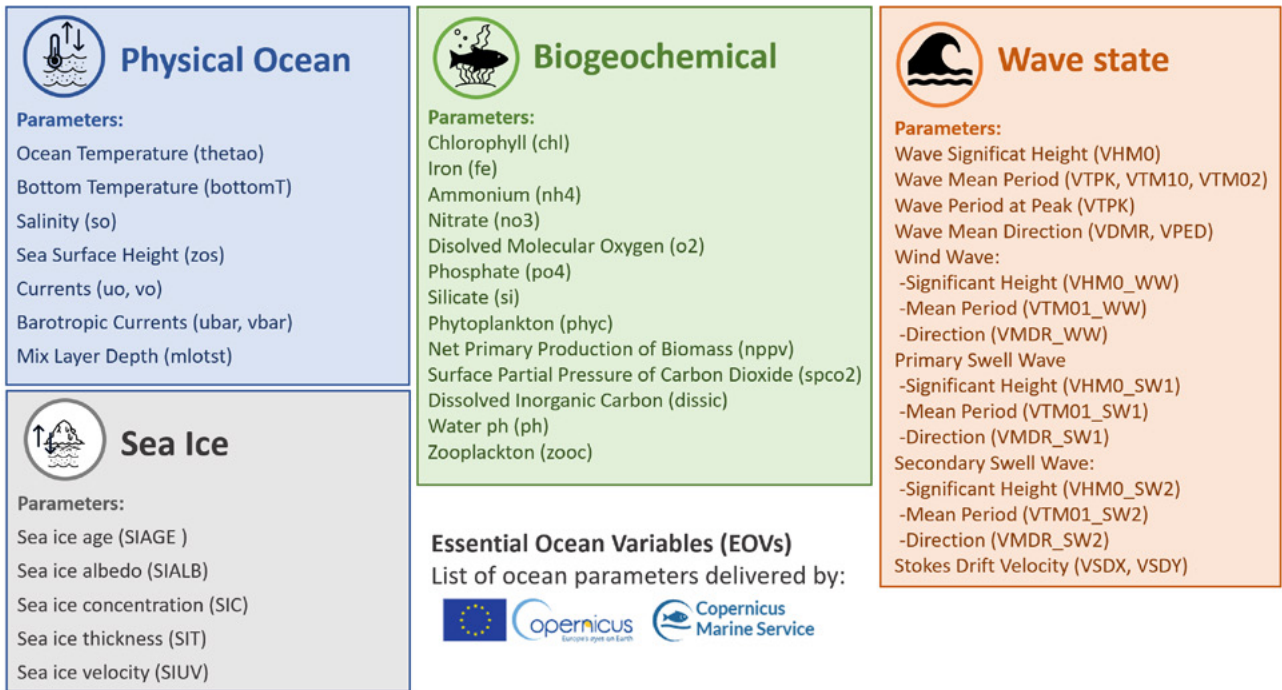
Figure 3.1. Essential Ocean Variables (EOVs): lists of parameters delivered by the Copernicus Marine Service for the physical ocean (including sea wave state), biogeochemistry and sea ice.

• 6 biogeochemical: Inorganic Carbon, Nitrous Oxide (including interior ocean N2O and N2O air-sea flux), Nutrients (including ocean concentrations of silicate, phosphate and nitrate), Ocean Colour (Chlorophyll-a Concentration), Oxygen, and Transient Tracers (CFCs, etc.).

• 2 Biological/Ecosystems: Marine Habitat Properties (Coral Reefs; Mangrove Forests, Seagrass Beds, Macroalgal Communities) and Plankton (Phytoplankton and Zooplankton).

Ocean monitoring and forecasting services focus their resources on covering most of these ocean ECVs. Actually, there is an expanded list of EOVs maintained by the GOOS (Sloyan et al., 2019) in collaboration with panels provided by the OOPC panel and the IOCCP. GOOS aims to periodically re-evaluate and update the EOVs list. Importantly, the EOVs include observable ecosystem and biogeochemical characteristics of the ocean that are needed for understanding the state and health of the marine environment, currently under pressure by human stressors and climate change. While networks that observe the physical ECVs/EOVs are generally well established, those working on biogeochemical and ecosystem EOVs are in most cases still in the concept or pilot phase. Nevertheless, acquisition of these data by regional and global observing systems is essential to the development of model-based forecasting capabilities. For further details on the on-going actions and the path forward to extend operational monitoring of these ocean variables see Muller-Karger et al. (2018).

Some marine services already go beyond the Ocean-ECV and EOV lists, delivering model and observation products for a broader set of variables. This is the case for the Copernicus Marine Service , which monitors Ocean-ECVs (as described in its "Ocean State Report (OSR)", Copernicus Marine Service, 2021b), but goes even further than the common list delivering more variables and indicators of interest for a wide-ranging end user community through its Product Portfolio (Copernicus Marine Service, 2021c). A summary of EOVs and parameters delivered by the Copernicus Marine Service is shown in Figure 3.1. Copernicus Marine Service is a good example of what occurs across most of the trans-national, national or regional ocean monitoring and forecasting services.

3.3.
The spatial scales: downscaling for higher resolutions

Ocean dynamics are described through equations of motion (the Navier–Stokes equations) that are well established for ocean physics (mass, momentum and heat). However, these equations formally apply to the continuum level, whereas in ocean forecasting they are solved on a computational grid with a finite number of cells and discrete resolution. Furthermore, in virtually all computational environmental fluid dynamics fields approximations are made to the governing equations to make their solution tractable. The trade-offs between model resolution, ocean dynamical processes resolved, and computational effort are discussed elegantly by Fox-Kemper (2018). At the outset, ocean modelers are confronted with the key decision of choosing the appropriate spatial resolution for each specific ocean model application. In global operational model applications, relatively coarse resolutions of the order 10s to 100s kilometers are common, whereas in coastal models far higher spatial resolution is needed (perhaps as little as hundreds of meters). The choice of spatial resolution inevitably sacrifices sub-grid-scale dynamical processes that are impractical to explicitly resolve and must instead be somehow parameterized.

Over the past 30 years there has been a steady evolution in ocean model resolution, in a direct proportion with enhancements and availability of computing resources. This resulted in a finer spatial resolution that allowed significant improvement in the simulation of oceanic flows. A major milestone in the evolution of ocean modeling was the introduction of eddy resolving models. This class of models, with spatial resolution (less than 1/4º in latitude and longitude; or around 25 km) sufficient to allow the spontaneous emergence of ocean mesoscale eddies, was a major ocean model achievement, improving the quality of global simulations and opening the door to accurate regional ocean modeling. However, as described in the next section, this resolution is now eclipsed in global operational systems.

The continuous increase of resolution along with the progressive enhancement of models was also due to the more explicit inclusion of higher frequency processes, such as the representation of tidal motions and the better representation of turbulence and mixing processes in shallow waters. These improvements have pushed the use of ocean models into the mesoscale resolved and sub-mesoscale-permitting regime, allowing their uses also for coastal purposes. As a result of this progressive evolution of ocean modeling, we have today an ocean model landscape composed of global, regional and local (coastal, littoral and estuarine) model applications.

The traditional, though in some way artificial, partition between spatial domain extent and model resolution, has been also favored by the fact that operational ocean forecasting centres generate their specific ocean model products for coastal and regional seas following a typical dynamical downscaling approach, which transfers information at large scales from the global solutions to the interior of the nested regional domains (Kourafalou et al., 2015). Spatial scales are directly linked to temporal ones, and adequate temporal resolution is also needed to simulate ocean processes at refined spatial resolution. Hydrodynamic model time steps are always matched to spatial resolution by virtue of numerical stability constraints, but consideration must be also given to adding temporal resolution in external inputs, such as specifying river inflow data at daily or shorter intervals, and resolving in this way the diurnal cycle of solar heating. It should be emphasized that temporal and spatial scales play important roles in ocean model performance, and inappropriate decisions on the spatial-temporal scales to be solved may result in modeling errors.

As pointed out by Holt et al. (2017), one of the greater challenges in Earth System Modeling science is to get an accurate representation of coastal and shelf seas in global ocean models. Furthermore, applying cutting-edge scientific progress in ocean model systems, which aim at solving the ocean state in the climate system or at supporting monitoring and forecasting systems, is another challenge of the operational ocean services.

Next sections describe ocean forecasting at the global, regional and coastal scales:

3.3.1. Global monitoring and forecasting systems

Numerous ocean modeling groups and individual researchers operate near real-time systems for the analysis and forecast of ocean mesoscale circulation in global and basin scale domains. They are gathered under the umbrella of the OceanPredict science network (🔗 ³) that evolved from the GODAE group established in 1999 at the behest of the GOOS sponsored OOPC panel. As a forum for knowledge exchange, OceanPredict fosters communication on best practices and new developments in global ocean modeling, engaging also with regional domain activities and the generation of mod-

---

3. https://oceanpredict.org

el-based information products. A component of these activities is the annual reporting on forecast systems run by national centers and multi-national consortia, which maintain a very high level of operational stability and reliability akin to national weather services. In many instances these ocean systems increasingly operate in strict collaboration with weather services, a trend that is strengthening with the emergence of seasonal to sub-seasonal prediction efforts. From OceanPredict 🔗[4] annual reports and system descriptions, it can be noted that horizontal resolutions of order 1/12°, or roughly 9 km at mid-latitudes, are widely considered adequate for delivering forecasts useful to numerous stakeholders and users, and to inform subsequent down-scaling efforts. Running global simulations at much higher resolution, such as the 1/48º (~2-3 km) MITgcm LLC4320 model (Su et al., 2020), has proven feasible, and this resolution improves the representation of processes such as the mesoscale to submesoscale turbulent cascade and submesoscale modulated vertical mixing. However, for global forecast systems, the substantial additional cost of advanced DA increases the computational demand of the analysis/forecast cycle by roughly an order of magnitude, making higher resolutions impractical at present. Moreover, there is evidence that existing global observing networks are not able to constrain higher resolutions. Jacobs et al. (2019) suggest that the horizontal scales of motion that are effectively constrained by available sustained observations is of order 36 to 54 km or larger, depending on the metric. When shorter length scales that were notionally resolved by their model (~5 to 10 times the grid resolution) but unconstrained by observation were filtered out of the model prior to computing Lagrangian drifter trajectories, the ensemble trajectory forecast error actually decreased.

3.3.2. Regional monitoring and forecasting systems

Many groups in the OceanPredict network also operate regional domain models encompassing single ocean basins or large marginal seas with enhanced resolutions of about 4 km or even finer, using output from global analysis/forecast systems as open boundary conditions. There are many reasons for this downscaling approach. The familiarity of local experts with regional ocean dynamics allows them to make choices in model configuration that yield more skillful results. For data assimilative systems, there is also the opportunity to incorporate local observations that were not utilized by the parent model operators. Furthermore, regional operators are often better acquainted with, and can be more responsive to, the information product requirements of regional stakeholders.

The nominal resolutions of some typical regional systems within OceanPredict 🔗[5] are for the seas around Korea of 1 to 3 km and ports at 300 m, the MedFS at 1/24º (~3.5 km), and the JMA at ~2.5 km. Numerous sub-domains in the Indian Ocean run by the INCOIS operate at similar resolutions.

Some of these systems include advanced DA in the forecast cycle initialization, such as the JMA regional model that uses 4-dimensional variational (4D-Var) assimilation, although this is not the norm. Several Regional Associations of the US IOOS operate down-scaling forecast systems using 4D-Var to incorporate local high-resolution data from autonomous vehicles and surface current measuring HF-radar in domains of several hundred kilometers in extent, but model resolution is in the range 4 to 10 km. The WCOFS operated by the US NOAA CO-OPS is an ambitious regional forecast system covering over 3000 km of the US west coast. Originally conceived as a 2-km model (Kurapov et al., 2017), this proved impractical for real-time DA. Operational WCOFS uses a 4 km grid, for which a complete cycle of 4D-Var takes 5 wall clock hours each day on 480 cores of the National Weather Service high performance computer.

However, computational cost remains a major constraint on regional model resolution, and the question of whether coastal ocean observing systems have sufficient resolution to inform finer scales remains open. Mixed resolution systems are in development, wherein the forecast model is run at a higher resolution than the DA analysis. In experimental systems there is evidence (Levin et al., 2021) that submesoscale resolving nested models can extract added information from closely spaced observing platforms that capture the unbalanced ageostrophic submesoscale.

Sotillo et al. (2021) describe an operational system with a model grid downscaling approach. It employs regional downscaling to order 4 km with the purpose of delivering improved resolution for continental shelf seas of the Iberian Peninsula, with subsequent downscaling to ~350 m on selected coastal sectors and further to ~70 m in ports. This hierarchical approach, using similar models at each level of refinement raises a question: what are the differences between a coastal and a regional model?

The regional forecasting system examples mentioned above mostly use model codes that solve the hydrostatic primitive equations on a structured grid. While the transition to very high-resolution might admit submesoscale stratified dynamics, shallow coastal waters are often well mixed vertically and the processes relevant to ocean prediction for maritime operations have horizontal scales that are long relative to the depth, and consequently the hydrostatic approximation remains valid (Fringer et al., 2019).

The distinction we have made in structuring this section is that coastal models differ from regional models in that sub-mesoscale processes are dramatically constrained by bathymetry while coastline scales are smaller than the Rossby deformation scale. Such processes include lateral and vertical flow separation, secondary flows, headland eddies, wakes, and frontal convergences. Resolution of topographic features that impact such processes is of paramount importance.

3.3.3. Coastal monitoring and forecasting systems

As previously noted, Sotillo et al. (2021) used a set of structured grids in their limited area one-way downscaled nested coastal models for selected ports and coastal segments. One advantage of this strategy is that the computational burden of short time steps demanded by high resolution is limited to the finest grid nests and does not impact the efficiency of the coarse parent grid.

More complex nested systems employ full coupling of parent and child nests on each time step, including two-way communication of fine scale variability back to the parent, a feature supported in some models such as the Coastal and Regional Ocean COmmunity model (CROCO; 🔗 [6]). A similar nesting framework has been used in the Regional Ocean Modeling System (ROMS; 🔗 [7]) model within the Coupled Ocean-Atmosphere-Wave-Sediment Transport system (COAWST; Warner et al. 2008) to perform numerous research studies of coastal and nearshore circulation and geomorphology, though implementation of this approach in operational systems is rare.

NOAA CO-OPS use the orthogonal curvilinear coordinate facility in ROMS to better represent details of irregular coastline shape and variable bathymetry in a number of estuaries of the U.S. coastal zone. For example, the Delaware Bay Operational Forecast System (DBOFS; 🔗 [8]) uses a curvilinear grid that adapts the model domain to the general shape of the estuary (Figure 3.2) and stretches the grid resolution from 4 km offshore to 40 m within the tidal river.

However, there are clear limits to the abilities and efficiencies of curvilinear structured grid models for coastal applications. By contrast, unstructured grid models (e.g. FVCOM, AD-CIRC, SELFE, SUNTANS; see Fringer et al. (2019) for references on these models) have enormous flexibility to resolve complex bathymetric features. They efficiently resolve multiscale features by adapting grid orientation to follow the coastline or the isobaths, telescoping the resolution to match anticipated scales in the circulation.

6. https://www.croco-ocean.org

7. https://www.myroms.org

8. https://tidesandcurrents.noaa.gov/ofs/dbofs/dbofs_info.html
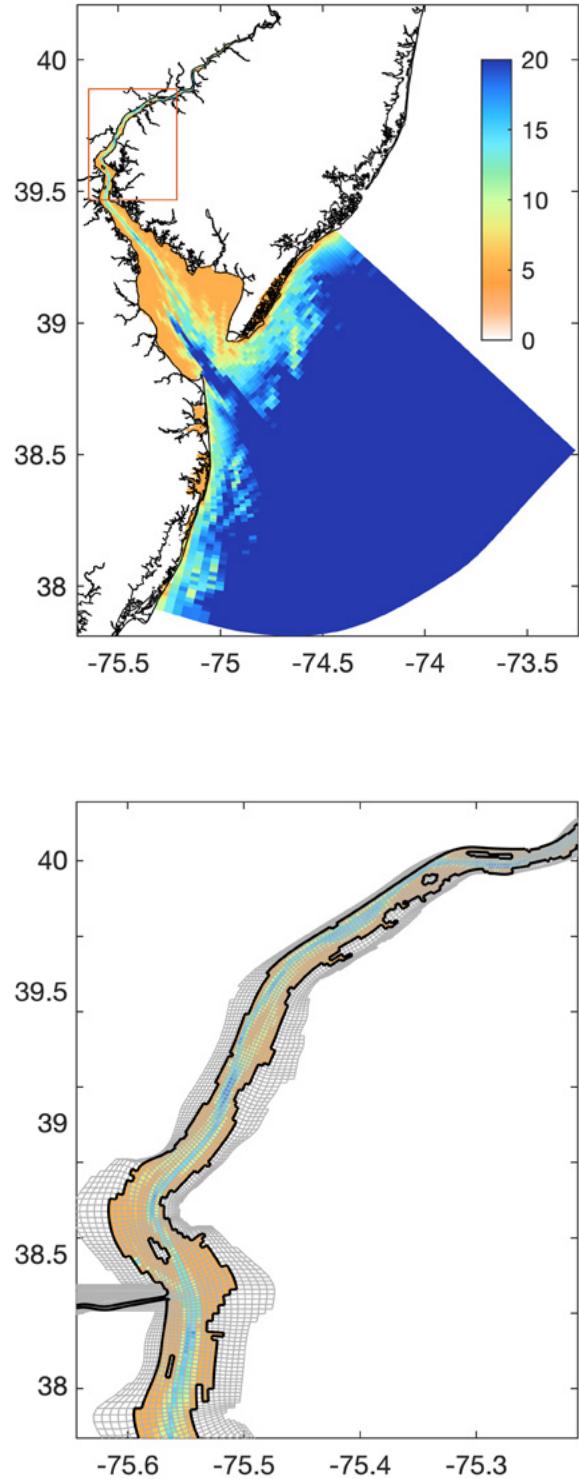
Figure 3.2. NOAA CO-OPS Delaware Bay Operational Forecast System (DBOFS) curvilinear grid domain and bathymetry (top) and enlarged view of inset area (bottom) showing the stretch mesh ~40 m resolution in the vicinity of the estuarine salt wedge and tidal river.

Conventional unstructured grid model configurations use the same time step throughout the domain, so regions of coarse resolution are often integrated with a time step vastly less than necessary for accuracy or stability, incurring in a loss of efficiency. But a well-crafted mesh will have a relatively small proportion of cells where the resolution is coarse. For example, the Great Barrier Reef model of Legrand et al. (2006) has 82% of the cells concentrated close to reefs and islands, whereas 25% of the area of the domain far from the coast is captured by less than 1% of cells.

As its name suggests, the SURF described by Trotta et al. (2021) demonstrates that both approaches to grid design can be implemented within a single system taking advantage of their respective strengths.

The ability of unstructured grids to resolve exceptional detail locally is illustrated by the application of the Stanford unstructured-grid, nonhydrostatic, parallel coastal ocean model (SUNTANS) to achieve ~1 m horizontal resolution at a convergence zone between tidal channels in the Snohomish River Estuary (Giddings et al., 2012). At this resolution, non-hydrostatic dynamics that are incorporated in the SUNTANS computational kernel can become important. However, in operational settings that encompass much larger domains, fully resolving such coastal submesoscale detail is not feasible, and some attempt at parameterization is necessary.

Approaches to parameterizing very high-resolution bathymetry in lower resolution models are discussed by Fringer et al. (2019), who draw particular attention to the sub-grid bathymetry method of Casulli (2009) for improved representation of wetting and drying processes for coastal sea level inundation. This approach, which preserves the cross-section area of cell faces on the basis of bathymetric data available at resolution finer than the model mesh, was used to great effect by MacWilliams et al. (2016) in simulations with the UnTRIM model (Casulli and Zanoli, 2005) of the San Francisco Estuary (Figure 3.3). Accuracy similar to the high-resolution (~10 m) version of the model was achieved with an order of magnitude fewer cells and a 40-fold speed-up in run time. For coastal inundation forecasting – an important application of operational coastal ocean modeling – is essential to follow these careful steps to represent coastal submesoscale bathymetric detail, as well as to achieve acceptable run-time for the timely delivery of forecast guidance.

The meaningful configuration of an operational system at such high resolution clearly requires the existence of comparable resolution bathymetric data. These are becoming more widely available with the increasing use of airborne LIDAR and concerted efforts to merge independently acquired data sets into unified gridded products with harmonized vertical datum. For example, coastal relief (both water and adjacent land) is digitized at 1/3 arc seconds (~10 m) for many sectors
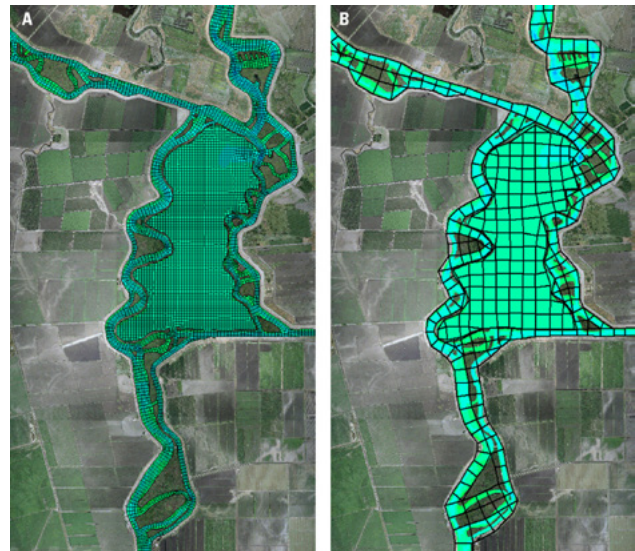
Figure 3.3. Comparison between high-resolution (left) and coarse-resolution (right) from the Bay–Delta model grids by the UnTRIM model in the region of Mildred Island, San Francisco Estuary, U.S., showing the savings in resolution with little loss in accuracy by the application of sub-grid-scale bathymetry parameterization – from MacWilliams et al. (2016).

of the US East coast that are subject to frequent storm surge inundation or at tsunami risk, and for most estuaries bathymetric data at 30 m resolution are available.

In contrast to the great challenge of adequately representing horizontal detail in coastal ocean models, vertical resolution is seldom a limitation in operational models. The widespread use in coastal models of terrain following coordinates retains vertical resolution in shallow water; in ROMS and CROCO this can be further stretched toward the surface or seafloor to give added resolution in frictional boundary layers.

Vertical turbulence closure schemes for operational coastal models are mature, including the parameterization of wave-current interaction processes that modify bed stress, wave radiation stress and Stokes drift, and models can exploit wave data or a wave model if they are available in conjunction with the circulation model. In this topic, there is active research and development on parameterizing the roles of sub-aquatic vegetation (Kalra et al. 2020) and semi-porous reefs on drag and circulation to adequately represent the drag in flooded areas during unusually severe inundation events.

Summarizing, the current best practices for multi-scale modeling from global to regional to coastal scales favor global and basin resolutions of order 1/12°, with downscaling to ~4 km in

regional seas and sub-kilometer scale in coastal applications, estuaries and ports. This hierarchy of scales in typical applications was corroborated also in reviews such as Holt et al. (2017).

For coastal domains, unstructured grid models remain popular for the substantial flexibility they offer in representing complex topographic regimes. At regional scales, the choice for the appropriate model is wide and this is reflected in the diversity of model codes used by operational agencies. It should be kept in mind that resolution is only one constraint on model fidelity. Forecast systems benefit from advanced data assimilation in the analysis step that informs the initial conditions of a forecast. While advanced data assimilation at global and basin scales is mature and widely employed in operational systems, these methods have yet to be applied seriously in operational coastal and estuarine environments.

When this happens, aided by the emergence of comprehensive high-resolution coastal observing networks, they place an added burden on computational effort and may demand reassessment of the resolution necessary to meet the information requirements of stakeholders.

While it seems unlikely that very small scale nonhydrostatic vertical processes will be resolved in operational systems in the near future, there is progress on their parameterization within conventional primitive equation models (e.g. Dong et al., 2021). There is further ongoing research in both coastal modeling techniques and parameterization of other processes (Fringer et al., 2019) for a comprehensive overview) and many of these developments are expected to advance from research to operations in due course.

3.4.

The temporal scales: different applications of numerical modeling to solve ocean problems

The ocean displays variability of physical parameters across a very wide range of spatial and temporal scales, from minutes to centuries and millennia and from centimeters to the dimension of ocean basins (Benway et al., 2019). As shown in Figure 3.4, this feature makes the ocean a greatly complex system, characterized by interactions between a great deal of processes at many different time/space scales (in which small scales can affect large ones and vice versa).

Operational forecasting services, as defined in Section 3.1, typically deal with problems with a forecast horizon from hours to days, and time intervals at which the solutions are presented to users can vary from hours to minutes. Nevertheless, ocean models can be used for other purposes at longer time scales, such as seasonal prediction and climate modeling. Climate models are based on well-established physical principles, and it has been shown that they can reproduce observed features of recent climate and past climate changes.

There is considerable confidence that AOGCMs provide credible quantitative estimates of future climate change, particularly at large scales, although uncertainties still remain. As stated in the Randall et al. (2007) contribution to the Physical Science Basis Contribution of Working Group I to the Fourth Assessment Report of the IPCC, there are different levels of skill in simulating the various ECVs.

Long-term climate change projections reflect how human activities and/or natural effects can alter the climate over decades and centuries. The principal driver of long-term warming is the large cumulative emission of CO_2 over time from many anthropogenic sources. In this context, it is important defining scenarios, using specific time series of emissions, land use, atmospheric concentrations or radiative forcing across multiple models, which allows for coherent climate model intercomparisons and synthesis. As stated by Collins et al. (2013), for the above purpose is used information from a range of different modeling tools, from simple energy balance models to the highly complex Earth System dynamical climate models. The CMIP Phase 5 utilizes an unprecedented level of information on base projections, including the more complete representation of forcings, and has produced new RCP scenarios (i.e. RCP2.6, RCP4.5, RCP6, and RCP8.5). Thanks to the coordination of model experiments and outputs by the CMIP5 group, the World Climate Research Program and its Working Group on Climate Models have been able to step up efforts to evaluate the ability of models to simulate past and current climate and to compare future climate change projections. This 'multi-model' approach is now a standard technique used by the climate science community to generate and assess projections of a specific climate variable.

Substantial progress has been made in understanding the climate scales, as well as in simulating important modes of
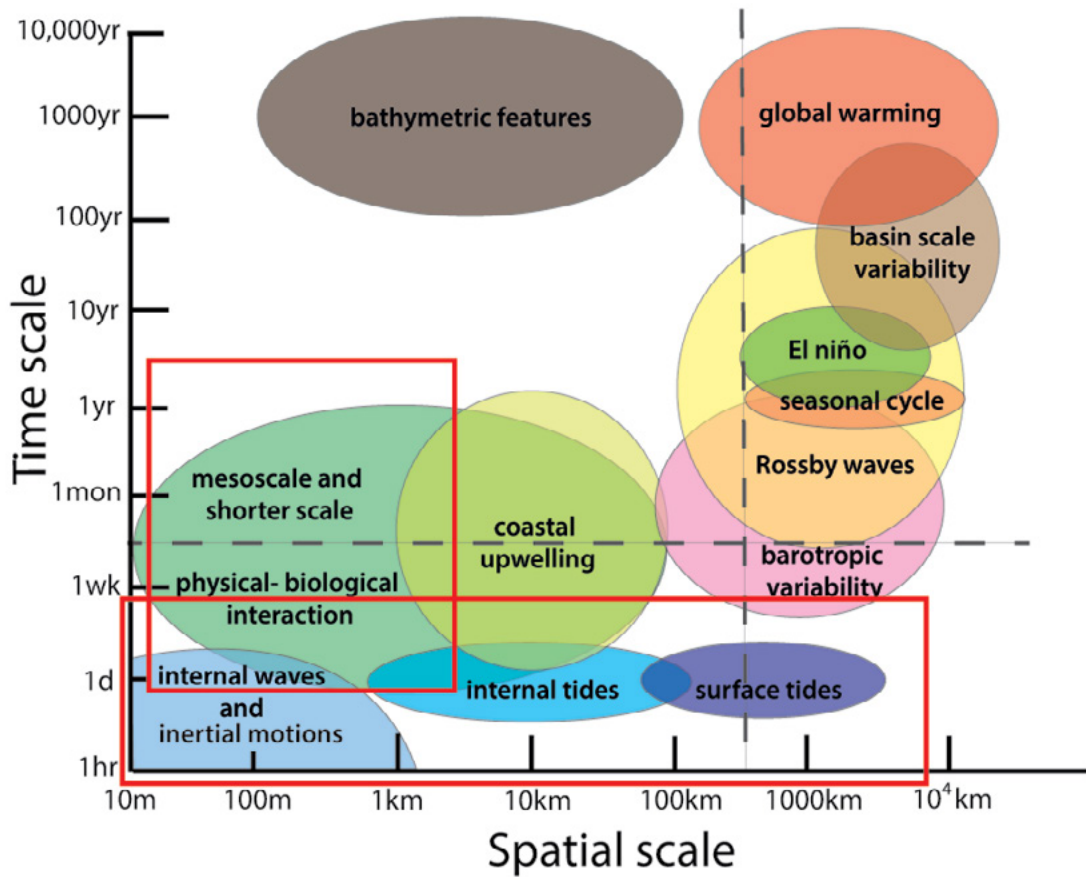
Source: modified from Dickey, 1991.

Figure 3.4.   Temporal and spatial scales of selected ocean processes.

climate variability; as a consequence, the overall confidence in the capacity of models to represent important climate processes has increased. These improvements in AOGCMs are due in large part to the continuous development of the oceanic model component in recent years. There have been improvements in terms of resolution, computational methods, and parametrizations; furthermore, additional new processes have been progressively added to the ocean models used to simulate multi-year periods and climate projections, enhancing the complexity of the ocean climate model component.

As previously mentioned, ocean model resolution has increased (currently, the state-of-the-art is eddy-resolving models) and ocean climate models, especially regional models, are abandoning the 'rigid lid' treatment of the ocean surface that filters out some high frequency processes. New physical numerical parametrizations, including true freshwater fluxes, and/or improved river and estuary mixing schemes, better advection and mixing schemes are now widely used. All these improvements have led to the reduction of the uncertainty associated with the use of less sophisticated parametrizations. Finally, it should be mentioned that there

has been substantial progress in developing the cryospheric components of AOGCMs. Almost all state-of-the-art AOGCMs now include sea ice, with more elaborate sea ice dynamics, while many also include several sea ice thickness categories with relatively advanced thermodynamics and rheology.

Efforts to enhance the quality of climate projections are always related to the computational resources dedicated to the ocean modeling component, but currently there is no consensus on the optimal way to divide computer resources among the following components: i) finer numerical grids, which allow for better simulations; ii) greater numbers of ensemble members, which allow for better statistical estimates of uncertainty; and iii) inclusion of a more complete set of processes (e.g. carbon feedbacks). Finally, it has to be mentioned that there is also an important ongoing activity in terms of ocean climate regionalization, which has been developed in the framework of national and regional climate services initiatives with special emphasis on coastal climate impacts and applications.

3.5.
References

Benway, H., Lorenzoni, L., White, A., Fiedler, B., Levine, N., Nicholson, D., and DeGrandpre, M., Sosik, H., Church, M., O'Brien, T., Leinen, M., Weller, R., Karl, D., Henson, S., Letelier, R. (2019). Ocean Time Series Observations of Changing Marine Ecosystems: An Era of Integration, Synthesis, and Societal Applications. *Frontiers in Marine Science*, 6, 393, https://doi.org/10.3389/fmars.2019.00393

Capet, A., Fernández, V., She, J., Dabrowski, T., Umgiesser, G., Staneva, J., Mészáros, L., Campuzano, F., Ursella, L., Nolan, G., El Serafy, G. (2020). Operational Modeling Capacity in European Seas - An EuroGOOS Perspective and Recommendations for Improvement. *Frontiers in Marine Science*, 7, 129, https://doi.org/10.3389/fmars.2020.00129

Casulli, V. (2009). A high-resolution wetting and drying algorithm for free-surface hydrodynamics. *International Journal for Numerical Methods in Fluids*, 60(4), pp.391-408, https://doi.org/10.1002/fld.1896

Casulli, V., Zanolli, P. (2005). High resolution methods for multidimensional advection-diffusion problems in free surface hydrodynamics. *Ocean Modelling*, 10, 137-151, https://doi.org/10.1016/j.ocemod.2004.06.007

Copernicus Marine Service (2021a). EU Copernicus Marine Service, https://marine.copernicus.eu/

Copernicus Marine Service (2021b). Ocean State Report (OSR), https://marine.copernicus.eu/access-data/ocean-state-report

Copernicus Marine Service (2021c). Ocean Variables monitored by Copernicus Marine Service and Product Portfolio https://marine.copernicus.eu/services/monitoring-ocean.

Collins, M., Knutti, R., Arblaster, J., Dufresne, J.-L., Fichefet, T., Friedlingstein, P., Gao, X., Gutowski, W.J., Johns, T., Krinner, G., Shongwe, M., Tebaldi, C., Weaver, A.J., Wehner, M. (2013). Long-term Climate Change: Projections, Commitments and Irreversibility. In "Climate Change 2013: The Physical Science Basis. Contribution of Working Group I to the Fifth Assessment Report of the Intergovernmental Panel on Climate Change [Stocker, T.F., D. Qin, G.-K. Plattner, M. Tignor, S.K. Allen, J. Boschung, A. Nauels, Y. Xia, V. Bex and P.M. Midgley (eds.)]". Cambridge University Press, Cambridge, United Kingdom and New York, NY, USA.

Dong, J., Fox-Kemper, B., Zhu, J., and Dong, C. (2021). Application of symmetric instability parameterization in the Coastal and Regional Ocean Community Model (CROCO). *Journal of Advances in Modeling Earth Systems*, 13(3), https://doi.org/10.1029/2020MS002302

Fox-Kemper, B. (2018). Notions for the motions of the oceans. In "New Frontiers in Operational Oceanography", Editors: E. P. Chassignet, A. Pascual, J. Tintoré, and J. Verron (Exeter: GODAE OceanView), 811, https://doi.org/10.17125/gov2018.ch02

Fringer, O.B., Dawson, C.N., He, R., Ralston, D.K. and Zhang, Y.J. (2019). The future of coastal and estuarine modeling: Findings from a workshop. *Ocean Modelling*, 143, 101458, https://doi.org/10.1016/j.ocemod.2019.101458

GCOS Global Climate Observing System. (2021). Essential Climate Variables https://gcos.wmo.int/en/essential-climate-variables

Giddings, S.N., Fong, D.A., Monismith, S.G., Chickadel, C.C., Edwards, K.A., Plant, W.J., Wang, B., Fringer, O.B., Horner-Devine, A.R., Jessup, A.T. (2012). Frontogenesis and frontal progression of a trapping-generated estuarine convergence front and its influence on mixing and stratification. *Estuaries and Coasts*, 35, 665-681, https://doi.org/10.1007/s12237-011-9453-z

Holt, J., Hyder, P., Ashworth, M., Harle, J., Hewitt, H. T., Liu, H., New, A. L., Pickles, S., Porter, A., Popova, E., Allen, J. I., Siddorn, J., and Wood, R. (2017). Prospects for improving the representation of coastal and shelf seas in global ocean models, *Geoscientific Model Development*, 10, 499-523, https://doi.org/10.5194/gmd-10-499-2017

Jacobs, G.A., D'Addezio, J.M., Bartels, B. and Spence, P.L. (2019). Constrained scales in ocean forecasting. *Advances in Space Research*, 68(2), 746-761, https://doi.org/10.1016/j.asr.2019.09.018

Kalra, T.S., Ganju, N.K., and Testa, J.M. (2020). Development of a submerged aquatic vegetation growth model in the Coupled Ocean-Atmosphere-Wave-Sediment Transport (COAWST v3.4) model. *Geoscientific Model Development*, 13(11), 5211-5228, https://doi.org/10.5194/gmd-13-5211-2020

Kourafalou, V. H., De Mey, P., Staneva, J., Ayoub, N., Barth, A., Chao, Y., Cirano, M., Fiechter, J., Herzfeld, M., Kurapov, A., Moore, A. M., Oddo, P., Pullen, J., Van der Westhuysen, A., and Weisberg, R., (2015). Coastal Ocean Forecasting: science foundation and user benefits. *Journal of Operational Oceanography*, 8:sup1, s147-s167, https://doi.org/10.1080/1755876X.2015.1022348

Kurapov, A. L., Pelland, N. A., and Rudnick, D. L. (2017). Seasonal and interannual variability in along-slope oceanic properties off the US West Coast: Inferences from a high-resolution regional model. *Journal of Geophysical Research: Oceans*, 122(7), 5237-5259, doi:10.1002/2017JC012721

Legrand, S., Deleersnijder, E., Hanert, E., Legat, V. and Wolanski, E. (2006). High-resolution, unstructured meshes for hydrodynamic models of the Great Barrier Reef, Australia. *Estuarine, Coastal and Shelf Science*, 68(1-2), 36-46, https://doi.org/10.1016/j.ecss.2005.08.017

Levin, J., Arango, H., Laughlin, B., Hunter, E., Wilkin, J., Moore, A. (2021), Observation Impacts on the Mid-Atlantic Bight Front and Cross-Shelf Transport in 4D-Var Ocean State Estimates, Part II – The Pioneer Array. *Ocean Modelling*, 157, 101731, https://doi.org/10.1016/j.ocemod.2020.101731

MacWilliams, M., Bever, A.J. and Foresman, E. (2016). 3-D simulations of the San Francisco Estuary with subgrid bathymetry to explore long-term trends in salinity distribution and fish abundance. *San Francisco Estuary and Watershed Science*, 14(2), https://doi.org/10.15447/sfews.2016v14iss2art3

Muller-Karger, F.E., Miloslavich, P., Bax, N.J., Simmons, S., Costello, M.J., Sousa Pinto, I., Canonico, G., Turner, W., Gill, M., Montes, E., Best, B.D., Pearlman, J., Halpin, P., Dunn, D., Benson, A., Martin, C.S., Weatherdon, L.V., Appeltans, W., Provoost, P., Klein, E., Kelble, C.R., Miller, R.J., Chavez, F.P., Iken, K., Chiba, S., Obura, D., Navarro, L.M., Pereira, H.M., Allain, V., Batten, S., Benedetti-Checchi, L., Duffy, J.E., Kudela, R.M., Rebelo, L.-M., Shin, Y., Geller, G. (2018). Advancing Marine Biological Observations and Data Requirements of the Complementary Essential Ocean Variables (EOVs) and Essential Biodiversity Variables (EBVs) Frameworks. *Frontiers in Marine Science*, 5:211, https://doi.org/10.3389/fmars.2018.00211

Pérez, B., Brouwer, R., Beckers, J., Paradis, D., Balseiro, C., Lyons, K., Cure, M., Sotillo, M. G., Hackett, B., Verlaan, M., Alvarez-Fanjul, E. (2012). ENSURF: multi-model sea level forecast implementation and validation results for the IBIROOS and Western Mediterranean regions. *Ocean Science*, 8, 211-226, https://doi.org/10.5194/os-8-211-2012

Randall, D.A., Wood, R.A., Bony, S., Colman, R., Fichefet, T., Fyfe, J., Kattsov, V., Pitman, A., Shukla, J., Srinivasan, J., Stouffer, R.J., Sumicand, A.,Taylor, K.E. (2007). Climate Models and Their Evaluation. In "Climate Change 2007: The Physical Science Basis. Contribution of Working Group I to the Fourth Assessment Report of the Intergovernmental Panel on Climate Change [Solomon, S., D. Qin, M. Manning, Z. Chen, M. Marquis, K.B. Averyt, M. Tignor and H.L. Miller (eds.)]". Cambridge University Press, Cambridge, United Kingdom and New York, NY, USA.

Schiller, A., Mourre, B., Drillet, Y., Brassington, G. (2018). An overview of operational oceanography. In "New Frontiers in Operational Oceanography", E. Chassignet, A. Pascual, J. Tintoré, and J. Verron, Eds., GODAE OceanView, 1-26, https://doi.org/10.17125/gov2018.ch01

Sloyan, B.M., Wilkin, J., Hill, K.L., Chidichimo, M.P., Cronin, M.F., Johannessen, J.A., Karstensen, J., Krug, M., Lee, T., Oka, E. and Palmer, M.D. (2019). Evolving the physical global ocean observing system for research and application services through international coordination. *Frontiers in Marine Science*, 6, 449, https://doi.org/10.3389/fmars.2019.00168

Sotillo, M.G., Mourre, B., Mestres, M., Lorente, P., Aznar, R., García-León, M., Liste, M., Santana, A., Espino, M., Álvarez, E. (2021) Evaluation of the Operational CMEMS and Coastal Downstream Ocean Forecasting Services During the Storm Gloria (January 2020). *Frontiers in Marine Science*, 8:644525, https://doi.org/10.3389/fmars.2021.644525

Su, Z., Torres, H., Klein, P., Thompson, A. F., Siegelman, L., Wang, J., Menemenlis, D., and Hill, C. (2020). High-frequency Submesoscale Motions Enhance the Upward Vertical Heat Transport in the Global Ocean. *Journal of Geophysical Research: Oceans*, 125(9), id. e16544, https://doi.org/10.1029/2020JC016544

Trotta, F., Federico, I., Pinardi, N., Coppini, G., Causio, S., Jansen, E., Iovino, D. and Masina, S. (2021). A Relocatable Ocean Modeling Platform for Downscaling to Shelf-Coastal Areas to Support Disaster Risk Reduction. *Frontiers in Marine Science*, 8, 317, https://doi.org/10.3389/fmars.2021.642815

Warner, J.C., Sherwood, C.R., Signell, R.P., Harris, C.K., and Arango, H.G. (2008). Development of a three-dimensional, regional, coupled wave, current, and sediment-transport model. *Computers and Geosciences*, 34(10), 1284-1306, https://doi.org/10.1016/j.cageo.2008.02.012

WMO World Meteorological Organization (2021). Definitions, requirements, and network information of ECVs (ECV-Ocean matrix) https://public.wmo.int/en/programmes/global-climate-observing-system/essential-climate-variables.

4.
Architecture of ocean monitoring and forecasting systems

CHAPTER COORDINATOR

Avichal Mehra

CHAPTER AUTHORS *(in alphabetical order)*

Roland Aznar, Stefania Ciliberti, Laurence Crosnier, Marie Drevillon, Yann Drillet, Begoña Pérez Gómez, Antonio Reppucci, Joseph Sudheer, Marcos Garcia Sotillo, Marina Tonani, P. N. Vinaychandranand, and Aihong Zhong.

4. Architecture of ocean monitoring and forecasting systems

4.1. Modelling systems architecture

4.1.1. Step 1 processes

4.1.1.1. Data access and pre-processing

4.1.1.2. Data assimilation: analysed fields

4.1.2. Step 2 processes

4.1.2.1. Forecast

4.1.3. Step 3 processes

4.1.3.1. Post-processing

4.1.3.2. Validation

4.1.3.3. Dissemination

4.1.3.4. Monitoring

4.2. Inputs required

4.2.1. Obtaining and preparing ocean data

4.2.1.1. Data retrieval and characterization

4.2.1.2. Quality Control

4.2.1.3. Data Formats

4.2.1.4. Data Delivery

4.2.2. Description of existing in-situ observational oceanographic data

4.2.2.1. Buoys

4.2.2.2. Tide gauges

4.2.2.3. Argo

4.2.2.4. Ship-of-opportunity program

4.2.2.5. Gliders

4.2.2.6. HF radars

4.2.2.7. Marine Mammals CTDs

4.2.2.8. Autonomous underwater vehicles

4.2.2.9. List of most relevant international in-situ data providers

4.2.3. Description of satellite observational oceanographic data

4.2.3.1. Satellite sea surface temperature

4.2.3.2. Satellite Altimeter

4.2.3.3. Satellite Sea Surface Salinity

4.1.
Modelling systems architecture

An OOFS, with a global to regional scale, is based on numerical modelling of the ocean dynamics, biogeochemistry, and wave and data assimilation schemes for blending observations into the model and for providing the most accurate initial condition for the forecast (Tonani et al. 2015). An OOFS at coastal scale may usually use information from global/regional scales in terms of initial and boundary conditions to initialise and force its ocean model core in a very limited area in order to provide very accurate spatial-temporal solutions and may not necessarily use data assimilation methods.

In general, to produce a forecast we need to:

1. know what the ocean is doing now (initial condition);
2. calculate how the ocean will change in future (forecast);
3. use oceanographic expertise to validate and refine the output (products).

These three steps, represented in Figure 4.1, are based on a few basic components: observations, numerical model, and oceanographic expertise. Most of the systems rely on data assimilation techniques (see Section 4.4 for a general introduction and Section 5.5 for more details about numerical schemes) for blending observation and models; therefore, data assimilation can be considered as one of the essential

components of the system. In the case of coastal forecasting systems, downscaling from global/regional scale is the preferred approach as described in Section 5.4.4.

Step 1 is the production of the most accurate initial condition about the variables the forecasting system is aiming to predict. This means that we need the best knowledge of the present status of each variable at every model grid point. This information is difficult to retrieve from observations because their spatial/temporal coverage is usually very sparse. Model simulations instead provide a uniform coverage in space and time and, thanks to data assimilation techniques observations, they can be blended into the model simulation, improving their accuracy. For data assimilation, it is common to use observations from multiple sources, maximising the data coverage and the type of variables measured by in situ and satellite instruments. The initial condition for the forecast is usually the result of a complex set of multiple simulations with data assimilation covering past hours or days. For global and regional oceanographic systems it is common to have a data assimilation cycle of the order of a few days. These simulations of the past provide not only the best knowledge for initialising the forecast of the present but also valuable information on the near present that can be included in the final product delivered to the users.
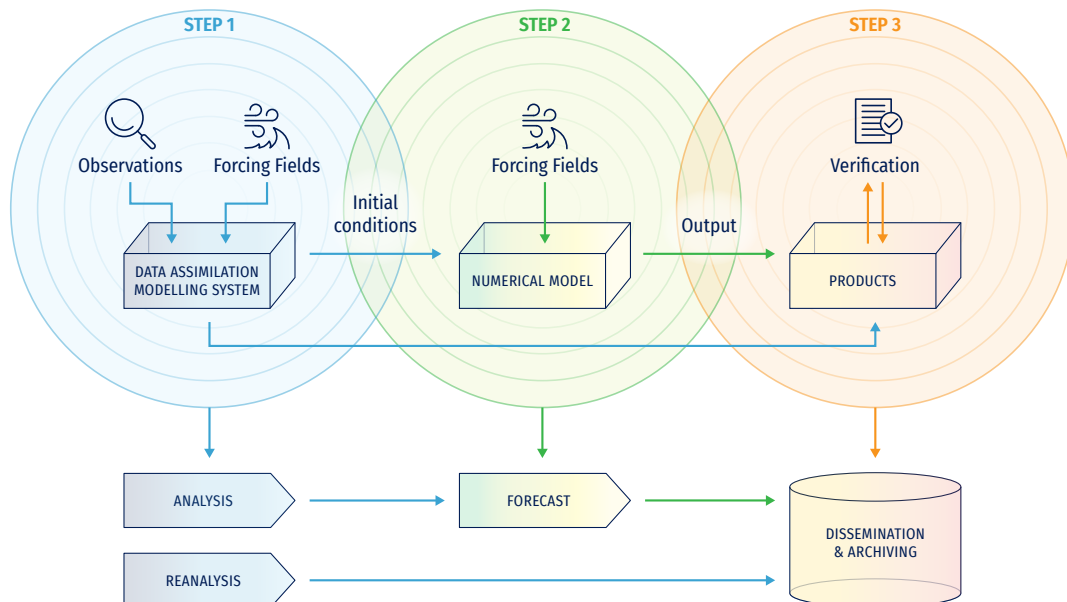
Figure 4.1.   Scheme of steps and main components of a forecasting system and of its architecture.

The model usually needs some external forcing as input. The type of information needed at its boundaries (e.g. ocean/atmosphere, lateral boundaries, along the coast, etc.) can vary from model to model. An ocean dynamical model usually needs an atmospheric forcing from a real time weather prediction system to resolve the processes at the ocean/atmosphere interface. A regional/coastal model requires river runoff data at the interface with the coast and input values for its variables at the lateral boundaries. In case of coupled models (see Chapter 5 and Chapter 10, for example), external forcing fields might not be needed.

Step 2 is the projection in the future, the production of the forecast that is done by running the numerical model for hours, days or months in the future. The forecast lead time can vary from hours to days. Many systems have a forecast lead time of 3-15 days. The same forcing fields described in Step 1 are needed also for the forecast. The forcing fields could be from another forecast like the atmospheric forcing, that usually is from a weather prediction system, or they can be provided by climatological values or persisting the last available value.

Once the model has produced the forecast, it is validated and its output post processed to a standard format for the delivery to the users (Step 3 in Figure 4.1). The validation of the forecast cannot be done via direct inter-comparison with observations but is based on the validation of its initial condition and on studies covering an extended period in the past of the model skills.

As explained before, observations are a key component but have to be made available in real time and in a standard format. Observations in real time are usually ready to be used within a few hours from their acquisition but sometimes they can have delays of more than 24 hours. Timing of data availability will influence the design of the production cycle that has to compromise between using the maximum number of the observations and reducing the delay in the forecast release. The choice to be made has also to consider the need to release a new forecast as soon as possible even if this could imply a degradation of its accuracy.

The timeliness of the forcing fields is another limiting factor in the design of the production chain. We can take as an example a wave forecasting system in which the accuracy of the predicted fields is strongly correlated with the accuracy of the winds. We have to wait until the latest and more accurate wind forecast is made available before starting our production. Different solutions can be implemented depending on the characteristics of each system. The computational time needed for running each of the three steps described is a very important aspect as, depending on the cost for running a specific system, it could be a limiting factor.

Timeliness is of paramount importance for the users and the production time should be reasonably short to avoid delivering forecasts referring to the past. A rule of thumb is that the production time needs to be consistently less than the production frequency. It means that for a daily cycle (production of a forecast once a day) the production time should be of the order of a few hours.

Even if the information provided in this section is focused on a forecasting system, with few modifications it can be also applied to a multi-year production system to produce a reanalysis. The main difference is that in this case you are not projecting in the future but in the past. This implies that you can blend observations and model simulations at each time step. The model is continuously corrected by the observations, increasing the accuracy of the simulations. The atmospheric forcing usually is also more accurate because it is an analysis and not a forecast, and hence the observations have been subject to a more restrictive data quality control compared to the real time ones.

The multi-year production is composed only of Step 1 and Step 3. In this case, in Step 1 the model and data assimilation cover a few hours/days spans over multiple decades of years. As the multi-year products are not limited by the timeliness, usually their major constraints are the computational time that can be extremely expensive as well as the availability of homogenous sources of forcing. These differences with respect to other forecast products have to be taken into account in the design of the production cycle.

In the next subsections the architecture details at the basis of an OOFS will be introduced.

4.1.1. Step 1 processes

4.1.1.1. Data access and pre-processing

The data access and pre-processing component should make available all the needed dataset that will be used to perform the analysis, and then the forecast (Step 2). Automatic acquisition of the data is mandatory for an operational system. It could be quite demanding depending on the dataset, the centres (or data providers) involved in data production and treatment, and the available network to connect the centres. For most of the dataset used in OOFS, at least a daily update is needed.

For atmospheric forcing the volume of the dataset can be big, and an efficient connection to Operational Meteorological Centres in charge of operational production of atmospheric analysis and forecast is critical. For example, the volume of hourly surface forcing fields from the ECMWF at global scale is 34 GB per day. Then, data pre-processing is necessary to interpolate the atmospheric fields to the ocean grid, if there

is inhomogeneity between frequency of available forcings during the length of the specific run, atmospheric datasets must also be interpolated temporally. When a regional ocean model is employed instead of a global model, the retreatment of the atmospheric dataset may substantially reduce the volume of the atmospheric dataset and reduce the overall storage cost.

In-situ ocean observations can be downloaded in real time using WMO GTS or from dedicated interface such as the service developed in the Copernicus Marine Service (Le Traon et al., 2019), in which in situ observations are made available, documented, quality controlled, and homogenised, all very important tasks to be performed before assimilating such dataset in an OOFS. Satellite observations need to be pre-processed by a dedicated centre before their assimilation in an ocean operational system. Satellite observations are processed at various levels ranging from Level 0 to Level 4 which need to be made available depending on the data type. For example, Copernicus Marine Service also provides a unique access point to download all the available satellite observations in real time.

4.1.1.2. Data assimilation: analysed fields

Ocean analysis is based on a model, observations, and data assimilation scheme to provide the initial state of the forecast on the basis of a minimum error principle, i.e. the data assimilation modelling system (Figure 4.1). This component is central processing unit (CPU) consuming and should be performed on a supercomputer. High performance computing power is one of the most important constraints to define the resolution of the analysis system, along with the number of observations that will be assimilated in the system and the frequency and length of the analysis cycle. In an operational framework, the analysis cycle should be performed in a range of a few minutes to a few hours (maximum), choosing the best compromise between performances, quality of the analysis, and robustness of the operational system. This component will provide the initial state for the ocean forecast. The resulting time series of analysed ocean state is defined as the best analysis time series.

To perform an ocean analysis, we need the initial state of the model, based on the prior state of the model at the end of the previous analysis cycle, in situ and satellite observations, and atmospheric forcing analysis fields, collected and formatted in the previous acquisition and pre-processing phase (including all the static files that are necessary for the data assimilation modelling system). Outputs of this component are 3D fields to update the best analysis time series and restart files to initialise the next ocean forecast. Other diagnostics, metrics or post-processing may be computed online directly during the analysis cycle to optimise the system, and used as additional products for dissemination and archiving.

Such products are also used during the validation phase (e.g. the mixed layer depth, the collocation between model output and observations, transports, etc.).

Note that in some coastal forecasting systems there is no direct data assimilation. If the model domain is small, in some occasions there is simply no available data to be assimilated. In these cases, the system relies totally on the boundary conditions and initial 3D fields derived from a larger scale model (see Section 5.4.4 for downscaling examples).

4.1.2. Step 2 processes

4.1.2.1. Forecast

The ocean forecast at some range is based on the numerical model initialised by the ocean analysis and forced by the atmospheric forecast fields as provided by the operational atmospheric centre. In most cases, the same model is used for both the forecast component and the analysis component, even if differences in terms of resolution and physical parameterizations could be envisaged especially in the framework of an ensemble forecast. The same constraints mentioned above about high performance computing apply in order to perform forecasts that are usually updated at least every day. Forecast range will also depend on the computing resources and on the main processes that have to be forecasted with a reasonable skill (to be defined by the developer of the forecasting system). The forecasting cycle should be performed in a range of a few minutes to a few hours. Inputs of the forecasting cycle are the initial state produced by the data assimilation modelling system (e.g. ocean analysis), all the static files needed to integrate the model, and the atmospheric forcing for the full forecast length. The forecast output is updated every day and consists of 3D and 2D ocean fields; it may include diagnostics, metrics and other post-processed dataset that can be useful to assess the quality of the product, to highlight specific features of the forecasted ocean properties and for the final delivery to users.

4.1.3. Step 3 processes

4.1.3.1. Post-processing

The post processing phase is devoted to building all the products that will be delivered to the users. It consists of files or datasets that are provided according to a) standard file format (e.g. according to CF Conventions, 🔗 [1]); b) on a specific grid; and c) with homogeneous variables and metadata. Such products may be then used to compute new products as ocean monitoring indicator (OMI), ensemble mean and standard deviation in the framework of ensemble forecast.

---

1. https://cfconventions.org/

This post processing should be performed on a supercomputer in which all datasets provided by the analysis and forecast components are stored in order to save resources in the computing centre. Computing cost of this stage could be really high (for example, due to the interpolation procedure in the case that the products are delivered on a specific grid) and would also include large data transfer and input/output access. The inputs of the post-processing component are represented by all datasets produced during the analysis and forecast cycles, while the outputs are all the products that will be delivered for internal and external users.

4.1.3.2. Validation

The objective of the validation component is to provide information on the quality of the operational system. The quality of the analysis is compared to already known or expected results (based on literature or climatological datasets) or to available observations. Quality of the forecast is performed by computing forecast skill in comparison to the analysis with the observation in delayed mode. The final step is to provide all this information to forecasters and users. Input of this component are model products, diagnostics and metrics computed during previous steps and the output could be numerical fields, time series and/or interactive maps that allows, through web interfaces or other kinds of applications, direct querying, comparison of different periods, and validation of the production.

4.1.3.3. Dissemination

The goal of the dissemination phase is to make all the products available to users on a dedicated infrastructure. This phase may be complex and the associated cost is very dependent on objectives and user needs. If the dissemination of the model is only internal, outputs could be made available through an intranet, using in-place storage capacities. Other approaches are mandatory for a more complex system providing a very large dataset and long-time series and designed to be accessed by several thousands of users, including a catalogue of products continuously maintained and updated, dedicated services for viewing, extracting and downloading the data. Cloud storage facilities are now the best infrastructure to disseminate operational ocean products.

4.1.3.4. Monitoring

The monitoring component is an important part of an operational system as it allows operators and forecasters to monitor the performances along all the production phases, from data access to dissemination. KPIs should be monitored during this phase, including availability of inputs and outputs during each phase, timeliness, time of delivery and delay of each component, anomaly and/or errors identified during each phase. Monitoring phase should be used to provide information to the users and to decide on a go/no-go to disseminate the products externally. Monitoring phase should be presented on a dedicated dashboard.

4.2.
Inputs required

To run an OOFS as part of Step 1, the following sources of information are needed:

- Observations of EOVs are extremely important for an OOFS as they are used for assimilation and validation purposes. The main sources of observations are:

  - In-situ observations:

    - **Buoys**. Typically used to measure directional waves, atmospheric parameters (wind, atmospheric pressure and air temperature), EOVs (currents, temperature and salinity) and, less frequently, biogeochemical parameters. Some stations measure only on the surface, while others extend their observations to the whole water column. These variables are used for all kinds of OOFS: Wave information is critical for validation and is occasionally used in assimilation; oceanographic data are widely used in circulation modelling and the scarse biogeochemical stations are critical to complement the existing climatological data;

    - **Tide gauges**. Measuring sea level, tide gauges are extremely useful for the validation of storm surge and circulation models, sometimes also used in data assimilation. In recent times, with the increased frequency sampling of modern tide gauges their use to validate wave models in coastal regions has extended;

    - **Argo drifters**. Typically measuring profiles of salinity and temperature. More recently, bio-geochemical parameters are also being incorporated.

This is an essential source of information for large scale circulation modelling;

• **Ship-of-opportunity**. Usually measuring SST and SSS via thermosalinograph or releasing Expendable Bathythermograph to measure temperature throughout the water column. These data are usually employed for circulation modelling;

• **Gliders**. Gliders can provide a 3D field of ocean structures that can be highly valuable for validation of circulation modelling and assimilation in regional and coastal scales. Gliders can also provide valuable biogeochemical information;

• **HF radars**. The surface current fields are used for validation and data assimilation in circulation models. Additionally, the wave measurements can be used for validation in wave forecasting systems;

• **Marine Mammals CTDs**. As in the case of the gliders, this is an increasingly important source of information that allows us to gather detailed information on small-scale ocean and coastal features.

• Satellite observations provide information on the following variables:

• **Sea level anomaly**. These data are a critical variable for data assimilation in large scale circulation models;

• **Sea surface temperature**. As the previous, usually it is employed in data assimilation as well as in validation of ocean circulation forecast systems;

• **Sea ice concentration**. Used for both validation and data assimilation in ice models, coupled to circulation models;

• **Waves**. This variable is being used in large scale wave forecast systems for data assimilation and, on some occasions, for validation;

• **Ocean colour.** Mainly employed for assimilation and validation in biogeochemical models. Can also be used as a secondary source for validation in circulations, since sometimes coastal structures are evident.

• Bathymetric datasets. Bathymetry is at the base of every OOFS and, therefore, it is indispensable for all systems;

• Surface forcing. Provided by operational NWP systems. These data are used for describing air-sea-sea

ice interactions. Momentum, heat and freshwater fluxes are of paramount importance for all the processes at sea. Therefore this forcing is needed in almost any OOFS, with only a few exceptions (for example, some very high resolution wave propagation systems can operate without it, because the influence of forcing is already considered on other larger scales);

• Land forcing fields (i.e. discharge of water and nutrients from rivers). Mainly used in circulation and biogeochemical modelling. This source of data is very relevant to provide accurate solutions at the coastline. Unfortunately, on some occasions real time data are not available and the modellers must rely on climatologies;

• Ocean fields. They are provided by OOFS at larger scale to work as initial and boundary conditions (for example 3D temperature fields for downscaling applications in circulation modelling). When nesting, it is indispensable to have these fields. It is a frequent technique in all kinds of regional scale and coastal OOFS;

• Climatologies. Sometimes climatologies are employed for validation or initialization when no other data are available. These data sources are also employed in validation processes, to check that the models do not depart too much from real values in regions where measurements are not frequent.

The following sections contain first an introduction on how to deal with ocean data from the perspective of the data provider, and then a description of the above mentioned data sources, including a list of international providers.

4.2.1. Obtaining and preparing ocean data

The quality of OOFS products is highly dependent on the availability of in situ and satellite observations; these are used, through data-assimilation, to constrain the analysis and the forecasting systems, and validate their outputs. However, prior to use these observations, they need to be properly retrieved, efficiently organised, and carefully quality controlled (Le Traon et al., 2009). In the architecture of an OOFS, this is accomplished by the so-called DMS, the data management component. The ultimate goal of this system is to ease the use of oceanographic observations, providing consistent and harmonised products ready to be used for data assimilation and validation.

Figure 4.2 shows how data flow should be organised in a DMS. To get the most out of information, a DMS is responsible for gathering and organising the ocean observations (satellite and in-situ) in high-quality products and then to disseminate them in a timely fashion that meets the requirements of modelling and data assimilation centres. Once acquired,
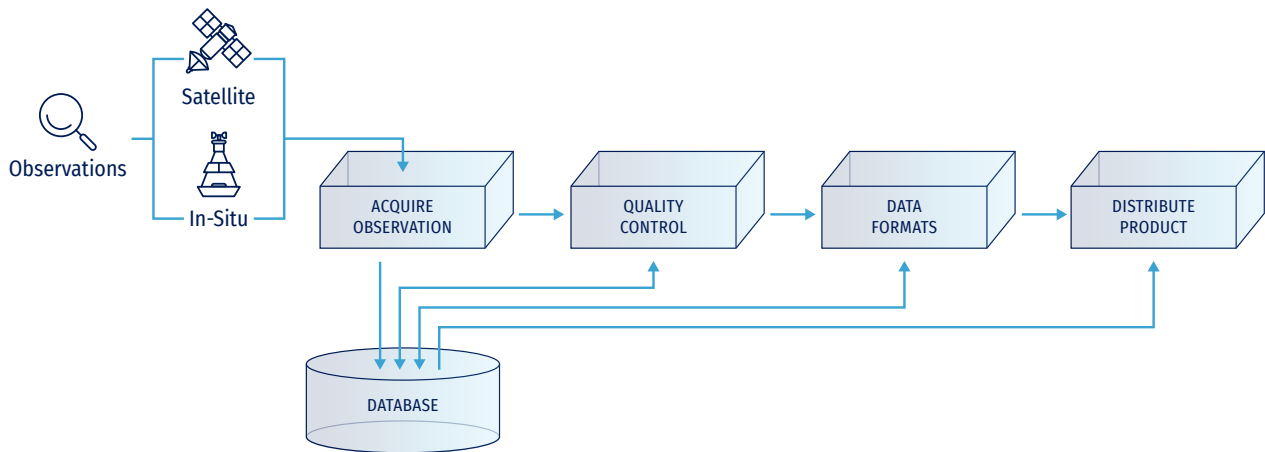
Figure 4.2. Typical DMS data flow from upstream international networks for OOFS.

observation must be supplemented by uncertainty estimates and quality flags (part of the quality control process), which are key for validation and data assimilation. Then, they are prepared according to the specific file formats and distributed to users.

4.2.1.1. Data retrieval and characterization

First task of a DMS is to gather observations available from selected data providers (e.g. space agencies, international in-situ data networks, etc.). The choice of observations to be retrieved, processed and delivered depends on a previous analysis of the needs expressed by the prediction systems. In general, a tight coordination, upstream with data providers and downstream with prediction systems, is necessary to keep needs updated and ensure that the required observations are provided timely.

Ocean observations are made using several sensors, including in situ and remotely sensed ones, covering a broad range of spatial and temporal scales. Ocean observations made by remote sensing sensors usually include data for monitoring sea level, SST, salinity, surface wind and currents, sea ice, and ocean colour; these observations are acquired on a global basis and distributed at several different levels of processing, ranging from raw data to detected geophysical variables. Space Agencies (e.g. ESA, NASA, EUMETSAT, JAXA) are responsible for the provision of such observations.

In-situ observations are of paramount importance for OOFS because they provide information about the ocean interior that cannot be observed from space. In-situ observations can locally sample high-frequency and high-resolution ocean processes, in particular in the coastal zone, that are essential for model and satellite validation activities. In-situ observations are acquired through various network programs at both global and regional scale.

Data from a global prediction system, to be used to define boundary conditions of a nested regional one, or terrain/ atmospheric forcing in certain scenarios will be part of the data to be inputted in the prediction system.

Knowledge of the processes that have been undertaken to produce a given observation and its characteristics is of high importance, as it allows a user to decide upon the product's fitness for a particular application. To this end, it is important to ensure that metadata associated with each of the retrieved dataset contain the appropriate information (e.g. instrument/platform characteristics, tests performed and failed, origins of the data stream, data processing history, and information about the datasets).

4.2.1.2. Quality Control

In general, a Prediction System needs two types of input data. Initially NRT data are needed for hourly to weekly forecasting activities; at a later stage and for applications in which long-term stability is needed (e.g. reanalysis, climate monitoring, and seasonal forecasting), DM data comes into play. Due to their different utilisation, quality control procedures for the two types of data are applied in different ways and with different methodologies.

NRT input data, delivered within a few hours to maximum one week from acquisition, are usually automatically quality

Code	Meaning	Comment
0	No QC was performed	-
1	Good data	All real time QC tests passed.
2	Probably good data	These data should be used with caution.
3	Bad data that are potentially correctable	These data are not to be used without scientific correction.
4	Bad data	Data have failed one or more of the tests.
5	Value changed	Data may be recovered after transmission error.
6	Value below detection/quantification	The level of the measured phenomenon was too small to be detected/quantified by the technique employed to measure it. The accompanying value is the detection/quantification limit for the technique or zero if that value is unknown.
7	Nominal value	-
8	Interpolated value	Missing data may be interpolated from neighbouring data in space or time.
9	Missing value	-

Table 4.1. Copernicus Marine quality control flags as applied to Global Ocean In-Situ Near-Real-Time Observations product (INSITU_GLO_NRT_OBSERVATIONS_013_030, 🔗 2).

controlled using a priori agreed upon procedures. For in-situ observations, quality control tests aim mainly at detecting outliers; these procedures check for inconsistencies in the measurements often using local statistics built from a long time series of similar data. Quality control of remotely sensed observations is performed by comparisons with in-situ observations when available, or by comparison to long-time series (i.e. climatologies) derived from the same product. These procedures aim at defining the accuracy of the product and detecting anomalous observations. As a result, for both in-situ and remotely sensed NRT products, quality flags are positioned to inform the users about the level of confidence and, where possible, the level of accuracy attached to the observations.

In-situ DM data are usually subject to an off-line quality control using statistical tests to check for spatial consistency and to a much more refined climatology test, usually with strong involvement of scientific experts in the quality-control process. Satellite observations delivered in DM usually

benefit from improved ancillary data (e.g. more precise satellite ephemerides, meteorological reanalysis, etc.) used in the retrieval process, resulting in a more accurate product.

Besides the activities aimed at establishing the quality of the required observations, a DMS shall also monitor the performance of the different providers in terms of availability, possible degradation of their sampling, and timeliness. This additional information also needs to be regularly provided to prediction systems making use of these observations.

A DMS should also set up a procedure to gather, in form of reports, regular information on the data that have not been used by the prediction systems, because they were deemed to be of inadequate quality; this procedure, often called "Blacklisting", has significant value for improving automated procedures for data quality control.

Table 4.1 shows the standard quality control (QC) indexes assigned to Copernicus Marine Service in-situ and satellite data.

2. https://doi.org/10.48670/moi-00036

4.2.1.3. Data Formats

Observations usually arrive at a DMS in a variety of formats, depending on the platform being used to acquire and broadcast them or on the software used to retrieve the variables of interest. For ease of use, a DMS will format all the incoming observations in data structures which satisfy the OOFS requirements. Data formats are usually defined during the development of the OOFS infrastructure in coordination with the prediction systems and detailed in dedicated documents. Besides a detailed description of the format in which the data or products will be stored, key subjects to be addressed in such documentation include:

- standards that will be used to build the data structures hosting the incoming observations (e.g. NetCDF format);

- semantics, provided by a recognized common convention (e.g., CF), which are then used to write metadata; and

- a description of the transformation algorithms for all data handling (e.g. transformation algorithms to/from standards).

To enhance interoperability and sharing of data, non-proprietary solutions commonly used by the community are favoured during the selection of data format.

4.2.1.4. Data Delivery

The ultimate task of a DMS is to deliver datasets required for assimilation and validation activities to prediction systems, including uncertainty estimates that are critical for the effective use of the data. For the best possible exploitation of this data, an easy-to-access and robust service to visualise and access present and past available observations and associated metadata must be deployed. Metadata include latency information on data availability as a key parameter in the data flow. It is important that new observations are made accessible to the prediction systems with the shortest possible delay.

Access to data can be achieved in different ways:

- "Pull services" enable users to request data according to their needs; this type of service should integrate tools that allow constraining the area of interest and time covered by the information;

- "Push Services" are often based on subscription, which literally push the data to users following prescribed specific requirements.

Beyond visual navigation of data, a dissemination service should also include utility tools allowing transformation (e.g. format conversion and coordinate transformation), aggregation, and integration of a given variable regardless of source.

Another aspect to be considered as key for a successful dissemination service is the ability to perform appropriate extractions according to different data geometries (e.g. gridded datasets, unstructured gridded data, vertical profiles etc.).

4.2.2. Description of existing in-situ observational oceanographic data

In the next sections, it will be introduced the main observational oceanographic data from in-situ platforms used by OOFS. Details about their usage in numerical modelling and validation, as well as providers, are described in Chapters 5 to 9.

4.2.2.1. Buoys

Operational drifting buoys are a primary source of data on ocean surface conditions. They are deployed and maintained by autonomous groups, subject to different intergovernmental agreements, under the coordination of the Data Buoy Cooperation Panel (DBCP, 🔗[3]). The Global Drifter Program (GDP) works in collaboration with national meteorological/oceanic agencies to routinely deploy large quantities of drifting buoys in support of their research and operational programs. Maintaining drifting buoy density distribution is a major challenge, due to the difficulty of high latitude deployments and because Lagrangian drifting buoys follow ocean currents and tend to cluster together near convergence zones.

Moored buoys are anchored at fixed locations, reporting temperature and salinity profiles, and are concentrated mostly in the tropical oceans and the coastal regions of Brazil, Europe, India, and the United States (🔗[4]). The different programs/agencies responsible for handling the tropical mooring networks are:

- the Tropical Atmosphere-Ocean/Triangle Trans-Ocean Buoy Network in the equatorial Pacific (TAO/TRITON) (McPhaden et al., 1998);

- the Prediction and Research Moored Array in the Tropical Atlantic (PIRATA) (Bourlès et al., 2008);

- the Research Moored Array for African-Asian-Australian Monsoon Analysis and Prediction (RAMA) in the Indian Ocean (McPhaden et al., 2009).

---

3. https://www.ocean-ops.org/board
4. https://www.ocean-ops.org/dbcp/platforms/types.html

The TAO/TRITON, PIRATA and RAMA moored arrays are part of the DBCP's moored buoy network through the Tropical Moored Buoy Implementation Panel (TIP).

Data from the DBCP GBN is transmitted through the GTS of the WMO and archived by the operational agencies. At present, the GBN has over 1,380 drifting buoys and 260 coastal/national moored buoys and 70 tropical arrays. While COVID-19 restrictions imposed stress on deployment opportunities, the drifting and moored buoy networks successfully maintained a healthy and resilient status in data quantity, quality, coverage and timeliness, due to the prolonged lifetime and improved performance of buoys (🔗 [5]).

4.2.2.2. Tide gauges

Tide gauges are instruments on fixed platforms, located usually along the coastline, that measure water level with respect to a local height reference. Their primary objective is to support coastal zone monitoring and management, tide prediction, datum definition, harbour operations and navigation; additionally, they are used in sea level hazard warning systems, for climate monitoring, model validation and assimilation, and to detect errors and drifts in satellite altimetry. Tide gauge data complement the sea surface height data provided by the spatial altimeters, by providing higher temporal sampling (up to 1 min or less, allowing detection of higher resolution sea level phenomena) from in-situ data at the coast, where the quality of altimetry is lower.

The Global Sea Level Observing System (GLOSS; 🔗 [6]) is the main international program responsible for collection, quality-control and archiving of tide gauge observations. The following data centres contribute to GLOSS data services:

• PSMSL (🔗 [7]), responsible for the global database of monthly and annual mean sea levels for long-term sea level change studies from tide gauges (🔗 [8]);

• UHSLC (🔗 [9]), in which high-frequency tide gauge data (hourly and daily) can be found. Two datasets are provided, with different levels of quality control: research quality (updated annually) and Fast-Delivery (updated every 1-2 months);

• IOC Sea Level Station Monitoring Facility (IOC/SLSMF: 🔗 [10]), maintained by Flanders Marine Institute (Belgium), provides access to real-time raw tide gauge data, with shorter time sampling (< 1min) for tsunami monitoring;

• SONEL (🔗 [11]) is the GLOSS data centre for GNSS time series at tide gauge locations, if available. This information is the source of vertical land movement at the site and provides an ellipsoidal height reference of the tide gauge.

Figure 4.3 shows the global distribution of tide gauges together with the total number of installed stations from 1800 to 2000s (Hamlington et al. 2016), collected by the PSMSL. It shows the sparse distribution of tide gauges stations in some areas, such as Africa and South America.

The EuroGOOS launched an initiative through its dedicated Tide Gauge Task Team (TGTT) working group (🔗 [12]) to capitalise the expertise, usage and further improvement of the tide gauges network in the continent. This working group has launched several actions to enhance the connection between GLOSS and European data portals such as EMODnet and Copernicus Marine Service. These data portals integrate tide gauge data with other in situ, satellite and model data, and provide a one-point access for most of the tide gauges data for operational and scientific activities.

4.2.2.3. Argo

Argo is a global array of approximately 4,000 free-drifting profiling floats, designed to measure the temperature and salinity of the upper 2,000m of the ocean. The array covers the global ocean reasonably well and is one of the main in-situ observation data sources for ocean data assimilation and validation.

Each standard float has a resting depth of 1000m for 9 days. Every 10 days it is programmed to descend to 2000 m and then ascend to the surface measuring temperature and salinity in the ocean column. Data is transmitted via satellite and distributed on the GTS in BUFR code. Similar real-time quality-controlled Argo profiles can be obtained from two Global Data Assembly Centres (GDACs) - based one in Monterey, USA, and the other in Brest, France - that were set up as part of the international GODAE. For their behind real-time analyses, some operational centres use real-time Argo floats from both the GTS and the two GDACs.

5. https://public.wmo.int/en/media/news/ocean-observing-system-report-card-2020

6. http://www.gloss-sealevel.org

7. https://www.psmsl.org/

8. https://www.psmsl.org/

9. http://uhslc.soest.hawaii.edu

10. http://www.ioc-sealevelmonitoring.org

11. http://www.sonel.org

12. https://eurogoos.eu/tide-gauge-task-team/
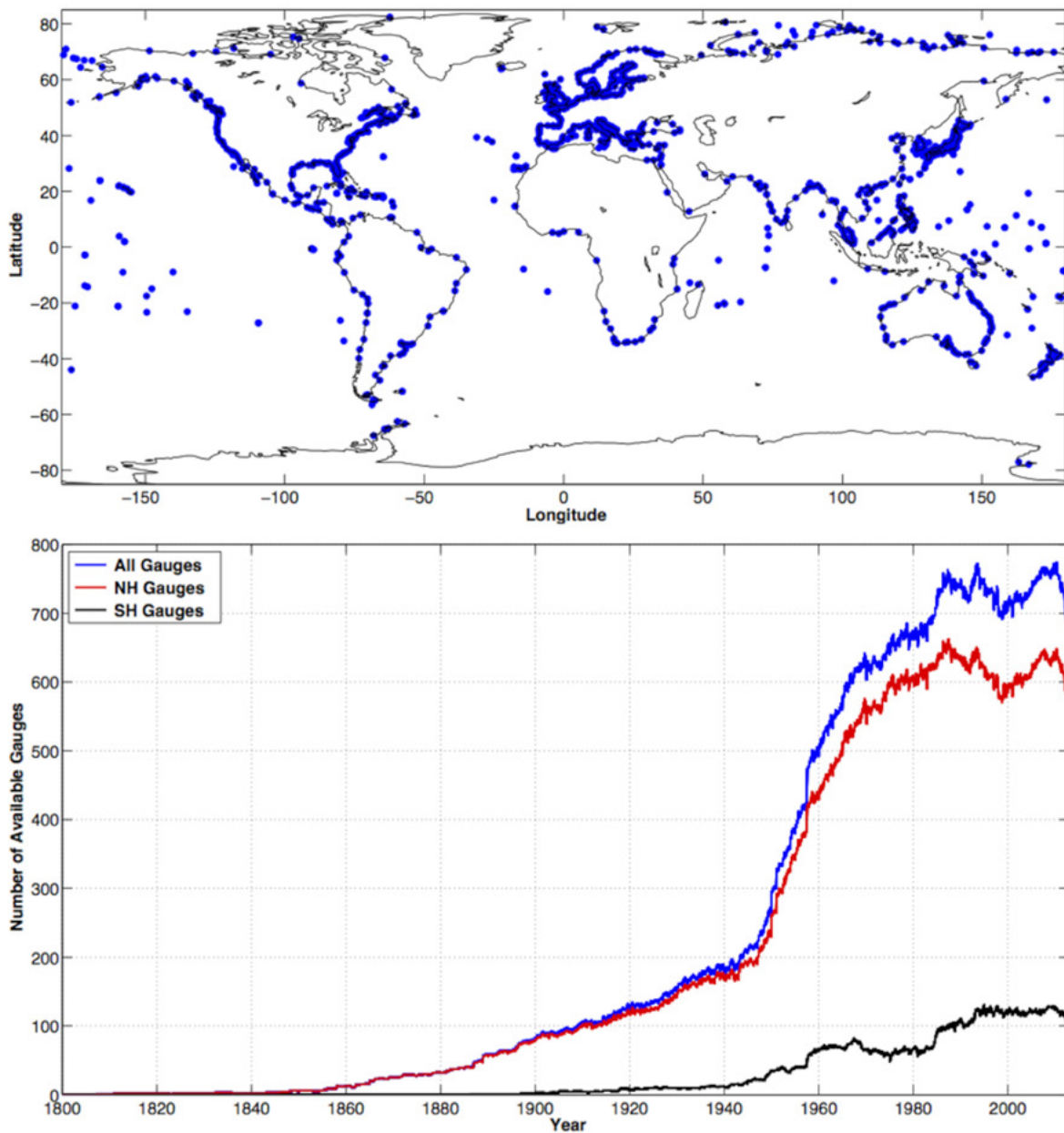
Figure 4.3. Top: global spatial distribution of the 1420 tide gauges in the PSMSL RLR dataset. Bottom: number of available tide gauges in the PSMSL RLR dataset through time (blue). Available gauges for the Northern Hemisphere (red) and Southern Hemisphere (black) are also shown for comparison (source: 🔗 13).

By 2020, Argo is collecting 12,000 data profiles each month (400 a day). The most updated picture of available operational Argo at global scale is shown in Figure 4.4. Further details are available at 🔗 14. There was a slight 10% decrease in daily data flow in early January 2021, but overall spatial-temporal coverage has progressed since 2020 despite the challenges of the worldwide pandemic.

Satellite-tracked surface drifting buoys are extremely cheap and useful to measure mixed layer currents, sea surface temperature, atmospheric pressure, winds, and salinity. They are part of the GDP and are able to reach a maximum 15 m depth. An updated map of operational surface drifters is shown in Figure 4.5. Further information is available at 🔗 15.

13. https://climatedataguide.ucar.edu/climate-data/tide-gauge-sea-level-data

14. https://argo.ucsd.edu

15. https://www.aoml.noaa.gov/phod/gdp/index.php.
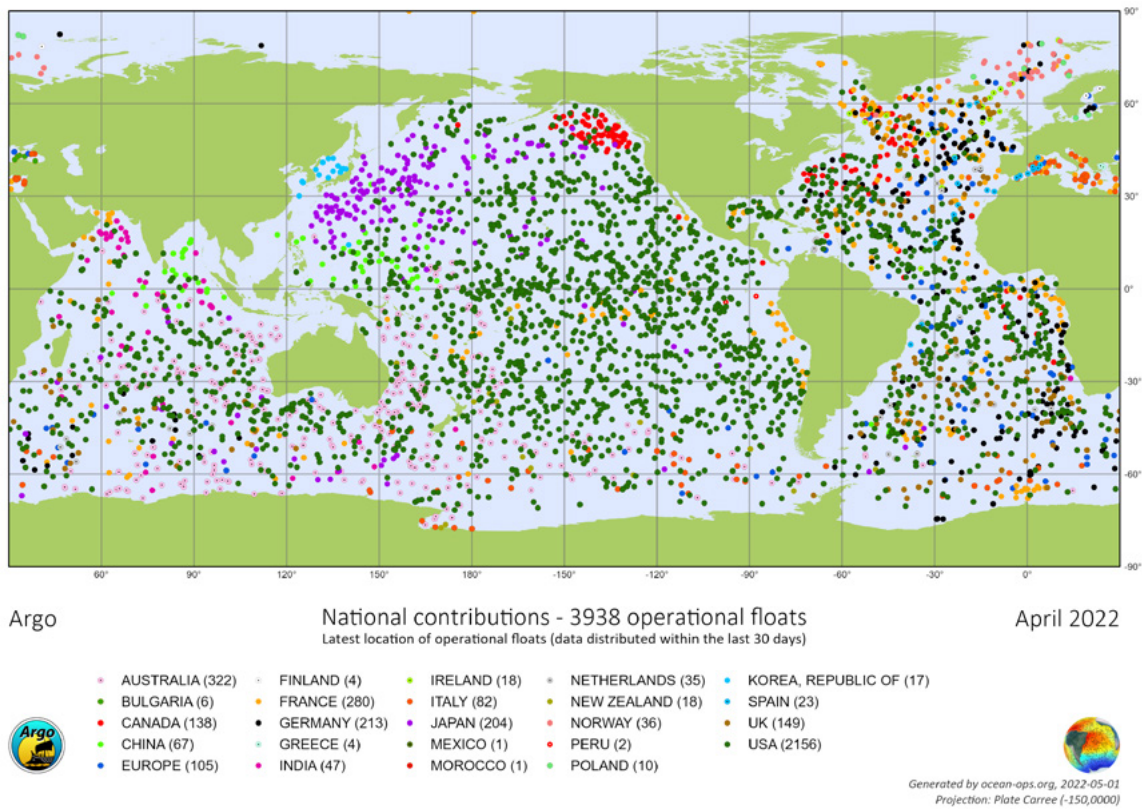
Figure 4.4. Global distribution of Argo network in January 2021 (source: 🔗 [16]).
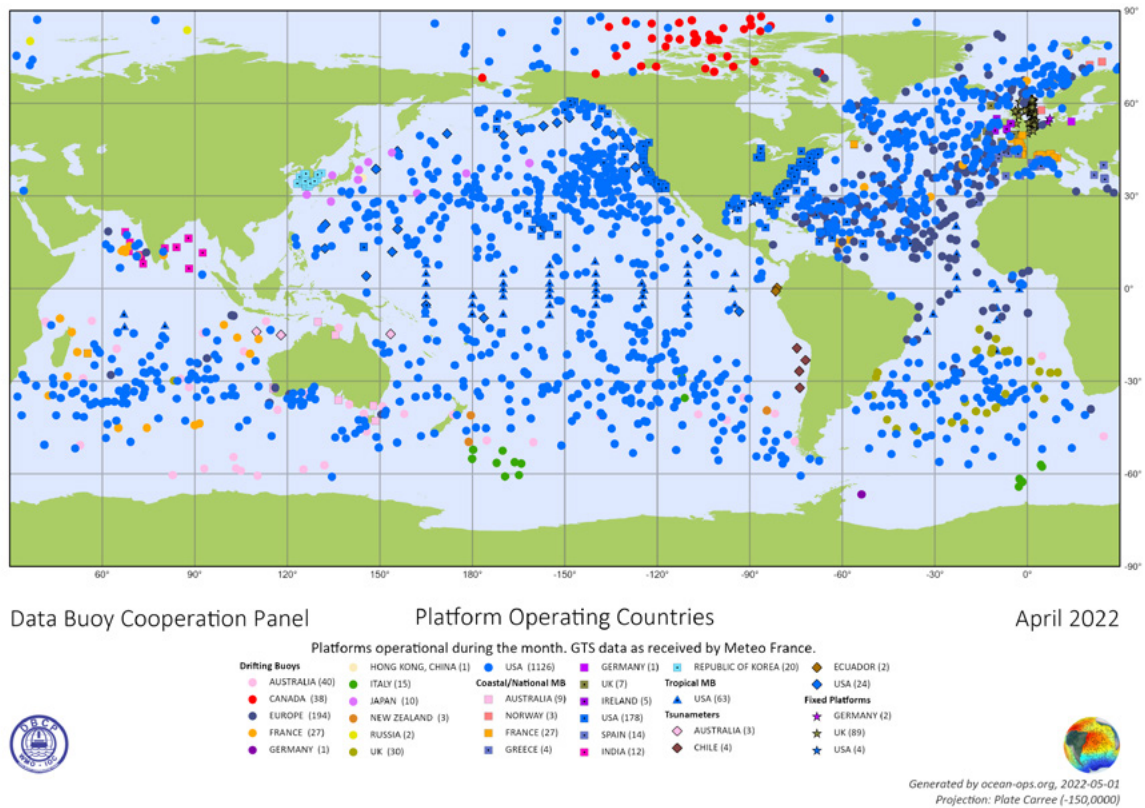
Figure 4.5. Global distribution of drifting buoys and moored buoys in January 2021, concentrated mostly in tropical oceans and coastal regions of Brazil, Europe, India, and the United States (source: 🔗 [17]).

4.2.2.4. Ship-of-opportunity program
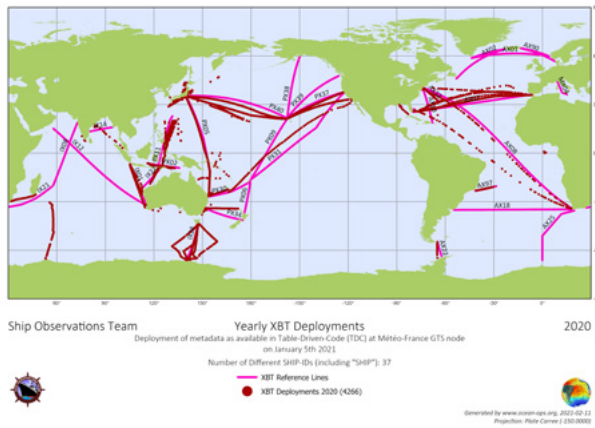
Figure 4.6.   The network status of global XBT lines provided from Ocean-OPS in December 2020. Purple indicates the XBT reference lines and red indicates deployment in 2020 (source: 🔗[18]).

The SOOP, promoted by the JCOMM, is a network of merchant and research ships equipped with sophisticated tools and technology that allow scientists to explore ocean environments. The instrumentation usually used are:

- XBT 🔗[19], used to collect temperature observations of the upper 1 km of the ocean (Figure 4.6). Data from the XBT drop is automatically generated, transmitted by satellite and distributed on the Global Telecommunications System (GTS) in the Binary Universal Form for the Representation of meteorological data (BUFR) format. For operational use, these messages from around the globe are decoded and stored in real-time databases by each operational centre. Approximately 20,000 XBTs are deployed annually by the scientific and operational communities;

- CTD 🔗[20], which detects how the conductivity and temperature of the water column changes relative to depth. Conductivity is a measure of how well a solution conducts electricity and it is directly related to salinity. By measuring the conductivity of seawater, the salinity can be derived from the temperature and pressure of the same water. The depth is then derived from the pressure measurement by calculating the density of water

from the temperature and the salinity. CTD are attached to a much larger metal frame called a rosette, which may hold water-sampling bottles that are used to collect water at different depths, as well as other sensors that can measure additional physical or chemical properties;

- TSG 🔗[21] are used for measuring sea surface temperature and sea surface salinity;

- ADCP 🔗[22] are able to measure how fast water is moving across an entire water column, using a principle of sound waves called the Doppler effect;

- Research vessels and voluntary observing ships participate in the SOOP 🔗[23]

The SOOP is directed primarily towards the continued operational maintenance and co-ordination of the XBT ship-of-opportunity network but other types of measurements, such as CTD probes, are also being made. The SOOP XBT program has been greatly impacted by the global COVID-19 pandemic. In early 2020, the program was temporarily suspended. However, almost half of lines resumed after June 2020, and by December 2020 there were 37 ships active on 25 lines (Figure 4.6), with 4266 profiles visible on GTS (source: 🔗[24]).

4.2.2.5. Gliders

Ocean gliders are autonomous underwater vehicles that move through the water column, ascending and descending with changes in buoyancy. Observations from ocean gliders have recently become an important data source in regional ocean data assimilation systems. The gliders are reusable and can be remotely controlled, making them a relatively cost-effective method for collecting repeated subsurface ocean observations. They also allow data acquisition in severe weather conditions. Equipped with a variety of sensors, the gliders are designed to measure ocean temperature, salinity and current profiles. Furthermore, the unique design of the gliders enables them to move horizontally through the water while collecting vertical profiles.

The OceanGliders program coordinates 27 nations' efforts, including 76 national and institutional glider programs (Figure 4.7). Despite the difficult context of Covid-19 restrictions, the OceanGliders program was able to operate over 200 gliders

16.   https://www.ocean-ops.org/board
17.   https://www.ocean-ops.org/board
18.   https://www.ocean-ops.org/board
19.   https://www.aoml.noaa.gov/phod/goos/xbt_network/
20.   https://oceanexplorer.noaa.gov/facts/ctd.html

21.   https://www.aoml.noaa.gov/phod/tsg/background.php
22.   https://oceanexplorer.noaa.gov/technology/acoust-doppler/acoust-doppler.html#:~:text=An%20acoustic%20Doppler%20current%20profiler,physical%20properties%20of%20the%20ocean.
23.   https://www.ocean-ops.org/sot/soop/
24.   https://public.wmo.int/en/media/news/ocean-observing-system-report-card-2020

Figure 4.7.   Active gliders in 2020-2021 (source: 🔗 25).

in 2020 (source: 🔗 26). Most of the glider groups share their real-time data via the GTS network.

4.2.2.6. HF radars

HF radar systems measure the speed and direction of ocean surface currents in real time in coastal areas. They utilise high frequency radio waves for performing such measurements: a pair of radar antennas are positioned on shore and can measure surface currents (over 1-2 m in the water column) up to 200 km offshore with a resolution spanning from 500 m to 6 km depending on the radar frequency (🔗 27). Figure 4.8 shows a sketch (adapted from Mantovani et al., 2020) of mutual functioning of a pair of antennas - Radar A and Radar B: they measure the radial components (vector in blue from Radar A and vector in green from Radar B) that may be used to compute total velocity inside each discrete cell (vector in orange). This technology is increasingly used in many applications to support downstream services for coast guard search and rescue activities, oil spill emergencies, water quality monitoring and marine navigation. Nevertheless, they are extremely useful for validating coastal models as well as assimilating OOFS at regional scale.

At international level, the GHFRN has been established as part of the GEO to promote high-frequency radar technology for scientific and operational activities along the coast. Roarty et al. (2019) include an updated list of countries and organisations providing surface current information to the GHFRN. Figure 4.9 shows the global distribution of HF radar stations organised within the three regions of the ITU.
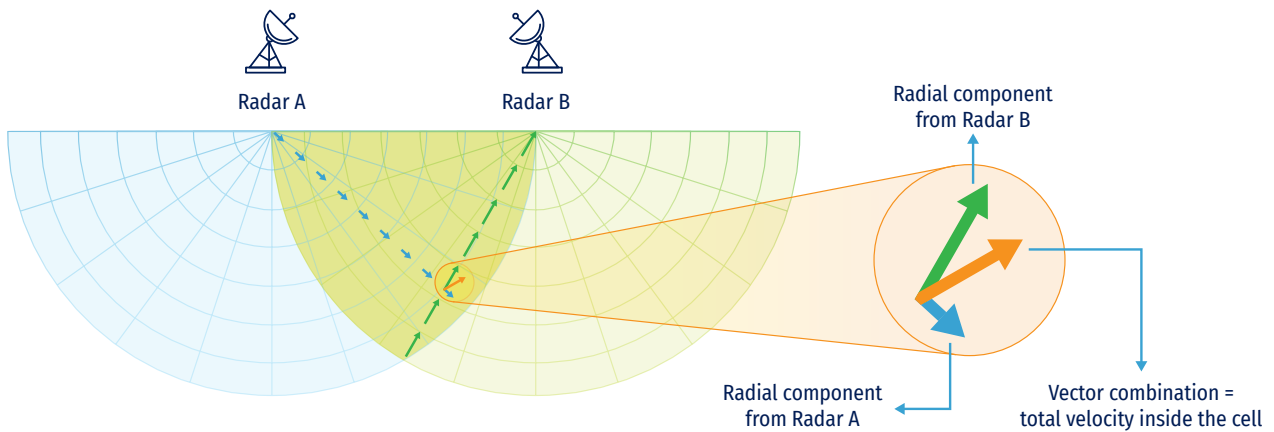
Figure 4.8.   Concept of surface current derivation from a two HF radar site network (adapted from Mantovani et al. 2020).

---

25. https://www.oceangliders.org/
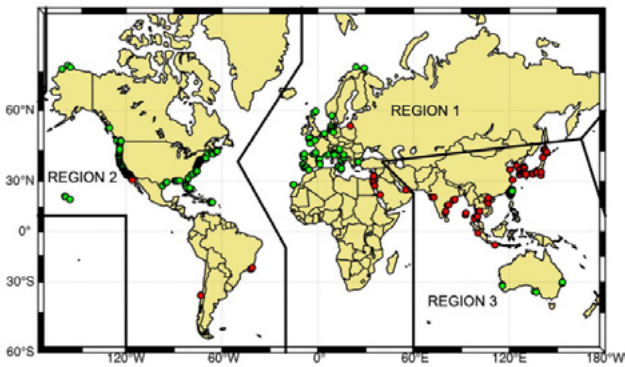
26. https://public.wmo.int/en/media/news/ocean-observing-system-report-card-2020

27. https://tidesandcurrents.noaa.gov/hfradar/

An example of an operational HF radar network is provided by that one managed by Puertos del Estado, operating in Spain, to monitor coastal and harbour zones. Figure 4.10 shows on the left the current operational HF radar network: selecting one of the regions in the red boxes - for example the Ebro Delta, on the right - the user may visualise the animation of the measurements collected during the reference observing period. Data may be accessed through the EMODnet Physics webportal.
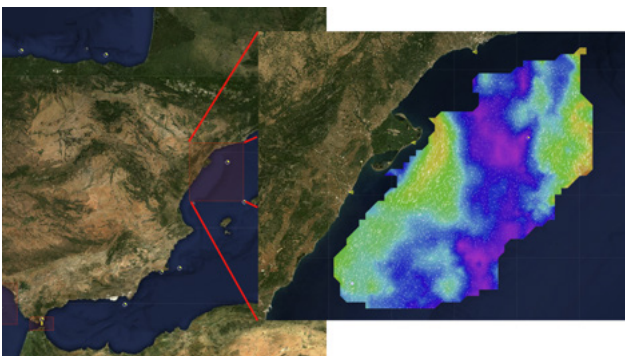
Figure 4.10.   An example of HF radar network: the case of the Ebro Delta monitored by Puertos del Estado (Spain) (source: 🔗²⁸).

4.2.2.7. Marine Mammals CTDs

Marine mammal CTD data are very important for ocean modelling and sea ice verification in high latitudes, particularly in the marginal sea ice zone. Since 2004, several hundred thousand profiles of temperature and salinity have been collected by instrumented animals (Figure 4.11). The use of elephant

28. http://www.puertos.es/

Figure 4.11.   Elephant seal with CTD tag ©JB Pons, in C. Guinet, 2018, CEBC/CNRS (available at 🔗²⁹).

seals has been particularly effective to sample the Southern Ocean and the North Pacific. These hydrographic data have been assembled in quality controlled databases that can be accessed through the MEOP consortium (🔗³⁰).

Currently, the MEOP data portal distributes three different databases:

• the MEOP-CTD database: quality-controlled CTD profiles;
• the MEOP-SMS database: submesoscale-resolving high density CTD data;
• the MEOP-TDR database: high spatial density temperature/light data.

Real-time marine mammal CTD data are uploaded to the GTS as shown at 🔗³¹.

4.2.2.8.   Autonomous underwater vehicles

An AUV is a self-propelled, unmanned, untethered, underwater vehicle capable of carrying out simple activities with little or no human supervision. Reasons for employing AUV range from the ability to obtain superior data quality (for example, obtaining high-resolution maps of the deep seafloor) to establishing a pervasive ocean presence (for example, using many small AUV to observe oceanographic fields) (Bellingham, 2009).

4.2.2.9. List of most relevant international in-situ data providers

Providers of international in-situ observations to be used for assimilation/validation are listed in Table 4.2.

29. https://www.cebc.cnrs.fr/wp-content/uploads/pub-lipdf/2019/GC124006.pdf
30. http://www.meop.net/
31. http://www.meop.net/meop-portal/ctd-srdl-technology.html

Provider	Description	Website
WOD	World Ocean Database provides uniformly formatted, quality controlled, publicly available ocean profiles	https://www.ncei.noaa.gov/products/world-ocean-database
Argo	Argo provides data access to Global Data Assembly Centres in Brest (France) and in Monterey (USA)	https://argo.ucsd.edu/about/status/
Copernicus Marine Service	Copernicus Marine Service through the INS TAC for the operational provisioning of near real time and reprocessed datasets used by the MFCs for assimilation and validation	https://marine.copernicus.eu/
SeaDataNet	SeaDataNet infrastructure, provides aggregated datasets (ODV collections of all unrestricted SeaDataNet measurements of temperature and salinity by sea basins) and climatologies (regional gridded field products) based on the aggregated datasets and data from external data sources such as the CORA and the WOD for all the European sea basins and the Global Ocean	https://www.seadatanet.org/
EMODnet	European Marine Observation and Data Network is a long-term, marine data initiative funded by the European Maritime and Fisheries Fund which, together with the Copernicus space programme and the Data Collection Framework for fisheries, implements the EU's Marine Knowledge 2020 strategy. EMODnet Physics provides a single point of access to validated in-situ datasets, products and their physical parameter metadata of European Seas and global oceans. More specifically, time series and datasets are made available, as recorded by fixed platforms (moorings, tide gauges, HF radars, etc.), moving platforms (Argo, Lagrangian buoys, ferryboxes, etc.) and repeated observations (CTDs, etc.)	https://www.emodnet.eu/ www.emodnet-physics.eu

Table 4.2. List of most relevant international in-situ data providers.

4.2.3. Description of satellite observational oceanographic data

Satellite altimetry is one of the most important techniques for operational oceanography. Figure 4.12, adapted from International Altimetry Team (2021), shows an overview of the radar altimetry constellation and timeline as available from early 90' and with a projection beyond 2030: it demonstrates how altimetry can be considered as a well-established Earth observation platform from space and its evolution contributes to scientific advances in ocean dynamics. Figure 4.12, in particular, reports the main international missions operational temporal framework: before 2020, we have a number of satellites that are not operational anymore (in orange) but that provide a huge and valuable source of historical observations. Then there are modern operational satellites for the provisioning of near real time altimetry data (in yellow): for some of them, the data provider is also able to report the degraded quality period. New missions (e.g., SWOT, Sentinel6) are planned to be launched starting from 2022. These missions should be able to provide very high quality and high resolution altimetry products (light yellow to green). Some of the operational satellite platforms are also part of the DUACS (in dark blue): these consist of a multi-mission merged dataset for measuring, in particular, ocean mesoscale dynamics (more details are also available at 🔗 [32]).

32. https://duacs.cls.fr/
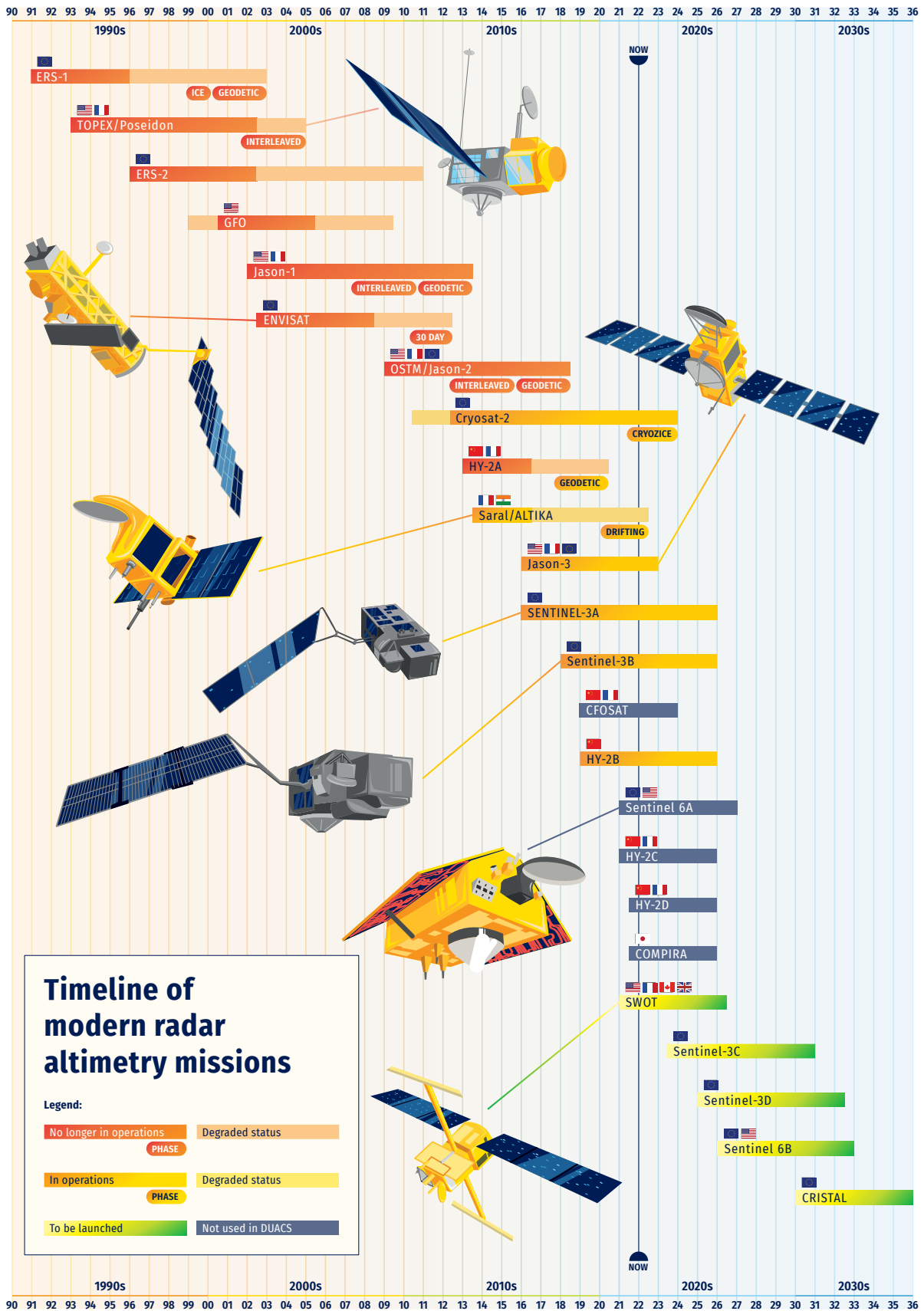
Figure 4.12. Altimetry satellites timeline (adapted from International Altimetry Team, 2021).

Satellite altimetry has substantially advanced understanding of the oceans by providing unprecedented observations of the surface topography at scales larger than 200 km, thus increasing our knowledge of global ocean circulation from the role of mesoscale eddies in shaping ocean circulation to the global sea level rise. The following sections describe the variables measured by satellites.

4.2.3.1. Satellite sea surface temperature

The SST is another important data source for ocean data assimilation and monitoring oceanic conditions. Since the beginning of operational satellite SST observations in 1981, the number and diversity of sensors have increased dramatically and are still evolving (O'Carroll, et al. 2019). A combination of infrared - onboard both LEO and geostationary orbit platforms - and passive microwave (LEO only) radiometers provide a comprehensive global SST coverage to meet the minimum data specification to be used in operational ocean models (as defined by GODAE in Bell et al., 2009).

Most satellite SST observations assimilated into ocean prediction systems are processed in accordance with guidelines and formats specified by the GHRSST (Donlon et al., 2009); an example of a multi-product ensemble is shown in Figure 4.13.
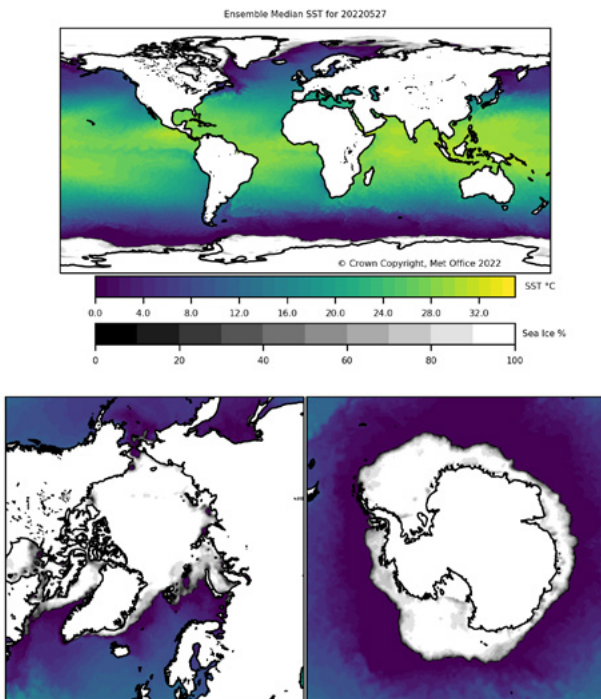
Figure 4.13.   Example of SST maps as provided by GHRSST multi-product ensemble (source: 🔗 33)

33. https://www.ghrsst.org/latest-sst-map/

GHRSST formatted products supply SST data either in satellite swath coordinates level 2 preprocessed (L2P) or level 3 composite (L3) gridded netCDF4 format files. L2P and L3 data products provide satellite SST observations together with a measure of uncertainty for each observation in a common GHRSST netCDF format (GHRSST Science Team, 2012). Auxiliary fields are also provided for each pixel as dynamic flags to filter and help interpret the SST data. These data are ideal for data assimilation systems or as input to analysis systems. Gridding a single L2P file produces an "uncollated" L3 file (L3U). Multiple L2P files are gridded to produce either a "collated" L3 file (L3C) from a single sensor or a "super-collated" L3 file from multiple sensors (L3S) (source: 🔗 34).

There are a wide range of satellite SST products in L2P or L3 format provided by various GHRSST regional and data assembly centres. The following is a list of SST products from different satellite sensors that are common to many ocean prediction systems:

• Passive Microwave Radiometers on LEO polar-orbiting satellites provide low spatial resolution SST at around 1 mm depth, with global coverage of the Earth at the equator up to twice daily and more frequently at higher latitudes. SST products obtained from passive microwave radiometers are effective at detecting ocean front variability in regions at least 50 km from land, under either clear or cloudy conditions but not precipitation. Most ocean prediction systems assimilate SST observations at ~25 km spatial resolution from the AMSR2 aboard the JAXA polar-orbiting satellite. These data are made available via the JAXA EORC (🔗 35) and Remote Sensing Systems (🔗 36).

• Infrared radiometers on LEO satellites provide high spatial resolution SST at around 10 micrometer depth, with global coverage of the Earth under clear sky conditions up to twice daily at the equator and more frequently at higher latitudes. SST products commonly used are measured by the Advanced Very High-Resolution Radiometer (AVHRR) instrument flown by the Meteorological Operational satellite (MetOp) series of polar-orbiting environmental satellites launched by the ESA and operated by the EUMETSAT. Two types of AVHRR SST products used in ocean prediction systems are: 1) the 1.1 to ~4 km spatial resolution FRAC AVHRR L2P and 2) the 4.4 to ~18 km resolution GAC AVHRR L2P, produced by the OSI SAF within EUMETSAT (🔗 37), OSPO (🔗 38), and NAVOCEANO.

34. https://www.ghrsst.org/ghrsst-data-services/products/
35. https://www.eorc.jaxa.jp/en/
36. http://www.remss.com/missions/amsr
37. http://www.osi-saf.org/?q=content/sst-products
38. https://www.ospo.noaa.gov/

The NAVOCEANO FRAC and GAC AVHRR L2P SST data are made available under the MISST (🔗 39) project sponsorship by the ONR and the PO.DAAC (🔗 40) operated by the NASA JPL. The newest NOAA JPSS satellites (Suomi-NPP and NOAA-20) are now equipped with the VIIRS sensors, that have a wide range of infrared channels, and provide SST at 0.75 km to 1.5 km resolution. In order to facilitate ingestion into real-time operational ocean systems, the VIIRS level 3 Uncollated (L3U) data are produced by the NOAA OSPO (🔗 41), and publicly available from NOAA OceanWatch (🔗 42) and PO.DAAC.

• Infrared radiometers on geostationary satellites above the equator provide high spatial (2~5 km) and temporal (10~60 minute) resolution SST observations over a fixed geographic region. There are several GEO satellites distributed around the equator and operated by different agencies (i.e. ESA, ISRO, NOAA, JMA, JAXA, KMA and CMA); they provide high temporal resolution SST that can improve clear-sky masking by using temporal information to separate the effects of faster moving clouds and other atmospheric features from the slower evolving SST fields (O'Carroll et al., 2019). One example is the AHI sensor of the JMA geostationary satellite "Himawari-8", which allows relatively high-frequency measurement of SST (every 10 minutes with horizontal resolution ~2 km) in a wide area of the Western Pacific (Kurihara et al., 2016). Data are made available by JAXA (🔗 43), NOAA (🔗 44) and the Australian Bureau of Meteorology via the National Computational Infrastructure (🔗 45).

Surface diurnal warming events occur in ocean regions of high solar radiation, clear skies, and calm seas. They are more common in the tropics (Zhang et al., 2016) but have also been observed at high latitudes (Eastwood et al., 2011). The warming events produce near-surface thermal gradients that create daytime near-surface or warm-layer temperatures up to 2-4°C warmer than nighttime (Donlon et al., 2002). Some operational centres exclude daytime satellite SST observations to reduce the diurnal warm bias and only use night-time satellite SST to assimilate into ocean analyses and forecast models. Most GHRSST L2P or L3U format SST data are cor-

rected for bias by subtracting the SSES bias value associated with each SST value (GHRSST Science Team, 2012), derived by data providers using recent matchups with SST observations from drifting buoys and tropical moorings (Petrenko et al., 2016) that produce SST estimates at around 0.2 m depth.

4.2.3.2. Satellite Altimeter

The main parameter that can be derived from satellite altimeters is SLA relative to a reference mean dynamic topography. SLA is fundamental for sea level monitoring and ocean data assimilation. Two freely available common data sources for real-time altimetry data retrieval are the RADS - which was developed by the DEOS and the NOAA Laboratory for Satellite Altimetry (Naeije et al., 2000; Scharroo, 2012) - and the Copernicus Marine Service (Figure 4.14).

The DEOS is building and developing the RADS database that incorporates validated and verified altimetry data products. The database is consistent in accuracy, correction, format and reference system parameters. The capability of such a database has attracted users with less satellite altimeter expertise. Currently, RADS enables users to extract the data from several present and past satellite altimeter missions like GEOSAT, ERS1, ERS2, ENVISAT, TOPEX/Poseidon (T/P), JASON1, JASON2, JASON3, CRYOSAT2, SENTINEL-3A, and SARAL 🔗 46.

The Level 3 SLA product from Copernicus Marine Service is another open accessible data source for SLA. It shares many of the most useful features of the RADS service, including adaptation to changes in the available satellite fleet and
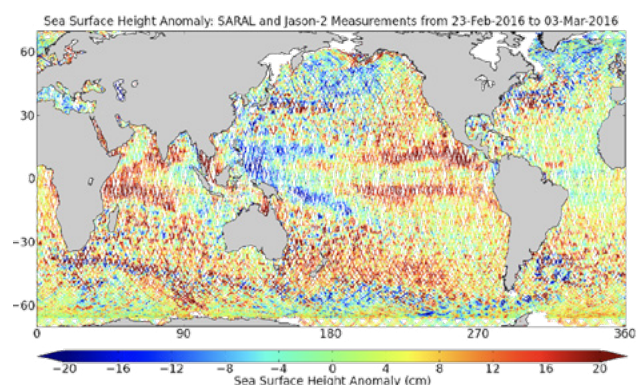
Figure 4.14.   Global ocean along track sea level anomaly (source: 🔗 47).

39. https://www.nopp.org/projects/multi-sensor-improved-sea-surface-temperature-misst

40. https://podaac.jpl.nasa.gov/

41. https://www.ospo.noaa.gov/

42. https://coastwatch.noaa.gov/cw/satellite-data-products/sea-surface-temperature.html

43. http://suzaku.eorc.jaxa.jp/GHRSST/

44. https://coastwatch.noaa.gov/cw/satellite-data-products/sea-surface-temperature/acspo-ahi.html

45. https://nci.org.au/

46. http://rads.tudelft.nl/rads/data/authentication.cgi

47. https://datastore.cls.fr/catalogues/global-ocean-along-track-sea-level-anomalies/

maintaining homogeneity. Although superficially RADS and Copernicus Marine Service seem providing the same type of SLA observation they are not identical and a detailed explanation of differences is non-trivial, as the RADS data includes many of the corrections used by Copernicus Marine Service, as well as the corrections applied in its own processing. Users are encouraged to explore the differences between these two data streams and choose the suitable satellite altimeter data source for their own data assimilation system.

4.2.3.3. Satellite Sea Surface Salinity

Measuring SSS from space is a relatively recent technique that relies on L-band radiometry (which has evolved to a point where useful information is provided every few days). Satellite SSS offers the advantages of global coverage and the ability to capture space and time scales not afforded by in-situ platforms such as vessels, moorings, and Argo profiling floats. Figure 4.15 shows a year of satellite SSS products from the ESA's SMOS and NASA Aquarius and SMAP missions. It is worth noting that regions of high variability of >0.2 psu - including coastal oceans, western boundary currents, the Indonesian Seas, and the Southern and Arctic Oceans - are either not sampled or poorly sampled by Argo (Vinogradova et al., 2019).
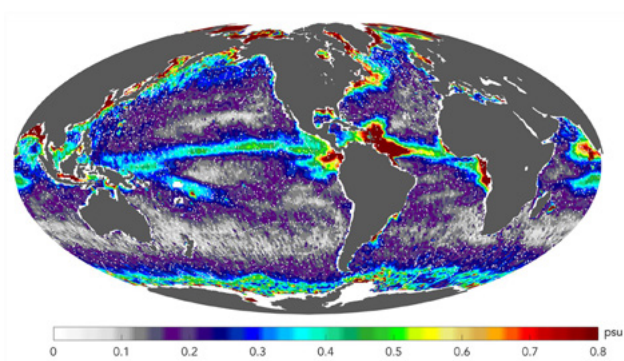
Figure 4.15. Variability in space-borne sea surface salinity during one year (colors) superimposed with locations of currently operational Argo floats (white dots) from Vinogradova et al. (2019).

Level 3 observations (L3 - provided on a grid but with no in-filling) with various temporal and spatial averaging from the SMOS, Aquarius, and SMAP satellites are available, as are level 2 data (L2; SSS values at the native swath resolution). For SMOS and Aquarius, L3 products are available daily, with separate files for the ascending and descending parts of the orbit. The products used are from the LOCEAN (🔗 [48]) and the JPL (🔗 [49]) respectively for SMOS and Aquarius. While there is

48. www.catds.fr
49. https://podaac.jpl.nasa.gov/
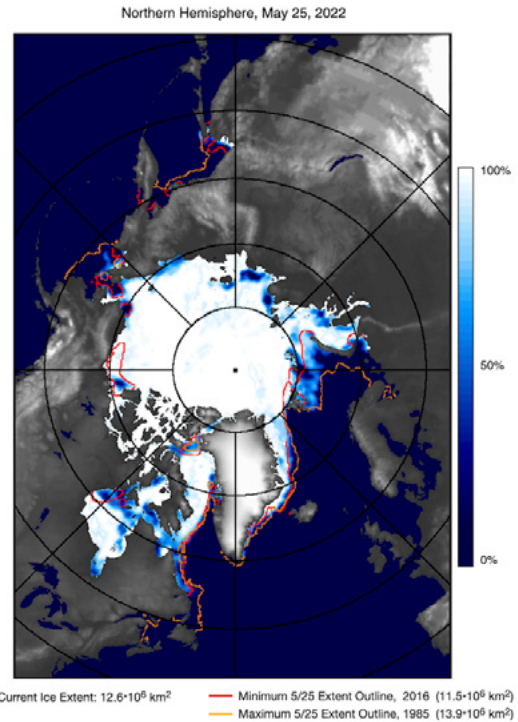
Figure 4.16. Example of satellite-based product for sea ice extension in the Northern Hemisphere (source: 🔗 [50]).

a daily L3 SMAP product, it is based on observations from an 8-day period that would require a complicated observation operator in the data assimilation.

The availability of SSS from SMOS, Aquarius and SMAP has enabled ocean forecast validation (e.g., Vinogradova et al., 2014; Martin, 2016). In recent years, efforts have been put into assimilating satellite SSS data, which is challenging for several reasons. Largely, these are related to the magnitude of errors in the data, particularly in the SSS products needed for operational-style forecasting systems that are required at high temporal resolution (Martin et al., 2019). Quality control of satellite SSS has proved to be a very important process for ocean data assimilation.

4.2.3.4. Satellite sea ice

The sea ice concentrations from Nimbus-7 SMMR sensor and DMSP SSM/I passive microwave data, are accessible from the NASA NSIDC DAAC (🔗 [51]) (Figure 4.16). This sea ice concentration dataset is generated from brightness tem-

50. https://earth.gsfc.nasa.gov/cryo/data/current-state-sea-ice-cover
51. https://doi.org/10.5067/8GQ8LZQVL0VL

perature data and is designed to provide a consistent time series of sea ice concentrations spanning the coverage of several passive microwave instruments. The data are provided in the polar stereographic projection at a grid cell size of 25 x 25 km. This is then interpolated to 10 km resolution, level 3 composite of SSMIS level 2 data, on a polar stereographic grid (🔗 52). Daily files are available within 24-48 hours after last satellite acquisition.

The same satellite sea ice concentration data originating from NSDIS SSM/I aboard the DMSP series of polar-orbiting sun-synchronous satellites, are provided by the OSI SAF (🔗 53). The global daily sea ice concentration is processed by OSI SAF at 10 km resolution as level 3 composites of SSMIS level 2 data on a Polar Stereographic grid. Northern Hemisphere and Southern Hemisphere daily files are available within 6 hours after last satellite acquisition.

4.2.3.5. Ocean Colour

Ocean colour measurement consists of detecting spectral variations in the water-leaving radiance (or reflectance), which is the sunlight backscattered out of the ocean after interaction with water and its constituents (Groom et al., 2019). This is a very significant measurement for the monitoring of ocean water quality, ocean acidification, or to understand the global carbon cycle, apart from using it for assimilation and validation. In the open ocean, the signal is largely influenced by the presence of phytoplankton and dissolved organic matter; in coastal waters, it is also influenced by resuspended particulate matter and river runoff that transports other kinds of anthropogenic particulate. In the framework of the Copernicus Marine Service, two types of products are delivered by the OC TAC (🔗 54):

• CHL is the phytoplankton chlorophyll concentration. For the global and regional seas, OC TAC selected the state-of-the-art product algorithm on the basis of optical characteristics of the basin and round robin procedure. For the regional seas, daily chlorophyll fields are produced by applying two different algorithms for open ocean (Case I) and coastal waters (Case II). The data are then merged into a single chlorophyll field providing a regional product with an improved accuracy of estimates in coastal waters.

• The OPTICS product includes all other variables retrieved from ocean colour sensors: IOP, such as absorption and scattering, the diffuse attenuation coefficient of light at 490 nm (Kd490), Secchi depth (transparency of water), spectral Rrs, PAR, CDOM, and the SPM.

Figure 4.17 shows an example of chlorophyll concentration at global scale from the MODIS Aqua satellite.
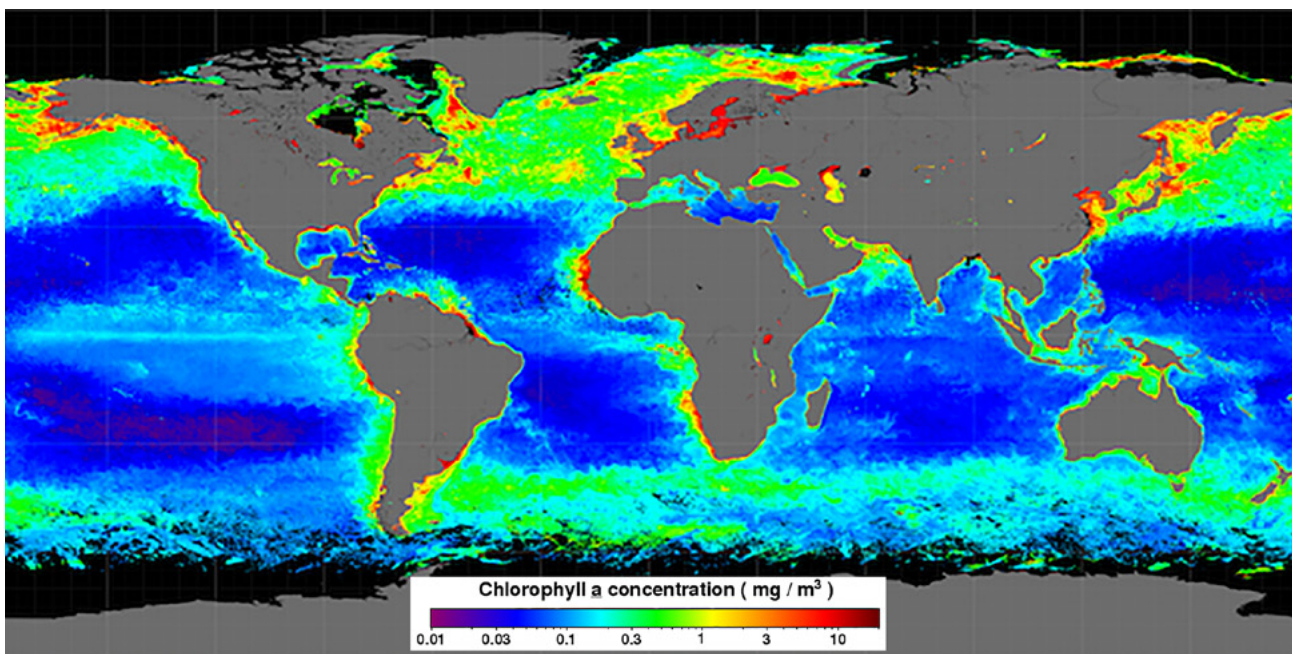
Figure 4.17.   MODIS Aqua chlor_a seasonal composite for Spring 2014 (source: 🔗 55).

52. https://nsidc.org/data/nsidc-0081

53. http://www.osi-saf.org/?q=content/sea-ice-products

54. https://marine.copernicus.eu/about/producers/oc-tac

55. https://oceancolor.gsfc.nasa.gov/atbd/chlr_a/
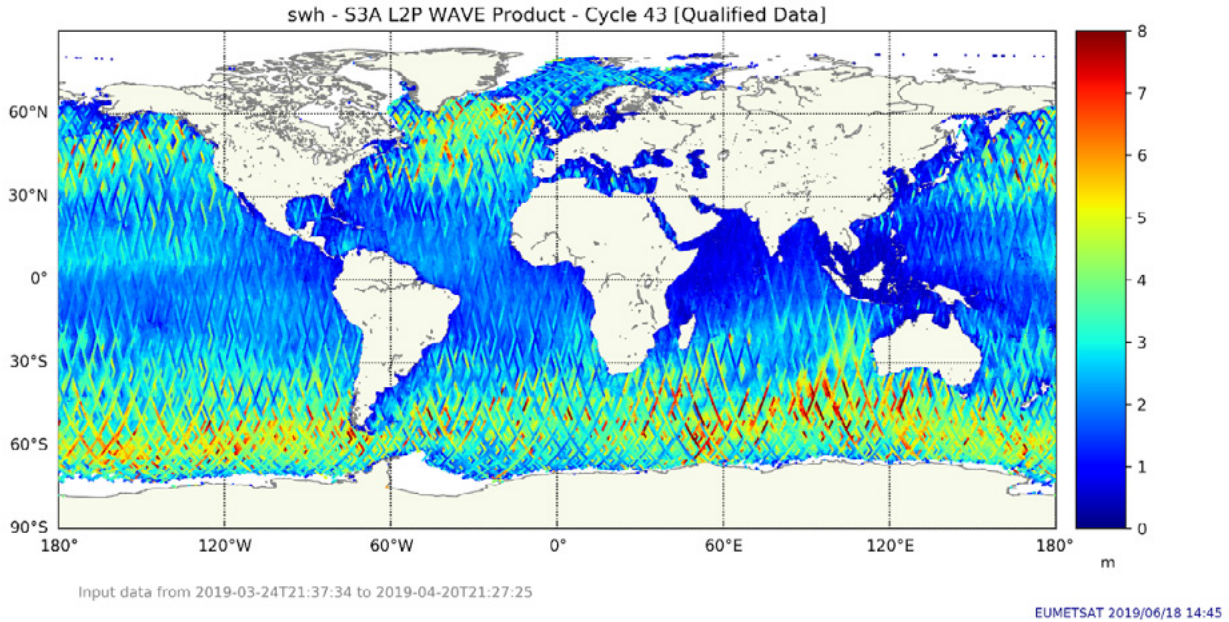
Figure 4.18.   Sentinel-3 SRAL significant wave height Level-2 global map (source: 🔗 56).

4.2.3.6. Significant Wave Height

The SWH (or Hs) is the average wave height (from trough to crest) of the highest third (33.33%) of the waves in a given sample period. The Sentinel-3 mission is able to monitor wave heights from 0 to 20 m. The marine sea state SWH product is a critical product for all maritime safety and rescue operations (from 🔗 57).

Figure 4.18 shows an example of SWH for the global ocean from Sentinel-3A measurements.

4.2.3.7. Providers of satellite data

Providers of satellite observations to be used for assimilation/validation are listed in Table 4.3.

4.2.4. Bathymetry

The term "bathymetry" refers to the ocean's depth relative to the sea level. It is an important element in any ocean model, since it allows us to represent the geographical and topographical peculiarities of the sea floor. It has a strong influence on the circulation, notably its barotropic and depth-integrated features, in particular (but not only) at sills and straits,
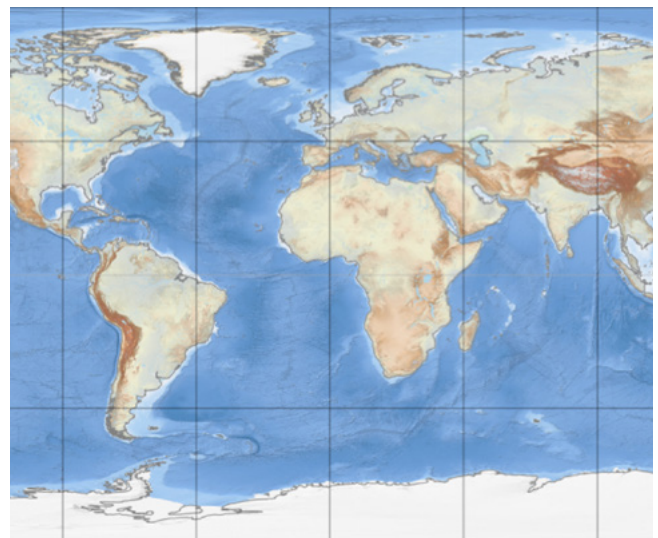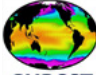
Figure 4.19.   An example of a bathymetric dataset: the EMODnet bathymetry (source: 🔗 58).

on coastal and in shelf seas. For this reason, its accuracy may determine the goodness of the ocean model, although there are issues of smoothing and grid mislocation that need to be considered and solved by using ad hoc spatial analysis.

---

56. https://www.eumetsat.int/new-S3-sral-wave-products

57. https://sentinels.copernicus.eu/web/sentinel/user-guides/sentinel-3-altimetry/overview/geophysical-measurements/significant-wave-height

58. https://www.emodnet-bathymetry.eu

Provider	Description	Website
Copernicus Marine Service	Copernicus Mawrine Service through the SL, SST, OC, WAVE TACs for the operational provisioning of near real time and reprocessed datasets used by the Monitoring and Forecasting Centres (MFCs) for assimilation and validation	Copernicus Marine Service https://marine.copernicus.eu/
GHRSST	The Group for High-Resolution Sea Surface Temperature (SST) (GHRSST) provides a new generation of global high-resolution (<10km) SST products to the operational oceanographic, meteorological, climate and general scientific community	GHRSST https://www.ghrsst.org/
AVISO++	AVISO++ provides altimeter data	AVISO⁺ https://www.aviso.altimetry.fr/en/home.html
EUMETSAT	EUMETSAT is the European operational satellite agency for monitoring weather, climate and the environment from space. In particular, it provides SST and altimeter data	EUMETSAT https://www.eumetsat.int/
NOAA NSIDC	NOAA National Snow and Ice Data Centre provides sea ice concentration in the polar region	NSIDC https://nsidc.org/

Table 4.3. List of most relevant international satellite data providers.

A bathymetric dataset needs to be interpolated onto the model's grid. Pre-processing of the bathymetric fields should be necessary for numerical reasons: since bathymetry datasets are usually finer than the model grid, they may need to be smoothed before inserted on the model grid. Effective resolution and vertical coordinates of the ocean model could also constrain the smoothness of the bathymetry.

Figure 4.19 shows an example of a bathymetric dataset as provided by EMODnet bathymetry.

Table 4.4 includes a list of public providers of bathymetric datasets (Marks and Smith, 2006).

4.2.5. Atmospheric forcing

Typically, NWP systems provide atmospheric surface forcing fields to OOFS in order to compute water, heat, and momentum fluxes. Such fields may be also supplemented by real-time or near real-time observations and other averaged datasets including climatology. Certainly, in a more complex modelling framework, an ad hoc atmospheric model can be developed at the same resolution of the ocean model in order to provide high resolution atmospheric fields (coupled systems, see Chapter 10 for further details).

In general, typical surface data input required by an OOFS that is provided by an NWP model includes:

- Sea ice coverage;
- Downward surface longwave radiation;
- Upward surface longwave radiation;
- Downward surface shortwave radiation;
- Upward surface shortwave radiation;
- Dewpoint depression at 2 m;
- Surface latent heat;
- Mean sea level pressure;
- Surface sensible heat;
- Specific humidity at 2 m;
- Air temperature at 2 m;
- Cumulative precipitation rates;
- Zonal and meridional wind components and wind speed at 10 m (or surface wind stresses);
- Short-wave radiation heat flux penetrating through ice;

Product	Description	Provider
DBDB2	Digital Bathymetric DataBase at 2 min by 2 min uniform grid global bathymetry and topography data developed for the ocean model. It was developed by the Naval Research Laboratory	https://www7320.nrlssc.navy.mil/DBDB2_WWW/
ETOPO1	1 arc-minute global relief model of Earth's surface that integrates land topography and ocean bathymetry. It was built from numerous global and regional data sets. Historic ETOPO2v2 and ETOPO5 global relief grids are depreciated but still available	National Centers for Environmental Information http://www.ngdc.noaa.gov/mgg/global/
GEBCO	Gridded Bathymetry Data for the World's oceans at 15 arc-second resolution. It operates under the joint auspices of the IHO and the UNESCO IOC	https://www.gebco.net/
SRTM+	Global bathymetry and topography. SRTM15+ is the last version at 15 arc-second resolution, built upon the latest compilation of ship-board sounding and satellite-derived predicted depths. V2.0 is part of the last release of GEBCO_2020 (Tozer et al., 2019)	http://topex.ucsd.edu/marine_topo/
EMODnet Bathymetry	It is part of the EMODnet project, funded by the European Commission, which brings together marine data into interoperable, continuous and publicly available bathymetric dataset for all the maritime basins in European waters and for the global ocean	EMODnet https://www.emodnet-bathymetry.eu/

Table 4.4. Bathymetric dataset products and providers.

- Ice freezing/melting heat flux;
- Zonal and meridional ice stress on ocean;
- Sea-Ice basal salt flux.

The above list is not exhaustive and inputs can vary based on the needs of the OOFS. For example, it can be used SST from the OOFS along with the air temperatures at 2 m to calculate sensible heat flux instead of using that provided by NWP. More details on thermodynamic and momentum forcing of the ocean can be found in Barnier (1998), Barnier et. al. (1995), Josey et al. (1999).

Figure 4.20 shows an example of surface forcing atmospheric fields from the ECMWF IFS.

A list of global NWP systems is provided in Table 4.5.

Base time: Mon 13 Jun 2022 00 UTC Valid time: Mon 13 Jun 2022 06 UTC (+6h) Interval (hr) : 6 Area : Global
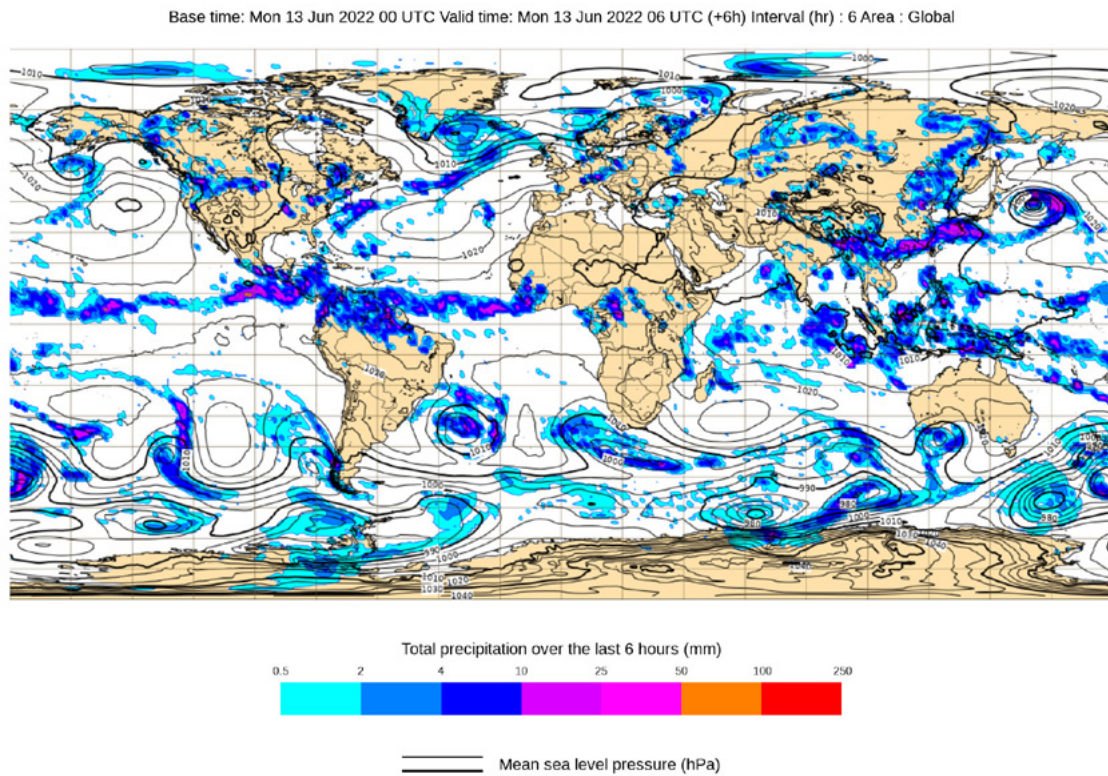
Figure 4.20. An example of surface forcing fields: rain and mean sea level pressure at global scale from ECMWF (source: [59]).

Dataset	Description	Provider
GFS	Global Forecast System, produced by the National Centers for Environmental Prediction (NCEP), provides analysis and forecast atmospheric fields for the global ocean at the resolution of about 28 km	https://www.ncdc.noaa.gov/data-access/model-data/model-datasets/global-forcast-system-gfs
NAVGEM	Navy Global Environmental Model runs by the United States Navy's Fleet Numerical Meteorology and Oceanography Center (FNMOC)	https://www.usno.navy.mil/FNMOC/meteorology-products-1m
ECMWF IFS and ERA5	European Center for Medium range Weather Forecasting that provides reanalysis, analysis and forecast atmospheric fields at medium, extended, and long range	**ECMWF** https://www.ecmwf.int/
Met Office UK	United Kingdom Meteorological Office that produces the Unified Model, a numerical model of the atmosphere used for both weather and climate applications	Met Office https://www.metoffice.gov.uk/
GEM	Global Environmental Multiscale model, an integrated forecasting and data assimilation system developed in the Recherche en Prévision Numérique (RPN), Meteorological Research Branch (MRB), and the Canadian Meteorological Centre (CMC)	Environment Canada https://collaboration.cmc.ec.gc.ca/

Table 4.5. Atmospheric forcing products and providers.

59. https://www.ecmwf.int/
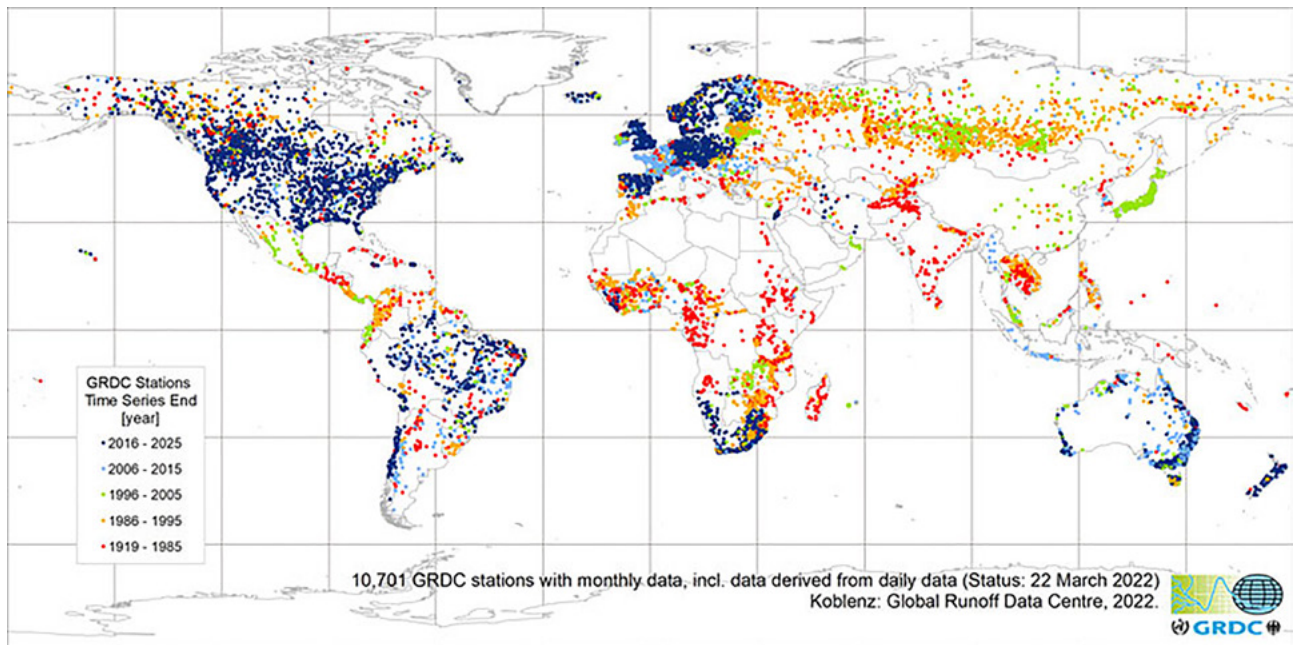
Figure 4.21.   An example of river runoff discharge data provider: worldwide distribution of stations contributing to GRDC (source: 🔗 60).
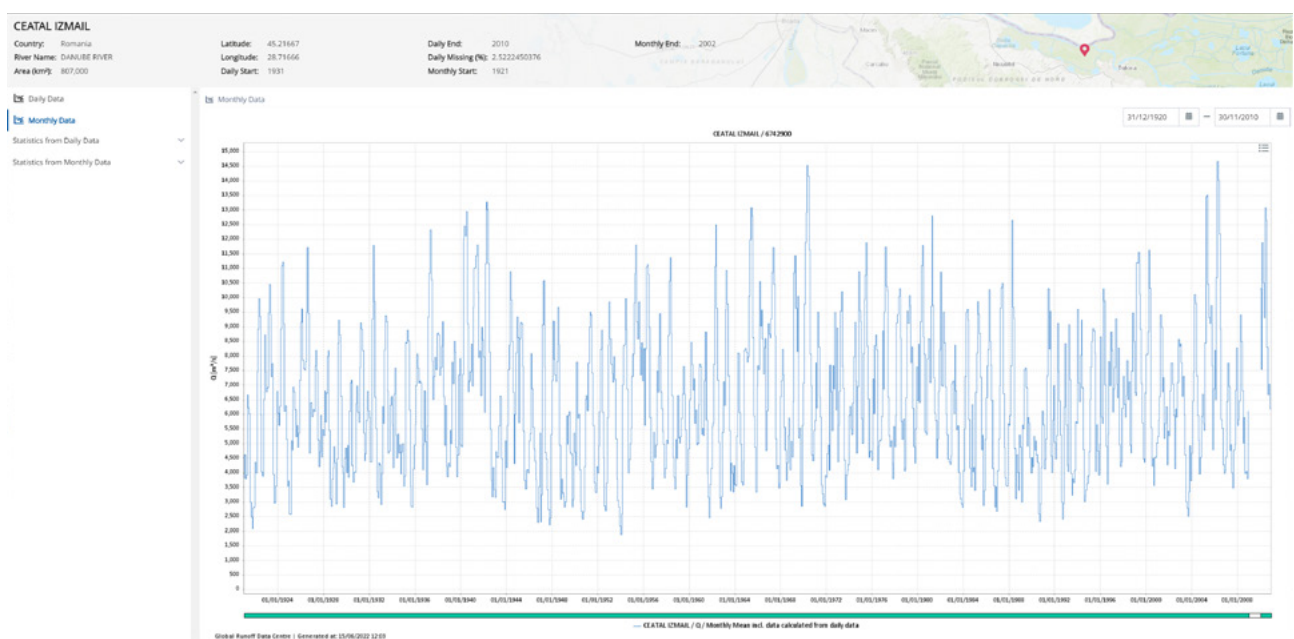
Figure 4.22.   An example of river runoff discharge (monthly data) time series from GRDC related to Ceatal Izmail station (Romania) that monitors the Danube basin (source: 🔗 61).

60. https://www.bafg.de/GRDC/EN/Home/homepage_node.html   61. https://www.bafg.de/GRDC/EN/Home/homepage_node.html

Dataset	Description	Provider
GRDC	Global Runoff Data Base, built on an initial dataset collected in the early 1980s from the responses to a WMO request to its member countries to provide global hydrological information	GRDC https://www.bafg.de/GRDC/EN/01_GRDC/13_dtbse/database_node.html
Dai and Trenberth	Dai and Trenberth Global River Flow and Continental Discharge Dataset contains time series of all available monthly river flow rates observed at the farthest downstream station for the world's largest 925 rivers, plus long-term mean river flow rates and continental discharge into the individual and global oceans, produced originally by Dai and Trenberth (2002) and Dai et al. (2009) and Dai (2021)	NCAR UCAR https://rda.ucar.edu/datasets/ds551.0
EFAS	European Flood Awareness System developed and operational within the Copernicus Emergency Management Service. It provides gridded modelled daily hydrological time series forced by meteorological observations. It includes river discharge, soil moisture for three soil layers and snow water equivalent	Emergency Management https://www.efas.eu/
GLOFAS	Global Flood Awareness System, operational within the Copernicus Emergency Management Service. It couples state-of-the art weather forecasts with a hydrological model and with its continental scale set-up, providing downstream countries with information on upstream river conditions as well as continental and global overviews	Emergency Management https://www.globalfloods.eu/
EMODnet Physics	EMODnet Physics gathers, harmonises and makes available near real time river runoff and in-situ river runoff trends (monthly and annual means), accessible through the website with MapViewer controllers	EMODnet https://map.emodnet-physics.eu/

Table 4.6.   River data providers.

4.2.6. Land forcing

Rivers represent the natural element connecting land and ocean through the coastline. They impact both coastal and basin-wide circulation and dynamics through net freshwater flux; additionally, they are responsible for biotic diversity and eutrophication, particularly in coastal waters.

Water discharges, nutrients, and organic materials represent sources of freshwater and biogeochemical fluxes for an OOFS, and we have to account for them once we set a numerical model. This kind of data may come from observations or from other models (hydrological or biogeochemical models). In particular, information about discharge, and possibly also salinity and temperature if available, should be provided for the river mouth at given coordinates.

As an example, in Figure 4.21 is shown the distribution at global scale of stations that operated/are operating in a certain temporal period contributing to the GRDC. Once the user selects one of the stations, the web service returns the water discharge timeseries (Figure 4.22) allowing to download and integrate it as an input dataset in the ocean model setup.

Table 4.6 provides a list of international databases for river data.

Below are listed some other initiatives for handling freshwater inputs with focus on icebergs and R&D project:

- Altiberg is a database for small icebergs (< 3km in length), detected by altimeters using the high-resolution waveforms (Tournadre et al., 2016), [62];

62. http://cersat.ifremer.fr/user-community/news/item/473-altiberg-a-database-for-small-icebergs

• BRONCO stands for "Benefits of dynamically modelled river discharge input for ocean and coupled atmosphere-land-ocean systems": it is a Service Evolution Project run in the framework of Copernicus Marine Service to improve and standardise input of river discharge into global, regional and coastal models, 🔗 [63];

• LAMBDA stands for Land-Marine Boundary Development & Analysis: it is another Service Evolution Project run in the framework of Copernicus Marine Service. It aims at improving the Copernicus Marine Service MFCs thermohaline circulation in coastal areas by better characterization of the land-marine boundary conditions, 🔗 [64].

4.2.7. OOFS fields as input for downscaling

An OOFS may be set also using information from other OOFSs: this is the case of the so-called nesting models (for major details see Section 5.4.4). For example, the GLO-PHY - herein referred to as parent model - provides lateral open boundary conditions to the Mediterranean Sea Forecasting System (MedFS) - herein referred to as child model. Both systems are part of the Copernicus Marine Service catalogue. Figure 4.23 shows a typical ocean field at global scale from GLO-PHY - in this case, we display sea surface temperature forecast product. The parent model provides temperature, salinity, sea surface height, zonal and meridional velocity components to the Mediterranean Sea through 3 open boundaries located in the Atlantic Ocean. Ocean fields from the parent model are spatially and temporally interpolated over the open boundary sections and provided to the ocean circulation model of the child domain. Figure 4.24 shows as example the Mediterranean Sea surface currents forecast product after integrating the numerical model accounting for the GLO-PHY ocean fields as lateral open boundary conditions.

For major details about the setup of both systems, please refer to the Copernicus Marine Service web pages dedicated to each product.

4.2.8. Climatology from observations

To describe the general oceanographic conditions at different time scales and spatial resolutions, climatological fields computed from observations can be used. They are defined as mean values of a certain variable in a certain period (e.g. month, season, etc.). They may be used for creating initial and/or boundary conditions for an ocean model, as well as validating numerical results and performing data assimilation.

Since observations are irregularly distributed in space, an objective analysis (Chang et al. 2009) is needed in order to
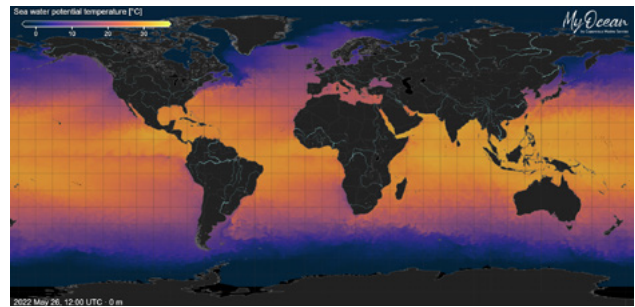
Figure 4.23.   The GLO-PHY sea surface temperature on 26 May 2022 (source: 🔗 [65] through the Ocean Viewer 🔗 [66]).

Figure 4.24.   The MedFS sea surface currents on 26 May 2022 (source: 🔗 [67] through the Ocean Viewer 🔗 [68]).

produce spatially gridded dataset that can be easily used by a numerical model. Numerical model results, being gridded, can be easily aggregated in time to produce a climatological field to be used as initial or boundary condition.

Climatologies may be also computed from NWP products to modify or to formulate ocean surface fluxes using mean momentum conditions from a reanalysis product (e.g., ECMWF ERA5, etc.) superposed with variability from the NWP fields. Additionally, observations such SSS and SST may be adopted for supplementing climatological data for surface flux relaxation to control model drifts. Finally, climatologies may be computed also from other ocean models to provide lateral open boundary conditions (numerics and methods will be presented in Chapter 5).

Figure 4.25 provides as an example of climatology the annual sea surface temperature computed over the period 1955-2017 for the global ocean by the WOA.

Table 4.7 provides a list of international atlases.

63. https://www.mercator-ocean.fr/en/portfolio/bronco-2
64. http://www.cmems-lambda.eu/

65. https://marine.copernicus.eu/
66. https://myocean.marine.copernicus.eu/
67. https://marine.copernicus.eu/
68. https://myocean.marine.copernicus.eu/
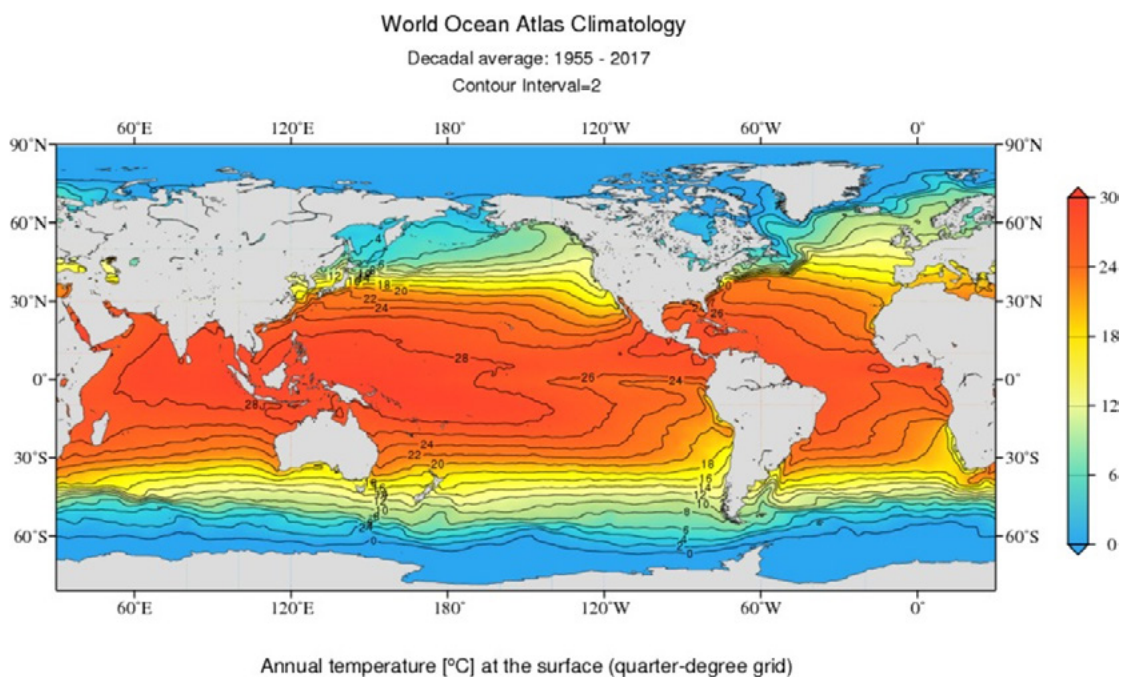
Figure 4.25. An example of climatology: temperature field from World Ocean Atlas Climatology (source: 🔗[69]).

Dataset	Description	Provider
WOA	World Ocean Atlas (Boyer et al., 2019) provides climatological temperature (ºC), salinity (unitless), density (kg/m3), mixed layer depth (m) and other biogeochemical parameters (for the latter, major details are provided in Chapter 9)	National Centers for Environmental Information https://www.ncei.noaa.gov/products/world-ocean-atlas
WOD	World Ocean Database (Boyer et al., 2019), is a continuation of the Climatological Atlas of the World Ocean (Levitus, 1982) and at present represents one of the world's largest collection of uniformly formatted, quality controlled, and publicly available ocean profiles data	National Centers for Environmental Information https://www.ncei.noaa.gov/products/world-ocean-database
SeaDataNet	SeaDataNet is a distributed Marine Data Infrastructure for the management of large and diverse sets of data deriving from in situ of the seas and oceans. It provides an online access to data on regional climatologies products – gridded fields of sea temperature and salinity - for the European seas (Arctic Sea, Baltic Sea, Black Sea, Mediterranean Sea, North Sea, North Atlantic Ocean) and for the global ocean	SeaDataNet https://www.seadatanet.org/Products/Climatologies

Table 4.7. Climatology products and providers.

69. https://www.ncei.noaa.gov/

4.3.
Data Assimilation

Through data assimilation, OOFS combines observations and the numerical model solution with the scope of producing the best reconstruction of the ocean state to be used as initial condition of the forecasting cycle. According to Moore et al. (2019) and considering Figure 4.27, we can assume that a priori state estimate of the ocean computed from the numerical model (blue line in Figure 4.26) together with a priori direct but incomplete state estimate from ocean observations (black dots in Figure 4.26) produce a posteriori state estimate which "combines" all available information considering uncertainties in both model and observations (green line in Figure 4.26).
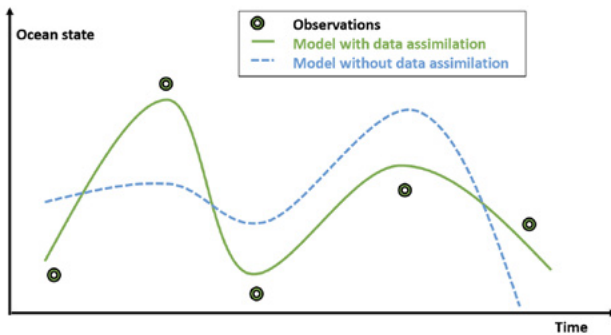
Figure 4.26.   Data assimilation models (green) are helped by observations to produce more realistic forecasts, closer to real observations (source: MEDCLIC project, SOCIB-La Caixa Foundation).

Ocean data assimilation is then defined mathematically through a rigorous process that combines ocean observation statistics with statistics of ocean model behaviour to extract the most useful information, possibly from sparse observations of time-varying ocean circulation (Cummings et al., 2009). Broadening Step 1 in Figure 4.1, the main characteristics of the data assimilation modelling system can be presented as in Figure 4.27, which shows the major components of the data assimilation modelling system, which are defined by:

- access to observations;
- data quality control;
- data assimilation scheme.

Access to observations, quality, providers as well as examples have been presented in Section 4.2. Data quality control is performed by an automatic procedure, native in the as-

simulation scheme or performed in offline mode at the submission of the analysis cycle, which selects the best observational dataset from the one accessed. To do such selection, the procedure takes as input the quality flag value associated with each specific observation (see Figure 4.3): usually, observations with QC flag = 1 and/or 2 are selected and make eligible to be used by the data assimilation scheme.

Depending on the specific characteristics of the basin on which the system is working, the data quality control may include further checks to reject data which are not sufficiently good to be assimilated. Such criterion may be implemented in offline mode as pre-processing steps of the data access and management. This is the case, for example, of the Mediterranean Forecasting System (MedFS) delivered in the framework of Copernicus Marine Service: the system performs additional checks for Argo and SLA observations rejection based on specific criteria, which are listed in Table 4.8.

Data assimilation scheme is really the core of the system since it performs the mathematical work of combining model state and observations. Existing data assimilation methods are classified in 2 major groups (Bouttier and Courtier, 2002):

- sequential method, which considers past observations until the time of analysis: this is the case of NRT products (analysis);

- non-sequential method, which uses "future" observation: this is the case of the multi-year products (e.g., reanalysis).

Another distinction can be made between continuous and intermittent assimilation in time:

- continuous assimilation: for a given period of time the observations are collected and the correction to the analysed state is smoothed over a specific assimilation window;

- intermittent assimilation: for a given period of time, the observations are collected within a specific assimilation window to compute a correction.
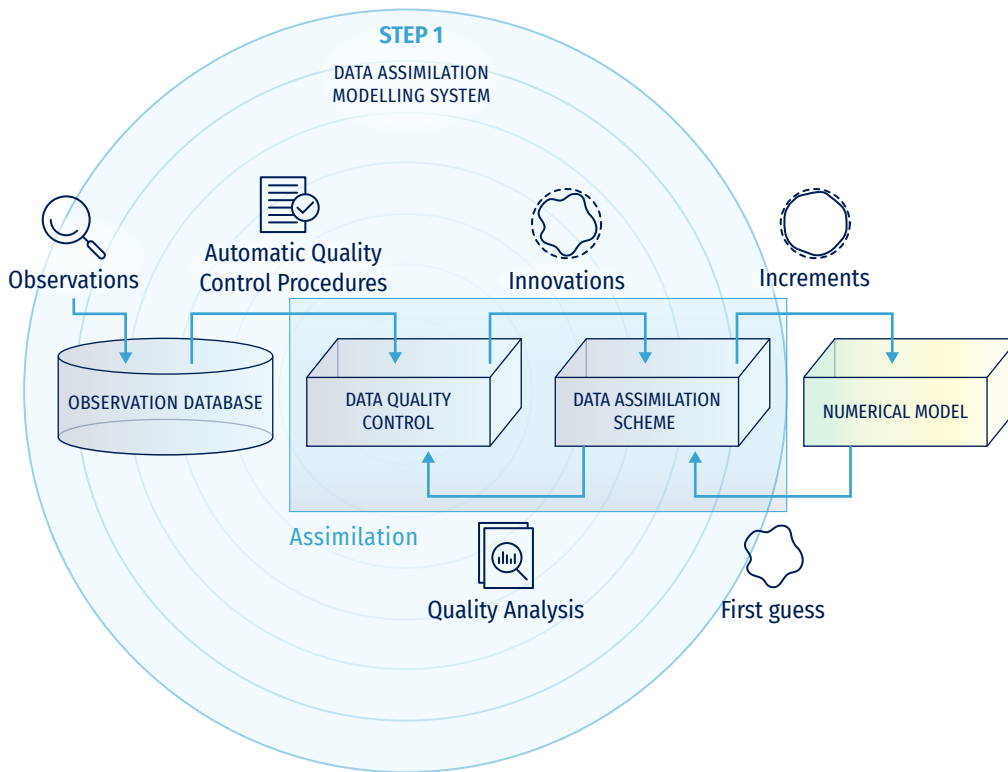
Figure 4.27. Major components of a data assimilation modelling system.

Carrassi et al. (2018) and De Mey (1997) detail more the nature of the assimilation schemes used in physical, biogeochemical, ice and wave forecasting systems, describing the formulation of the problem and numerical approximation. These concepts are detailed in the theoretical chapters from 5 to 9, which are dedicated to show how such methods are used for setting up an OOFS.

From the scheme in Figure 4.27, we can derive some key definitions at the basis of the assimilation cycle: the innovation, defined as the difference between the first guess (or forecast) and the observation. The data assimilation method tries to estimate with less uncertainty than either the model prediction or observation: it deals with the computation of the increment, defined as the analysis minus the model first guess. The data assimilation system itself has been used to monitor observations and data quality control (Hollingsworth et al., 1986) by computing statistics involving observations, such as observation increments used to setup the blacklisting; this is a list of observations that the data assimilation has rejected and represents valuable information to be shared also with data providers in order to fix potential issues or bugs in the observational datasets.

ARGO QC1	Check on the date and location quality flags: only the profiles with both flags equal to 1 are taken into account
ARGO QC2	Out of the Mediterranean Sea region
ARGO QC3	Retain only ascending profiles (descending are rejected)
ARGO QC4	Check on the values of the quality flags of pressure, temperature and salinity for each depth: if one of the flags is not equal to 1, the layer is deleted
ARGO QC5	Check on the values of the temperature and salinity, data outside the following ranges are rejected: $0<T<35$; $0<S<45$
ARGO QC6	Check on the thermocline: if distance between two subsequent measurements of temperature and salinity in the first 300 meters is larger than 40 m, the profile is rejected
ARGO QC7	Measurement between 0 and 2 m are rejected
SLA QC1	Check on the values of date, latitude, longitude, sea level anomaly and DAC: if one of these values is equal to missing value the measurement of sea level anomaly is rejected. Check on the quality flag of sea level anomaly: if the flag is not equal to 1 the measurement of sea level anomaly is rejected

Table 4.8.   Quality control criteria adopted by the Mediterranean Analysis and Forecasting System (MedFS, 🔗[70]) for in-situ (Argo) and SLA.

4.4.
Numerical Ocean models

4.4.1. Definition and types of models

Ocean numerical models are the very core of the OOFS (see Figure 4.1). A numerical ocean model is a computational tool used to understand and predict oceanic variables (Griffies, 2006). A set of equations governing the dynamics and thermodynamics of the ocean are solved numerically to obtain a three dimensional dataset of simulated variables, which typically consist of EOV such as wave fields, velocity components, temperature, salinity and sea level, at any instant of time.

Depending on the problem and variables to be treated, different numerical models are employed:

• Temperature, salinity and currents fields are solved by means of ocean circulation models (see also Chapter 5);

• Ice models (see also Chapter 6);

• Sea level uses ocean circulation models, although typically are running under simplified equations (see also Chapter 7);

• Growth, propagation and decay of waves due to winds are calculated by wave models (see also Chapter 8). The rate of change of the wave spectrum is governed by transfer of energy from wind, wave-wave interaction and dissipation. Interaction with ocean bottom is critical at high resolution coastal processes; different models, with different physics, are available to solve this scale (mild-slope, Boussinesq, etc.);

• Biogeochemical processes in the ocean can be represented by biogeochemical models (see also Chapter 9), using coupled differential equations. Examples of such processes include cycles of carbon, nitrogen, iron, etc. Additional equations are used for time evolution of phytoplankton, zooplankton, etc., at varying levels of complexity. The chemistry and ecosystem equations are combined with the physical OGCM for the time-dependent estimation of variables.

70. https://medfs.cmcc.it/

4.4.2. Coupled models

Various dynamical components of the Earth system, such as NWP systems, OOFS, Sea Ice forecast systems, wave forecast systems, Land/Hydrological forecast systems, etc., can be coupled together (see also Chapter 10). The coupling is facilitated by using a common framework - like the ESMF - which allows the various dynamical components to exchange forcing data with other components. Couplers are then designed to provide appropriate output/input information on model grids at every time step, as required. This provides a much more "tight" exchange of forcing data, which otherwise would be prohibitively expensive to provide using traditional file I/O. Different couplers allow for data exchange at different time scales. For example, atmosphere and sea ice can be coupled at smaller time intervals while ocean and sea-ice exchange information at much slower time intervals in the same coupled environment.

A significant application of such "tight" coupling is for wind-waves. Feedback from wave models in terms of radiation stress can be used to modify drag coefficients for calculating wind stresses. These can be particularly useful for complex seas driven by hurricanes.

4.5.
Validation and Verification

Operational ocean services provide routine marine products to an ever-widening community of users and stakeholders. Some of the products delivered are generated by means of ocean models (i.e. forecasts, analyses, or reanalyses). Ocean models are powerful computational tools able to produce useful information in the absence of (or in between) ground truth information. The reliability of this information depends on the realism of the model itself, but also on the accuracy of its initial and boundary conditions, as well as on the capacity to constrain this model with contemporaneous high-quality observations. This information on models' quality and performance is almost more crucial for the end-users than the model solutions themselves. Thus, the reliability of model solutions must be assessed, and the MPQ must be quantified at the analysis, forecast, and reanalysis stages; it has also to be properly documented for end-users.

The purpose of this section is to give a general overview of the commonly used methodology and processes applied by existing operational ocean services to validate and verify their ocean model products. In particular, standard validation metrics and protocols were designed for oceanography model analyses and forecasts, and agreed among the community of OceanPredict forecasters (Hernandez et al, 2015, 2018). This section is focused on describing these validation methodologies and standards for model products. Specific details on the thematic (process oriented) validation for each kind of model use in the OO community (i.e., waves, storm surge, ocean circulation, biogeochemical, etc.), along with examples, illustrations and use cases, can be found in Chapters 5 to 9.

4.5.1. Basis statistical tools for time series validation

Several metrics can be computed for a quantitative analysis of the model-data time series validation: bias, maximum error *MaxErr*, *RMSE*, Pearson correlation coefficient (*R*) or Scatter Index (*SI*) are some of the most common examples and are obtained as:

$$bias = \sum_{i=1}^{N}(O_i - P_i) \tag{4.1}$$

$$MaxErr = O_i - P_i \tag{4.2}$$

$$bias = \sum_{i=1}^{N}(O_i - P_i) \tag{4.1}$$

$$RMSE = \sqrt{\frac{\sum_{i=1}^{N}(P_i - O_i)^2}{N}} \tag{4.3}$$

$$R = \frac{\sum_{i=1}^{N}(P_i - \bar{P})(O_i - \bar{O})}{\sqrt{\sum_{i=1}^{N}(P_i - \bar{P})^2}\sqrt{\sum_{i=1}^{N}(O_i - \bar{O})^2}} \tag{4.4}$$

$$SI = \sqrt{\frac{\sum_{i=1}^{N}[(P_i - \bar{P}) - (O_i - \bar{O})]^2}{\sum_{i=1}^{N}O_i^2}} \tag{4.5}$$

where P_i and O_i refer to the forecasted and observed signals respectively, N is the number of time records, and ($\bar{}$) is the mean operator. Other type of skill scores can be used, such as the Coefficient of Efficiency (COE) (Legates and McCabe, 1999, 2013) obtained as:

$$COE = 1 - \frac{\sum_{i=1}^{N} |\, O_i - P_i \,|}{\sum_{i=1}^{N} |\, O_i - \bar{O} \,|} \qquad (4.6)$$

A perfect model has a COE = 1.0, COE = 0.0: this implies that the model is no more able to predict the measured values than the measured mean; a negative COE value would indicate that the computed signal performs worse than the measured mean.

4.5.2. Ocean forecasting standard metrics for validation and intercomparison

There are different types of model products (i.e. forecast, analysis, reanalysis) and different types of model evaluation methodologies, which are mostly based on the comparison with reference values, aiming at building performance and skill scores. Among others, some of the most applied methods to assess OO models are:

1. Analysis (or forecast at various forecast lengths) versus contemporaneous observations (in situ, but also satellite) in the observations' space. This type of comparison to observations is also performed by the data assimilation system, so it is usually extensively used in operational oceanography. Since ocean in-situ observations are sparse and unevenly distributed, representativeness issues are frequent. Depending on the observation's coverage, the comparisons are either local (at one given observation location) or the statistics of the differences between model solutions and the observations are computed over rather large areas or long periods of time.

2. Model forecast versus model analysis (or observation only). In this case, the model forecast for a specific day is compared to the analysis of the same day, assuming that the analysis is the best available estimate of the ocean state for that day; this methodology can be applied only in delayed mode, when the analysis is available. The forecast can also be compared with gridded observations (an analysis of observations only, for instance satellite L4 observations).

3. Forecast versus persistence. Model fields at various forecast lengths are compared to their initial condition. The forecast is compared with the persistence of the last analysis available (or observations), in other words it is compared to what would have been the best estimate of the ocean state of that day if no model forecast were available. This comparison is performed expect-

ing that the model forecast is more accurate than persistence and allows to quantify the skill of the forecast.

4. Analysis (or forecast) versus climatology or versus literature estimates for less observed quantities. This approach is commonly used with currents or transports.

5. Observed versus modelled feature structure. In this case, the structure (location or intensity) of an observed feature (such as an ocean front or eddy) is compared to its modelled counterpart. Categorical scores can be defined from this type of model validation, possibly introducing space and/or time lags.

The results of these comparisons between model outputs and reference values can be combined in different ways to derive MPQ monitoring scores or metrics. In the numerical weather prediction community, there is a long tradition in model forecast verification methods with vigorous progresses related to the advent of probabilistic methods into operational numerical weather prediction (Jolliffe and Stephenson, 2003; Nurmi, 2003). On the other hand, the OO forecasting community, conditioned by the limited number of oceanic observations and their uneven distribution (mostly of them, surface ones), has shown that quality assessment
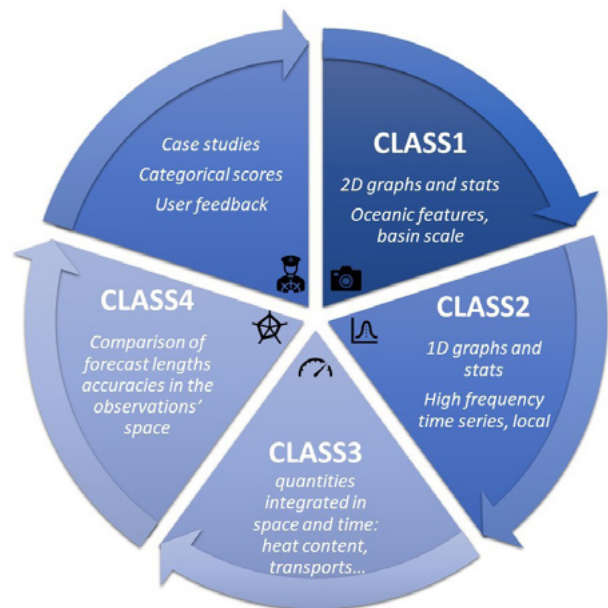
Figure 4.28. Classes of metrics currently used in the OceanPredict community to monitor the quality of ocean analyses and forecasts: a complete range of statistics and comparisons in space and time are necessary to assess the consistency, representativeness, accuracy, performance, and robustness of ocean model outputs.

must include four types of metrics to properly assess the consistency, representativeness, accuracy, performance, and robustness of ocean model outputs (Crosnier and Le Provost, 2007; Hernandez et al., 2009). These four classes of metrics (Figure 4.28) were adopted by GODAE OceanPredict and they have been extensively used in different OO initiatives. For instance, these four classes (with specific computation methods and definition of reference geographical areas) have allowed regular intercomparison exercises between global and regional ocean forecasts (see Ryan et al. (2015) for a global ocean forecasts intercomparison). A last type of metrics, defined from user feedback and called "user oriented" (such as categorical scores point 5), is also instrumental for the quantification of uncertainties dedicated to specific applications (Maksymczuk et al., 2016). Categorical scores using space and time lags or specific case studies, can also help considering the double penalty effect that can lower statistical performance while comparing high resolution model outputs with observations, as pointed out by Crocker, et al. (2020).

4.5.3. Qualification, validation and verification processes in support of operational ocean models' production

Qualification, validation and verification are terms commonly used in the quality control of OO model products. Usually, qualification refers to model quality assessment at the development stage, during which model parameters are optimised. In OO services, such as the Copernicus Marine Service, the qualification phase refers to a comprehensive scientific assessment of any new/updated operational ocean model application, which is performed before the entry into service of the proposed system (Sotillo et al., 2021). This qualification phase is often used to quantify the added value of the updated model system with respect to its previous existing version, comparing the performances of both system versions (V_{n+1} versus V_n) against a well-defined list of metrics, and using the same referential observational data. On the other hand, validation refers to the operational ocean analyses and forecast performance assessment, while in operation. Finally, verification is defined by Hernandez et al. (2015) as the a posteriori quantification of operational ocean forecast skill, preferentially based on independent data, which means observational products not used to constrain the model products; for instance, by means of any kind of data assimilation.

Achieving the best possible MPQ is a major objective for OO centres, and a MPQ itself is a key performance indicator for any OO service. Several model quality assessment stages can be defined along the life of an OO model product. Figure 4.29 illustrates the typical MPQ assurance loop adopted by OO services to ensure and quantify the quality of their model products. This approach is becoming popular across OO services to deal with MPQ at each major stage of development of an operational oceanography model (i.e. development, transition into operations, operational routine, and "after sales service" including delayed mode validation and expertise), using dedicated model assessment processes, and it counts with a long tradition in the operational meteorological and climate community.
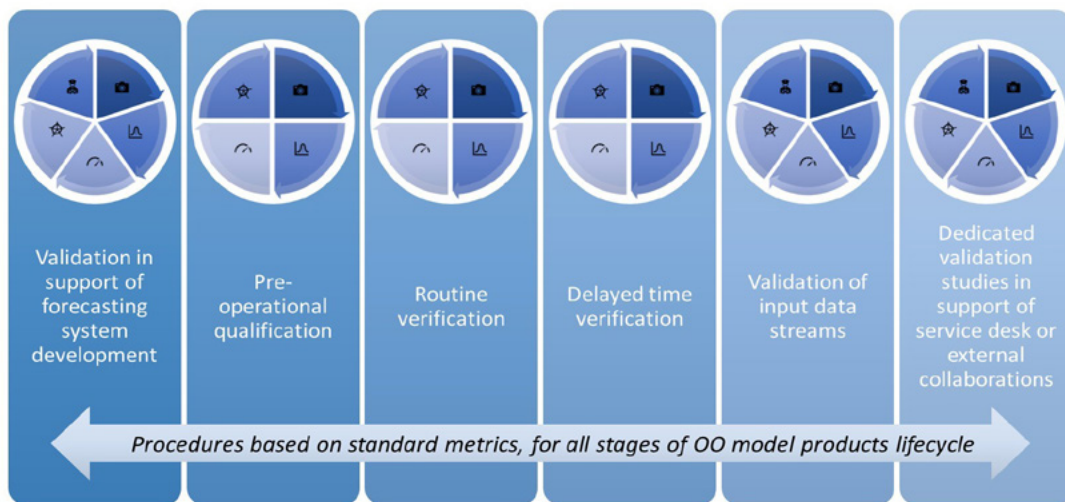
Figure 4.29. Schematic view of different Model Product Quality assessment processes applied along the life of an Operational Oceanography (OO) service product in the development and dissemination stages. All processes rely on the use of the standard metrics (Figure 4.28) to compare the model product with observations as well as with other model solutions.

As shown in Figure 4.29, six main steps or phases can be distinguished within the MPQ assurance process. The first one, focused on research and development activities, supports the implementation/update of new/existing model products to be operationally delivered. At this research and development phase, relevant scientific quality information is developed - and that can also later published in peer reviewed publications - mostly ensuring that the ocean model application is state-of-the-art and based as much as possible on cutting-edge science. Both model versus observations (model-obs) comparisons and intercomparisons with other available model solutions (model-model intercomparisons) can be performed in support of this forecasting system development phase, and they are the basis for the evaluation of model sensitivity tests and scenarios. User oriented metrics, such as categorical scores or Lagrangian drift evaluations, (Drévillon et al, 2013) can be used in specific case studies to quantify the impact of changes in the model system, either during the system development phase or to prepare specific OSEs and OSSEs.

When the new model set-up application is scientifically tested and before the model system is scheduled for entry into service, there is a pre-operational qualification stage, along which the expected (reference) products' quality is established. In the qualification phase, it is critical that the model solution tested is generated in a pre-operational environment that ensures analogous conditions (i.e. same model applications, same type of forcing data, and analogous observational data sources to be assimilated) to the ones that are later applied in operations. It is also important to compare the quality of the product with its previous versions to ensure that there is no regression in terms of MPQ. The stability in time of the performance of the model is also assessed, using a data record of at least one year. Finally, as an outcome from this phase, the OO services can issue the "static" reference documentation on the quality of the product using the different assessment metrics computed. The document can be later delivered to end-users together with the product itself; for instance, see the QUID delivered together with any Copernicus Marine Service ocean product.

Once the model system is in operation, the OO centres perform the scientific validation and verification of the model products delivered on a routine online near-real-time basis, together with the control of the operational production. This on-line validation usually includes forecast model assessments with the available observational data sources (specially from NRT operational products) or with other model solutions (more recent available analysis or, in the case of regional models, comparisons with the parent solution in which are nested). This first on-line validation process is later completed with an extra assessment done in delayed mode. This delayed-mode validation, performed typically monthly, allows to generate more complete and robust validation metrics, extending the obs-model comparisons using observational information from extra data sources or more quality-controlled ones and more complete series of analyses and forecast cycles.

Finally, user feedback focused on specific processes, areas or events, as well as extra model product assessments performed by the producers themselves or by producers in collaborative frameworks (such as scientific research projects or other initiatives with targeted end-users) can significantly enhance the knowledge of the model products.

OO services are continuously progressing towards the regular delivery of up-to-date quality information, although there are remaining gaps in operational capacities to assess model solutions, mostly linked to shortcoming in the availability of ocean observations, and specially in NRT. Observational data used for model skill assessment and validation are mainly originating from drifting profilers, fixed mooring platforms, tide gauges, and remote sensing data. In their review on the operational modelling capacity in the European Seas, Capet et al. (2020), point out that only 20% of operational model services provide a dynamic uncertainty together with the forecast products. This uncertainty would be required for a real-time provision of confidence levels associated with the forecasts as, for instance, is usual in weather forecasts. This lack of uncertainty information, associated with a lack of observations, affects also the data assimilation capacity (Capet et al. (2020) noted that data assimilation is only implemented for 23% of the surveyed models, remaining exceptional in biogeochemical systems). The development of ensemble forecasting and that of probabilistic uncertainty information may help to fill this gap in the future. Peng et al. (2021) stressed the need for findability, accessibility, interoperability and reusability (FAIR data principles) of the information in earth science datasets. This confirms that pertinent product quality information has to be developed further as part of OO services.

4.6.
Output preparation

4.6.1. Introduction

The OOFSs aim at delivering, by means of numerical ocean models, essential information on the ocean state to a wide community of stakeholders and users.

To meet users' requirements, the variables to be supplied must be carefully selected among the large amount of data produced by the OOFSs. In addition, spatial and temporal resolution at which these variables are obtained must also be well defined. Furthermore to these specifications, the efficient storage and delivery of the information supplied by the OOFS is of paramount importance to allow later manipulation. For this purpose, the outputs obtained from the modelling systems should be saved in standard formats that enable their easy use, treatment, and exchange.

The purpose of this section is to provide information and recommendations on the characteristics of the outputs to be delivered in the frame of OOFSs, to maximise their utility and ensure that they meet the requirements demanded by the users.

4.6.2. Products and datasets

The data related to forecast systems are provided through products and datasets.

A "product" is a usable set of data (or one or more datasets) with its descriptive information (metadata). A product is the association of one or several datasets with some static and/or dynamic metadata.

A "dataset" is the aggregation of analysis and forecast with the same geospatial structure or feature type: profiles, point series, trajectories, points, grids, grid series, etc. A dataset is composed of one or several data files. The aggregation is done so that the content of the dataset is predictable for the user (list of variables, predefined geographical bounding box) and expandable when the product is updated (time axis). A dataset can be accessed through an "Access service". A dataset is gridded when the data are stored in raster data files (e.g. in NetCDF format), and each file of the dataset contains some variables on the same geographical coverage. The difference between two files composing a gridded dataset shall be the time coverage of the variable(s).

4.6.3. Variables

The EOVs identified by the GOOS Expert Panels as fundamental measurements needed to address the current scientific and societal ocean-related issues, can play an overriding role as guidelines to incorporate the most relevant ocean information in the final OOFS output products and their inclusion is thus strongly encouraged.

These variables provide an optimal global representation of the state of the ocean (Lindstrom et al., 2012) and the affordable and technically feasible to generate information they give is particularly relevant for main ocean themes such as ocean health or climate.

Among these EOVs, the most important ones regarding ocean physics are mainly surface and subsurface temperature, salinity, currents, sea surface height, sea ice, and surface stress. In biogeochemistry, some of the most relevant are nutrients, oxygen, dissolved organic carbon, and particulate matter, whereas phytoplankton, zooplankton, and algal cover stand for major variables for biology and ecosystems.

4.6.4. Spatial resolution

Ocean modelling systems deliver outputs over discretized grids at specific horizontal and vertical resolutions. Usually, the most used horizontal grids are structured Arakawa B or C, which avoid the existence of a singularity point in the computational domain by locating north mesh poles on land instead. This particularity entails that those models generate data in non-regular meshes that can be more complex to handle. Other models can also produce unstructured data gridded in irregular patterns composed by simple shapes such as triangles or tetrahedra that allow the mesh to adjust to more complex geographical areas. Likewise, spatial resolution can be increased in specific regions presenting features or events of particular interest (e.g. coastal areas) by way of nesting techniques that allow the dynamic exchange of information between model parent and child domains.

Three dimensional grids of ocean circulation models are vertically discretized following different vertical coordinate systems. These coordinate systems are based on different ways of discretizing, such as the cartesian depth-following z-coordinate, the isopycnal ρ-coordinate, the terrain-following σ-coordinate, or the pressure p-coordinate. Their choice

is especially important since each of them has advantages and disadvantages in accurately representing the different ocean layers features.

To slightly simplify the managing of outputs for the model users, some later horizontal interpolation can be performed to generate final outputs in easier regular user-defined coordinate systems, although this must be achieved always ensuring that the information loss is minimised and the highest possible product quality is reached.

4.6.5. Time resolution

Final model outputs are typically distributed as time-averaged means or instantaneous values encompassing a wide range of time frequencies. The selected frequencies may depend on the variability of each variable and on the scope of the study for which the outputs would be employed, but hourly, daily, or monthly means are the most demanded outputs. Anyway, this feature is configurable in the models and hence can be modified as needed; for consistency, increases in spatial resolution usually should go hand in hand with rises of temporal resolution and therefore also higher-frequency outputs. In any case, later procedures can be applied to organize the final outputs as wished, splitting, or gathering the produced variables in different datasets, or computing averages for specific time periods.

4.6.6. Data format

Outputs formats constitute an essential aspect of the OOFS production. Formats highly depend on the models employed to generate outputs. In that sense, the utilisation of standard formats is especially significant to ease the data reading or processing with specific software or to improve the exchange between different systems, since they structure data in setups easily interpretable according to well-defined rules.

Among these formats, the most recommended is certainly the Network Common Data Form (NetCDF), a set of free software libraries and data interfaces widely applied in meteorology, oceanography, and earth sciences, and specifically designed for creating, accessing, and sharing array-oriented scientific data (🔗 71).

NetCDF format features are:

- Self-Describing: netCDF files show information (metadata) on the contained data;
- Appendable: Data may be added to an already existing netCDF file without altering its structure;

- Scalable: Datasets from netCDF files can be easily subset through interfaces;
- Portable: netCDF files can be effectively retrieved from computing machines with different architectures;
- Shareable: netCDF files allow simultaneous access;
- Archivable: The access to earlier forms of netCDF data is possible with newer versions.

NetCDF also includes data access libraries for, among other programming languages, Fortran, Java, C, C++, as well as utility programs to open and manipulate the data files.

Metadata contained in the netCDF files are a key component since they supply major information on the data characteristics. To promote the sharing of such files, there are conventions specifically designed for defining common climate and forecast metadata, such as the COARDS CF conventions. These conventions allow the NetCDF files to accurately describe each variable data, as well as define their spatial and temporal properties. Thus, they simplify the process of comparing quantities between different sources and enhance the design of specific applications.

In particular, the CF metadata convention is an extension of the COARDS conventions especially intended for model-generated data. According to this convention, specific attributes provide a general explanation of the netCDF file contents, whereas others deliver associated descriptions of each variable included in the file. Furthermore, when following the CF convention, a special treatment is given to the essential model outputs coordinates (latitude, longitude, vertical and time). More information on CF conventions can be found at 🔗 72.

4.6.7. Display and analysis tools

Numerous tools are available for displaying, analysing, and handling ocean modelling output data, particularly when data are structured according to common formats such as NetCDF. Its libraries include helpful command lines such as "ncdump" that allows to quickly view a text representation of data and metadata information included in the file. Another command, "ncgen", is used to generate a netCDF file or the C/Fortran programs needed to create it from a description of the netCDF file previously obtained in a small language known as Compiler Description Language (CDL).

Aside from the previously mentioned netCDF libraries commands, many well-known packages and programming languages can open, manipulate (e.g. for modifying information, calculating arithmetic operations, computing statistics, etc.), or visualize netCDF files.

71. https://www.unidata.ucar.edu/software/netcdf/

72. https://www.unidata.ucar.edu/software/netcdf/

Among them, the most popular are:

- Ferret (https://www.unidata.ucar.edu/software/netcdf/),
- NCO (http://nco.sourceforge.net),
- CDO (https://code.mpimet.mpg.de/projects/cdo),
- Python (https://www.python.org/),
- Matlab (https://www.mathworks.com/),
- GrADS (http://cola.gmu.edu/grads),
- IDL (ttps://www.harrisgeospatial.com/Software-Technology/IDL),
- IDV (https://www.unidata.ucar.edu/software/idv),
- Panoply (https://www.giss.nasa.gov/tools/panoply),
- NCL (http://www.ncl.ucar.edu),
- ncview (ttp://cirrus.ucsd.edu/ncview),
- ncBrowse (https://www.pmel.noaa.gov/epic/java/ncBrowse).

4.6.8. Output dissemination

The OOFSs require an accessible and reliable service to effectively distribute the data generated. This service must implement interfaces interoperable with the oceanography community (NetCDF outputs following CF convention, quality control procedures, etc.), and use common tools and protocols (e.g. Thredds-OpenDAP) for accessing the data.

The service mentioned should be based on systems that have been effectively serving users for years, ensuring that the outputs are provided considering the user requirements. In addition, all service components should be properly managed and maintained.

The model outputs should be archived in easy-to-access services from where users may obtain them, either requesting them through dedicated interfaces (pull service) or, for subscribed users, receiving the files via any well-known protocol such as ftp, ssh, etc. These services should also allow the users to subset the requested data from the original outputs.

4.7.
User management and outreach

A marine service is the provision of marine information to assist decision making. The service must respond to user needs, must be based on scientifically credible information and expertise, and requires appropriate engagement between users and providers. It should be an integrated service gathering all ocean products into a single catalogue sustained on the long term.

The first mandatory step is to define the service to be provided and answer the following questions:

- What is the target audience of the service? It can include one or all the following users: national/local public environmental agencies, scientists and academia, citizens, private companies, etc.

- Which data policy is applied to the service? It can be an open service (open to all users with or without registration) or a restricted access service. It can also be a free of charge or a paid service.

- Which operational commitments and service level agreement are available to users? To engage through a

transparent and trust relationship with users, service commitments should be made publicly available.

Depending on the answers to the 3 above questions, the service will develop a patchwork of the following assets:

- Communication assets (both on and offline), ocean literacy tools, and societal awareness can for example include the activities below. These are designed to deliver the operational oceanography service expertise to a wider audience through the translation from scientific language and findings for different target audiences, and to distribute the tools to drive uptake.

  - Digital website, digital tools, social media (Twitter, Linkedin, Youtube, etc.);
  - Editorial (News, Events web section, etc.) and press relations (Newsletters, etc.);
  - Ocean Literacy and Outreach activities (outreach events, partner initiatives, museum exhibitions, etc.).

- An ocean data portal including the catalogue of ocean products should be made available online to download and visualise marine data.

• A searchable online catalogue of products should be made available including product metadata description and search parameters such as: free text, geographical areas, marine parameters, models or observations (satellite or in situ), resolution (spatial and temporal), coverage (spatial and temporal), update frequency, etc. It should also allow the user to download the selected data product (with or without registration, and with or without charges, depending on the definition of the service). The online catalogue should be compliant with the highest standards of usability and interoperability.

• Another major asset includes viewing tools to visually explore the different ocean products. Such tools can include the ability to create 2D maps, cross sections, select regions, and generate graphs with selected variables. Layering and superimposing layers with different opacities can be made possible allowing users to compare multiple datasets. In addition, the selected maps and time frames can be exported as videos, images or embedded elsewhere.

• Such ocean data portal encompasses product management activities to carefully and closely manage the product portfolio and each product life cycle. Product management allows to carefully track all product changes impacting users along with product metadata updates and homogenisation, which in turn need to be carefully communicated to the users.

• The user support desk is the point of contact for all questions and comments from users and its objective is to optimise user experience throughout the service. Various means can be used to initiate or conduct exchanges with users (e.g. chat box, e-mail address, online forms, phone, video-conferencing, etc.). The user support desk is also responsible for informing users of operational issues on products and services, such as incidents, maintenance, and improvements. In addition, it also provides an internal link between users and scientific and technical experts. Finally, it is also very involved in the training activity described below and participates in all such events. A client-oriented approach for specific users can be developed if needed for specific major accounts.

• User learning services or training activities allow to strengthen user uptake: its objective is to train, answer questions, facilitate user experience, share knowledge, and collect requirements. Training workshops are designed to train existing, new or beginner users. The target audience needs to be clearly defined and the training resources need to be developed accordingly. For example, participants can learn about products and services and their possible applications across a wide range of subjects during plenary and practical training sessions. Participants should be enabled to share their experiences as well as express their needs and requirements for future new products to be included in the portfolio. Finally, tutorial videos and jupyter notebooks (i.e. open-source web application that allows experts to create practical exercises and share codes) can be shared with participants to help them for their own code programming and understanding of how to use products.

• A service monitoring activity: the service should be monitored through key performance indicators (KPIs), reported quarterly and annually. Such KPIs assess the service reliability against operational commitments and service level agreement (timeliness, robustness, etc.). The service monitoring activity encompasses many KPIs to steer the service and its uptake, and for example provides figures about the product portfolio evolution, variation in the number of subscribers and their detailed characteristics, as well as monitoring of the service availability and product timeliness.

• User feedback and user satisfaction should be measured, monitored, analysed, and injected back into the service through the implementation of new or updated products and services to better fit user's demand.

• User engagement and market expansion activities can be developed to foster uptake of marine products, develop market intelligence, and seek novel opportunities for data use in new communities. Such activities include targeting developing blue markets, explaining the marine offer to new audiences, showcasing the use of data through use cases, launching marketing campaigns, organising or participating in events advocating the marine services and liaising with new partners and communities.

4.8.
References

Barnier, B., Siefridt, L., and Marchesiello, P. (1995). Thermal forcing for a global ocean circulation model using a three-year climatology of ECMWF analyses. Journal of Marine Systems, 6(4), 363-380, https://doi.org/10.1016/0924-7963(94)00034-9

Barnier, B. (1998). Forcing the ocean. In "Ocean Modeling and Parameterization", Editors: E. P. Chassignet and J. Verron, Eds., Kluwer Academic, 45-80.

Bell, M.J., Lefèbvre, M., Le Traon, P.-Y., Smith, N., Wilmer-Becker, K. (2009). GODAE the global ocean data assimilation experiment. *Oceanography, 22, 14-21*, https://doi.org/10.5670/oceanog.2009.62

Bellingham, J. (2009). Platforms: Autonomous Underwater Vehicles. In "Encyclopedia of Ocean Sciences", Editors-in-Chief: J. K. Cochran, H. Bokuniewicz, P. Yager, ISBN: 9780128130827, doi:10.1016/B978-012374473-9.00730-X

Bourlès, B., Lumpkin, R., McPhaden, M.J., Hernandez, F., Nobre, P., Campos, E., Yu, L. Planton, S., Busalacchi, A., Moura, A.D., Servain, J., and Trotte, Y. (2008). The PIRATA program: History, accomplishments, and future directions. *Bulletin of the American Meteorological Society*, 89, 1111-1125, https://doi.org/10.1175/2008BAMS2462.1

Boyer, T.P., Baranova, O.K., Coleman, C., Garcia, H.E., Grodsky, A., Locarnini, R.A., Mishonov, A.V., Paver, C.R., Reagan, J.R., Seidov, D., Smolyar, I.V., Weathers, K.W., Zweng, M.M. (2019). World Ocean Database 2018. A. V. Mishonov, Technical Editor, NOAA Atlas NESDIS 87.

Bouttier, F., and Courtier, P. (2002). Data assimilation concepts and methods. Meteorological training course lecture series, ECMWF, 59. Available at https://www.ecmwf.int/en/elibrary/16928-data-assimilation-concepts-and-methods

Capet, A., Fernández, V., She, J., Dabrowski, T., Umgiesser, G., Staneva, J., Mészáros, L., Campuzano, F., Ursella, L., Nolan, G., El Serafy, G. (2020), Operational Modeling Capacity in European Seas - An Euro-GOOS Perspective and Recommendations for Improvement. *Frontiers in Marine Science*, 7:129, https://doi.org/10.3389/fmars.2020.00129

Carrassi, A., Bocquet, M., Bertino, L., Evensen, G. (2018). Data assimilation in the geosciences: An overview of methods, issues, and perspectives. *Wiley Interdisciplinary Reviews: Climate Change*, 9(5), e535, https://doi.org/10.1002/wcc.535

Chang, Y.-S., Rosati, A. J., Zhang, S., and Harrison, M. J. (2009). Objective Analysis of Monthly Temperature and Salinity for the World Ocean in the 21st century: Comparison with World Ocean Atlas and Application to Assimilation Validation. *Journal of Geophysical Research: Oceans*, 114(C2), https://doi.org/10.1029/2008JC004970

Crocker, R., Maksymczuk, J., Mittermaier, M., Tonani, M., and Pequignet, C. (2020). An approach to the verification of high-resolution ocean models using spatial methods. *Ocean Science*, 16, 831-845, https://doi.org/10.5194/os-16-831-2020

Crosnier, L., and Le Provost, C. (2007). Inter-comparing five forecast operational systems in the North Atlantic and Mediterranean basins: The MERSEA-strand1 Methodology. *Journal of Marine Systems*, 65(1-4), 354-375, https://doi.org/10.1016/j.jmarsys.2005.01.003

Cummings, J., Bertino, L., Brasseur, P., Fukumori, I., Kamachi, M., Martin, M.J., Mogensen, K., Oke, P., Testut, C.-E., Verron, J., Weaver, A. (2009). Ocean data assimilation systems for GODAE. *Oceanography*, 22, 96-109, https://doi.org/10.5670/oceanog.2009.69

Dai, A., and Trenberth, K. E. (2002). Estimates of freshwater discharge from continents: Latitudinal and seasonal variations. *Journal of Hydrometeorology*, 3(6), 660-687, https://doi.org/10.1175/1525-7541(2002) 003<0660:EOFDFC>2.0.CO;2

Dai, A., Qian, T., Trenberth, K. E., Milliman, J. D. (2009). Changes in continental freshwater discharge from 1948-2004. *Journal of Climate*, 22(10), 2773-2791, https://doi.org/10.1175/2008JCLI2592.1

Dai, A. (2021). Hydroclimatic trends during 1950–2018 over global land. *Climate Dynamics*, 4027-4049, https://doi.org/10.1007/s00382-021-05684-1

De Mey, P. (1997). Data assimilation at the oceanic mesoscale: A review. Journal of Meteorological of Japan, 75(1b), 415-427, https://doi.org/10.2151/jmsj1965.75.1B_415

Carrassi, A., Bocquet, M., Bertino, L., Evensen, G. (2018). Data assimilation in the geosciences: An overview of methods, issues, and perspectives. Wiley Interdisciplinary Reviews: Climate Change, 9(5), e535, https://doi.org/10.1002/wcc.535

Donlon, C, Minnett, P., Gentemann, C., Nightingale, T.J., Barton, I., Ward, B., Murray, M. (2002). Toward improved validation of satellite sea surface skin temperature measurements for climate research. Journal of Climate, 15:353-369, https://doi.org/10.1175/1520-0442(2002)015<0353:TIVOSS>2.0.CO;2

Donlon, C., Casey, K., Robinson, I., Gentemann, C., Reynolds, R, Barton, I., Arino, O., Stark, J., Rayner, N., Le Borgne, P., Poulter, D., Vazquez-Cuervo, J., Armstrong, E., Beggs, H., Llewellyn-Jones, D., Minnett, P., Merchant, C., Evans, R. (2009). The GODAE High-Resolution Sea Surface Temperature Pilot Project. *Oceanography*, 22, 34-45, https://doi.org/10.5670/oceanog.2009.64

Drévillon, M., Greiner, E., Paradis, D., et al. (2013). A strategy for producing refined currents in the Equatorial Atlantic in the context of the search of the AF447 wreckage. *Ocean Dynamics*, 63, 63-82, https://doi.org/10.1007/s10236-012-0580-2

Eastwood, S., Le Borgne, P., Péré, S., Poulter, D. (2011). Diurnal variability in sea surface temperature in the Arctic. *Remote Sensing of Environment*, 115(10), 2594-2602, https://doi.org/10.1016/j.rse.2011.05.015

GHRSST Science Team (2012). The Recommended GHRSST Data Specification (GDS) 2.0, document revision 5, available from the GHRSST International Project Office, available at https://www.ghrsst.org/governance-documents/ghrsst-data-processing-specification-2-0-revision-5/

Griffies, S. M. (2006). Some ocean model fundamentals. In "Ocean Weather Forecasting", Editoris: E. P. Chassignet and J. Verron, 19-73, Springer-Verlag, Dordrecht, The Netherlands, doi:10.1007/1-4020-4028-8_2

Groom, S., Sathyendranath, S., Ban, Y,. Bernard, S., Brewin, R., Brotas, V., Brockmann, C., Chauhan, P., Choi, J-K., Chuprin, A., Ciavatta, S., Cipollini, P. Donlon, C., Franz, B., He, X., Hirata, T., Jackson, T., Kampel, M., Krasemann, H., Lavender, S., Pardo-Martinez, S., Mélin, F., Platt, T., Santoleri, R., Skakala, J., Schaeffer, B., Smith, M., Steinmetz, F., Valente, A., Wang, M. (2019). Satellite Ocean Colour: Current Status and Future Perspective. *Frontiers in Marine Science*, 6:485, https://doi.org/10.3389/fmars.2019.00485

Hamlington, B.D., Thompson, P.,. Hammond, W.C., Blewitt, G., Ray, R.D. (2016). Assessing the impact of vertical land motion on twentieth century global mean sea level estimates. Journal of Geophysical Research, 121(7), 4980-4993, https://doi.org/10.1002/2016JC011747

Hernandez, F., Bertino, L., Brassington, G.B., Chassignet, E., Cummings, J., Davidson, F., Drevillon, M., Garric, G., Kamachi, M., Lellouche, J.-M., et al. (2009). Validation and intercomparison studies within GODAE. *Oceanography*, 22(3), 128-143, https://doi.org/10.5670/oceanog.2009.71

Hernandez, F., Blockley, E., Brassington, G B., Davidson, F., Divakaran, P., Drévillon, M., Ishizaki, S., Garcia-Sotillo, M., Hogan, P. J., Lagemaa, P., Levier, B., Martin, M., Mehra, A., Mooers, C., Ferry, N., Ryan, A., Regnier, C., Sellar, A., Smith, G. C., Sofianos, S., Spindler, T., Volpe, G., Wilkin, J., Zaron, E D., Zhang, A. (2015). Recent progress in performance evaluations and near real-time assessment of operational ocean products. *Journal of Operational Oceanography*, 8(sup2), https://doi.org/10.1080/1755876X.2015.1050282

Hernandez, F., Smith, G., Baetens, K., Cossarini, G., Garcia-Hermosa, I., Drevillon, M., ... and von Schuckman, K. (2018). Measuring performances, skill and accuracy in operational oceanography: New challenges and approaches. In "New Frontiers in Operational Oceanography", Editors: E. Chassignet, A. Pascual, J. Tintoré, and J. Verron, GODAE OceanView, 759-796, doi:10.17125/gov2018.ch29

Hollingsworth, A., Shaw, D. B., Lönnberg, P., Illari, L., Arpe, K., and Simmons, A. J. (1986). Monitoring of Observation and Analysis Quality by a Data Assimilation System. *Monthly Weather Review*, 114(5), 861-879, https://doi.org/10.1175/1520-0493(1986)114<0861:MOOAAQ>2.0.CO;2

International Altimetry Team (2021). Altimetry for the future: building on 25 years of progress. Advances in Space Research, 68(2), 319-363, https://doi.org/10.1016/j.asr.2021.01.022

Kurihara, Y., Murakami, H., and Kachi, M. (2016). Sea surface temperature from the new Japanese geostationary meteorological Himawari-8 satellite. *Geophysical Research Letters*, 43(3), 1234-1240, https://doi.org/10.1002/2015GL067159

Josey, S.A., Kent, E.C., Taylor, P.K. (1999). New insights into the ocean heat budget closure problem from analysis of the SOC air-sea flux climatology. *Journal of Climate*, 12(9), 2856-2880, https://doi.org/10.1175/1520-0442(1999)012<2856:NIITOH>2.0.CO;2

Jolliffe, I.T., and Stephenson, D.B. (2003). Forecast Verification: A Practitioner's Guide in Atmospheric Sciences, John Wiley & Sons Ltd., Hoboken, 296 pages, ISBN: 978-0-470-66071-3

Legates, D.R., McCabe, G.J. Jr. (1999). Evaluating the use of "Goodness of Fit" measures in hydrologic and hydroclimatic model validation. *Water Resources Research*, 35, 233-241, https://doi.org/10.1029/1998WR900018

Legates, D., and Mccabe, G. (2013). A refined index of model performance: A rejoinder. *International Journal of Climatology*, 33(4), 1053-1056, https://doi.org/10.1002/joc.3487

Le Traon, P.Y., Larnicol, G., Guinehut, S., Pouliquen, S., Bentamy, A., Roemmich, D., Donlon, C., Roquet, H., Jacobs, G., Griffin, D., Bonjean, F., Hoepffner, N., Breivik, L.A. (2009). Data assembly and processing for operational oceanography 10 years of achievements. Oceanography, 22(3), 56-69, https://doi.org/10.5670/oceanog.2009.66

Levitus, S. (1982). Climatological Atlas of the World Ocean. NOAA/ERL GFDL Professional Paper 13, Princeton, N.J., 173 pp. (NTIS PB83-184093).

Lindstrom, E., Gunn, J., Fischer, A., McCurdy, A. and Glover L.K. (2012). A Framework for Ocean Observing. IOC Information Document;1284, Rev. 2, doi:10.5270/OceanObs09-FOO

Maksymczuk J., Hernandez, F., Sellar, A., Baetens, K., Drevillon, M., Mahdon, R., Levier, B., Regnier, C., Ryan, A. (2016). Product Quality Achievements Within MyOcean. *Mercator Ocean Journal #54*. Available at https://www.mercator-ocean.eu/en/ocean-science/scientific-publications/mercator-ocean-journal/newsletter-54-focusing-on-the-main-outcomes-of-the-myocean2-and-follon-on-projects/

Mantovani C., Corgnati, L., Horstmann, J. Rubio, A., Reyes, E., Quentin, C., Cosoli, S., Asensio, J. L., Mader, J., Griffa, A. (2020). Best Practices on High Frequency Radar Deployment and Operation for Ocean Current Measurement. Frontiers in Marine Science, 7:210, https://doi.org/10.3389/fmars.2020.00210

Marks, K., and Smith, W. (2006). An Evaluation of Publicly Available Global Bathymetry Grids. Marine Geophysical Researches, 27, 19-34, https://doi.org/10.1007/s11001-005-2095-4

Martin, M.J. (2016). Suitability of satellite sea surface salinity data for use in assessing and correcting ocean forecasts. *Remote Sensing of Environment*, 180, 305-319. https://doi.org/10.1016/j.rse.2016.02.004

Martin, M.J, King, R.R., While, J., Aguiar, A.B. (2019). Assimilating satellite sea-surface salinity data for SMOS Aquarius and SMAP into a global ocean forecasting system. *Quarterly Journal of the Royal Meteorological Society*, 145(719), 705-726, https://doi.org/10.1002/qj.3461

McPhaden, M. J., Busalacchi, A.J., Cheney, R., Donguy, J.R., Gage, K.S., Halpern, D., Ji, M., Julian, P., Meyers, G., Mitchum, G.T., Niller, P.P., Picaut, J., Reynolds, R.W., Smith, N., Takeuchi, K. (1998). The Tropical Ocean-Global Atmosphere (TOGA) observing system: A decade of progress. *Journal of Geophysical Research*, 103, 14169-14240, https://doi.org/10.1029/97JC02906

McPhaden, M. J., Meyers, G., Ando, K., Masumoto, Y., Murty, V. S., Ravichandran, M., Syamsudin, F., Vialard, J., Yu, L., and Yu, W. (2009). RAMA: The Research Moored Array for African-Asia-Australian Monsoon Analysis and Prediction. *Bulletin of the American Meteorological Society*, 90, 459-480, https://doi.org/10.1175/2008BAMS2608.1

Moore, A.M., Martin, M.J., Akella, S., Arango, H.G., Balmaseda, M., Bertino, L., Ciavatta, S., Cornuelle, B., Cummings, J., Frolov, S., Lermusiaux, P., Oddo, P., Oke, P.R., Storto, A., Teruzzi, A., Vidard, A., Weaver, A.T. (2019). Synthesis of Ocean Observations Using Data Assimilation for Operational, Real-Time and Reanalysis Systems: A More Complete Picture of the State of the Ocean. Frontiers in Marine Science, 6:90, https://doi.org/10.3389/fmars.2019.00090

Naeije, M., Schrama, E., and Scharroo, R. (2000). The Radar Altimeter Database System project RADS. Published in "IGARSS 2000. IEEE 2000 International Geoscience and Remote Sensing Symposium. Taking the Pulse of the Planet: The Role of Remote Sensing in Managing the Environment", doi:10.1109/IGARSS.2000.861605

Nurmi P. (2003). Recommendations on the verification of local weather forecasts (at ECMWF member states). Consultancy report to ECMWF Operations Department. Available at https://www.cawcr.gov.au/projects/verification/Rec_FIN_Oct.pdf

O'Carroll, A.G., Armstrong, E.M., Beggs, H., Bouali, M., Casey, K.S., Corlett, G.K., Dash, P., Donlon, C.J., Gentemann, C.L., Hoyer, J.L., Ignatov, A., Kabobah, K., Kachi, M. Kurihara, Y., Karagali, I., Maturi, E., Merchant, C.J., Minnett, P., Pennybacker, M., Ramakrishnan, B., Ramsankaran, R., Santoleri, R., Sunder, S., Saux Picart, S., Vazquez-Cuervo, J., Wimmer, W. (2019). Observational needs of sea surface temperature, *Frontiers in Marine Science*, 6:420, https://doi.org/10.3389/fmars.2019.00420 .

Peng, G., Downs, R.R., Lacagnina, C., Ramapriyan, H., Ivánová, I., Moroni, D., Wei, Y., Larnicol, G., Wyborn, L., Goldberg, M., Schulz, J., Bastrakova, I., Ganske, A., Bastin, L., Khalsa, S.J.S., Wu, M., Shie, C.-L., Ritchey, N., Jones, D., Habermann, T., Lief, C., Maggio, I., Albani, M., Stall, S., Zhou, L., Drévillon, M., Champion, S., Hou, C.S., Doblas-Reyes, F., Lehnert, K., Robinson, E. and Bugbee, K., (2021). Call to Action for Global Access to and Harmonization of Quality Information of Individual Earth Science Datasets. *Data Science Journal*, 20(1), 19, http://doi.org/10.5334/dsj-2021-019

Petrenko, B., Ignatov, A., Kihai, Y., Dash, P. (2016). Sensor-Specific Error Statistics for SST in the Advanced Clear-Sky Processor for Oceans. Journal of Atmospheric and Oceanic Technology, 33(2), 345-359, https://doi.org/10.1175/JTECH-D-15-0166.1

Roarty, H., Cook, T., Hazard, L., George, D., Harlan, J., Cosoli, S., Wyatt, L., Alvarez Fanjul, E., Terrill, E., Otero, M., Largier, J., Glenn, S., Ebuchi, N., Whitehouse, Br., Bartlett, K., Mader, J., Rubio, A., Corgnati, L., Mantovani, C., Griffa, A., Reyes, E., Lorente, P., Flores-Vidal, X., Saavedra-Matta, K. J., Rogowski, P., Prukpitikul, S., Lee, S-H., Lai, J-W., Guerin, C-A., Sanchez, J., Hansen, B., Grilli, S. (2019). The Global High Frequency Radar Network. *Frontiers in Marine Science*, 6:164, https://doi.org/10.3389/fmars.2019.00164

Ryan, A. G., Regnier, C., Divakaran, P., Spindler, T., Mehra, A., Smith, G. C., et al. (2015). GODAE OceanView Class 4 forecast verification framework: global ocean inter-comparison. *Journal of Operational Oceanography*, 8(sup1), S112-S126, https://doi.org/10.1080/1755876X.2015.1022330

Scharroo, R. (2012). RADS version 3.1: User Manual and Format Specification. Available at http://rads.tudelft.nl/rads/radsmanual.pdf

Sotillo, M. G., Garcia-Hermosa, I., Drévillon, M., Régnier, C., Szczypta, C., Hernandez, F., Melet, A., Le Traon, P.Y. (2021). Communicating CMEMS Product Quality: evolution & achievements along Copernicus-1 (2015-2021). *Mercator Ocean Journal #57*. Available at https://marine.copernicus.eu/it/node/19306

Tonani, M., Balmaseda, M., Bertino, L., Blockley, E., Brassington, G., Davidson, F., Drillet, Y., Hogan, P., Kuragano, T., Lee, T., Mehra, A., Paranathara, F., Tanajura, C., Wang, H. (2015). Status and future of global and regional ocean prediction systems. *Journal of Operational Oceanography*, 8, s201-s220, https://doi.org/10.1080/1755876X.2015.1049892

Tournadre, J., Bouhier, N., Girard-Ardhuin, F., Remy, F. (2015). Large icebergs characteristics from altimeter waveforms analysis. *Journal of Geophysical Research: Oceans*, 120(3), 1954-1974, https://doi.org/10.1002/2014JC010502

Tozer, B., Sandwell, D.T., Smith, W.H.F., Olson, C., Beale, J. R., and Wessel, P. (2019). Global bathymetry and topography at 15 arc sec: SRTM15+. *Earth and Space Science*, 6, 1847-1864, https://doi.org/10.1029/2019EA000658

Vinogradova, N.T., Ponte, R.M., Fukumori, I., and Wang, O. (2014). Estimating satellite salinity errors for assimilation of Aquarius and SMOS data into climate models. *Journal of Geophysical Research: Oceans*, 119(8), 4732-4744, https://doi.org/10.1002/2014JC009906

Vinogradova N., Lee, T., Boutin, J., Drushka, K., Fournier, S., Sabia, R., Stammer, D., Bayler, E., Reul, N., Gordon, A., Melnichenko, O., Li, L., Hackert, E., Martin, M., Kolodziejczyk, N., Hasson, A., Brown, S., Misra, S., and Linkstrom, E. (2019). Satellite Salinity Observing System: Recent Discoveries and the Way Forward. *Frontiers in Marine Science*, 6:243, https://doi.org/10.3389/fmars.2019.00243

Zhang H., Beggs, H., Wang, X.H., Kiss, A. E., Griffin, C. (2016). Seasonal patterns of SST diurnal variation over the Tropical Warm Pool region. Journal of Geophysical Research: Oceans, 121(11), 8077-8094, https://doi.org/10.1002/2016JC012210

5.
Circulation modelling

CHAPTER COORDINATOR

Stefania Ciliberti

CHAPTER AUTHORS *(in alphabetical order)*

Nadia Ayoub, Jérôme Chanut, Mauro Cirano, Anne Delamarche, Pierre De Mey-Frémaux, Marie Drévillon, Yann Drillet, Helene Hewitt, Simona Masina, Clemente Tanajura, Vassilios Vervatis, and Liying Wan

5. Circulation modelling

5.1. General introduction to circulation models

5.1.1. Objective, applications and beneficiaries

5.1.2. Circulation Physics

5.2. Circulation forecast and multi-year systems

5.2.1. Ocean-Earth system as basis for OOFS

5.2.2. Architecture singularities

5.3. Input data

5.4. Modelling component: general circulation models

5.4.1. Mathematical model

5.4.2. Basic discretization techniques

5.4.2.1. Horizontal grids

5.4.2.2. Vertical discretization

5.4.2.3. Time stepping

5.4.2.4. Numerical techniques

5.4.3. List of Ocean General Circulation Models

5.4.4. Downscaling large-scale solutions to regional/coastal circulation models

5.5. Data assimilation systems

5.5.1. Basic concepts

5.5.2. Sequential methods

5.5.3. Variational methods

5.5.4. Modelling errors

5.5.5. Overview of current data assimilation systems in operational forecasting

5.6. Ensemble modelling

5.6.1. Basic concepts

5.6.2. Ocean model uncertainties

5.6.3. Towards ocean EPS

5.1.
General introduction to circulation models

5.1.1. Objective, applications and beneficiaries

The main objective of any OOFS is to provide users with the best reliable and easy access information available on the state of the ocean in near real-time. The service is meant for any user, and especially downstream service providers who use the information as an input to their own value-added services.

A forecasting system relies on a numerical ocean model and, in many cases, on a data assimilation component able to assimilate the available observations and provide a complete dataset that can be used as initial conditions by the ocean circulation model. The availability of relevant observations is crucial to the success of an OOFS and the development of models and numerical techniques, along with data assimilation schemes that combine all the information taking into account the uncertainties of the observations and models.

The circulation modelling component represents one of the main cores of operational marine monitoring and forecasting systems: it provides an overall description of ocean physical essential variables (i.e. temperature, salinity, currents, sea surface height, etc.) for ocean predictions and for supporting climate studies. Ocean models are able to describe the sea state from global to coastal scales and to predict its variability and evolution in time (from short to mid-term to long-term). This is done by numerically solving a set of partial differential equations, based on an approximated version of the Navier-Stokes equations.

At the beginning of the XX century, Bjerknes (1914) described a practical method that could solve the mathematical dynamic and thermodynamic equations at least for a finite amount of time. He defined two factors that were necessary to make predictions a reality: (1) knowledge of the initial conditions as accurately as possible, and (2) the development of an accurate predictive model. The latter consisted of discretizing the equations and using numerical methods to solve for the time derivative. Based on this approach, the first successful meteorological forecast became operational at the end of the 1960s, while ocean forecasting began in the 1980s; a joint venture between Harvard University and the Naval Postgraduate School in Monterey, both in the United States, completed the first successful forecast of ocean mesoscales in a limited ocean area (see Pinardi et al., 2017, for an overview of the ocean prediction science). Earlier examples of wave forecasting during the second World War responded to the need to know the sea state during landing operations (O'Brien and Johnson, 1947).

During the last decades of the 20th century and the first decades of the 21st century, ocean forecasting has become an operational activity and, thanks to the increase of computing power, today we are able to numerically integrate the governing equations at very high resolution in space and time, to study multi-scale ocean processes, physical properties and their impacts on the climate, and human activities affecting the environment. In modern ocean prediction, stochastic approaches and ensemble estimates complement deterministic solutions, accounting for the different sources of uncertainties (e.g. errors in the initial conditions, in the forcing functions, in the physics of the numerical model, and in the bathymetry) that unavoidably affects the final solution and tends to increase over the forecast period.

To improve the quality of predictions, data assimilation and ensemble techniques are widely used, and their primary scope is to rigorously and systematically combine available observations (in situ and satellite) with numerical ocean models to provide the best estimate of the forecasting cycle. However, in case of very high-resolution nested models and when observation availability is limited, operational systems do not use a data assimilation procedure. When possible, an OOFS system needs to retrieve data observations from a wide variety of observing platforms and systems over the domain of interest for prediction. Satellite based observing systems provide a large source of observational data for an OOFS as well.

An OOFS needs to access information from a numerical weather prediction system in order to provide surface boundary forcing information. The OOFS will also require information on other parameters that influence the ocean such as river outflows, etc. Depending on the domain of interest, the OOFS may also require information about sea ice (see Section 4.2 for the input data and Chapter 6 for understanding sea ice modelling basics). Observations are also used to provide a quantitative understanding of the capacity of the ocean model to make predictions by means of validation and calibration techniques and, consequently, to measure and monitor the accuracy of the forecasting product (see Section 4.5). Routine validation and verification information will tell the OOFS operators when a model is not performing well. The errors identified through validation and verification can be used to set priorities for further development of the OOFS. Despite the enormous improvements reached nowadays by operational forecasting systems ranging from global to coastal scales, much research is still needed to advance in ocean prediction. Developments include access to additional innovative autonomous multi-scale observing technologies observations, both remote and in situ (Le Traon et al., 2019), to new model developments (Fox-Kemper et al., 2019), up to next-generation computational methods and data assimilation schemes supported by the recently expanding applica-

tions of machine learning techniques in this field (De Mey-Frémaux et al., 2019).

The ultimate purpose for operating an OOFS is the production, preparation, and delivery of operational ocean forecasts to users in forms that meet their needs. There is a growing list of users relying on the products and services from operational ocean forecasting systems. Ocean predictions will continue to produce an increasing number of marine applications and services: e.g. for maritime safety, marine resources, coastal and marine environment (Chapter 11). This is because the new systems allow informed management and emergency decisions to be made based on physical knowledge resolved at unprecedented space and time resolution, with known quality and accuracy.

The emergence of operational organisations for delivering real-time forecasts and analyses will encourage the development of value-added products, including forecasts for extreme weather driven events (such as storm surges), pollution, oil spills, acoustic properties (e.g. the speed of sound), sea ice, ecosystem management, safe offshore activities, search and rescue operations, optimal energy extraction, and maritime safety and transport. In addition, ocean forecast products and services can also be providers of information for aquaculture, fishery research, and regional fishery organisations, contributing to the protection and sustainable management of living marine resources. Availability of predictions on the ocean helps to limit damages in the case of floods, storm surges, heat waves and other dangers associated with sea conditions. Furthermore, detailed and accurate forecasts are also useful to assist decision making to plan long-term strategies aiming at managing the risks associated with the impacts of climate change on the sea and coasts, such as sea level rise and marine heat waves.

A predicted ocean where society has the capacity to understand current and future ocean conditions is one of the proposed seven outcomes of the United Nations Decade of Ocean Sciences for Sustainable Development.

Scope of this chapter is to present all elements that make an OOFS and provides a detailed understanding of the main circulation modelling components. For each component, a comprehensive description is provided in dedicated chapter subsections, including the presentation of some state-of-the-art examples of ocean models currently working in operational frameworks. In addition, basic concepts of data assimilation systems and validation strategies will be presented as well, since an essential part of operating a model is to conduct the necessary validation and verification procedures to maintain a continuous quality control of the system outputs.

5.1.2. Circulation Physics

The physical processes, properties and circulation of the ocean are described numerically by the approximated Navier-Stokes equations (details in Section 5.4.1). The equations allow the spatial and temporal distribution of the temperature, salinity, density, pressure, and currents to be described. Numerical ocean models are the building block of operational oceanography and fundamental for near real time to seasonal to decadal forecasts and climate projections. In operational oceanography, they are used alongside data assimilation techniques to accurately represent the state of the ocean at a particular point in time and space, and to produce the initial condition of the forecasting system.

The governing equations for a real fluid are the Navier-Stokes equations, together with conservation of salt and heat and an equation of state; these equations support fast acoustic modes and involve nonlinearities in many terms that make their solution both difficult and expensive. A series of approximations are made to simplify and yield the "primitive equations", which are the basis of most general circulation models. The assumptions that are made in ocean models are described in Section 5.4.

Ocean circulation models aim to represent key processes. These include: 1) transport of heat by the ocean; 2) the effect of evaporation, precipitation and runoff on ocean salinity and density; and 3) the role of ocean currents which, along with wind waves and tides, drive ocean mixing and water mass transformation. Ocean circulation models discretize the governing equations on a horizontal and vertical grid (Section 5.4 expands on this). The details of whether processes can be explicitly resolved in models or they must be parameterised depend on the resolution of the grid used to solve the approximate numerical system.

Figure 3.4 (see Chapter 3) shows the order of magnitude of spatial and temporal scales of specific ocean processes. If the model resolves scales of 100 km, ocean models should be able to resolve Kelvin and Rossby waves; indeed, the representation of Equatorial dynamics has been shown to be important for forecasting the evolution of El Nino on seasonal timescales (Latif et al., 1994). On shorter timescales but with similar spatial scales, surface tides are key processes to represent. Moving to spatial scales of ~10 km to 100 km, the ocean mesoscale can start to be represented; this scale includes boundary currents and mesoscale eddies (Hewitt et al., 2020). At even finer scales, coastal upwelling, internal tides, and internal waves can be represented. Interactions with bathymetry can be important at the scale of the bathymetry. For example, choke points can determine the exchange between the deep ocean and inland seas, such as the Gibraltar Strait. Horizontal resolution choices are discussed further in Section 5.4.

While a primary consideration is the horizontal scales (Figure 3.4), the choice of vertical resolution and coordinate is also an important consideration. These choices are discussed further in Section 5.4, along with the numerical methods that are employed to solve the equations and some of the parameterisation choices to be made.

The ocean has strong links to other aspects of the Earth system, such as sea ice, which is particularly important for modulating temperature and salinity at high latitudes. Global ocean models include a sea ice component. State-of-the-art sea ice models represent the ice thermodynamics including meltponds and the ice dynamics, with a representation of the ice rheology. Many sea ice models also capture the variations in ice thickness or ice age within a typical ocean grid box. Current status of sea ice modelling and the applicability of models for operational forecasting is discussed in Hunke et al. (2020).

This chapter provides complementary information on the way to set an OOFS, which core is the circulation model. Section 5.3 will provide a list of input data needed for setting up an ocean model, from static datasets such the bathymetry to operational products such atmospheric forcing, to other OOFS for the provisioning of initial/boundary conditions in case of regional/coastal models, to observations used for assimilation and validation. Section 5.4 focuses on the mathematical formulation of the primitive equations, providing some basic information to numerical methods for discretization and numerical integration of such equations. Section 5.5 is devoted to presenting the basic mathematics for the data assimilation schemes commonly used in global and regional OOFS. Section 5.6 deals with ensemble modelling and, finally, Sections 5.7 and 5.8 provide major details on the validation approaches and the OOFS output. The last part of this chapter provides an inventory of OOFS, including multi-year systems, operating at international level, from global to coastal scale.

5.2.
Circulation forecast and multi-year systems

5.2.1. Ocean-Earth system as basis for OOFS

The ocean is a system that interacts with other systems. Figure 5.1 shows a simplified representation of the Earth system interaction in weather and ocean forecasting. Focusing on the ocean, we can identify (Madec et al., 2022):

- **Connection with land:** in particular with rivers and lakes which exchange freshwater flux with the ocean;

- **Connection with the atmosphere:** the ocean receives precipitation and returns evaporation. The atmosphere and the ocean also exchange horizontal momentum (wind stress) and heat;

- **Connection with sea ice:** the ocean exchanges heat, salt, freshwater and momentum with sea ice. The sea surface temperature is constrained to be at the freezing point of the interface. Sea ice salinity is very low (~4-6 PSU) compared to that of the ocean (~34 PSU). The cycle of freezing/melting is associated with freshwater and salt fluxes and cannot be neglected;

- **Connection with solid earth:** heat and salt fluxes through the seafloor are small, hence no flux of heat and salt is considered across solid boundaries. For mo-

mentum instead, we express the kinematic boundary condition. Additionally, the ocean exchanges momentum with the Earth through friction; this needs to be parameterized in terms of turbulent fluxes using bottom and lateral boundary conditions.

These connections will be detailed along this chapter and represent the core of the OOFS architecture introduced in the next subsection.

5.2.2. Architecture singularities

An OOFS that would provide the prediction, as well as the past reconstruction of the past state of the ocean, is based on several components that are strongly linked. A general introduction to OOFS architecture singularities is provided in Chapter 4, which includes for each system component, input and output data, as well as links between some of the components, are described. Complexity of the system, components of the system, infrastructure, maintenance of the code, and monitoring of the whole data flow should be defined depending on needs, robustness and operationality. Of course, the cost of the development, maintenance and evolution of the system depends on operational constraints.
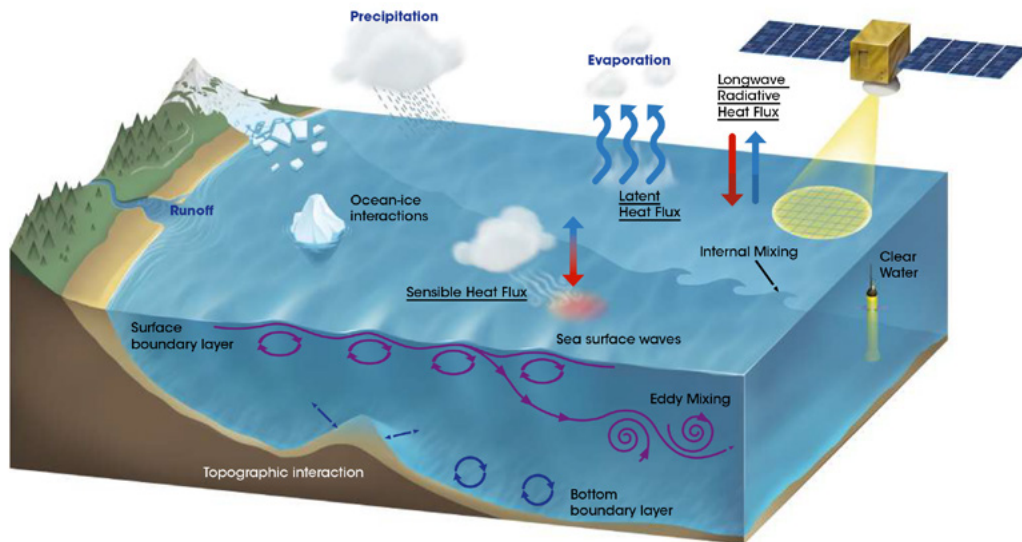
Figure 5.1. Representation of the ocean processes and connections with the Earth.

5.3.
Input data

Elements needed to run a circulation model for operational forecasting:

- **Observations.** These are used for:

  - Validation (including forecast verification) and calibration, further described in Section 5.7;
  - Data assimilation, which basic concepts are introduced in Section 5.5;

  Sources of observations are:

  - In-situ observations for the following variables: temperature, salinity, sea surface height, and sea surface currents. See Section 4.2.2. for more information on in-situ ocean observations;
  - Satellite observations for the following list of variables: sea level anomaly, sea surface temperature, and sea ice concentration. Recently, other parameters such as sea surface salinity and sea ice thickness have been remotely measured. See Section 4.2.2. for more information on in-situ ocean observations.

- **Bathymetry.** It is an indispensable topographical information for an Ocean Circulation Forecasting System. Its resolution may significantly drive the modeller during the setup of the circulation model to address specific scales and resolution. For example, in coastal models we may need bathymetric datasets, whose resolution can be even lower than 100 m, to properly represent the physical structural peculiarities of both coastline and shelf area, allowing the representation of small-scale physics. See more information on bathymetric data sets in Section 4.2.4.

- **Atmospheric forcing.** Generated by NWP services, it is vital to provide momentum, heat, and freshwater fluxes to the OOFS. More info on atmospheric forcing can be found in Section 4.2.5.

- **Land forcing.** Provides freshwater fluxes from rivers. More details on this data source are in Section 4.2.6.

- **Initial and boundary conditions from other OOFS.** 3D fields from parent models are required when downscaling to obtain higher resolutions (see Sections 4.2.7. and 5.4.4. for more information).

- **Climatological fields.** These serve as complement to the other data sources or might be used to substitute the previous if no other data are available. See Section 4.2.8 for more information on climatologies.

5.4.
Modelling component: general circulation models

An ocean model is a numerical and computational tool used to understand and predict ocean variables (Griffies, 2006), providing a discrete solution of the geophysical fluid dynamic equations. It represents a rigorous way of linking the ocean state parameters through mathematical equations representing the physics that governs the oceans.

In the next subsections, we will introduce the different components of an OGCM, that is part of the OOFS (steps 1 and 2 as in Figure 4.1), focusing on mathematical equations, numerical methods, and spatial discretization techniques. A list of available numerical ocean models is provided in Table 5.1 in Section 5.4.3. Data assimilation methods used in OOFSs are instead presented in Section 5.5.

5.4.1. Mathematical model

The Navier-Stokes equations represent the fundamental laws of fluid dynamics; they are based on conservation of momentum, conservation of mass, and an equation of state.

Oceans are also represented by the following equations (although with some significant simplifications as explained in Madec et al., 2022):

- **Spherical Earth approximation:** the geopotential surfaces are assumed to be oblate spheroids that follow the Earth's bulge, and are approximated by spheres which gravity is locally vertical (parallel to the Earth's radius) and independent from latitude;

- **Thin-shell approximation:** the ocean depth is neglected compared to the Earth's radius;

- **Turbulent closure hypothesis:** the turbulent fluxes - which represent the effect of small-scale processes on the large scale - are expressed in terms of large scale features;

- **Boussinesq hypothesis:** density variations are neglected, except in their contribution to buoyancy force:

$$\rho = \rho(T, S, p) \qquad (5.1)$$

- **Hydrostatic hypothesis:** the vertical momentum equation is reduced to a balance between the vertical pressure gradient and the buoyancy force (this removes convective processes from the initial Navier-Stokes equations and so convective processes must be parameterized instead):

$$\frac{\partial p}{\partial z} = -\rho g \qquad (5.2)$$

- **Incompressibility hypothesis:** the 3D divergence of the velocity vector U is assumed to be zero:

$$\nabla \cdot U = 0 \qquad (5.3)$$

- **Neglect of additional Coriolis terms:** the Coriolis terms that vary with the cosine of latitude are neglected.

Because the gravitational force dominates in the equations of large-scale motions, it is useful to choose an orthogonal set of unit vectors (i,j,k) linked to the Earth such that k is the local upward vector and (i,j) are 2 vectors orthogonal to k. Let us define additionally: U the vector velocity, T the potential temperature, S the salinity, ρ the insitu density. The vector invariant form of the primitive equations in the (i,j,k) vector system provides the following equations:

- The momentum balance:

$$\frac{\partial U_h}{\partial t} = -\left[(\nabla \times U) \times U + \frac{1}{2}\nabla(U^2) \right]_h$$
$$-fk \times U_h - \frac{1}{\rho_0}\nabla_h p + D^U + F^U \qquad (5.4)$$

- The heat and salt conservation equations:

$$\frac{\partial T}{\partial t} = -\nabla \cdot (TU) + D^T + F^T \qquad (5.5)$$

$$\frac{\partial S}{\partial t} = -\nabla \cdot (SU) + D^S + F^S \qquad (5.6)$$

where ∇ is the generalised derivative vector operator in (i,j,k) directions, t is the time, z is the vertical coordinate, ρ is the in-situ density given by Eq. 5.1, ρ_0 is the reference density, p is the pressure, f$=2\Omega \cdot k$ is the Coriolis acceleration (where Ω is the Earth's angular velocity vector) and g is the gravitational acceleration. D^U, D^T and D^S are the parameterizations of small-scale physics for momentum, temperature and salinity, while F^U, F^T and F^S are surface forcing terms.

OGCMs are able to resolve the mesoscale in some regions but not in others; additionally, once applied for climate research, they cannot entirely reproduce the rich mesoscale eddy activity we observe in reality. For this reason, mixing associated with sub-grid scale turbulence needs to be parameterized.

A common problem an ocean modeller is facing when he/she deals with primitive equations is the numerical discretization in space and time. As described in Hallberg (2013), numerical ocean models need to represent the effects of mesoscale eddies, which are the typical horizontal scales of less than 100 km and timescales in the order of a month. When defining the spatial grid for the numerical integration of the primitive equations, it is important to account for the ratio of a model's grid spacing to the deformation radius, defined as:

$$L_{Def} = \sqrt{\frac{c_g^2}{f^2 + 2\beta c_g}} \qquad (5.7)$$

where c_g is the first-mode internal gravity wave speed, f is again the Coriolis parameter, and β is its meridional gradient (Chelton et al., 1998).

Figure 5.2 shows the ocean model resolution required for the baroclinic deformation radius to be twice the grid spacing, based on an eddy-permitting ocean model after one year of spin-up from climatology (Hallberg, 2013).

5.4.2. Basic discretization techniques

The next step towards the setup of a numerical model is the discretization phase, which involves the spatial discretization and the equation discretization.

The spatial discretization consists in defining a grid or mesh that would represent the space continuum with a finite number of points where the numerical values of the physical variables must be determined. In Section 5.4.2.1-2, basic concepts for dealing with horizontal grids and vertical discretization will be introduced. Once the mesh is defined, we move to the final step related to the primitive equations discretization by using numerical methods, which consist in transforming the mathematical model into an algebraic, nonlinear system of equations for the mesh-related unknown quantities. The concepts on the basis of the time stepping are treated in Section 5.4.2.3. With the definition of the time-dependent numerical formulation, we finally select the discretization method to use for the equations, described in Section 5.4.2.4.
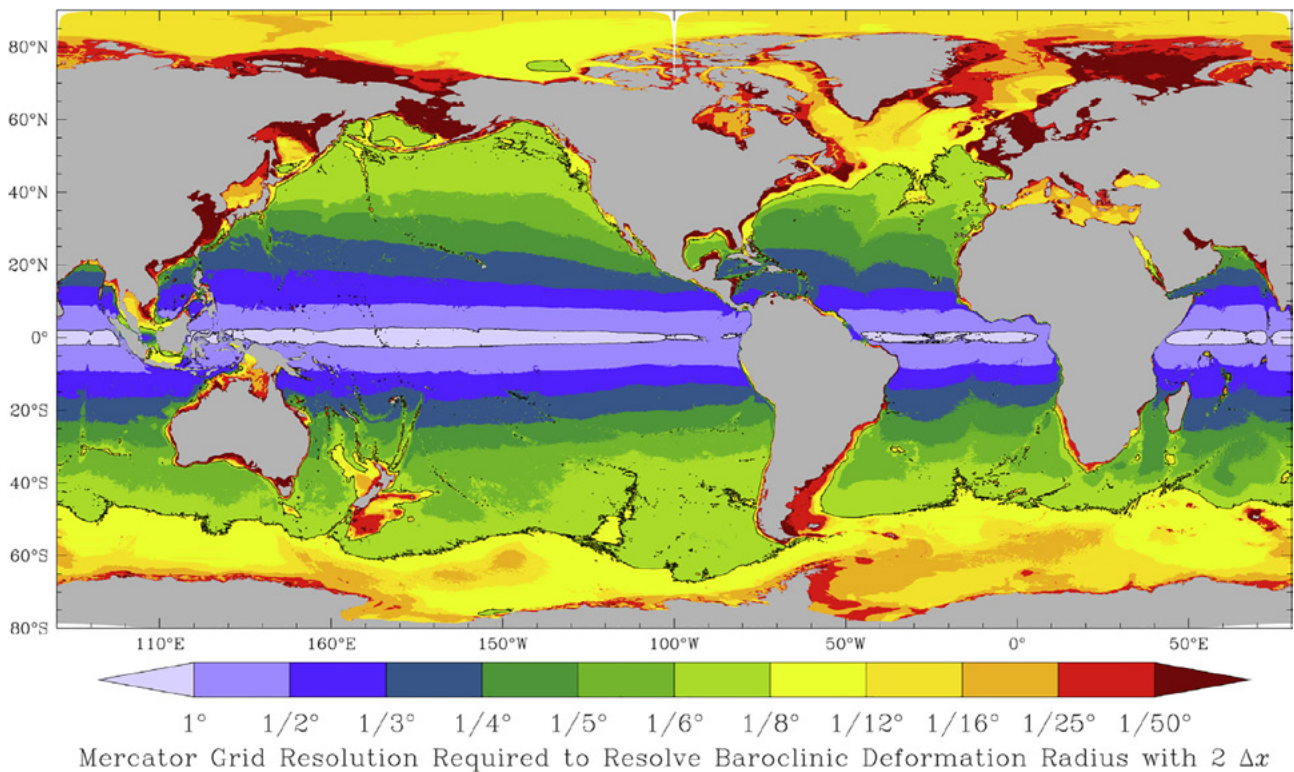
Figure 5.2. The horizontal resolution needed to resolve the first baroclinic deformation radius with two grid points, based on a 1/8º model on a Mercator grid on Jan 1 after one year of spinup from climatology (from Hallberg, 2013).

5.4.2.1. Horizontal grids

In numerical methods, we can use:

- Structured grids
- Unstructured grids

A mesh is structured when the grid cells have the same number of sides and the same number of neighbouring cells. Typically, in ocean models three kinds of grids may be used (Figure 5.3): the Arakawa-A grid, the Arakawa-B grid and the Arakawa C-grid. In the Arakawa-A grid (Figure 5.3A), all variables are evaluated at the same location. Then, the B and C grids have been developed respectively for coarse and fine resolution models. In the Arakawa-B grid (Figure 5.3B) both u (Northwards current component, in orange) and v (Eastwards current component, in green), for example, are evaluated at the same point and the velocity points are situated at the point that is equidistant from the four nearest elevation points (Elevation, in blue). In the Arakawa-C grid (Figure 5.3C), the u points lie east and west of elevation points, while the vpoints lie north and south of the elevation points .

Unstructured grids (Figure 5.4C) allow one to tile a domain using more general geometrical shapes (most commonly triangles) that are pieced together to optimally fit details of the geometry. They are extremely attractive for ocean modelling, especially for coastal models, in which the high-quality representation of geometrical features of a given domain is essential, and from the numerical point of view they may reach a significant level of complexity (Griffies et al., 2000).

Besides their ability to better represent coastlines, unstructured grid approaches also offer the possibility to smoothly increase the resolution over a region of interest or depending on physical parameters (Sein et al., 2017). This is also possible with structured curvilinear grids (for example, see the BLUElink Australian prediction model grid in Brassington et al., 2005, and Figure 5.4A), though with likely more constraints on the grid deformation properties. However, in any of the two cases, numerical stability is dictated by the smallest grid element, which substantially increases the computational problem. An additional difficulty is that sub-grid parameterizations have to be valid throughout the domain, whatever the grid size and eddy resolution regime are (Hallberg, 2013). In the structured grid case, block structured refinement techniques enable to circumvent some of the aforementioned difficulties by allowing a stepwise change (over a given grid patch) of the space and time resolutions (by integer factors, Figure 5.5B). Parameterizations and numerical schemes can also be changed accordingly. Grid exchanges can either be "one-way" if finer grids only receive information at their dynamical boundaries from the outer grid, or "two-way" if they also feed information back to the underlying mesh. In the latter case, data transferred at each model time step allows for a nearly seamless transition at the interface and possibly guarantees perfect conservation of prognostic quantities (Debreu et al., 2012).

Several libraries do facilitate the implementation of block structured refinement. Among them, the AGRIF library (Debreu et al., 2008) has been successfully used in HYCOM, MARS, NEMO and ROMS models. It is noteworthy that refinement techniques can eventually be adaptive, hence refinement regions can move

A) Arakawa A grid   **B) Arakawa B grid**   **C) Arakawa C grid**

Legend:
- Northwards current
- Eastwards current
- Elevation
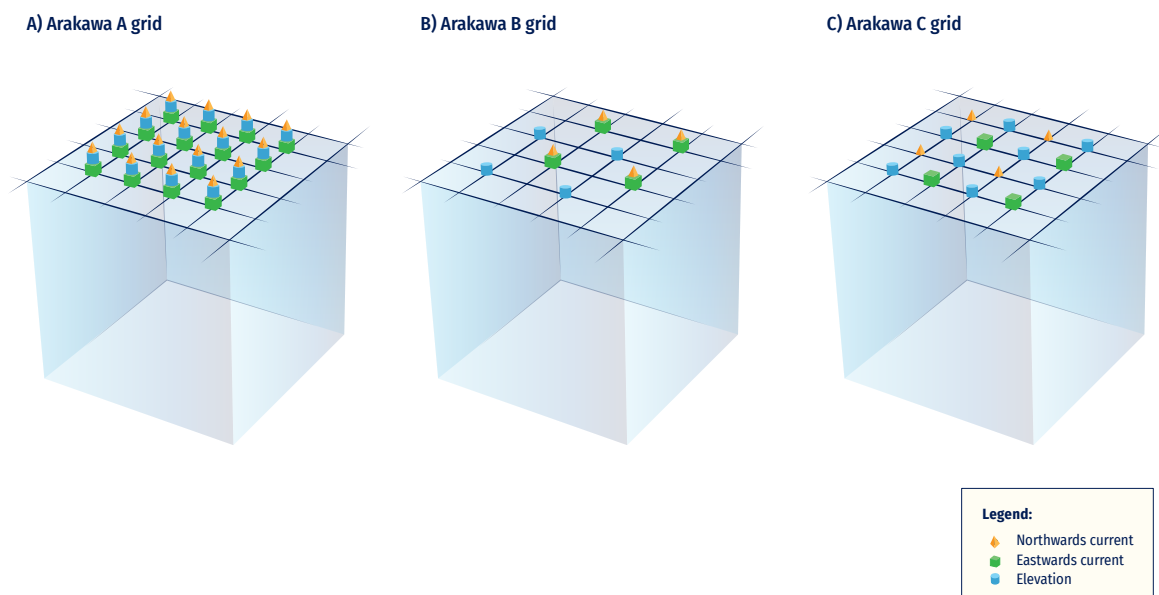
Figure 5.3.   The three Arakawa types of grids (adapted from Dyke, 2016).

Legend:
+ Resolution level 0
Resolution level 1
Resolution level 2
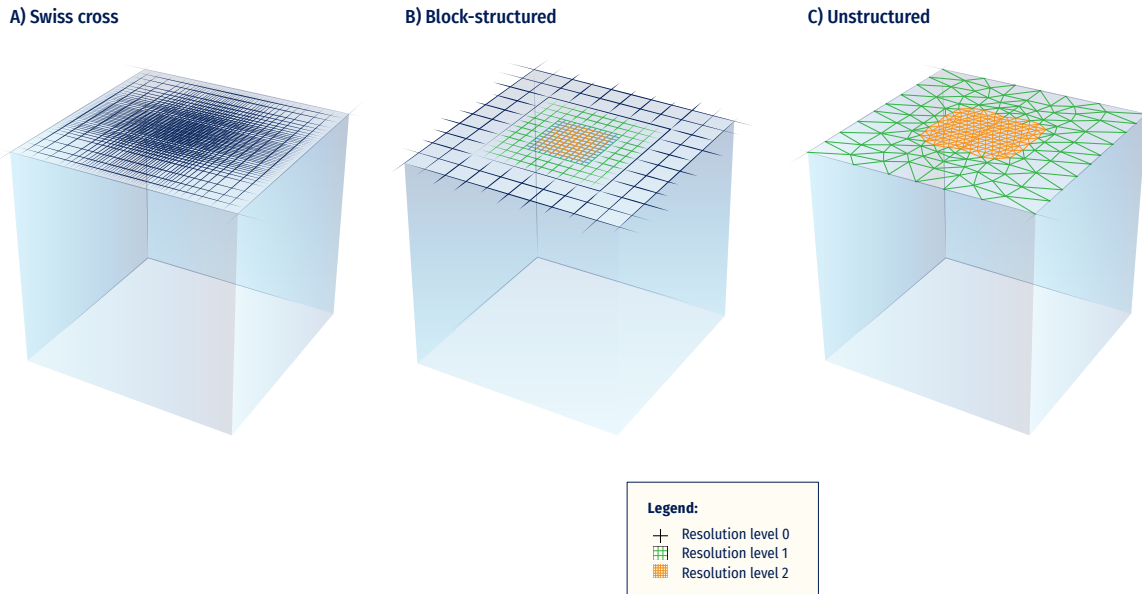
Figure 5.4. Possible ways to get a local increase of resolution: a) Progressive deformation of a structured grid; b) Block structured refinement; and c) Stretching of unstructured grid cells (adapted from Gerya, 2019).

over the course of the model integration (Blayo and Debreu, 1999). Resolution is in that case increased only where needed, depending on a local numerical or physical criterion, to save computing resources. The use of AMR techniques in realistic ocean models is nevertheless still poorly documented.

5.4.2.2. Vertical discretization

The problem of vertical discretization is connected to physical processes that the modeler wants to resolve and it must address questions related to: a) the representation of pressure gradients; b) the representation of sub-grid scale processes; c) the need to concentrate the resolution in a specific region (e.g. the shelf, the coastal areas, etc.); and d) the comparison with observations. Griffies et al. (2000) distinguished among three traditional approaches (Figure 5.5):

- Depth/geopotential vertical coordinates;
- Terrain-following;
- Potential density (isopycnic) vertical coordinates.

Geopotential (z-) coordinates (Figure 5.5A) have been largely used in ocean and atmospheric models because of their simplicity and straightforward nature for parameterizing the surface boundary layer. On the contrary, they are not able to adequately represent the effect of topography on the large-scale ocean models. Terrain-following coordinate systems (Figure 5.5B) are used especially in coastal applications, where bottom boundary layers and topography need to be well resolved. As z-coordinates, they suffer from spurious di-

apycnal mixing due to problems with numerical advection. In isopycnic vertical coordinates (Figure 5.5C), the potential density is referred to a given pressure. This system basically divides the water column into distinct homogeneous layers, which thicknesses can vary from place to place and from one time step to the next. This choice of coordinate works well for modelling tracer transport, which tends to be along surfaces of constant density. While both layered and isopycnal models use density as the vertical coordinate, there are subtle differences between the two types. Griffies et. al. (2000) and Chassignet et al. (2006), provide a discussion on the advantages and disadvantages of each vertical coordinate system.

5.4.2.3. Time stepping

Once the model is set from the spatial point of view and discretization in horizontal and vertical is defined, the time step for the computation needs to be considered as well. In the numerical schemes used to integrate the primitive equations, the time step must be small enough to guarantee computational stability. The Courant-Friedrichs-Lewy criterion (CFL) is the stability condition that states that the velocity c at which the information is propagating at times the time step Δt must be less than the horizontal grid spacing Δx:

$$C = \frac{u\Delta t}{\Delta x} \leq C_{max} \tag{5.8}$$

where C is the Courant number and C_{max} depends on the specific used scheme: explicit schemes allow to advance the solution to the next time level, one spatial grid point at a time, and are quite simple to implement (Kantha and Clayson, 2000);

A)   B)   C)
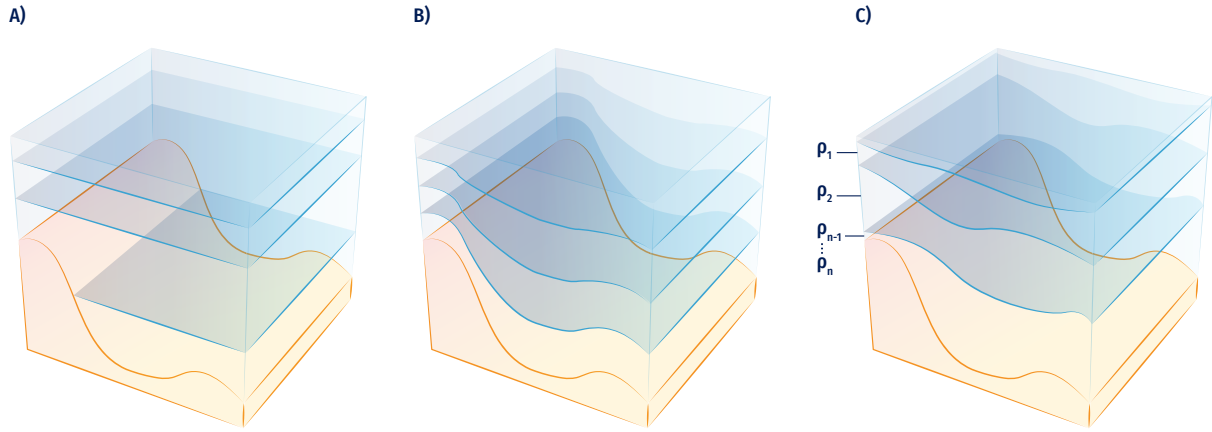
Figure 5.5. Vertical grid types: a) depth/geopotential vertical coordinates; b) terrain-following; and c) potential density (isopycnic) vertical coordinates.

in an implicit time-stepping scheme, the solution at the next time level must be derived for all grid points simultaneously. These schemes are computationally more intensive, but are unconditionally stable, thus permitting larger time steps to be taken than would otherwise be required.

5.4.2.4. Numerical techniques

Three families of methods are available for discretizing the space derivatives that enters in the primitive equations:

- Finite difference Method (FDM);
- Finite Volume Method (FVM);
- Finite Elements Method (FEM).

Here we provide an introduction to each method but for more detailed explanation refer to Hirsch, 2007.

The FDM is based on the properties of the Taylor expansions: it corresponds to an estimation of a derivative by the ratio of two differences according to the theoretical definition of the derivative, like the following:

$$u_x = \frac{\partial u}{\partial x} = \frac{u(x + \Delta x) - u(x)}{\Delta x} \qquad (5.9)$$

If we remove the limit in Eq. 5.9, we obtain a finite difference: additionally, if Δx is "small" but finite, the expression on the RHS of Eq. 5.9 is an approximation of the exact value of u_x. Since Δx is finite, an error is introduced, called truncation error, which goes to zero for Δx tending to zero. The power of Δx with which this error tends to zero, is caller order of accuracy of the difference approximation and can be obtained by a Taylor series of $u(x+\Delta x)$ around point x (Eqq. 5.10 and 5.11):

$$u(x + \Delta x) = u(x) + \Delta \frac{\partial u}{\partial x}$$
$$+ \frac{\Delta x^2}{2} \frac{\partial^2 u}{\partial x^2} + \frac{\Delta x^3}{3!} \frac{\partial^3 u}{\partial x^3} + \dots \qquad (5.10)$$
$$\frac{u(x + \Delta x)}{\Delta x} = \frac{\partial u}{\partial x} + \frac{\Delta x}{2} \frac{\partial^2 u}{\partial x^2} + \frac{\Delta x^2}{6} \frac{\partial^3 u}{\partial x^3} + \dots \qquad (5.11)$$

Equation 5.11 shows that:

- The RHS of Eq. 5.9 is an approximation of the first derivative u_x in the point x;
- The remaining terms in the RHS represent the error associated with this formula.

If we restrict the truncation error to its dominant term, that is the lower power of Δx, we see that this approximation for $u(x)$ goes to zero like the first power of Δx and is said to be the first order in Δx:

$$\frac{u(x + \Delta x)}{\Delta x} \cong \frac{\partial u}{\partial x} + \frac{\Delta x}{2} \frac{\partial^2 u}{\partial x^2} = u_x(x) + O(\Delta x) \quad (5.12)$$

where $O(\Delta x)$ is the truncation error.

The FVM is a numerical technique by which the integral formulation of the conservation laws is discretized directly in the physical space. It is based on cell-averaged values, which makes this method totally different from FDM and FEM where the main numerical quantities are the local function values at the mesh points. For each cell, a local finite volume, also called control volume, is associated to each mesh point and applies the integral conservation law to this local volume. For this reason, the FVM is considered a conservative method. The essential property of this formulation is the presence of the surface integral and the fact that the time variation of a generic variable u inside the volume only depends on the surface values of the fluxes.

The FVM requires:

- The subdivision of the mesh, obtained from the space discretization, into finite small volumes, one control volume being associated to each mesh point;
- The application of the integral conservation law to each of these finite volumes.

The FEM originates from the field of structural analysis and it has two common points with the FVM:

- The space discretization is considered a set of volumes or cells, called elements;

- It requires an integral formulation as a starting point that can be considered as a generalisation of the FVM.

The FEM requires:

- Discretization of the spatial domain into a set of elements of arbitrary shapes;
- In each element, a parametric representation of the unknown variables, based on families for interpolating or shape functions, associated to each element or cell is defined.

Model	Grid topology	Numerical methods	Nesting capabilities	Website
NEMO	Structured grid	Finite Difference	Yes, with AGRIF	https://www.nemo-ocean.eu/
HYCOM	Structured grid	Finite Volume	Yes, with AGRIF	https://www.hycom.org/
MITgcm	Structured grid	Finite Difference	Yes	https://mitgcm.org/
ROMS	Structured grid	Finite Volume	Yes, with AGRIF	https://www.myroms.org/
CROCO	Structured grid	Finite Difference	Yes, with AGRIF	https://www.croco-ocean.org/
FVCOM	Unstructured grid	Finite Volume	Yes, with AGRIF	http://fvcom.smast.umassd.edu/
SHYFEM	Unstructured grid	Finite Element		https://sites.google.com/site/shyfem/project-definition
SCHISM	Unstructured grid	Finite Element		http://ccrm.vims.edu/schism-web/
FESOM	Unstructured grid	Finite Element		https://fesom.de/
MPAS	Unstructured grid	Finite Element		https://mpas-dev.github.io/
MOM	Structured grid	Finite Volume		https://www.gfdl.noaa.gov/ocean-model

Table 5.1. List of available ocean models used from global to coastal scales.

Such nice properties of the FEM as conservation of energy, that is common for all variational methods of solving differential equations, treatment of boundary conditions, and flexibility of irregular meshes have made them quite attractive, since they are also well suited to parallel computing. For this reason, it is considered as an interesting alternative to FDM commonly used in ocean modelling (Danilov et al., 2004).

5.4.3. List of Ocean General Circulation Models

In Table 5.1, are summarised some of the most used ocean models that integrate numerically the primitive equations for a wide range of spatial domains, from global ocean to coastal scales.

5.4.4. Downscaling large-scale solutions to regional/coastal circulation models

The need to resolve the small scales of ocean circulation in coastal seas, as well as the impracticability to run models at suf-

ficiently high resolution and detailed physics at global scales, led to the development of downscaling approaches for both the direct modelling and the data assimilation problems.

Two families of modelling approaches can be distinguished: (1) models running at global scales with mesh refinement in the coastal areas of interest; and (2) one-way or two-way nesting of coastal models into regional or global ones. In practice, the first one is achieved by setting variable-mesh grids, such as unstructured or curvilinear structured grids (as discussed in 5.4.2.1). To our knowledge, only 2D (i.e. barotropic) unstructured models dedicated to storm surges and/or tides modelling, such as the tidal atlas FES2014 (Lyard et al., 2021), are running over the global ocean and satisfy the resolution requirements in shallow waters. In the second approach, the large-scale global (or regional) model, i.e. the 'parent' model, provides open-boundary conditions to the coastal ('child') model; in case of two-way nesting, both models are coupled and the child model returns an estimate of the ocean state at its boundary, which is used in turn to
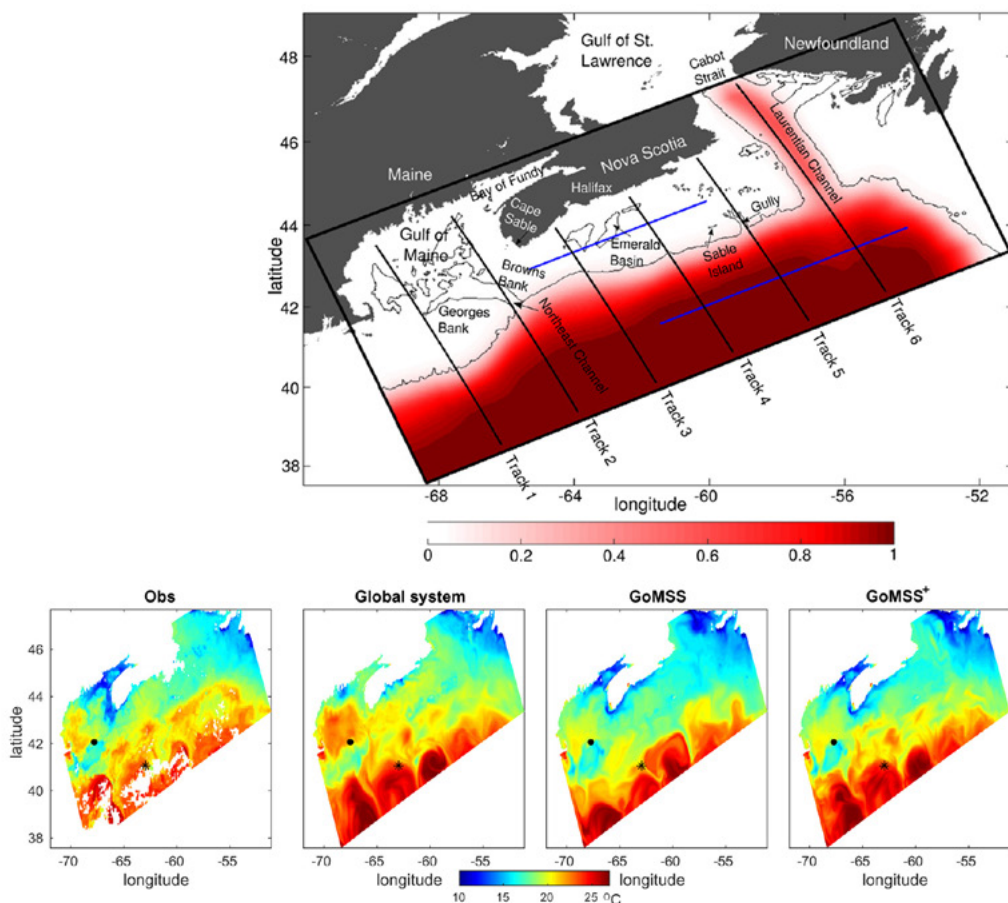
Figure 5.6.   Spectral nudging in the Gulf of Maine; top: spatial domain; bottom: snapshots of sea surface temperature on 22 Jul 2012 from observations, global system, regional configuration and regional configuration with spectral nudging (from Katavouta and Thompson, 2016).

force the parent simulation. General resolution issues for both approaches and practical considerations are discussed in Greenberg et al. (2007).

However, nesting methods do not just consist in reproducing the large-scale solution with more details. Indeed, the child model may represent different processes from those solved by the parent model (e.g. tides, surface gravity waves, etc.) or may rely on different parameterizations or parameters. Besides, due to the strong nonlinearity of the ocean flow, the internal variability of the child model may decouple from that of the parent, leading to divergent solutions (Katavouta and Thompson, 2016). Figure 5.6 shows an example of spectral nudging in the Gulf of Maine as in Katavouta and Thompson (2016). The spatial domain is given in Figure 5.6-top: the black box represents the bounding box of the regional model GoMSS (NEMO, 1/36° horizontal resolution), which is nested into the HYCOM+NCODA global 1/12° analysis system. GoMSS+ is the regional configuration with spectral nudging where temperature and salinity variables are directly updated. By adopting such a nesting approach, the regional configuration significantly improves the quality of the solution as shown in Figure 5.6-bottom: it represents the sea surface temperature snapshots for 22 July 2012 based on satellite ("Obs"), the global system ("Global system"), the regional system ("GoMSS"), and that implementing the spectral nudging ("GoMSS+"). The GoMSS+ exhibits an improved version of the coastal sea surface temperature representation, which is typical for a higher resolution model that takes into account coastal processes (e.g., tides). At the same time, it is able to capture the warm slope water and cold shelf waters as shown in the observations, which are well represented in the global model thanks to data assimilation. For further details, please refer to Katavouta and Thompson (2016).

In 2007, the GODAE Coastal and Shelf seas Working Group (De Mey et al., 2007) noted that: "It is becoming increasingly clear that specifying the offshore boundary conditions of coastal models by using forecasts from a hydrodynamical large-scale ocean model has the potential (1) to provide better local estimates by adding value to GODAE products, (2) to extend predictability on shelves, and (3) to enhance the representativeness of local observations." Despite considerable efforts since 2007 on both coastal modelling capabilities and nesting methods, downscaling still raises obvious numerical and physical issues. In the following paragraphs an attempt has been made, but not exhaustively, to present the various difficulties that arise and the solutions found in the literature to address them.

The coastal ocean is subject to both local (e.g. atmosphere, river mouths) and remote forcings (e.g. astronomical potential, coastal waveguide, wind fetch, biogeochemical connectivity). Therefore, the boundaries of a coastal model, which

also intercept strong bathymetry gradients, play a critical role. In addition, solving primitive equations on a limited area domain with OBC does not lead to a unique physically realistic solution. Consequently, a variety of ad hoc methods to set-up practical OBC have been developed with a dependence upon flow dynamics, model resolution, types of information at the open boundaries, etc., as reviewed by Blayo and Debreu (2005). A simple view of the OBC issues consists in viewing the problem because of inconsistencies between the parent and child models which, as mentioned previously, arise due to different physics of the model, to different forcing (e.g. atmospheric, runoff, bathymetry), and to truncated information at the open boundary. The last refers to the fact that the parent information is provided as discrete fields in space and time (e.g. daily or hourly averages); high-frequency motions are therefore filtered out or aliased.

The example of tides is particularly enlightening on these limitations. Even though the parent model resolves tides, forcing the child with the parent tidal waves (either barotropic or both barotropic and baroclinic) implies the availability of the large-scale forcing at very high frequency (a few minutes). In practice, especially for operational systems, this is very difficult to achieve as it requires huge storage capacities. Therefore, coastal models are usually forced by low-frequency dynamics and tidal constituents, both of which not necessarily stemming from the same parent models (tidal constituents are often chosen from accurate global tidal atlases). Herzfeld and Gillibrand (2015) noted that conditions for incoming tidal waves may be reflective for the low-frequency external data and propose OBC based on dual relaxation time scales. Furthermore, the difference of bathymetry and representation of the coastline between the parent and child models may lead to large inconsistencies between the tidal solutions in both models, with a risk of spurious patterns developing in the coastal domain close to the open boundaries (e.g. rim currents). Toublanc et al. (2018) proposed a simple approach that reduces such inconsistencies by pre-processing the tidal forcing using a 2D simulation with a dedicated 2D tidal model. At last, filtering out the high-frequency 3D incoming information by using for instance hourly or daily averages from the parent simulation, may lead to a loss of energy in the coastal domain, in particular because of the missing internal waves forcing, as recently evidenced by Mazloff et al. (2020).

Another difficulty in one-way nesting arises from the possibility that the child model develops an internal variability that diverges from the parent's one. In many operational systems, global or large-scale solutions stem from a data assimilation system in which the mesoscale dynamics are constrained by satellite data (e.g. altimetry). If no data assimilation is performed in the coastal domain, the developing mesoscale (and a fortiori submesoscale) may deviate from reality leading to the undesirable case in which the parent solution is closer
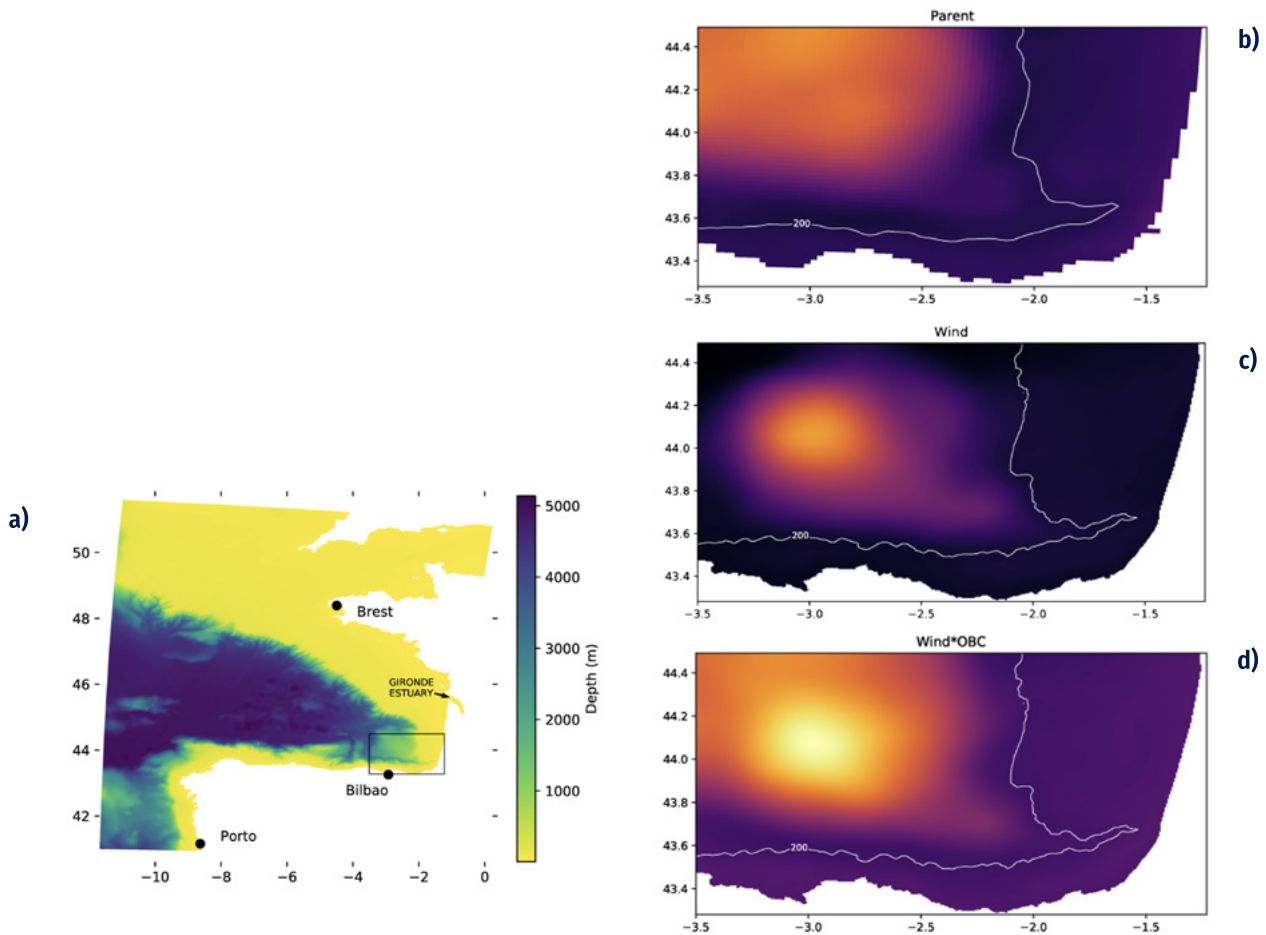
Figure 5.7. A case study in the south-east Bay of Biscay: a) bathymetry of the parent model and bounding box (black box) of the child domain; ensemble spread in SSH over 3 months period (Jan-Feb-Mar) from 50 ensemble members perturbing; b) wind in parent model; c) wind in the child domain; and d) wind and OBC in the child domain (from Ghantous et al., 2020).

to observations at large-scale and mesoscale than the child. Sandery and Sakov (2017) report that even with data assimilation, increasing the resolution does not automatically improve the skill of the forecast, because of the inverse cascade of unconstrained submesoscale towards mesoscale. Methods such as spectral nudging are developed to ensure that the large-scale patterns, e.g. eddies or meandering jets that are accurately represented in the parent model, are maintained in the child; an example of such method can be found in Katavouta and Thompson (2016).

A last but not least issue concerns quantifying the errors in the child simulations due to the nesting process. The errors originate from the OBC scheme (numerical implementation and physical assumptions) and from the uncertainties on the parent forcing fields. In the latter case, the question is how the parent model errors are downscaled. Ensemble approaches can help to characterise and estimate the downscaling of parent errors, as for instance explored in Ghantous et al. (2020).

Figure 5.7 shows an example of ensemble downscaling of a coastal ocean model (Symphonie model, 500 m resolution) for the south-east Bay of Biscay in an ensemble of a regional model (NEMO, 1/36°) (Ghantous et al., 2020). Figure 5.7a presents the regional domain, in particular the parent domain over the map, while the blue box is the domain of the child model. Figures 5.7b-d show the ensemble spread (standard-deviation) in sea surface height (SSH) in the domain of the child model for ensembles of 50 members. In particular, Figure 5.7b is the parent ensemble, generated by perturbing the wind in the parent domain; Figure 5.7c is the child ensemble, generated by perturbing the wind in the child domain; Figure 5.7d is the child ensemble generated by perturbing both the wind and the OBC conditions (the OBC perturbations stem from the parent ensemble). The numerical experiment reveals that, on average over the period of study, the spread in SSH is greatest where the mesoscale eddies are present (in the deeper area of the domain). It also reveals that the contribution from the OBC uncertainties is larger than the impact
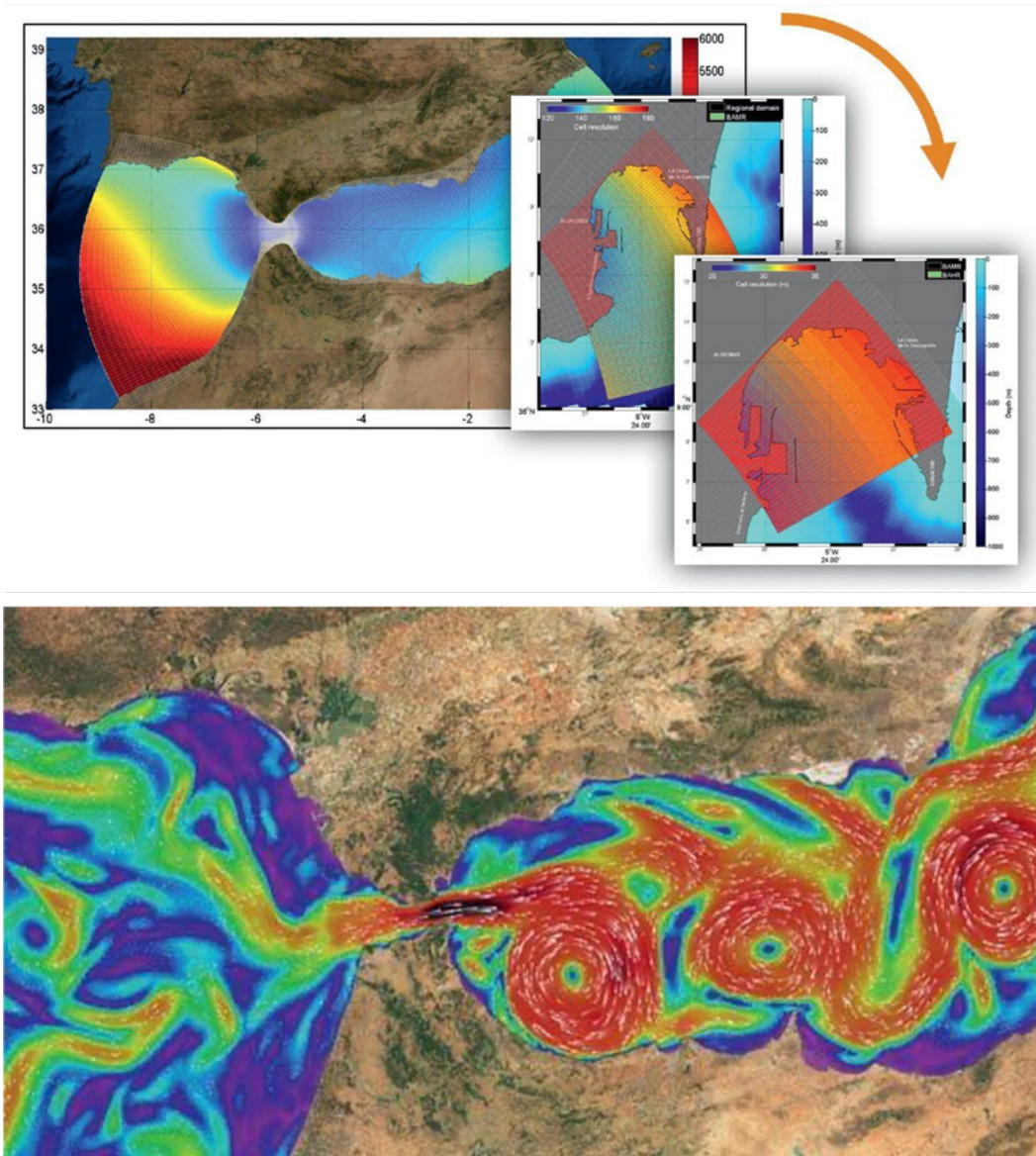
Figure 5.8. Gulf of Cadiz and the Alborán Sea: example of downscaling capacities. Source: Puertos del Estado and Universidad de Málaga.

of local wind uncertainties. It is a valuable result for the next generation of ensemble data assimilation systems.

An example of nesting capacities of circulation modelling in short-term forecast is shown in Figure 5.8. This is the result of downscaling the Copernicus Marine Service Iberia-Biscay-Ireland – Monitoring and Forecasting Centre (IBI-MFC, 🔗¹) product on a higher spatial grid; in the bottom panel it can be seen a detail of surface currents in the Gulf of Cadiz and Alborán Sea.

The downscaling approach is extremely powerful to allow the modeller to set up an OOFS at high resolution, and every OOFS may be used to build another OOFS in a seamless way. In Section 5.9 can be found an initial but exhaustive list of OOFSs' providers from which the modeller may select to nest her/his new OOFS.

1. https://resources.marine.copernicus.eu/product-detail/
IBI_ANALYSISFORECAST_PHY_005_001/INFORMATION

5.5.
Data assimilation systems

An introduction to the data assimilation concept can be found in Section 4.3. This Section focuses on the numerical characteristics of the DAS largely used in circulation modelling.

5.5.1. Basic concepts

In ocean forecasting the objective is to produce an estimate x_a of the true state x_t of the ocean at initial time to initialise forecasts. Ide et al., 1997, De Mey-Frémaux et al. (1998), and Bouttier and Courtier (2002) provide an extensive introduction to DAS basic concepts and herein are recalled and summarised.

DA consists in calculating the «best» estimate of the state of a physical system, of its evolution in time, given observations and a prognostic numerical model.

The basic objective information that can be used to produce the analysis is a collection of observed values provided by observations of the true state. If the model state is overdetermined by the observations, then the analysis is reduced to an interpolation problem. In most cases the analysis problem is under-determined because data are sparse and only indirectly related to the model variables. In order to make it a well-posed problem, it is necessary to rely on some background information in the form of an a priori estimate of the model state.

A discrete model for the evolution of the ocean from t_i to t_{i+1} is governed by the following Eq. 5.13:

$$\mathbf{x}^f(t_{i+1}) = M_i \left[\mathbf{x}^f(t_i) \right] \quad (5.13)$$

where $\mathbf{x}$ is the so-called state vector (velocities, temperature, salinity, etc., at model grid positions) and M is the corresponding dynamics operator. The state vector has dimension n. The dynamic operator in Eq. 5.13 is commonly non linear and deterministic, while the true ocean state may differ from Eq. 5.13 by random and systematic error.

Observations $\mathbf{y}^o_t$ at time t_i are defined by Eq. 5.14:

$$\mathbf{y}^o_t = H_i \left[\mathbf{x}^t(t_i) \right] + \epsilon_i \quad (5.14)$$

where H is an observation operator and ϵ is a noise process. The observation vector has dimension p_i. A major problem of data assimilation is that typically $p_i \ll n$. The observation operator H can be also non-linear like M and both can contain explicit time dependence in addition to the implicit dependence via the state vector $x^f_i \equiv x^f(t_i)$. The noise process ϵ is commonly used to have zero mean and we denote its covariance matrix by R: it consists of instrumental and representativeness errors which covariance matrices are E and F, respectively, with $R=E+F$.

The key of the analysis is the use of discrepancies between observations and state vector:

$$y^o - H(x) \quad (5.15)$$

When calculated with the background x_b it is called innovations and with the analysis x_a analysis residuals.

In the following, we present two data assimilation types of approaches: the sequential methods and the variational methods.

5.5.2. Sequential methods

Several schemes have been proven useful and implemented using a sequential-estimation approach including the Bluelink Ocean Data Assimilation System (BODAS) (Oke et al., 2008) and the Singular Evolutive Extended Kalman (SEEK) filter (Pham et al., 1998). An extensive literature is available on related methods, such as OI (Daley, 1991), EnOI, and EnKF (Evensen, 2003).

Following Ide et al., (1997), the true ocean fluid $\mathbf{x}^f$ is assumed to differ from that of the numerical model (Eq. 13) by stochastic perturbations:

$$\mathbf{x}^f(t_{i+1}) = M_i \left[\mathbf{x}^f(t_i) \right] + \eta(t_i) \quad (5.16)$$

where η is a noise process with zero mean and covariance matrix $\mathbf{Q}$. The EKF consists of a forecast step based on previously obtained state variables, which include previous assimilation steps, $\mathbf{x}^f(t_{i+1})$ and an updated probability function described by $P^f(t_i)$:

$$\mathbf{x}^a(t_i) = M_i \left[\mathbf{x}^a(t_{i-1}) \right] \quad (5.17)$$

$$\mathbf{P}^f(t_i) = \mathbf{M}_{i-1}\mathbf{P}^a(t_{i-1})\mathbf{M}_{i-1}^T + \mathbf{Q}(t_{i-1}) \quad (5.18)$$

The core of the Kalman Filter method is an update step in which the observations available at time i is blended with the previous information, taking account of their joint probability distributions and carried forward by the forecast step:

$$\mathbf{x}^a(t_i) = \mathbf{x}^f(t_i) + \mathbf{K}_i\mathbf{d}_i \quad (5.19)$$

$$\mathbf{P}^a(t_i) = (\mathbf{I} - \mathbf{K}_i\mathbf{H}_i)\mathbf{P}^f(t_i) \qquad (5.20)$$

where the observation residual or innovation vector is defined by:

$$\mathbf{d}_i = \mathbf{y}_i^0 - H_i\left[\mathbf{x}^f(t_i)\right] \qquad (5.21)$$

The Kalman gain $\mathbf{K}_i$ is defined by:

$$\mathbf{K}_i = \mathbf{P}^f(t_i)\mathbf{H}_i^T\left[\mathbf{H}_i\mathbf{P}^f(t_i)\mathbf{H}_{i-1}^T + \mathbf{R}_i\right]^{-1} \qquad (5.22)$$

The innovation vector $\mathbf{d}_i$ is evidently a displacement of the modelled forecast toward the observed data, scaled by the Kalman gain. The Kalman gain accounts for the weighting required by the joint probability function for the model and observation variability. In practice, various simplifications are introduced to describe $\mathbf{P}$ to overcome the computational burden involved in the matrix calculation (Oke et al., 2008; Pham et al., 1998).

Another example is the *OI* that is quite frequently used in oceanography and meteorology. It is a particular suboptimal filter, in which the EKF's error covariance matrix P^f is replaced by an approximation, $\mathbf{B}$, computed as a product of variances placed in the diagonal matrix $\mathbf{D}$ and of correlations placed in a matrix $\mathbf{C}$ with unit diagonal (Ghil and Malanotte-Rizzoli, 1991):

$$\mathbf{B} = \mathbf{D}^{1/2}\mathbf{C}\mathbf{D}^{1/2} \qquad (5.23)$$

The state vector is still given by Eq. 5.13. The *OI* gain writes:

$$\mathbf{K}_i^{OI} = \mathbf{B}^f(t_i)\mathbf{H}_i^T\left[\mathbf{H}_i\mathbf{B}^f(t_i)\mathbf{H}_i^T + \mathbf{R}_i\right]^{-1} \qquad (5.24)$$

where $H_i B^f(t_i)\mathbf{H}^T_i$ is evaluated from the correlation model, and the state update is given by:

$$\mathbf{x}^a(t_i) = \mathbf{x}^f(t_i) + \mathbf{K}_i^{OI}\mathbf{d}_i \qquad (5.25)$$

5.5.3. Variational methods

Several schemes have been implemented using variational methods such as 3D-Var, e.g. the Navy Coupled Ocean Data Assimilation (NCODA) (Cummings, 2005) and the Forecasting Ocean Assimilation Model (FOAM) (Martin et al., 2007). 4D-Var methods are used extensively in Numerical Weather Prediction and are one of the future directions for ocean prediction systems. The NEMOVAR system (Mogensen et al., 2012) is able to handle both categories of variational approaches for the NEMO modelling system.

Following Ide et al. (1997), 4D-Var minimises the objective function J that measures the weighted sum of distance J^b to the background state $\mathbf{x}^b$ and J^o to the observation $\mathbf{y}^o$ distributed over a time interval $[t_0, t_n]$:

$$J[\mathbf{x}(t_0)] = \frac{1}{2}\left[\mathbf{x}(t_0)) - x^b(t_0)\right]^T\mathbf{B}_0^{-1}\left[\mathbf{x}(t_0)) - \mathbf{x}^b(t_0)\right]$$
$$+ \frac{1}{2}\sum_{i=0}^{N}\left[\mathbf{y}_i - \mathbf{y}_i^0\right]^T\mathbf{R}_i^{-1}\left[\mathbf{y}_i - \mathbf{y}_i^0\right] \qquad (5.26)$$

where $\mathrm{y}_i \equiv H_i[\mathrm{x}(t_i)]$. Here B^{-1} is an a priori weight matrix, with B meant to approximate the error covariance matrix x^b, and a minimization is done with respect to the initial state $x(t_0)$.

Equation 5.25 reflects the imposition of a strong constraint (Sasaki, 1970). Alternative formulations based on a weak constraint are given by Bennett (1992) and by Menard and Daley (1996). Efficient methods for performing the minimization of J require its partial derivatives with respect to the elements of $\mathrm{x}(t_0)$ given by:

$$\left[\frac{\partial J}{\partial x(t_0)}\right] = \mathbf{B}_0^{-1}\left[\mathbf{x}(t_0) - \mathbf{x}^b(t_0)\right]$$
$$+ \sum_{i=0}^{N}\mathbf{M}(t_{i+1}, t_0)^T\mathbf{H}_i^T\mathbf{R}_i^{-1}(\mathbf{y}_i - \mathbf{y}_i^0) \qquad (5.27)$$

where:

$$\mathbf{M}(t_i, t_0)^T = \Pi_{j=0}^{i-1}\mathbf{M}(t_{j+1}, t_j)^T \qquad (5.28)$$

This follows from:

$$\left[\frac{\partial J}{\partial\mathbf{x}_{i+1}^f}\right]^T = \mathbf{M}(t_{i+1}, t_i)^T\left[\frac{\partial J}{\partial\mathbf{x}_i^f}\right]^T \qquad (5.29)$$

$$\left[\frac{\partial J}{\partial\mathbf{x}_i}\right]^T = \mathbf{H}_i^T\left[\frac{\partial J}{\partial\mathbf{y}_i}\right]^T \qquad (5.30)$$

$\mathbf{M}(t_{i+1}, t_i)^T$ is usually called adjoint model and $\mathbf{H}^T_i$ is the adjoint observation operator. 4D-Var reduces to three-dimensional variational assimilation (3D-Var) if the time dimension is taken out.

Figure 5.9 shows an example of 4D-Var capacity: x_a is used as the initial state for a forecast, then by construction of 4D-Var one is sure that the forecast will be completely consistent with the model equations and the 4D distribution of observations until the end of the 4D-Var time interval n (the cutoff time).
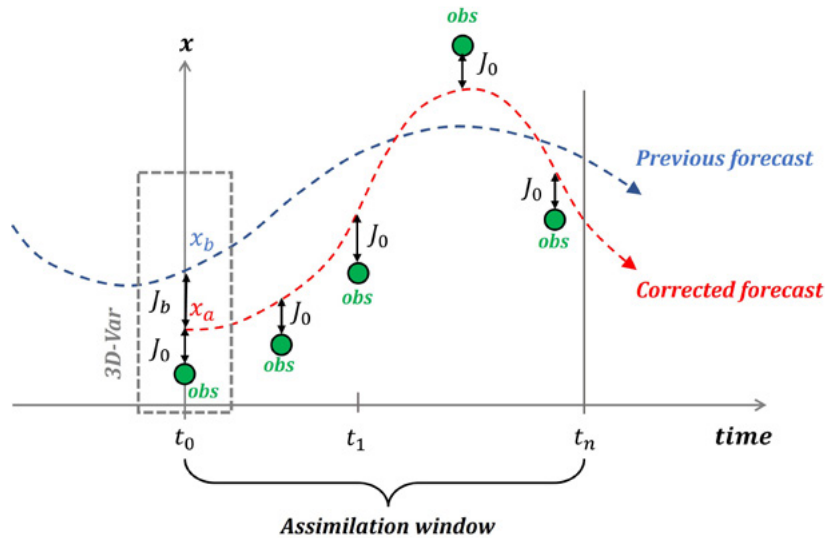
Figure 5.9. Example of 4D-Var intermittent assimilation in a numerical forecasting system (adapted from Bouttier and Courtier 2002).

5.5.4. Modelling errors

As reported in Bouttier and Courtier (2002), to represent the fact that there is some uncertainty in the background and in the analysis, we need to assume some model of the errors between these vectors.

Given a background field $\mathbf{x}_b$ just before doing an analysis, we define the vector of errors that separates it from the true state:

$$\epsilon_b = \mathbf{x}_b - \mathbf{x}_t \qquad (5.31)$$

If we are able to repeat each analysis experiment a large number of times, under exactly same conditions but with different realisation of errors generated by unknown causes, b would be different every time. It can be represented through a probability density function (PDF), able to provide all statistics, including the average (or expectation) -b and the variances. A popular model of scalar pdf is the Gaussian function, that can be generalised to a multivariate PDF.

The errors in the background and in the observations are modelled as follows:

- Background errors. They are the estimation errors of the background state, given by the difference between the background state vector and its true value;
- Observation errors. They contain errors in the observation process (i.e instrumental errors), errors in the design of the operator H, and representativeness errors (i.e. discretization errors which prevent x^t from being a perfect image of the true state;

- Analysis error. Defined through the trace of the covariance matrix $\mathbf{A}$:

$$Tr(\mathbf{A}) = \overline{\| \epsilon_a - \bar{\epsilon}_a \|^2} \qquad (5.32)$$

They are the estimation errors of the analysis state, which is what we want to minimize. In a scalar system, the background error covariance is the variance:

$$\mathbf{B} = var(\epsilon_b) = var\overline{| \epsilon_b - \bar{\epsilon}_b |^2} \qquad (5.33)$$

In a multidimensional system, B is a square symmetric matrix with n×n dimension. The diagonal of B contains the variances, while the off-diagonal contains the cross-covariances between a pair of variables in the model. The off-diagonal terms can be transformed into error correlations:

$$\rho(e_i, e_j) = \frac{cov(e_i, e_j)}{\sqrt{var(e_i)var(e_j)}} \qquad (5.34)$$

The error statistics are functions of the physical processes governing the meteorological or the ocean state and the observing network. They depend on a priori knowledge of the errors: variances reflect our uncertainty in features of the background or the observations. To estimate statistics, it is necessary to assume that they are stationary over a period and uniform over a domain, so that one can take a number of error realisations and make empirical statistics.

In setting a DAS, the estimated statistics is very difficult and we can rely on diagnostics of an existing data assimilation system using the observational method.

5.5.5. Overview of current data assimilation systems in operational forecasting

Data assimilation techniques, schematically introduced in previous paragraphs and that are widely documented in Daley (1991), Evensen (2003) and Zaron (2011), represent the baseline of the modelling framework with general circulation models for operational forecasting and reanalysis. At international level, the GODAE's OceanView (Bell et al., 2015) and OceanPredict initiatives have promoted strong synergies with GOOS, ETOOFS and GEO BluePlanet contributing to a value chain from observations, data, information systems, predictions, and scientific assessments to end users, with the aim to promote the use and impact of observations and ocean predictions for societal benefit, and increasing visibility of operational oceanography advances.

Martin et al. (2015) presents an overview of the main characteristics of the data assimilation used in each GODAE OceanView systems; this is a list of the adopted numerical techniques:

- Bluelink (Oke et al., 2013) adopts MOM4 ocean model and EnOI algorithm;
- GIOPS (Smith et al., 2016) uses NEMO ocean model and SEEK (with fixed basis) for the ocean component, and 3DVar for assimilation in the ice component;
- ECMWF (Balmaseda et al., 2013) uses NEMO ocean model and 3DVar for the assimilation component (+ bias correction technique);
- FOAM (Waters et al., 2014) uses NEMO ocean model and 3DVar for the assimilation component (+ bias correction technique);
- GOFS (Cummings and Smedstad, 2013) uses HYCOM ocean model with 3DVar data assimilation scheme;
- Mercator Ocean (Lellouche et al., 2013) uses NEMO ocean model with SEEK-FGAT (with fixed basis) and 3DVar bias correction;
- MOVE (Usui et al., 2006) uses MRI COM model and 3DVar data assimilation scheme;
- TOPAZ (Sakov et al., 2012) uses HYCOM with EnKF techniques.

Description of the operational initiatives is also provided at GODAE OceanView website (🔗 ²) and OceanPredict website (🔗 ³).

5.6.
Ensemble modelling

Numerical models, applied to nonlinear dynamical systems such as the ocean, inevitably approximate the solution of the so-called Navier-Stokes shallow-water equations, because of limitations in computer power to resolve the whole spectrum of geophysical processes. In addition, numerical modelling is subject to numerous inherent uncertainties related to modelling parameters, to forcing functions, to initial and boundary conditions. This is why a single forecast is, to some extent, uncertain, and we use ensemble modelling to answer how uncertain a forecast is. Ensemble prediction systems (EPS) are well-known in atmospheric science communities for more than 25 years (Palmer, 2018) but are more recent in operational oceanography, with marked advances in the last decade (e.g., TOPAZ system, Sakov et al., 2012). EPS uses ensemble modelling and adds other components, such as probabilistic outputs and soon machine learning under varying flavours, with prediction as objective. In most cases, EPS also incorporates ensemble-based data assimilation (DA) to decrease forecast errors.

Due to the chaotic nature of the ocean, the probabilistic approach is an interesting alternative beyond the classic deterministic approach, and it can help users to interpret model predictions supplemented by their uncertainties. Ensemble modelling consists of possible ocean states using Monte Carlo techniques to sample the probability density function (pdf) of the model forecast. Each model simulation is called an ensemble member. This approach is illustrated in Figure 5.10a. The ensemble is initialised by a sample of different initial conditions (e.g. perturbed analyses in DA). The model operator (which can be also perturbed during integration) is then used to bring forward in time each member and produce an ensemble of model simulations. The ensemble members may diverge radically or remain broadly similar, resulting in a forecast PDF. A quantitative assessment of the ensemble is depicted in Figure 5.10b. The ensemble mean and spread (estimating model uncertainty) are calculated as first and second order statistical moments from the members, and can be compared with the unperturbed deterministic simulation and the climatology (and to observations, if available). The ensemble spread is flow-dependent

2. https://www.godae-oceanview.org/
3. http://oceanpredict19.org
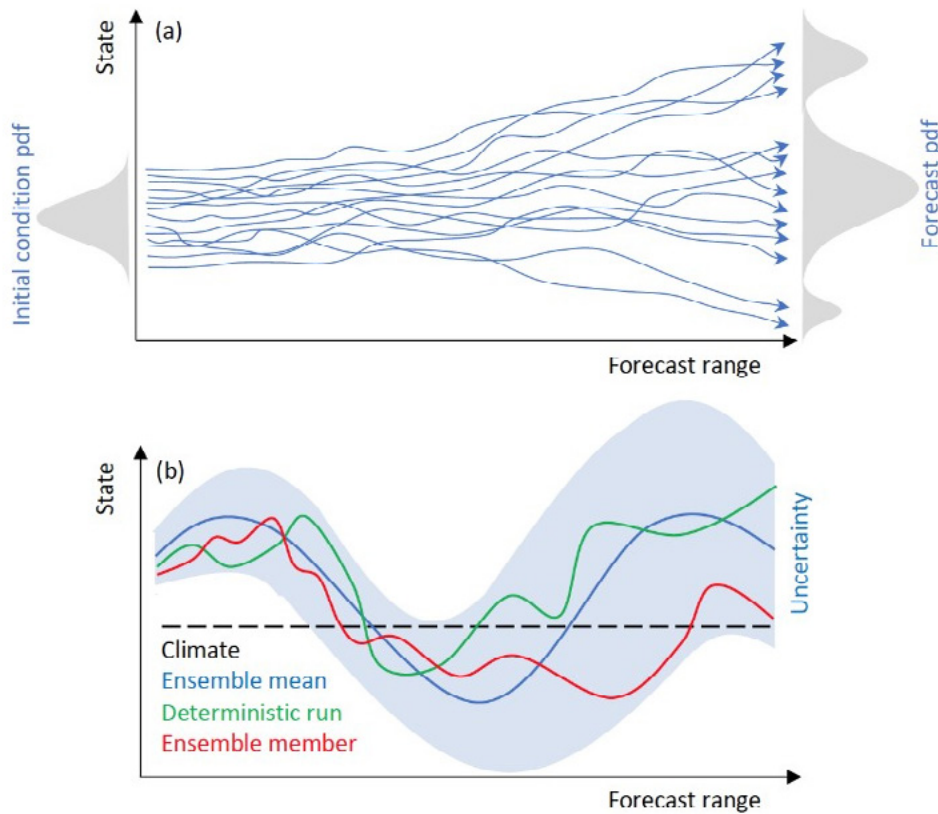
Figure 5.10. (a) Schematic of an ensemble simulation with equiprobable forecasts (blue trajectories); the forecast pdf gives an indication of the likelihood of occurrence of the different states; (b) Schematic of the flow-dependent ensemble spread in relation to the ensemble mean, an individual member, the unperturbed deterministic run, and the climatology (credits: 🔗 4).

and varies for different state variables. Ensemble forecasting aims at quantifying this flow-dependent uncertainty. EPS are highly demanding systems in terms of computational resources and can be run efficiently in HPC facilities. A major challenge for the next generation of OOFSs is to improve their services by integrating ensemble capabilities in their systems.

5.6.1. Basic concepts

There are three main categories of ocean model ensembles: (a) multi-model ensembles, e.g. Copernicus Marine Service multi-model products and CMIP6 coupled models for climate studies (🔗 5); (b) stochastic model ensembles, used in research e.g. the OCCIPUT project (Penduff et al., 2014), and less frequently in operational oceanography due to their computational cost; and (c) ocean model response to an atmospheric EPS, e.g. using the ECMWF-EPS atmospheric forcing(🔗 6).

The focus here is on the practical aspects for the implementation of a stochastic ocean model, mainly for short- to medium-range forecasting applications. The notion "stochastic model" for a system exhibiting chaotic behaviour can be defined by the partial differential Fokker-Planck equation, describing the temporal evolution of the state pdf, controlled by stochastic diffusion and advection processes, and local model tendencies. Stochastic modelling is used to represent model errors and as an ulterior step can be integrated in ensemble-based DA. Several methods and tools to produce stochastic model ensembles have been discussed in the literature following the SANGOMA project (🔗 7).

The main objectives of (ensemble) stochastic modelling are: (a) the estimation of model uncertainties providing realistic error bars and confidence intervals at useful ranges for ocean predictions; and (b) using model uncertainties in a DA framework to enrich background error covariances with flow-dependent errors and improve model prediction at the range of the outer loop of the DA scheme. The most useful

4.https://confluence.ecmwf.int/
5. https://www.wcrp-climate.org
6. https://www.ecmwf.int/en/forecasts

7. http://www.data-assimilation.net

statistical properties are the ensemble mean, the covariances and spread given by the diagonal of the covariance matrix, and sometimes the higher order moments (Quattrocchi et al., 2014). Stochastic ensembles are not used solely for DA but can be applied also as a machine learning base for artificial intelligence applications, guiding observational strategies based on array design (Charria et al., 2016; Lamouroux et al., 2016), and enabling probabilistic forecasting (Cheng et al., 2020), e.g. occurrence of ocean upwelling or bloom events, occurrence of sea level and storm surge exceeding a particular threshold, sea ice concentration, etc.

The main elements to be decided and identified when generating an ocean model ensemble are: (a) the relevant quantities to perturb; (b) the stochastic parameterizations; and (c) the dynamical balances that must be preserved, if any (which in turn influence choices in (a)). These notions are often combined under the term "stochastic physics".

The ensemble verification is an important integral part of the ensemble modelling and EPS-developing process. An ensemble empirical consistency aims at verifying a posteriori the model pdf approximated by the ensemble of forecasts, with respect to existing observations and their pdfs. The underlying notion is the model and data joint probability on the right-hand-side of the equal sign in the Bayes theorem. Empirical consistency can be explored by specific criteria and analysis tools, e.g. from rank histograms being the simplest measuring "reliability" (Candille and Talagrand, 2005) to Desroziers et al. (2005) consistency diagnostics on innovations and ensemble pattern-selective consistency analysis (Vervatis et al., 2021a). The "reliability" measures to which degree the forecast probabilities agree with outcome frequencies and is an important attribute for the development of probabilistic scores. Such scores are for example the Continuous Rank Probability Score (CRPS) (Hersbach, 2000; Candille and Talagrand, 2005) and the Brier Score measuring, in addition to "reliability", the attribute of "resolution". For a reliable EPS, "resolution" is the ability to separate cases when an event occurs or not, i.e. probabilities being close to 0 or 1. The ensemble consistency evaluation framework provides important information to test the relevance of an EPS when the system is set-up (e.g. the ensemble size).

5.6.2. Ocean model uncertainties

Ocean model uncertainties emerge from sources of errors relevant to the ocean state, including physics, biogeochemistry, and sea ice, as well as errors in the initial state and boundary conditions (i.e. atmospheric forcing and lateral open boundary conditions). Model uncertainties in ocean physics have a significant impact in all other system components as, for example, in biogeochemistry and sea ice. The choice of the perturbed model quantities depends: (a) on the ocean application, e.g. global vs regional and coastal configurations,

and short- to medium- or seasonal-range forecasts; (b) on the processes resolved by the model (or not, such as sub-grid scale processes); (c) on choices in the DA framework, e.g. variational and Kalman filter approaches, variables and parameters included in the control vector, assimilated observations etc.; and (d) on the dynamical balances the user wants to preserve in the perturbation space, e.g. leaving velocities unperturbed tends to preserve the degree of geostrophy of the ocean state.

Recent advances in NEMO incorporated an easy-to-use modelling framework for the production of ocean model ensembles (Brankart et al., 2015), including the following schemes applied also in NWP systems: SPPT (Buizza et al., 1999), SPUF (Brankart, 2013), SPP (Ollinaho, et al., 2017) and SKEB (Berner et al., 2009). The stochastic parameterizations in all schemes are implemented via first-order autoregressive Markov processes, i.e. a statistical model based on the assumption that the past value of uncertainty determines the present within some error. Several studies expand the NEMO ensemble framework (Bessières et al., 2017; Vervatis et al., 2021b), incorporating a stochastic ocean physics package (Storto and Andriopoulos, 2021).

The SPPT perturbs the net parameterized model tendencies, assumed to contain upscaled ocean model errors due to sub-grid parameterizations. The SPUF scheme is based on random walks sampling gradients (which represent the sub-grid unresolved scales) from the state vector and adding them to the models' solution; the random walks consist of independent consecutive steps in all directions. The SPP introduces perturbations at each time step to parameters within the model parameterization schemes. The SKEB adds perturbations to the barotropic stream function, upscaling a fraction of the dissipated energy back to the resolved flow, which is often useful assuming that the inverse cascade of energy is underestimated in ocean models due to unresolved sub-grid processes.

Selecting the appropriate perturbation scheme and properly tuning the stochastic parameterizations for the autoregressive processes (for each of the perturbed model quantities) are essential steps to produce meaningful stochastic ensembles. All stochastic perturbation schemes have their advantages and disadvantages (e.g. energy and mass conservation laws, production of over/under-dispersive ensembles, etc.), though the SPPT scheme appears to be the most effective (in terms of generating sufficient model spread) and easiest to use (in terms of stochastic parameterizations) for many model quantities.

A common approach to generate stochastic ocean model ensembles is by using a pseudorandom combination of multivariate empirical orthogonal functions (EOFs) to perturb the wind forcing (Vervatis et al., 2016). The wind has a large impact on upper-ocean model uncertainties because it controls the Ekman and geostrophic components of the Sverdrup dynamics; it

also largely drives the shelf-seas dynamics in addition to tides. In general, all surface atmospheric forcing variables constitute major sources of ocean model uncertainties. Momentum, heat, and freshwater fluxes are key quantities coupling the air-sea processes and are parametrized in terms of bulk coefficients. These model parameters can also be stochastically perturbed (in addition to atmospheric forcing) with spatiotemporal varying patterns (or by applying simple Gaussian noise, if there is no information available regarding their scales).

Complementary to stochastic approaches, ocean model uncertainties can be introduced by making use of an atmospheric ensemble. Using an atmospheric EPS does not necessarily outperform the stochastic modelling approach in terms of ocean model spread. In general, it takes longer for the ensemble to spin-up and increase its spread, and the method also requires a large amount of data to process. On the other hand, the main advantage of using an atmospheric EPS is the realism of the fields in terms of conserved quantities. A common approach of a marine EPS generated by an atmospheric EPS, used successfully at operational centres, is the ocean wind-wave ensemble forecasting (Janssen, 2004).

In the ocean interior below the seasonal thermocline, model uncertainties can be introduced effectively by perturbing the ocean boundary conditions and the water column properties. Such perturbations are usually difficult to implement because of the need to ensure physical consistency in the water column, and because errors in the prescribed boundary fields are usually unknown. A favourable solution for the open boundaries is when a coarse parent ensemble is available providing uncertainty estimates to the nested child model (Ghantous et al., 2020).

Methods incorporating polynomial chaos expansions along with EOF-based perturbations of temperature and salinity profiles in isopycnal coordinate space, can be applied efficiently in estimating model error propagation in the open boundaries (Thacker et al., 2012). Model uncertainties affecting also the water column properties can be applied in the equation of state by perturbing the temperature and salinity state, using the SPUF method aimed at representing sub-grid unresolved scales. Other quantities that can be perturbed in the ocean interior and its boundaries are the model bathymetry influencing the barotropic and baroclinic states (Lima et al., 2019), the bottom drag coefficient affecting the bottom Ekman flow transport and tidal mixing in shelf-seas (Vervatis et al., 2021b), and the SSH together with depth integrated velocities in tidal open boundaries (Barth et al., 2009).

Inflation methods and bred vectors for short-range ocean prediction systems can be used to initialise an ensemble of forecasts. The choice of perturbing initial conditions is also relevant to DA, for example using ensemble-based hybrid variational methods such as the 4D-EnsVar controlling (possibly among other quantities) the initial conditions.

Ensemble-based DA methods are used to improve the predictive skill of biogeochemical and sea-ice models. In these Earth system components, model errors stem from unresolved diversity, unresolved scales, and multiple model parameterizations. The unresolved diversity refers for example to the biodiversity restriction, including only a few species in the biogeochemical model, and to restrictions in the categorization of sea-ice in an effort to reduce complexity and state variables. These diversity restrictions often lead to missing model processes that are instead approximated by parameterizations. On the other hand, the unresolved scales depend on the model resolution (in a way similar to the unresolved scales for physics).

In this context, the most common quantities to perturb in biogeochemical models are the sources and sinks (e.g. photosynthesis, respiration, death, and grazing), and the biogeochemical parameters controlling some of these processes (e.g. growth and mortality rates, nutrient limitations, grazing, etc.) (Santana-Falcón et al., 2020). Other biogeochemical model state uncertainties depend on the water column optical properties and the penetrative solar radiation, affecting photosynthesis and primary production (Ciavatta et al., 2014). An anamorphosis transformation in lognormal space is required for any use of the stochastic biogeochemical outputs that involve Gaussian distributions, such as variance analysis or DA (Simon and Bertino, 2009). This latter attribute of selecting a positive distribution function to introduce model uncertainties is also followed for sea-ice perturbations, e.g. using a gamma distribution for the sea-ice strength variable to improve DA and model performance for sea-ice concentration and sea-ice thickness (Juricke et al., 2013).

5.6.3. Towards ocean EPS

A summary of the practical aspects and challenges of a road-map towards ocean probabilistic forecasting for the next generation of OOFS is as follows. Initially, ensemble forecasting should be developed and tested without the use of DA. This will allow operational centres to coordinate their activities, such as: (a) preparing OGCM platforms for the production of ensembles, e.g. several choices among regional centres tuning the stochastic parameterizations; (b) integrating ensembles in their operational chain assessing the computational cost (doubled for DA) and which variables are essential to archive; and (c) providing tools for the interpretation of uncertainty estimates as well as guiding users to extract information from ensembles, e.g. ocean indices for the probabilistic detection of events. An open issue in this first step, without DA, is how ensembles are going to be initialised in an operational context. In a second step, within a DA framework, the initialization of the ensemble is part of the DA process.

5.7.
Validation strategies

As explained in Section 4.5.2, four classes of metrics (Figure 4.30) were defined and adopted by GODAE OceanPredict and have been extensively used for the validation of OO model products since the first validation and intercomparisons exercises (Crosnier and Le Provost, 2007; Ryan et al., 2015). It is indeed necessary to use a complete range of statistics and comparisons in space and time to properly assess the consistency, representativeness, accuracy, performance, and robustness of ocean model outputs. One of the first steps at all stages of the validation procedure is usually to compare the surface temperature (analysed, and at various forecast length) with contemporaneous satellite observations, which is a good example of CLASS1 metrics (Figure 5.11). Sea surface temperature is a signature of ocean-atmosphere interactions and it is critical for many maritime applications, while being one of the major sources of uncertainty for ocean model analyses and forecasts. This type of comparison allows a day-to-day control of atmospheric forcing inconsistencies

and large scale features of the systematic biases can also be monitored on the longer terms.

Another important step is to check the local behaviour of the model analyses and forecast for several time frequencies (tidal, non-tidal) using fixed buoys observations, for instance for sea surface height against tide gauges (CLASS2 metrics, Figure 5.12). This type of metrics is essential for the overall assessment of the representativeness of a physical model solution. Many statistical estimators can be used to compare models to observations within this CLASS1 and CLASS2 framework, but also spectral analysis, extreme events characterization, and mesoscale feature detection can be performed at this stage. This surface "satellite" approach (2-dimensional with time) and local approach (1-dimension with time) must be combined with the monitoring of the basin scale or global scale behaviour of the ocean, integrated in space (3-dimensions) and/or time, such as the validation and intercomparison
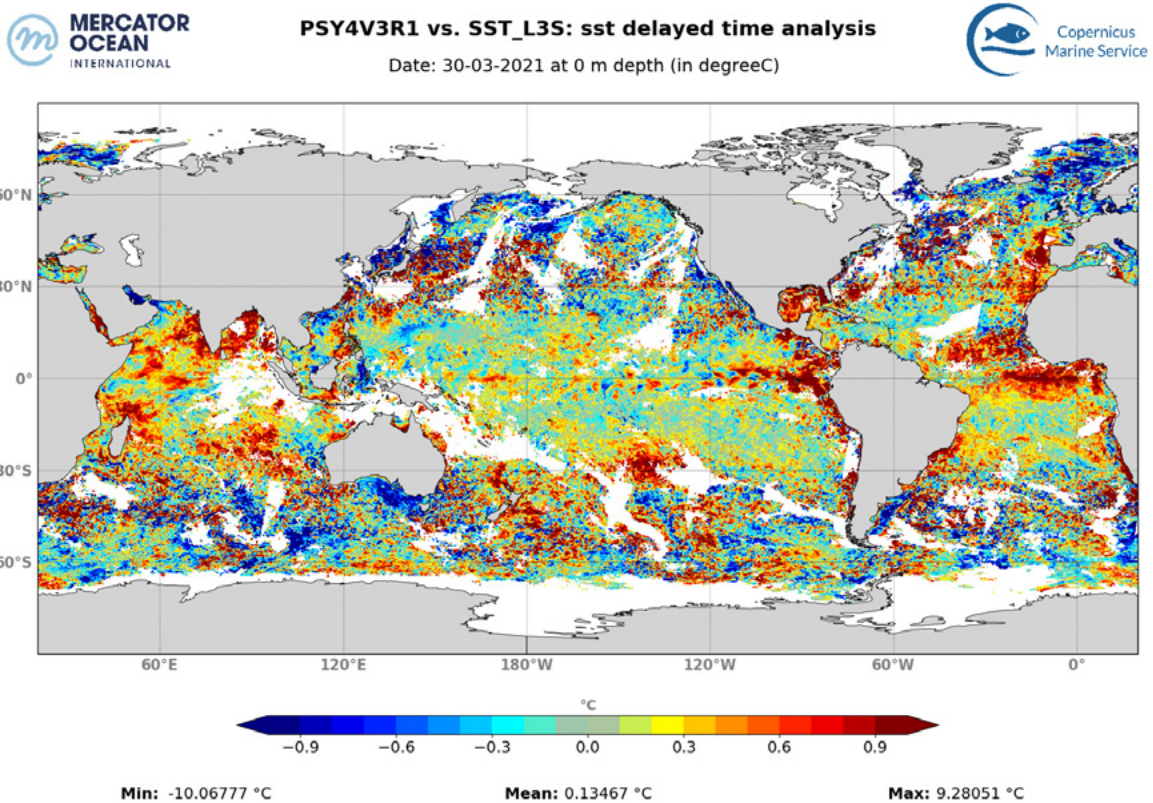
Figure 5.11. Copernicus Marine Service global model SST analysis minus gridded supercollated SST observations on 03/30/2021 (°C).
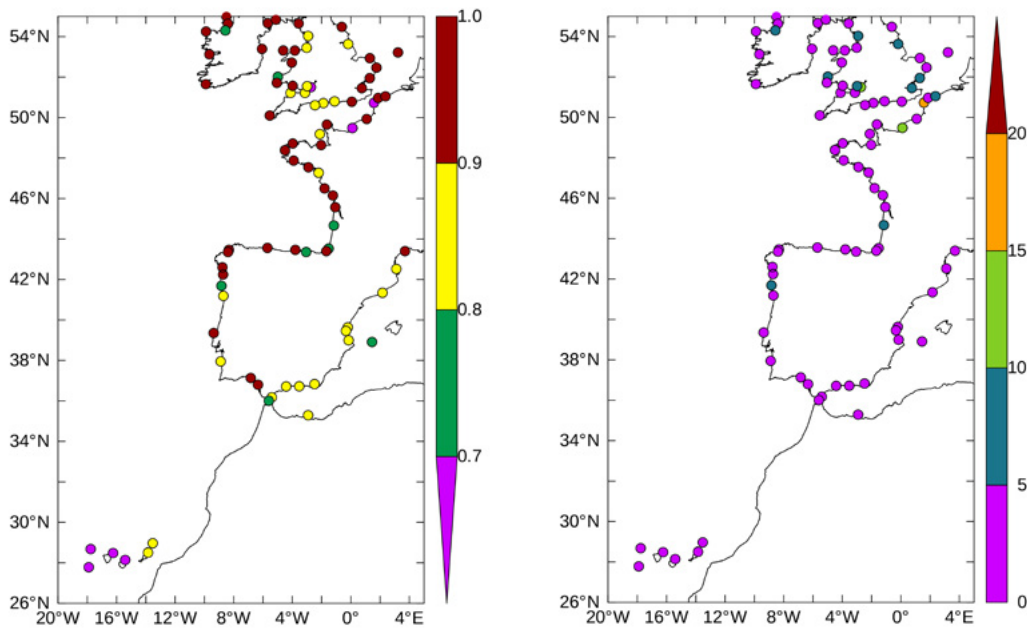
Figure 5.12. Correlation (left) and RMS difference (cm)(right) between the Iberia-Biscay-Ireland model analyses by Copernicus Marine Service and the observations of the residual elevation at tide gauges´ locations (January 2017 to December 2018) (courtesy of Bruno Levier, Mercator Océan).
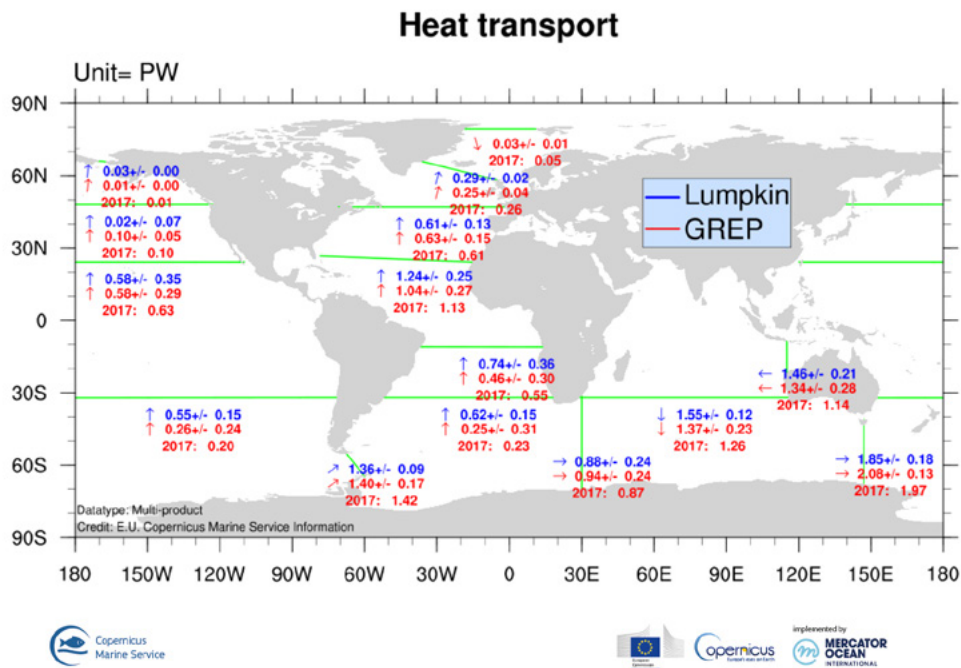
Figure 5.13. Heat transport (PW) from Copernicus Marine Service global reanalysis ensemble product (🔗 8) compared with estimates of Lumpkin and Speer (2007). Uncertainty ranges are derived from the ensemble standard deviation. Arrows indicate the direction of the mean flow through the sections.

8.https://marine.copernicus.eu/access-data/ocean-monitoring-indicators/mean-heat-transport-across-sections

of ocean monitoring indicators. The intercomparison of integrated heat transports (CLASS3 metrics, Figure 5.12) with values from the literature (Lumpkin and Speer, 2007) is a good example of diagnostic which can help identify biases, drifts or limitations in the model's representation of the ocean circulation, while it also provides valuable information on the ocean state and variability. Additionally, the intercomparison of several model estimates, whenever possible, allows to derive a range of likely values for ocean monitoring indicators, and to assess the robustness of the model solution. In Figure 5.13 the standard deviation between four ocean reanalyses (varying in their configuration and data assimilation
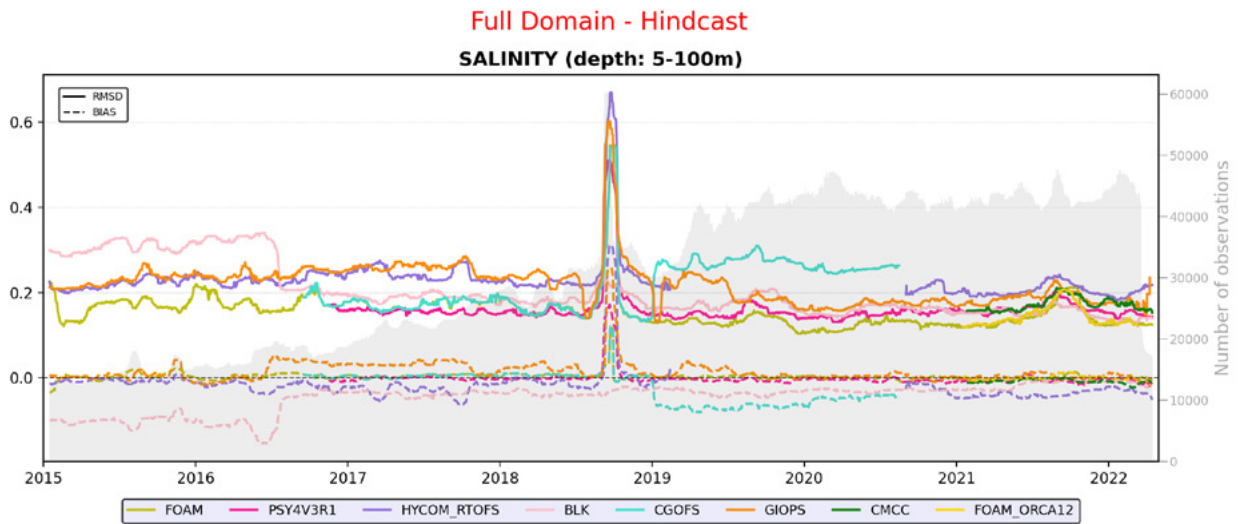
Figure 5.14. Performance of GODAE OceanPredict global forecasting systems, in terms of global mean departures from salinity in-situ profiles observations (psu) in the 0-500m layer. The time evolution of the mean bias between the model forecast (12h) and the observations is shown by dotted lines, and the root mean square difference is shown by solid lines (courtesy of Charly Régnier, Mercator Ocean).
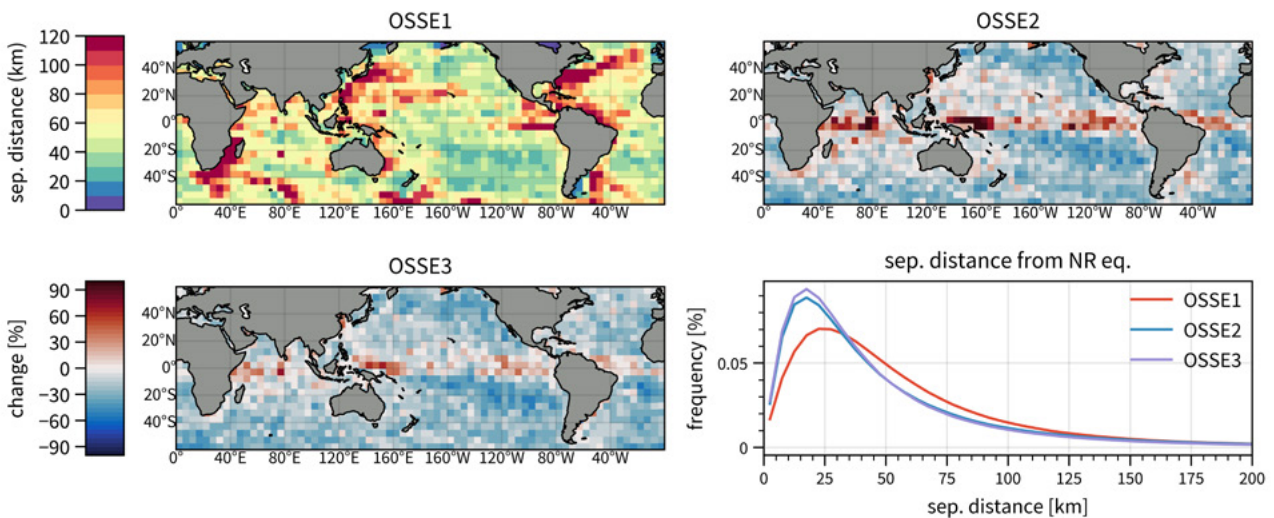
Figure 5.15. Results of a Lagrangian experiment. Panels: a) the metric corresponds to the distance separating the true position of the particle in NR with that of the OSSE1 (3Nadir) after 7 days, averaged in 5-degree bins; b) and c) show the average change in separation distance (reduction in blue) obtained when using instead OSSE2 and OSSE3 surface currents, with an overall improvement; and d) global distributions of the separation distance in each experiment (courtesy of Simon van Gennip, Mercator Ocean).

settings) based on the same model (NEMO) were used to derive the uncertainty associated with each heat transport estimate.

Finally, CLASS1-2-3 must be complemented by quality indicators averaged in space at basin scale, and possibly in time, in order to monitor and quantify the individual performance of model solutions. To this aim, data assimilation misfits (innovations and residuals) are extensively used, as observation operators, developed within data assimilation schemes, usually provide the most adequate transposition of the model solution into the observations' space. CLASS4 metrics can be computed offline in delayed time, outside of the data assimilation process, to add the possibility to compare residual differences with one given observation between various forecast lengths, to compare with climatology and persistence, and finally to derive forecast skill scores. Hence, independent observations (not assimilated) can be used to compute CLASS4 metrics, and reference datasets can be defined to build robust

intercomparison frameworks. For instance, ARGO floats measurements are only used by the GODAE OceanPredict community in order to measure performance in salinity as illustrated by Figure 5.14 (Ryan et al., 2015). A spike in the statistics corresponds to a campaign at sea in the Arctic in 2018, which shows that, despite a growing observing network, these statistics suffer from representativeness issues.

As at high resolution (a few km or less) the small scales are not constrained by observations, the performance measured by direct or statistical comparisons to observations may not be as good as for coarser model solutions, which is referred to as the "double penalty" effect (Ebert, 2009). Neighbourhood metrics (Mittermaier et al., 2013, 2021) focus on the ability of a model to forecast a range of events within a neighbourhood in space and time, and for which the direct or statistical comparisons to observations at all time and space scales would not be informative.
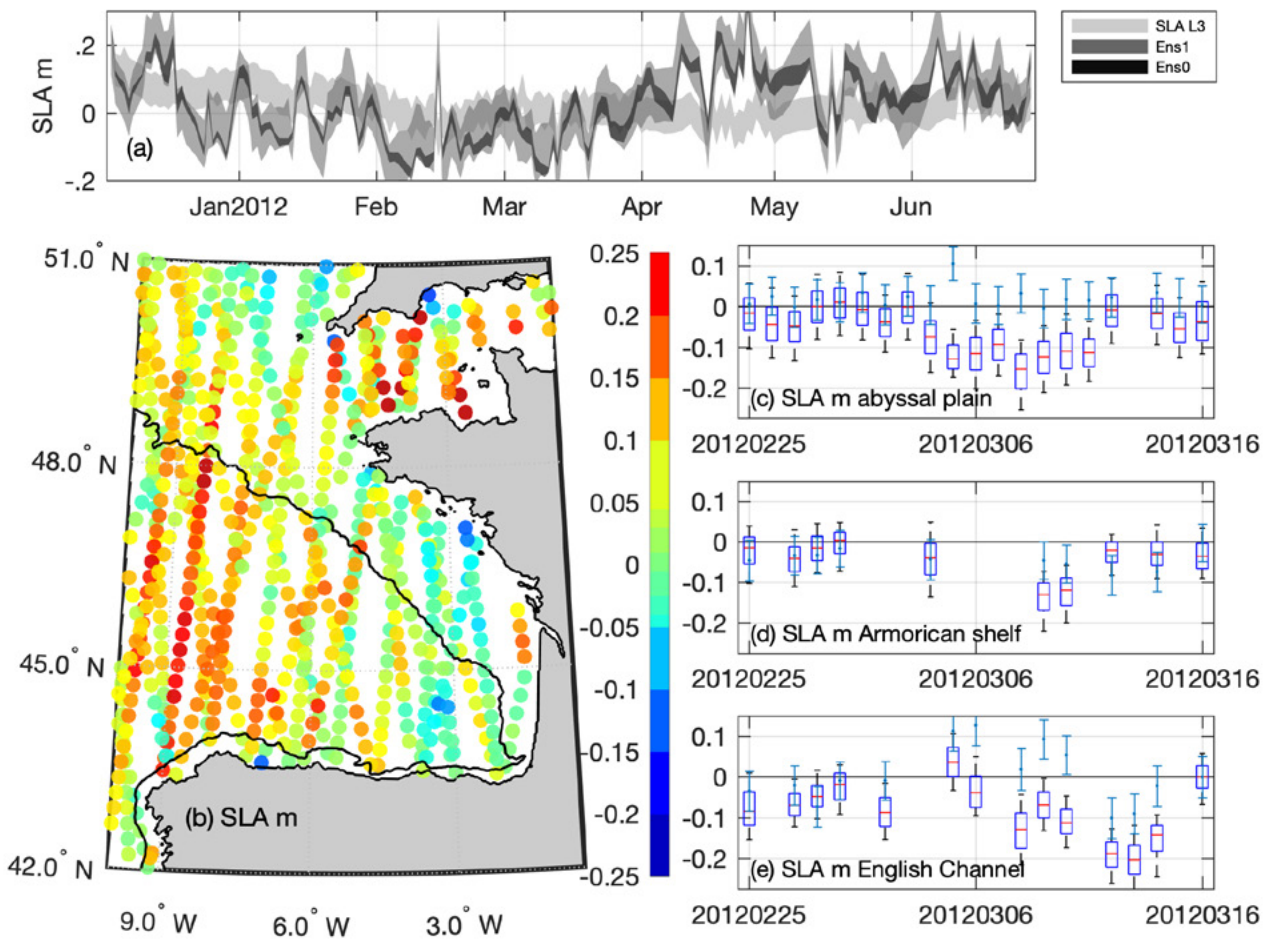
Figure 5.16.   a) SLA along track L3 observation distribution (in meters) and two model ensembles in data space; (b) "Observation minus Ensemble" map for a period starting on 25 February 2012 and for three consecutive weeks; (c) box-whisker plots and observation error bars averaged over the abyssal plain; (d) the Armorican shelf; and (e) the English Channel.

Additionally, "user oriented" metrics focusing on processes or using downstream applications can reduce this effect and allow to better assess the fit-for-purpose of ocean analyses and forecasts, among which we can cite eddies (Mason et al., 2014), fronts detection (Ren et al., 2021), and lagrangian drift scores. Lagrangian separation distance scores and distributions (shown in Figure 5.15) are a primary validation diagnostic when studying the impact of changes in the observations network (Tchonang et al., 2021). Figure 5.15 shows, in particular, results of a Lagrangian experiment wherein particles seeded in every model grid cell (1/12 degree resolution) and advected for 7 days in the Nature Run and three different OSSEs surface currents (OSSE1 collecting and assimilating 3 nadir-like satellite altimeters, and OSSE2 SWOT-like satellite altimeter, and OSSE3 nadir-like and one SWOT-like satellite altimeters).

Ensemble scores applied to ensemble forecasts (see Section 5.6) also allow better study of predictability and, eventually, to validate and quantify the skill of the forecast. This is needed in particular for mesoscale features (Thoppil et al,. 2021). In the near future, it is essential to add this type of verification and quantification of uncertainty to the range of validation metrics. Figure 5.16 illustrates examples of ensemble diagnostics (Vervatis et al., 2021a) important to be checked in the development phase and during the production to verify consistency between ensemble model distribution and observation. Figure 5.16a compares the distribution of observations (light grey) and of two ensemble simulations (dark grey); a good quality criterion is the distribution of ensemble members overlapping the distribution of the observations, if this should not be investigated. Figure 5.16b shows the bias between ensemble members and observations in the observations' space for a dedicated period. Errors can also be quantified in physically consistent domains as illustrated in Figure 5.16c, where the consistency between box-whisker plots of the ensemble members distributions and error bars can be assessed for observations in the same area.

5.8.
Outputs

Information on formats and types of outputs of all kinds of OOFS can be found in Chapter 4. The following section treats only some specific aspects related to circulation modelling.

5.8.1. Variables/EOV

The circulation modelling variables describe any system related to the production of 3D ocean dynamics variables.

The main physics variables (with their abbreviation or acronym) are:

- Temperature

  - temperature [T]
  - sea surface temperature [SST]
  - bottom temperature bottom [bottomT]

- Density [D]
- Salinity [S]
- Sea Surface Height [SSH]

  - above sea level
  - above geoid
  - geopotential height

- Velocity
- Velocity [UV/W]

  - geostrophic velocity [UV/UVG]
  - barotropic velocity [UVB]

- Mixed Layer Depth [MLD]
- Sea Ice

  - sea ice concentration [SIC]
  - sea ice edge [SIE]
  - sea ice extent [SIE]
  - sea ice thickness [SIT]
  - sea ice velocity [SIUV]
  - sea ice drift [SIUV]
  - snow [SNOW]
  - iceberg [ICBG]
  - sea ice age [SIAGE]
  - sea ice albedo [SIALB]
  - sea ice temperature [IST]

The variables follow the CF standards. The CF Metadata Conventions are a widely used standard for atmospheric, ocean, and climate data. Standard names are defined in a CF Standard Name Table (see 🔗 [9]).

9. http://cfconventions.org/standard-names.html

5.9.
Inventories

The purpose of this section is to provide an initial inventory of the operational Near Real Time (NRT) and Multi Year (MY) systems operating at international level. Details about the specific system, resolution, implemented circulation model, and data assimilation are provided in the following lists, along with the observations used for assimilation and assessment, summary of the main offered product catalogue and, where existing, the website address to directly link to systems products and other relevant information.

5.9.1. Inventory of operational global to regional to coastal to local forecasting systems

The present state-of-the-art operational systems for NRT products from global to local scale is presented in Table 5.2. This proposed inventory has been prepared in collaboration with the Coastal and Shelf Seas (COSS-TT) Working Group, one of the OceanPredict Task Teams. An evolutive list of Regional/Coastal Ocean Forecasting Systems (R/COFS) is maintained by the COSS-TT in the System Information Table (SIT) (latest version available at 🔗[10]). Due to the shorter lifespan and more frequent updates in coastal systems compared to global and basin-scale systems, the SIT is frequently refreshed and then please refer to the latest online version for up-to-date information. In addition to operational/NRT systems, the online SIT contains also tools (e.g. used for applications, crisis-time scenarios, etc.), research and pre-operational models, etc.

5.9.2. Inventory of multi-year systems

Starting from the list in Balmaseda et al. 2015, an initial inventory of state-of-the-art MY systems has been prepared (Table 5.3). As in Table 5.2, for each system is provided scale (from global to regional), resolution, models, and providers, as well as relevant links to web pages that the reader may consult for further details.

---

10. https://oceanpredict.org/science/task-team-activities/coastal-ocean-and-shelf-seas/#section-sit

Table 5.2. Initial inventory of global (G) to regional (R) to coastal (C) to local (L) operational forecasting systems.

Scale	System	Area	Resolution	Circulation model	Data used for assimilation and assessment	Downscaling/ nesting	Products	Website
G	OceanMAPS, BLUElink (Bureau of Meteorology)	Global ocean	0.1 degree grid spacing at the Australia region	MOM4	BODAS is an ensemble optimal interpolation system used to assimilate available in-situ and satellite obs.	N/A	Daily T, S, SSH and UV	https://re-search.csiro.au/bluelink/global/fore-cast/
G	CONCEPTS GIOPS (Government of Canada)	Global ocean	1/4° horizontal resolution	NEMO	SEEK scheme, using INS, SLA, SST obs.	N/A	Daily 10-days forecast for T, S, SSH, UV, sea ice concentration	https://science.gc.ca/eic/site/063.nsf/eng/h_97631.html
G	ECCO: Estimating the Circulation and Climate of the Ocean	Global ocean	The horizontal resolution varies spatially from 22 km to 110 km	MITgcm	Assimilation of INS, SLA, SST obs.	N/A	Daily forecast for T, S, SSH, UV, fluxes, sea ice	https://ec-co-group.org/products-EC-CO-V4r4.htm
G	FOAM: Forecast Ocean Assimilation Model system	Global ocean	1/4° horizontal resolution	NEMO	NEMOVAR (3D-Var scheme) using INS, SLA, SST obs.	N/A	Daily mean, analysis and five-day forecast for T, S, SSH, UV, sea ice	https://www.metoffice.gov.uk/research/weather/ocean-fore-casting
G	NAVOCEANO, the US Naval Oceanographic Office (US)	Global ocean	1/12° horizontal resolution	HYCOM	Hybrid data assimilation scheme	N/A	Daily forecast for ocean fields	https://www.metoffice.gov.uk/research/weather/ocean-fore-casting
G	INCOIS, the Indian National Centre for Ocean Information Service	Global ocean	horizontal resolution at 1/4° with 40 vertical sigma levels	ROMS	N/A	N/A	Daily 5 days forecast for surface UV, SST, MLD, waves and winds	https://in-cois.gov.in/

Scale	System	Area	Resolution	Circulation model	Data used for assimilation and assessment	Downscaling/ nesting	Products	Website
G	GOFS16 CMCC Global Ocean Forecasting System	Global ocean	1/16° horizontal resolution and 98 vertical levels	NEMO	OceanVar (3D-Var scheme) using INS, SL, SST, SICE obs.	N/A	Daily analysis and 7 days forecast for T, S, SSH, UV, sea ice	https://gofs.cmcc.it/
G	Global MFC by Copernicus Marine Service (MOI, France)	Global ocean	1/12° horizontal resolution and 50 vertical levels	NEMO	SAM2 (SEEK scheme) using INS, SLA, SST obs.	N/A	Daily analysis and 10 days forecast for T, S, SSH, UV, sea ice	https://marine.copernicus.eu
G/R	MOVE/MRI.COM-JPN (MRI, Japan)	Global, North Pacific, Japan	Double nested system consisting of global (GLB), North Pacific (NP) and Japan area (JPN) models Ocean model : MRI.COM with resolutions: (JPN) 1/33° x 1/50°, 60 levels; (NP) 1/11° x 1/10°, 60 levels; (GLB) 1°x1/2° (tripolar), 60 levels	MRI.COM	4DVAR (applied to a reduced grid version of NP model). Assessment: Tide gauge, In-situ observations (buoy, T-S profiles), HF radars, satellite (SST, SSH, sea ice concentration), volume transport at repeated hydrographic sections.	Downscaling: one/two-way nesting with IAU initialization	Real time monitoring and prediction, re-analysis of: T, S, UV, SSH, sea ice concentration, tropical cyclone heat potential (TCHP)	https://ds.data.jma.go.jp/tcc/tcc/products/elnino/move_mricom-g2_doc.html
R	Arctic MFC by Copernicus Marine Service (NERSC, Norway)	Arctic Region	12.5 km at the North Pole	HYCOM	EnKF assimilation scheme using INS, SLA, SST and SICE obs.	N/A	Daily analysis and 10 days forecast for T, S, SSH, UV, sea ice	https://marine.copernicus.eu
R	Baltic MFC by Copernicus Marine Service (SHMI, Sweden)	Baltic Sea	0.028 degrees x 0.017 degrees in horizontal and 56 levels	NEMO	PDAF LESTKF univariate for SST	1-way nested into NWS-MFC Copernicus Marine Service regional product	Daily analysis and 6 days forecast for T, S, SSH, MLD, UV	https://marine.copernicus.eu
R	Mediterranean Sea MFC by Copernicus Marine Service (CMCC, Italy)	Mediterranean Sea	1/24° in horizontal and 141 vertical levels, 2-way coupled to WW3 wave model	NEMO	OceanVar (3D-Var scheme) using INS, SL, SST obs.	1-way nested into GLO-MFC Copernicus Marine Service (1/12°, 50 vertical levels)	Analysis and 10 days forecast for T, S, SSH, UV, MLD, fluxes, sea icea	https://marine.copernicus.eu, https://medfs.cmcc.it/

Scale	System	Area	Resolution	Circulation model	Data used for assimilation and assessment	Downscaling/ nesting	Products	Website
R	Irish-Biscay-Iberian shelves MFC by Copernicus Marine Service (Mercator Ocean International, France / Spain)	Irish-Biscay-Iberian shelves	1/36° in horizontal and 50 vertical levels	NEMO	SEEK scheme, using INS, SL, SST obs.	1-way nested into GLO-MFC Copernicus Marine Service (1/12°, 50 vertical levels)	Analysis and 5 days forecast for T, S, SSH, UV, MLD	https:// marine. copernicus.eu
R	North-West shelf MFC by Copernicus Marine Service (Met Office, UK)	European North-West shelf Seas	1.5 km in horizontal and 51 hybrid s-sigma terrain-following coordinates on the vertical	NEMO	NEMOVAR (3D-Var scheme) using INS, SL, SST obs.	1-way nested into Met Office FOAM NATL (1/12°; 6 hourly fields) and Baltic Sea physics by Copernicus Marine Service (2 km, 1 hourly fields)	Analysis and 5 days forecast for T, S, SSH, UV, MLD	https:// marine. copernicus.eu
R	Black Sea MFC by Copernicus Marine Service (CMCC, Italy)	Black Sea	1/40° in horizontal and 121 vertical levels	NEMO	OceanVar (3D-Var scheme) using INS, SL, SST obs.	Lateral open boundary conditions from the Unstructured Turkish Straits System (U-TSS, Ilicak et al. 2021)	Analysis and 10 days forecast for T, S, SSH, UV, MLD	https:// marine. copernicus.eu
R	High Resolution Data Assimilative Model for Coastal and Shelf Seas around China (Institute of Atmospheric Physics/Chinese Academy of Sciences, China)	Northwest Pacific, coastal seas around China			Assessment: SST, SLA, temperature, buoys, ship cruises	2-way nesting	Daily averaged 3-D fields of UV, T, S	

Scale	System	Area	Resolution	Circulation model	Data used for assimilation and assessment	Downscaling/ nesting	Products	Website
R/C	MARC: Modelling and Analyses for Coastal Research and ILICO: Coastal Ocean and Nearshore Observation Research Infrastructure (Ifremer, France)	Bay of Biscay / English Channel / Northwestern Mediterranean Sea	2.5 km horizontal resolution and 40 levels	MARS3D	SST, HF Radar (sea state + currents), Moored buoys (T,S)	Spectral nudging, one-way nesting using GLO-MFC products and 2D models for tides	1 hr output in Bay of Biscay, 3 hr output in Mediterranean Sea, HF observations (20min)	MARC: http://marc.ifremer.fr ILICO: https://www.ir-ilico.fr/en
R/C	SOMISANA (SAEON/DFFE, South Africa)	Algoa Bay, south coast, South Africa	Horizontal grid that decreases from ~3km at the edges to 500 m within the bay	CROCO	No DA. Assessment is based on Underwater Temperature Recorder (UTR) and ADCP data	1-way nested into GLO-PHY (1/12°, 50 vertical levels)	SSH, 3D T, S and UV, trajectories from hypothetical oil spills	http://ocim-stest.ocean.gov.za/aloga_bay_model
R/C	CNAPS Coupled Northwest Atlantic Prediction System (North Carolina State University, USA)	Northwest Atlantic coast ocean, including the entire east coast of U.S., the Gulf of Mexico and Caribbean seas	Horizontal resolution < 7 km	ROMS	HF Radar, buoy, ship, satellite observations	1-way nesting with Mercator Ocean GLO-PHY; Global HyCOM; WWIII	Daily nowcast and 3-day forecast for UV, T, S, ocean waves and atmospheric variables	http://omgsrv1.meas.ncsu.edu:8080/CNAPS/
R/C	REMO Oceanographic Modeling and Observation Network (Brazilian Navy Hydrographic Center, Brazil)	Region between latitudes 35.5°S and 7°N and longitude 20°W to the Brazilian coast	2 grids, at 1/12° and 1/24° horizontal resolutions for the eastern, southeastern and southern regions	HYCOM	The system assimilates vertical profiles of temperature (T) and salinity (S) from the ARGO system, XBTs, CTDs, Sea Level Anomaly, SST; assessment using AVISO SL, SST, INS	TPXO 7.1 for tides; one-way nesting from the 1/12° resolution to the 1/24° resolution grid	4-day forecasts (T, UV and SSH) at 6-hour intervals updated daily on 2 different grids	https://www.marinha.mil.br/chm/dados-do-smm-modelagem-numerica-te-la-de-chama-da/modela-gem-numerica

Scale	System	Area	Resolution	Circulation model	Data used for assimilation and assessment	Downscaling/nesting	Products	Website
R/C	DREAMS: Data assimilation Research of the East Asian Marine System (RIAM, Kyushu University, Japan)	Northwestern Pacific with focus on marginal seas	DREAMS_marginal seas model at ~7.4km horizontal resolution. Coastal models at ~1.5km along the Japan Sea coast nested in DREAMS_marginal seas model	RIAM	Assessment: Volume transport through the Tsushima Strait, U, V and T measurements by fishing vessels	OBC from climatological run	T, S, U, V, sea level, mixed layer depth, density	https://dreams-c1.riam.kyushu-u.ac.jp/vwp
R to L	BSH Operational Model System (BSH, Germany)	North and Baltic Sea, German coastal waters	Horizontal resolution is 3 km for the North and Baltic Sea, 0.5 km for German coastal waters	HBM	Assimilation with PDAF scheme using AVHRR SST/Sentinel-3 SST and validation using Copernicus Marine Service data	2-way nesting among regional and coastal models	120-hour forecast from 0 and 12 UTC and a 78-hour forecast from 6 and 18 UTC; water level, T, S, UV, ice products and biogeochemical variables	https://www.bsh.de/EN/DATA/Predictions/predictions_node.html
R to L	COSYNA	North Sea, German Bight, German Wadden Sea	3 nested models: i) North Sea Baltic Sea model (5 km), ii) German Bight model (1 km, varying unstructured-grid, 1km), iii) Estuarine model (varying unstructured-grid, 20-200 m)	GETM	Assessment with independent ADCP observations, FerryBox data, dedicated profile measurements, intercomparison with products from other operational systems	MyOcean ECOOP, OSTIA, MERIS color data Downscaling using 3 different grids	Surface UV, T, S, suspended matter, wind wave characteristics in the German Bight	http://codm.hzg.de/codm

Scale	System	Area	Resolution	Circulation model	Data used for assimilation and assessment	Downscaling/ nesting	Products	Website
C	PCOMS: Portuguese Coastal Operational Modelling System (MARETEC, Portugal)	Western Iberia region and subregions	5.6 km in horizontal and 50 vertical layers	MOHID 3D	N/A	1-way nesting into Mercator-Ocean PSY2V4 in the North Atlantic; tidal levels computed by a 2D version of MOHID, forced by FES2004, running on a wider region. Climatological profiles from WOA09 for nutrients.	Hindcasts and 3-day forecasts of SSH and 3D UV, T, S and biogeochemical model	http://forecast.maretec.org
C	SANIFS (CMCC, Italy)	Southern Adriatic Northern Ionian coastal Forecasting System	Horizontal resolution from 3 km in open-sea to 100-20 m in coastal areas	SHYFEM	No DA. Assessment using available observations from Copernicus Marine Service, EMODnet and national observing network	1-way nesting using the Copernicus Marine Service Mediterranean MFC regional forecast products (at 1/24°)	Short term forecast (3 days) of SSH, 3D UV, T, S	http://sanifs.cmcc.it
C/L	SAMOA (Puertos del Estado, Spain)	Regional areas at ~ 2 km resolution; model applications consist of 2 nested regular grids with spatial resolution of ~350 m and ~70 m for the coastal and harbour domains	Regional areas at ~ 2 km resolution; model applications consist of 2 nested regular grids with spatial resolution of ~350 m and ~70 m for the coastal and harbour domains	ROMS	No DA. Assessment using in-situ obs. from mooring buoys, ADCPs, tide gauges and drifter buoys; SST satellite data and surface currents from HF radar	1-way nesting using the IBI-MFC Regional Forecast products (at 1/36°)	Daily operational short-term (+72h) met-ocean forecast	http://opendap.puertos.es/thredds/catalog.html ; http://www.puertos.es/es-es/proyectos/Paginas/SAMOA.aspx

Scale	System	Area	Resolution	Circulation model	Data used for assimilation and assessment	Downscaling/ nesting	Products	Website
C/L	NYHOPS: New York Harbor Observation and Prediction System (Jupiter Intelligence, USA)	New York and East Coast of US	7.5 km at the open ocean boundary to less than 50 m	POM	N/A	Offshore boundary tides, surges, waves. Real time data from Ntl Ocean Service, Adv. Hydrologic Prediction Service, Ntl. Climatic Data Center.	72 hr forecasts, nowcasts, 24 hr hindcasts initiated every 6 hrs; Variables: SSH, T, S, UV, winds, coastal waves - height, period and direction, biogeochemical variables	https://hudson.dl.stevens-tech.edu/maritimeforecast/index.shtml
C/L	SWITCH – Georgia Coasts (CMCC / GeorgiaTech, Italy / USA)	Georgia coast, US	1km in open ocean to 100m in coastal areas to 10m in the rivers	SHYFEM	No DA, assessment is based on tide gauges at coast and along rivers	1-way nested into GLO-PHY (1/12°, 50 vertical levels)	3-days forecast for SSH, 3D UV, T, S	https://savannah.cmcc.it
L	Tagus Mouth operational model (MARETEC / IST, Portugal)	Tagus Estuary and Mouth region	Variable horizontal resolution, ranging from 2 km off the coast up to 400 m inside the estuary, 50 layers in the vertical	MOHID 3D	No DA. Assessment: Argo and buoys data from IBI-ROOS and the Portuguese hydrographic institute, satellite images (ODYSSEA, Ocean Colour and HF radar)	1-way nesting using the PCOMS	Hindcasts and 3-day forecasts of SSH and 3D UV, T, S and biogeochemical model	http://forecast.maretec.org/tagusmouth

Table 5.3. Initial inventory of global (G) to regional (R) to coastal (C) to local (L) multi-year systems.

Scale	System	Area	Resolution	Circulation model	Data Assimilation scheme	Downscaling/ nesting	Timeseries	Website
G	CFSR by the Climate Prediction Center	Global Ocean	~ 38 km horizontal resolution and 64 vertical levels	MOM4	3D-Var scheme for the assimilation of SST, INS, SICE obs.	N/A	1979-2010	https://rda.ucar.edu/#!lfd?n-b=y&b=proj&v=NCEP%20Climate%20Forecast%20System%20Reanalysis
G	C-GLORS by the Euro-Mediterranean Center on Climate Change Foundation	Global Ocean	1/4° horizontal resolution and 50 to 75 levels	NEMO	OceanVar (3D-Var scheme) using INS, SLA, SST and SICE obs.	N/A	1990-2016	http://c-glors.cmcc.it/index/index.html
G	ECCO by JPL-NASA	Global Ocean	The horizontal resolution varies spatially from 22 km to 110 km	MitGCM	4D-Var scheme for the assimilation of SLA, SST and INS obs.	N/A	1992-2017	www.ecco-group.org
G	GECCO by University of Hamburg	Global Ocean		MitGCM	4D-Var scheme for the assimilation of SLA, SST and INS obs.	N/A	1948-2018	www.ecco-group.org
G	ECDA by the Geophysical Fluid Dynamics Laboratory	Global Ocean	1° horizontal resolution and 50 vertical levels	MOM4	EnKF scheme using INS, SST and SLA obs.	N/A	Integration for the 20th Century	http://www.gfdl.noaa.gov/ocean-data-assimilation
G	GloSea5 (UK MetOffice, UK)	Global Ocean	1/4° horizontal resolution and 75 levels	NEMO	3D-Var scheme using SLA, SST, INS and SICE obs.	N/A	1993-2015	https://www.metoffice.gov.uk/research/

Scale	System	Area	Resolution	Circulation model	Data Assimilation scheme	Downscaling/ nesting	Timeseries	Website
G	K7-ODA (Japan Agency for Marine-Earth Science and Technology)	Global Ocean	1° horizontal resolution and 45 levels	MOM3	4D-Var adjont method for the assimilation of INS, SLA, SST obs.	N/A	1957-2009	http://www.godac.jam-stec.go.jp/estoc/e/
G	PEODAS (Centre for Australian Weather and Climate Research - Bureau of Meteorology)	Global Ocean	1° x 2° horizontal resolution	MOM2	EnKF for the assimilation of INS and SST obs.	N/A	2000-2010	https://www.cawcr.gov.au/
G	ORAS5 (ECMWF, UK)	Global Ocean	1° horizontal resolution	NEMO	3D-Var scheme using SLA, INS and SST obs.	N/A	1979-present	https://www.ecmwf.int/en/research/climate-re-analysis/ocean-re-analysis
G	MOVE-C RA (Japan Meteorological Agency)	Global Ocean	1° horizontal resolution	MRI.COM2	3D-Var scheme using SLA, INS and SST obs.	N/A	1950-2011	https://www.mri-jma.go.jp/
G	SODA (National Center for Atmospheric Research Staff, US)	Global Ocean	1/4° horizontal resolution	POP2.1	OI for INS and SST obs.	N/A	1869-2010	https://climatedataguide.ucar.edu/climate-data/soda-simple-ocean-data-assimilation
G	Global Ocean MFC by Copernicus Marine Service (MOI, France)	Global Ocean	1/12° horizontal resolution, 50 vertical levels	NEMO	Reduced-order Kalman filter for assimilating SLA, SST, INS and SICE obs.	N/A	1993-2019	https://marine.copernicus.eu
R	Arctic MFC by Copernicus Marine Service (NERSC, Norway)	Arctic Region	12.5 km horizontal resolution and 12 levels	HYCOM	DEnKF for assimilating satellite and INS obs.	N/A	1991-2019	https://marine.copernicus.eu

Scale	System	Area	Resolution	Circulation model	Data Assimilation scheme	Downscaling/ nesting	Timeseries	Website
R	Baltic MFC by Copernicus Marine Service (SHMI, Sweden)	Baltic Sea	0.05556 degrees x 0.03333 degrees horizontal resolution and 56 vertical levels	NEMO	LSEIK data assimilation scheme	At the lateral boundaries in the western English Channel and along the Scotland-Norway boundary, the sea levels are prescribed using a coarse (24 nautical miles resolution) storm-surge model called NOAMOD (North Atlantic Model). Climatological monthly mean values of salinity and temperature are used at the boundary, and it is assumed there is no sea ice	1993-2019	https:// marine. copernicus.eu
R	North-West shelf MFC by Copernicus Marine Service (Met Office, UK)	North West Shelf Seas	7 km horizontal resolution and 24 vertical levels	NEMO	NEMOVAR (3D-Var scheme) using SST and INS obs.	1-way nested into the Global Ocean MFC and Baltic MFC reanalysis products	1993-2019	https:// marine. copernicus.eu
R	Irish-Biscay-Iberian shelves MFC by Copernicus Marine Service (Puertos del Estado, Spain)	Irish-Biscay-Iberian shelves	1/12° horizontal resolution	NEMO	SEEK scheme, using INS, SL, SST obs.	1-way nested into the Global Ocean MFC reanalysis product at 1/4° horizontal resolution	1993-2019	https:// marine. copernicus.eu
R	Mediterranean Sea MFC by Copernicus Marine Service (CMCC, Italy)	Mediterranean Sea	1/24° in horizontal and 141 vertical levels	NEMO	OceanVar (3D-Var scheme) using INS, SLA, SST obs.	1-way nested into C-GLORS	1993-2019	https:// marine. copernicus.eu
R	Black Sea MFC by Copernicus Marine Service (CMCC, Italy)	Black Sea	3 km horizontal resolution and 31 vertical levels	NEMO	OceanVar (3D-Var scheme) using INS, SLA, SST obs.	N/A	1993-2019	https:// marine. copernicus.eu

5.10.
References

Balmaseda, M. A., Mogensen, K., and Weaver, A.T. (2013). Evaluation of the ECMWF ocean reanalysis system ORAS4. Quarterly Journal of the Royal Meteorological Society, 139, 1132-1161, https://doi.org/10.1002/qj.2063

Balmaseda, M.A., Hernandez, F., Storto , A., Palmer, M.D., Alves, O., Shi, L., Smith, G.C. Toyoda, T., Valdivieso, M., Barnier, B., Behringer, D., Boyer, T., Chang, Y-S., Chepurin, G.A., Ferry, N., Forget, G., Fujii, Y., Good, S., Guinehut, S., Haines, K., Ishikawa, Y., Keeley, S., Köhl, A., Lee, T., Martin, M.J, Masina, S., Masuda, S., Meyssignac, B., Mogensen, K., Parent, L., Peterson, K.A., Tang, Y.M., Yin, Y., Vernieres, G., Wang, X., Waters, J., Wedd, R., Wang, O., Xue, Y., Chevallier, M., Lemieux, J.F., Dupont, F., Kuragano, T., Kamachi, M., Awaji, T., Caltabiano, A., Wilmer-Becker, K., Gaillard, F. (2015). The Ocean Reanalyses Intercomparison Project (ORA-IP). Journal of Operational Oceanography, 8(sup1), s80-s97, https://doi.org/10.1080/1755876X.2015.1022329

Barth, A., Alvera-Azcárate, A., Beckers, J.M., Weisberg, R. H., Vandenbulcke, L., Lenartz, F., and Rixen, M. (2009). Dynamically constrained ensemble perturbations–application to tides on the West Florida Shelf. Ocean Science, 5, 259-270, https://doi.org/10.5194/os-5-259-2009

Bell, M., Schiller, A., Le Traon, P-Y., Smith, N.R., Dombrowsky, E., Wilmer-Becker, K. (2015). An introduction to GODAE OceanView. Journal of Operational Oceanography, 8, 2-11, https://doi.org/10.1080/1755876X.2015.1022041

Bennett, A.F. (1992). Inverse Methods in Physical Oceanography, Cambridge University Press, Cambridge, UK.

Berner, J., G. Shutts, M. Leutbecher, and T. Palmer. (2009). A spectral stochastic kinetic energy backscatter scheme and its impact on flow-dependent predictability in the ECMWF ensemble prediction system. Journal of the Atmospheric Sciences, 66, 603-626, https://doi.org/10.1175/2008JAS2677.1

Bessières, L., Leroux, S., Brankart, J.M., Molines, J.M., Moine, M.P., Bouttier, P.A., Penduff, T., Terray, L., Barnier, B., Sérazin, G. (2017). Development of a probabilistic ocean modelling system based on NEMO 3.5: Application at eddying resolution. Geoscientific Model Development, 10, 1091-1106, https://doi.org/10.5194/gmd-10-1091-2017

Bjerknes, V. (1914). Meteorology as an exact science. Monthly Weather Review, 42(1), 11-14, https://doi.org/10.1175/1520-0493(1914)42<11:MAAES>2.0.CO;2

Blayo, E., and Debreu, L. (1999). Adaptive mesh refinement for finite-difference ocean models: first experiments. Journal of Physical Oceanography, 29(6), 1239-1250, https://doi.org/10.1175/1520-0485(1999)029<1239:AMRFFD>2.0.CO;2

Blayo, E., and Debreu, L. (2005). Revisiting open boundary conditions from the point of view of characteristic variables. Ocean Modelling, 9(3), 231-252, https://doi.org/10.1016/j.ocemod.2004.07.001

Bouttier, F., and Courtier, P. (2002). Data assimilation concepts and methods, March 1999. ECMWF Education material, 59 pp., https://www.ecmwf.int/en/elibrary/16928-data-assimilation-concepts-and-methods

Brankart, J.-M., (2013). Impact of uncertainties in the horizontal density gradient upon low resolution global ocean modelling. Ocean Modelling, 66, 64-76, http://dx.doi.org/10.1016/j.ocemod.2013.02.004

Brankart, J.-M., Candille, G., Garnier, F., Calone, C., Melet, A., Bouttier, P.-A., Brasseur, P., Verron, J., (2015). A generic approach to explicit simulation of uncertainty in the NEMO ocean model. Geoscientific Model Development, 8, 1285-1297, https://doi.org/10.5194/gmd-8-1285-2015

Brassington, G.B., Warren, G., Smith, N., Schiller, A., Oke, P.R. (2005). BLUElink> Progress on operational ocean prediction for Australia. Bulletin of the Australian Meteorological and Oceanographic Society, Vol.18 p. 104.

Buizza, R., Miller, M., Palmer, T.N. (1999). Stochastic representation of model uncertainties in the ECMWF ensemble prediction system. Quarterly Journal of the Royal Meteorological Society, 125, 2887-2908, http://dx.doi.org/10.1002/qj.49712556006

Candille, G., and Talagrand, O. (2005). Evaluation of probabilistic prediction systems for a scalar variable. Quarterly Journal of the Royal Meteorological Society, 131, 2131-2150, https://doi.org/10.1256/qj.04.71

Charria, G., Lamouroux, J., De Mey, P. (2016). Optimizing observational networks combining gliders, moored buoys and FerryBox in the Bay of Biscay and English Channel. J. Mar. Syst., 162, 112-125. http://dx.doi.org/10.1016/j.jmarsys.2016.04.003

Chassignet, E. P., Hurlburt, H. E., Smedstad, O. M., Halliwell, G. R., Hogan, P. J., Wallcraft, A. J., and Bleck, R. (2006). Ocean prediction with the hybrid coordinate ocean model (HYCOM). In "Ocean weather forecasting", 413-426, Springer, Dordrecht, doi:10.1007/1-4020-4028-8_16

Chelton, D. B., DeSzoeke, R. A., Schlax, M. G., El Naggar, K., and Siwertz, N. (1998). Geographical variability of the first baroclinic Rossby radius of deformation. Journal of Physical Oceanography, 28(3), 433-460, https://doi.org/10.1175/1520-0485(1998)028<0433:GVOTFB>2.0.CO;2

Cheng, S., Aydoğdu, A., Rampal, P., Carrassi, A., Bertino, L. (2020). Probabilistic Forecasts of Sea Ice Trajectories in the Arctic: Impact of Uncertainties in Surface Wind and Ice Cohesion. Oceans, 1, 326-342, https://doi.org/10.3390/oceans1040022

Ciavatta, S., Torres, R., Martinez-Vicente, V., Smyth, T., Dall'Olmo, G., Polimene, L., and Allen, J. I. (2014). Assimilation of remotely-sensed optical properties to improve marine biogeochemistry modelling. Progresses in Oceanography, 127, 74-95, https://doi.org/10.1016/j.pocean.2014.06.002

Crosnier, L., and Le Provost, C. (2007). Inter-comparing five forecast operational systems in the North Atlantic and Mediterranean basins: The MERSEA-strand1 Methodology. Journal of Marine Systems, 65(1-4), 354-375, https://doi.org/10.1016/j.jmarsys.2005.01.003

Cummings, J. A. (2005). Operational multivariate ocean data assimilation. Quarterly Journal of the Royal Meteorological Society, 131(613), 3583-3604, https://doi.org/10.1256/qj.05.105

Cummings, J.A., and Smedstad, O.M. (2013). Variational data analysis for the global ocean. In: S.K. Park and L. Xu (Eds.), Data Assimilation for Atmospheric, Oceanic and Hydrologic Applications Vol. II., doi:10.1007/978-3-642-35088-7_13, Springer-Verlag Berlin Heidelberg.

Daley, R. (1991). Atmospheric Data Analysis. Cambridge University Press. 457 pp.

Danilov, S., Kivman, G., and Schröter, J. (2004). A finite-element ocean model: principles and evaluation. Ocean Modelling, 6(2), 125-150, https://doi.org/10.1016/S1463-5003(02)00063-X

Debreu, L., Marchesiello, P., Penven, P., and Cambon, G. (2012). Two-way nesting in split-explicit ocean models: Algorithms, implementation and validation. Ocean Modelling, 49, 1-21, https://doi.org/10.1016/j.ocemod.2012.03.003

Debreu, L., Vouland, C., and Blayo, E. (2008). AGRIF: Adaptive grid refinement in Fortran. Computers & Geosciences, 34(1), 8-13, https://doi.org/10.1016/j.cageo.2007.01.009

De Mey-Frémaux and the Groupe MERCATOR Assimilation (1998). Scientific Feasibility of Data Assimilation in the MERCATOR Project. Technical Report, doi: https://doi.org/10.5281/zenodo.3677206

De Mey P., Craig P., Kindle J., Ishikawa Y., Proctor R., Thompson K., Zhu J., and contributors (2007). Towards the assessment and demonstration of the value of GODAE results for coastal and shelf seas and forecasting systems, 2nd ed. GODAE White Paper, GODAE Coastal and Shelf Seas Working Group (CSSWG), 79 pp. Available online at: http://www.godae.org/CSSWG.html

De Mey-Frémaux, P., Ayoub, N., Barth, A., Brewin, R., Charria, G., Campuzano, F., Ciavatta, S., Cirano, M., Edwards, C.A., Federico, I., Gao, S., Garcia-Hermosa, I., Garcia-Sotillo, M., Hewitt, H., Hole, L.R., Holt, J., King, R., Kourafalou, V., Lu, Y., Mourre, B., Pascual, A., Staneva, J., Stanev, E.V., Wang, H. and Zhu X. (2019). Model-Observations Synergy in the Coastal Ocean. Frontiers in Marine Science, 6:436, https://doi.org/10.3389/fmars.2019.00436

Desroziers, G., Berre, L., Chapnik, B., Poli, P. (2005). Diagnosis of observation, background and analysis-error statistics in observation space. Quarterly Journal of the Royal Meteorological Society, 131, 3385-3396, http://dx.doi.org/10.1256/qj.05.108

Dyke, P. (2016). Modelling Coastal and Marine Processes. 2nd Edition, Imperial College Press, https://doi.org/10.1142/p1028

Ebert, E. E. (2009). Neighborhood verification - a strategy for rewarding close forecasts. Weather and Forecasting, 24(6), 1498-1510, https://doi.org/10.1175/2009WAF2222251.1

Evensen, G. (2003). The ensemble Kalman filter: Theoretical formulation and practical implementation. Ocean dynamics, 53, 343-367, https://doi.org/10.1007/s10236-003-0036-9

Fox-Kemper, B., Adcroft, A., Böning, C.W., Chassignet, E.P., Curchitser, E., Danabasoglu, G., Eden, C., England, M.H., Gerdes, R., Greatbatch, R.J., Griffies, S.M., Hallberg, R.W., Hanert, E., Heimbach, P., Hewitt, H.T., Hill, C.N., Komuro, Y., Legg, S., Le Sommer, J., Masina, S., Marsland, S.J., Penny, S.G., Qiao, F., Ringler, T.D., Treguier, A.M., Tsujino, H., Uotila, P., and Yeager, S.G. (2019). Challenges and Prospects in Ocean Circulation Models. Frontiers in Marine Science, 6:65, https://doi.org/10.3389/fmars.2019.00065

Gerya, T. (2019). Introduction to Numerical Geodynamic Modelling. 2nd edition, Cambridge University Press, https://doi.org/10.1017/9781316534243

Ghantous, M., Ayoub, N., De Mey-Frémaux, P., Vervatis, V., Marsaleix, P. (2020). Ensemble downscaling of a regional ocean model. Ocean Modelling, 145, http://dx.doi.org/10.1016/j.ocemod.2019.101511

Ghil, M., and Melanotte-Rizzoli, P. (1991). Data Assimilation in Meteorology and Oceanography. Advances in Geophysics, 33, 141-266, https://doi.org/10.1016/S0065-2687(08)60442-2

Greenberg, D.A., Dupont, F., Lyard, F., Lynch, D., Werner, F. (2007). Resolution issues in numerical models of oceanic and coastal circulation. Continental Shelf. Research, 27(9), https://doi.org/10.1016/j.csr.2007.01.023

Griffies, S. M., Pacanowski, R. C., and Hallberg, R. W. (2000). Spurious diapycnal mixing associated with advection in a z-coordinate ocean model. Monthly Weather Review, 128, 538-564, https://doi.org/10.1175/1520-0493(2000)128<0538:SDMAWA>2.0.CO;2

Griffies, S. M. (2006). Some ocean model fundamentals. In "Ocean Weather Forecasting", Editoris: E. P. Chassignet and J. Verron, 19-73, Springer-Verlag, Dordrecht, The Netherlands, doi:10.1007/1-4020-4028-8_2

Hallberg, R. (2013). Using a resolution function to regulate parameterizations of oceanic mesoscale eddy effects. Ocean Modelling, 72, 92-103, https://doi.org/10.1016/j.ocemod.2013.08.007

Hersbach H. (2000). Decomposition of the continuous ranked probability score for ensemble prediction systems. Weather and Forecasting, 15(5), 559-570, https://doi.org/10.1175/1520-0434(2000)015<0559:DOTCRP>2.0.CO;2

Herzfeld, M., and Gillibrand, P.A. (2015). Active open boundary forcing using dual relaxation time-scales in downscaled ocean models. Ocean Modelling, 89, 71-83, https://doi.org/10.1016/j.ocemod.2015.02.004

Hewitt, H.T., Roberts, M., Mathiot, P. et al. (2020). Resolving and Parameterising the Ocean Mesoscale in Earth System Models. Current Climate Change Reports, 6, 137-152, https://doi.org/10.1007/s40641-020-00164-w

Hirsch, C. (2007). Numerical Computation of Internal and External Flows - The Fundamentals of Computational Fluid Dynamics. 2nd Edition, Butterworth-Heinemann.

Hunke, E., Allard, R., Blain, P., Blockey, E., Feltham, D., Fichefet, T., Garric, G., Grumbine, R., Lemieux, J.-F., Rasmussen, T., Ribergaard, M., Roberts, A., Schweiger, A., Tietsche, S., Tremblay, B., Vancoppenolle, M., Zhang, J. (2020). Should Sea-Ice Modeling Tools Designed for Climate Research Be Used for Short-Term Forecasting? Current Climate Change Reports, 6, 121-136, https://doi.org/10.1007/s40641-020-00162-y

Ide, K., Courtier, P., Ghil, M., and Lorenc, A. C. (1997). Unified notation for data assimilation: Operational, sequential and variational (Special Issue Data Assimilation in Meteorology and Oceanography: Theory and Practice). Journal of the Meteorological Society of Japan, Ser. II, 75(1B), 181-189, https://doi.org/10.2151/jmsj1965.75.1B_181

Janssen, P.A.E.M., Abdalla, S., Hersbach, H., Bidlot, J.R. (2007). Error estimation of buoy, satellite, and model wave height data. Journal of Atmospheric and Oceanic Technology, 24(9), 1665-1677, https://doi.org/10.1175/JTECH2069.1

Juricke, S., Lemke, P., Timmermann, R., Rackow, T. (2013). Effects of Stochastic Ice Strength Perturbation on Arctic Finite Element Sea Ice Modeling. Journal of Climate, American Meteorological Society, 26(11), 3785-3802, https://doi.org/10.1175/JCLI-D-12-00388.1

Kantha, L. H., & Clayson, C. A. (2000). Numerical models of oceans and oceanic processes. Elsevier, 1-940, ISBN: 978-0-12-434068-8.

Katavouta, A., Thompson, K.R. (2016). Downscaling ocean conditions with application to the Gulf of Maine, Scotian Shelf and adjacent deep ocean. Ocean Modelling, 104, 54-72, https://doi.org/10.1016/j.ocemod.2016.05.007

Lamouroux, J., Charria, G., Mey, P. De, Raynaud, S., Heyraud, C., Craneguy, P., Dumas, F., Le Hénaff, M. (2016). Objective assessment of the contribution of the RECOPESCA network to the monitoring of 3D coastal ocean variables in the Bay of Biscay and the English Channel. Ocean Dynamics, 66(4), 567-588, http://dx.doi.org/10.1007/s10236-016-0938-y

Latif, M., Barnett, T.P., Cane, M.A. et al. (1994). A review of ENSO prediction studies. Climate Dynamics, 9, 167-179.

Le Traon, P. Y., Reppucci, A., Alvarez Fanjul, E., Aouf, L., Behrens, A., Belmonte, M., ... and Zachariouda-ki, A. (2019). From observation to information and users: the Copernicus Marine Service perspective. Frontiers in Marine Science, 6, 234, https://doi.org/10.3389/fmars.2019.00234

Lellouche, J.-M., Le Galloudec, O., Drévillon, M., Régnier, C., Greiner, E., Garric, G., Ferry, N., Desportes, C., Testut, C.-E., Bricaud, C., Bourdallé-Badie, R., Tranchant, B., Benkiran, M., Drillet, Y., Daudin, A., De Nicola, C. (2013). Evaluation of global monitoring and forecasting systems at Mercator Océan. Ocean Science, 9, 57-81, 2013, https://doi.org/10.5194/os-9-57-2013

Lima, L.N., Pezzi, L.P., Penny, S.G., and Tanajura, C.A.S., (2019). An investigation of ocean model uncertainties through ensemble forecast experiments in the Southwest Atlantic Ocean. Journal of Geophysical Research: Oceans, 124, 432-452. https://doi.org/10.1029/2018JC013919

Lumpkin, R., and Speer, K. (2007). Global Ocean Meridional Overturning. Journal of Physical Oceanography, 37(10), 2550-2562, https://doi.org/10.1175/JPO3130.1

Lyard, F. H., Allain, D. J., Cancet, M., Carrere, L., and Picot, N. (2021). Fes2014 global ocean tides atlas: design and performances. Ocean Science, 17, 615-649, https://doi.org/10.5194/os-17-615-2021

Madec, G., and NEMO System Team, (2022). "NEMO ocean engine", Scientific Notes of Climate Modelling Center (27) – ISSN 1288-1619, Institut Pierre-Simon Laplace (IPSL), doi:10.5281/zenodo.6334656

Martin, M. J., Hines, A., and Bell, M. J. (2007). Data assimilation in the FOAM operational short-range ocean forecasting system: a description of the scheme and its impact. Quarterly Journal of the Royal Meteorological Society, 133(625), 981-995, https://doi.org/10.1002/qj.74

Martin, M. J., Balmaseda, M., Bertino, L., Brasseur, P., Brassington, G., Cummings, J., ... and Weaver, A. T. (2015). Status and future of data assimilation in operational oceanography. Journal of Operational Oceanography, 8(sup1), s28-s48, https://doi.org/10.1080/1755876X.2015.1022055

Mason, E., Pascual, A., and McWilliams, J.C. (2014). A new sea surface height–based code for oceanic mesoscale eddy tracking. Journal of Atmospheric and Oceanic Technology, 31(5), 1181-1188, https://doi.org/10.1175/JTECH-D-14-00019.1

Mazloff, M. R., Cornuelle, B., Gille, S. T., Wang, J. (2020). The importance of remote forcing for regional modeling of internal waves. Journal of Geophysical Research: Oceans, 125, e2019JC015623, https://doi.org/10.1029/2019JC015623

Menard, R., and Daley, R. (1996). The application of Kalman smoother theory to the estimation of 4DVAR error statistics. Tellus A: Dynamic Meteorology and Oceanography, 48, 221-237, https://doi.org/10.3402/tellusa.v48i2.12056

Mittermaier, M., Roberts, N., and Thompson, S.A. (2013). A long-term assessment of precipitation forecast skill using the Fractions Skill Score. Meteorological Applications, 20(2), 176-186, https://doi.org/10.1002/met.296

Mittermaier, M., North, R., Maksymczuk, J., Pequignet, C., & Ford, D. (2021). Using feature-based verification methods to explore the spatial and temporal characteristics of forecasts of the 2019 Chlorophyll-a bloom season over the European North-West Shelf. Ocean Science, 17, 1527-1543, https://doi.org/10.5194/os-17-1527-2021

Mogensen, K, Balmaseda, A., Alonso, W.M. (2012). The NEMOVAR ocean data assimilation system as implemented in the ECMWF ocean analysis for System 4. Technical memorandum, doi:10.21957/x5y9yrtm

O'Brien, M.P., and Johnson, J.W. (1947). Wartime research on waves and surf. The Military Engineer, 39, pp. 239-242.

Oke, P. R., Brassington, G. B., Griffin, D. A., and Schiller, A. (2008). The Bluelink ocean data assimilation system (BODAS). Ocean Modelling, 21(1-2), 46-70, https://doi.org/10.1016/j.ocemod.2007.11.002

Ollinaho, P., Lock, S., Leutbecher, M., Bechtold, P., Beljaars, A., Bozzo, A., Forbes, R.M., Haiden, T., Hogan, R.J., Sandu, I. (2017). Towards process-level representation of model uncertainties: stochastically perturbed parametrizations in the ECMWF ensemble. Quarterly Journal of the Royal Meteorological Society, 143, 408-422, http://dx.doi.org/10.1002/qj.2931

Palmer, T. (2018). The ECMWF ensemble prediction system: Looking back (more than) 25 years and projecting forward 25 years. Quarterly Journal of the Royal Meteorological Society, 145, 12-24, https://doi.org/10.1002/qj.3383

Penduff, T., Barnier, B., Terray, L., Sérazin, G., Gregorio, S., Brankart, J.-M., Moine, M.-P., Molines, J.-M., Brasseur, P. (2014). Ensembles of eddying ocean simulations for climate. In: CLIVAR Exchanges, 65(19), 26-29. Available at: https://www.clivar.org/sites/default/files/documents/exchanges65_0.pdf

Pham, D. T., Verron, J., and Roubaud, M.C. (1998). A singular evolutive Kalman filters for data assimilation in oceanography. Journal of Marine Systems, 16(3-4), 323-340, https://doi.org/10.1016/S0924-7963(97)00109-7

Pinardi, N., Lermusiaux, P.F.J., Brink, K.H., Preller, R. H. (2017). The Sea: The science of ocean predictions. Journal of Marine Research, 75(3), 101-102, https://doi.org/10.1357/002224017821836833

Quattrocchi, G., De Mey, P., Ayoub, N., Vervatis, V., Testut, C.-E., Reffray, G., Chanut, J., Drillet, Y., (2014). Characterisation of errors of a regional model of the bay of biscay in response to wind uncertainties: a first step toward a data assimilation system suitable for coastal sea domains. Journal of Operational Oceanography, 7(2), 25-34, https://doi.org/10.1080/1755876X.2014.11020156

Ren, S., Zhu, X., Drevillon, M., Wang, H., Zhang, Y., Zu, Z., Li, A. (2021). Detection of SST Fronts from a High-Resolution Model and Its Preliminary Results in the South China Sea. Journal of Atmospheric and Oceanic Technology, 38(2), 387-403, https://doi.org/10.1175/JTECH-D-20-0118.1

Ryan, A. G., Regnier, C., Divakaran, P., Spindler, T., Mehra, A., Smith, G. C., et al. (2015). GODAE OceanView Class 4 forecast verification framework: global ocean inter-comparison. Journal of Operational Oceanography, 8(sup1), S112-S126, https://doi.org/10.1080/1755876X.2015.1022330

Sakov, P., Counillon, F., Bertino, L., Lisæter, K.A., Oke, P.R., Korablev, A., (2012). TOPAZ4: an ocean-sea ice data assimilation system for the north atlantic and arctic. Ocean Science, 8 (4), 633–656, http://dx.doi.org/10.5194/os-8-633-2012

Sandery, P.A., and Sakov, P. (2017). Ocean forecasting of mesoscale features can deteriorate by increasing model resolution towards the submesoscale. Nature Communications, 8, 1566, http://dx.doi.org/10.1038/s41467-017-01595-0

Santana-Falcón, Y., Brasseur, P., Brankart, J.M., and Garnier, F. (2020). Assimilation of chlorophyll data into a stochastic ensemble simulation for the North Atlantic Ocean. Ocean Science, 16, 1297-1315, https://doi.org/10.5194/os-16-1297-2020

Sasaki, Y. (1970). Some basic formalisms in numerical variational analysis. Monthly Weather Review, 98(12), 875-883.

Sein, D.V., Koldunov, N.K., Danilov, S., Wang,Q., Sidorenko, D., Fast, I., Rackow, T., Cabos, W., Jung, T. (2017). Ocean Modelling on a Mesh With Resolution Following the Local Rossby Radius. Journal of Advances in Modelling Earth Systems, 9:7, 2601-2614, https://doi.org/10.1002/2017MS001099

Simon, E., and Bertino, L. (2009). Application of the Gaussian anamorphosis to assimilation in a 3-D coupled physical-ecosystem model of the North Atlantic with the EnKF: a twin experiment. Ocean Science, 5, 495-510, 2009, https://doi.org/10.5194/os-5-495-2009

Smith, G.M., Roy, F., Reszka, M., Surcel Colan, D., He, Z., Deacu, D., Belanger, J.-M., Skachko,S., Liu, Y., Dupont, F., Lemieux, J.-F., Beaudoin, C., Tranchant, B., Drévillon, M., Garric, G., Testut, G.-E., Lellouche, J.-M., Pellerin, P., Ritchie, H., Lu, Y., Davidson, F., Buehner, M., Caya, A., Lajoie, M. (2016). Sea ice forecast verification in the Canadian Global Ice Ocean Prediction System. Quarterly Journal of the Royal Meteorological Society, 142(695), 659-671, https://doi.org/10.1002/qj.2555

Storto, A., and Andriopoulos, P., (2021). A new stochastic ocean physics package and its application to hybrid-covariance data assimilation. Quarterly Journal of the Royal Meteorological Society, 147, 1691-1725, https://doi.org/10.1002/qj.3990

Tchonang, B.C., Benkiran, M., Le Traon P.-Y., Van Gennip, S.J., Lellocuhe, J.M., Ruggiero, G. (2021). Assessing the impact of the assimilation of SWOT observations in a global high-resolution analysis and forecasting system. Part 2: Results. Frontiers in Marine Science, 8:687414, https://doi.org/10.3389/fmars.2021.687414

Thacker, W.C., Srinivasan, A., Iskandarani, M., Knio, O.M., Le Hénaff, M., (2012). Propagating boundary uncertainties using polynomial expansions. Ocean Modelling, 43-44, 52-63, http://dx.doi.org/10.1016/j.ocemod.2011.11.011

Thoppil, P.G., Frolov, S., Rowley, C.D. et al. (2021). Ensemble forecasting greatly expands the prediction horizon for ocean mesoscale variability. Communications Earth & Environment, 2, 89, https://doi.org/10.1038/s43247-021-00151-5

Toublanc, F., Ayoub, N.K., Lyard, F., Marsaleix, P., Allain, D.J., 2018. Tidal downscaling from the open ocean to the coast: a new approach applied to the Bay of Biscay. Ocean Modelling, 214, 16-32. http://dx.doi.org/10.1016/j.ocemod.2018.02.001

Usui, N., Ishizaki, S., Fujii, Y., Tsujino, H., Yasuda, T., Kamachi, M. (2006). Meteorological Research Institute multivariate ocean variational estimation (MOVE) system: Some early results. Advances in Space Research, 37(4), 806-822, https://doi.org/10.1016/j.asr.2005.09.022

Vervatis, V. D., Testut, C.E.. De Mey, P., Ayoub, N., Chanut, J., Quattrocchi, G. (2016). Data assimilative twin-experiment in a high-resolution Bay of Biscay configuration: 4D EnOI based on stochastic modelling of the wind forcing. Ocean Modelling, 100, 1-19, https://doi.org/10.1016/j.ocemod.2016.01.003

Vervatis, V.D., De Mey-Frémaux, P., Ayoub, N., Karagiorgos, J., Ciavatta, S., Brewin, R., Sofianos, S., (2021a). Assessment of a regional physical-biogeochemical stochastic ocean model. Part 2: empirical consistency. Ocean Modelling, 160, 101770, http://dx.doi.org/10.1016/j.ocemod.2021.101770

Vervatis, V. D., De Mey-Frémaux, P., Ayoub, N., Karagiorgos, J., Ghantous, M., Kailas, M., Testut, C.-E., and Sofianos, S., (2021b). Assessment of a regional physical-biogeochemical stochastic ocean model. Part 1: ensemble generation. Ocean Modelling, 160, 101781, https://doi.org/10.1016/j.ocemod.2021.101781

Waters, J., Lea, D.L., Martin, M.J., Mirouze, I., Weaver, A., While, J. (2014). Implementing a variational data assimilation system in an operational 1/4 degree global ocean model. Quarterly Journal of the Royal Meteorological Society, 141(687), 333-349, https://doi.org/10.1002/qj.2388

Zaron, E.D. (2011). Introduction to Ocean Data Assimilation. In: Schiller, A., Brassington, G. (eds) "Operational Oceanography in the 21st Century". Springer, Dordrecht. https://doi.org/10.1007/978-94-007-0332-2_13

6.
Sea Ice modelling

CHAPTER COORDINATOR

Laurent Bertino

CHAPTER AUTHORS *(in alphabetical order)*

Ed Blockley, Johnny A. Johannessen, and Einar Örn Ólason

6. Sea Ice modelling

6.1. General introduction to sea ice models

6.1.1. Objective, applications and beneficiaries

6.1.2. Fundamental theoretical background

6.2. Sea Ice forecast and multi-year systems

6.2.1. Architecture singularities

6.2.2. Input data: available sources and data handling

6.2.3. Modelling component

6.2.3.1. Basic equations and modelling choices

6.2.3.2. Sea ice rheology

6.2.3.3. Community sea-ice models

6.2.3.4. Coupling of sea ice to atmosphere and ocean

6.2.3.5. Model setup

6.2.4. Ensemble Modelling

6.2.5. Data Assimilation systems

6.2.5.1. Ensemble-based methods

6.2.5.2. Variational methods

6.2.5.3. Challenges with coupled data assimilation

6.2.6. Validation strategies

6.2.7. Outputs

6.2.8. Examples of operational sea ice forecasting systems

6.3. References

6.1.
General introduction to sea ice models

6.1.1. Objective, applications and beneficiaries

The main objective of an operational sea ice forecasting system is to provide users with a reliable estimate of the state of the ice cover and its temporal evolution. To meet this purpose, the system needs to be coupled to, or use data from, ocean and atmosphere forecasting systems. Some form of data assimilation is also required to counteract errors due to the chaotic nature of the atmosphere-ocean-ice system. Users of sea ice forecasting systems are either stakeholders operating in the Arctic or downstream service providers who use the information as an input to their own services. With a changing climate and a warming Arctic, the number of stakeholders interested in operating in that region is growing.

The Arctic is getting warmer with temperatures rising at approximately twice the rate of the global average (Overland et al., 2016) but also more attractive for business as its natural resources are becoming available for exploitation and transport for the first time in our history. These include about 13% of the world's oil and gas resources as estimated by the United States Geological Survey (Gautier et al., 2009), gold and other metals, and 5.5% of the freshwater resources stored on Greenland (Kundzewicz et al., 2007). Changing environmental conditions are modifying ecosystems in diverse ways. In the Barents Sea, the cod are thriving thanks to warming conditions (Kjesbu et al., 2014). A migration behaviour of boreal generalist fishes to cooler waters is also observed in the Bering Sea (Mueter and Litzow, 2008). These changes have implications for fisheries management and more generally for the Arctic ecosystem. Cruise tourism in the Arctic is also developing fast since operators can offer comfortable icebreaker cruises all the way to the North Pole.

The NSR along the Russian coast of the Arctic, which was heavily used by the Soviet Union until the 1990's, could again become an attractive alternative to reach East Asia from Western Europe. The route is indeed shorter than the one crossing Suez Passage (17000 km instead of 22000 km for a Rotterdam-Shanghai voyage) and would save fuel. However, in case of accidents, cargo and fuel would pose serious threats for the Arctic environment. Coastguards and navies of the Arctic nations must then be prepared for assisting vessels, performing search and rescue operations, and remediating oil spills in ice-infested waters, with frequently poor communication capabilities that may hinder access to new information.

The oil and gas exploration and production need sea ice forecasting both on local scales, to simulate individual ice floes on the theatre of their operations, and on large scales, to predict the time of the freeze up and break-up of the ice. It is expected that the exploration and production activities will be more active in relatively mild ice conditions than in severe ice conditions, which means that forecasts will have higher value
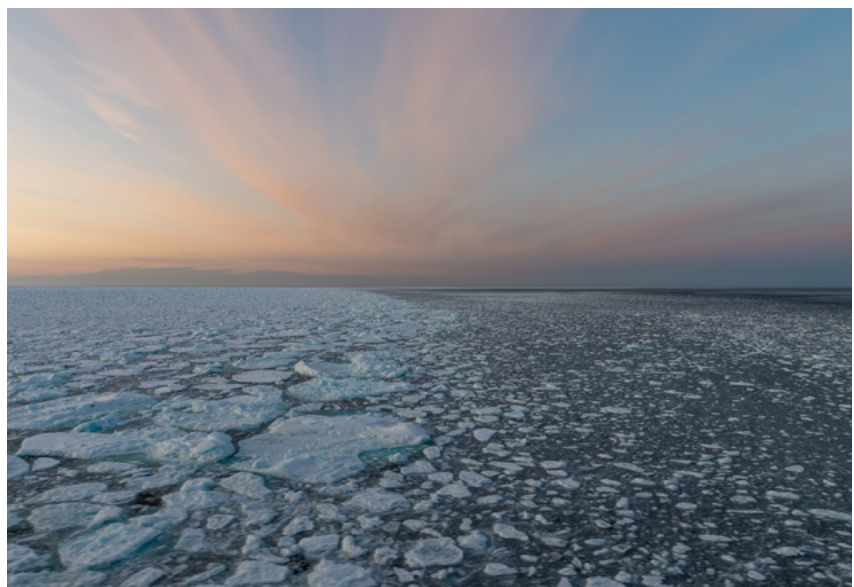
Figure 6.1. Pack ice showing a pressure ridge on the left; Marginal Ice Zone with ice floes on the right. (Photos: E. Storheim, INTAROS/NERSC).

for the MIZ than for the ice pack. The MIZ, defined as the ice-covered region under the influence of surface waves from the open ocean, is particularly in need of forecasts to prevent risks such as ice floe's projections under the action of waves.

There are fewer stakeholder interests in the Southern Ocean, due to the reduced commercial activities in that region. However, ice-ocean predictions can provide information for tourism or scientific operations in the region, including access to Antarctic research stations and support for scientific research vessels. The complex rescue of a joint tourist-research vessel stuck within the Antarctic sea ice in December 2013 (A. Luck-Baker, BBC News, 21 January 2014, 🔗[1]), requiring assistance from two icebreakers and a helicopter, highlighted the need for reliable predictions even in such a remote region. On longer timescales, changing sea ice conditions have implications for ice-dependent wildlife in the region, such as emperor penguins (e.g., Jenouvrier et al., 2012), which raises associated wildlife management concerns.

The shipping industry is primarily concerned with very detailed ice concentration, thickness and compression (and marginally snow depths, because deep snow can also impede the progression of an icebreaker). On the other hand, in the aftermath of oil spills in ice-infested waters, search and rescue operations and forecasting are both dependent on ice motion and their diffusive properties that increase the search radius with time. The question of spatial and temporal resolution is especially critical for the latter case because of the strong scale-dependence of sea ice deformation rates (Rampal et al., 2008). In addition, the diffusion is higher in the chaotic MIZ than in the ice pack (Figure 6.1). The oil industry would ultimately need a detailed forecast of the position of each ice floe surrounding their operations for the day-to-day management of their activities, which can be only delivered by discrete-element models (Herman 2015, Rabatel et al., 2015). How to nest discrete-element models into the continuum sea ice models, considered in this chapter, remains an open question.

6.1.2. Fundamental theoretical background

The physical processes simulated by sea ice models are commonly split into two: vertical processes, related to thermodynamic growth and melt, and mechanical and dynamical processes giving rise to horizontal movement of ice (Figure 6.2).
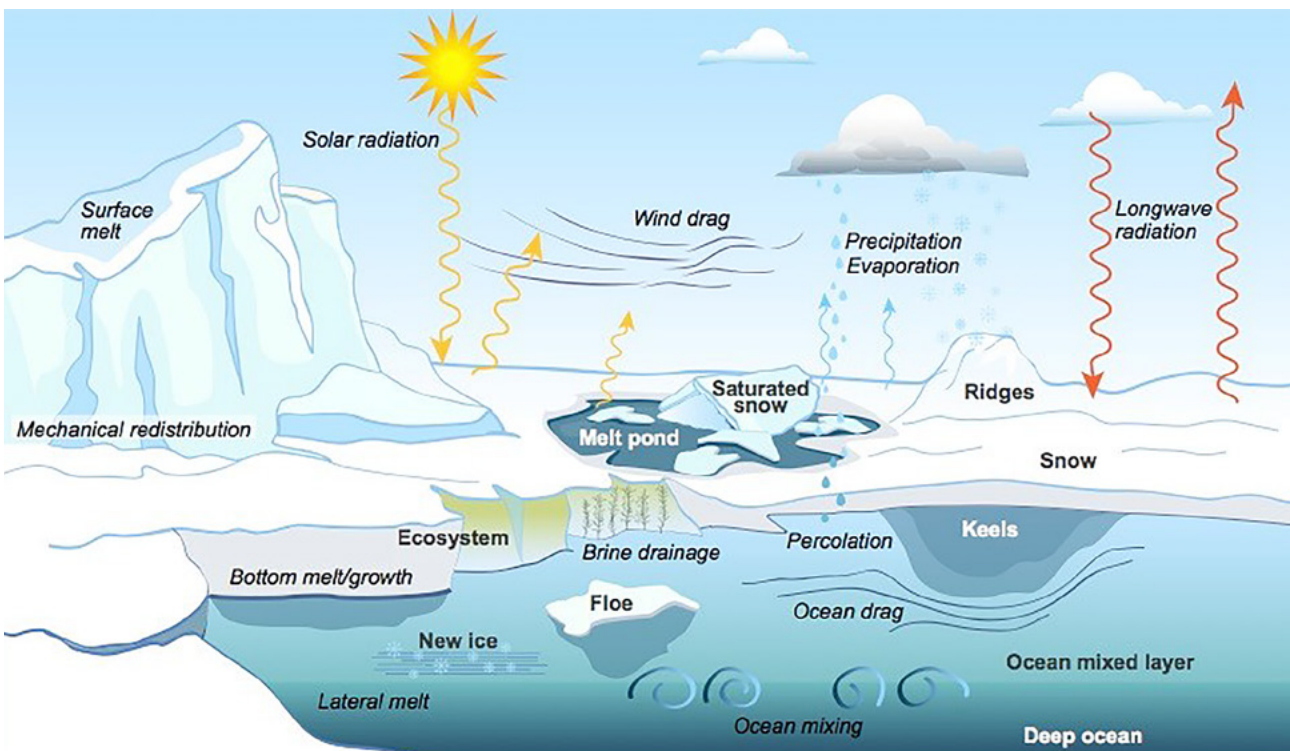
Figure 6.2. A CICE Consortium graphic of sea-ice physics illustrates the complexity and breadth of variables at play (From 🔗[2]).

1. https://www.bbc.com/news/science-environment-25833307

2. https://www.lanl.gov/discover/science-briefs/2021/March/0322-cice.php

The thermodynamic growth and melt of ice can be thought of as the result of the diffusion of heat between ocean and atmosphere, through the ice. Additional complications arise primarily due to the presence of salt or brine pockets in the ice, and the presence of snow. The brine pockets affect the heat conductivity and heat capacity of the ice, while both heat conductivity and heat capacity of the snow, as well as its density, are affected by the state and type of snow, as well as snow metamorphosis.

The basics of thermodynamic modelling of sea ice have been well established since the early 70s (Maykut and Untersteiner, 1971), with the notable improvement in theoretical understanding brought by the application of mushy-layer theory to sea ice (Feltham et al., 2006), and substantial work relating to the dynamics of brine drainage and the multi-phase nature of sea ice (Vancoppenolle et al., 2007; Notz and Worster, 2009; Griewank and Notz, 2013). In terms of model development though, progress has been made in improving numerical performance and in technical aspects, such as conservation of heat, energy, and enthalpy (e.g., Semtner, 1976; Bitz and Libscomb, 1999; Winton, 2000; Huwald et al., 2005). Recently, the more advanced multi-phase physics have also found its way into large-scale sea-ice models (Turner et al., 2013; Turner and Hunke, 2015).

The fundamentals of ice dynamics modelling are less firmly rooted in basic theoretical understanding. While most of the terms of the momentum equation are well understood and follow the basic formulation of the Navier-Stokes equation on a rotating sphere, the formulation of internal stresses is less certain. These describe the response of the ice to external forcing and are, as such, at the heart of sea ice dynamical modelling.

Sea ice is a solid material and, as such, can only move once fractured or broken. In most sea ice models this is taken into account by assuming a rate-independent (von Mises) plasticity. This approach was originally proposed by Coon et al. (1974) but reshaped into a more computationally tractable form in the viscous-plastic model proposed by Hibler (1979), in which the ice is assumed to deform in a linear-viscous manner until it reaches a plastic threshold, representing the fracturing or breaking of the ice. The fracturing process is, as such, simulated explicitly at the grid scale.

However, the process of ice fracturing has been shown to be the result of the propagation of fracturing events from small spatial scales to large ones (Weiss and Marsan, 2004). This results in fractal characteristics of the deformation rates (e.g., Marsan et al., 2004; Rampal et al., 2008; Stern and Lindsay, 2009¸ Schulson and Hibler, 2017). It means that a sea ice model hoping to correctly capture the deformation of the ice must account for this propagation of fracturing events from small to large scales. As the propagation starts at very small spatial and temporal scales (Oikkonen et al., 2017), a geophysical scale model must account for this through a sub-grid scale parameterisation.

The role and importance of fracture dynamics is still a hotly debated subject within the sea ice modelling community. The fractal nature of sea ice deformation is generally accepted and the scaling of deformation rates is recognised as a potential tool and metric for model evaluation and improvement (Rampal et al., 2016; Spreen et al., 2017; Hutter et al., 2018; Rampal et al., 2019; Bouchat et al., 2021). At the same time, it is still unresolved the question of whether to explicitly simulate the fracturing process at a very high resolution (Hutter et al., 2019) or to use a sub-grid scale parameterisation of the fracturing process at a more modest resolution (Dansereau et al., 2016; Rampal et al., 2016).

6.2.
Sea Ice forecast and multi-year systems

6.2.1. Architecture singularities

This section and the next one focus on the "forward integration" spot in the centre of Figure 4.1, designing the architecture of an OOFS.

Sea ice drift forecasts are affected by multiple sources of uncertainties. The surface winds are one of the most important external forces driving the motion of the sea ice in the central Arctic (Thorndike and Colony, 1982). More-over, the uncertainties in the atmospheric reanalysis in the Arctic are higher than those at the mid-latitudes, and observations are insufficient to estimate the statistical characteristics (scale, amplitudes) of the errors. Rabatel et al. (2018) investigated the sensitivity of sea ice drift using neXtSIM-EB for the uncertainties of the surface winds. They concluded that, in regions of highly compact ice cover, the accuracy of surface wind forcing and sea ice rheology are both important for the probabilistic forecast skill of sea ice trajectories.

Passive-µwaves	Scatterometer	SAR	Altimeter	Spectrometer	InfraredRadi- ometer
SMOS	Metop-B/C ASCAT	Sentinel-1A/B	CRYOSAT-2	Sentinel-3 A/B	Sentinel-3 A/B
			Sentinel-3 A/B	Sentinel-2 A/B	Metop AVHRR
AMSR-2	CFOSAT	Radarsat2	Altika	Aqua MODIS	Aqua MODIS
SMAP	Oceansat2	Radarsat constellation	ICESat/ICESat 2		
		CFOSAT*	CFOSAT*		
CIMR	Metop second generation	Sentinel-1 C/D	SWOT	Sentinel-3 C/D	Sentinel-3 C/D
		Rose-L	Cristal	Sentinel-2 C/D	
		HARMONY**			
		BIOMASS			

Table 6.1. Overview of operating and approved satellites and sensors for the sea ice observations grouped into: ESA and Eumetsat missions (yellow), 3rd Party Missions (green) and new approved missions from ESA and NASA/CNES (blue). Spectrometers and infrared radiometers are only sensing in cloud free conditions. Note (*) that CFOSAT flies a combined altimeter and real aperture radar at five distinct incidence angles up to 10 degrees. Harmony (**) comprises two bi-static satellites that will fly in convoy with Sentinel-1.

The ocean below the ice contains large quantities of heat and momentum, enough to melt the sea ice and to cause ice drift and deformations. Uncertainties in ocean temperature, vertical mixing, and currents are then very meaningful for the sea ice. The surface ocean salinity is important, as the melting point temperature depends on it. However, measuring ocean properties and particularly currents below the sea ice is challenging and uncertainties are rather high.

Uncertain initial conditions, particularly the sea ice thickness, persist a long time (Chevallier and Salas-Mélia, 2012). Blockley and Peterson (2018) showed that the sea ice conditions in spring persist typically a few months into the summer and are an important source of large-scale predictability. Errors in the position of the ice edge at the beginning of a forecast are usually persistent throughout the forecast run and ought to be post-processed for practical use.

Finally, sea ice models are dependent on their numerous model parameters, both in the sea ice dynamics and thermodynamics (Urrego-Blanco et al. 2016).

6.2.2. Input data: available sources and data handling

Initialized forecasts are critically dependent on the observations used for their initialization. To be useful for operational systems, observations are needed in near real-time for short-term forecasts and with limited time lag for seasonal and longer forecasts. There are unique challenges involved in polar observations because of its remoteness, harsh conditions, and long polar night. However, forecasting systems are making use of satellite observations for initialization, most routinely for sea ice concentration. Additionally, new products, such as sea ice thickness and drift, are becoming available and may ultimately improve the predictive capabilities.

Sea ice reconnaissance flights were mostly occasional until after the second world war, with the exception of the USSR which started systematic flights with Polar Aviation as early as 1929 to monitor the Northern Sea Route. The USA and Japan gradually increased the frequency of their flights at the turn of the 1950's and adopted the WMO sea ice charting standard proposed in 1952 (WMO, 1970). These flights are still used nowadays, mostly in Canada, but have elsewhere been superseded by satellite data.

Regular and routine sea ice observations are today performed by a variety of satellite-based measurements provided by several space agencies (as grouped in the matrix in Table 6.1 and organised by satellite sensor classes). This has been accomplished thanks to a large number of major technical and scientific milestones and achievements over more than 40 years, as further addressed below. Note that spectrometers and radiometers are only sensing in cloud free conditions.

Started in 1978, the longest satellite record to cover the whole Arctic comes from polar orbiting passive microwave sensors onboard the satellites SMMR, SSM/I, AMSR-E and AMSR2 (Cavalieri and Parkinson, 2012) which provide the sea ice areal concentration. Their main advantage is that they can see through clouds but still a few issues remain, especially with the summer ice, because the sensor does not properly discriminate between open water and signatures from wet snow and melt ponds. This and other technical issues are accommodated differently in a multitude of algorithms that calculate sea ice concentrations from the raw passive microwave retrievals (Ivanova et al., 2014, 2015). This is an important matter for data assimilation as we will see in Section 6.2.5. The resolution of passive microwaves depends on the frequency band used, with the most precise low-frequency channels having the largest footprint (as large as 60 km). However, gridded sea ice concentration data can be found at resolutions between 6 and

25 km, which is consistent with current operational models of the whole Arctic but still coarse with respect to the needs of any operational users navigating in ice-infested waters. SAR and satellite data in the visible channels (VIIRS, AVHRR, MODIS, SPOT) provide much more detail at spatial resolutions finer than 1 km, which is what the ship captain would need, for example to detect and sail along a lead. However, both types of data suffer from poor coverage, SAR images because the acquisition frequency may be limited, and visible data because they are impaired by the frequent cloud coverage and by Arctic winter darkness.

For short-term forecasts, it is important to assess how the sea ice is moving. Various sea ice drift products are obtained from different satellites and can be split in two types: 1) the coarse resolution, full spatial coverage products using passive microwave radiometers and scatterometers (most accurate retrievals in winter because of the aforementioned limitations of passive microwave data during summer; see review by Sumata et al., 2014); and 2) the high resolution but reduced coverage SAR-based products (Kwok 2006). The SAR coverage has recently significantly improved by the launch of the ESA Sentinel-1 A/B missions offering full daily coverage in high latitudes (Korosov and Rampal. 2017). In comparison, drifting buoys on sea ice still provide the longest (more than 40 years) data record of the IABP but with limited spatial coverage.

Satellite Sensors	Extent and concentration	Sea Ice type	Sea Ice thickness	Snow depth	Sea Ice drift	Open leads	Melt ponds	Waves in ice
Passive microwaves	X	First and multi-year ice	Less than 50 cm thick from L-band		X			
Scatterometer	(X)	(X)			X			
SAR	(X)	(X)			X	X	X	X
Altimeter (radar, laser)			Thicker than ~ 50 cm	X	X			
Spectrometer *	(X)	Ridges, rough and flat ice			(X)	X	X	(X)
Infrared Radiometer *	(X)					X	(X)	

Table 6.2. Overview of sea ice variables observed per group of satellite sensors listed in Table 6.1. Note (*) that spectrometers and radiometers are only sensing in cloud free conditions.

Sea ice thickness observations from satellites have recently become routinely available. These use different principles to obtain either: sea ice freeboard of thick ice, for example from the satellite altimetry missions ICESat, ICESat2 (Kwok et al., 2007), CryoSat-2 (Laxon et al., 2013) and Sentinel-3; and the thickness of thin ice, derived from the SMOS (Tian-Kunze et al., 2014). These observations are quite complex and come with relatively high uncertainties (Zygmuntowska et al, 2014, Tian-Kunze et al., 2014). As discussed above, sea ice thickness is an important source of sea ice predictability on seasonal and longer timescales. Other aspects of the sea ice, such as snow cover, snow thickness and melt pond characteristics, may also be important for sea ice forecasts on seasonal and longer timescales. Remote sensing is used to characterise these aspects of the sea ice. For example, snow depth information is being provided through the NASA Operation Ice-Bridge airborne campaign (Kurtz et al., 2013), and melt pond fractions have been derived from satellite data in the visible channels (Rösel et al., 2012). Combined use of IceSAT-2, Cryo-Sat-2 and Altika has also demonstrated promising capabilities to recover reliable snow depth estimates during winter (Guerreiro et al., 2016). Ice mass buoys are also providing in-situ measurements of snow depth and other sea ice characteristics (Richter-Menge et al., 2006; Perovich et al., 2008). However, only limited work has been done to quantify the possible influence of these types of observations for forecasting systems.

As already indicated in Table 6.1, the continuity of sea ice observations from satellites are indeed assured by the approved future satellite missions such as CIMR, Cristal, and ROSE-L Copernicus Sentinel Expansion missions under preparation by ESA. However, more dedicated field campaigns are still needed to assess the uncertainties of the satellite-based retrievals, as well as to harvest the multi-sensor synergies as can be noted
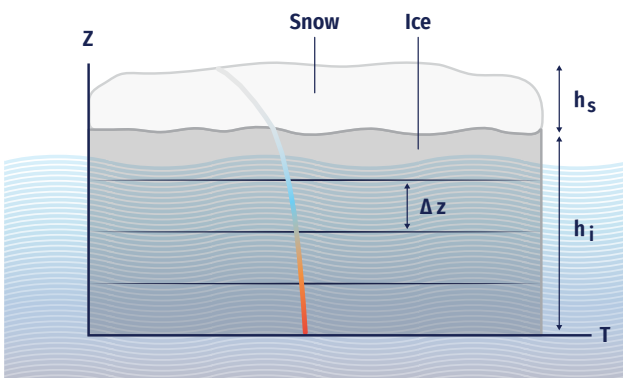
Figure 6.3.   Illustration of a vertical temperature profile in a column consisting of sea ice of thickness hi and topped by snow of depth hs. The heat conduction equation is discretized in the vertical by Δz-thick levels. (adapted from Lisæter 2009).

from Table 6.2. In turn, this would improve the quality and use of satellite data, and expectedly advance the forecast skill of sea ice on seasonal to interannual timescales.

6.2.3. Modelling component

6.2.3.1. Basic equations and modelling choices

Most modern large-scale sea ice models are based on very similar foundations. The ice is generally modelled as a continuum using a Eulerian perspective, with the sea ice moving in a horizontal plane, subject to both external and internal forces. The dynamic evolution of the sea ice cover is described using two continuity equations and the momentum equation. The thermodynamic evolution is modelled within each column of the grid and is modelled as a heat diffusion process within the slab of sea ice. There are substantially varying degrees of complexity in the treatment of the thermodynamic processes, ranging from treating all the ice as being of a single thickness (Hibler, 1979) and treating the heat diffusion without resolving the temperature profile (Semtner, 1976), to using multiple thickness categories (Hibler, 1979, and numerous later variations) and treating the heat diffusion using mushy-layer dynamics (Feltham, et al., 2006).

The main equations for a simple dynamic model of sea ice with two categories (ice and open water) are the two continuity equations and the momentum equation. The continuity equation for mass is:

$$\frac{\partial m}{\partial t} + \nabla \cdot (vm) = S_m \qquad (6.1)$$

where m is the sea ice mass per unit area, S_m is a thermodynamic source/sink term and v is velocity. In the case of a single sea ice category the continuity equation for the sea ice distribution takes the basic form:

$$\frac{\partial A}{\partial t} + \nabla \cdot (vA) = S_A \qquad (6.2)$$

with A is the sea ice concentration and S_A is a source/sink term. In addition, the condition $A \leq 1$ is imposed. This can be interpreted as a ridging condition since m can increase even if A does not (Hibler, 1979). Together these equations describe the advection of the sea ice in a given velocity field.

The momentum equation is generally written as (Connolley et al., 2004):

$$m\frac{\partial v}{\partial t} = A(\tau_a + \tau_w) - mf\widehat{k} \times v - mg\nabla H - \nabla \cdot \sigma \quad (6.3)$$

Here $\hat{k}$ is a unit vector normal to the surface, τ_a and τ_w are the air and water stresses, f is the Coriolis parameter, g is the gravitational acceleration, ∇H is the gradient of the sea surface height and σ is the sea ice stress tensor. The acceleration term on the left-hand side may be set to zero, depending on

A)

B)
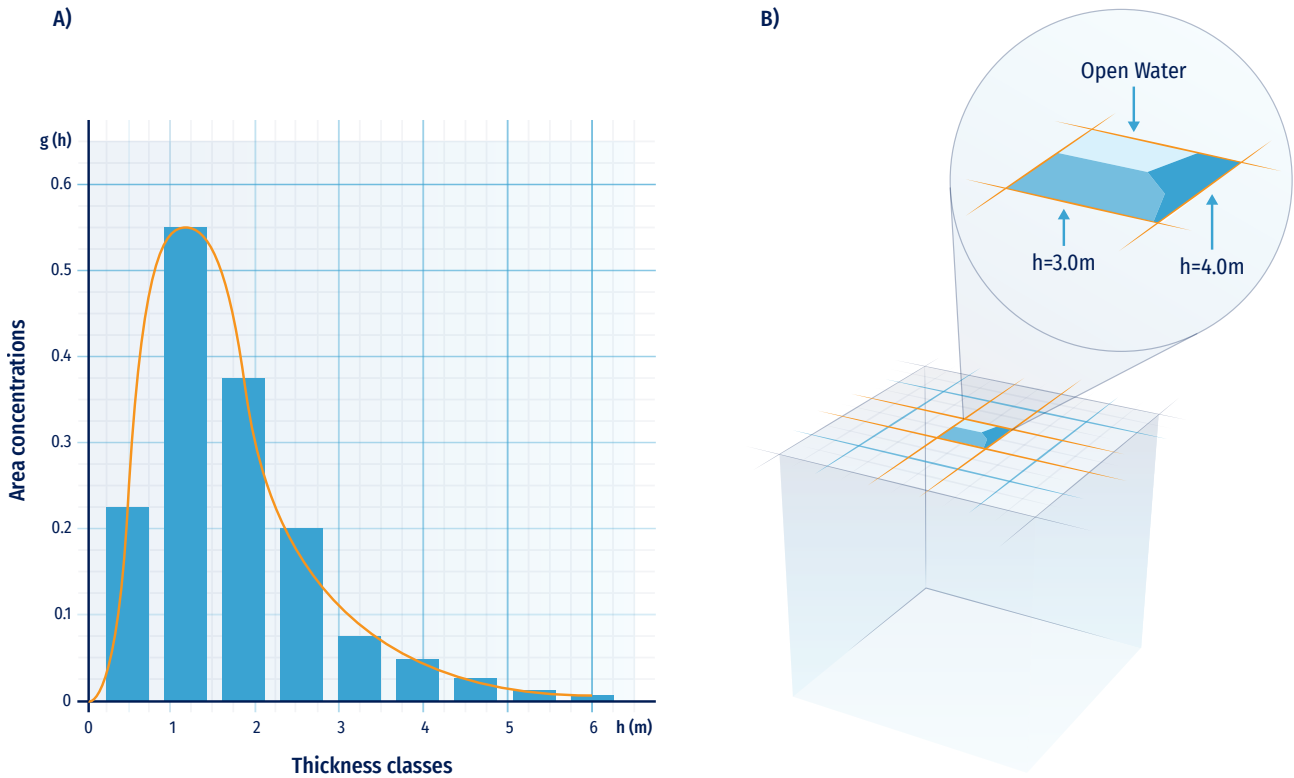
Figure 6.4. Left: a schematic example of an ice thickness distribution, the thickness classes are in x-axis and the y-axis relates to the area concentrations. The continuous distribution is shown with a solid line, while the discretized version is shown in filled bars. Right: illustration of the subgrid-scale ice thickness distribution in a sea ice model (only two classes of 3 and 4 m thickness for the sake of illustration) (adapted from Lisæter, 2009).

the model implementation. The last term on the right hand side $\nabla \cdot \sigma$, describes forces due to internal stress while the other terms are all external factors. Wind and water stresses are generally treated as quadratic drag (e.g., McPhee, 1975). In the absence of internal stress, the sea ice is in "free drift" and the model simplifies drastically. Free drift forecasts have therefore been used for a long time (Grumbine 1998) are still used operationally.

The thermodynamic equation is the heat diffusion equation:

$$\rho c \frac{\partial T}{\partial t} = k \frac{\partial^2 T}{\partial t^2} \qquad (6.4)$$

where ρc is the heat capacity of sea ice or snow and k is the heat conductivity. This equation can be solved in various ways (see Figure 6.3) (e.g., Maykut and Untersteiner, 1971; Semtner, 1976; Bitz and Libscomb, 1999; Winton, 2000; Huwald et al., 2005), discretized in the vertical (Figure 6.3). These take into account different physical properties and numerical solutions in solving the equation.

In addition to these grid-scale quantities, many models consider various sub-grid scale information and parameterisations. The most important of those is arguably the ice thickness distribution (ITD). This assumes that each grid cell of

the model contains not is of uniform thickness, but of varying thicknesses described by an ice thickness distribution g (see Figure 6.3). This is in principle a continuous distribution of thicknesses, which is modified through dynamic and thermodynamic processes. The governing equation of evolution of the ice thickness distribution is (e.g., Thorndike et al., 1975):

$$\frac{\partial g}{\partial t} = -\nabla \cdot (vg) - \frac{\partial}{\partial h}(fg) + \Psi \qquad (6.5)$$

where f is the thermodynamic growth or melt rate, h is the ice thickness, and Ψ is a mechanical redistribution function.

In practice, sea ice models must use a discretized version of the ice thickness distribution, resulting in models with several distinct thickness categories (Figure 6.4 right, for a top view of a grid cell). The thickness distribution then becomes (Bitz et al., 2001):

$$g(h) = g_0 \delta(h) + \sum_{i=1}^{M} g_i \delta(h - H_i) \qquad (6.6)$$

where M is the number of thickness categories, M_i is the thickness of category i, and $\delta(h)$ is the Dirac delta function. Various implementations exist, but the one from Bitz et al., (2001) with five thickness categories remains a popular choice.
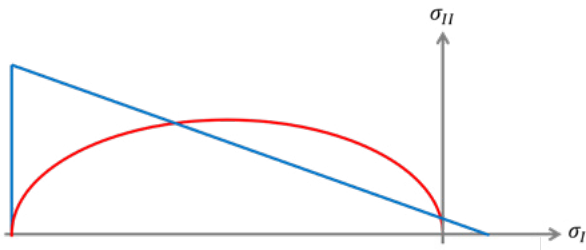
Figure 6.5. Two yield curves commonly associated with sea ice rheology: in red the elliptic yield curve used in the (E)VP models, and in blue a Mohr-Coulomb yield curve, for instance used in the brittle rheology of neXtSIM.

In addition to these two basic components, a large number of sub-grid scale processes can and should be represented, depending on the use cases for each model. These include simulation of melt points (Flocco et al., 2010; Hunke et al., 2013), changes in atmospheric and oceanic drag due to sea ice roughness (Tsamados et al., 2014), and salt rejection from freezing sea ice (Vancoppenolle et al. 2009).

6.2.3.2. Sea ice rheology

The relationship between the internal stress and resulting deformation is referred to as rheology. Basically, all continuum, geophysical-scale sea ice models currently employ the VP rheology proposed by Hibler (1979) or some direct descendant of that work. The VP rheology treats the sea ice as a continuum and assumes it deforms in a viscous manner with a high viscosity until the internal stress reaches a plastic threshold, determined by a yield curve which usually has an elliptic shape (see Figure 6.5). Several important improvements have been made to the original VP rheology (e.g. Hunke and Dukowicz, 1997; Lemieux et al., 2010; Bouillon et al., 2013; Kimmritz et al., 2017), but the physical principles remain the same.

The VP rheology has enjoyed tremendous success and is used for time scales from days to centuries and spatial scales from tens of kilometres to basin scales. However, the VP rheology is not without faults when it comes to both the underlying assumptions (see in particular Coon et al., 2007) and the results it produces. In model inter-comparison studies, there is generally a very large spread - well beyond observed variability - in key prognostic variables such as sea ice thickness, concentration, and drift (Chevallier et al., 2017; Tandon et al., 2018). The sharp gradients in velocities, which are known as LKFs that are related to ridge and lead formation, are also poorly reproduced in any VP-based model running at a coarser resolution than about 2 km - a resolution that is an order of magnitude higher than the observational data (Spreen et al., 2017; Hutter et al., 2019).

Therefore, several authors, such as Tremblay and Mysak (1997), Wilchinsky and Feltham (2004), Schreyer et al. (2006), Girard-Ardhuin and Ezraty (2012), Dansereau et al. (2016), and Ólason et al. (2022), have suggested alternative approaches to the VP rheology. The EAP rheology of Wilchinsky and Feltham (2004) was implemented in the CICE model (Tsamados et al., 2013) and has been used in several studies, although it was not widely adopted yet (Bouchat et al., 2021; Hutter et al. 2021). The brittle rheologies of Girard et al. (2011), Dansereau et al. (2016), and Ólason et al. (2022) have all been implemented in the neXtSIM model (Bouillon and Rampal 2015; Rampal et al., 2019; Ólason et al., 2022) and used for forecasting and scientific research by the team involved in the model. The current neXtSIM version uses the BBM rheology of Ólason et al. (2022).

6.2.3.3. Community sea-ice models

Practically all sea ice models used in modern forecasting platforms are based on the principles described above. They use a Eulerian reference frame and use some version of the VP or the Elastic-Viscous-Plastic (EVP) rheologies. The thermodynamic growth and melt of ice are described through the diffusion of heat between ocean and atmosphere, through the ice. As such, they all follow the same general design philosophy. The main differences exist in the form of different choices of parameterisation and differences in data assimilation approaches.

Today, the CICE model (e.g. Hunke et al., 2021) is likely the most widely used sea ice model for operational forecasts. This model was developed at the Los Alamos National Laboratory and was originally designed to be part of the CCSM. Thanks to its clean and modular design, the model has been used in other multiple modelling systems, as a stand-alone model, part of sea ice-ocean models, and part of climate and earth-system models. The LIM and SI3 models (Rousset et al., 2015), which are part of the NEMO modelling system, are also very widely used, but only within the NEMO modelling system. Other sea-ice models include the SIS (Adcroft et al., 2019), which is part of the GFDL ocean modelling system MOM, the MITgcm sea-ice model (Losch et al., 2010) and the FESOM sea-ice model (FESIM, Danilov et al., 2015).

In contrast, only a few stand-alone sea ice models have used moving Lagrangian coordinates (Hopkins 2004), among which the neXtSIM model (Rampal et al., 2016; Rampal et al., 2019; Ólason et al., 2022) and the DEMSI model (Turner et al., 2022). neXtSIM-F is unique among forecasting models as it uses both a moving Lagrangian mesh and a newly developed brittle rheology, the Brittle Bingham-Maxwell (Williams et al., 2021; Ólason et al., 2022). This setup gives results that are clearly different from the classical systems, and arguably more realistic (Rampal et al., 2016; Rampal et al., 2019; Ólason et al., 2020; Ólason et al., 2022). The key improvement is a

much more realistic representation of the deformation statistics of the ice cover, which gives more realistic leads and ridges in the model. Sea ice drift simulated by neXtSIM is also very realistic, and the pan-Arctic ice-thickness distribution is also quite good (Williams et al., 2021).

6.2.3.4. Coupling of sea ice to atmosphere and ocean

Sea ice models are integral parts of Earth system models. The reason for this is that at high latitudes sea ice insulates the relatively warm ocean from the cold atmosphere. Over an unbroken sea ice cover, the atmosphere can therefore cool much more than it could if it was not insulated by the presence of sea ice. This has an impact on all ocean-atmosphere interactions in the polar regions, and therefore a global climate or Earth system model without a sea ice model can simply not function.

Sea ice interacts with the atmosphere through heat, moisture, and momentum exchanges. In summer incoming short-wave radiation melts the ice surface but would warm up the ocean surface in the absence of sea ice. In winter, heat conduction from the ocean and through the ice only results in a very modest amount of heat flux to the atmosphere. However, the dominant heat flux source is radiant cooling through long wave radiation from the surface. This happens because surface cooling through long wave radiation is much more efficient than the heat conduction through ice from the ocean, resulting in a surface that is colder than the lowest layers of the atmosphere. The result is a predominant temperature inversion and a stable atmospheric boundary layer. This reduces even further the latent and sensible heat fluxes from the surface. However, openings in the ice (leads and polynyas) expose the relatively warm ocean surface to the atmospheric boundary layer, which causes mixing and breaks down the stable boundary layer.

Momentum transfer between ice and atmosphere happens through wind stress at the surface of the ice. This is the main driver of ice movement and exerts a drag on the atmosphere, slowing down the wind. The amount of momentum transferred between ice and atmosphere is determined primarily by the stability of the atmospheric boundary layer (Gryanik and Lüpkes, 2017) and the roughness of the ice. While parameterisations and studies on the ice surface roughness have been proposed (Lüpkes et al., 2012, Castellani et al., 2014), consistent and basin-scale observations of the atmospheric drag coefficient over sea ice are currently unavailable (Petty et al., 2017). In a modelling context, our ability to predict ice surface roughness is severely limited, as most ice-atmosphere coupled models do not take surface roughness into account when calculating atmosphere-ice momentum exchanges.

Sea ice interacts with the ocean through heat, fresh-water, and salt exchanges, as well as momentum exchanges. During summer, the mixed layer may warm up due to shortwave heating through openings in the ice. This makes the ice melting from below, causing release of both freshwater and salt into the ocean. In winter, the atmosphere extracts heat from the ocean through the ice, causing new ice to form at the bottom of the existing ice pack. This causes a net heat and freshwater flux out of the ocean. However, most of the salt present in the ocean cannot enter the ice, since the ice is much fresher than the ocean (ca. 15 vs 30 PSS for newly formed ice in the Arctic). This results in a layer of very salty water forming below the ice, which then sinks into the mixed layer. The resulting salt plumes generally reach the bottom of the halocline but may also be mixed into the mixed layer in the presence of turbulence.

Momentum transfer between ice and ocean happens through interface stress between ocean and ice. The momentum coupling of ice and ocean is much stronger than that of ice and atmosphere, and the ice can be considered as the first layer in the ocean's Ekman spiral. Ice-ocean stress drives most geostrophic flows in ice covered areas, as well as some larger scale circulation patterns.

It is also worth mentioning the interaction between sea ice and ocean waves. Waves entering the ice pack may mechanically fracture it into smaller sea ice floes. This can widen the MIZ, which may also be viewed as the area where the ice is fractured by waves. Fracturing the ice into smaller floes increases the mobility of the ice cover, the momentum transfer between atmosphere, ocean, and ice, and this may cause enhanced melting of the ice through lateral melt. The ice in turn dampens the waves causing an attenuation of the wave amplitude, so that waves will only penetrate a limited distance into the ice pack, depending on the size of the waves and the compactness of the pack. Wave-ice interactions are of major importance in the Southern Ocean, but less so in the Arctic, where much less of the ice edge is exposed to open ocean.

Virtually all climate or earth-system models today include sea-ice models of the classical description above, i.e., a Eulerian reference frame, VP or EVP rheology, and thermodynamics and column physics of varying complexity. They generally include very simplistic formulations for the momentum transfer between atmosphere, ocean, and ice, and no ice-wave interactions. This is true for all the CMIP6 models. In fact, the sea ice models used in today's forecasting models were all designed for climate modelling, the only current exception is the above mentioned neXtSIM model. It is not clear how this lineage of the models affects the quality of their short-term predictions. It could be argued that a good large-scale sea ice model should be able to represent scales from ca. 1 km up to the basin scales and from hours to centuries. This is not the current case, but the discussion of why it is this way and how to address it is still in its infancy (Hunke et al., 2020; Blockley et al., 2020).
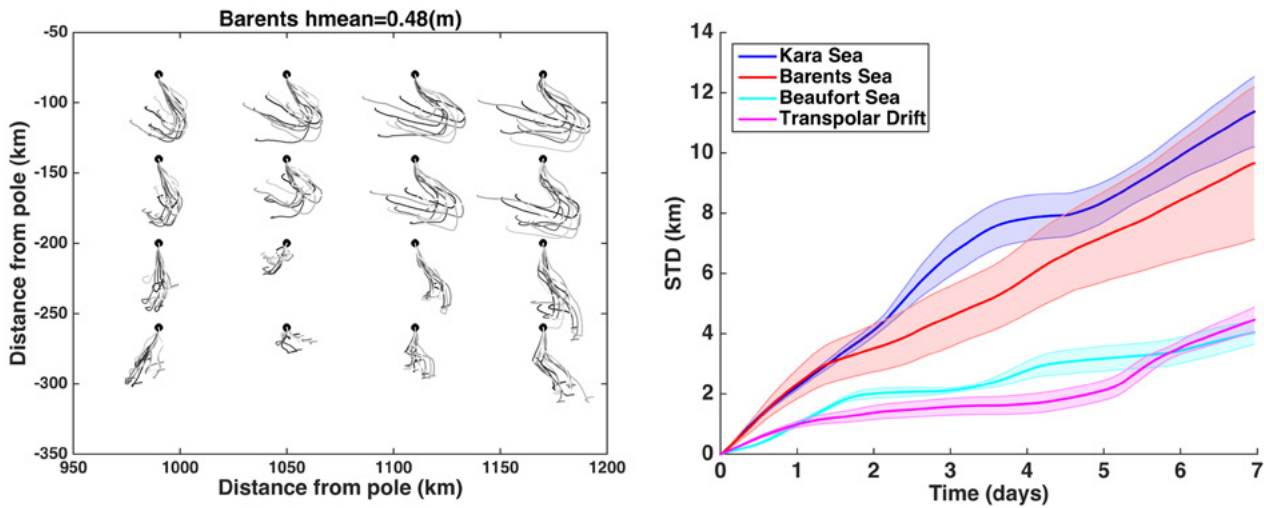
Figure 6.6.   Left: example of ice trajectories from an ensemble of 10 members of 7-days sea ice drift of synthetic floats in an area of the Barents Sea from the TOPAZ system using randomly perturbed winds. The mean sea ice thickness is indicated above. Right: illustration of the ensemble spread in end point positions increasing as a function of the forecast length. The uncertainty growth depends strongly on the region (from Bertino et al., 2015).

6.2.3.5. Model setup

In nearly all forecasting platforms, the sea ice model is coupled to an ocean model. There are platforms that use fully coupled atmosphere-ocean-sea ice models and only a few platforms using a stand-alone sea ice model. The reasons for this are partly historical: most sea ice models are written as parts of ocean models. Ocean forecasting and re-analysis platforms have tended to include a sea ice model from the start, making a dedicated sea ice forecasting platform redundant. In addition, the coupling between sea ice and ocean is quite strong, so running a separate sea ice forecasting platform can bring its own set of challenges. On the other hand, a stand-alone sea ice forecasting platform can be run at a higher resolution and can be used as a technology preview, as in the case of the neXtSIM-F platform.

6.2.4. Ensemble Modelling

Probabilistic forecasts, which are widely used in weather forecasting (Molteni et al., 1996; Leutbecher and Palmer, 2008), are still in their infancy in sea ice forecasting. Probabilistic predictions rely on an ensemble of model simulations (e.g. a Monte Carlo simulation) used to describe the forecast uncertainty stemming from errors in the model parameters, initial and boundary conditions, and any external forcing. The resulting range of model outputs is used to retrieve statistical information, such as the ensemble mean and its spread (i.e. the standard deviation), which are thus used instead of the deterministic forecast to estimate the associated uncertainty (see Figure 6.6). The multiple simultaneous sources of errors usually make the forecast accuracy of the ensemble mean ex-

ceed that of the single deterministic prediction (Leith, 1974), although the spread often underestimates the actual forecast error when the sources of error are not all adequately accounted for (Buizza et al., 2005). Monte Carlo techniques are already common practice in different areas (e.g. Dobney et al., 2000; Hackett et al., 2006; Breivik and Allen, 2008; Melsom et al., 2012; Motra et al., 2016; Duraisamy and Iaccarino, 2017) and a common tool for sensitivity analysis.

6.2.5. Data Assimilation systems

As introduced in the previous section, a sea ice forecast needs to regularly assimilate operational observations, which, at present, are mostly satellite data. The most tempting way forward is to insert directly the satellite observed concentrations and thicknesses into the model. However, this is not as easy as it sounds in a complex sea ice code where a large number of model variables are dependent on each other. Hence, various data assimilation methods are used for sea ice models, similar to those used for ocean physical, biogeochemical models or weather models. The most common method is nudging, which is less disruptive than direct insertion: the data are introduced gradually over a given time scale (Lindsay and Zhang, 2006). The nudged model is then assumed to adjust itself progressively using its own equations. But how much can we rely on such adjustments?

When the ocean mixed layer is too warm to sustain sea ice but observations show the presence of sea ice, a data assimilation system updating only sea ice would add sea ice on top of the warm waters, but the huge heat capacity of the ocean would then melt the added sea ice almost immediately. The

ocean mixed layer temperature and salinity must be adjusted accordingly. This suggests that when used in a coupled ice-ocean system, assimilation of sea ice observations ought to be coupled in the sense that it should update both the sea ice and the ocean properties consistently. In data assimilation jargon, this means that the sea ice observation should be projected down to the ocean column using a multivariate forecast error covariance matrix.

6.2.5.1. Ensemble-based methods

Dynamical model ensembles are a practical way to estimate the covariances mentioned above. In data assimilation terminology, the state vector must include all prognostic variables of the coupled model (ocean and sea ice variables) and the ensemble of model runs can be used to calculate empirically the cross-covariances between sea ice and ocean variables. Similarly, observations of the ocean are used to update sea ice variables, although this situation is less common. Using an EnKF (see section 5.5.2), Lisæter et al. (2003) demonstrated that the coupled assimilation of sea ice properties can modify the ocean surface temperatures in rather systematic ways (adding sea ice cools down the water), but not ocean salinities. However, according to sea ice halodynamics, the freezing of sea ice injects salty brines to the ocean mixed layer and the melting releases fresher water, but these simple relationships explain only a part of the sea ice-salinity cross-covariances and a relationship may arise in other situations without the intervention of sea ice thermodynamics: the wind may occasionally blow the sea ice on top of more saline water. Sakov et al. (2012) showed how the sea ice-salinity cross-covariance can change sign on either side of the ice edge in the Barents Sea: the sea ice-salinity correlation turns negative on the ocean side because the main process responsible for melting is the advection of warm and saline Atlantic water near the surface, thus the sea ice-salinity correlation is made through the intermediate of the surface temperature variable. The last finding does not hold in locations where the sea ice is isolated from the Atlantic water, but such isolation may not remain forever if the open water mixing reaches these warm waters (Rippeth et al., 2015). The assimilation of sea ice concentrations with the EnKF described in Lisæter et al. (2003) was included in the near-real-time TOPAZ forecasts in 2003.

6.2.5.2. Variational methods

An alternative to ensemble methods is the use of an adjoint model as in the 4D-variational (4D-Var) data assimilation method. The adjoint model and the tangent linear model calculate the sensitivity of observed variables to the control variables within the duration of the assimilation window. If tangent linear and adjoint models are available both for the ocean and the sea ice models, they can exchange information about the interface variables, like the heat, salt, and momentum fluxes. Since these correlations are usually monovariate at the beginning of the assimilation window, the length of the assimilation window should be as long as possible. The most recent experiments report successful applications of the 4D4D-VarVAR in an Arctic regional configuration for durations of one year or longer (Fenty and Heimbach 2013; Fenty et al., 2015); an adjoint model for the EVP sea ice rheology has been introduced later (Toyoda et al. 2019). The advantage of the 4D-Var method is that it returns one optimised model trajectory, which is very useful for oceanographic interpretation (Kauker et al., 2009) and quantitative network design (Kaminski et al., 2015) but, to our knowledge, 4D-Var is not used for operational sea ice-ocean forecasting.

A computationally simplified variant of 4D-Var is known as 3D-Var, in which the same increment is used to compute the model equivalent of the observation-minus-reference state differences at all times in the assimilation. Owing to the relatively low cost of the scheme compared with the full 4D-Var, 3D-Var is commonly used by operational forecasting centres around the world (Usui et al., 2006; Mogensen et al., 2012; Hebert et al., 2015; Tonani et al., 2015; Waters et al., 2015; Smith et al., 2016, see Table 6.3 below).

6.2.5.3. Challenges with coupled data assimilation

Coupled multivariate covariances do not necessarily cure all the troubles of assimilating sea ice observations. Another source of problems is the lack of respect of the traditional Gauss-linear assumptions underlying classical data assimilation methods. By definition, sea ice concentrations have bounded values between zero and one, while other sea ice tracer variables (thickness, snow depth) have positive values only. Ocean temperatures are not allowed below the freezing point. While it should be easy for a monovariate assimilation method, based on a heuristic covariance function, to preserve monotonicity and therefore the bounds of variables (Wackernagel, 2003), an ensemble-based covariance (or a tangent linear model) may generate values out of bounds. Honouring the bounds can be forced by different means, either by nonlinear transformations of the variables (a method called Gaussian anamorphosis in geostatistics; Bertino et al., 2003, Barth et al., 2015) or by including inequality constraints in the cost function (Lauvernet et al., 2009; Simon et al., 2012; Janjic et al., 2014). Altogether, the benefits of multivariate flow-dependent covariances still outbeat the inconvenience of values out of bounds.

There are continuous improvements to data assimilation methods in chaotic high-dimensional systems, such as coupled sea ice-ocean models. But new models and new observations always call for further developments in data assimilation. In particular, sea ice models expressed in Lagrangian grids with automatic remeshing are uncommon targets for data assimilation. Ensemble Kalman Filtering techniques rely
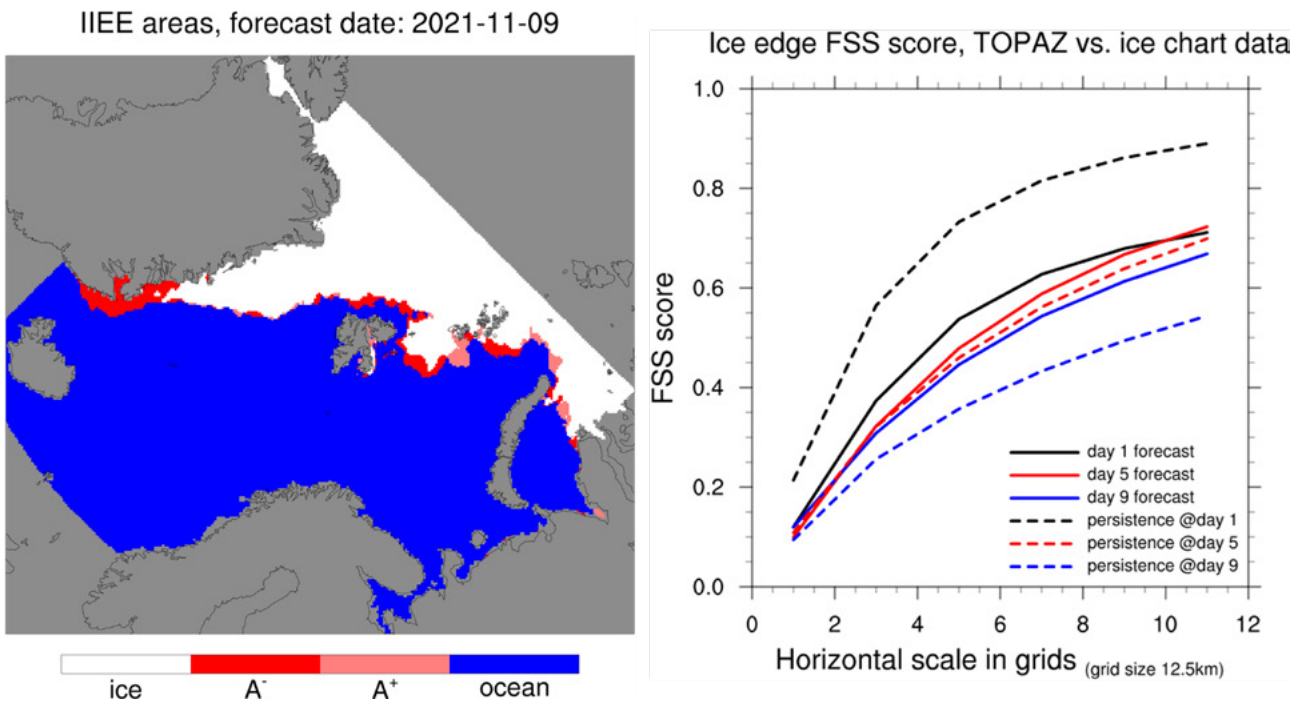
Figure 6.7.   Left: example of areas of excess ice (A+) and missing ice (A-) for a given TOPAZ forecast in the European Arctic; the validation data is the Norwegian Ice Charts. Right: associated Fraction Skill Scores showing that the forecast beats persistence at +5 and +9 days lead time irrespective of spatial scales for that specific forecast (both from ⌘³ of Copernicus Marine Service).

on cross-covariances between observed and unobserved variables, which implies that the grid cells have to be uniquely identified across different members of the ensemble. This also becomes difficult when adaptive remeshing is turned on, unless the Lagrangian model output is interpolated on a fixed grid, at the risk of smoothing the very localised kinematic features (long cracks, ridges and leads) that they are meant to simulate (Aydoğdu et al., 2019). Lagrangian models do not offer any easy differentiation/automatic adjoint capabilities, thus preventing the use of variational techniques. It should also be noted that a coupling framework such as CESM is sufficiently flexible to allow several instances of a model component to be run (for example, the atmosphere) for each instance of another (for example, the ocean), thus allowing to use different data assimilation methods for the sea ice, ocean, land, and atmosphere. An important aspect in view of coupled data assimilation and ensemble forecasting is that the uncertainties are consistent across these compartments; the error statistics at the base of the atmosphere are consistent with those at the surface of the sea ice and similarly between the bottom of the sea ice and the ocean surface. This is possible to enforce if all components of the coupled system use an ensemble to represent the errors.

3. https://cmems.met.no/ARC-MFC/

6.2.6. Validation strategies

Since a measure of RMS errors of sea ice concentrations depend on arbitrary choices made by the person doing the scoring (these errors diminish as more open ocean is included in the validation area), more targeted sea ice validation metrics express the skill as distance of the forecast from the observed ice edge (Dukhovskoy et al., 2015). In the Arctic, the skill of the 24-hour forecast of ice edge location is about 50 km for the TOPAZ (including both seasonal biases and RMS errors, updated at http://cmems.met.no/ARC-MFC/) and 40 km down to 30 km depending on the input data sources in the ACNFS (Hebert et al. 2015; Posey et al., 2015), although both methods may differ and be sensitive to special configurations of the ice edge. The area of discrepancy is accepted as an objective metric with the IIEE introduced by Goessling et al. (2016). The dependence of such metrics on spatial scales can be further included in the evaluation using the FSS (Melsom et al., 2019) and an extension of the IIEE metric proposed by Goessling and Jung (2018) for the evaluation of ensemble forecasts of the ice edge. Examples of IIEE and FSS are shown in Figure 6.7.

It should be noted that the metrics related to isolines (like the ice edge, classically defined at the 15% ice concentration isoline, or at other critical values such as 50% and 85%) ap-
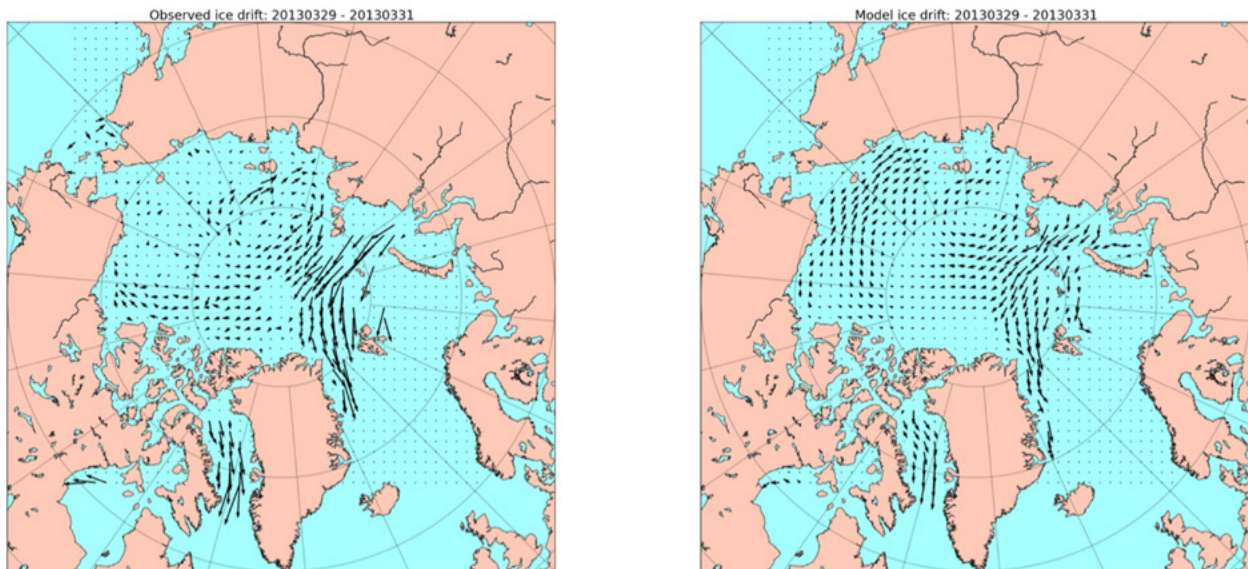
Figure 6.8.   Typical Example of a two-day sea ice drift from satellite observations (OSI-SAF, left) and a model (TOPAZ4, right) (courtesy of A. Melsom, MET Norway).

ply also to other isolines, like the frontier between FYI and MYI, or to theMIZ/pack boundary. Contingency tables are also a valuable approach to the validation of sea ice concentrations (Smith et al., 2016), as well as the threat scores or the Heidke Skill Score.

The forecast skills for sea ice drift have received comparatively less attention but errors in sea ice drift are important, both for their contribution to the displacement of the sea ice edge and for their cumulative contribution to the sea ice thickness distribution. Long climate simulations hint for a seasonal dependence of the forecast skills, also noted in free drift simulations (Grumbine 1998). Biases of sea ice drift have been revealed in IPCC simulations (Tandon et al., 2018) related to the seasonal cycle. To our knowledge, there are no signs that these shortcomings are corrected in recent forecast models (Xie et al., 2017, for the TOPAZ system; Hebert et al., 2015 for the ACNFS), although a review of global reanalysis systems shows that some models simulate correctly the minimum sea ice drift in March (Chevallier et al., 2017). Hebert et al. (2015) also noted that the forecast of drifter positions beats persistence although the forecast of drift speed does not, indicating that the drift direction is better forecasted than the drift speed. How to remedy these shortcomings? Although adjusting the mean speed of sea ice can be easily achieved by tuning the drag coefficients, there is no simple tuning that can make the sea ice accelerate over years or shift its seasonal cycle.

The assimilation of sea ice drift data has been so far less successful than that of sea ice concentrations: Stark et al. (2008) showed a 50% reduction of errors in ice speed but no

benefit to ice concentrations and Sakov et al. (2012) indicated a low sensitivity of the sea ice drift to external perturbations in the wind forcing, which points to a shortcoming of the TOPAZ4 version of the EVP sea ice rheology. Qualitatively, the large-scale patterns of sea ice drift can be reproduced by such a model (see a typical situation in Figure 6.8) but the observed gradients between areas of low sea ice drift (North of Greenland) and strong sea ice drift (North of the Barents Sea) are smoothed by the model, which tends to simulate intermediate values of the sea ice drift speed. The forecast of 24-hours ice trajectories and locations exhibits an RMS error of 6.3 km in TOPAZ4 (Melsom et al., 2015), which does not seem to beat a simple free drift predictor (5 km in Grumbine, 1998). It should be noted that the validation is done against different data sources (sea ice drift from satellite SAR images versus IABP buoys) and at different periods (years 2012-2015 versus 80's and 90's decades). The SIDFEx (Goessling et al., 2020), carried out in the framework of the Multidisciplinary drifting Observatory for the Study of Arctic Climate (MOSAiC) ice camp, has been the first to collect forecasts from international systems and has shown that a consensus forecast could be successfully used to order detailed satellite images of the ice camp in advance. Beyond the use of RMS errors, several alternative metrics for sea ice drift validation have been reviewed by Grumbine (2013). Validation metrics for an ensemble of trajectories from a probabilistic ice drift forecast have been proposed by Rabatel et al. (2018) and refined in Cheng et al. (2020) based on an analogy with Search and Rescue operations, in which the ensemble of trajectories define a search ellipse; the success of the forecast is the probability of containment of the target inside the ellipse.

The forecast of sea ice thickness also suffers from excessive smoothness: thick sea ice is too thin and thin sea ice is too thick (Johnson et al., 2012) and errors reach easily one to two metres. There is a dynamical contribution to these errors with the too high sea ice drift speed North of Greenland exaggerating the transport of thick sea ice into the Beaufort Gyre. However, thermodynamic contributions cannot be excluded either (in particular from snow and melt ponds). More generally, any error in the model initial conditions, atmospheric and ocean boundary conditions or its inherent parameters will eventually accumulate in sea ice thickness biases, which means that different errors can cancel each other and yield a correct sea ice thickness for the wrong reasons. It is worth stressing the important role of snow on sea ice as an effective insulator, its presence can inhibit both the growth and melt of sea ice and thus reduce its seasonal cycle. Snow predictions in sea ice-ocean models are very dependent on the quality of precipitation from weather analyses and forecasts which are difficult to validate and usually vary from one product to another (Lindsay et al., 2014).

6.2.7. Outputs

Information on formats and types of outputs by all kinds of OOFS can be found in Chapter 4. In this Section, we list the variables related to sea ice forecasts:

- sea ice concentration (SIC)
- sea ice thickness (SIT)

- sea ice drift velocity in x- and y- directions (SIUV)
- snow depth (SNOW)
- sea ice age
- sea ice albedo (SIALB)
- sea ice temperature

Sea ice forecasting systems generally comply with CF standards. The CF metadata conventions are a widely used standard for atmospheric, ocean, and climate data. Standard names are defined in a CF Standard Name Table (see 🔗 4). Standard variable names from the CMIP nomenclature can be found in Notz et al. (2016).

6.2.8. Examples of operational sea ice forecasting systems

Most present day short-term forecast systems (listed in Table 6.3) assimilate sea ice concentration and are therefore expected to perform well at forecasting the ice edge. These systems include the Canadian RIOPS (Smith et al., 2021), the United States ACNFS/GOFS3.1 (Hebert et al., 2015), the Italian GOFS16 (Iovino et al,. 2016) the Global and the Arctic Marine Forecasting System (TOPAZ, Sakov et al. 2012) by the Copernicus Marine Services. Stand-alone sea ice models, like neXtSIM-F (Williams et al., 2021), are also used for forecasting purposes and, given that their control vector excludes the ocean, they can be initialised more flexibly than coupled ice-ocean systems. Baltic forecasting systems are omitted for brevity. Ocean data assimilated are also omitted from Table 6.3.

Table 6.3.   List of present-day short-term global and Arctic forecast systems. Note that the output spatial resolution may differ from the native resolution.

Area	System	Resolution (km)	Model	Assimilation (method and sea ice data)	Variables	Website
Arctic	ArcIOPS	18 km	MITgcm	LESTKF SIC, SIT	SIC, SID, SIT	http://www.oceanguide.org.cn/IceIndexHome/ThicknessIce
Arctic	NOAA (Bob Grumbine)	N/A	Free drift	N/A	SIUV	https://mag.ncep.noaa.gov/model-guidance-model-parameter.php?group=Model%20Guidance&model=ICE-DRIFT&area=POLAR&ps=area#
Global	RTOFS	3.5 km	HYCOM-CICE5	3DVAR SIC	SIC, SIT, SIUV	https://polar.ncep.noaa.gov/global/

4. http://cfconventions.org/standard-names.html

Area	System	Resolution (km)	Model	Assimilation (method and sea ice data)	Variables	Website
Arctic	TOPAZ4	12.5 km	HYCOM-CICE3	EnKF SIC, SIUV, SIT	SIC, SIT, SIUV. SNOW, SIALB	https://marine.copernicus.eu/
Arctic	neXtSIM-F	7.5 km*	neXtSIM	Nudging SIC	SIC, SIT, SIUV, SNOW	https://marine.copernicus.eu/
Global	MOi	3.5 km	NEMO-LIM2	SEEK SIC	SIC, SIT, SIUV	https://marine.copernicus.eu/
Global	GIOPS	12 km	NEMO-CICE4	3DVAR SIC	N/A	CONCEPTS - Science.gc.ca
Arctic	RIOPS	3.5 km	NEMO-CICE4	3DVAR SIC	N/A	https://science.gc.ca/eic/site/063.nsf/eng/h_97620.html
Global	GOFS3.1	3.5 km	HYCOM-CICE4	3DVAR SIC	SIC, SIT, SIUV	https://www7320.nrlssc.navy.mil/GLBhycomcice1-12
Global	ECMWF	12 km	NEMO-LIM2	3DVAR SIC	SIC, SIT	https://www.ecmwf.int/en/forecasts/datasets/set-i
Arctic	DMI	10 km	HYCOM-CICE4	Nudging SIC	N/A	http://ocean.dmi.dk/models/hycom.uk.php
Global	Met Office coupled DA	12 km	NEMO-CICE5	3DVAR SIC	SIC, SIT, SIUV	https://marine.copernicus.eu/
Global	Met Office FOAM	3.5 km	NEMO-CICE5	3DVAR SIC	N/A	
Arctic**	VENUS	2.5km	IcePOM	N/A	SIC, SIT	https://ads.nipr.ac.jp/venus.mirai/#/mirai

* Note that the resolution of a Lagrangian triangular mesh is not comparable to square grids, thus the output resolution is 3 km.
** VENUS is deployed on demand.

6.3.
References

Adcroft, A., Anderson, W., Balaji, V., Blanton, C., Bushuk, M., Dufour, C. O., et al. (2019). The GFDL global ocean and sea ice model OM4.0: Model description and simulation features. *Journal of Advances in Modelling Earth Systems,* 11, 3167-3211, https://doi.org/10.1029/2019MS001726

Aydoğdu, A., Carrassi, A., Guider, C.T., Jones, C. K. R. T., and Rampal, P. (2019). Data assimilation using adaptive, non-conservative, moving mesh models. *Nonlinear Processes in Geophysics,* 26(3), 175-193, https://doi.org/10.5194/npg-26-175-2019

Barth, A., Canter, M., Van Schaeybroeck, B., Vannitsem, S., Massonnet, F., Zunz, V., Mathiot, P., Alvera-Azcárate, A., Beckers, J.-M. (2015). Assimilation of sea surface temperature, ice concentration and ice drift in a model of the Southern Ocean. *Ocean Modelling,* 93, 22-39, https://doi.org/10.1016/j.ocemod.2015.07.011

Bertino, L., Bergh, J., and Xie, J. (2015). Evaluation of uncertainties by ensemble simulation, ART JIP Deliverable 3.3. NERSC, Bergen, Norway.

Bertino, L., Evensen, G., Wackernagel, H. (2003). Sequential Data Assimilation Techniques in Oceanography. *International Statistical Review* 71(2), 223-241, http://www.jstor.org/stable/1403885

Bitz, C. M. and Lipscomb, W. H. (1999). An energy-conserving thermodynamic model of sea ice. *Journal of Geophysical Research: Oceans,* 104(C7), 15669-15678, https://doi.org/10.1029/1999JC900100

Bitz, C. M., Holland, M. M., Weaver, A. J., and Eby, M. (2001). Simulating the ice-thickness distribution in a coupled climate model. *Journal of Geophysical Research: Oceans,* 106(C2), 2441-2463, https://doi.org/10.1029/1999JC000113

Blockley, E. W. and Peterson, K. A. (2018). Improving Met Office seasonal predictions of Arctic sea ice using assimilation of CryoSat-2 thickness. *The Cryosphere,* 12, 3419-3438, https://doi.org/10.5194/tc-12-3419-2018

Blockley, E., Vancoppenolle, M., Hunke, E., Bitz, C., Feltham, D., Lemieux, J., Losch, M., Maisonnave, E., Notz, D., Rampal, P., Tietsche, S., Tremblay, B., Turner, A., Massonnet, F., Ólason, E., Roberts, A., Aksenov, Y., Fichefet, T., Garric, G., Iovino, D., Madec, G., Rousset, C., Salas y Melia, D., Schroeder, D. (2020). The future of sea ice modeling: Where do we go from here? *Bulletin of the American Meteorological Society*, 101, E1302-E1309, https://doi.org/10.1175/BAMS-D-20-0073.1

Bouchat, A., Hutter, N.C., Chanut, J., Dupont, F., Dukhovskoy, D. S., Garric, G., Lee, Y. J., Lemieux, J.-F., Lique, C., Losch, M., Maslowski, W., Myers, P. G., Ólason, E., Rampal, P., Rasmussen, T.A.S., Talandier, C., Tremblay, B. (2021). Sea Ice Rheology Experiment (SIREx), Part I: Scaling and statistical properties of sea-ice deformation fields. Journal of Geophysical Research: Oceans, 127(4), e2021JC017667, https://doi.org/10.1029/2021JC017667

Bouillon, S., Fichefet, T., Legat, V., and Madec, G. (2013). The elastic-viscous-plastic method revisited. *Ocean Modelling,* 71, 2-12, https://doi.org/10.1016/j.ocemod.2013.05.013

Bouillon, S., and Rampal, P. (2015). On producing sea ice deformation data sets from SAR-derived sea ice motion. *The Cryosphere,* 9, 663-673, https://doi.org/10.5194/tc-9-663-2015

Breivik, Ø. and Allen, A. A. (2008). An operational search and rescue model for the Norwegian Sea and the North Sea. *Journal of Marine Systems,* 69(1-2), 99-113, https://doi.org/10.1016/j.jmarsys.2007.02.010

Buizza, R., Houtekamer, P. L., Pellerin, G., Toth, Z., Zhu, Y., and Wei, M. (2005). A Comparison of the ECMWF, MSC, and NCEP Global Ensemble Prediction Systems. *Monthly Weather Review,* 133(5), 1076-1097, https://doi.org/10.1175/MWR2905.1

Castellani, G., Lüpkes, C., Gerdes, R., Hendricks, S. (2014). Variability of Arctic sea ice topography and its impact on the atmospheric surface drag. *Journal of Geophysical Research: Ocean,* 119(10), 6743-6762, https://doi.org/10.1002/2013JC009712

Cavalieri, D. J., Parkinson, C. L. (2012). Arctic Sea ice variability and trends, 1979-2010. *The Cryosphere,* 6, 881-889, https://doi.org/10.5194/tc-6-881-2012

Cheng, S., Aydoğdu, A., Rampal, P., Carrassi, A., Bertino, L. (2020). Probabilistic Forecasts of Sea Ice Trajectories in the Arctic: Impact of Uncertainties in Surface Wind and Ice Cohesion. *Oceans,* 1(4), 326-342, https://doi.org/10.3390/oceans1040022

Chevallier, M., and Salas-Melia, D. (2012). The role of sea ice thickness distribution in the Arctic sea ice potential predictability: A diagnostic approach with a coupled GCM. *Journal of Climate,* 25(8), 3025-3038, https://doi.org/10.1175/JCLI-D-11-00209.1

Chevallier, M., Smith, G. C., Dupont, F., Lemieux, J.-F., Forget, G., Fujii, Y., et al. (2017). Intercomparison of the Arctic sea ice cover in global ocean-sea ice reanalyses from the ORA-IP project. *Climate Dynamics,* 49, 1107-1136, https://doi.org/10.1007/s00382-016-2985-y

Connolley, W. M., Gregory, J. M., Hunke, E., McLaren, A. J. (2004). On the Consistent Scaling of Terms in the Sea-Ice Dynamics Equation. *Journal of Physical Oceanography,* 34(7), 1776-1780, https://doi.org/10.1175/1520-0485(2004)034<1776:OTCSOT>2.0.CO;2

Coon, M. D., Maykut, G. A., Pritchard, R. S., Rothrock, D. A., Thorndike, A. S. (1974). Modeling the pack ice as an elastic-plastic material. *AIDJEX Bulletin*, 24, 1-106, Univ. of Wash., Seattle, 1974.

Coon, M., Kwok, R., Levy, G., Pruis, M., Schreyer, H., Sulsky, D. (2007). Arctic Ice Dynamics Joint Experiment (AIDJEX) assumptions revisited and found inadequate. *Journal of Geophysical Research: Ocean,* 112, C11S90, https://doi.org/10.1029/2005JC003393

Danilov, S., Wang, Q., Timmermann, R., Iakovlev, N., Sidorenko, D., Kimmritz, M., Jung, T., and Schröter, J. (2015). Finite-Element Sea Ice Model (FESIM), version 2. Geoscientific Model Development, 8, 1747-1761, https://doi.org/10.5194/gmd-8-1747-2015

Dansereau, V., Weiss, J., Saramito, P., and Lattes, P. (2016). A Maxwell elasto-brittle rheology for sea ice modelling. *The Cryosphere,* 10, 1339-1359, https://doi.org/10.5194/tc-10-1339-2016

Dobney, A., Klinkenberg, H., Souren, F., and Van Borm, W. (2000). Uncertainty calculations for amount of chemical substance measurements performed by means of isotope dilution mass spectrometry as part of the PERM project. *Analytica chimica acta*, 420, 89-94.

Dukhovskoy, D. S., Ubnoske, J., Blanchard-Wrigglesworth, E., Hiester, H. R., and Proshutinsky, A. (2015). Skill metrics for evaluation and comparison of sea ice models. *Journal of Geophysical Research: Oceans,* 120(9), 5910-5931. https://doi.org/10.1002/2015JC010989

Duraisamy, K. A., and Iaccarino, G. (2017). Assessing turbulence sensitivity using stochastic Monte Carlo analysis. Physical Review Fluids, https://arxiv.org/abs/1704.05187

Feltham, D. L., Untersteiner, N., Wettlaufer, J. S., and Worster, M. G. (2006). Sea ice is a mushy layer. *Geophysical Research Letters,* 33(14), L14501, ISSN 0094-8276, https://doi.org/10.1029/2006GL026290

Fenty, I., and Heimbach, P. (2013). Coupled sea ice–ocean state estimation in the Labrador Sea and Baffin Bay. *Journal of Physical Oceanography,* 43(5), 884-904, https://doi.org/10.1175/JPO-D-12-065.1

Fenty, I., Menemenlis, D., and Zhang, H. (2015). Global coupled sea ice-ocean state estimation. *Climate Dynamics,* 49, 931-956, https://doi.org/10.1007/s00382-015-2796-6

Flocco, D., Feltham, D., Turner, A. (2010). Incorporation of a physically based melt pond scheme into the sea ice component of a climate model. Journal of Geophysical Research: Oceans, 115, C08012, https://doi.org/10.1029/2009JC005568

Gautier, D. L., Bird, K. J., Charpentier, R. R., Grantz, A., Houseknecht, D. W., Klett, T. R., ... Wandrey, C. J. (2009). Assessment of Undiscovered Oil and Gas in the Arctic. *Science,* 324, 1175-1179, https://doi.org/10.1126/science.1169467

Girard, L., Bouillon, S., Weiss, J., Amitrano, D., Fichefet, T., and Legat, V. (2011). A new modeling framework for sea-ice mechanics based on elasto-brittle rheology. *Annals of Glaciology,* 52, 123-132, doi:10.3189/172756411795931499

Girard-Ardhuin, F., and Ezraty, R. (2012). Enhanced Arctic Sea Ice Drift Estimation Merging Radiometer and Scatterometer Data. IEEE Transactions on Geoscience and Remote Sensing, 50(7), 2639-2648, doi:10.1109/TGRS.2012.2184124

Goessling H., Tietsche, S., Day, J.J., Hawkins, E., Jung, T. (2016). Predictability of the Arctic sea ice edge. *Geophysical Research Letters,* 43(4), 1642-1650, https://doi.org/10.1002/2015GL067232

Goessling, H. F., and Jung, T. (2018). A probabilistic verification score for contours: Methodology and application to Arctic ice-edge forecast. *Quarterly Journal of the Royal Meteorological Society,* 144, 735-743, https://doi.org/10.1002/qj.3242

Goessling, H. F. and the SIDFEx Team (2020). Making Use and Sense of 75,000 Forecasts of the Sea Ice Drift Forecast Experiment (SIDFEx), EGU General Assembly 2020, Online, 4-8 May 2020, EGU2020-18867, https://doi.org/10.5194/egusphere-egu2020-18867

Griewank, P. J., Notz, D. (2013). Insights into brine dynamics and sea ice desalination from a 1-D model study of gravity drainage. *Journal of Geophysical Research: Oceans,* 118, 3370-3386, doi:10.1002/jgrc.20247

Grumbine, R. W. (1998). Virtual Floe Ice Drift Forecast Model Intercomparison. *Weather and Forecasting,* 13, 886-890, https://doi.org/10.1175/1520-0434(1998)013<0886:VFIDFM>2.0.CO;2

Grumbine, R. W. (2013). Long Range Sea Ice Drift Model Verification. Camp. Springs, Maryland.

Guerreiro, K., Fleury, S., Zakharova, E., Rémy, F., and Kouraev, A. (2016). Potential for estimation of snow depth on Arctic sea ice from CryoSat-2 and SARAL/AltiKa missions. *Remote Sensing of Environment,* 186, 339-349, https://doi.org/10.1016/j.rse.2016.07.013

Gryanik, V. M., and Lüpkes, C. (2017). An Efficient Non-iterative Bulk Parametrization of Surface Fluxes for Stable Atmospheric Conditions Over Polar Sea-Ice. *Boundary-Layer Meteorology,* 166, 301-325, https://doi.org/10.1007/s10546-017-0302-x

Hackett, B., Breivik, Ø., Wettre, C. (2006). Forecasting the drift of objects and substances in the ocean. In E.P. Chassignet and J. Verron (ed.s) "Ocean Weather Forecasting, An Integrated View of Oceanography", 507-524, Springer, Dordrecht.

Hebert, D. A., Allard, R. A., Metzger, E. J., Posey, P. G., Preller, R. H., Wallcraft, A. J., Phelps, M. W., and Smedstad, O. M. (2015). Short-term sea ice forecasting: An assessment of ice concentration and ice drift forecasts using the U.S. Navy's Arctic Cap Nowcast/Forecast System. *Journal of Geophysical Research: Oceans,* 120, 8327-8345, https://doi.org/10.1002/2015JC011283

Herman, A. (2015). Discrete-Element bonded particle Sea Ice model DESIgn, version 1.3a - model description and implementation. *Geoscientific Model Development,* 9, 1219–1241, https://doi.org/10.5194/gmd-9-1219-2016

Hibler, W. D. (1979). A dynamic thermodynamic sea ice model. *Journal of Physical Oceanography,* 9, 817-846.

Hopkins, M. (2004). A discrete element Lagrangian sea ice model. *Engineering Computations,* 21, 409-421, https://doi.org/10.1108/02644400410519857

Hunke, E., and Dukowicz, J. (1997). An elastic-viscous-plastic model for sea ice dynamics. *Journal of Physical Oceanography,* 27(9), 1849-1867, https://doi.org/10.1175/1520-0485(1997)027<1849:AEVPMF>2.0.CO;2

Hunke, E., Hebert, D., Lecomte, O. (2013). Level-ice melt ponds in the Los Alamos sea ice model, CICE. *Ocean Modelling,* 71, 26-42, https://doi.org/10.1016/j.ocemod.2012.11.008

Hunke, E., Allard, R., Blain, P. et al. (2020). Should Sea-Ice Modeling Tools Designed for Climate Research Be Used for Short-Term Forecasting? *Current Climate Change Reports,* 6, 121-136, https://doi.org/10.1007/s40641-020-00162-y

Hunke, E., Allard, R., Bailey, D.A., Blain, P., Craig, A., Dupont, F., DuVivier, A., Grumbine, R., Hebert, D., Holland, M., Jeffery, N., Lemieux, J.F., Osinski, R., Rasmussen, T., Ribergaard, M., Roberts, A., Denise, W. (2021). CICE Version 6.3.0. http://doi.org/10.5281/zenodo.1205674

Hutter, N., Losch, M., and Menemenlis, D. (2018). Scaling properties of Arctic sea ice deformation in a high-resolution viscous-plastic sea ice model and in satellite observations. *Journal of Geophysical Research: Oceans,* 123, 672-687, https://doi.org/10.1002/2017JC013119

Hutter, N., Zampieri, L., Losch, M. (2019). Leads and ridges in Arctic sea ice from RGPS data and a new tracking algorithm. *The Cryosphere,* 13, 627-645, https://doi.org/10.5194/tc-13-627-2019

Huwald, H., Tremblay, L.-B., Blatter, H. (2005). A multilayer sigma-coordinate thermodynamic sea ice model: Validation against Surface Heat Budget of the Arctic Ocean (SHEBA)/Sea Ice Model Intercomparison Project Part 2 (SIMIP2) data. *Journal of Geophysical Research: Oceans,* 110, C05010, https://doi.org/10.1029/2004JC002328

Iovino, D., Masina, S., Storto, A., Cipollone, A., and Stepanov, V. N. (2016). A 1/16° eddying simulation of the global NEMO sea-ice–ocean system. *Geoscientific Model Development,* 9, 2665–2684, https://doi.org/10.5194/gmd-9-2665-2016

Ivanova, N., Johannessen, O. M., Pedersen, L. T., and Tonboe, R. T. (2014). Retrieval of Arctic Sea Ice Parameters by Satellite Passive Microwave Sensors: A Comparison of Eleven Sea Ice Concentration Algorithms, IEEE Transactions on Geoscience and Remote Sensing, 52, 7233-7246, doi:10.1109/TGRS.2014.2310136

Ivanova, N., Pedersen, L. T., and Tonboe, R. T. (2015). Inter-comparison and evaluation of sea ice algorithms: towards further identification of challenges and optimal approach using passive microwave observations. *The Cryosphere,* 9, 1797-1817, https://doi.org/10.5194/tc-9-1797-2015

Janjić, T., McLaughlin, D., Cohn, S. E., and Verlaan, M. (2014). Conservation of Mass and Preservation of Positivity with Ensemble-Type Kalman Filter Algorithms. *Monthly Weather Review,* 142(2), 755-773, https://doi.org/10.1175/MWR-D-13-00056.1

Jenouvrier, S., Holland, M., Strœve, J., Barbraud, C., Weimerskirch, H., Serreze, M., Caswell, H. (2012). Effects of climate change on an emperor penguin population: analysis of coupled demographic and climate models. Available at https://core.ac.uk/download/pdf/9584173.pdf

Johnson, M., Proshutinsky, A., Aksenov, Y., Nguyen, A.T., Lindsay, R., Haas, C., Zhang, J., Diansky, N., Kwok, R., Maslowski, W., Häkkinen, S., Ashik, I., de Cuevas, B. (2012). Evaluation of Arctic sea ice thickness simulated by Arctic Ocean Model Intercomparison Project models. *Journal of Geophysical Research: Oceans,* 117(C8), https://doi.org/10.1029/2011JC007257

Kaminski, T., Kauker, F., Eicken, H., and Karcher, M. (2015). Exploring the utility of quantitative network design in evaluating Arctic sea ice thickness sampling strategies. *The Cryosphere,* 9, 1721-1733, https://doi.org/10.5194/tc-9-1721-2015

Kauker, F., Kaminski, T., Karcher, M., Giering, R., Gerdes, R., and Voßbeck, M. (2009). Adjoint analysis of the 2007 all time Arctic sea-ice minimum. *Geophysical Research Letters,* 36, L03707, doi:10.1029/2008GL036323

Kimmritz, M., Losch, M., Danilov, S. (2017). A comparison of viscous-plastic sea ice solvers with and without replacement pressure. *Ocean Modelling,* 115, 59-69, https://doi.org/10.1016/j.ocemod.2017.05.006

Kjesbu, O.S., Bogstad, B., Devine, J.A., Gjøsæter, H., Howell, D., Ingvaldsen, R.B., Nash, R.D. M., and Skjæraasen, J. E. (2014). Synergies between climate and management for Atlantic cod fisheries at high latitudes. *Proceedings of the National Academy of Sciences of the United States of America,* 111(9), 3478-3483, https://doi.org/10.1073/pnas.1316342111

Korosov, A. A., and Rampal, P. (2017). A Combination of Feature Tracking and Pattern Matching with Optimal Parametrization for Sea Ice Drift Retrieval from SAR Data. *Remote Sensing,* 9(258), https://doi.org/10.3390/rs9030258

Kundzewicz, Z. W., Mata, L. J., Arnell, N. W., Doll, P., Kabat, P., Jimenez, B., Miller, K., Oki, T., Zekai, S. and Shiklomanov, I. (2007) Freshwater resources and their management. In: Parry, M. L., Canziani, O. F., Palutikof, J. P., van der Linden, P. J. and Hanson, C. E. (eds.) "Climate Change 2007: Impacts, Adaptation and Vulnerability. Contribution of Working Group II to the Fourth Assessment Report of the Intergovernmental Panel on Climate Change". Cambridge University Press, 173-210, ISBN 9780521880091

Kurtz, N., Farrell, S. L., Studinger, M., Galin, N., Harbeck, J. P., Lindsay, R., Onana, V. D., Panzer, B., and Sonntag, J. G. (2013). Sea ice thickness, freeboard, and snow depth products from Operation IceBridge airborne data. *The Cryosphere,* 7, 1035-1056, https://doi.org/10.5194/tc-7-1035-2013

Kwok, R. (2006). Contrasts in sea ice deformation and production in the Arctic seasonal and perennial ice zones. *Journal of Geophysical Research: Oceans,* 112(C2), https://doi.org/10.1029/2005JC003172

Kwok, R., Cunningham, G. F., Zwally, H. J., and Yi, D. (2007). Ice, Cloud, and land Elevation Satellite (ICESat) over Arctic sea ice: Retrieval of freeboard. *Journal of Geophysical Research: Oceans,* 112(C12), https://doi.org/10.1029/2006JC003978

Lauvernet, C., Brankart, J.-M. M., Castruccio, F., Broquet, G., Brasseur, P., and Verron, J. (2009). A truncated Gaussian filter for data assimilation with inequality constraints: Application to the hydrostatic stability condition in ocean models. *Ocean Modelling,* 27(1-2), 1-17. https://doi.org/https://doi.org/10.1016/j.ocemod.2008.10.007

Laxon S. W., Giles, K. A., Ridout, A. L., Wingham, D. J., Willatt, R., Cullen, R., Kwok, R., Schweiger, A., Zhang, J., Haas, C., Hendricks, S., Krishfield, R., Kurtz, N., Farrell S., and Davidson, M. (2013). CryoSat-2 estimates of Arctic sea ice thickness and volume. *Geophysical Research Letters,* 40, 732-737, https://doi.org/10.1002/grl.50193

Leith, C. E. (1974). Theoretical skill of Monte Carlo forecasts. *Monthly Weather Review,* 102(6), 409-418, https://doi.org/10.1175/1520-0493(1974)102<0409:TSOMCF>2.0.CO;2

Lemieux, J.-F., Tremblay, B., Sedlácek, J., Tupper, P., Thomas, S., Huard, D., and Auclair, J.-P. (2010). Improving the numerical convergence of viscous-plastic sea ice models with the Jacobianfree Newton Krylov method. *Journal of Computational Physics,* 229(8), 2840-2852, https://doi.org/10.1016/j.jcp.2009.12.011

Leutbecher, M., and Palmer, T. N. (2008). Ensemble forecasting. *Journal of Computational Physics,* 227(7), 3515-3539, https://doi.org/10.1016/j.jcp.2007.02.014

Lindsay, R. W., and Zhang, J. (2006). Assimilation of Ice Concentration in an Ice-Ocean Model. *Journal of Atmospheric and Oceanic Technology,* 23(5), 742-749, https://doi.org/10.1175/JTECH1871.1

Lindsay, R., Wensnahan, M., Schweiger, A., and Zhang, J. (2014). Evaluation of seven different atmospheric reanalysis products in the Arctic. *Journal of Climate,* 27(7), 2588-2606, https://doi.org/10.1175/JCLI-D-13-00014.1

Lisæter, K. A., Rosanova, J., Evensen, G. (2003). Assimilation of ice concentration in a coupled ice-ocean model, using the Ensemble Kalman filter. *Ocean Dynamics,* 53, 368-388, https://doi.org/10.1007/s10236-003-0049-4

Lisæter, K. A. (2009). A multi-category sea-ice model. Technical report 304. NERSC, Thormøhlensgt. 47, N-5006 Bergen, Norway.

Losch, M., D. Menemenlis, J.-M. Campin, P. Heimbach, and C. Hill, 2010. On the formulation of sea-ice models. Part 1: Effects of different solver implementations and parameterizations. *Ocean Modelling,* 33(1-2), 129-144, https://doi.org/10.1016/j.ocemod.2009.12.008

Lüpkes, C., Gryanik, V. M., Hartmann, J., Andreas, E. L. (2012). A parameterization, based on sea ice morphology, of the neutral atmospheric drag coefficients for weather prediction and climate models. *Journal of Geophysical Research: Atmospheres,* 117(D13), https://doi.org/10.1029/2012JD017630

Marsan, D., Stern, H., Lindsay, R., Weiss, J. (2004). Scale Dependence and Localization of the Deformation of Arctic Sea Ice. *Physical Review Letter,* 93(17), https://link.aps.org/doi/10.1103/PhysRevLett.93.178501

Maykut, G. A., and Untersteiner, N. (1971). Some results from a time-dependent thermodynamic model of sea ice. *Journal of Geophysical Research (1896-1977),* 76, 1550-1575, https://doi.org/10.1029/JC076i006p01550

McPhee, M. G. (1975). Ice-ocean momentum transfer for the AIDJEX ice model. *AIDJEX Bullettin,* 29 , 93-111.

Melsom, A., Counillon, F., LaCasce, J. H., Bertino, L. (2012). Forecasting search areas using ensemble ocean circulation modeling. *Ocean Dynamics,* 62(8), 1245-1257, https://doi.org/10.1007/s10236-012-0561-5

Melsom, A., Palerme, C., Müller, M. (2019). Validation metrics for ice edge position forecasts. *Ocean Science,* 15(3), 615-630, https://doi.org/10.5194/os-15-615-2019

Mogensen, U. B., Ishwaran. H., Gerds, T. A. (2012). Evaluating Random Forests for Survival Analysis using Prediction Error Curves. *Journal of Statistical Software,* 50(11), 1-23, doi: 10.18637/jss.v050.i11

Molteni, F., Buizza, R., Palmer, T. N., Petroliagis, T. (1996). The ECMWF Ensemble Prediction System: Methodology and validation. *Quarterly Journal of the Royal Meteorological Society,* 122, 73-119, https://doi.org/10.1002/qj.49712252905

Motra, H. B., Stutz, H., Wuttke, F. (2016). Quality assessment of soil bearing capacity factor models of shallow foundations. *Soils and Foundations,* 56(2), 265-276, https://doi.org/10.1016/j.sandf.2016.02.009

Mueter, F. J., Litzow, M. A. (2008). Sea ice retreat alters the biogeography of the Bering Sea continental shelf. *Ecological Applications,* 18(2), 309-20, https://doi.org/10.1890/07-0564.1

Notz, D., and Worster, M. G. (2009). Desalination processes of sea ice revisited. *Journal of Geophysical Research: Oceans,* 114(C5), https://doi.org/10.1029/2008JC004885

Notz, D., Jahn, A., Holland, M., Hunke, E., Massonnet, F., Stroeve, J., ... Vancoppenolle, M. (2016). The CMIP6 Sea-Ice Model Intercomparison Project (SIMIP): Understanding sea ice through climate-model simulations. *Geoscientific Model Development,* 9(9), 3427-3446, https://doi.org/10.5194/gmd-9-3427-2016

Oikkonen, A., Haapala, J., Lensu, M., Karvonen, J., Itkin P. (2017). Small-scale sea ice deformation during N-ICE2015: From compact pack ice to marginal ice zone. *Journal of Geophysical Research: Oceans,* 122(6), 5105-5120, https://doi.org/10.1002/2016JC012387

Ólason, E., Rampal, P., and Dansereau, V. (2021). On the statistical properties of sea-ice lead fraction and heat fluxes in the Arctic. *The Cryosphere,* 15, 1053-1064, https://doi.org/10.5194/tc-15-1053-2021

Ólason, E., Boutin, G., Korosov, A., Rampal, P., Williams, T., Kimmritz, M., Dansereau, V. (2022). A new brittle rheology and numerical framework for large-scale sea-ice models. Submitted to Journal of Modelling the Earth System (JAMES), https://doi.org/10.1002/essoar.10507977.2

Overland, J.E, Dethloff, K., Francis, J.A., Hall, R.J., Hanna, E., Kim, S.-J., Screen, J.A., Shepherd, T.G., Vihma, T. (2016). Nonlinear response of mid-latitude weather to the changing Arctic. *Nature Climate Change,* 6, 992-999, https://doi.org/10.1038/nclimate3121

Perovich, D. K., Richter-Menge, J. A., Jones, K. F., Light, B. (2008). Sunlight, water, and ice: Extreme Arctic sea ice melt during the summer of 2007. *Geophysical Research Letters,* 35(11), https://doi.org/10.1029/2008GL034007

Petty, A. A., Markus, T., Kurtz, N. (2017). Improving our understanding of Antarctic sea ice with NASA's Operation IceBridge and the upcoming ICESat-2 mission. *US CLIVAR Variations,* 15(3), doi:10.5065/D6833QQP

Posey, P. G., Metzger, E.J., Wallcraft, A.J., Hebert, D.A., Allard, R.A., Smedstad, O.M., Phelps, M.W., Fetterer, F. , Stewart, J.S., Meier, W.N., and Helfrich, S.R. (2015). Improving Arctic sea ice edge forecasts by assimilating high horizontal resolution sea ice concentration data into the US Navy's ice forecast systems. *The Cryosphere,* 9, 1735-1745, https://doi.org/10.5194/tc-9-1735-2015

Rabatel, M., Labbé, S., and Weiss, J. (2015). Dynamics of an Assembly of Rigid Ice Floes. J. *Journal of Geophysical Research: Oceans,* 120(9), 5887-5909, https://doi.org/10.1002/2015JC010909

Rabatel, M., Rampal, P., Carrassi, A., Bertino, L., and Jones, C.K.R T. (2018). Impact of rheology on probabilistic forecasts of sea ice trajectories: Application for search and rescue operations in the Arctic. *The Cryosphere,* 12, 935-953, https://doi.org/10.5194/tc-12-935-2018

Rampal, P., Weiss, J., Marsan, D., Lindsay, R., and Stern, H. (2008). Scaling properties of sea ice deformation from buoy dispersion analysis. *Journal of Geophysical Research: Oceans,* 113(C3), C03002, https://doi.org/10.1029/2007JC004143

Rampal, P., Bouillon, S., Ólason, E., and Morlighem, M. (2016). NeXtSIM: A new Lagrangian sea ice model. *The Cryosphere,* 10, 1055-1073, https://doi.org/10.5194/tc-10-1055-2016

Rampal, P., Dansereau, V., Olason, E., Bouillon, S., Williams, T., Korosov, A., and Samaké, A. (2019). On the multi-fractal scaling properties of sea ice deformation. *The Cryosphere,* 13, 2457-2474, https://doi.org/10.5194/tc-13-2457-2019

Richter-Menge, J. A., Perovich, D. K., Elder, B. C., Claffey, K., Rigor, I., Ortmeyer, M. (2006). Ice mass-balance buoys: a tool for measuring and attributing changes in the thickness of the Arctic sea-ice cover. *Annals of Glaciology,* 44(1), 205-210, doi:10.3189/172756406781811727

Rippeth, T.P. et al. (2015). Tide-mediated warming of Arctic halocline by Atlantic heat fluxes over rough topography. *Nature Geoscience,* 8(3), 191-194, https://doi.org/10.1038/ngeo2350

Rousset, C., Vancoppenolle, M., Madec, G., Fichefet, T., Flavoni, S., Barthélemy, A., Benshila, R., Chanut, J., Levy, C., Masson, S., and Vivier, F. (2015). The Louvain-La-Neuve sea ice model LIM3.6: global and regional capabilities. *Geoscientific Model Development,* 8, 2991-3005, https://doi.org/10.5194/gmd-8-2991-2015

Rösel, A., Kaleschke, L., and Birnbaum, G. (2012). Melt ponds on Arctic sea ice determined from MODIS satellite data using an artificial neural network. *The Cryosphere,* 6, 431-446, https://doi.org/10.5194/tc-6-431-2012

Sakov, P., Counillon, F., Bertino, L., Lisæter, K. A., Oke, P., and Korablev, A. (2012). TOPAZ4: an ocean-sea ice data assimilation system for the North Atlantic and Arctic. *Ocean Science,* 8, 633-656, https://doi.org/10.5194/os-8-633-2012

Schreyer, H. L., Sulsky, D. L., Munday, L. B., Coon, M. D., Kwok, R. (2006). Elastic-decohesive constitutive model for sea ice. *Journal of Geophysical Research: Oceans,* 111(C11), https://doi.org/10.1029/2005JC003334

Schulson, E. M., Hibler, W. D. (2017). The fracture of ice on scales large and small: Arctic leads and wing cracks. *Journal of Glaciology,* 27(127), 319-322, https://doi.org/10.3189/S0022143000005748

Semtner, A. J. (1976). A Model for the Thermodynamic Growth of Sea Ice in Numerical Investigations of Climate. *Journal of Physical Oceanography,* 6(3), 379-389. https://doi.org/10.1175/1520-0485(1976)006<0379:AMFTTG>2.0.CO;2

Simon, E., Samuelsen, A., Bertino, L., and Dumont, D. (2012). Estimation of positive sum-to-one constrained zooplankton grazing preferences with the DEnKF: a twin experiment. *Ocean Science,* 8(4), 587-602, https://doi.org/10.5194/os-8-587-2012

Smith, G. C., Roy, F., Reszka, M., Surcel Colan, D., He, Z., Deacu, D., Belanger, J.-M., Skachko, S., Liu, Y., Dupont, F., Lemieux, J.-F., Beaudoin, C., Tranchant, B., Drévillon, M., Garric, G., Testut, C.-E., Lellouche, J.-M., Pellerin, P., Ritchie, H., Lu, Y., Davidson, F., Buehner, M., Caya, A. and Lajoie, M. (2016). Sea ice forecast verification in the Canadian Global Ice Ocean Prediction System. *Quarterly Journal of the Royal Meteorological Society,* 142(695), 659-671, https://doi.org/10.1002/qj.2555

Smith, G. C., Liu, Y., Benkiran, M., Chikhar, K., Surcel Colan, D., Gauthier, A.-A., Testut, C.-E., Dupont, F., Lei, J., Roy, F., Lemieux, J.-F., and Davidson, F. (2021). The Regional Ice Ocean Prediction System v2: a pan-Canadian ocean analysis system using an online tidal harmonic analysis. *Geoscientific Model Development,* 14, 1445-1467, https://doi.org/10.5194/gmd-14-1445-2021

Spreen, G., Kwok, R., Menemenlis, D., and Nguyen, A. T. (2017). Sea-ice deformation in a coupled ocean–sea-ice model and in satellite remote sensing data. *The Cryosphere,* 11, 1553-1573, https://doi.org/10.5194/tc-11-1553-2017

Stark, J. D., Ridley, J., Martin, M., and Hines, A. (2008), Sea ice concentration and motion assimilation in a sea ice-ocean model. *Journal of Geophysical Research: Oceans,* 113(C5), https://doi.org/10.1029/2007JC004224

Stern, H., Lindsay, R. (2009). Spatial scaling of Arctic sea ice deformation. *Journal of Geophysical Research: Oceans,* 114(C10), https://doi.org/10.1029/2009JC005380

Sumata, H., Lavergne, T., Girard-Ardhuin, F., Kimura, N., Tschudi, M. A., Kauker, F., Karcher, M., Gerdes, R. (2014). An intercomparison of Arctic ice drift products to deduce uncertainty estimates. *Journal of Geophysical Research: Oceans,* 119(8), 4887-4921, https://doi.org/10.1002/2013JC009724

Tandon, N. F., Kushner, P. J., Docquier, D., Wettstein, J. J., and Li, C. (2018). Reassessing sea ice drift and its relationship to long-term Arctic sea ice loss in coupled climate models. *Journal of Geophysical Research: Oceans,* 123, 4338-4359. https://doi.org/10.1029/2017JC013697

Thorndike, A. S., Rothrock, D. A., Maykut, G. A., Colony, R. (1975). The thickness distribution of sea ice. *Journal of Geophysical Research: Oceans,* 80(33), 4501-4513, https://doi.org/10.1029/JC080i033p04501

Thorndike, A. S., Colony, R. (1982). Sea ice motion in response to geostrophic winds. *Journal of Geophysical Research: Oceans,* 87(C8), 5845-5852, https://doi.org/10.1029/JC087iC08p05845

Tian-Kunze, X., Kaleschke, L., Maaß, N., Mäkynen, M., Serra, N., Drusch, M., and Krumpen, T. (2014). SMOS-derived thin sea ice thickness: algorithm baseline, product specifications and initial verification. *The Cryosphere,* 8, 997-1018, https://doi.org/10.5194/tc-8-997-2014

Tonani M., et al. (2015). Status and future of global and regional ocean prediction systems. *Journal of Operational Oceanography,* 8(sup2), s201-s220, http://doi.org/10.1080/1755876X.2015.1049892

Toyoda, T., Hirose, N., Urakawa, L. S., Tsujino, H., Nakano, H., Usui, N., Fujii, Y., Sakamoto, K., and Yamanaka, G. (2019). Effects of Inclusion of Adjoint Sea Ice Rheology on Backward Sensitivity Evolution Examined Using an Adjoint Ocean-Sea Ice Model. *Monthly Weather Review,* 147(6), 2145-2162, https://doi.org/10.1175/MWR-D-18-0198.1

Tremblay, L.-B., and Mysak, L. A. (1997). Modeling Sea Ice as a Granular Material, Including the Dilatancy Effect. *Journal of Physical Oceanography,* 27(11), 2342-2360. https://doi.org/10.1175/1520-0485(1997)027<2342:MSIAAG>2.0.CO;2

Tsamados, M., Feltham, D. L., and Wilchinsky, A. V. (2013). Impact of a new anisotropic rheology on simulations of Arctic sea ice. *Journal of Geophysical Research: Oceans,* 118, 91-107, https://doi.org/10.1029/2012JC007990

Tsamados, M., Feltham, D. L., Schroeder, D., Flocco, D., Farrell, S. L., Kurtz, N., Bacon, S. (2014). Impact of Variable Atmospheric and Oceanic Form Drag on Simulations of Arctic Sea Ice. *Journal of Physical Oceanography,* 44, 1329-1353, https://doi.org/10.1175/JPO-D-13-0215.1

Turner, A. K., and Hunke, E. C. (2015). Impacts of a mushy-layer thermodynamic approach in global sea-ice simulations using the CICE sea-ice model. *Journal of Geophysical Research: Oceans,* 120, 1253-1275, https://doi.org/10.1002/2014JC010358

Turner, A. K., Hunke, E. C., and Bitz, C. M. (2013). Two modes of sea-ice gravity drainage: A parameterization for large-scale modeling. *Journal of Geophysical Research: Oceans,* 118, 2279-2294, https://doi.org/10.1002/jgrc.20171

Turner, A. K., Peterson, K. J., and Bolintineanu, D. (2022). Geometric remapping of particle distributions in the Discrete Element Model for Sea Ice (DEMSI v0.0). *Geoscientific Model Development,* 15, 1953-1970, https://doi.org/10.5194/gmd-15-1953-2022

Urrego-Blanco, J. R., Urban, N. M., Hunke, E. C., Turner, A. K., and Jeffery, N. (2016). Uncertainty quantification and global sensitivity analysis of the Los Alamos sea ice model. *Journal of Geophysical Research: Oceans,* 121, 2709-2732, https://doi.org/10.1002/2015JC011558

Usui, N., Ishizaki, S., Fujii, Y., Tsujino, H., Yasuda, T., Kamachi, M. (2006). Meteorological Research Institute multivariate ocean variational estimate (MOVE) system: Some early results. *Advances in Space Research,* 37(4), 806-822, https://doi.org/10.1016/j.asr.2005.09.022

Vancoppenolle, M., Bitz, C. M., and Fichefet, T. (2007). Summer landfast sea ice desalination at Point Barrow, Alaska: Modeling and observations. *Journal of Geophysical Research: Oceans,* 112(C4), https://doi.org/10.1029/2006JC003493

Vancoppenolle, M., Fichefet, T., Goosse, H., Bouillon, S., Madec, G., and Maqueda, M. A. M. (2009). Simulating the mass balance and salinity of Arctic and Antarctic sea ice. 1. Model description and validation. *Ocean Modelling,* 27(1-2), 33-53, https://doi.org/10.1016/j.ocemod.2008.10.005

Wackernagel, H. (2003). Multivariate Geostatistics. An Introduction with Applications. Springer Science & Business Media, 12 feb 2003 - 388 pp.

Waters, J., Lea, D.J., Martin, M.J., Mirouze, I., Weaver, A., and While, J. (2015). Implementing a variational data assimilation system in an operational 1/4 degree global ocean model. *Quarterly Journal of the Royal Meteorological Society,* 141(687), 333-349, https://doi.org/10.1002/qj.2388

Weiss, J., and Marsan, D. (2004). Scale properties of sea ice deformation and fracturing. *Comptes Rendus Physique,* 5(7), 735-751, https://doi.org/10.1016/j.crhy.2004.09.005

Wilchinsky, A. V., and Feltham, D. L. (2004). A continuum anisotropic model of sea-ice dynamics. *Proceedings of the Royal Society A,* 460(2047), https://doi.org/10.1098/rspa.2004.1282

Williams, T., Korosov, A., Rampal, P., Ólason, E. (2021). Presentation and evaluation of the Arctic sea ice forecasting system neXtSIM-F. *The Cryosphere,* 15, 3207-3227, https://doi.org/10.5194/tc-15-3207-2021

Winton A. (2000). A Reformulated Three-Layer Sea Ice Model. *Journal of Atmospheric and Oceanic Technology,* 17(4), 525-531, https://doi.org/10.1175/1520-0426(2000)017<0525:ARTLSI>2.0.CO;2

WMO (1970). Sea-ice nomenclature, terminology, codes and illustrated glossary. WMO Rep. WMO/OMM/BMO 259, 121 pp.

Xie, J., Bertino, L., Counillon, F., Lisæter, K. A., and Sakov, P. (2017). Quality assessment of the TOPAZ4 reanalysis in the Arctic over the period 1991–2013. *Ocean Science,* 13(1), 123-144, http://doi.org/10.5194/os-13-123-2017

Zygmuntowska, M., Rampal, P, Ivanova, N., and Smedsrud, L. H. (2014). Uncertainties in Arctic sea ice thickness and volume: new estimates and implications for trends. *The Cryosphere,* 8, 705-720, https://doi.org/10.5194/tc-8-705-2014

7.
Storm surge modelling

CHAPTER COORDINATOR

Fujiang Yu

CHAPTER AUTHORS *(in alphabetical order)*

David Byrne, Jianxi Dong, Begoña Pérez Gómez, and Shichao Liu

7. Storm surge modelling

7.1. General introduction to storm surge

7.1.1. Overview of storm surge disaster

7.1.1.1. Disasters and forecasting

7.1.1.2.The impact of climate change on storm surge

7.1.2. Basic description of storm surge phenomena

7.1.3. Physics of storm surge

7.1.3.1. Meteorological forcing

7.1.3.2. The influence of topography and bathymetry

7.2. Storm surge modelling

7.2.1. Architecture components and singularities

7.2.2. Input data: available sources and data handling

7.2.2.1. Bathymetry and geometry

7.2.2.2. Tidal boundaries

7.2.2.3. Meteorological inputs

7.2.3. Modelling component

7.2.3.1. Governing equations

7.2.3.2. 2D barotropic and 3D baroclinic models for storm surge

7.2.3.3. Wetting and drying scheme

7.2.3.4. Grid types

7.2.3.5. Discretization method

7.2.3.6. Existing models for storm surge modelling

7.2.4. Data assimilation systems

7.2.4.1. Sources of error in storm surge models

7.2.4.2. Assimilated data sources for storm surge modelling

7.2.4.3. Application of data assimilation to real time forecasting systems

7.2.4.4. Examples from real operational systems

7.2.5. Ensemble modelling

7.2.6. Validation strategies

7.2.7. Outputs

7.2.7.1. Time series outputs

7.2.7.2. Maximum elevation field

7.2.7.3. Ensemble forecast field

7.2.7.4. Animation output

7.2.8. Existing operational storm surge forecasting systems

7.3. References

7.1.
General introduction to storm surge

Many natural phenomena can cause the sea to rise and fall, such as wind, air pressure, celestial gravity, earthquakes, etc. The sea level changes caused by different phenomena have different periods. For example, wind waves have a period of several seconds, tsunami waves of few minutes to tens of minutes, and the period of storm surge and astronomical tide is about several hours to several days (Figure 7.1).

Among them, the storm surge brings huge economic losses and risks to coastal countries every year (Murty, 1988). In order to reduce the impact of storm surge disasters on coastal residents, understanding and forecasting storm surge have always been an important objective for marine forecasters.

This chapter will introduce the main overview and elements of storm surge modelling, to guide technical personnel to engage in related work and give full play to the role of storm surge numerical models in various fields.

7.1.1. Overview of storm surge disaster

7.1.1.1. Disasters and forecasting

Storm surge refers to the phenomenon of abnormal water level rise in a coastal or inland body caused by strong atmospheric disturbances, such as tropical cyclones (typhoons, hurricanes), extratropical cyclones, strong winds from cold fronts, and sudden change in atmospheric pressure.

Figure 7.2. The impact of the storm surge caused by the super typhoon Haiyan on the Philippines, the coastal villages of Tacloban were destroyed (Credits: Photography Marcel Crozet, ILO, 11-2013).

As a complex coastal dynamic process of major coastal marine disasters, storm surge has received much attention by major affected countries all over the world. Storm surge disasters are mainly caused by the abnormal water level rise and by flooding. The disaster causing factors include not only the storm surge, but also coupling with the effect of astronomical tide and nearshore waves. Storm surge disasters (Figure 7.2, Figure 7.3, and Figure 7.4) not only include the damage to ports,
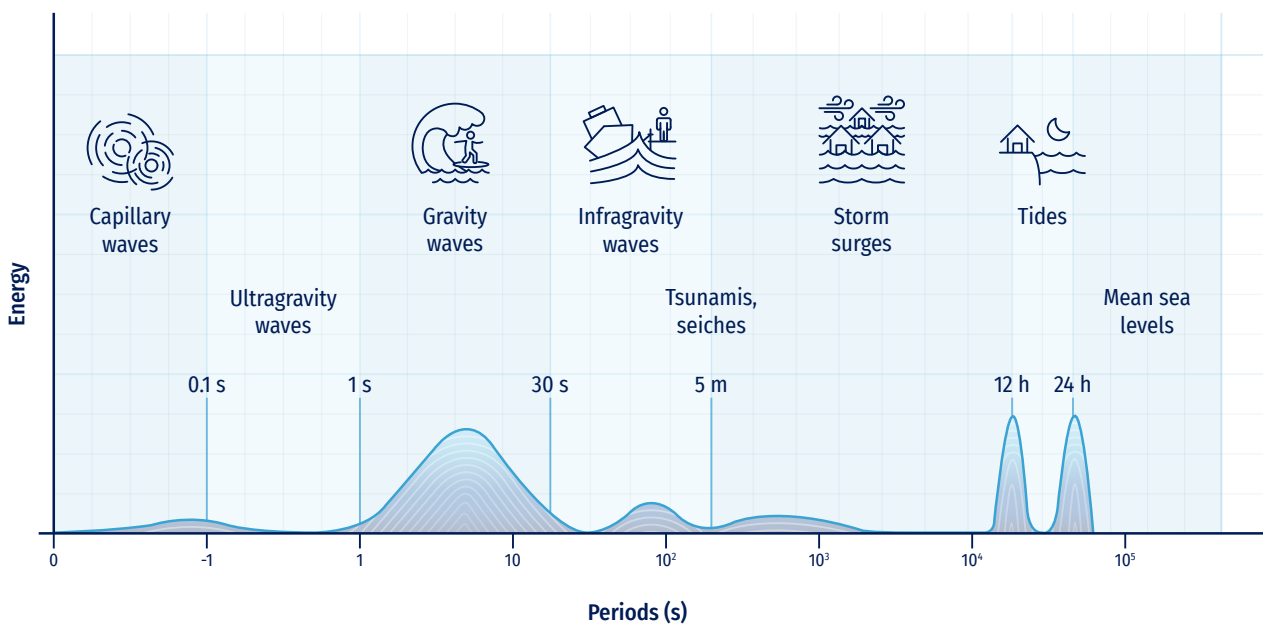
Figure 7.1. Frequencies and periods of the vertical motions of the ocean surface (adapted from Pérez et al., 2013).

Figure 7.3. People walk among debris next to a ship washed ashore in the aftermath of super typhoon Haiyan in Tacloban, Philippines, 11 November 2013. (Credits: ILO, 11-2013).

wharfs, dykes, but also include the disasters caused by flooding houses, farmland, and aquaculture facilities.

Areas with severe storm surges are shown on a global map (Figure 7.5). The Gulf Coast of North America and the eastern coast of the United States are affected by storm surges generated by Atlantic hurricanes. In Europe, the North Sea coast is often affected by extratropical cyclones, which bring storm surge disaster. The coast of the Bay of Bengal in the Indian Ocean is threatened by storm surges caused by typhoons in the Indian Ocean. On the western Pacific Ocean coast, China, Japan, and the Philippines are frequently affected by storm surges caused by typhoons, and the north coast of China is also affected by extratropical cyclones.

In addition to the areas severely affected by the storm surge mentioned above, other countries or regions may also be affected by the storm surge. Areas with low elevation may face the threat of storm surge inundation, and the approaching channel may not meet the navigation requirements due to the drop in water level. For example, 20% of the land in the Netherlands is below mean sea level, and large areas of flooding may be caused without a very severe storm surge. For this reason, they built the famous Storm Surge Barriers

(Mooyaart and Jonkman, 2017). In Spain, surges of 60 cm contribute significantly to inundation processes.

Figure 7.4. The impact of the storm surge caused by the super typhoon Haiyan on the Philippines, the coastal villages of Tacloban were inundated with water (Credits: Photography Marcel Crozet, ILO, 11-2013).

Figure 7.5. Areas severely affected by storm surge.

Storm surge forecasting is an important means of reducing disasters and losses, and a very necessary link in disaster prevention and mitigation. The methods of storm surge forecasting can be divided into two categories: empirical statistical forecasting and numerical forecasting. With the rapid development of computer technology, numerical models play an increasingly important role in storm surge forecasting. The establishment of a storm surge numerical model will provide strong support for storm surge forecasting. In addition to providing help for disaster prevention and mitigation, the numerical model of storm surge can also be used in offshore engineering design and marine disaster risk assessment of coastal cities.

In recent years, with the rapid economic development of coastal cities and the urgent needs of disaster prevention and mitigation, more and more ocean forecasting centres have started to establish operational storm surge models to provide relevant services for the above activities and purposes (more information in Section 7.2.8).

7.1.1.2. The impact of climate change on storm surge

Coastal cities are directly affected by global warming, sea temperature continues to increase, sea level fluctuates and rises, and natural disasters such as storm surges and huge waves show an increasing trend. Statistics show that there is a significant increase in global super typhoons (or category 4 and 5 hurricanes). In the 1970s, the number of super

typhoons accounted for 20% of the total tropical cyclones, while it rose to 35% in the 1990s. Among them, the most evident increase was in the North Pacific, Indian Ocean, and Southwest Indian Ocean, while the increase was the least in the North Atlantic (Webster et al., 2005). Therefore, storm surge disasters caused by typhoons showed an increasing trend, as well as the risk of storm surge disasters in coastal cities. The tide observation data also shows this characteristic. After the storm surge of typhoon Hato (2017) and typhoon Mangkhut (2018) affected coastal cities such as Zhuhai and Shenzhen in China, the return period of coastal tide levels changed significantly. The Hengmen Station, located on the west bank of the Pearl River Estuary (China), has shown that the tide level return period has been reduced from 200 years to 50 years, as well as the original 100 years tide level return period been reduced to 50 years at the Sanzao Station, and the Chiwan Station on the east bank of the Pearl River Estuary.

Sea level rise directly leads to the expansion of storm surge inundation area, increases the mean sea level, and various characteristic tide levels. The increased water depth and enhanced nearshore waves further strengthen the impact of storm surges.

7.1.2. Basic description of storm surge phenomena

Storm surges have periods of several hours to several days, and are usually superimposed on tides, wind waves and
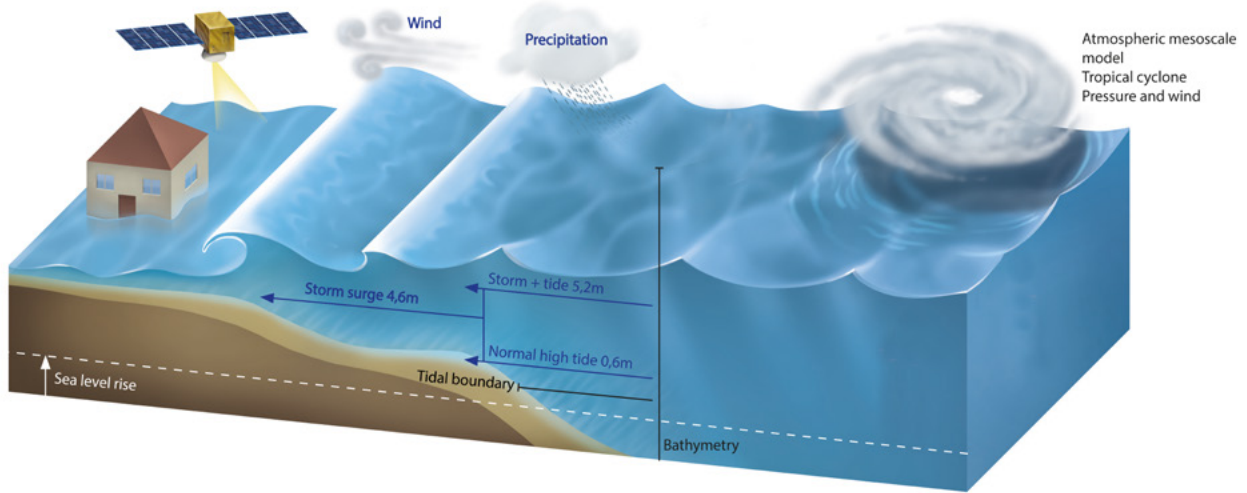
Figure 7.6.   Storm surge components and drivers.

swells (with a period of several seconds). Combination of these three factors causes extreme rise of coastal water level and often leads to huge storm surge disasters. However, sometimes the opposite situation can also be encountered: the wind blowing away from the direction of the open coast for a long time causes the water level to drop sharply along the shore and shoals exposed. In this case, the normal navigation is seriously affected, as well as anchoring of ships, especially large oil tankers.

The spatial range of storm surges is generally between tens and thousands of kilometres, and the time scale or period is about several to hundreds hours, which is between a tsunami and the astronomical tide. Since the area affected by storm surges moves with the movement of meteorological forcing, sometimes a storm surge process can affect a coastal area of 1000-2000km, and the impact time can be up to several days. In addition, the period of water level change by a storm surge ranges from some hours to several days, excluding seiches, tsunamis and wind waves.

According to its standard definition, a storm surge is caused by atmospheric disturbance, specifically abnormal alterations in water surface due to strong winds and atmospheric pressure changes. Storm surge can also occur in inland bodies, such as the Great Lakes in the US. In recent years, studies have shown that the nearshore waves breaking can also cause rise of the water level, in the range of tens of centimetres to metres, called wave setup. With the perspective of changes occurred in modern times, the definition of storm surges should be revised as the following: "storm surge refers to strong atmospheric disturbances, such as tropical cyclones (typhoons and hurricanes), extratropical cyclones, strong wind due to cold fronts, and sudden changes in atmospheric pressure inducing

abnormal water level rise combined with nearshore wave set-up" (Yu et al., 2020). See representation of storm surge components and drivers in Figure 7.6.

Meteorological tsunami, or meteotsunami, is caused by strong winds and sudden changes in atmospheric pressure and its period is equivalent to a tsunami. In the Tsunami Glossary ($\mathscr{O}$[1]) by the IOC's ITIC, meteotsunami is defined as following: "Tsunami-like phenomena generated by meteorological or atmospheric disturbances. These waves can be produced by atmospheric gravity waves, pressure jumps, frontal passages, squalls, gales, typhoons, hurricanes and other atmospheric sources. Meteotsunamis have the same temporal and spatial scales as tsunami waves and can similarly devastate coastal areas, especially in bays and inlets with strong amplification and well defined resonant properties (e.g. Ciutadella Inlet, Baleric Islands; Nagasaki Bay, Japan; Longkou Harbour, China; Vela Luka, Stari Grad and Mali Ston Bays, Croatia)."

The water level recorded at coastal or estuarine tide stations usually include a combination of changes caused by astronomical tides, storm surges, tsunamis, and other long waves. Generally, tide gauges filter out sea surface fluctuations caused by short-period waves in the order of seconds. The separation of storm surge phases is obtained by linear subtracting the harmonic analysis forecast astronomical tide from the hourly data (Figure 7.7 and Figure 7.8).

1. http://itic.ioc-unesco.org/index.php?option=com_content&view=category&id=2339&Itemid=2433
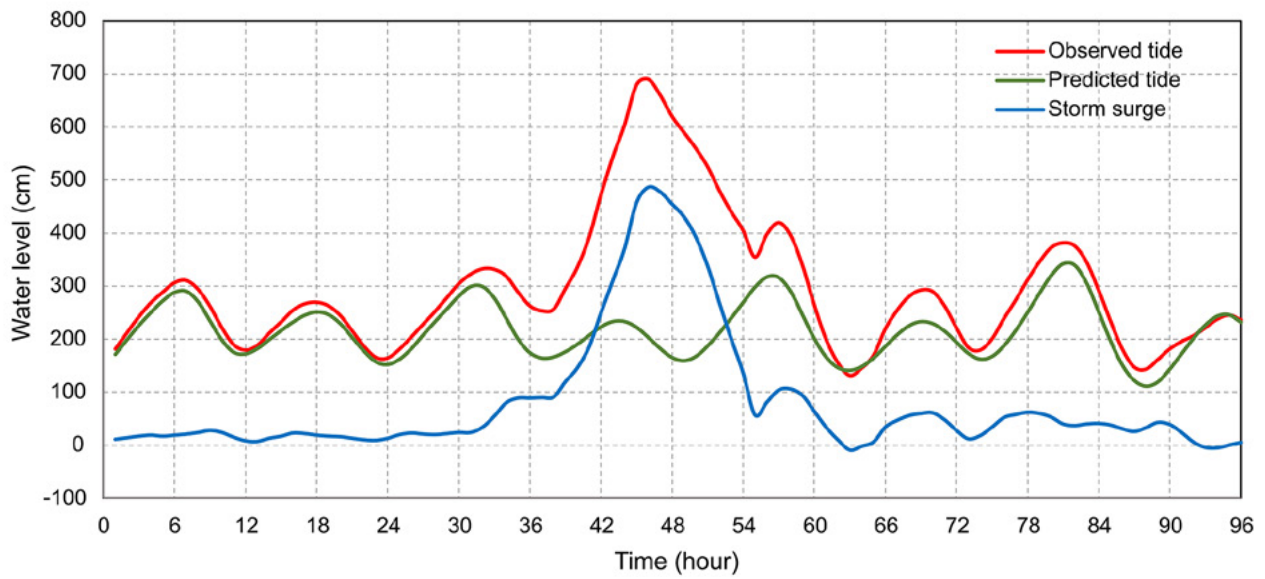
Figure 7.7. Observed water level, astronomical tide, and storm surge (water level subtracting astronomical tide); data from Zhanjiang tide station (China).
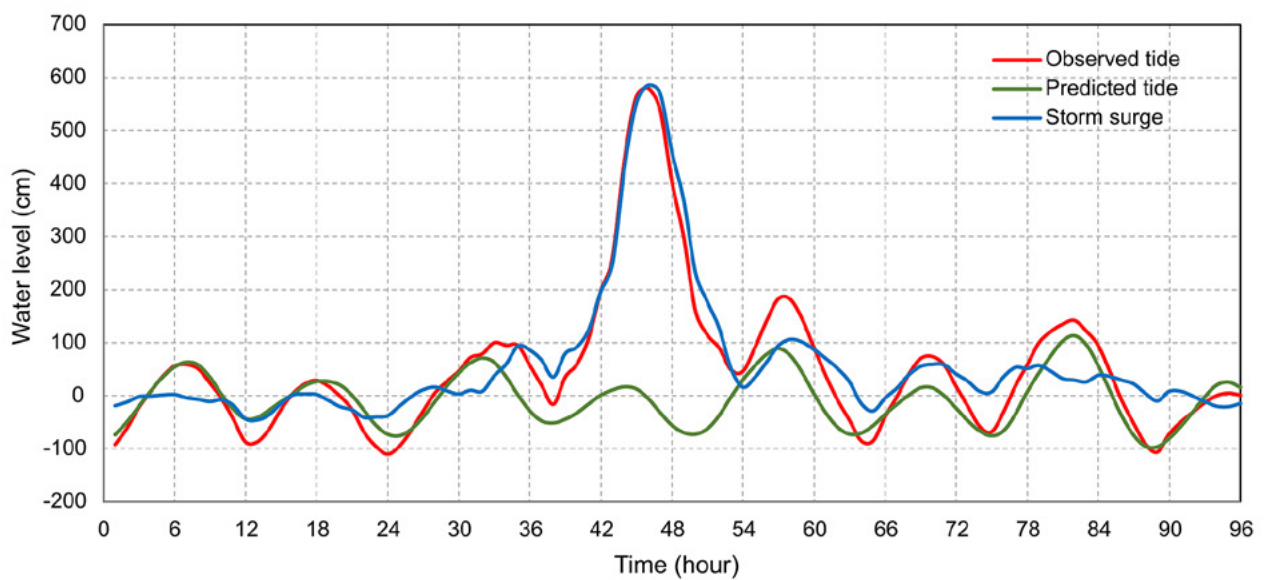
Figure 7.8. Observed water level, astronomical tide, and storm surge (water level subtracting astronomical tide); data from Nandu tide station (China).

7.1.3. Physics of storm surge

7.1.3.1. Meteorological forcing

Meteorological forcing is the main driver for storm surges. When a storm passes over the open sea, the low centre pressure of the storm will cause the water level to rise. The height of the surge is related to the barometric pressure drop of the storm, i.e. 1 mbar decrease corresponds approximately to 1 cm increase in sea level (Schalkwijk, 1948; Myers, 1954; Pore, 1964). The raised sea surface will propagate with the movement. At the same time, a kind of free long wave, induced by raised sea surface, could spread outward from the storm centre. This process will typically take place near the coast when interactions with bathymetry changes become relevant. If the pressure disturbance is moving at a speed comparable to the shallow water wave speed, the water level disturbance may be greatly amplified by resonance (Harris, 1957).

Compared with the long wave effect, the wind shear stress is the dominating forcing of storm surges in shallow water of nearshore and estuaries (Miller, 1958; Pore, 1964). With the wind blowing continuously, water accumulates at the coastal line causing the water level to rise. This phenomenon is referred to as "wind set-up" and its magnitude is inversely proportional to water depth. The wind set-up is particularly evident in semi-enclosed seas, such as Bohai Bay in China.

7.1.3.2. The influence of topography and bathymetry

Storm surge is not only influenced by astronomical tide and waves, but also by topography and bathymetry. Due to the shoreline block, storm surge propagates from ocean to nearshore. The surge is generated by water accumulation at the shoreline. The magnitude of the surge is controlled by the shape of the shoreline. In case of onshore direction, semi-enclosed bays or estuaries contribute to intensify storm surge than straight shoreline. That is because the shape of the semi-enclosed bay and estuary hinder water flow out. The water accumulates in the semi-enclosed bay or estuary continuously, resulting in a greater storm surge.

Another factor that can impact storm surge is the variation of bathymetry from the continental shelf to estuaries and coasts. Generally, the water depth of estuaries and coasts is shallower than the continental shelf, and the propagation speed of the storm surge wave is approximately proportional to the square root of the water depth. Therefore, the speed of the wave propagation at estuaries and coasts is slower than at the continental shelf. The storm surge waves converge at estuaries and coasts, causing the water level to increase.

On the other hand, in the process of storm surge wave propagation, the water depth at the crest is greater than at the preceding trough, and the movement of the crest is faster. So, the more waves move inland, the smaller the interval between the crests. This is more pronounced where the continental shelf is longer, for example in the North Sea, and hence larger storm surges will be caused due to the long continental shelf extension.

The propagation speed of storm surge waves is controlled by the water depth: it moves faster at high tide than at low tide. The wind effect is inversely proportional to the total water depth, and the same wind speed will produce a greater surge at low tide than at high tide. Combining the two effects above, surge in an estuary tends to be greater on the rising stage of the tide (Doodson, 1929; Doodson, 1956; Rossiter, 1961).

Extremely accurate topography and bathymetry, especially for shallow water areas, is key to storm surge modelling.

7.2.
Storm surge modelling

7.2.1. Architecture components and singularities

Storm surge models are generally based on the two-dimensional shallow water equation to compute the water level and velocity. According to different modelling purposes, the storm surge model can be divided into: i) storm surge model without tide; ii) storm surge model including astronomical tide; and iii) storm surge flooding model considering inundation.

In a storm surge model without tide, only the effect of the meteorological forcing needs to be considered. Obtained result is only the water level rising and falling under the effect of atmospheric pressure and wind. The role of this model is generally to provide forecasters with a reference for the magnitude of storm surge when making forecasts, and it cannot truly reflect the fluctuations of water level.

Based on the former model, the tidal boundary conditions and tidal potential are introduced in the total water level storm surge model, in which the nonlinear interaction between
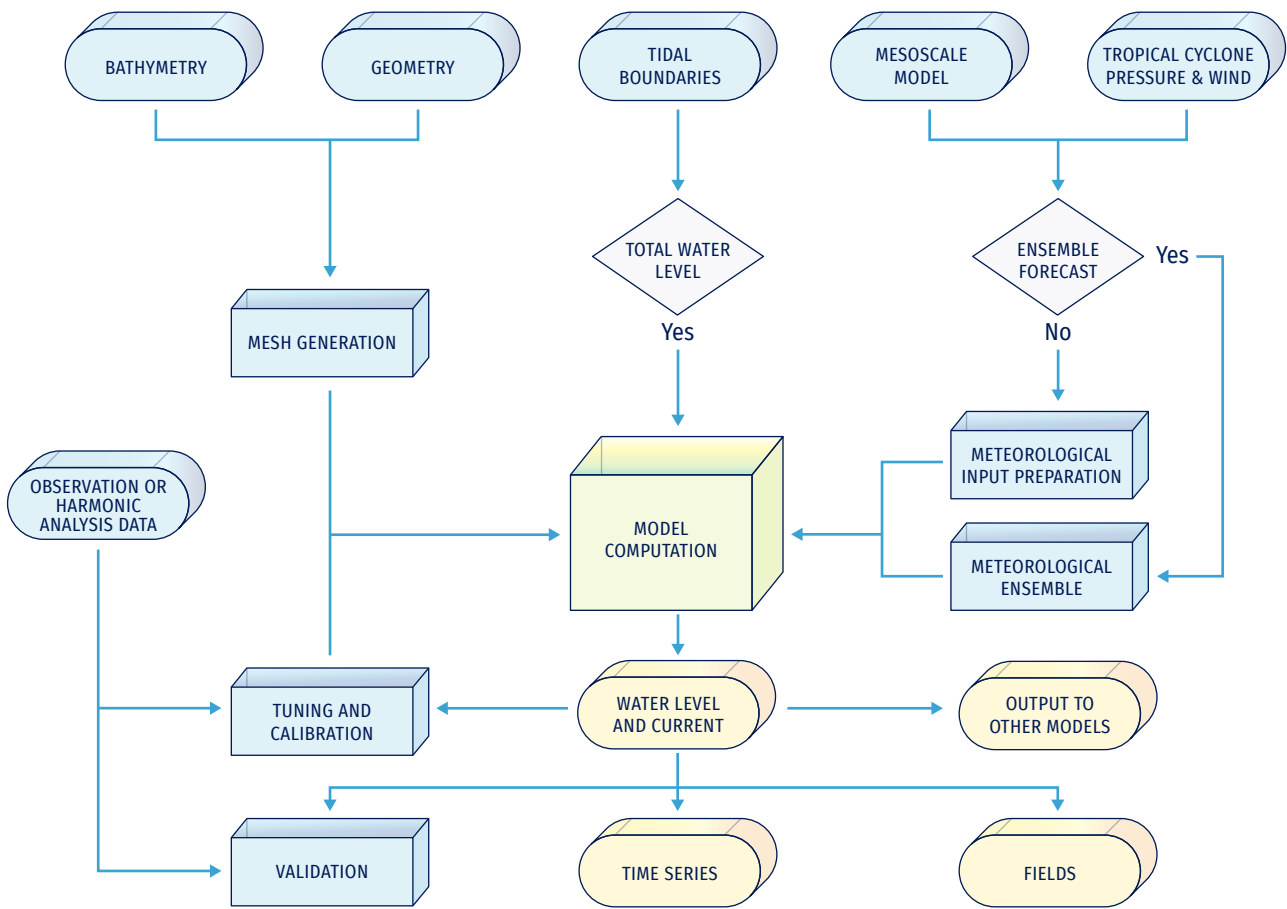
Figure 7.9.   Storm surge modelling flow chart.

storm surge and astronomical tide can be fully considered in the model. This model can be used for releasing storm surge numerical forecast products and providing reference for coastal response to storm surge disasters. It can also provide the water level changes in the target area under the influence of extreme weather conditions for coastal engineering (such as harbours, wharfs, seawalls, offshore wind farms, etc.).

The storm surge flooding model considering inundation is more complicated than the previous two models. The interaction of storm surge and astronomical tide, and the interaction of storm surge and wave are also considered in the model. The inundation range and depth of the coastal area can be obtained by a storm surge simulation. Figure 7.9 shows the main storm surge modelling components used by a forecasting system and that will be detailed in the next sections.

7.2.2. Input data: available sources and data handling

7.2.2.1. Bathymetry and geometry

Reliable and accurate shoreline and bathymetry data are the basis for modelling of storm surge, tidal, and storm surge flooding models. In the process of model setup, the computational grid should be determined according to the demand, and then the data of shoreline and bathymetry should be collected according to the location and scope.

Sources of bathymetric data can be found on Section 4.2.4. These data need to be used with caution when establishing high-resolution storm surge models. As the bathymetry of coastal or estuary changes rapidly over time, these upstream data may not be able to be updated in time. Therefore, the correctness of the data needs to be verified before it is used.

When the published upstream data do not meet the requirements, it is preferable to use the latest sea chart or high-resolution DEM data. In addition, the datum of the data needs to be confirmed as, due to different sources of data, the datum could be different. In order to truly reflect the effects of bathymetry on storm surges, data from different sources need to be unified on the same datum.

7.2.2.2. Tidal boundaries

In the storm surge and storm surge flooding modelling, tidal waves are generally used as open boundary conditions. Open boundary conditions can be velocity, water level, or harmonic constant.

Tidal height at any location and time can be written as a function of harmonic constituents according to the following general relationship:

$$H(t) = H_0 + \sum_{n=1}^{N} f_n H_n \cos[a_n t + (V_0 + u)_n - g_n] \qquad (7.1)$$

where

$H(\mathrm{t})$ = height of the tide at any time t

H_0 = mean water level above some defined datum such as mean sea level

H_n = mean amplitude of tidal constituent n

f_n = factor for adjusting mean amplitude H_n values for specific times

a_n = speed of constituent n in degrees/unit time

t = time measured from some initial epoch or time, i.e., t=0 at t_0

$(V_0 + u)_n$ = value of the equilibrium argument for constituent n at Greenwich and when t=0

g_n = epoch of constituent n, i.e., phase shift from tide-producing force to high tide from t_0

In Eq. 7.1, for a tidal component, the f_n and the $(V_0 + u)_n$ will change with time, and the H_n and the g_n will change with the geographical location. Therefore, according to the start time of simulation, the f_n and $(V_0 + u)_n$ of the proposed tidal component should be set in the model, and the H_n and the g_n boundary conditions should be given according to the position of the boundary grid node.

The location of the tidal open boundary is critical. First of all, it is necessary to ensure that the grid can completely cover the definition area. Secondly, it is better to set the open boundary near the tidal station, because the tidal constituent data near the tidal station is more accurate. Finally, it is preferable not to set the open boundary at the amphidromic point nearby, because too small amplitude will bring uncertainty to the simulation.

The data for tidal boundaries can be obtained by downloading publicly available data on tidal harmonic constants covering most of the oceans. TPXO (Egbert et al., 1994; Egbert and Erofeeva, 2002) is a widely used global tidal data. It is a series of fully global models of ocean tides, which best fits, in a least squares sense, the Laplace Tidal Equations and altimetry data. The TPXO models include eight primary (M2, S2, N2, K2, K1, O1, P1, Q1), two long period (Mf, Mm) and 3 non-linear (M4, MS4, MN4) harmonic constituents (plus 2N2 and S1 for TPXO9 only). More detailed information can be found at 🔗[2]. In addition, also the NAO.99b tide model (Matsumoto et al., 2000 and 2001), which is developed by assimilating TOPEX/POSEIDON Altimeter Data into Hydrodynamical Model, can provide global tide data. This model provides 16 short-period harmonic constituents (M2, S2, K1, O1, N1, N2, P1, K2, Q1, M1, J1, OO1, 2N2, Mu2, Nu2, L2, L2, and T2), 7 long-period harmonic constituents (Mf, Mm, Msf, Msm, Mtm, Sa, Ssa) data with of 0.5 degrees, and provides 16 short-period harmonic constants around Japan with a resolution of 5 minutes. More detailed information can be found at 🔗[3].

Once the model and tidal boundaries have been established, they need to be tuned and calibrated before using. The model can be run with tidal boundaries and tidal potential. The tidal results are more sensitive to changes in the bottom friction coefficient and the bathymetry. By calibrating the tidal simulation, a reasonable bottom friction coefficient can be set for the model. At the same time, the difference in the tidal results caused by the bathymetry from dissimilar sources helps to find more suitable bathymetry data for the model.

7.2.2.3. Meteorological inputs

In storm surge or storm surge flooding modelling, the input from meteorological forcing mainly includes surface wind shear stress and atmospheric pressure at sea surface level. In deep water, the sea level rises are mainly caused by the atmospheric pressure gradient, i.e. the water level rises approximately 1 cm at every reduction in pressure of 1 mbar. In shallow water, estuary and nearshore, wind shear stress is the dominant force of the storm surge, and the sea level rise is proportional to the square of wind speed. Therefore, accurate meteorological inputs, especially sea surface wind, is essential for storm surge modelling. The accuracy of storm surge results depends largely on the quality of meteorological data.

---

2. https://www.tpxo.net/global

3. https://www.miz.nao.ac.jp/staffs/nao99/index_En.html

Depending on the storm surge modelling purposes, the types of meteorological forcing input are different. At present, there are two main sources of wind field for storm surge modelling: atmospheric model and empirical formula. Atmospheric models can provide global or regional meteorological fields; the main elements required for storm surge calculation are sea level pressure and 10 metres wind. The horizontal resolution of these data is between ten and tens of kilometres, and the forecast period can reach up to 240 hours. This kind of meteorological field is mainly used in the calculation of storm surge caused by extratropical cyclones. Compared with extratropical cyclones, tropical cyclones are smaller in scale but stronger in intensity, and atmospheric models cannot resolve the structure of tropical cyclones well. Therefore, the meteorological field from atmospheric models is not applicable to the typhoon storm surge calculation. Empirical formulas for tropical cyclone pressure and wind are often applied to create meteorological forcing fields for tropical storm surge models. Since the wind speed and pressure structure of tropical cyclones are close to axisymmetric, their distribution can be reasonably represented with an empirical formula for the radial distribution of wind or pressure.

The commonly used empirical formulas for pressure distribution mainly include the following:

Takahashi (1939):

$$\frac{P(r) - P_0}{P_\infty - P_0} = 1 - \frac{1}{1 + \frac{r}{R}} \tag{7.2}$$

Myers (1954):

$$\frac{P(r) - P_0}{P_\infty - P_0} = 1 - \frac{1}{\sqrt{1 + 2\left(\frac{r}{R}\right)^2}} \tag{7.3}$$

Myers (1954):

$$\frac{P(r) - P_0}{P_\infty - P_0} = e^{\frac{-R}{r}} \tag{7.4}$$

Jelesnianski (1965):

$$\frac{P(r) - P_0}{P_\infty - P_0} = \frac{1}{4}\left(\frac{r}{R}\right)^3, 0 \le r < R$$

$$\frac{P(r) - P_0}{P_\infty - P_0} = 1 - \frac{3R}{4r}, R \le r < \infty \tag{7.5}$$

Bjerknes (1921):

$$\frac{P(r) - P_0}{P_\infty - P_0} = 1 - \left[1 + \left(\frac{r}{R}\right)^2\right]^{-1} \tag{7.6}$$

Holland (1980):

$$\frac{P(r) - P_0}{P_\infty - P_0} = e^{-\frac{A}{R^B}} \tag{7.7}$$

where:

P_∞ = the ambient pressure;

P_0 = the pressure at the tropical cyclone centre;

$P(r)$ = the pressure at r from tropical cyclone centre;

A and B = empirical parameters that control the tropical cyclone size.

The tropical cyclone wind field is formed by the superposition of two vector fields (Ueno, 1981). The first vector field is a wind field symmetrical to the centre of the cyclone. The wind vector passes through the isobar and points to the left with a 20° deflection angle.

The wind speed is proportional to the gradient wind, which can be expressed by the following formula:

$$V_v = V_r \frac{2Rr}{R^2 + r^2} \tag{7.8}$$

V_r = the maximum wind speed;

R = the radius of the maximum wind.

The second vector field caused by the movement of cyclone is superimposed on the wind system for the stationary symmetric cyclone, and that the wind velocity $\vec{V}_f$ is:

$$\vec{V}_f = \vec{V}_t \exp\left(-\frac{\pi}{4}\frac{|r - R|}{R}\right) \tag{7.9}$$

$\vec{V}_t$ = velocity of typhoon;

R = the radius of the maximum wind.

Consequently, the wind velocity $\vec{W}$ is:

$$\vec{W} = \vec{V}_v + \vec{V}_f \tag{7.10}$$

The typhoon centre pressure, maximum wind speed, moving speed and other parameters can be obtained from websites of national meteorological agencies.

7.2.3. Modelling component

7.2.3.1. Governing equations

The governing equations of numerical simulation were determined by the flow dynamic theory.

The three-dimensional flow equations are as follows:

- Continuity equation:

$$\frac{\partial u}{\partial x} + \frac{\partial v}{\partial y} + \frac{\partial w}{\partial z} = 0 \qquad (7.11)$$

- Momentum equation:

$$\frac{\partial u}{\partial t} + \frac{\partial(uu)}{\partial x} + \frac{\partial(uv)}{\partial y} + \frac{\partial(uw)}{\partial z} - fv =$$
$$-\frac{1}{\rho}\frac{\partial p}{\partial x} + \frac{1}{\rho}\left(\frac{\partial \tau_{xx}}{\partial x} + \frac{\partial \tau_{xy}}{\partial y} + \frac{\partial \tau_{xz}}{\partial z}\right) \qquad (7.12a)$$

$$\frac{\partial v}{\partial t} + \frac{\partial(vu)}{\partial x} + \frac{\partial(vv)}{\partial y} + \frac{\partial(vw)}{\partial z} - fu =$$
$$-\frac{1}{\rho}\frac{\partial p}{\partial y} + \frac{1}{\rho}\left(\frac{\partial \tau_{xy}}{\partial x} + \frac{\partial \tau_{yy}}{\partial y} + \frac{\partial \tau_{yz}}{\partial z}\right) \qquad (7.12b)$$

$$\frac{\partial p}{\partial z} = -\rho g \qquad (7.12c)$$

Based on hydrostatic approximations and incompressible assumption of fluid, the depth integrated two-dimensional storm surge governing equations can be written as:

- Continuity equation:

$$\frac{\partial \xi}{\partial t} + \frac{\partial}{\partial x}[(\xi + h)u] + \frac{\partial}{\partial y}[(\xi + h)v] = 0 \qquad (7.13)$$

- Momentum equation:

$$\frac{\partial u}{\partial t} + u\frac{\partial u}{\partial x} + v\frac{\partial u}{\partial y} - fv + g\frac{\partial \xi}{\partial x} \pm \frac{\tau_{x,s} - \tau_{x,b}}{\rho H}$$
$$+ \frac{1}{\rho}\frac{\partial P}{\partial x} = \epsilon\left(\frac{\partial^2 u}{\partial x^2} + \frac{\partial^2 u}{\partial y^2}\right) \qquad (7.14a)$$

$$\frac{\partial v}{\partial t} + u\frac{\partial v}{\partial x} + v\frac{\partial v}{\partial y} - fu + g\frac{\partial \xi}{\partial y} \pm \frac{\tau_{y,s} - \tau_{y,b}}{\rho H}$$
$$+ \frac{1}{\rho}\frac{\partial P}{\partial y} = \epsilon\left(\frac{\partial^2 u}{\partial x^2} + \frac{\partial^2 u}{\partial y^2}\right) \qquad (7.14b)$$

where:

ξ= free surface elevation relative to the geoid;

h = water depth;

f = Coriolis coefficient;

ρ = density of water;

g = gravitational acceleration;

$(\tau_{x,s}$, $\tau_{x,b})$ = free-surface shear stress in x and y direction;

$$(\tau_{x,b}, \tau_{y,b}) = C_d\rho_a|\underline{W}|(W_x, W_y)$$

$\underline{W}$ = wind speed at 10 metres above sea surface;

W_x , W_y = wind speed components in x and y direction;

C_d = wind Drag coefficient which is relevant to wind speed;

$\tau_{x,b}$, $\tau_{y,b}$ = bottom shear stress in x and y direction;

$$(\tau_{x,b}, \tau_{y,b}) = \frac{\rho g\sqrt{u^2 + v^2}}{C^2}(u, v)$$

C = Chezy coefficient, $\quad C = \dfrac{h^{1/6}}{n} \quad$ n is roughness coefficient;

u, v = depth-averaged horizontal velocity components in x and y direction;

$$u = \frac{1}{\xi + h}\int_{-h}^{\xi} u\,dz$$

$$v = \frac{1}{\xi + h}\int_{-h}^{\xi} v\,dz$$

P = atmospheric pressure at the free surface;

ε = depth-averaged horizontal eddy viscosity.

7.2.3.2. 2D barotropic and 3D baroclinic models for storm surge

Hydrodynamic models are generally divided into vertically averaged 2D barotropic, 3D barotropic, or 3D baroclinic models. These types of models can be used for storm surge modelling. Minato (1998) first studied the effect of a 3D model on storm surge results and simulated the water level change caused by Typhoon 7010 in Tosa Bay, Japan. The results showed that the difference between the 3D model and the 2D model is about 2 to 10%. Weisberg and Zheng (2008) found that under the condition of setting the same bottom friction coefficient, the 3D model simulates higher extreme water level than the 2D model. Subsequently, simulating the storm surge of Hurricane Ike in the Gulf of Mexico, Zheng et al. (2013) pointed out that the 2D and the 3D models have differences in the trend and peak values of water level, but the calibration of the bottom friction is more important. Ye et al. (2020) studied the influence of baroclinic models on storm surge simulation results. Sensitivity tests show that the impact of the baroclinic model on storm surge is not significant, but it has a greater impact on current.

Since the vertical velocity distribution structure of the 2D model is different from that of the 3D model, the vertical average velocity is greater than that near the bottom layer, so that the bottom shear stress of the 2D model will be greater. Satisfactory results can be obtained for both types of models by calibrating the bottom friction.

Regarding operational storm surge modelling, computational efficiency is a factor that must be considered. 3D models generally divide the water body into multiple layers vertically, so they require more computing time than 2D models. If the purpose of storm surge modelling is to obtain water level, rather than currents, the 2D models are the best choice for balancing calculation efficiency and accuracy. Most of the existing operational storm surge forecasting systems are 2D models.

7.2.3.3. Wetting and drying scheme

During the simulation of storm surge inundation, the grid points close to the coastline in the model will be either wet or dry due to the fluctuation of water level. Therefore, the model needs to determine the dry and wet state of a grid point according to the state of the surrounding grid points.

Assuming that the state of a certain grid point is wet, if the calculated water level makes the water volume less than zero, then this grid point will become a dry grid point and will not participate in the next calculation. In practical calculations, to prevent the negative value of the water volume at a grid point, which makes the momentum equation and continuity equation meaningless, a threshold value greater than zero is usually selected. When the water volume is less than the threshold value, the state of the grid point is defined as dry.

Assuming that the state of a certain grid point is dry, the first step is to check how many of the surrounding grid points are wet grid points. If more than one is wet grid point, then the water level is averaged over these wet grid points. If the averaged water level is greater than the threshold water level, the state of this grid point may become wet, otherwise it still remains as a dry one. In the second step, it is necessary to further check the transport over the cross-section area between the grid point and the surrounding wet grid points. If these transport cross-section areas are all positive, then the dry grid point becomes a wet grid point and participates in the next calculation; otherwise, it is still a dry grid point.

7.2.3.4. Grid types

The grids used in most sea level models are mainly divided into two categories: structured and unstructured grids. The structured grid nodes are arranged in an orderly manner, and the connection relationship between adjacent nodes is fixed. In contrast, the unstructured grid nodes are arranged in an unordered manner and the adjacent nodes have no fixed connection relationship. Differently from structured grids, unstructured grids with triangular elements allow to adjust the resolution flexibly to depict complex shapes of coastline and estuary (Figure 7.10).
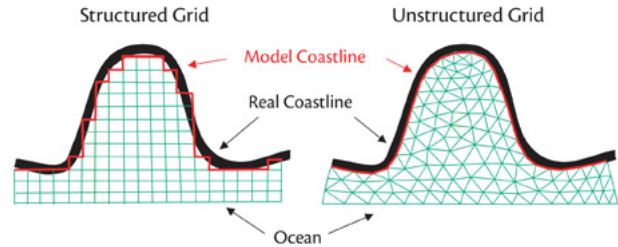
Figure 7.10. Structured grid and unstructured grid at coastal area.

Structured grids mainly have two forms: rectangular grids and curvilinear grids. Relatively speaking, the curvilinear grid can adapt better to the complex shape of the coastline, and it can also realise the change of grid resolution that is more advantageous for storm surge simulation in estuary area (Figure 7.11).
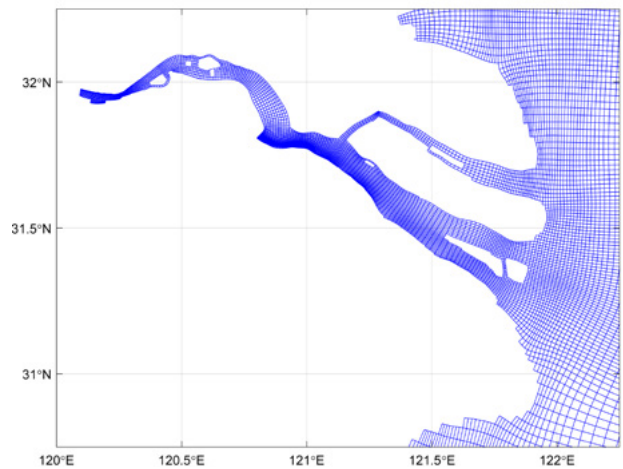
Figure 7.11. An example of curvilinear grid.

Triangular grids were the main forms of unstructured grids until a new form of unstructured grids, the SCVTs (Figure 7.12), appeared in ocean modelling a decade ago (Ringler et al., 2013). Like the triangular grids, the SCVTs can adapt well to complex coastline, and facilitate a smooth transition from coarse resolution grid cell to high resolution grid cell. In addition, they also solve the computational instability problem caused by small acute angles in the triangular grid. At present, the SCVTs model has been used in the China Sea (as shown in Figure 7.13).
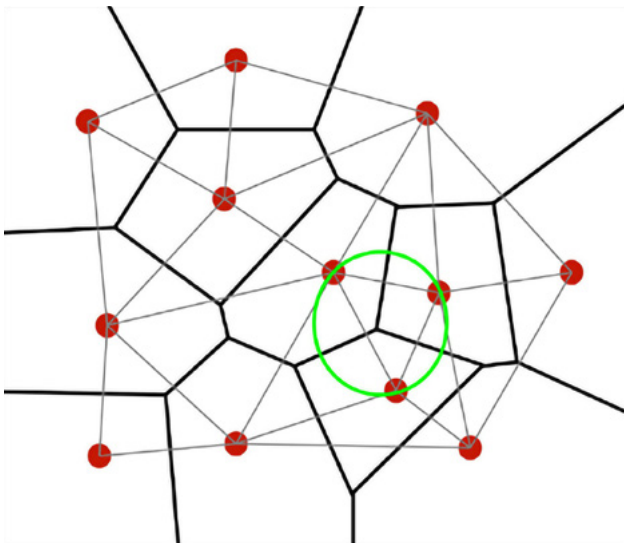
Figure 7.12. An example of Voronoi tessellation schematic diagram: centroid in red, Voronoi circle in green, edges in grey.

7.2.3.5. Discretization method

The main discretization methods include finite difference method, finite element method, and finite volume method. Discretization methods also correspond to the types of grids used. The finite difference method is generally used for structured grids, while the finite element method and finite volume method are generally used for unstructured grids.

The FDM is one of the simplest and oldest methods to solve the storm surge problems, and it is still widely used. This method divides the solution domain into differential grids, replacing the continuous solution domain with a finite number of grid nodes. By using the Taylor series expansion, the derivative of the governing equation is discretized by the difference quotient of the function value on the grid node, so as to establish the algebraic equations with the value on the grid node as the unknown quantity. This method is an approximate numerical solution that directly transforms a differential problem into an algebraic problem. The mathematical concept is intuitive and simple to express. It is an earlier and relatively mature numerical method.
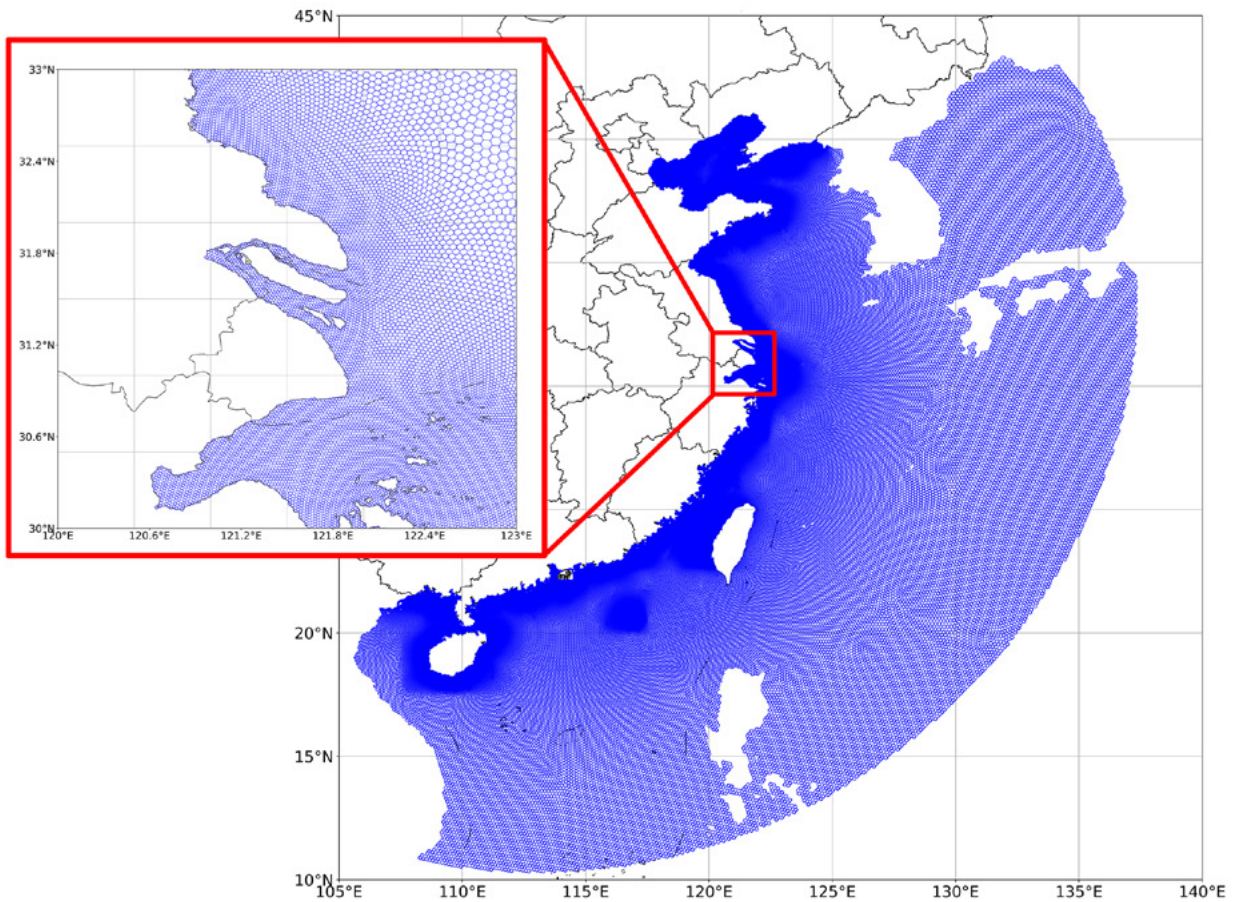
Figure 7.13. A storm surge model grid based on SCVTs applied to the China Sea.
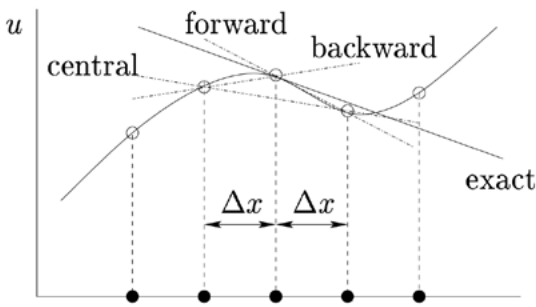
$$\left(\frac{\partial u}{\partial x}\right)_i \approx \frac{u_{i+1}-u_i}{\Delta x} \qquad \text{forward difference}$$

$$\left(\frac{\partial u}{\partial x}\right)_i \approx \frac{u_i-u_{i-1}}{\Delta x} \qquad \text{backward difference}$$

$$\left(\frac{\partial u}{\partial x}\right)_i \approx \frac{u_{i+1}-u_{i-1}}{2\Delta x} \qquad \text{central difference}$$

Figure 7.14.   Geometric interpretation of difference expression.

The basic difference expression mainly has three forms (Figure 7.14): forward difference, backward difference, and centre difference. The first two formats are first-order derivatives, while the last format is second-order derivatives. Different computational schemes can be obtained through the combination of several different formats of time and space.

According to the precision of the scheme, we can distinguish among first-order, second-order, and high-order accuracy schemes. Depending on the influence of the time factor, the difference scheme can also be divided into explicit scheme, implicit scheme, explicit and implicit alternate scheme.

The FEM is based on variational principle and weighted residual method. The basic solution idea is to divide the computational domain into a finite number of non-overlapping elements. In each element, some appropriate nodes are selected as interpolation points of the solution function. The variable in the differential equation is changed into a linear expression composed of the node value of each variable or its derivative and the selected interpolation function. The differential equation is solved discretely by means of variational principle or weighted residual method.

According to the difference of the weight function and the interpolation function, the finite element method is divided into several computational schemes. For the choice of weight function, there are collocation methods, moment method, least square method, and Galerkin method. According to the shape of the computing cell grid, there are triangular grid, quadrilateral grid, and polygonal grid. Triangular grids are commonly used in storm surge modelling. The accuracy of the interpolation function is divided into linear interpolation functions and high-order interpolation functions. Different combinations also constitute different finite element calculation schemes.

The FVM is also called the control volume method. The basic idea is to divide the computational domain into a series of non-overlapping control volumes, and make a control volume around each grid point. Integrate the differential equa-

tions to be solved for each control volume to obtain a set of discrete equations. The unknown is the value of the dependent variable at the grid point. In order to obtain the integral of the control volume, it is necessary to assume the changing law of the value between grid points, i.e. the distribution profile (continuous or segmented) of the assumed value. From the selection method of the integral region, the finite volume method belongs to the subregion method in the weighted residual method. From the approximate method of the unknown solution, the finite volume method is a discrete method using local approximation. The physical meaning of the discrete equation is the conservation principle of the dependent variable in a finite controlled volume, just as the differential equation expresses the conservation principle of the dependent variable in an infinitely small controlled volume. The discrete equation obtained by the finite volume method requires the integral conservation of the dependent variable to be satisfied for any set of control volumes, and naturally also for the entire computation area. This is the attractive advantage of the finite volume method. Some discrete methods, such as the finite difference method, only satisfy the integral conservation if the grid is extremely fine. The finite volume method shows accurate integral conservation even in the case of coarse grids. As far as the discrete method is concerned, the finite volume method can be regarded as an intermediate between the finite element method and the finite difference method.

7.2.3.6. Existing models for storm surge modelling

Numerical simulation of storm surges began in the 1950s. After decades of development, it has emerged that many numerical models can be used to storm surge simulations. Commercial models include MIKE21 and TuFlow, while examples of free models are: ADCIRC, Delft3D-FLOW, POM, FVCOM, ROMS, and SCHISM. Free numerical models generally provide the source code of the model, so that the model can be modified as needed when establishing a forecasting system. The models listed in Table 7.1.can be used to establish a complete operational storm surge forecasting system.

Model	Grid topology	Numerical methods	Nesting capabilities	Website
MIKE21	Structured curvilinear grid and unstructured grid	Alternating direction implicit method for structured grid. Cell-centered finite volume method for unstructured grid	Nesting is not possible	https://www.mikepoweredbydhi.com/products/mike-21-3
TuFlow	Structured grid and unstructured grid	2nd order semi-implicit matrix solver for structured grid. Finite-Volume for unstructured grid	Sub-Grid	https://www.tuflow.com/
ADCIRC	Unstructured grid	Finite element method in space and finite difference method in time	Not available	https://adcirc.org/
Delft3D-FLOW	Structured curvilinear grid	Alternating direction implicit method	Nested boundary conditions	https://oss.deltares.nl/web/delft3d/
POM	Structured curvilinear grid	Finite difference scheme	Not available	http://www.ccpo.odu.edu/POMWEB/index.html
FVCOM	Unstructured grid	Finite volume method	Nesting at the boundaries	http://codfish.smast.umassd.edu/fvcom/
ROMS	Structured curvilinear grid	Second-order finite differences	One-way nesting	https://www.myroms.org/
SCHISM	Unstructured mixed triangular/quadrangular grid	Semi-implicit Galerkin finite element method	One-way nesting	http://ccrm.vims.edu/schismweb/

Table 7.1. Geometric interpretation of difference expression.

7.2.4. Data assimilation systems

Data assimilation techniques are used to combine model and observed data to obtain the best estimate of the state of a system (see Chapter 4.3 for more details). Statistical techniques are often employed to find a solution which, ideally, minimises some error metric. For storm surges, this is done to obtain fields of sea surface height that can help us to better understand past events or to improve the quality of forecasts. An overview of the application of data assimilation to storm surge modelling and forecasting is provided in this section. Henceforth, references to errors mean some metric distance between the model and observations.

7.2.4.1. Sources of error in storm surge models

In order to reduce errors in storm surge models, especially for forecasting in which the accuracy may influence real-time decision making, it is important to understand the sources of error. Some of the main sources are given below.

Quality of input datasets

This includes atmospheric surface forcing and tidal forcing at the boundaries (see Section 7.2.2). Storm surges are largely forced phenomena; therefore, the accuracy of forcing is key and errors in the related datasets may be transferred into the

storm surge component of the modelled sea surface height. Errors in input datasets may arise from similar sources as the storm surge model, including model and instrument errors.

For example, errors in tidal amplitudes and phases at the boundaries will propagate with the tidal waves into the domain. As discussed in Section 7.2.1, interactions with the tides can influence both timing and height of a storm surge, so it is important to have an accurate tidal component in the model. The accuracy of the surface atmospheric forcing is important as well, especially the components of wind and surface pressure. Due to the forced nature of storm surges, this is one of the largest sources of error in storm surge forecasts (Horsburgh et al., 2011).

Tuning of model parameters

It is common practice to adjust various model parameters to obtain a better solution. For example, it could include the tuning of bottom/surface friction coefficients. It is very unlikely to find a perfect parameter set, and the iterative processes often used can lead to non-optimal solutions. See Section 7.2 for more information about parameters used in storm surge models.

Representativity errors

Representativity errors arise from models' ability to represent variables and processes such as resolution (Daley, 1991). For example, a coarse model may not be able to resolve finer scale features, which is present in the observations. For storm surges, this is particularly important nearby complex coastlines and estuaries. Similarly, coarser models may mean smoother bathymetry in these areas, which can significantly affect the modelled surge.

A model may not simulate all processes required to accurately model a storm surge. For example, if tides are not included in the model, only the atmospherically forced component of sea surface height is being generated, and contributions from tide-surge interactions will be missing. Other examples include the lack of tidal processes such as self-attraction and loading, or not including the inverse barometer effect in the model.

7.2.4.2. Assimilated data sources for storm surge modelling

An attempt to reduce the impact of the errors described in the previous section can be made using data assimilation. For storm surge modelling, assimilation of observations may occur directly into the model or indirectly via input datasets.

Datasets used as atmospheric forcing often contain assimilated observations. The generation of the storm surge

is highly dependent on the model's interaction with these datasets and it is vital that they are accurate. For example, the forecasted atmospheric fields used at the UK Met Office use assimilation of atmospheric observations. There are also many reanalysis datasets available, such as the ECMWF ERA5 dataset (Hersbach et al., 2020) that assimilates observations from multiple sources to generate atmospheric data. While these examples are suitable for extratropical storm surges, they may not sufficiently resolve intense tropical cyclones, meaning that parametric methods may be a better option (see Section 7.2.2.3). There are also assimilative alternatives, such as the MTCSWA datasets (Knaff et al., 2011), which blend together parametric fields and observations. These have been shown to have some benefit for forecasting (Byrne et al., 2017). The same is true for the datasets used to derive tidal signals at the model boundaries. Examples of such datasets include TPXO (Egbert et al., 2002) and FES (Lyard et al., 2021), which incorporate data from satellite altimetry and tide gauges. See Section 7.2.2.2 for more information on these tidal datasets.

Sea surface height may also be assimilated directly into the modelled sea surface. There are two sources used, both with advantages and disadvantages: tide gauges and satellite altimetry. Tide gauges (and other fixed instruments such as bottom pressure recorders) offer information that is frequent and consistent in time, making them useful for capturing ocean processes of all frequencies (including storm surges). However, they are generally spatially sparse. On the other hand, altimetry data offer good spatial coverage but are less consistent in time, as a satellite only returning to the same location once every number of days. This makes the data useful for longer periods of periodic ocean processes.

Tide gauge data are currently assimilated for storm surge forecasting at some institutions (see Section 7.2.4.4). There are representativity challenges that must be considered when using these data. Most importantly, modelled sea surface height variables and observed variables must represent the same physical quantity. For example, do both datasets contain the same components of sea level such as tides and inverse barometer effect? The datum on which the data are based must also be considered. The sea level anomaly can be used to overcome these problems if a long enough record is available.

7.2.4.3. Application of data assimilation to real time forecasting systems

For real time forecasting, data assimilation is used to generate an improved initial condition for a forecast model run. The forward propagation of errors can be reduced by creating a more realistic initial condition. This is important to improve the lead times over which good forecasts may be given. The use of data assimilation for storm surge forecasting has been shown to offer improvements over short lead
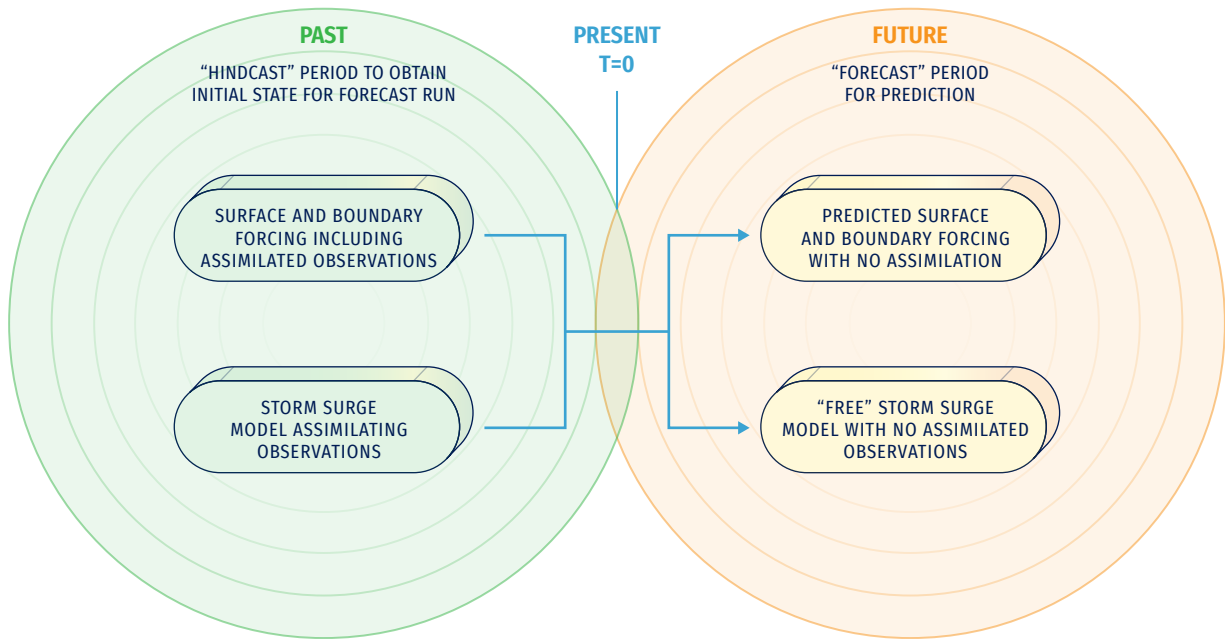
Figure 7.15.   Illustration of two distinct stages of sequential data assimilation for forecasting storm surges.

times (Heemink, 1986; Verlaan et al., 2005; Madsen al., 2015; Zijl et al., 2015; Byrne, 2021). However, the duration of these improvements may be limited to a few hours of forecast, due to the forced nature of storm surges.

This improved initial condition can be generated by running the model for some historical period up until today, including forcing with assimilated observations and potentially direct assimilation of sea surface height. This model run can effectively be seen as a continuous simulation with assimilative steps at some predefined frequency, for example every 6 hours. When a forecast is desired, the most recent state from this model can be taken and used as the initial condition. A forecast simulation is then done using no assimilation, as no observations are available in the future. This means that the atmospheric forcing used is also a forecast. Figure 7.15 illustrates this process.

There are several methods that have been used with success in storm surge modelling, including Optimal Interpolation (Gandin, 1966; Lorenc, 1981 and 1986; Daley, 1991), variational assimilation (Lorenc, 1986), Kalman filters (Kalman, 1960) and Ensemble Kalman Filters, (Evensen, 2004). In all methods, a key step is the estimation of spatial error covariances in both the model and the observations. This can be parametrically, as shown in the example in Figure 7.16, or by deriving covariances from an ensemble of model states. An example of the latter is described in Section 7.2.4.4.

Data assimilation has the potential to add significantly to the computation and time resources required, especially for en-

semble systems. As noted, for real-time forecasting systems is vital that a balance is made between accuracy and speed, i.e. useful forecasts need to be delivered in a timely manner (Horsburgh et al., 2011).
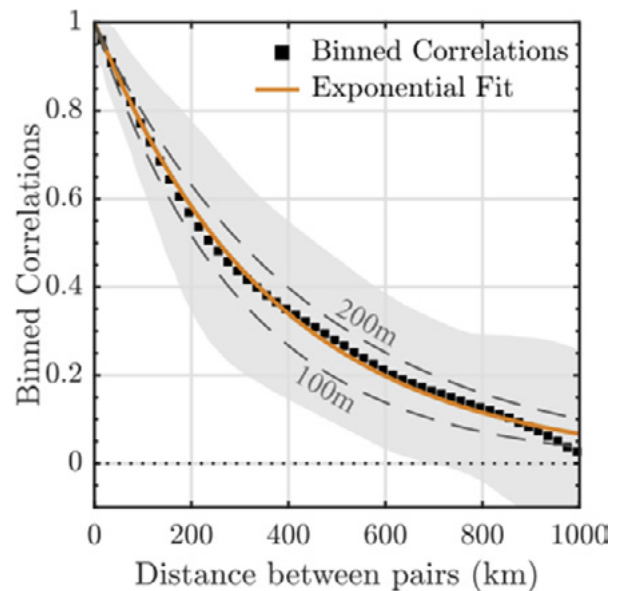
Figure 7.16.   An example of correlation length scale estimation for assimilation of sea surface height into a barotropic storm surge model of the North Sea (Byrne et al. 2021). Such a length scale could be used to assimilate tide gauge observations.

7.2.4.4. Examples from real operational systems

The examples below are correct at the time of writing.

UKMO

The UK Met Office provides storm surge forecasting for the United Kingdom. Its 2D operational model does not currently assimilate any data into the model sea surface height. The atmospheric forcing used does include assimilated observations and comes from UKMO or the European Centre for Medium-Range Weather Forecasts (ECMWF) models, depending on the system. They also have more general operational 3D models that assimilate temperature, salinity and sea level anomaly, but the last is only done in deep water.

Rijkswaterstaat

Rijkswaterstaat provides storm surge forecasts for The Netherlands. Its system assimilates information from tide gauges around the Northwest European Shelf, especially in the North Sea (Verlaan et al., 2005; Zijl et al., 2015). They use a steady-state Kalman Filter (SSKF), which uses a stationary Kalman gain derived from an ensemble of states, such as might be used for the ensemble Kalman filter (EnKF). SSKF offers more computational efficiency than EnKF, and potentially a better representation of the error covariance than the standard Kalman Filter. Additional localization steps are also applied to the assimilation, to limit the distance from observations over which information is assimilated.

7.2.5. Ensemble modelling

Like any other forecasts, sea level predictions have an associated uncertainty. The threat to life and property of extreme sea level events makes estimation of this uncertainty and the generation of a range of possible water levels (probabilistic forecast) particularly important for risk managers and decision-makers. The error of a single forecast time series can be assessed by comparison with in-situ tide gauges at specific locations and grid points. However, uncertainty of the forecast and its dependence on the forcing, model characteristics, and set up is usually unknown.

Uncertainty of sea level forecasts depends on several factors and may contain errors in both the tide and the non-tidal residuals (storm surge) components. During a storm, the storm surge is mainly driven by the weather conditions at the sea surface. This is considered to be the dominant source of uncertainty in sea level forecasts and may change significantly depending on the meteorological conditions. For this reason, ensemble storm surge forecasts based on weather ensemble prediction systems (EPS) are the most common approach to generate probabilistic forecasts (forecast plus a confidence interval).

The weather is a chaotic system highly sensitive to the initial state (Lorenz, 1965) that can only be deterministically predicted for about 10 days. Therefore, the standard procedure for dealing with forecasts uncertainty, i.e. the combination of different model solutions or ensemble modelling, was initially applied to meteorological forecasts (Leith, 1974; Hamill et al., 2000). Conceptual background of ensembles is chaos theory; they are a valuable tool to deal with equations in which several nonlinear processes and interacting variables are present. This is the case of meteorological models but also of ocean models and, particularly, of tide and surge models. Hence, their application is today strongly recommended in oceanography.

An EPS is based on the combination of a set of forecasts with different controlled changes in the initial conditions, the model physics or the open boundary conditions (Palmer and Williams, 2010; Flowerdew et al., 2010). All these modifications are designed to represent the uncertainties in the knowledge of the weather state. For example, different initial conditions allow to include those perturbations that grow most rapidly in time, in a context where slight changes to the initial conditions may lead to significantly different forecasts (Buizza and Palmer, 1995). Slight modifications of the set of equations (including different values in the parameterization constants representing different processes) also provide estimation of model uncertainties contributing to the forecast error.

Deviation of wind and sea level pressure fields from their actual evolution will determine a corresponding deviation on the predicted sea level. Therefore, their uncertainty derived from weather EPS will cause an uncertainty in the evolution of the sea level, linked to the meteorological forcing and affecting mainly the storm surge component. If different weather predictions are used to drive different sea level simulations, the probability distribution function of the forecast sea level values allows estimating the uncertainty of the sea level forecast and the probability of exceeding a given sea level threshold.

The ECMWF EPS has been operational since 1992 (Molteni et al., 1996). It was first applied to storm surge operational forecasts in the North Sea by Flowerdew et al. (2010 and 2013), who provided skilled probabilistic forecasts of sea level and showed that ensemble spread was a reliable indicator of uncertainty during large surge events.

Storm surge ensemble predictions have been used to forecast sea level in Venice by Mel and Lionello (2014a). They used a 50 members ensemble to simulate 10 events showing that EPS slightly increases the accuracy of the prediction with respect to the deterministic forecast, and that the probability distribution of maximum sea level produced by the EPS is acceptably realistic. They also showed that the storm surge peaks correspond to maxima of uncertainty and that the uncertainty of such maxima increases linearly with the forecast range. The same procedure was used by Mel and Lionello (2014b) for the simulation

of the operational forecast practice for a three-month period (fall 2010). It revealed that uncertainty for short and long lead times of the forecast is mainly caused by the uncertainty of the initial condition and of the meteorological forcing, respectively. The probability forecast based on this ensemble technique has a clear skill in predicting the actual probability distribution of sea level. A computationally cheap alternative, called ensemble dressing method, has been proposed by Mel and Lionello (2016). It replaces the explicit computation of uncertainty by ensemble forecast with an empirical estimate. Instead of performing multiple forecasts, the procedure "dresses" the forecast of sea level with an error distribution form, which includes, on one hand, a dependence of the uncertainty on surge level and lead time and, on the other hand, of the uncertainty of the meteorological forcing. This computationally cheap alternative also provides acceptably realistic results.

Apart from the meteorological input, other sources of error on sea level forecasts can be attributed to the ocean model characteristics and/or to the setup of the system: bathymetry, spatial resolution, model domain, tidal forcing, temporal resolution of the meteorological input, barotropic or baroclinic models, ocean open boundary conditions, etc. Currently, sea level variations on timescales of hours/days are operationally forecasted through different barotropic and baroclinic models, sometimes over the same area. Therefore, another option is the combination of existing operational models with different characteristics, forcings and even physics (multi-model forecast).

A multi-model storm surge forecast was first implemented by Deltares (an independent Dutch institute) in 2008, combining existing operational storm surge forecasts from different countries in the North Sea. The system included the use of the Bayesian Model Average (BMA) statistical technique

for validation of the different members and generation of a combined improved prediction, with a confidence interval (Beckers et al., 2008). In the same year, this methodology was tested for the Spanish coast by Puertos del Estado (Spain) (Pérez et al., 2012), combining the output of Nivmar (Álvarez-Fanjul et al., 2001), an existing storm surge forecasting system, with circulation (baroclinic) models already operating in the region. Nowadays, at Puertos del Estado is operational a multi-model surge forecast named ENSURF that combines Nivmar with two Copernicus Marine Service regional operational models, IBI-MFC (Sotillo et al., 2015) and MedFS (Clementi et al., 2021).

The BMA technique requires near-real time access to tide gauge data and automatic quality control of this data (as required by the Nivmar system as well), and specific data tailoring of model outputs. It is applied to the surge or non-tidal residual component of sea level because this can be approximated by a normal distribution (which is not the case for total sea level including tides, especially for strong semidiurnal regimes). So, observations from tide gauges and model data for those models providing total sea level must be previously decided. This could be considered a limitation but, in practice, it is the best way of optimising the final total sea level forecast by using the tidal component obtained from historical tide gauge observations at each site. ENSURF is also a valuable operational validation tool that allows a detailed assessment of the skills of different models to forecast coastal sea levels. A first deterministic forecast is provided by the old Nivmar solution early in the morning every day and, when later the Copernicus Marine Service forecasts become available, they are integrated with the tide gauge data and, by means of the BMA technique, a probabilistic forecast band is generated for each harbour (Pérez-González et al., 2017, Pérez-Gómez et al., 2019) (Figure 7.17).
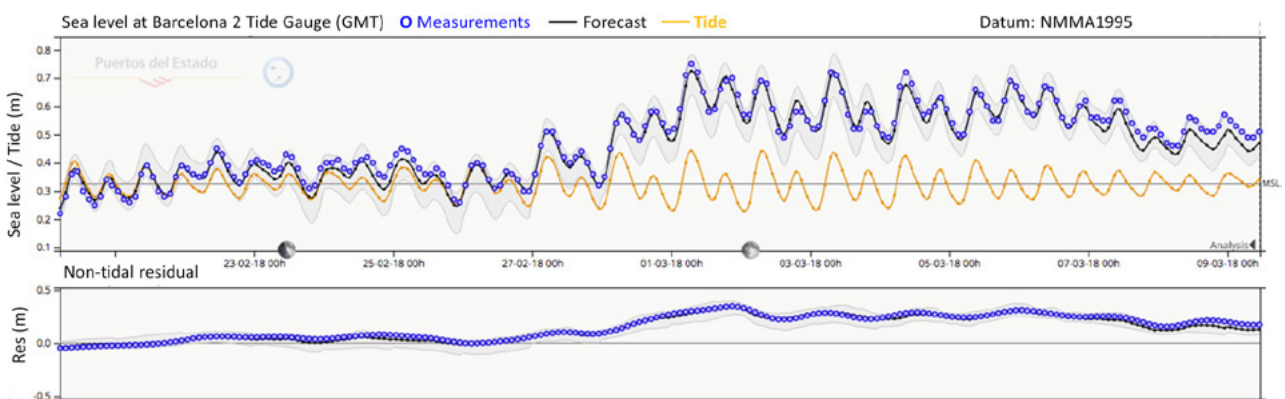
Figure 7.17.   Example of sea level probabilistic forecast generated by the multi-model ENSURF for the Barcelona harbour, validated against Barcelona tide gauge (hourly data). Top panel: total sea level; bottom panel: surge component. Blue: tide gauge data; orange: tide prediction; black: BMA forecast; grey: BMA confidence interval.

Generally, use of the probabilistic methodology improves the forecast and gives significant added value to existing operational systems, as there is no single model that outperforms at all tidal stations and synoptic conditions. However, further work must be done with the BMA technique to predict the storm peaks which, in some weather conditions, are better captured by single systems.

A multi-model ensemble forecasting system has been recently developed for the Adriatic Sea combining 10 models predicting sea level height (either storm surge or total water level) and 9 predicting waves characteristics (Ferrarin et al., 2020). Other examples of this technique can be found in New York (Di Liberto et al., 2011) and the North Sea (Siek and Solomatine, 2011).

7.2.6. Validation strategies

Storm surge models have been traditionally validated with time series of coastal sea level measured by tide gauges. These data allow assessing the skills of the model to reproduce observed water heights at specific points along the coast. Note the advantages this application presents with respect to sea level data from satellite altimetry, less reliable along the coastal strip and with a lower temporal resolution. Fortunately, there are hundreds of tide gauges around the world that become a very valuable and reliable dataset for storm surge validation (Muis et al., 2016 and 2020, Fernández-Montblanc et al., 2020). In some cases, these stations provide ancillary meteorological data, such as wind and atmospheric pressure, which can also be used to validate the model meteorological forcing. In addition, tide gauges transmit data in near-real time that can be integrated in an operational validation of the forecasting system (Álvarez-Fanjul et al., 2001).

In most cases, the forecast will provide the tide and storm surge signals (hourly to daily timescales), usually dominant at the tide gauge records, but will not be able to reproduce higher-frequency sea level oscillations such as infragravity waves, seiches or meteotsunamis, with periods of the order of a few minutes. It is important to define which observed "sea level" product will best fit the validation purpose, according to the physical processes included in the system. The most adequate standard product for existing operational storm surge forecasting systems are filtered hourly values from tide gauges. As new models include additional processes (e.g. fully coupled models including wave effects), higher resolution bathymetries, and forcing fields, the use of lower temporal sampling data will become more important and the validation process more challenging.

Normally, the model output at the grid point closer to the tide gauge is selected. However, the validation results will depend on the resolution and quality of the bathymetry data, as well as on the location of the tide gauge: if it is in an open site or inside a harbour or bay with important local effects, it may not be resolved by the model.

A careful validation of both tide and surge components should be performed to verify not only the final total sea level forecast, but also the quality of the tidal signal in the model, which can be an important source of error especially on shallow waters with high tidal range. For these reasons, model and tide gauge data must be de-tided, applying a harmonic analysis to both time series, as well as computing the tide prediction for the analysed period, and the surge or non-tidal residual after tide subtraction. The performance assessment can then be made in terms of comparison of the harmonic constants (amplitude and phase) from model and observations, and in terms of model data time series comparison of tide, surge and total sea level.

It is important to mention that sea levels measured by the tide gauge will be related to a local, regional or national datum. The model forecast is theoretically referred to mean sea level, though this mean sea level may be affected by the model setup implementation, domain, etc. Therefore, the mean should be subtracted from both time series at each location before comparison.

Metrics for time series validation can be found at Section 4.5.1. Most of these metrics describe the overall performance of the model for a time period of several days (the storm duration), months or years. However, they do not reflect the predictive skill for extreme surge events. This can be better evaluated, for example, in terms of the differences in the highest percentiles (e.g.: 95th, 99th percentiles) or the maximum observed and modelled value. For validation of long time series (multi-decadal hindcasts), it is possible to use annual maxima, annual percentiles, and extreme sea levels for specific return periods, obtained through extreme sea level analysis (Muis et al., 2020).

Taylor diagrams can be used to graphically indicate the performance of different competing models or solutions, providing information of the Pearson correlation coefficient, the standard deviation and the RMSE at each tide gauge.

Progressively, the storm surge models will consider inundation, and additional validation of the flooding extent will be required. This is less straightforward and requires other types of data, such as locations of flooded points, marks left by the water or reports about the flood chronology (Le Roy et al., 2015). This information is commonly available after the event for a delayed mode validation; e.g. for validation of inundation, Loftis et al. (2017) used crowdsourced GPS data and maps of flooded areas obtained by drones.

7.2.7. Outputs

The main outputs of storm surge models are: time series output, maximum elevation field output (extreme values at every time step for water surface elevation), ensemble forecast elevation field output, animation output.

7.2.7.1. Time series outputs

The time series output is usually plotted in a two-dimensional rectangular coordinate system, the abscissa is time and the ordinate is water level. The time series output of storm surge models are the water level changes at a certain location. In order to facilitate the comparison between the results of simulations and the observation data, multiple result curves can be plotted in the same coordinate system.

Generally, the results of storm surge models (without tide) can be directly used for plotting time series diagrams, but sometimes attention should be paid to the change of the total water level at a certain point. Therefore, there is a way to output the total water level, that is the results of the storm surge model without astronomical tide directly superimposed on the astronomical tide from harmonic analysis, obtaining in this way the time series results of the total water level. Figures 7.18 and 7.19 show examples of time series model storm surge result and storm surge superimpose on harmonic analysis tide.
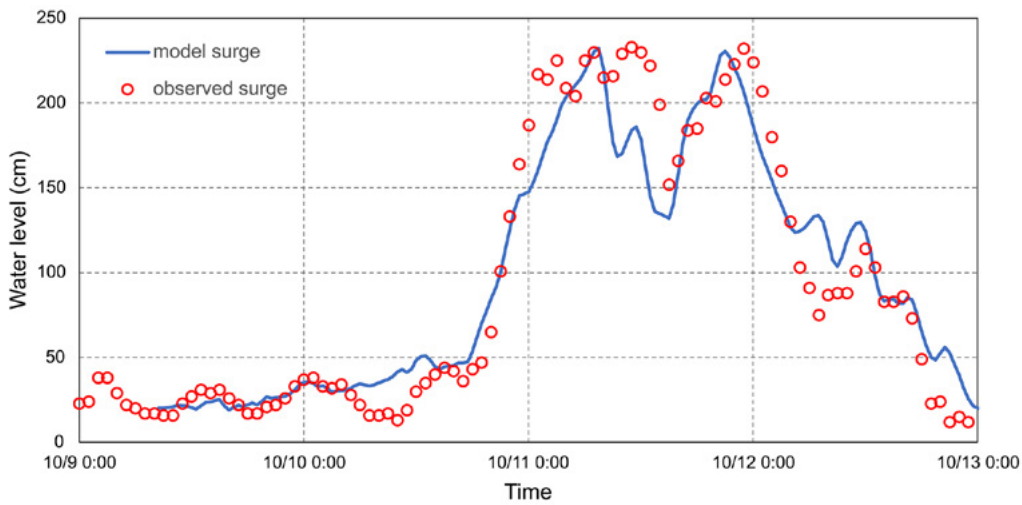
Figure 7.18.   Time series model storm surge result (blue line) and observed storm surge (red circle).
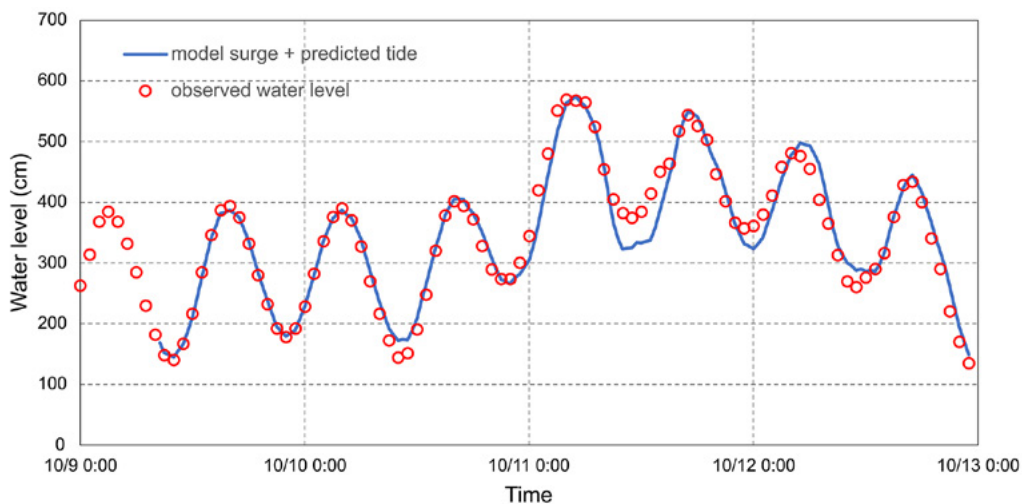
Figure 7.19.   Time series model storm surge result superimposed on predicted tide (blue line) and observed water level (red circle).

7.2.7.2. Maximum elevation field

Among the output methods of storm surge models, there is an output form called maximum elevation field. This kind of field output is not the water level field at a certain time, but extracts the highest water level value of each grid point in the calculation process to form the maximum elevation field. The maximum water level field can be used to grasp the distribution of the maximum water level during a Typhoon and to identify the more severely affected areas along the coast. Figure 7.20 shows the maximum storm surge field during 2019 Typhoon Mitag (1918).
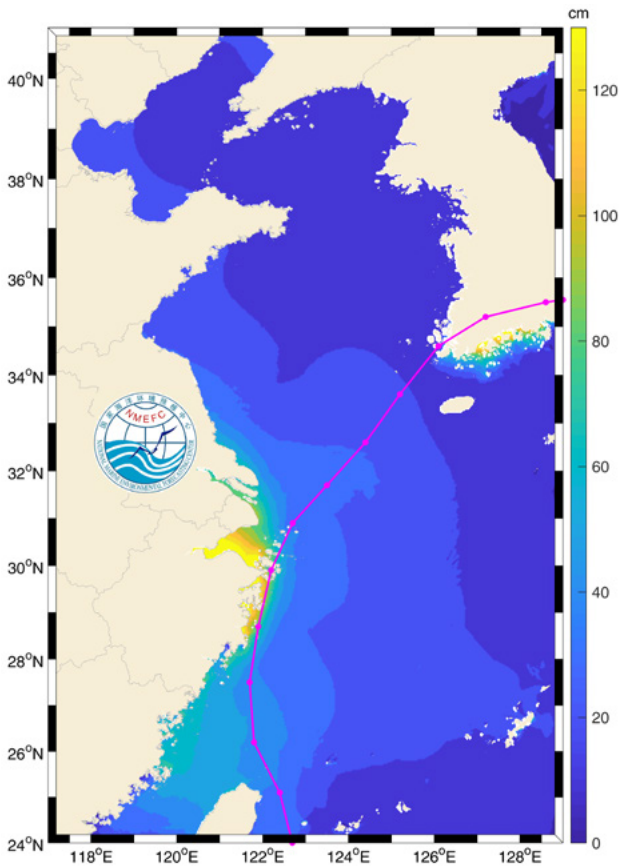
Figure 7.20. The maximum storm surge field during 2019 Typhoon Mitag (1918).

7.2.7.3. Ensemble forecast field

The storm surge ensemble forecast usually uses the respective meteorological forcing fields of the ensemble members to calculate the storm surge separately. The output of ensemble forecast fields mainly includes the following forms: (a) ensemble mean field; (b) probability field; and (c) postage stamp maps.

a. Ensemble mean storm surge field

In order to obtain a definite forecast result, it is necessary to synthesise the respective results of the ensemble members. It is generally used to assign different weights to the results of each member and to superimpose the results of all members, i.e. the weighted average method (Wang et al., 2010). The superimposed result is output in the form of the elevation field, and the ensemble forecast field is obtained as result.

The track map of Typhoon Mitag can be seen in Figure 7.21. The storm surge results of the subjective typhoon forecast track, fast track, slow track, left track, and right track are used to synthesise the ensemble forecast water level field applying the weighted average method (Figure 7.22). In this example, the weight of the storm surge result of the subjective forecast typhoon track is 60%, while the weight of the storm surge result of the other tracks are all 10%.

b. Probability storm surge field

The typhoon ensemble forecasting tracks for storm surge numerical simulation can describe the surge field
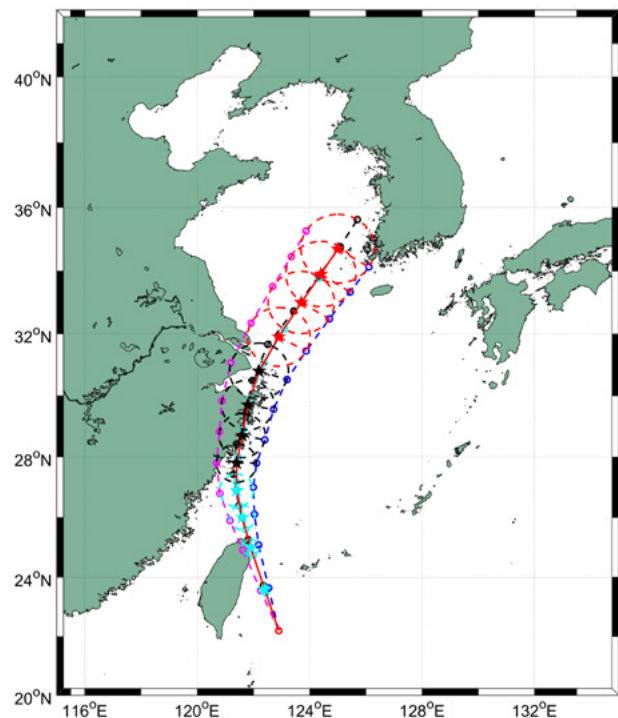
Figure 7.21. Track map of Typhoon Mitag. Red line: middle track; black line: fast track; cyan line: slow track; magenta line: left track; blue line: right track.
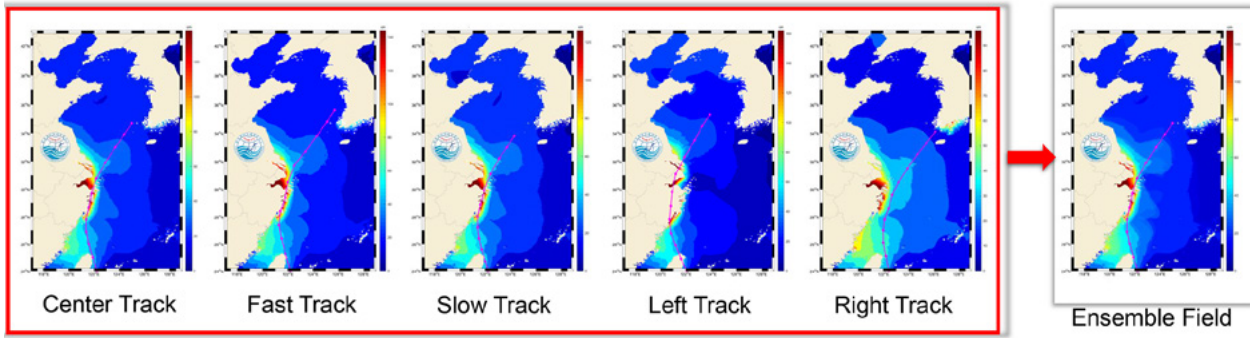
Figure 7.22.   Synthesis of ensemble forecast water level field.

under different typhoon track scenarios. By equitably assigning weights to different track results, the probability field distributions under different extreme values of storm surges can be clearly displayed, and the intensity probability of coastal storm surges can be more intuitively presented (Liu et al., 2020). Figures from 7.23 to 7.25 show the probability distribution of forecast storm surge over 0.5m, 1.0m and 2.0m of Typhoon Mitag.

c. Postage stamp maps

A postage stamp map is a set of small storm surge maps drawn by the results of the individual members (Figure 7.26). Forecasters can learn about the possible situation of each ensemble member through the postage stamp map, thereby estimating the magnitude of the maximum storm surge and the range of impact. (WMO, 2012)
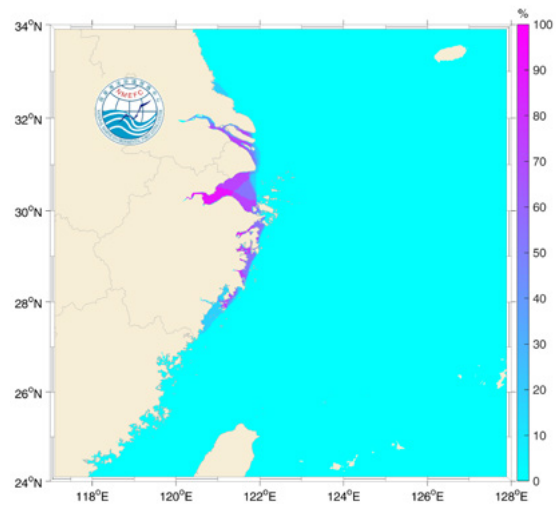
Figure 7.24.   Distribution of probability forecasting of storm surge over 1.0m.
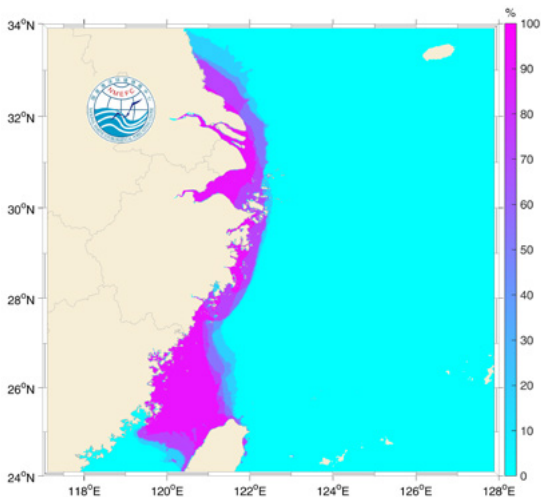
Figure 7.23.   Distribution of probability forecasting of storm surge over 0.5m.
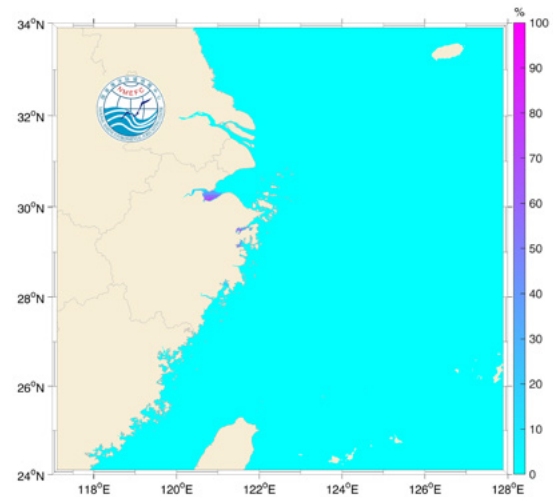
Figure 7.25.   Distribution of probability forecasting of storm surge over 2.0m.
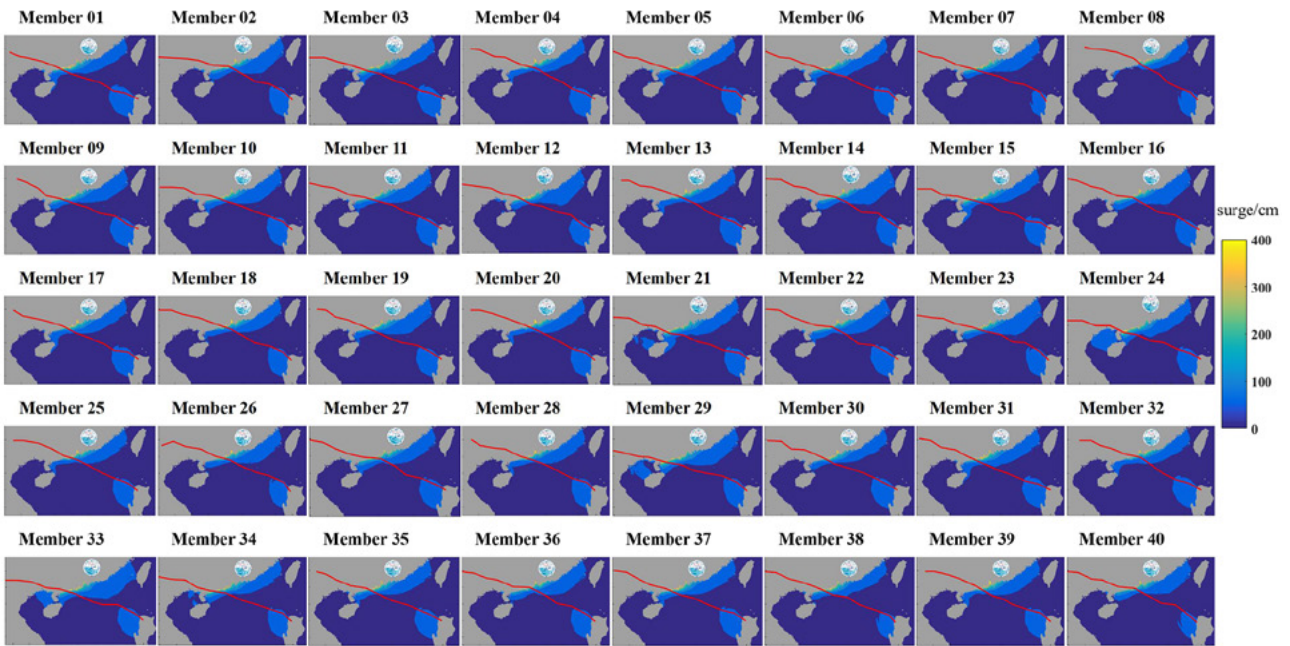
Figure 7.26. Postage stamp map of storm surge field of Typhoon Mangkhut.

7.2.7.4. Animation output

The output of the water level field is very helpful for grasping the distribution of the storm surge process over a whole region. The output of the storm surge water level field is the elevation value of all grid points at a certain time. The elevation field figure at each moment is taken as a frame of the animation, and all the frames are connected to form the elevation field animation (Figure 7.27). The elevation field animation can intuitively reflect the changes in the water level of the entire area during the impact of the storm surge.
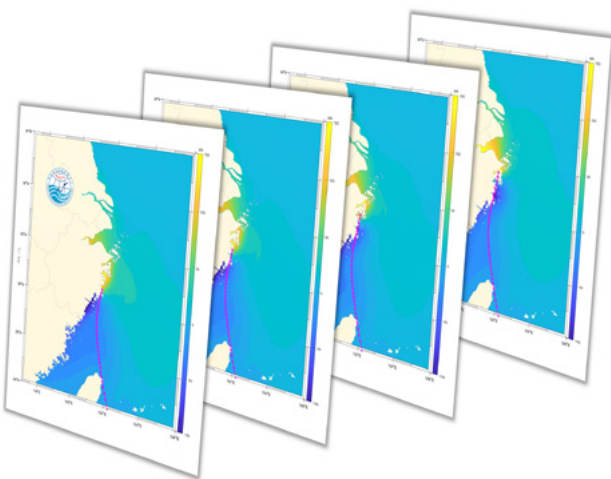
Figure 7.27. Synthesis of elevation field animation.

7.2.8. Existing operational storm surge forecasting systems

After decades of development of storm surge numerical models, many countries have established their own operational storm surge forecasting models. For example, in the United States a storm surge forecasting system is operating through the SLOSH model, in which the wind field is established based on the cyclone path, maximum wind speed radius, storm centre, and environmental pressure difference; it provides operational forecast products and storm surge inundation guidance products (Jarvinen and Lawrence,1985). China established ver3.0 of the PMOST forecasting system, which is based on a depth-averaged two-dimensional shallow water equation in the vector invariant form, and uses a SCVTs grid. It can enhance the resolution in key areas and fit the coastline. The system is able to couple astronomical tides and simulate flooding processes. With the GPU acceleration technology, the efficiency of storm surge simulation along the coast of China can reach 60 sec/day. The system can also perform ensemble forecasts based on multiple typhoon events and storm surge probability forecasting. The Indian Institute of Technology storm surge model was developed in the 1980s and applied to storm surge forecasts in the Indian Ocean and the Arabian Sea. It uses rectangular Cartesian coordinates and separates land and water during calculations. It has been applied throughout the north Indian Ocean (Dube et al., 1984, Dube et al., 1985).

The two-dimensional storm surge model developed by the Japan Meteorological Agency also uses rectangular coordinates (Hasegawa et al., 2015). In the numerical calculation, the water and land are separated with the flexible mesh, i.e. fine grid is used in shallow water and coarse grid is used in deep water. The system can also provide ensemble forecasting products. In the mid-1980s, the Netherlands developed a numerical fluid dynamics model called the DCSM, which uses a depth integrated shallow water equation. The driving force of the model is provided by a high-resolution regional meteorological model. In the early 1990s, the Kalman filtering method was used in DCSM to assimilate the water level (Verlaan et al., 2005; de Vries, 2009). The UKMO developed the storm surge forecasting model CS3X, which is a tide-storm surge model. In this operational storm surge forecasting system, the interaction of tide and storm surge is considered. In recent years, a storm surge ensemble forecasting has been developed in this system (Flowerdew et al., 2013). A storm surge model covering the French overseas territories has been operated since the 1990s by Meteo-France (Daniel et al., 2009); it was established based on the spherical nonlinear shallow water equation. In order to solve the problem of the shore boundary, the C-grid difference format was adopted, with meteorological forcing provided by the Holland model (see Section 7.2.2.3). Table 7.2 provides a list and features of storm surge forecasting systems currently operating in various countries.

Table 7.2.   List and features of operational storm surge forecast models.

Model	Area	Type	Grid	Country
HAMSOM, Nivmar	Mediterranean Sea and Iberian Peninsula	Vertically integrated barotropic	10 minutes	Spain
Mike 21 pre-operational 3-D 2-D finite element MOG2D	North Sea, Baltic Sea	2-D hydrodynamic	Finite difference 9 nmi, 3 nmi, 1 nmi, 1/3 nmi	Denmark
Coupled ice–ocean NPAC	Grand Banks, Newfoundland, Labrador NE Pacific, 120°W–160°W, 40°N–62°N	3-D circulation based on the Princeton Ocean Model	Approximately 20 km x 20 km Finite difference curvilinear C-grid 1/8 degree	Canada
Mike 21 pre-operational 3-D 2-D finite element MOG2D	North Sea, Baltic Sea	2-D hydrodynamic	Finite difference 9 nmi, 3 nmi, 1 nmi, 1/3 nmi	Denmark
JMA Storm Surge	23.5°N–46.5°N, 122.5°E–146.5°E	2-D linearized shallow water	Staggered Arakawa C-grid. 1 minute latitude/longitude	Japan
KMA Storm Surge	20°N–50°N, 115°E–150°E	2-D barotropic surge and tidal current based on the Princeton Ocean Model	Approximately 8 km x 8 km, finite difference curvilinear C-grid 1/12 degree	Republic of Korea

Model	Area	Type	Grid	Country
NIVELMAR	Portuguese mainland coastal	Shallow water	1 minute latitude x 1 minute longitude	Portugal
SMARA storm surge	Shelf sea 32°S–55°S, 51°W–70°W. Rio de la Plata	2-D depth-averaged	Geographical Arakawa C-grid, 1/3 degree latitude x 1/3 degree longitude 1/20 degree latitude x 1/20 degree longitude	Argentina
BSH circulation (BSHcmod) BSH surge (BSHsmod)	North-east Atlantic, North Sea, Baltic	3-D hydrostatic circulation 2-D barotropic surge	Regional spherical, North Sea, Baltic 6 nmi, German Bight Western Baltic, 1 nmi, surge North Sea, 6 nmi, north-east Atlantic 24 nmi	Germany
Caspian Storm Surge	Caspian Sea 36°N–48.5°N, 45°E–58°E North Caspian Sea 44.2°N–48°N, 46.5°E–55.1°E	2-D hydrodynamic, based on MIKE 21 (DHI Water & Environment)	10 km x 2 km	Kazakhstan
HIROMB/NOAA	North-east Atlantic, Baltic	3-D baroclinic	C-grid, 24 nmi	Sweden
WAQUA-in-Simona/DCSM98	Continental shelf 48°N–62°N, 12°E–13°E	2-D shallow water, ADI method, Kalman filter data assimilation	1/8 degree longitude x 1/12 degree latitude	Netherlands
Derived from MOTHY oil spill drifts model	Near-Europe Atlantic (Bay of Biscay, Channel and North Sea) 8.5°E–10°E, 43°N–59°N West Mediterranean basin (from the Strait of Gibraltar to Sicily) Restricted area in overseas departments and territories	Shallow-water equations	Arakawa C-grid 5' of latitude x 5' of longitude Finer meshes	France
SLOSH	Sea area south of Hong Kong within 130 km	Finite difference	Polar, 1 km near to 7 km, South China Sea	Hong Kong, China
Short-term sea-level and current forecast	Caspian Sea and near-shore low-lying zones	3-D hydrodynamic baroclinic	3 nmi horizontal, 19 levels	Russian Federation

Model	Area	Type	Grid	Country
IIT–Delhi, IIT–Chennai, NIOT–Chennai	East and west coasts of India and high-resolution areas	Non-linear, finite element, explicit finite element	For inundation model average spacing of 12.8 km offshore direction and 18.42 km along shore	India
CS3 tide surge	North-west European shelf waters	Finite difference, vertically averaged	C-grid 12 km, nested finer resolution	United Kingdom
SLOSH	Atlantic and gulf coasts	2-D depth integrated	625 meters	United States
PMOST 3.0	China sea 10°N~45°N, 105°E~140°E	2-D depth-averaged barotropic	SCVTs unstructured grid, 10km at boundary and 500m along shoreline	People's Republic of China

7.3.
References

Álvarez-Fanjul, E., Perez Gomez, B., Sanchez Arevalo, I.R. (2001). Nivmar: A storm surge forecasting system for Spanish Waters. *Scientia Marina*, 65(S1), https://doi.org/10.3989/scimar.2001.65s1145

Beckers J. V. L., Sprokkereef, E., and Roscoe, K. L. (2008). Use of Bayesian model averaging to determine uncertainties in river discharge and water level forecasts, Proceeding of "4th International Symposium on Flood Defence: Managing Flood Risk, Reliability and Vulnerability", Toronto, Ontario, Canada, 6–8 May, 2008.

Bjerknes, V. (1921). On the dynamics of the circular vortex with applications to the atmosphere and atmospheric vortex and wave motions. *Quarterly Journal of the Royal Meteorological Society*, 48(204), 375-376. https://doi.org/https://doi.org/10.1002/qj.49704820414

Buizza, R., and Palmer, T.N. (1995). The Singular-Vector Structure of the Atmospheric Global Circulation. *Journal of the Atmospheric Sciences*, 52(9), 1434-1456, https://doi.org/10.1175/1520-0469(1995)052<1434:TSVSOT>2.0.CO;2

Byrne, N. J. (2017). Deterministic models of Southern Hemisphere circulation variability. Ph.D. thesis, University of Reading, 105 pp.

Byrne, D., Horsburgh, K., and Williams, J. (2021). Variational data assimilation of sea surface height into a regional storm surge model: Benefits and limitations. *Journal of Operational Oceanography*, 1-14, https://doi.org/10.1080/1755876X.2021.1884405

Clementi, E., Aydogdu, A., Goglio, A. C., Pistoia, J., Escudier, R., Drudi, M., Grandi, A., Mariani, A., Lyubartsev, V., Lecci, R., Cretí, S., Coppini, G., Masina, S., and Pinardi, N. (2021). Mediterranean Sea Physical Analysis and Forecast (CMEMS MED-Currents, EAS6 system) (Version 1) set. Copernicus Monitoring Environment Marine Service (CMEMS), https://doi.org/10.25423/CMCC/medsea_analysisforecast_PHY_006_013_EAS6

Daley, R. (1991). Atmospheric Data Analysis. Cambridge University Press: Cambridge, UK

Daniel, P., Haie, B., and Aubail, X. (2009). Operational Forecasting of Tropical Cyclones Storm Surges at Meteo-France. *Marine Geodesy*, 32(2), 233-242. https://doi.org/10.1080/01490410902869649

de Vries, H. (2009). Probability Forecasts for Water Levels at the Coast of The Netherlands. Marine Geodesy, 32(2), 100-107, https://doi.org/10.1080/01490410902869185

Di Liberto, T., and Colle, B.A. (2011). Verification of a Multimodel Storm Surge Ensemble around New York City and Long Island for the Cool Season. *Weather and Forecasting*, 26, 922-939.

Doodson, A. T. (1929). Report on Thames Floods. *Geophysical Memoir*s, Great Britain Meteorological Office, 5(47), 1-26.

Doodson, A. T. (1956). Tides and storm surges in a long uniform gulf. Proceedings of the Royal Society of London. Series A. *Mathematical and Physical Sciences*, 237(1210), 325-343.

Dube, S. K., Sinha, P. C., Rao, A. D., and Rao, G. S. (1985). Numerical modelling of storm surges in the Arabian Sea. *Applied Mathematical Modelling*, 9(4), 289-294, https://doi.org/https://doi.org/10.1016/0307-904X(85)90067-8

Dube, S. K., Sinha, P. C., and Roy, G. D. (1984). Numerical simulation of storm surges induced by tropical storms impinging on the Bangladesh coast. *Coastal Engineering Proceedings*, 1(19), https://doi.org/10.9753/icce.v19.13

Egbert, G. D., Bennett, A. F., and Foreman, M. G. G. (1994). TOPEX/POSEIDON tides estimated using a global inverse model. *Journal of Geophysical Research*: Oceans, 99(C12), 24821-24852, https://doi.org/https://doi.org/10.1029/94JC01894

Egbert, G. D., and Erofeeva, S. Y. (2002). Efficient Inverse Modeling of Barotropic Ocean Tides. *Journal of Atmospheric and Oceanic Technology*, 19(2), 183-204, https://doi.org/10.1175/1520-0426(2002)019<0183:Eimobo>2.0.Co;2

Evensem, G. (2004). Sampling strategies and square root analysis schemes for the EnKF. *Ocean Dynamics*, 54, 539-560, https://doi.org/10.1007/s10236-004-0099-2

Fernández-Montblanc, T., Vousdoukas, M.I., Mentaschi, L., Ciavola, P. (2020). A Pan-European high resolution storm surge hindcast. *Environment International*, 135, 105367, https://doi.org/10.1016/j.envint.2019.105367

Ferrarin, C., Valentini, A., Vodopivec, M., Karic, D., Massaro, G., Bajo, M., De Pascalis, F., Fadini, A., Ghezzo, M., Menegon, S., Bressan, L., Unguendoli, S., Fettich, A., Jerman, J., Licer, M., Fustar, L., Papa, A.. Carraro, E. (2020). Integrated sea storm management strategy: the 29 October 2018 event in the Adriatic Sea. *Natural Hazards and Earth System Sciences*, 20, 73-93, https://doi.org/10.5194/nhess-20-73-2020

Flowerdew, J., Horsburgh, K., Wilson, C., and Mylne, K. (2010). Development and evaluation of an ensemble forecasting system for coastal storm surges. *Quarterly Journal of the Royal Meteorological Society*, 136(651), 1444-1456, https://doi.org/10.1002/qj.648

Flowerdew, J., Mylne, K., Jones, C., and Titley, H. (2013). Extending the forecast range of the UK storm surge ensemble. *Quarterly Journal of the Royal Meteorological Society*, 139(670), 184-197, https://doi.org/https://doi.org/10.1002/qj.1950

Fujita, T. (1952). Pressure distribution within typhoon. *Geophysical Magazine*, 23, 437-451.

Gandin, L.S. (1963). Objective analysis of meteorological fields. Translated from Russian.

Hamill, T. M. , Snyder, C., and Morss, R.E. (2000). A comparison of probabilistic forecasts from bred, singular vector, and perturbed observation ensembles. *Monthly Weather Review*, 128(6), 1835-1851, https://doi.org/10.1175/1520-0493(2000)128<1835:ACOPFF>2.0.CO;2

Harris, D.L. (1957). The Effect of a Moving Pressure Disturbance on the Water Level in a Lake. In: "Interaction of Sea and Atmosphere". Meteorological Monographs, vol 2. American Meteorological Society, Boston, MA. https://doi.org/10.1007/978-1-940033-15-0_4

Hasegawa, H., Kohno, N., and Itoh, M. (2015). Development of Storm Surge Model in Japan Meteorological Agency. Available at http://www.waveworkshop.org/14thWaves/Papers/JCOMM_2015_J4.pdf

Heemink, A.W. (1986). Storm surge prediction using Kalman filtering. Dissertation TU Twente, Hydraulic Engineering Reports. Available at http://resolver.tudelft.nl/uuid:8a7c65f5-f8f5-4033-b796-adaef2eb39a7

Hersbach, H. Bell, B., Berrisford, P., Hirahara, S., Horányi, A., Muñoz-Sabater, J., Nicolas, J., Peubey, C., Radu, R., Schepers, D., Simmons, A., Soci, C., Abdalla, S., Abellan, X., Balsamo, G., Bechtold, P., Biavati, G., Bidlot, J., Bonavita, M., De Chiara, G., Dahlgren, P., Dee, D., Diamantakis, M., Dragani, R., Flemming, J., Forbes, R., Fuentes, M., Geer, A., Haimberger, L., Healy, S., Hogan, R.J., Hólm, E., Janisková, M., Keeley, S., Laloyaux, P., Lopez, P., Lupu, C., Radnoti, G., de Rosnay, P., Rozum, I., Vamborg, F., Villaume, S., Thépaut Hersbach, J.N. (2020). The ERA5 global reanalysis. *Quarterly Journal of the Royal Meteorology Society*, 146(730), 1999-2049, https://doi.org/10.1002/qj.3803

Holland, G. J. (1980). An Analytic Model of the Wind and Pressure Profiles in Hurricanes. *Monthly Weather Review*, 108(8), 1212-1218. https://doi.org/10.1175/1520-0493(1980)108<1212:Aamotw>2.0.Co;2

Horsburgh, K., and de Vries, H. (2011). Guide to Storm Surge Forecasting. WMO-No. 1076. ISBN 978-92-63-11076-3

Jarvinen, B. R., and Lawrence, M. B. (1985). An evaluation of the SLOSH storm-surge model. *Bulletin of the American Meteorological Society*, 66(11), 1408-1411.

Jelesnianski, C. P. (1965). A numerical calculation of storm tides induced by a tropical storm impinging on a continental shelf. *Monthly Weather Review*, 93(6), 343-358. https://doi.org/10.1175/1520-0493(1993)093<0343:Ancos>2.3.Co;2

Kalman, R. E. (1960). A New Approach to Linear Filtering and Prediction Problems. *Journal of Basic Engineering*, 82(1), 35-45. https://doi.org/10.1115/1.3662552

Knaff, J.A., De Maria, M., and Molenar, D.A. (2011). An automated, objective, multiple satellite platform tropical cyclone surface wind analysis. *Journal of Applied Meteorology and Climatology*, 50(10), pp. 2149-2166, https://doi.org/10.1175/2011JAMC2673.1

Le Roy, S., Pedreros, R., André, C., Paris, F., Lecacheux, S., Marche, F., and Vinchon, C. (2015). Coastal flooding of urban areas by overtopping: dynamic modelling application to the Johanna storm (2008) in Gâvres (France). *Natural Hazards and Earth System Sciences*, 15, 2497-2510, https://doi.org/10.5194/nhess-15-2497-2015

Leith, C.E. (1974). Theoretical Skill of Monte Carlo Forecasts. *Monthly Weather Review*, 102 (6), 409-418, https://doi.org/10.1175/1520-0493(1974)102<0409:TSOMCF>2.0.CO;2

Liu, Q., Jiang, J., Yu, F., Zhang, C., Dong, J., Song, X., and Wang, Y. (2020). Typhoon storm surge ensemble forecast based on GPU technique. *Acta Oceanologica Sinica*, 39(5), 77-86, https://doi.org/10.1007/s13131-020-1570-8

Loftis, J.D., Wang, H., Forrest, D., Rhee, S., Nguyen, C. (2017). Emerging flood model validation frameworks for street-level inundation modeling with StormSense. SCOPE '17: Proceedings of the 2nd International Workshop on Science of Smart City Operations and Platforms Engineering, April 2017, 13-18, https://doi.org/10.1145/3063386.3063764

Lorenc, A. (1981). A global three-dimensional multivariate statistical interpolation scheme. *Monthly Weather Review*, 109, 701-721.

Lorenc, A. (1986). Analysis methods for numerical weather prediction. *Quarterly Journal of the Royal Meteorology Society*, 112, 1177-1194.

Lorenz, E.N. (1965). A study of the predictability of a 28-variable atmospheric model. Massachusetts Institute of Technology, Cambridge, Massachusetts. *Tellus*, 17(3), 321-333.

Lyard, F.H., Allain, D.J., Cancet, M., Carrere, L., Picot, N. (2021). FES2014 global ocean tide atlas: design and performance. *Ocean Science*, 17, 615-649, https://doi.org/10.5194/os-17-615-2021

Madsen, K.S., Hoyer, J., Fu, W., Donlon, C. (2015). Blending of satellite and tide gauge sea level observations and its assimilation in a storm surge model of the North Sea and Baltic Sea. *Journal of Geophysical Research: Oceans*, 20(9), 6405-6418, https://doi.org/10.1002/2015JC011070

Matsumoto, K., Sato, T., Takanezawa, T., and Ooe, M. (2001). GOTIC2: A program for computation of oceanic tidal loading effect. *Journal of the Geodetic Society of Japan*, 47(1), 243-248, https://doi.org/10.11366/sokuchi1954.47.243

Matsumoto, K., Takanezawa, T., and Ooe, M. (2000). Ocean Tide Models Developed by Assimilating TOPEX/POSEIDON Altimeter Data into Hydrodynamical Model: A Global Model and a Regional Model around Japan. *Journal of Oceanography*, 56(5), 567-581, https://doi.org/10.1023/A:1011157212596

Mel, R., and Lionello, L. (2014a). Storm Surge Ensemble Prediction for the City of Venice. *Weather and Forecasting*, 29(4), 1044-1057, https://doi.org/10.1175/WAF-D-13-00117.1

Mel, R., and Lionello, P. (2014b). Verification of an ensemble prediction system for storm surge forecast in the Adriatic Sea. *Ocean Dynamics*, 64(12), 1803-1814, https://doi.org/10.1007/s10236-014-0782-x

Mel R. and Lionello, P. (2016). Probabilistic Dressing of a Storm Surge Prediction in the Adriatic Sea. *Advances in Meteorology*, 3764519, 8, https://doi.org/10.1155/2016/3764519

Miller, A. R. (1958). The Effects of Winds on Water Levels on the New England Coast 1. *Limnology and Oceanography*, 3(1), 1-14.

Minato, S. (1998). Storm surge simulation using POM and a revisitation of dynamics of sea surface elevation short-term variation. *Oceanographic Literature Review*, 7(45), 1103.

Molteni, F., R. Buizza, T. N. Palmer, and T. Petroliagis (1996). The ECMWF Ensemble Prediction System: Methodology and validation. *Quarterly Journal of the Royal Meteorological Society*, 122, 73-119, https://doi.org/10.1002/qj.49712252905

Mooyaart, L., and Jonkman, S. N. (2017). Overview and design considerations of storm surge barriers. *Journal of Waterway, Port, Coastal, and Ocean Engineering*, 143(4), 06017001.

Muis, S., Verlaan, M., Winsemius, H.C., Aerts, J.C.J.H., Ward, P.J. (2016). A global reanalysis of storm surges and extreme sea levels. *Nature Communications*, 7, 11969, https://doi.org/10.1038/ncomms11969

Muis, S., Irazoqui Apecechea, M., Dullaart, J., de Lima Rego, J., Madsen, K.S., Su, J., Yan, K., and Verlaan M. (2020). A High-Resolution Global Dataset of Extreme Sea Levels, Tides, and Storm Surges, Including Future Projections. *Frontiers in Marine Science*, 7(263), https://doi.org/10.3389/fmars.2020.00263

Murty, T. (1988). List of major natural disasters, 1960-1987. *Natural Hazards*, 1(3), 303-304.

Myers, V.A. (1954). Characteristics of United States hurricanes pertinent to levee design for Lake Okeechobee, Florida. US Government Printing Office.

Palmer, T., and Williams, P. (2010). Stochastic Physics and Climate Modelling. Cambridge University Press.

Pérez, B., Álvarez Fanjul, E., Pérez, S., de Alfonso, M., Vela, J. (2013). Use of tide gauge data in operational oceanography and sea level hazard warning systems, *Journal of Operational Oceanography*, 6(2), 1-18, https://doi.org/10.1080/1755876X.2013.11020147

Pérez, B.,Brouwer, R., Beckers, J., Paradis, D., Balseiro, C., Lyons, K., Cure, M., Sotillo, M.G., Hackett, B., Verlaan, M., Fanjul, E.A. (2012). ENSURF: Multi-model sea level forecast-implementation and validation results for the IBIROOS and Western Mediterranean regions. *Ocean Science*, 8(2), 211-226, https://doi.org/10.5194/os-8-211-2012

Pérez-Gómez, B., Pérez González, I., Sotillo, M. G., and Álvarez-Fanjul, E. (2019). Retos de los sistemas de observación y predicción en los riesgos asociados al nivel del mar. *Ribagua*, 6, 1-5, https://doi.org/10.1080/23863781.2019.1595212

Pérez González, I., Pérez-Gómez, B., Sotillo, M. G., and Álvarez-Fanjul, E. (2017). Towards a new sea level forecast system in Puertos del Estado. In Proceedings of the 8th EuroGOOS Conference, Bergen.

Pore, N. A. (1964). The relation of wind and pressure to extratropical storm surges at Atlantic City. *Journal of Applied Meteorology and Climatology*, 3(2), 155-163.

Ringler, T., Petersen, M., Higdon, R. L., Jacobsen, D., Jones, P. W., and Maltrud, M. (2013). A multi-resolution approach to global ocean modeling. *Ocean Modelling*, 69, 211-232, https://doi.org/10.1016/j.ocemod.2013.04.010

Rossiter, J. R. (1961). Interaction between tide and surge in the Thames. *Geophysical Journal International*, 6(1), 29-53.

Schalkwijk, W.-F. (1948). A contribution to the study of storm surges on the Dutch coast. *Ciel et Terre*, 64, 188.

Siek, M., and Solomatine, D. (2011). Real-time Data Assimilation for Chaotic Storm Surge Model Using NARX Neural Network. *Journal of Coastal Research*, 1189-1194, https://www.jstor.org/stable/26482362

Sotillo, M.G., Cailleau, S., Lorente, P., Levier, B., Aznar, R., Reffray, G., Amo-Baladron, A., Chanut, J., Benkiran, M., Alvarez-Fanjul, E. (2015). The MyOcean IBI Ocean Forecast and Reanalysis Systems: operational products and roadmap to the future Copernicus Service. *Journal of Operational Oceanography*, 8(1), https://doi.org/10.1080/1755876X.2015.1014663

Takahashi, K. (1939). Distribution of pressure and wind in a typhoon. *Journal of the Meteorological Society of Japan*, 17(2), 417-421.

Ueno, T. (1981). Numerical computations of the storm surges in tosa bay. *Journal of the Oceanographical Society of Japan*, 37(2), 61-73, https://doi.org/10.1007/BF02072559

Verlaan, M., Zijderveld, A., de Vries, H., and Kroos, J. (2005). Operational storm surge forecasting in the Netherlands: developments in the last decade. *Philosophical Transactions of the Royal Society A: Mathematical, Physical and Engineering Sciences*, 363(1831), 1441-1453, https://doi.org/doi:10.1098/rsta.2005.1578

Wang, P., Yu, F., Liu, Q., and Dong, J. (2010). Research and application of fine ensemble numerical forecasting technology for typhoon storm surge in Fujian coastal. *Marine Forecasts* (in Chinese), 27(05), 7-15.

Webster, P. J., Holland, G. J., Curry, J. A., and Chang, H.-R. (2005). Changes in Tropical Cyclone Number, Duration, and Intensity in a Warming Environment. *Science*, 309(5742), 1844-1846, https://doi.org/10.1126/science.1116448

Weisberg, R. H., and Zheng, L. (2008). Hurricane storm surge simulations comparing three-dimensional with two-dimensional formulations based on an Ivan-like storm over the Tampa Bay, Florida region. *Journal of Geophysical Research: Oceans*, 113(C12), https://doi.org/10.1029/2008JC005115

WMO. (2012). Guidelines on Ensemble Prediction Systems and Forecasting.

Ye, F., Zhang, Y. J., Yu, H., Sun, W., Moghimi, S., Myers, E., Nunez, K., Zhang, R., Wang, H. V., and Roland, A. (2020). Simulating storm surge and compound flooding events with a creek-to-ocean model: Importance of baroclinic effects. *Ocean Modelling*, 145, 101526, https://doi.org/10.1016/j.ocemod.2019.101526

Yu, F., Fu, C., Guo, H., and Liu, Q. (2020). Modern technologies and Application in storm surge forecasting. Science Press (in Chinese).

Zheng, L., Weisberg, R. H., Huang, Y., Luettich, R. A., Westerink, J. J., Kerr, P. C., Donahue, A. S., Crane, G., and Akli, L. (2013). Implications from the comparisons between two- and three-dimensional model simulations of the Hurricane Ike storm surge. *Journal of Geophysical Research: Oceans*, 118(7), 3350-3369, https://doi.org/10.1002/jgrc.20248

Zijl, F., Sumihar, J., Verlaan, M. (2015). Application of data assimilation for improved operational water level forecasting on the northwest European shelf and North Sea. *Ocean Dynamics*, 65, 1699-1716, https://doi.org/10.1007/s10236-015-0898-7

8.
Wave modelling

CHAPTER COORDINATORS

Lotfi Aouf and Gabriel Diaz-Hernandez

CHAPTER AUTHORS *(in alphabetical order)*

Alexander Babanin, Jean Bidlot, Joanna Staneva, and Andy Saulter

8. Wave modelling

8.1. General introduction to wave characterization

8.1.1. Objective, applications, and beneficiaries

8.1.2. General characteristic of waves

8.1.2.1. General concepts

8.1.2.2. Definitions

8.1.3. Deep water wind-generated wave theory

8.1.4. Nearshore transformation of waves

8.1.4.1. Shoaling

8.1.4.2. Refraction

8.1.4.3. Diffraction

8.1.4.4. Wave current interaction

8.1.4.5. Dissipation (breaking and bottom friction)

8.1.4.6. Wave-structure interaction

8.2. Wave forecast and multi-year systems

8.2.1. Architecture singularities

8.2.1.1. Levels of complexity from deep to shallow water

8.2.1.2. Hybrid and clustering technique

8.3. Input data, available sources, data handling, and model pre-processing

8.3.1. Bathymetry and geometry

8.3.2. Forcing fields

8.3.3. Observations

8.3.4. Pre-processing and definition of the numerical problem

8.3.5. Boundary and initial conditions

8.4. Modelling component: general wave generation and propagation models

8.4.1. Types of models

8.4.1.1. Deep water

8.4.1.2. Shallow water

8.4.2. Discretization methods

Figure 8.1.   Waves panorama (credits: Gabriel Barajas Ojeda, IHCantabria).

8.1.
General introduction to wave characterization

Waves are extremely important in OOFS. This section gives an overview of the main challenges foreseen by OOFS for predictions to be able to numerically represent some relevant processes like that in Figure 8.1.

8.1.1. Objective, applications, and beneficiaries

Why is a comprehensive and reliable wave forecast so important?

In the last decade, the worldwide seas were hit by severe storms (see ECMWF, 2020), which caused serious damages in offshore and coastal zones, and attracted public attention on the importance of having reliable and comprehensive wave forecasts, especially when extreme events occur (Figure 8.2). Additionally, human activities, such as offshore wind power industry, oil industry, and coastal recreation also necessitate regular operational sea state information with high resolution in space and time.

Furthermore, extreme waves can cause serious impacts over coastal environments and infrastructures. The design of coastal and offshore structures requires a reliable estimation of maximum wave height. Efforts of sea state information are directed towards the improvement of environmental loads definition for lifetime of a ship or structure (e.g. wind energy turbines or oil and gas platforms). For example, long-term statistical and high-resolution predictions of significant wave height are necessary for planning the maintenance operations of offshore wind farms. Subject to wave forecasts, in the days and hours preceding a mission, "go/no go" decisions are made on operations and maintenance activities in offshore wind farms. Indeed, a reduction of uncertainties on metocean conditions will have a direct impact on structure and mooring loads, both for ultimate limit state and fatigue design, as well as for warning criteria for ships. These results can be obtained through hindcast and forecast studies including maximum wave parameters, which also aim at expanding the wave Copernicus Marine Service products catalogue[1] by providing novel wave diagnostics.

---

1. https://myocean.marine.copernicus.eu/
data?view=catalogue&initial=1
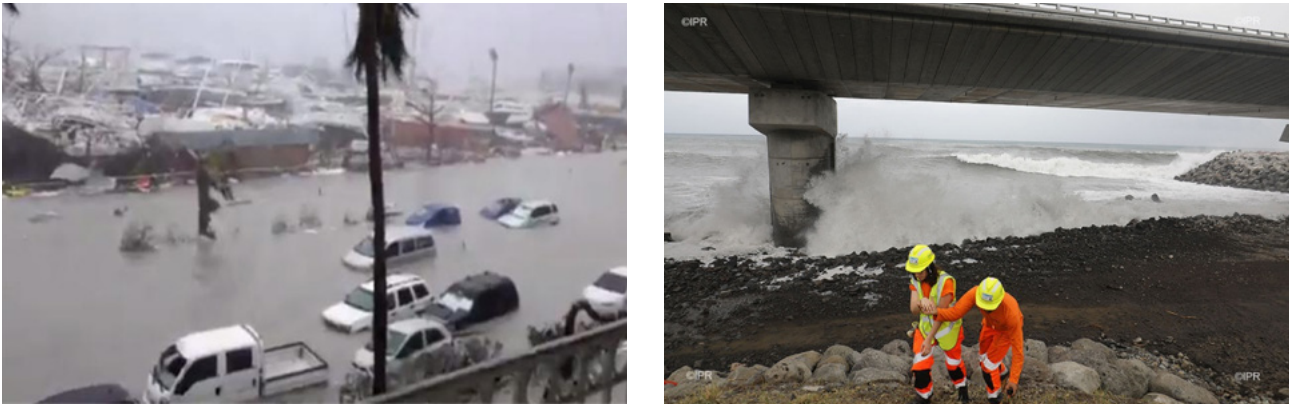
Figure 8.2. Left: high waves flooding after passage of Hurricane Irma in Saint Martin (Atlantic Ocean) in September 2017 (source: RCI-Guadeloupe). Right: high waves warning after passage of tropical cyclone Eliakim in La Réunion (Indian Ocean) on 15 March 2018 (copyright IPR Imaz Press Réunion).
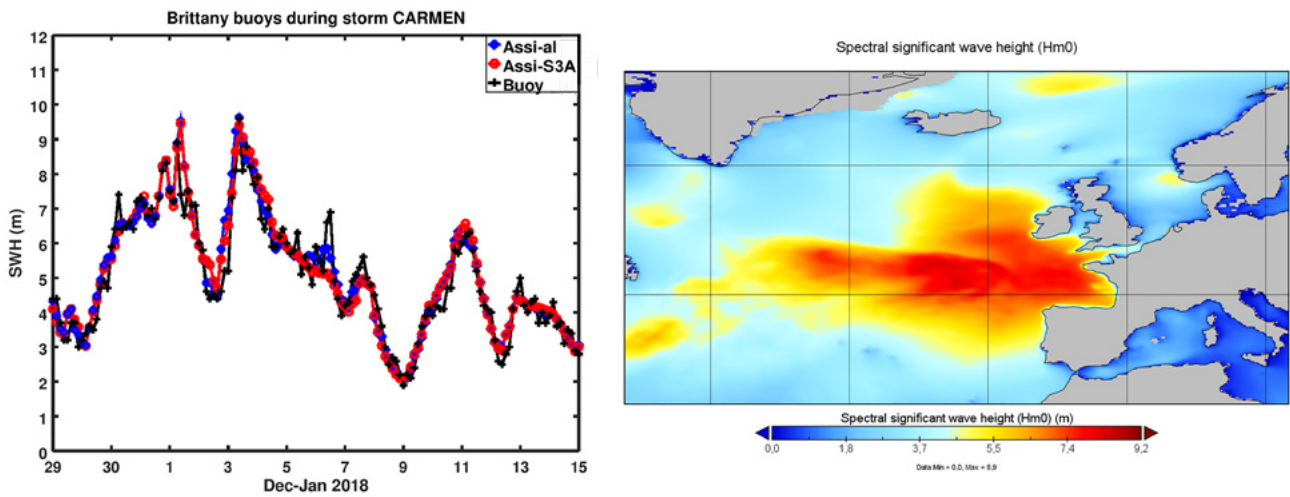
Figure 8.3. Left: time series of significant wave height at Brittany (France) buoy location during storm Carmen on 1 January 2018. Blue, red and black colours stand for hindcast from wave model MFWAM, analysis from model with assimilation of Sentinel-3 SWH and buoy SWH, respectively. Right: SWH map (in metres) from Copernicus Marine Service global wave reanalysis at peak of 1 January 2018 event, 09 UTC (source: Copernicus Marine Service).

The level of performance of wave forecasting products is of crucial importance. The assimilation of novel satellite data in global Monitoring and Forecasting Centres has pointed out the skill of the systems during storms generating high waves (Aouf, 2018). The joined satellite and model analyses also demonstrate the capability of the wave forecasting products to cover from global to regional scales (Copernicus Marine Service, OSR[2]), as well as the potential benefits of merging observational and modelled products (such as those shown in Figure 8.3) provided by the Copernicus Marine Service.

2. https://marine.copernicus.eu/access-data/ocean-state-report

Monitoring and forecasting

Monitoring and forecasting of wind waves are, in most cases, closely linked with ocean and atmospheric observations and modelling. The availability of systematic near-real time ocean observations is a prerequisite for the quality of weather and ocean state forecasts. Novel satellite wave observations are crucial for reducing the uncertainties in prediction skills for the wave simulations. Given that most of the buoy observations are coastal, remote sensing data are needed for tuning and validating the models offshore. On the other hand, ocean waves have a clear signature in most ocean remote sensing
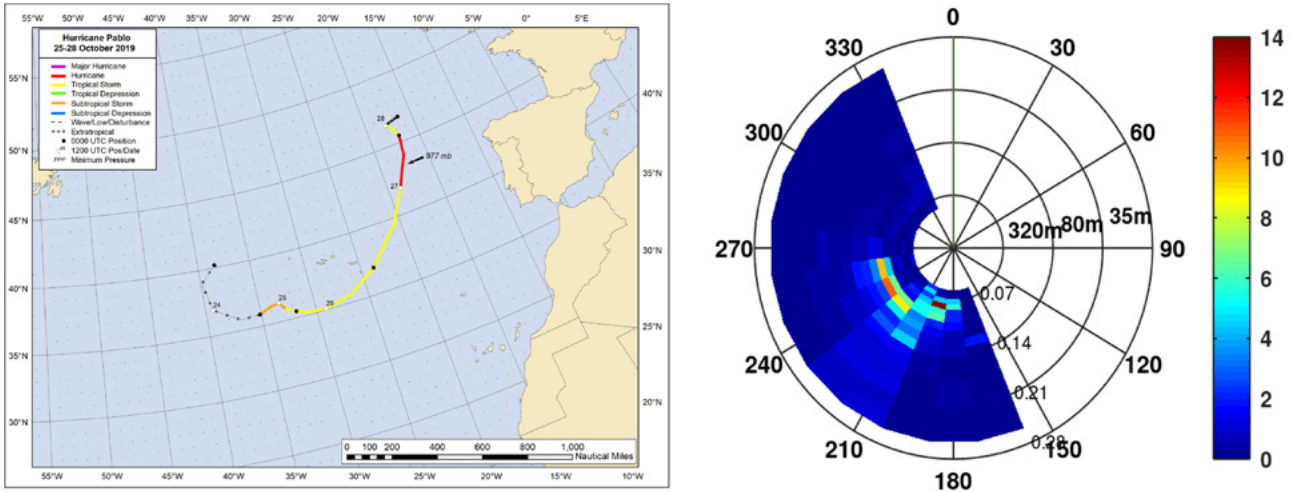
Figure 8.4.   Left: trajectory of hurricane Pablo from 25 to 28 October 2019, NHC-NOAA tropical cyclone report. Right: wave spectrum observed by CFOSAT near the trajectory of hurricane Pablo (17°W-45°N) on 27 October 2019 at 18 UTC (source: Beven, 2019).

techniques, either adding noise or biases, and stable corrections and detection are very important for sea level and velocity estimates from altimetry (Climate Change Initiative Coastal Sea Level Team, 2020; Marti et al., 2021). It is important to underline that future regular monitoring of maximum wave heights is expected to improve understanding of the conditions that favour the generation of very large waves in the global ocean.

Sea state information for applications

There is a steady growth of the already intense interest in the wave conditions in coastal areas at different time scales. Increasing maritime traffic, recreational activities, urban development, ecosystem restoration, renewable energy industry, offshore management, all push in this direction (Cavaleri et al., 2018). Indeed, sea state affects most of the activities at sea (shipping, oil and gas industry, fisheries, offshore aquaculture, etc.), on the coast (marine protected areas, harbours, marine renewable energy, tourism, etc.). These activities require precise information on the sea state (hindcast, nowcast and forecast) and, in particular, on wave extremes. In addition to activities directly linked to the ocean, wind waves are of general interest to the Earth system.

Extreme events

Wind waves constitute the most relevant ocean process affecting the human activities and nearshore environment. The sea state and its related spatio-temporal variability dramatically affect maritime activities and the physical connectivity between offshore waters and coast-

al ecosystems, impacting also on the biodiversity of marine protected areas (Hewitt, 2003; González-Marco et al., 2008). Given their destructive effects in both the shoreline environment and human infrastructures, significant efforts have been devoted to predict extreme wave height events, prompting a wide range of adaptation strategies to deal with natural hazards in coastal areas (Hansom et al., 2015). In addition, there is also the emerging question about the effects of anthropogenic global climate change on present and future sea state conditions.

Tropical cyclones are commonly linked to devastation by hurricane force winds, storm surges and strong rainfall. They are also responsible for large exchanges of heat in the upper ocean and the atmosphere, and the transport of water from ocean to land. However, the dynamics inside these extremes are poorly sampled and understood. SAR overcomes these situations, but it is only able to recover one-dimensional information, which limits the ac<Zcuracy of estimated quantities like wind speed, total surface current, and wave spectra. In tropical cyclones, wave spectra (e.g. from Sentinel or by the CFOSAT) can only partly be recovered, as the quickly changing sea surface limits the resolution of SAR in the azimuth direction (Ardhuin et al., 2020) and from SWIM instrument of CFOSAT mission (Figure 8.4).

Coupling with circulation

The combined effect of high waves and sea level surge aggravate the storm risk potential. Integration of local wave and sea level forecasting systems (Álvarez-Fanjul et al., 2018; Staneva et al., 2020) and their associated alerts demonstrated
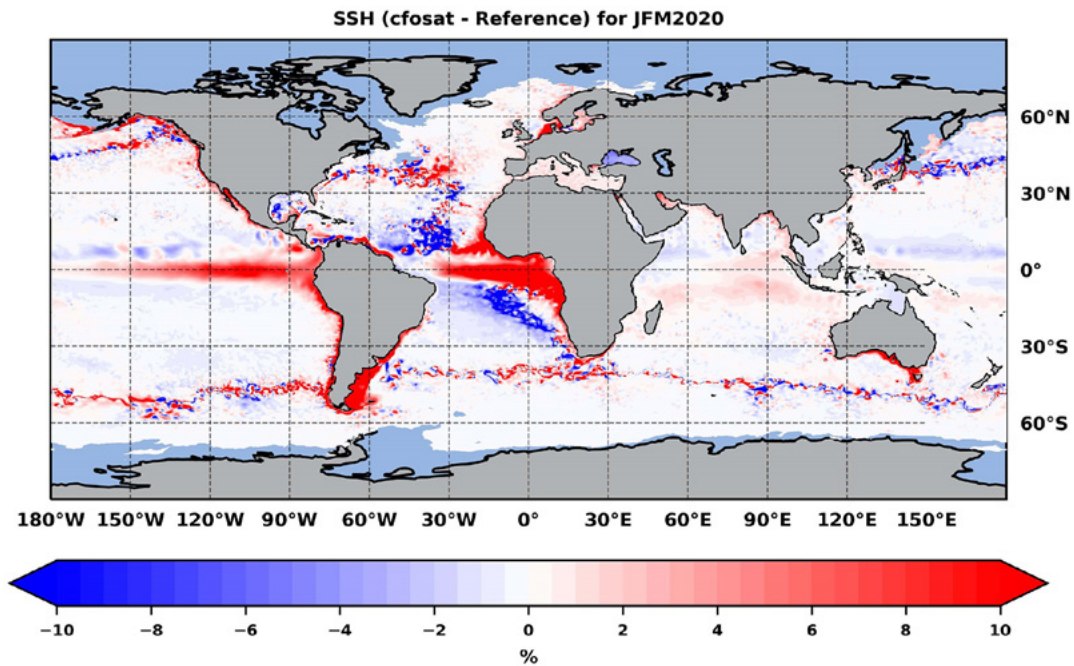
Figure 8.5. Mean difference (in percentage) of sea surface temperature induced by wave forcing in comparison with reference NEMO without waves (surface stress, Stokes drift and wave breaking inducing turbulence in the ocean mixed layer) for austral summer (January to March 2020) (source: Aouf et al., 2021).

the urgent need for such services. In respect to deep open waters, the relevance of currents is a difference emerging often. In the past, especially in the deep ocean, surface currents did not reach velocities to substantially affect wave conditions, which led to ignoring the wave induced currents in the ocean forecasts. However, close to the coast, the currents (barotropic and baroclinic) are geographically enhanced reaching values that, if not considered, can lead to substantial errors in wave model results (Cavaleri et al., 2018). Coupling between wind waves and circulation model waves can also affect the predictions of water levels, and thus of storm surges through changes in the stress of the upper-ocean mixing and circulation (Thomas et al., 2008; Staneva et al., 2021), providing more accurate offshore wave spectra (Cavaleri et al., 2018). Besides, forecasting the Lagrangian behaviour of surface currents is a key to identify high-risk scenarios for pollution of coastal areas, search and rescue, marine plastic, or quantify transport and retention of larvae or other planktonic organisms, with impact for fishery and Marine Protected Areas management.

Mixing

Human activities that take place at the atmospheric and ocean mixed layer (e.g. offshore wind energy sector) are largely driven by the air-sea exchanges of momentum, heat, and gas transfer. The fluxes between atmosphere and ocean are usually parameterized using bulk formulations, in which coefficients are often a function of wind speed alone. For example,

ocean waves largely define air-sea fluxes and upper ocean mixing (Babanin et al., 2012; Veron, 2015). A considerably enhanced momentum transfer from the atmosphere to the wave field is found during growing sea state (young sea) (Janssen, 1989). A wind stress formulation depending on wind stress and the wind–wave momentum released to the ocean was proposed by Janssen (1991). When running stand-alone ocean or atmosphere models, the surface waves that represent the air-sea interface are not taken into account. This can cause biases about the upper ocean, due to insufficient or, in some cases, too strong mixing (Breivik et al., 2015), or even because the momentum transfer is shifted in time and space compared to how the fluxes would behave in the presence of waves. Recent analyses show a moderate impact for intermediate wind speeds (Edson et al., 2013), even though it is expected that the surface roughness caused by waves should play a role (Donelan, 2004), although it is often correlated with the wind speed. The impact of waves on upper ocean mixing and sea surface temperature, in particular in cases of shallow mixed layers, is clearer at global and regional scales (Janssen, 2012; Staneva et al., 2017; Law Chune et al., 2018); see an example in Figure 8.5.

Engineering and near coastal applications

In order to design and operate ocean and coastal infrastructures (e.g. dikes, harbours, etc.) wave climate data and wave statistics are crucial. High-resolution, high-skill wave forecasts are important for coastal and marine engineering, given that waves can damage marine infrastructures and affect the safety
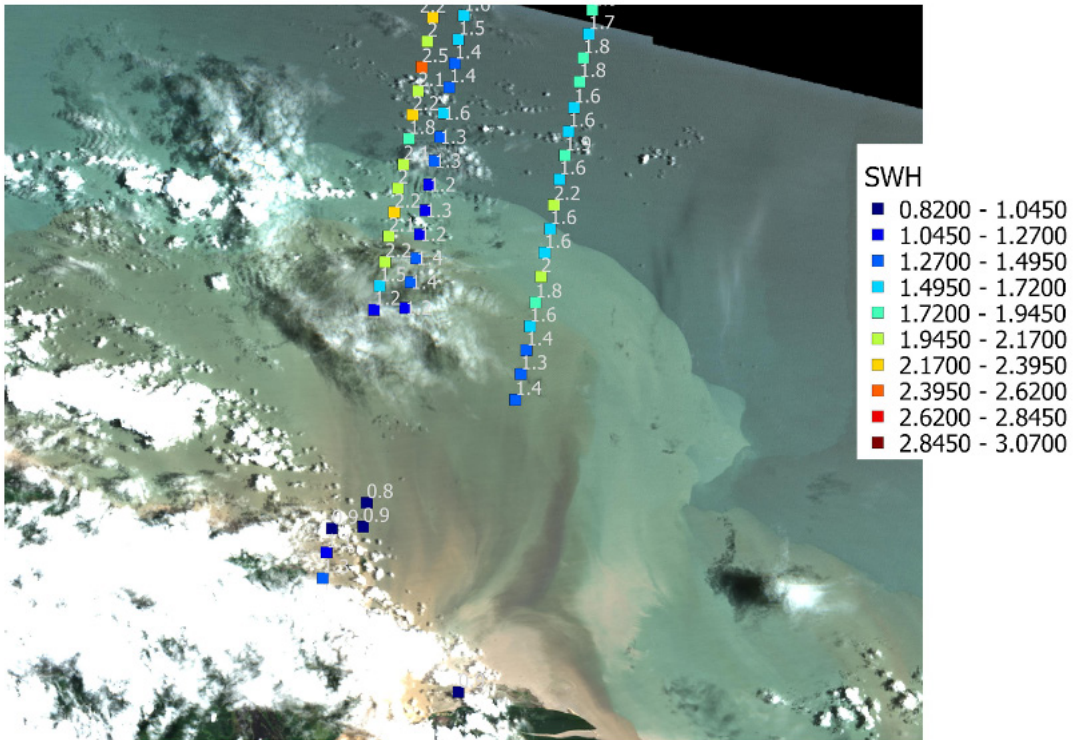
Figure 8.6. Sentinel-2 image observing coastal changes at Maroni estuary (French Guyana) overlapped by high resolution (1 km) significant wave heights on CFOSAT nadir tracks in March 2021. CFOSAT captures the decrease of SWH induced by very shallow water depth processes (courtesy of A. Dalphinet, MeteoFrance).

of shipping, ports, and offshore operations. Waves contribute to a large extent to shoreline erosion and flooding, which can influence coastal ecosystems and affect coastal communities. Realistic assessment and good understanding of historical wave climate is important to successfully address challenges and opportunities caused by present and future climate change, such as reduction of sediment supply by rivers to sand mining, blocking of longshore sediment transport by ports and other structures, sea level rise, particularly near tidal inlets, and land subsidence. Wind waves force coastal bathymetry changes and in coastline evolution, especially during extreme events or large swell events, waves can damage beaches, dunes, and/or dikes.

Early warning systems and risks

Warnings from integrated high-resolution wind waves surge forecasting systems can be sent in advance to the users. Several actions can be carried out to mitigate the impact of extreme hydrometeorological events. For example, harbours would stop operations to prevent accidents and assure safety. In some events material damages can be considerable but, as a result of preventive actions, personal injury can be avoided. Thanks to freely available satellite imagery (e.g.

Sentinel), it is now possible to observe from nadir altimeters, with good accuracy and increased sampling, the coastline changes by significant wave height, as shown in Figure 8.6.

The assimilation of newly available satellite-based wave data in wind wave models allows to more accurately hindcast and forecast coastal evolution in remote and ungauged areas, and to assess the effectiveness of coastal management strategies. Wind wave forecasts directly may improve the safety of people working offshore, such as those on oil platforms, fishers, etc. Professional sailors are constantly looking for wave forecast products that improve their knowledge and forecasts of sea state to be able to make the best decisions about routes and actions they will take during month-long competitions.

Sea state and coastal ecosystems

Some coastal ecosystems, such as salt marshes, coral reefs, mangroves, and seagrass meadows, play a fundamental role in shaping nearshore processes in a large portion of the world's coastline. Due to their capacity to naturally mitigate coastal flooding and erosion, the management and protection of these ecosystems is increasingly advocated within nature-based

coastal protection initiatives. Awareness that Nature-based solutions (NBS) can tackle societal challenges by utilising environmentally safe operations for vulnerability and risk assessment processes is growing. For example, marine seagrass is highly considered as a useful NBS, as it is capable of attenuating the impact of storm surges and coastal erosion. Ecosystem models usually have significant uncertainty in predictions. Understanding and better predicting wave-driven nearshore processes would help to improve our knowledge of hydrodynamic interactions with ecosystems across different time and space. Furthermore, wave forecast data are needed for activities involving protection, development, and enhancement of coastal and marine environments. Besides, sea state information can provide technical and scientific support to policy makers and stakeholders for environmental governance.

Wave data and the industry (e.g. marine energy sector, shipping operations, emergency response, etc.)

Wave data are critical for safe and efficient design, installation and operation of assets of the marine energy sector. High-resolution regional and coastal wave models can help to improve downscaling of general sea state forecasts, identify hotspots of different wave height properties, and prioritisation of maintenance jobs in offshore wind turbines, reducing their maintenance cost. Applications can further include initial resource assessment (wave power), environmental assessment, and planning (e.g. for installation and execution, operation and maintenance).

Sea state conditions have a significant impact on the design and structure of how vessels are built. The changes of the sea state impact on vessels operations and have always been a challenge for seafarers to which they have had to continually adapt. Besides, shipping/cargo operations are highly impacted by sea state and weather conditions. In addition, wave forecasts are needed for oil spill and emergency responses. The industry has developed various ways to adapt to the strength of the ocean. As evolving design and commercial needs push the boundaries of vessels' size and capacity, the demand for accurate sea state information increases.

Climate and waves as a part of the Earth system models

In our "blue" planet, interactions between the atmosphere and the ocean are crucial for the climate, and sea-related research plays a key role for a sustainable future (Visbeck, 2018), as advocated by international initiatives like the United Nations Decade of Ocean Science for Sustainable Development (2021-2030). Recent studies (e.g., Hewitt et al., 2017) have shown the relevance of air-sea interaction for a wide variety of phenomena (e.g. tropical/extratropical cyclogenesis, storm tracks, and global energy/radiation balances). Moreover, the IPCC has recognized the relevance of ocean waves for natural hazards in coastal areas, pointing out the

need for more mature regional (coupled) downscaling. Furthermore, air-sea transfers will become even more critical in the future, due to enhanced interface transients, temperature gradients, and possible other factors. To address the uncertainty and sensitivity of future projections due to global warming, it is necessary to fill the knowledge gaps related to air-sea feedbacks, which also limit present weather modelling, advancing from semi-empirical (bulk) formulations to sea-state dependent equations with an enhanced process basis. There is also an urgent need to advance the understanding and improve the modelling capabilities of the air-sea boundary, in which wind-waves play a key role.

The atmosphere-ocean feedback has now become state-of-the-art in weather prediction, but their bearing in climate simulations is somewhat limited and warrants a more detailed assessment (Breivik et al., 2015). The modulation of the active air-sea interface alters atmospheric and oceanic dynamics, as well as the associated bio-geo-chemical fluxes (e.g. CO_2 fluxes and storage at sea). Sea-state coupling should be accounted for in predictions/projections, so that the wave modulating effect on weather and climate evolution can be properly reproduced (Parkinson and Cavalieri 2012). Within an appropriate coupling and downscaling/nesting strategy, gaining understanding of air-sea interactions would reduce uncertainty in forecasting and be a critical advance for climate projections. Air-sea interface may have a role well beyond that conventionally accepted, and non-linear feedback should become more crucial under changing climate.

It is then essential to introduce the role of sea-state in both global and regional models for climate projection, addressing the resulting implications for bio geochemical and boundary (sea-ice and land) processes. Enhanced ESMs can be supported by new satellites (e.g. CFOSAT, Sentinel data, etc.) to achieve improved predictions for energetic conditions (e.g. tropical cyclones or Mediterranean tropical-like cyclones, often referred to as medicanes) and projections. In an ESM, the sea state needs to be considered at both global and regional scales, ensuring consistency and contributing to overcome uncertainties of projections at both short-term and long-term time scales. The advances on air-sea-wave-ice interactions in coupled models (including the land boundary) will contribute to bridge the gap between predictions/projections.

8.1.2. General characteristic of waves

8.1.2.1. General concepts

Within the catalogue of physical meteo-oceanographic variables and processes offered by any OOFS, waves can be considered one of the most relevant elements. Waves have high interaction with human activities located on the coast (coasts, ports, river mouths, etc.) given their energetic importance, and their cyclical and continuous presence in nature. Figure 8.7 dis-
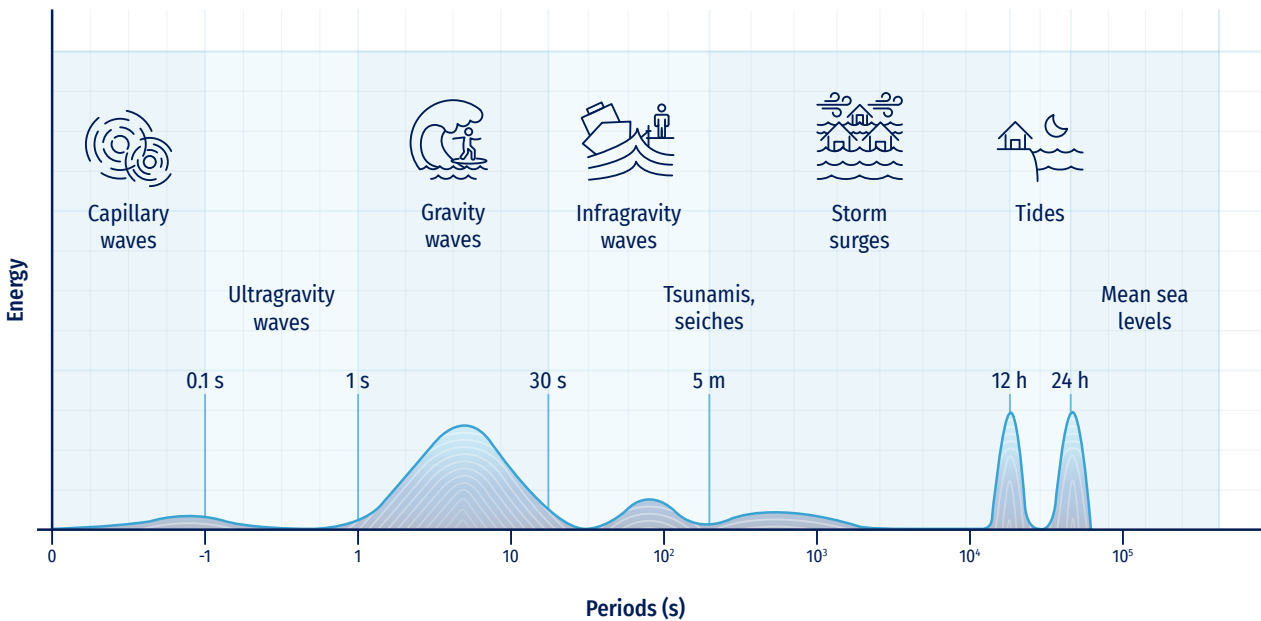
Figure 8.7. Frequencies and periods of the vertical notions of the ocean surface (adapted from Pérez et al. 2013, Holthuijsen (2007), after Munk (1950)).

plays the energetic relevance of wind-generated waves (with typical periods between 1 and 30s), in comparison with other oscillatory variables in the marine physical environment.

Traditionally, observations of ocean waves were obtained through visual databases (Gulev et al., 2003) limited in space and time, and with a high uncertainty about their qualitative genesis. Likewise, instrumental wave databases (Chelton and McCabe, 1985), obtained at discrete points in ocean and coastal areas, have been relevant in the understanding, quantification, and exploitation of this variable. However, only records of no more than two decades duration, generally non-continuous and acquired by equipment with non-homogeneous hardware characteristics, were available.

More recently, thanks to satellite technology it is possible to rely on a more extensive, continuous, accurate and homogeneous wave database (Barstow et al., 2004; Ribal and Young, 2019), with approximately two decades of development in the state of the art. The major disadvantage of this type of data consists in the spatial discontinuity conditioned by the satellite's own translation, which only manages to cover narrow trajectories (see Chapter 4, Section 4.2.3).

In the same way, thanks to technological advances in computers, in recent years it has been possible to obtain continuous, homogeneous, and realistic wave databases with global coverage (Saha et al., 2010; Reguero et al., 2012; Perez et al., 2017), in line with directional calibration techniques for post-processing this type of series. These new databases are in turn fed by global climate models of wind, pressure, ice cover, and other variables (Tolman, 2010). See in Figure 8.8 a general scheme of variables and processes for wind-generated waves.

The wave variable represents one of the fundamental bases of meteo-oceanographic knowledge, due to its energy and interactions with natural and human activities in open and coastal areas. Therefore, it is important to have a good quantification of wave characteristics, either from a statistical (long-term or multi-year / hindcast databases) or predictive (short- to medium-term / forecast strategies) approach. This information is needed to design, construct, and operate maritime activities from coastal areas to offshore locations exposed to extreme events, as well as for environmental management, climate analysis, and all situations in which the complex processes of wave transformation occur.
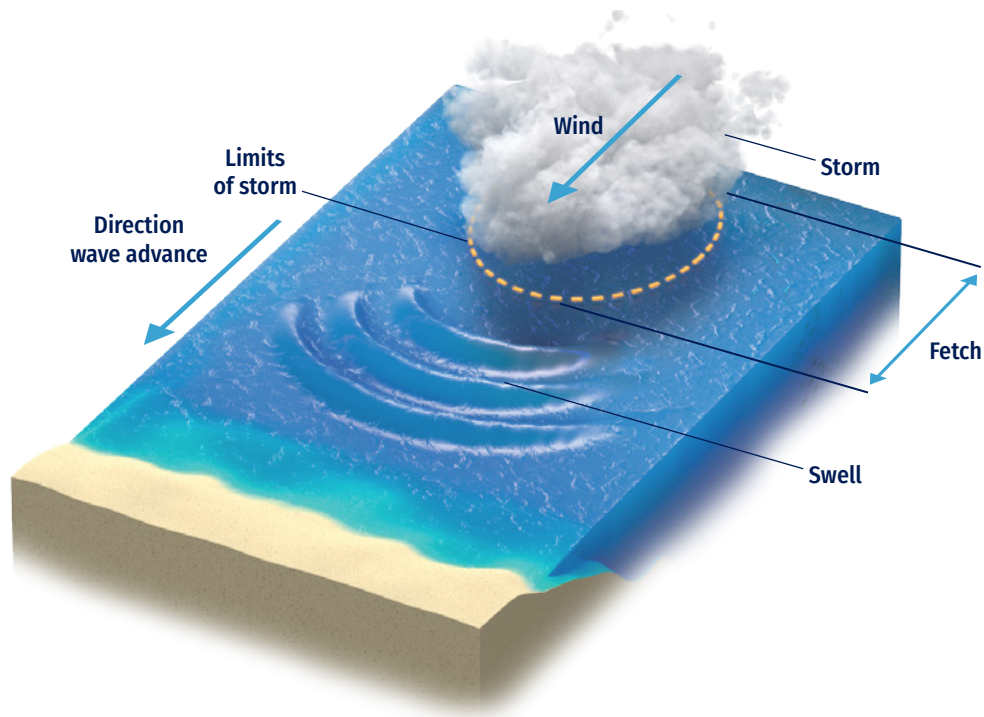
Figure 8.8. General scheme of variables and processes for wind-generated waves' characterization from offshore to coastal zones.

The current techniques require long-time (historical) series on the most relevant wave variables, associated to sea states (generally hourly) with a global coverage. These databases are already available, often free of charge, thanks to important technological efforts of different institutions worldwide (Rascle et al., 2008; National Centers for Environmental Prediction, 2012; Le Traon et al., 2019). This reliable information is subjected to validation, assimilation, and calibration protocols with instrumental data (Thomas, et al., 2008; Stopa, 2018) but, as it is only limited to open water areas, does not usually include the transformation processes that waves undergo in intermediate to reduced waters. Then, to include these relevant processes, it is necessary to address the concept of wave downscaling, and additional physics is needed to characterise in detail and with high resolution the waves in coastal areas, harbours, beaches, etc.

Modern downscaling relies almost entirely on the support of numerical models that, over the last decade, have evolved enormously in terms of resolution, including physical processes, spatial extensions; also the variables to be obtained go beyond the basic wave variables. However, the new processes/variables to be obtained, along with the new numerical tools, tend to increase the complexity of the solutions, since they call upon for increasingly sophisticated mathematical formulations, rise the dimensions of the computational scheme (from two-dimensional to three-dimensional scopes) and, consequently, boost the computational time for their solution.

This trend represents an important technical constraint in the assembly of numerical solutions for obtaining the wave variables, from hourly to multi-annual statistical analysis, as well as for any analytical project in the predictive or forecast environment, in which the results are expected to be available on a daily basis and within a calculation window of a few minutes/hours.
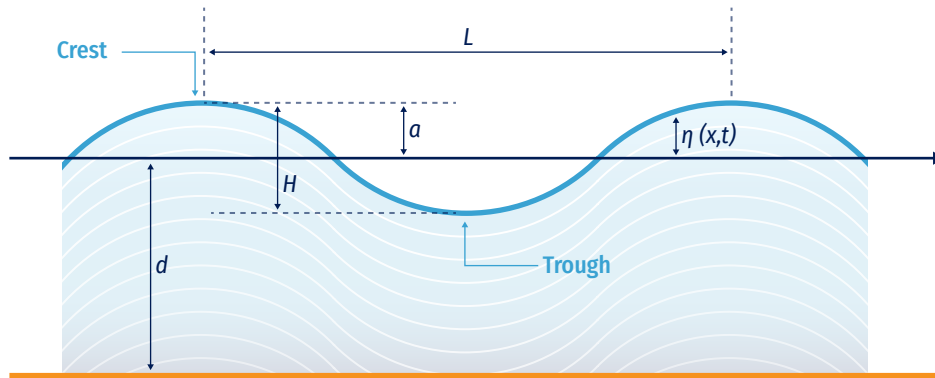
Figure 8.9.   Characteristics of a 2D linear water wave.

Different methods have been proposed in the literature (Gaslikova and Weisse, 2005; Camus, et al. 2011 and Camus, et al. 2013) to overcome this problem, with the purpose of a better understanding of the complexity of the physical processes associated with the generation / propagation of waves, without paying a computational cost that moves the climate solution away from its practical and efficient objective.

In this chapter are discussed the most relevant concepts on the quantification of the wave variable in the meteo-oceanographic field, focusing on how to obtain time series (hourly) of this variable in the multi-annual field (hindcast) and the predictive field that are part of an OOFS. Basic concepts are:

- Theoretical definition of waves;

- Techniques, tools, and numerical models that are currently commonly used worldwide;

- Architecture and singularities in the solution schemes, assembly, and general approximation methods for the adequate exploitation of the tools;

- Basic and advanced variables associated with waves that can be obtained in different geographical areas;

- Some examples of multi-annual and forecast systems currently operating at the global level.

In line with the ten challenges of the UN Decade of Ocean Science for Sustainable Development, this chapter aims at making the readers able to obtain general and basic knowledge of wave climate, enabling them to establish their own multi-annual statistical prediction and interpretation systems for studies and projects in coastal engineering, offshore maritime works, beach design, integrated coastal management, harbour agitation, forensic analysis of extreme events, design formulations for coastal engineering, marine construction aid systems, etc.

8.1.2.2. Definitions

This section describes the general terminology for the physical features of the ocean waves. Theoretical water waves are described by their length (L), height (H), amplitude (a) or height (H), and water propagation depth (d). Other variables, such as velocities, pressures and accelerations can be explicitly mathematically calculated from the three basic quantities: amplitude (a), wavelength (L) and period (T). Two-dimensional wave schematic is traditionally visualised (Dean and Dalrymple, 1991) to better understand the wave main characteristics (Figure 8.9).

This scheme exemplifies ocean waves a as simple sinusoidal wave, where a represents the oscillatory and cyclic vertical distance between the mean water level and the crest height, and η(x,t) represents the vertical position of the free surface at a specific location x and time. The coordinate axis used to describe wave motion is located on the still water line z=0 and bottom of the water z=-d. Wavelength (L) can be defined using the dispersion relation (as described in Eq. 8.1), defined as the horizontal distance between two successive wave crests or troughs (wave lowest point) and directly related with the wave period (T, as the required time for two successive crests to pass from a fixed point in space or time respectively), over a water depth.

As waves propagate, water mass moves in orbital trajectories. Also, wave phase velocity or celerity (C), is equivalent to $C=L/T$.

This idealisation rarely appears in nature, neither in frequency nor in direction. Thus, irregular waves or real field waves can be organised as a superposition of a large number of sinusoidal components (monochromatic waves) going in multiple directions, each of them with different frequencies or periods, amplitudes and random phases. This idea allows the use of a classical Fourier analysis, statistical techniques, and well-known energy-spectral techniques to adequately

assimilate and describe ocean waves that exist within any location and time window (generally within 1 hour as sea-state definition).

Random or irregular ocean waves, as a summation of independent harmonic waves, can be described in detail with linear theory for surface gravity waves, only valid for small amplitude waves. Linear theory (also called Airy theory, or Airy waves), after a clear definition of basic governing equations and contour conditions, gives the solution of a long-crested harmonic propagating wave in the x-direction, as follows:

$$\eta(x, t) = a \sin(\omega t - kx) \tag{8.1}$$

That yields the general dispersion equation that relates the angular frequency $\omega = 2\pi/T$ and wavenumber $\omega = 2\pi/L$:

$$\omega^2 = gk \tanh(kd) \tag{8.2}$$

So, dispersion conditions can be used to calculate the wave propagation velocity at any depth, based only on the wave period. As a result, long waves travel faster compared to short waves. These waves, whose propagation speed depends on the wavelength and frequency, are called dispersive waves.

When waves travel and propagate in the ocean, they form groups of different components. Since the difference between the spectral sea-state frequencies is infinitely small (difference between adjacent wave numbers is also infinitely small), the velocity of the group (C_g) can be calculated from the phase velocity (C) as shown below:

$$C_g = \frac{1}{2} \left(1 + \frac{2kd}{\sinh(2kd)} \right) \tag{8.3}$$

It indicates that the phase velocity (speed of an individual wave) is always equal or greater than the speed of the group. The dependence of the group velocity on frequency results in the disintegration of the wave groups: this is physically visible as longer waves travel faster ahead of the shorter waves and wave energy disperses across the ocean. A consequence of this is the transformation of an irregular sea (called SEA-type) created by a storm into a more regular and phase-ordered sea (or SWELL-type).

In the basic linear theory, these variables can define three zones that clearly differentiate the overall behaviour of waves as they are generated and propagated towards the coast, as follows:

- **Deep water**: limited by *d>0.5 L* where wave-induced velocities decrease exponentially with increasing distance from the surface. Water particles move in circles of decreasing radius towards the sea bottom. Eventually, the amplitude of the wave is equal to the radius of

the biggest circle on the free surface. Individual waves of the group travel faster than the group.

- **Shallow water**: limited between *d<0.05 L*, for shallow waters, particle kinematics shows that the amplitude of the horizontal velocity is constant over the vertical axis and it does not depend on the depth; also the amplitude of the vertical velocity increases linearly from the seabed to the surface. The orbits of the particles in shallow waters are elliptic. The celerity (*C*) is calculated only by the depth (*d*) and the wavelength (*L*) is proportional to the wave period (*T*). Individual components travel at the same speed of the group, maintaining their position in the group.

- **Intermediate depth**: all other cases in which both water depth and period (or wavelength) have a significant influence on the solution of linear wave theory. In addition, individual waves of the group travel faster than the group (as in deep waters).

This definition of waves into different theoretical zones allows to classify the physical behaviour of the oscillatory flow in three categories:

a. Wave generation in deep water by wind action;
b. Wave propagation and dispersion from deep to intermediate waters;
c. Wave transformation and dissipation towards the coastal zone, and its interaction with bathymetry, natural and artificial structures.

The general knowledge of these processes allows understanding their degree of complexity, importance, and application in statistical or predictive climate systems. It is imperative to properly identify the experimental, mathematical or numerical tools to be selected to solve processes (based on the most relevant wave transformation characteristics), to generate a hierarchy of the variables and processes to be considered and to establish the hypotheses in assembling climate systems.

The following sections discuss these topics, with the purpose of enabling the setup of a climatic (multi-year) or predictive system for ocean waves from deep water to the coast, tailored to the processes that the user wants to include, considering pros and cons of each numerical module, as well as the inherent and concatenated uncertainties of the integrated system.

8.1.3. Deep water wind-generated wave theory

Ocean wind-generated waves are one of the most challenging research objects in meteo-oceanographic physics. They are generated and forced by the wind fields acting at global

scale (Janssen, 2004, Chalikov, 2016) and are subject to important dissipation and strong nonlinear effects (Babanin, 2011), which drive the evolution of wave spectra at the scale of tens of thousands of wave periods (Hasselmann, 1962, Zakharov, 1968). Generation, dissipation, and interaction dynamics are the three main non-separable pillars for any wave model: once the waves are produced by the wind, no matter how small they are, the mechanisms of their attenuation and energy exchanges with other wave components within the wave spectrum are immediately activated. Moreover, each pillar is not a single physical process, but rather a plethora of various processes, often concurrent and with varying relative significance over the course of wave evolution.

The three main dynamics are always present but in particular circumstances, or from the point of view of a particular application, other processes can become relevant or even dominate. For example, various influences of surface currents (Babanin et al., 2017), sea ice (Thomson et al., 2018) or surface tension, as well as other forcings (Cavaleri et al., 2007).

In shallow-water environments and with extreme winds, waves become a different physical object and their respective wave models are notable for a lesser degree of physics and a larger degree of parametric and ad hoc tuning. For finite depths, dispersion is reduced or even ceases, nonlinearity grows but active nonlinear mechanisms change, balance between energy input and dissipation is no longer maintained, and a variety of new physical processes come into existence because of various wave-bottom interactions and sediment response (Young, 1999, Holthuijsen, 2007).

When winds exceed 30 m/s, a simultaneous change of physical regime takes place in all the three air-sea environments, i.e. atmospheric boundary layer, sea surface, and upper ocean (Babanin, 2018). For the waves on the ocean surface, this modifies wind input processes in which frequent flow separation and massive production of spray alters wind-wave exchanges and leads to the known effect of saturation of the sea drag. Wave breaking and dissipation are now driven by completely different dynamics, i.e. by direct wind forcing rather than nonlinear wave evolution.

8.1.4. Nearshore transformation of waves

Any ocean wave reanalysis (multi-year database) or prediction system, focusing on shallow waters of the coastal zone, will require detailed information on the most important processes involved in the transformation of ocean wave characteristics, which originated in deep water. This subsection presents a comprehensive description of these processes, their basic equations and the physics that need to be taken into account.

It is important to underline that the theories presented here treat each process as an isolated entity but, in reality, all these processes appear together and act concomitantly. Hence, it is necessary to create a hierarchy of the relevant processes for each sub-area of wave propagation towards the coast, so that developers of climate and forecasting systems can be aware and consider them appropriately.

8.1.4.1. Shoaling

Shoaling happens when waves start to interact with the ocean's bottom or bathymetry configuration. As the wave propagates over intermediate and shallow waters zones, it reduces its celerity and maintains its frequency (linear theory main hypothesis); both wavelength and phase speed decrease, and wave amplitude trends to grow (Figure 8.10). In other words, in shallow waters, ocean waves become less dispersive, meaning that the phase speed is less dependent on the wave frequency.
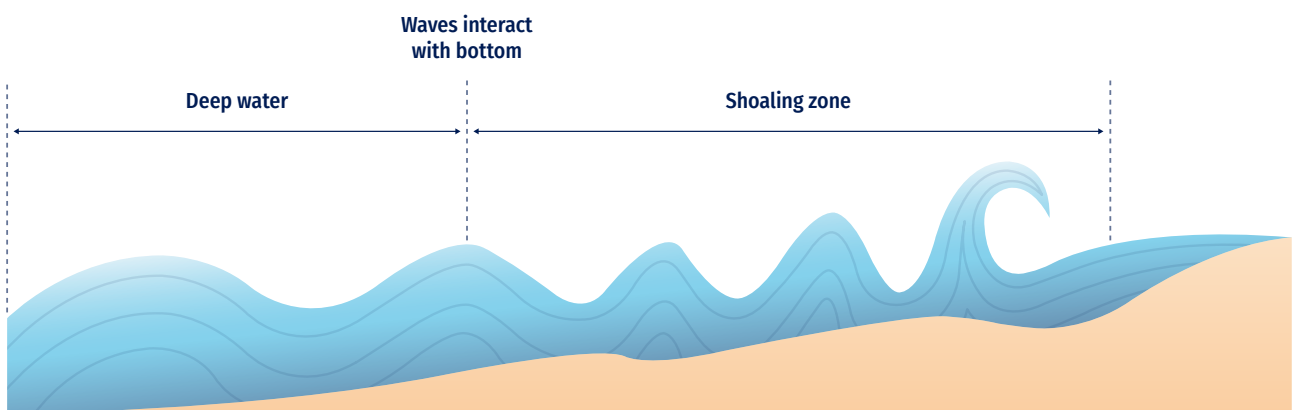
Figure 8.10.   Ocean wave shoaling main characteristics.
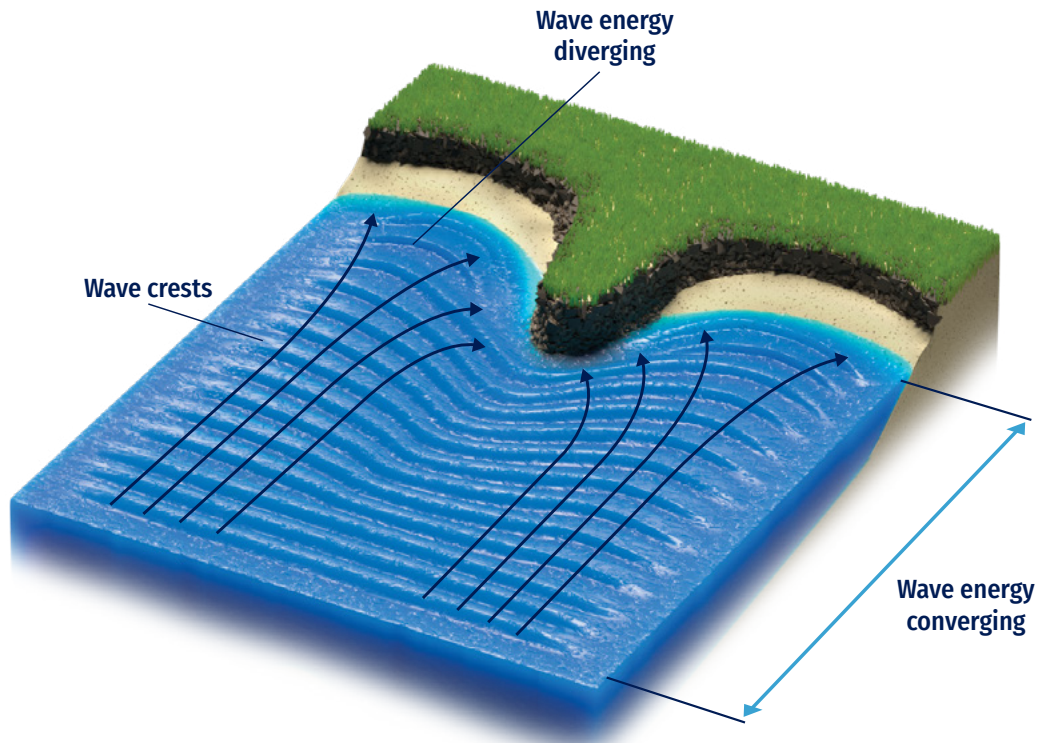
Figure 8.11.   Ocean wave refraction main characteristics.

The change in the wave height due to shoaling can be calculated from the following general relationship thorough a shoaling coefficient, K_s:

$$H_2 = H_1 \sqrt{\frac{C_{g1}}{C_{g2}}} = H_1 \cdot K_S \qquad (8.4)$$

In practice, wave shoaling phenomena can be observed as a local increase of wave heights due the reduction of the bathymetry profile or depths. Also can occur also in a reverse form, i.e. shoaled waves travelling into progressively deeper water. This results in a wavelength increase effect (wave speed also increases), while wave height decreases.

8.1.4.2. Refraction

When ocean waves change their direction of propagation from the bottom or for a bathymetry interaction, a refraction occurs, mainly due to the change of a same wave front travelling at different bathymetric depths, yielding partial reduction of its celerity. One section of a travelling wave moves faster than the other part, resulting in the wave fronts turning towards the coast (Figure 8.11). Ocean waves will al-ways turn towards the region with lower propagation speed. Physically, wave refraction satisfies Snell's law:

$$\frac{\sin \theta}{C} = \frac{\sin \theta_0}{C_0} \qquad (8.5)$$

As waves propagate towards a coast, waves crests tend to become parallel to the coastline. Refraction can be visualised as the gradual change in waves' direction when they tend to approach a coastline at an angle 0°, known as oblique incidence.

Additionally, refraction can have an important effect (partial wave height reduction or increase) calculated with a refraction coefficient (K_R) as follows:

$$K_R = \sqrt{\frac{\cos \alpha_0}{\cos \alpha}} \qquad (8.6)$$

Finally, combined wave refraction and shoaling are always present simultaneously and affect wave height as follows:

$$H_2 = H_1 \sqrt{\frac{C_{g1}}{C_{g2}}} \sqrt{\frac{\cos \alpha_0}{\cos \alpha}} = H_1 \cdot K_S \cdot K_R \qquad (8.7)$$

Wave diffraction around an obstacle

Wave diffraction through a gap

Wave diffraction around an obstacle
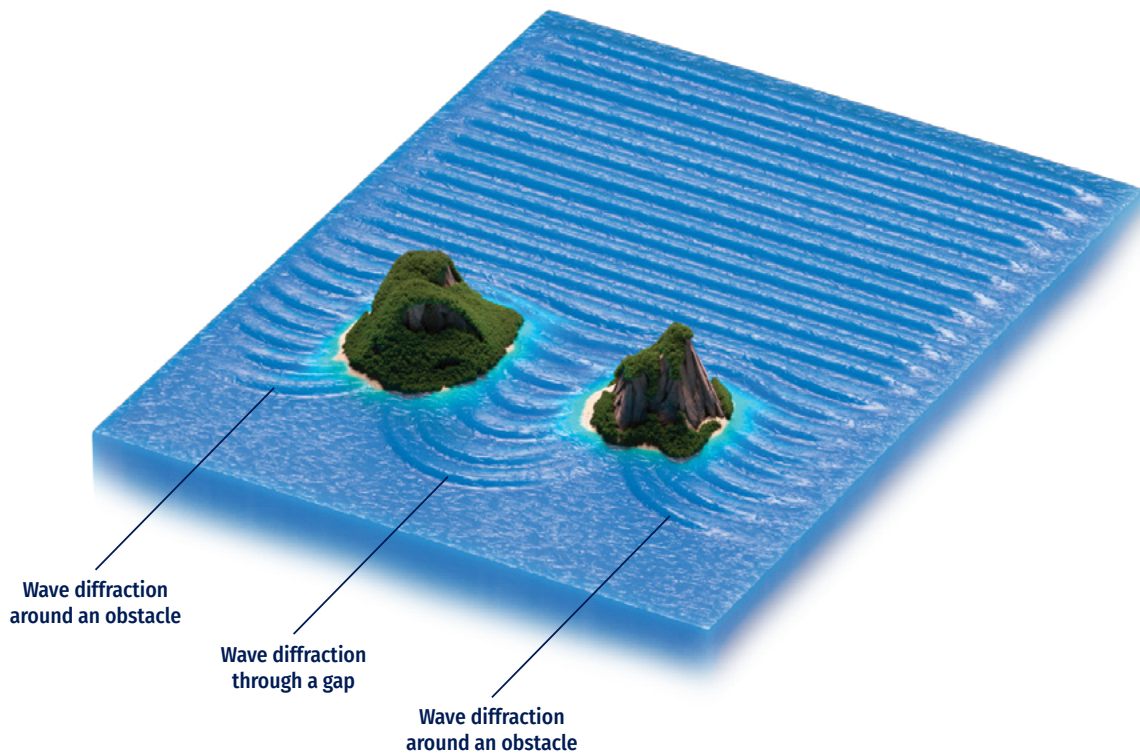
Figure 8.12.   Ocean wave diffraction behind semi-infinite obstacles.

8.1.4.3. Diffraction

When ocean waves reach and interact with any structure (natural or artificial, totally or partially emerged), wave diffraction occurs, which is described as the blocking and spreading of energy laterally perpendicular to the dominant direction of wave propagation. The result is that wave fronts, angles, and energy spreads behind (so-called lee side) the obstacle and wave heights appear lower in sheltered areas (Figure 8.12). Also, wave fronts rearrange into more structured and radial/focused wave propagation patterns.

The circular pattern adopted by diffracted wave crests, as they penetrate in the lee side of obstacles, diminishes rapidly as waves are diffracted further behind the obstacles. This behaviour could be relevant for any OOFS near bays, harbours, islands, and peninsulas areas.

Diffracted waves are also still affected with both refraction and shoaling effects, especially for large sheltered zones with relevant bathymetric changes. Also, semi-diffraction effects can occur for those semi-submerged structures (break-

waters and/or steep bathymetric bodies) with a clear refraction-diffraction combined effect.

Analytical solution for diffracted waves can be handled through a diffraction coefficient for an idealised constant bathymetry and semi-infinite emerged bodies (CERC, 1984), ignoring wave reflection effects, and using instead graphical diagrams as a function of the wavelength, the angle of incidence between the emerged body and the distance between the head of the breakwater and the point of calculation (Koutitas, 1990). For more realistic configuration, numerical approaches (phase averaging or resolving strategies) should be invoked.

8.1.4.4. Wave current interaction

Ocean waves are also affected by currents (tides, storm surges, river discharges, ambient currents, etc.). Changes in the amplitude, frequency, and direction of the incident waves are expected (Dean and Dalrymple, 1991).

Current-derived local shoaling might occur if waves get blocked by a current. Also, current-induced refraction can induce chang-
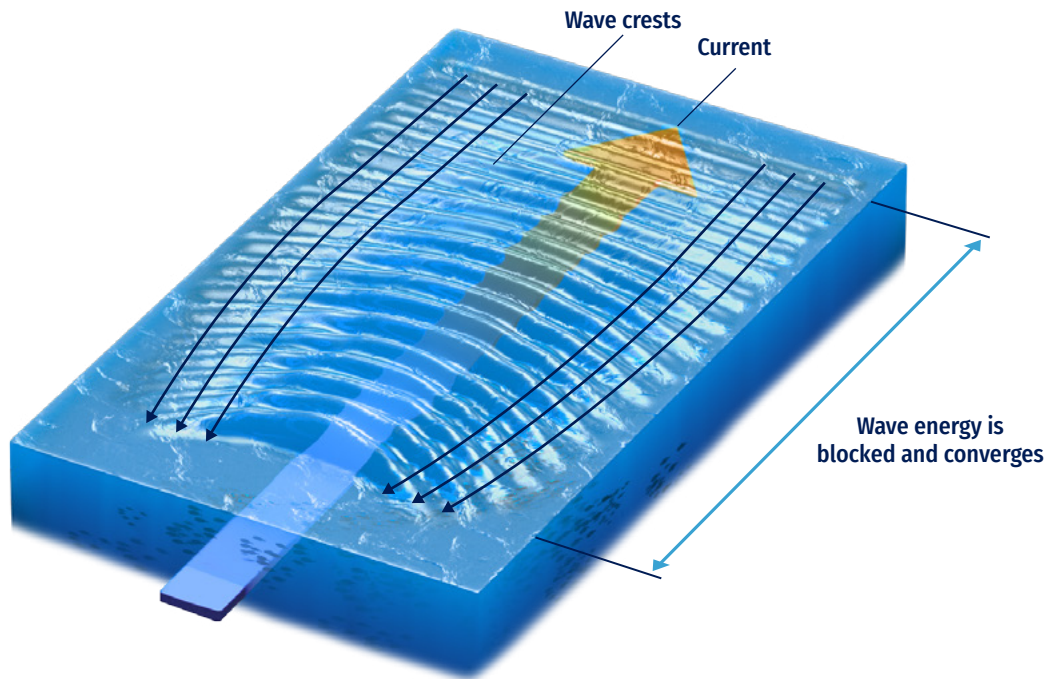
Figure 8.13.   Example of wave-current interaction.

es in the direction of speed/wave propagation, as well as energy exchange between the current and the wave can be present at coastal/mouth of the river zones and in some harbour entrances affected by littoral currents (Figure 8.13).

Linear theory is still valid and dispersion equation can be adapted to take into account currents (vertical integrated depth) as follows:

$$\omega = \sigma + kU_n \tag{8.8}$$

where U_n is the component of the current in the wave direction.

8.1.4.5. Dissipation (breaking and bottom friction)

Wave breaking is maybe one of the most energy-dissipating phenomena that waves can experience. It occurs when a shoaling/growing wave propagates over a limited depth profile, reaching its own water volume stability. As waves propagate towards shallow water, they become steeper until a stability-limit when they break, generating a complex mechanism related to fluid turbulence and vorticity.

Depending on water wave incoming characteristics such as frequency, direction, and height, and the bathymetric char-

acteristics (slope), different types of wave breaking are expected to occur. A parameter called the Iribarren number (also known as surf similarity parameter) can be employed for these classifications (see Figure 8.14), defined as a function of the bottom gradient and wave steepness as:

$$\xi = \frac{\tan \alpha}{\sqrt{\frac{H}{L_0}}} \tag{8.9}$$

where α is the bottom slope, H is the incident wave height and L_0 is the deep-water wavelength.

A simple way to estimate breaking limit depth is based on the breaking height equal to a fraction of the water depth, as established by McCowan (1984):

$$H_b = k \cdot h_b \tag{8.10}$$

where *k=0.78.*

For coastal wave climate or forecast applications, realistic characterization of wave breaking could be one of the most challenging issues and should be handled numerically when dealing with prediction of structure damaged by waves inside the surf zone of the breaker line at beach profile.

Spilling

Spilling breaking which spans within the whole surf zone for mild-slope beaches.

Plunging

Plunging breaking what waves curls forward and impinges formatting a partial tube.

Collapsing

Collapsing breaking and it comprises of a combination of plunging and surging breaking (Dean & Dalrymple, 1991).

Surging

Surging breaking for very steep beaches forming a very narrow or even non-existing surf line or zone. Wave reflection in this case is relevant.

Figure 8.14.   Wave breaking type based on Iribarren number.

Additionally, wave dissipation due to bottom friction can be relevant when waves propagate into shallow water. Friction between the bottom and the orbital motion of water wave particles dissipates wave energy; it depends on both the orbital velocity and the roughness of the bottom.

8.1.4.6. Wave-structure interaction

As wave fronts reach any coastal obstacle, part of the total-incident wave energy travels back into the open sea, basin, or sheltered area (Figure 8.15). Some of the original wave energy is reflected and some is dissipated. The amount of energy is reflected (stated as reflection coefficient or K_f) depending on both the vertical structure typology (natural cliffs, beaches, artificial breakwaters, quays, etc.) and the incident wave characteristics (mainly due to wave frequency).

An idealised vertical structure can reflect a 100% of the incoming wave energy ($K_R=1$) but in real imperfect coastal perimeters this value is commonly below ($K_f<1$), due to the combination of complex physical processes (e.g. wave break-ing, friction, percolation, run-up, etc.) that occur in the structure-water interface.

For shallow water zones adjacent to coastal structures, it is important to include wave reflection in the list of relevant wave transformation processes, especially for those wave climate or forecast systems that needs a good characterization for both incident and reflected waves at the study zone (i.e. propagation of collateral reflection effects from far areas such harbours, cliffs, reefs, jetties, harbour agitation, etc.).

The mathematical description of wave reflection deals with the calculation of wave motion as a linear sum of the incident wave and the (partially) reflected wave, as a transient or standing wave effect (for a constant deep domain and 1D approach). This can be complex for real bathymetry and coastal perimeter configuration, when irregular wave trains interact with different structures and coastal typologies and, in this case, an ad-hoc numerical approach should be used.

Partial wave reflection can also be relevant for semi-submerged structures and/or steep bathymetric changes (e.g. dredged navigation channels), as it interacts with wave shoaling, diffraction, and refraction effects. For example, harbour agitation phenomena deal with a complex computation of diffracted and partially reflected wave patterns.

Along with wave reflection effect and wave breaking on coasts and rubble-mound structures, waves' energy and frequencies can overtop these elements, tide instants, and each particular structure's typologies and characteristics.

Within wave climate or forecast systems, for a detailed definition of wave effects interaction with coastal structures (natural or artificial) could be important: i) wave run-up height, defined as (Ru2%) the wave level, measured vertically from the still water line which is exceeded by 2% of the number of incident waves; and ii) wave overtopping discharge (Figure 8.16), defined as the average water discharge per linear metre of width of the structure.

In recent times, forecast systems dealing with wave overtopping along a pedestrian coastal zone are delivered worldwide. The precision of these early-alert systems depends on a good reproduction of both incoming water waves and the geometry of the structure (freeboard, crest width, roughness, slope, permeability, and porosity). In order to calculate these derived variables, EurOtop Manual (Van der Meer et al., 2016) gathered some empirical formulae
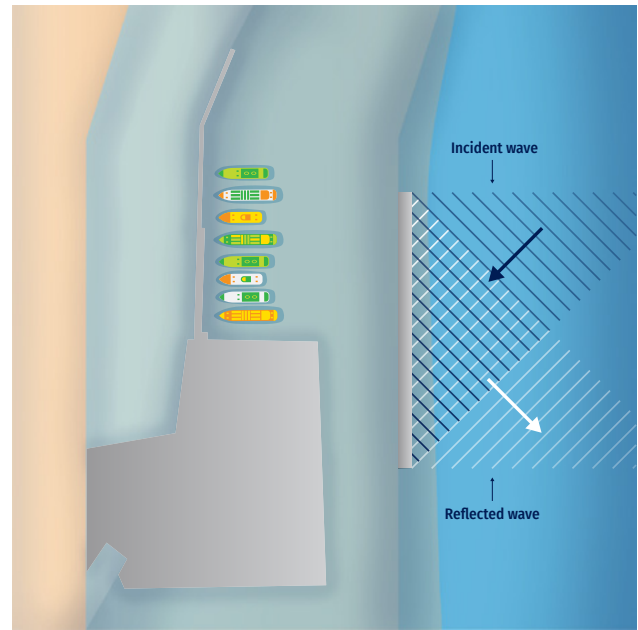
Figure 8.15.   Ocean wave reflection.

to easily obtain them. Also, some advanced numerical models (based on Computational Fluid Dynamics) are available to obtain, with a very good approximation, overtopping values and discharge volumes (Losada et al., 2008).
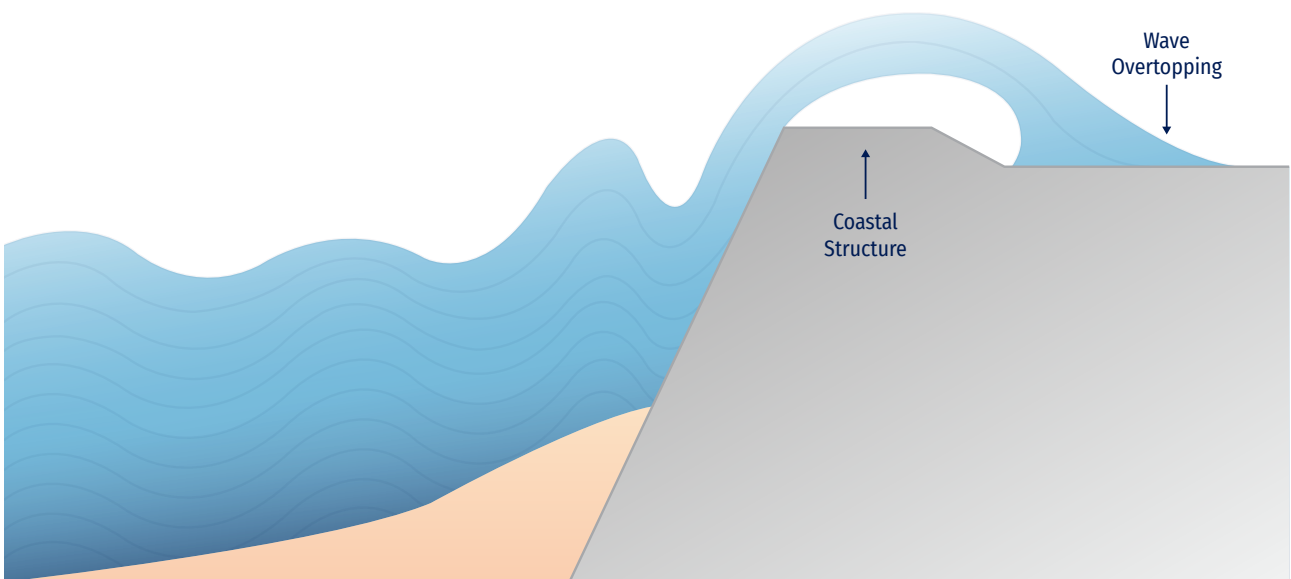
Figure 8.16.   Wave overtopping on a coastal perimeter example.

8.2.
Wave forecast and multi-year systems

Wave forecasting consists in describing the evolution of waves under the action of wind on the ocean surface and their propagation following interactions with currents, ice, and obstacles. Wave models numerically solve the variation of the wave spectrum from the energy balance equation taking into account the energy gain and loss terms. The evolution of wave models has followed improvements in the key processes of wind-wave growth, swell dissipation, and nonlinear wave interactions. Experimental works (Mitsuyasu, 1970; Hasselmann et al., 1973) have highlighted the importance of nonlinear wave interactions and wind-wave growth.

This has led to the improvement of wave models with, for example, a better simulation of the overshoot phenomenon which describes the transition of wave energy from high to low frequencies. Wave models must consider the computation time to ensure an operational forecast in near-real time conditions. So far, non-linear wave interactions have been simulated in the models in an approximate way, which sometimes generate errors.

Wave prediction is primarily a short-term process to ensure the safety of people, property, and maintenance of operation-

Level of Complexity

1	2	3
Spectral ocean wave variables	Shoaling	Thresholds
Statistical ocean wave variables	Refraction	Downtime
Spectral wave shapes	Diffraction	Functionality
Extreme waves	Reflection	Safety
Free surface series	Breaking	Management
Wake waves	Friction	Performance
Wind-wave effects	Run-up and overtopping	Performance (KPI)
Infragravity waves	6-DOF ship	Economics
Tsunamis	Mooring line stress	Social impacts
Meteo-tsunamis	Pressure over structures	Environmental impacts
Wave-current effects	Harbour agitation and resonance	
Directional wave attack	Structure stability	
	Erosion	
	Surf-beat	
	Navigation	
	Wave-structure interaction	

Figure 8.17. Variables included in ocean wave OOFS grouped in levels from 1 to 3 depending on their complexity and codependency.

al activities that require an accurate description of the sea state. In addition, wave forecasting is necessary for long-term analysis of the wave climate, to learn lessons from extreme wave events, and to upgrade and improve operational wave forecasting systems. These last actions are part of wave reanalysis or so-called multi-year products, of which the most known by users are ERA5, WAVERYS - Global Ocean Waves Reanalysis - and CFSR.

8.2.1. Architecture singularities

8.2.1.1. Levels of complexity from deep to shallow water

Every OOFS, designed to provide ocean wave-related products for both historical (multi-year) and future predictions, would require a modular architecture and a common approach methodology (see Chapter 4).

The main components of a forecasting system and of its architecture (Figure 4.1) can be considered valid for almost any OOFS architecture as they are based on three general steps:

a. Forcing and observations for data assimilation;
b. Numerical model:
c. Post-processing tools and final product information (including validation, monitoring, and dissemination).

These steps should be followed when wave OOFS is used for deep water. However, when the main process to be assessed within the OOFS are ocean waves in the coastal zone, the second step could be a major problem if not well conceptualised. The reason is that the type of numerical models to be used would not be able to obtain the results efficiently or fast enough, especially for those forecast systems that need a robust and recurrent architecture for a 24/7 output. In addition, numerical wave propagation in the coastal zone could turn rapidly into a high-CPU requirement problem, especially when singular wave physics should be solved, such as wave reflection, wave current interaction, wave overtopping over structures, etc.

Usually, wave OOFS at deep water only provides simple prediction of basic variables (called here level 1). In coastal zones, downscaling approaches were not able to obtain more complex solutions involving derived variables (called level 2 and 3), because they could not be based on direct/trivial solutions but needed complex numerical calculations, and the use of advanced tools with high requirement of CPU time. A general list of the variables to be considered for each level (from 1 to 3) of sophistication and complexity within a wave OOFS, is shown in Figure 8.17.

The variables included will define the main architecture of the OOFS in which, through a method, effects, physical behaviour, and final prediction are linked, but allowing the pos-

sible future exchange/substitution of variables and methods in a simple and direct way.

The general architecture of modern ocean wave OOFS needs to meet certain characteristics of quality, interoperability, operation, and reliability. These characteristics should prevent anomalies that can lead to serious operational drawback such as:

- Unrealistic results without any protocol of quality control, with solutions only found with a dynamic approach (real-time sea-state by sea-state numerical runs, as explained by Rusu et al., 2008);
- Limited tools due to daily availability of CPU time;
- No learning/(feedback);
- Limited in space, geometrically inert (non-evolutionary);
- Unknown uncertainties (no error control/ measure);
- No communication between modules, only based on a deterministic nature.

To overcome these possible shortcomings, it is then necessary to identify some architectural specificities, which are described below.

a. Efficiency and speed of predictions. The need of creating a sufficiently agile and efficient system that can provide results within the time window pre-established by the future use. Generally, this window is reduced to the very competitive time of around 1 hour, necessary to trigger all processes, obtain results, and publish them. Therefore, the general assembly method, based on a hybrid architecture combining clustering methods, should be invoked, especially for the high-CPU modelling for shallow waters.

b. Robustness (24/7). The workflow must be light and computationally ordered, to guarantee an adequate triggering of the processes and obtaining of results.

c. Modular design. This refers to the ability of the system to interchange methods and tools directly, without major modifications to the backbone architecture of the system (plug & play). This way of working requires an adequate standardisation of the intercommunication formats between modules (input and output, I/O), so that the connection of each part is compatible with the coding of the general system.

d. Reliable and realistic results. This is one of the most important characteristics for a wave OOFS as it refers to the reliability of the tool, the credibility of the general method adopted, and the satisfaction of the end user. For this purpose, there should be proposed methods for validating the tool and its results with information measured in-situ. A common practice in the development

of this method is to prepare a document with instructions on how to carry out field campaigns, indicating locations, variables to be measured and type of equipment to be used, recommended schedules, suggested post-processing algorithms, and final validation products. It is important to note that the measurements will reflect the logical evolution/growth of the study area in the operational system (modification of bathymetries, evolutionary shelter elements, etc.).

e. Ad-hoc mathematical and numerical tools. This is closely related to the idea of a modular system mentioned above, and it is based on the precise integration of those tools aiming at the solution of physical processes of special interest. It is achieved through the appropriate use and adaptation of wave propagation tools (e.g. CFD models, Non-Linear Shallow Water Equations, Boussinesq-type equations, Mild Slope equations, third-generation wave generation and propagation models, etc.).

f. Self-diagnosis of results. This feature is based on the use of statistical methods that allow a detailed diag-

nosis of the results provided by the system on a daily basis, to identify and quantify the errors and uncertainties that are triggered throughout the execution of the system. This concept, closely linked to the "cascade of uncertainty" theory (Wilby and Dessai, 2010), makes it possible to optimise each method and reduce errors and uncertainties.

g. Nowcast integration. This refers to the capacity of the wave OOFS to take advantage of in-situ measurements provided continuously and in parallel with the use of the system during its operational phase. Algorithms should be developed for accessing, reading, post-processing, and assimilating the information measured to compare it with the predictions provided by the system, with the final capacity to generate readjustments of certain control parameters and, thus, of the predictions. This self-learning capacity of the system guarantees that, in a few months, the system will reach a mature operational level.

h. Tailor-made results. This is the OOFS's capacity to correctly prepare the formats in which the results are pre-
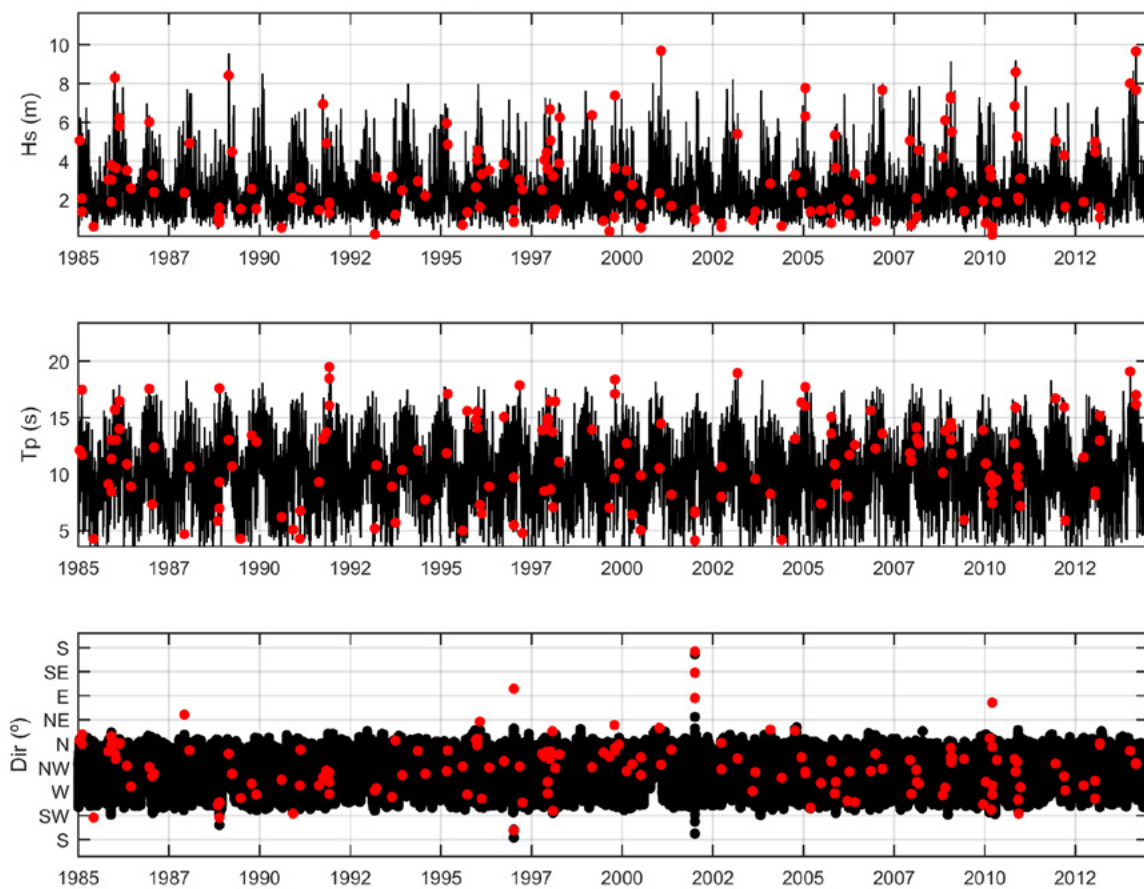
Figure 8.18. Wave climate clustering using Max-Diss algorithm (source: University of Cantabria).

sented (summary tables, email bulletins, and web pages) for the appropriate decision-making process, adapting the formats to the user needs and showing the general uncertainties in the predictions.

The architecture specificities proposed here are able to provide: i) a multi-year wave (hindcast) and b) an operational/ predictive product.

8.2.1.2. Hybrid and clustering technique

A hybrid approach has been recommended (Groeneweg et al., 2006, Stansby et al., 2006) when the complexity of the physics involved in the wave propagation assessment arises conditioning: i) the numerical model (CPU time) to be used; ii) the spatial resolution of the domains to be taken into account; and iii) the temporal relevance of new variables (such as variables above level 1) to be included in the final system/solution.

This approach allows a fast assessment of variables from level 2 to 3, regardless of the sophistication of the tool that performs it. This happens thanks to the concept of "pre-executed catalogue of cases" or clustering technique (also known as pre-cooked catalogue), which is responsible for assimilating the statistics of all the casuistry of processes involved, from the forcing involved to the final response.

The hybrid method, as described in various articles (Gaslikova and Weisse, 2006; Breivik et al., 2009, Herman et al. 2009), always follows the same steps:

- Access to the original forcing database (generally at deep water, sea-states, wind, and sea level series);

- Apply a self-selection algorithm of N pre-selected families of cases to be run, which will cover all the physics of the climate at the outer point (Figure 8.18);

- Transform level 1 variables to levels 2 and 3 through the execution of the N cases with the use of mainly mathematical/numerical tools;

- Statistically reconstruct the original database (Kalra et al., 2005; Browne et al., 2007) at the transfer point after having gone through the transformation processes, e.g. from the outer harbour zone to the quay area, making use of an algorithm that statistically interrelates the pre-run catalogue of N cases with the complete statistics of the forcing in the outer zone;

- Diagnose the data for historical diagnostic use.

8.3.
Input data, available sources, data handling, and model pre-processing

8.3.1. Bathymetry and geometry

Any global ocean wave OOFS needs accurate bathymetry data (see Section 4.2.4 for information about sources of bathymetric data). For systems downscaled towards the coastal/ harbour zone, it is recommended a detailed bathymetry with resolution grid between 5 and 20 m.

Some solutions and models developed along the ocean wave OOFS strategy also need a topography (DEM). Main beach topographies, artificial structure sections, and elevations are recommended, with resolution grid below 5 m. In addition, vertical datumreference should be known and used to integrate all the different bathymetric, sections, topography references, along with sea level time series.

8.3.2. Forcing fields

Deep-water wave OOFS commonly need the following forcing met-ocean variables:

- Wind maps;
- Pressure maps;
- Ice coverage maps.

Shallow water / coastal / downscaled wave OOFS commonly need the following forcing met-ocean variables (generally obtained from the previous deep-water module or other hindcast/forecast global providers):

- Wave spectra in the form of:

  - Integrated variables (Hm0, Tp, Dir);
  - N-modal integrated variables (i.e. 2 SWELL and 1 SEA);
  - Wave spectral real forms if available;

- Sea level time series (both meteorological and astronomical tides);
- Mid to high-resolution wind maps;
- Free-surface elevation time series.

8.3.3. Observations

Observations are used as the main source for validation and calibration. The following observations are required.

For deep-water approach:

- Satellite observations of Hm0, Tp and Dir;
- Directional wave spectra definition (buoy).

For shallow-water approach:

- Directional wave spectra definition (buoy);
- Pressure gauge time series (burst with more than 20 minute length);
- Non-directional wave buoy;
- Wave overtopping measurements if available (non-intrusive camera deployment).

8.3.4. Pre-processing and definition of the numerical problem

Modern ocean wave OOFS uses a numerical model strategy to simulate the generation and propagation of the main phenomena in ocean (deep water) and coastal regions (shallow water). These numerical codes commonly contain three main elements: i) pre-process; ii) mathematical solver; and iii) post-process.

The first step takes place before the model execution and it is included in the pre-processing stage. Within this stage, the following sub-parts should be accomplished:

- Definition of the computational domain geometry where the equations will be applied and solved. This area is commonly discretized as cells, control volumes, or elements (depending on the solver-type), and all of them conform to a grid domain.

- Integration and adaptation of bathymetry data with the generated mesh (this is relevant for an adequate physical representation of the variables and for the stability of the model).

In general, accuracy increases with a greater number of cells but a longer computational time will be required. The choice will depend on the computer power available, on the type of architectural scope, and on the method to be used (for example, a hybrid approach could help to minimise the CPU time required). In general, the balance CPU-cost / physical definition can be tackled with the use of non-uniform meshes that have their nodes in the regions of special interest or where high variations of the physics properties take place.

Recently developed numerical wave models have incorporated self-adaptive meshes. That means that the mesh automatically adjusts its resolution (according to some tolerance criteria / physical mesh design defined by the user).

8.3.5. Boundary and initial conditions

Boundary conditions are the forcing values on the perimeters of the computational domain needed by any wave numerical model. In some cases, in the vicinity of any other body or another model incorporated in the domain.

Initial conditions are commonly the values of water waves that define a sea-state simulation (commonly with 1-hour frequency rate data for regional OOFS).

The following recommendations should be considered:

- Select an input forcing of the model (boundary conditions), adapt the formats, and assimilate the input data to a form that can be used later by the solver equations (data normalisation stage). Note to establish correct sea levels and DATUM elevations.

- Define any symmetry and cyclic boundary conditions at the perimeter boundaries.

- Define any open boundary conditions that are used to freely radiate water waves through infinite.

- For wave reflection models, define each individual reflection coefficient to be taken into account.

8.4.

Modelling component: general wave generation and propagation models

8.4.1. Types of models

Ocean wave modelling efforts and applications can be broadly classified into two large groups: i) phase resolving (or direct) models; and ii) phase average (usually spectral) models. Direct models can explicitly simulate basic equations of fluid mechanics for the water, air, or even two-phase media, and therefore extend the analytical research beyond its traditional range of approximate and asymptotic solutions of such equations. At oceanic scales, however, such models are not practical and not feasible, and therefore spectral models are employed for wind-wave forecasts.

In the next subsections, for both deep and shallow water analysis is given a general description, mathematical model, limitations, and main applications for each type of model.

8.4.1.1. Deep water

Spectral models

Evolution of wind-generated waves in water of finite depth d can be described by the wave action $N=F/\omega$ balance equation:

$$\frac{\partial N}{\partial t} + \cdot[(\mathbf{c}_g + \mathbf{U})N] + \nabla_{\mathbf{k}} \cdot [\mathbf{c_k}N] = \frac{I + L + D + B}{\omega} \quad (8.11)$$

where $F(\omega,\mathbf{k})$ is the wave energy density spectrum, ω is intrinsic (from the frame of reference relative to any local current) radian frequency, $\mathbf{k}$ is wavenumber (bold symbols signify vector properties). In the linear case, temporal and spatial scales of the waves are linked through the dispersion relationship (see Eq. 8.2).

The left-hand side of Eq. 8.11 represents time/space evolution of the wave action density because of the energy source terms on the right. On the left, $\mathbf{c}_g$ is group velocity, $\mathbf{c}_k$ means the spectral advection velocity, $\mathbf{U}$ is the current speed, and we note that $c=\omega/_k$ is phase speed of the waves. ∇ here is the horizontal divergence operator, and ∇_k is such an operator in spectral space.

On the right, source terms are physically represented by wind energy input from the wind, I; nonlinear interactions of various orders within the wave spectrum, L, whose role

is to redistribute the energy within the spectrum; dissipation energy sinks, D; wave-bottom interaction processes, B; and more sources are possible in specific circumstances. Note that all the source terms, as well as the group and advection velocities, and the advection current are spectra themselves. Please refer to Cavaleri et al. (2007) for further details.

Among the source functions, L is a conservative term, i.e. its integral is zero, but the other integrals define energy fluxes in and out the wave system:

$$E_I = \int I(\omega, \mathbf{k})d\omega d\mathbf{k} \quad (8.12)$$

is the total flux of energy from the wind to the waves. Note that, depending on the relative speed of wind $\mathbf{U}_{10}$ and wave speeds $\mathbf{c}(\omega,\mathbf{k})=\omega/\mathbf{k}$, contributions to the total flux can be both positive (from the wind to the waves if $U_{10}>c$) and negative (from the waves to the wind if $U_{10}<c$). In the tropics, for example, where the wave climate is dominated by swells produced at high latitudes, the local winds are typically light and therefore the wind climate can be actually dominated by wave-induced winds (Hanley et al., 2010).

It should be noted that the energy input to the waves is generally accepted as a purely atmospheric exchange. In principle, however, energy input from the ocean side to the surface waves of scales accommodated in Eq. 8.11 is perceivable. For example, upper-ocean currents, tides, or internal waves can provide such dynamics. Given the amount of energy stored in the ocean movements, this could have large impacts on surface wave fields, even if localised, but it is fair to say that it has not been considered by the wave-ocean modelling community in practical terms.

Integrating the momentum-input spectrum gives the total momentum flux:

$$\tau_w = \int \frac{I(\omega, \mathbf{k})}{c(\omega, \mathbf{k})}d\omega d\mathbf{k} = \int I(\omega, \mathbf{k})\frac{\mathbf{k}}{\omega}d\omega d\mathbf{k} \quad (8.13)$$

which is an important measure of wind-wave interactions (Tsagareli et al., 2010). Together with the tangential viscous stress τ_v it forms the total wind stress at the ocean surface

$$\tau = \tau_w + \tau_v \quad (8.14)$$

and this stress is known independently (usually through empirical parameterisations of the so-called drag coefficient) and thus can be used as a constraint or for validation of the wind input term I. On the other hand, the total stress is often the main, if not the only property which expresses dynamic exchanges in large-scale air-sea models. Apart from situations of light winds, the wave-induced form drag (Eq. 8.12) provides a dominant contribution to this total stress (Kudryavtsev et al., 2001) and thus, if the wave-model physics is well defined and validated, such models can provide explicit rather than empirical estimates of fluxes for general circulation models if those are appropriately coupled with wave models.

The dissipation function D has a similar meaning in the context of wave-ocean dynamic exchanges, but with some essential distinctions. First, the integral

$$E_D = \int D(\omega, \mathbf{k}) d\omega d\mathbf{k} \qquad (8.15)$$

is the total flux of energy out of the wave field. The energy passed to the ocean is largely spent on generating turbulence near the surface and on work against buoyancy forces acting on bubbles injected during the wave breaking.

Unlike the input, however, which only occurs on the air side of the interface, the loss (8.15) can go both to the ocean below and to the atmosphere above the ocean surface. Numerical simulations of Iafrati et al. (2013) showed that up to 80% of wave energy due to breaking can be actually dissipated through the atmospheric turbulence.

The momentum-loss integral of dissipation function gives the so-called radiation stress:

$$\tau_r = \int D(\omega, \mathbf{k}) \frac{\mathbf{k}}{\omega} d\omega d\mathbf{k} \qquad (8.16)$$

which is presumed to be going to the currents (although some of it may in fact be going back to the wind, or to the bottom in shallow areas). In the present wave models, radiation stress is parameterized in terms of wave-height difference along the propagation direction. Obviously, such parameterization does describe the energy dissipation, and can then be used to estimate the momentum loss, but only in the areas where dissipation (Eq. 8.14) is much larger than the energy input (Eq. 8.14), i.e. usually in shallow waters. In deep water, the mean wave height is not a proxy for the energy loss. In fact, it may grow under wind action or not change if this action is balanced by the whitecapping dissipation, but the integral (Eq. 8.16) and hence the radiation stress is not zero.

Wave-ocean-bottom interactions in infinite depths, depicted by term B in Eq. 8.11, are very rich. Finite depths are characterised by the condition of $\mathbf{k}d{\sim}1$ (wavelength is comparable with the water depth d), and shallow non-dispersive environments by $\mathbf{k}d{<<}1$. Dispersive-wave nonlinear dynamics slowdown in finite and shallow depths, weaken or cease, but other nonlinear behaviours come into existence.

Wave exchanges with the bottom include bottom friction, formation of ripples, sediment suspension and transport if the sea bed is sandy, generation of bottom waves if the bottom is muddy, and percolation. Long-shore, cross-shore, and rip currents result from radiation stresses (Eq. 8.15), infragravity waves are produced by combined action of wave breaking and nonlinear wave groups, which can be subsequently reflected back to the deep ocean or trapped by coastal bays.

An example of this deep-water approach is the WAM (Hasselmann et al., 1988), perhaps the first one proposed as third-generation model, able to explicitly represent all the physics relevant for the development of the sea state in two dimensions, such as wind generation, whitecapping, quadruplet wave-wave interactions, and bottom dissipation. This modes is mainly forced by a two-dimensional ocean wave spectrum that develops freely with no constraints on the spectral shape, so that: a) a transfer source function of the same degree of freedom as the spectrum itself need to be developed; and b) the energy balance had to be closed by defining the dissipation source function. Hasselmann et al., (1985) and Komen et al., (1984) were employed to deal with these aspects, respectively. The dissipation was selected in order to replicate the observed fetch-limited wave growth and the fully developed Pierson-Moskowitz spectrum (WAMDI group, 1988).

Constant improvements and updates have led to a third-generation WAM model. A third-generation wave model explicitly represents all the physics relevant to the development of the sea state in two dimensions. Numerical solutions of the momentum balance of air flow over growing surface gravity waves have been presented in a series of studies by Janssen et al. (1989), and Janssen (1991). The main conclusion was that the growth rate of the waves generated by wind depends on the ratio of friction velocity and phase speed and on several additional factors, such as the atmospheric density stratification, wind gustiness, and wave age. This work has also introduced the surface stress dependency with the sea state, and the feedback of wave-induced stress on the wind profile in the atmospheric boundary layer.

WAM is an Eulerian phase-averaged model. Designed as a deep-water model, it can be used to predict directional spectra and wave properties (significant wave height, mean wave direction and frequency, swell wave height). The model can be used in finite depth as well by introducing bottom dissipation source function and refraction. The model runs on a spherical latitude-longitude grid.

The first WAVEWATCH model was developed at TU Delft (Tolman, 1989; Tolman 2014), followed by the NASA Goddard

Space Flight Centre in 1992. Recently, WAVEWATCH III was presented as a worldwide used and full-spectral third-generation wind-wave model. It was developed at NOAA/NCEP and it is based on the first WAM model's principles. This latest version includes many improvements in the governing equations, model structure, numerical schemes, and physical parameterizations. The model solves the random phase spectral action density balance equation for wavenumber-direction spectra. The medium properties, namely the water depth and current properties, as well as the wave field, vary in time and space in scales much larger than a single wave. WAVEWATCH is an open-source model that is freely available[3], including the whole source code and all documentation.

The discretization of the wave energy spectra in all directions is achieved by using a constant directional increment and a spatially varying wavenumber grid, which corresponds to an invariant logarithmic intrinsic frequency. In order to achieve high accuracy, both first order and third order schemes are available for wave propagation. For the integration of source terms in time, a semi-implicit scheme is used similar to that used in WAM, which includes a dynamically adjusted time stepping algorithm.

Following the work of Battjes and Janssen (1978), WAM and WAVEWATCH III models have been upgraded to account for the dissipation by wave breaking induced by depth in the surf zone. However, wave models still have difficulties with strong three-wave interactions that occur in finite-depth and shallow waters. That has led to simplified empirical calculations with large errors, especially for complex wave trains with multi-model spectra. In addition, both models lack of diffraction processes, which implies that only open coastal zones could be solved accurately, plus only linear behaviour of wave propagation could be assessed and non-linear corrections to linear wave should be imposed, by triad and quadruplet wave-wave interactions in shallow waters, where the waves break (Booij et al., 1999).

8.4.1.2. Shallow water

Spectral models

For shallow water domains and wave propagation (Eckart, 1952), the SWAN model could be a good choice. This also is a third-generation wave model developed at the Delft University of Technology, with the purpose of obtaining realistic estimates of wave parameters in coastal areas, lakes, and estuaries from given wind, bottom, and current conditions. The SWAN model can be also used on any scale relevant for wind-generated surface gravity waves. The model equations are based on the wave action balance equation with sources and sinks.

3. https://polar.ncep.noaa.gov/waves/wavewatch/wavewatch.shtml

SWAN has been developed to simulate coastal wave conditions (with friction, breaking, whitecapping, triad, and quadruplet wave-wave interaction). SWAN can be also coupled with previous models such as WAM or WAVEWATCH III, and inherit the boundary conditions. SWAN can provide a computational representation of directional and no directional spectrum at one point, and several spectral and time-dependent parameters of waves, such as significant wave height, peak or mean period, direction, and direction of energy transport. SWAN is a freely available[4] open-source software.

SWAN model is based on the spectral action balance equation, which describes the evolution of the wave spectrum (Booij et al., 1999).

In Cartesian coordinates the evolution of the action density is governed by the following balance equation:

$$\frac{\partial N}{\partial t} + \frac{\partial (C_x N)}{\partial x} + \frac{\partial (C_y N)}{\partial y} + \frac{\partial (C_\theta N)}{\partial \theta} + \frac{\partial (C_\sigma N)}{\partial \sigma} = \frac{S_{total}(x, y, t, \theta, \sigma)}{\sigma} \quad (8.17)$$

where σ is the wave frequency, θ is the wave direction component, t is the time, x and y the 2D coordinates in space, N the wave action density spectrum defined as:

$$N(x, y, t, \theta, \sigma) = \frac{E(x, y, t, \theta, \sigma)}{\sigma} \quad (8.18)$$

where E is the wave energy density spectrum; S_{total} is the source term and C,S are the wave propagation velocities in space and wavenumber, given by:

$$C_x = C_g \cos \theta + U_x \quad (8.19)$$

$$C_y = C_g \sin \theta + U_y \quad (8.20)$$

$$C_\sigma = -\frac{\partial \sigma}{\partial h} \frac{\partial h}{\partial s} - K \frac{\partial U}{\partial s} \quad (8.21)$$

$$C_\theta = -\frac{\partial \sigma}{\partial h} \frac{\partial h}{\partial m} - K \frac{\partial U}{\partial m} \quad (8.22)$$

where k is the wavenumber, C_g is the group velocity; s is a coordinate in θ direction and m is a coordinate perpendicular to s; h is the mean water depth and K the wavenumber vector.

The left hand side of Eq. 8.16 corresponds to the kinematic terms, as derivatives for the propagation in space; and are the propagation velocities. The term with the derivative with respect to θ is the refraction term. The term with respect to σ causes a change of frequency. The right hand side is the

4. https://swanmodel.sourceforge.io/
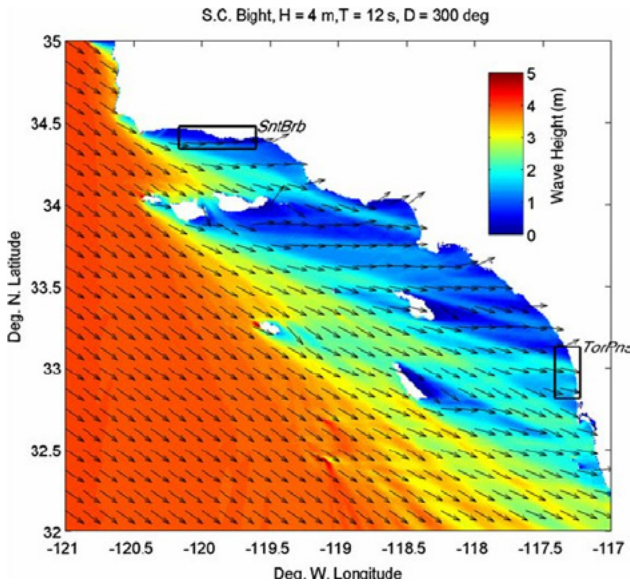
Figure 8.19. Example wave height and direction output from SWAN wave transformation model over the Southern California Bight (source: University of Florida).

source term and contains the effects of wind generation, whitecapping, dissipation, bottom friction, surf breaking, and nonlinear wave-wave interaction. This equation is implemented with finite difference schemes in all directions: time, geographic space, and spectral space.

The essential input data to run the model is the bathymetry for a sufficiently large area, the incident wave field, and the wind field. Various general and nested grids can be selected, depending on the availability of high-resolution data and the computational efficiency. Nesting is a very important implementation that can save computational time and increase accuracy. The model is validated with analytical solutions, field observations and experimental measurements, and has shown good agreement (Booij et al., 1999). Moreover, SWAN can operate with unstructured grids as well. Zijlema (2009) presented a method of vertex-based, fully implicit, and finite differences that is designed for unstructured meshes with high variability in geographic resolution. It is useful for complex bottom topographies in shallow areas and irregular shorelines.

SWAN is basically designed for applications in open coastal scale, with no-diffraction effects. That means that the model should be used in areas where variations in wave height are large within a horizontal scale of a few wavelengths.

SWAN organises its output in tables, maps (Figures 8.19 and 8.20) and time series, as well as 1D and 2D spectra, significant wave height and periods, average wave direction and directional spreading, one- and two-dimensional spectral

source terms, root-mean-square of the orbital near-bottom motion, dissipation, wave induced force (based on the radiation-stress gradients), set-up, diffraction parameter, etc.

Mild slope equations models

MSE originally developed to describe the propagation of the waves over low gradient seabeds. MSE is commonly used in coastal engineering, since it can account well the effects of simultaneous diffraction and refraction of the waves due to coastlines or structures (Berkhoff, 1972). Mild-slope equations are a type of depth-averaged equation, within a x-y domain (2DH), applied in both deep and shallow waters for monochromatic waves (Lin, 2008).

The equations can be found in various forms, including the effects of wave breaking, nonlinearity of waves, wave-current interactions, and seabed friction. They calculate the wave amplitude or wave height but, if there is a constant water depth, the mild-slope equation reduces to the Helmholtz equation for wave diffraction. First introduced by Berkhoff (1972), the MSE assumed that the wave is linear and the slope is mild, obtaining the following main equation, improved by including the effects of friction dissipation and wave breaking:

$$\nabla(CC_g\nabla\widehat{\eta}) + \left(\frac{C_g}{C}\sigma^2 + i\sigma w + iC_g\sigma\gamma\right)\widehat{\eta} = 0 \qquad (8.23)$$

where C is the wave celerity and C_g the group velocity; $\hat{\eta}$ is the complex wave surface function; k is the wavenumber; σ is the wave frequency; w is a friction factor and γ is a wave breaking parameter. Friction is then obtained with:

$$w = \left(\frac{2n\sigma}{k}\right)\left[\frac{2f_r}{3\pi}\frac{ak^2}{2kh + \sinh(2kh)\sinh(kh)}\right] \qquad (8.24)$$

where a is the wave amplitude, and f_r is a Reynolds dependent friction coefficient related to the bottom roughness; n is the Manning dissipation coefficient.

For weave breaking parameter, the following formulation is commonly used:

$$\gamma = \frac{0.15}{h}\left(1 - \frac{0.4^2 h^2}{4\sigma^2}\right) \qquad (8.25)$$

The original MSE has limitations because it is only applicable to linear waves and on mild bottom geometry. In addition, the equation does not contain energy dissipation, but in recent years there have been numerical advances to include energy dissipation and weakly non-linear waves with steeper bottom slopes. Mild-slope equation has been developed with different formulations that can be described by hyperbolic (Dingemans, 1997), elliptic (Berkhoff, 1972), and parabolic (Lin, 2008) formulation of the mild-slope equation respectively.

The practical application of wave transformation usually requires the simulation of directional random waves; thus, the

principle of superposition of different wave frequency components can be applied. In general, MSE models for spectral wave conditions require inputs of the incoming directional random sea at the offshore boundary. The two-dimensional input spectra are discretized into a finite number of frequency and direction wave components.

For the parabolic approach, the evolution of the amplitudes of all the wave components is computed simultaneously. Based on the calculations for all components and assuming a Rayleigh distribution, statistical quantities such as the significant wave height Hs can be calculated at every grid point. Figure 8.20 shows an example for a near-coast wave propagation obtained with a parabolic approximation of the mild slope equation for spectral wave conditions.
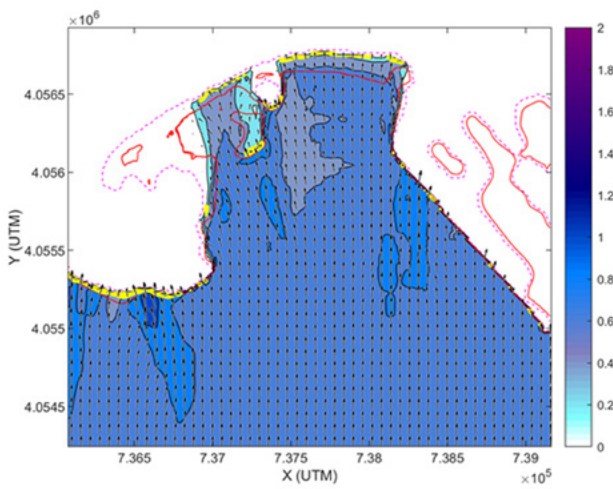
Figure 8.20.   Significant wave height propagation map for Los Galeones Beach (Cadiz, Spain) computed with a parabolic Mild-Slope based model (REF-DIFF, OLUCA model) (source: University of Cantabria).

When wave reflection becomes relevant for wave propagation and transformation (i.e. within bays, harbours, sheltered areas, etc.), models should be based on the elliptical approximation of the mild-slope equation (Berkhoff, 1972; Madsen and Larsen, 1987; Tsay et al., 1989). This approach allows engineers to obtain the energetic response of reflected (totally or partially) waves, under the penetrating wave action.

Elliptic mild slope models solve the extended mild-slope equation to reproduce the main processes that control dynamics of waves when approaching coastal areas and entering into harbours (Figure 8.21): geometric refraction, shoaling, diffraction by obstacles, and full or partial reflection. Radiation conditions and free infinite outflow conditions are also available in the model. It also considers the complete

spectral frequency distribution and the directional spreading of the wave energy spectrum.

In addition to the above mechanisms, nonlinear waves may be simulated by incorporating amplitude-dependent wave dispersion, which has been demonstrated to be important in certain situations (Kirby and Dalrymple, 1983).

This practical approach for harbour agitation and wave propagation can be assessed with the following, among others, commercial and non-commercial models: CGWAVE; ARTEMIS MIKE21; PHAROS, and MSP.
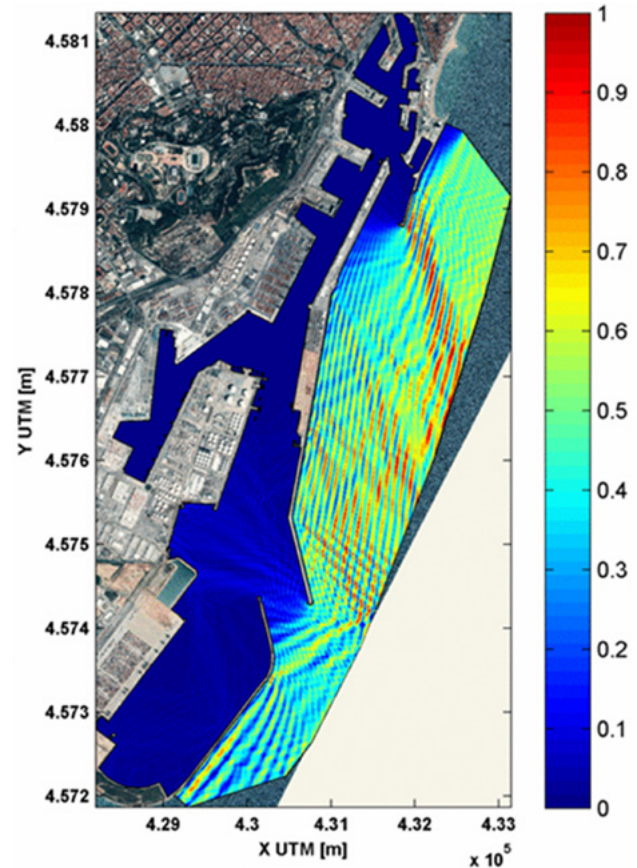
Figure 8.21.   Significant wave height map within Barcelona Port computed with an elliptic Mild-Slope based model (MSP model) (source: University of Cantabria and Puertos del Estado).

Phase resolving models (SWE, NSWE, and Boussinesq)

The Shallow Water Equations (SWE) are applied when water waves enter very shallow domains. Particles move basically horizontally and the vertical accelerations are negligible.

In this case, the propagation of the wave can be described by the SWE (Holthuijsen, 2007). These equations are derived from averaging the depth of the Navier-Stokes equations (NSE) assuming that the horizontal length scale is much greater than the vertical. The profile is uniform in depth and the vertical components very small. Using the conservation of mass, it can be shown that the vertical velocity is small, while using the momentum equation the vertical pressure gradients are hydrostatic. Therefore, the velocity profile is uniform in depth and the vertical components very small, and this is the reason for which SWE are also known as "long-wave equations", given that they can be applied only to waves which are much larger to the bottom depth.

In the case of ignoring the Coriolis force, the frictional and viscous forces, the formulas of SWE are:

$$\frac{\partial \eta}{\partial t} + \frac{\partial (\eta u)}{\partial x} + \frac{\partial (\eta v)}{\partial y} = 0 \tag{8.26}$$

$$\frac{\partial (\eta u)}{\partial t} + \frac{\partial}{\partial x}\left(\eta u^2 + \frac{1}{2}g\eta^2\right) + \frac{\partial (\eta uv)}{\partial y} = 0 \tag{8.27}$$

$$\frac{\partial (\eta v)}{\partial t} + \frac{\partial}{\partial y}\left(\eta v^2 + \frac{1}{2}g\eta^2\right) + \frac{\partial (\eta uv)}{\partial x} = 0 \tag{8.28}$$

Equation 8.26 is derived from mass conservation and Eqq. 8.27 and 8.28 from momentum conservation, where η is the total fluid column height, (u,v) - a 2D vector - is the fluid's horizontal velocity in the xy 2D domain.

To represent the ocean waves frequencies and physical behaviour, an improvement within the original SWE is needed, including the non-linearity terms and dispersive functions. The solution for this is the NSWE, as a non-hydrostatic wave-flow solution model. It can be used for predicting transformation of dispersive surface waves from offshore to the beach, solving the surf zone and swash zone dynamics, wave propagation and agitation in bays and harbours, and rapidly varied shallow water flows typically found in coastal flooding (e.g. dike breaks, tsunamis and flood waves, density driven flows in coastal waters), as well as large-scale ocean circulation, tides and storm surges (typically solved by the original SWE models).

Main governing equation considers a 2DH wave motion over a domain represented in a Cartesian coordinate system (x,y). The depth-averaged, non-hydrostatic, free-surface flow can be described by the NSWE and comprise the conservation of mass and momentum. These equations are given by:

$$\frac{\partial \zeta}{\partial t} + \frac{\partial (hu)}{\partial x} + \frac{\partial (hv)}{\partial y} = 0 \tag{8.29}$$

$$\frac{\partial u}{\partial t} + u\frac{\partial u}{\partial x} + v\frac{\partial u}{\partial y} + g\frac{\partial \zeta}{\partial x}$$
$$+ \frac{1}{h}\int_{-d}^{\zeta}\frac{\partial q}{\partial x}dz + C_f\frac{u\sqrt{u^2+v^2}}{h} \tag{8.30}$$
$$= \frac{1}{h}\left(\frac{\partial h\tau_{xx}}{\partial x} + \frac{\partial h\tau_{xy}}{\partial v}\right)$$

$$\frac{\partial v}{\partial t} + u\frac{\partial v}{\partial x} + v\frac{\partial v}{\partial y} + g\frac{\partial \zeta}{\partial y}$$
$$+ \frac{1}{h}\int_{-d}^{\zeta}\frac{\partial q}{\partial y}dz + C_f\frac{u\sqrt{u^2+v^2}}{h} \tag{8.31}$$
$$= \frac{1}{h}\left(\frac{\partial h\tau_{yx}}{\partial x} + \frac{\partial h\tau_{yy}}{\partial v}\right)$$

where t is the time; ζ is the free surface elevation, d is the water depth and $h=d+\zeta$, u and v are depth-averaged flow velocities, q is the non-hydrostatic pressure, g the gravitational acceleration, C_f the bottom friction coefficient, and the group of τ are the horizontal turbulent stress terms.

The SWASH (Zijlema et al., 2011) is one of the latest world-wide available 🔗5 NSWE models. It is a numerical tool for simulating unsteady, non-hydrostatic, free-surface, rotational flow, and transport phenomena in coastal waters as driven by waves, tides, buoyancy, and wind forces. It provides a general basis for describing wave transformations from deep water to the beach, port or harbour, as well as complex changes to
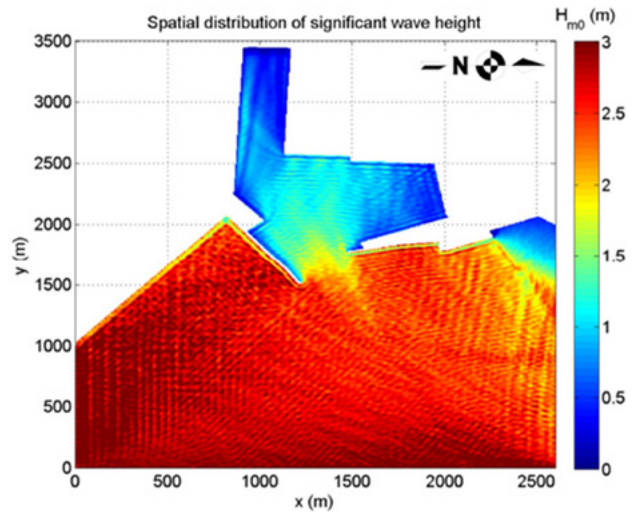
Figure 8.22. Results from the SWASH model for the wave condition at Limassol Port (Cyprus) (from Van der Ven et al., 2018).

rapidly varied flows, and density driven flows in coastal seas, estuaries, lakes, and rivers. SWASH is an efficient and robust model that allows the application of a wide range of time and space scales of surface waves and shallow water flows in complex environments (Figure 8.22). The model can be also

5. https://swash.sourceforge.io/

employed to resolve the dynamics of wave transformation, buoyancy flow, and turbulent exchange of momentum, salinity, heat, and suspended sediment in shallow seas, coastal waters, estuaries, reefs, rivers, and lakes.

SWASH may be run in depth-averaged mode or multi-layered mode in which the computational domain is divided into a fixed number of vertical terrain-following layers. SWASH improves its frequency dispersion by increasing the number of layers rather than increasing the order of derivatives of the dependent variables like Boussinesq-type wave models do.

BE can be applied as an alternative to NSWEs as the region between deep and shallow waters can be also well described by the Boussinesq model. In BE models, the horizontal component of the velocity is assumed to be constant in the water column and the vertical component of the velocity varies almost linearly over depth (2DH hypothesis). Essentially, these equations are the shallow-water equations with corrections for the vertical acceleration, and third order derivatives are the result of the Laplace equation forcing the vertical velocity of the velocity potential function to be expressed in terms of the horizontal velocity distribution. These equations can be readily expanded into two horizontal dimensions.

Researchers have introduced many different implementations of the Boussinesq equations, creating Boussinesq-type models to be applied for propagation in deep water and the process of wave-breaking (Brocchini, 2013). A vast majority of Boussinesq equations models (for fully non-linear approach) can be presented as follows:

$$\eta_t = -\nabla \cdot [(h + \epsilon\eta)(V + \mu^2 M] + O(\mu^4) \tag{8.32}$$

$$V_t + \frac{\epsilon}{2}\nabla(V^2) = -\nabla\eta - \mu^2\left[\frac{1}{2}z_\alpha^2\nabla\nabla \cdot V_t + z_\alpha\nabla\nabla \cdot (hV_t)\right]$$
$$+ \epsilon\mu^2\nabla(D_1 + \epsilon D_2 + \epsilon^2 D_3) + O(\mu^4) + N + E \tag{8.33}$$

with

$$M = \left[\frac{1}{2}z_\alpha^2 - \frac{1}{6}(h^2 - \epsilon h\eta + \epsilon^2\eta^2)\right]\nabla\nabla \cdot V$$
$$+ \left[z_\alpha + \frac{1}{2}(h - \epsilon\eta)\right]\nabla\nabla \cdot (hV) \tag{8.34}$$

$$D_1 = \eta\nabla \cdot (hV_t) - \frac{1}{2}z_\alpha^2 V \cdot \nabla\nabla V$$
$$- z_\alpha V \cdot \nabla\nabla \cdot (hV) - \frac{1}{2}(\nabla \cdot (hV))^2 \tag{8.35}$$

$$D_2 = \frac{1}{2}\eta^2\nabla \cdot V_t + \eta V \cdot \nabla\nabla \cdot (hV)$$
$$- \eta\nabla \cdot (hV)\nabla \cdot V \tag{8.36}$$

$$D_3 = \frac{1}{2}\eta^2[V \cdot \nabla\nabla \cdot V - (\nabla \cdot V)^2] \tag{8.37}$$

where index of t denotes time; h is the equilibrium depth; η is the free-surface elevation, V is the horizontal velocity, and ∇ is the 2DH gradient operator. N and E respectively represent bottom drag and diffusion (artificial).

On the other hand, a similar family of equations exist and are applied in the region between deep and shallow waters; the Boussinesq equation-based model. For this approach, the main hypothesis is that the horizontal component of the velocity is assumed to be constant in the water column, and the vertical component of the velocity varies almost linearly over depth.

One of the most complete Boussinesq models, the fully non-linear Boussinesq wave model (FUNWAVE) in its TVD version known as FUNWAVE-TVD model (Fengyan, et al., 2012), was developed at the Centre for Applied Coastal Research at the University of Delaware (USA). It includes several enhancements: i) a more complete set of fully nonlinear Boussinesq equations; ii) a MUSCLE-TVD finite volume scheme together with adaptive Runge Kutta time stepping; iii) shock-capturing wave breaking scheme, iv) wetting-drying moving boundary condition with HLL construction method for the scheme; and v) code parallelization using MPI method. The development

Figure 8.23. Free surface snapshot from the FUNWAVE-TVD applied in Sardinero Beach and Santander Bay (Spain) outer and inner zone (source: University of Cantabria).

of the FUNWAVE-TVD was prompted by the need to model tsunami waves in regional and coastal scale, coastal inundation, and wave propagation at basin scale (Figure 8.23). FUNWAVE is an open-source model available to the public 🔗 [6].

6. https://fengyanshi.github.io/build/html/index.html

Numerical solutions of Boussinesq equations can be significantly corrupted if truncation errors, arising from the differencing of the leading order wave equation terms, are allowed to grow in size and become comparable to the terms describing the weak dispersion effects. All errors involved in solving the underlying nonlinear SWE are reduced to 4th order in grid spacing and time step size. Due to non-linear interaction in the model, higher harmonic waves will be generated as the program runs. These super harmonic waves could have very short wavelengths and the classic Boussinesq model is not valid. For this reason, a numerical filter suggested by Shapiro (1970) can be used.

In summary, both Boussinesq and NSWEs modelling approaches are the preferred solutions in their respective physical regions: Boussinesq where nonlinearity and dispersion are both significant, typically prior to breaking; and NSWE where nonlinearity predominates, from the mid-surf to inner surf zone shoreward, although it should be noted that there can be a significant overlap of these regions. Therefore, the NSWE models, which work well from the surf zone shoreward and naturally model wave breaking and the moving shoreline, find their main weakness in the absence of frequency dispersion, so that in deeper water waves will propagate incorrectly at the shallow water wave speed and, sooner or later, break again, which is not usual and correct in this region.

Two- and three-dimensions wave structure interaction model

CFD utilises numerical approaches to examine fluid flows, heat transfer and chemical reactions. Therefore, within wave propagation and structure interaction problems, the CFD term mainly refers to computer codes that solve the fully nonlinear Navier-Stokes equations in all three dimensions (3D).

CFD is then a state-of-the-art techniques for industrial and research applications, although its often high computation cost demands the use of high-performance computers. Within the wave propagation and wave structure interaction field, two of the most used CFD programs are: IH2VOF (two-dimension approach, derived from COBRAS original model) and OpenFOAM (three-dimension approach); these two codes are also well validated for many marine and ocean engineering applications.

As a classic Eulerian approach, both models are based on the RANS equations. These equations represent the continuum properties of the flow. By averaging the Navier-Stokes equations, more recent VARANS equations are obtained. The VARANS equations can have different terms, depending on the assumptions applied; for example, they include a k-ω turbulence model closure within the porous media, which make them the most suitable formulation for coastal engineering as the advantages of VARANS equations are numerous. The solving process yields very detailed solutions, both in time and space. Pressure and velocity fields are obtained

cell-wise, even inside the porous zones, so that the whole three-dimensional flow structure is solved. Furthermore, non-linearity is inherent to the equations, and therefore all the complex interactions among the different processes are also taken into consideration. Finally, the effects of turbulence within the porous zones can be also easily incorporated with closure models.

IH2VOF model (Lara et al., 2006) solves 2D RANS equations for the oscillatory fluid and VARANS equations for the porous media. This 2D model can simulate the most relevant hydrodynamic near-field processes that take place in the interaction between waves and low-crested breakwaters. It considers wave reflection, transmission, overtopping, and breaking due to transient nonlinear waves, including turbulence in the fluid domain and in the permeable regions for any kind of geometry and number of layers. This model is highly validated, with different wave conditions and breakwater configurations, achieving a high degree of agreement with all the studied magnitudes, free surface displacement, pressure inside the porous structure, and velocity field.

IH2VOF is based on the decomposition of the instantaneous velocity and pressure fields into mean and turbulent components, the κ-ε equations for the turbulent kinetic energy κ, and its dissipation rate ε. This permits the simulation of any kind of coastal structure (e.g. rubble mound, vertical or mixed breakwaters). The free surface movement is tracked by the volume of fluid (VOF) method for one phase only, water and void. In order to replicate solid bodies immersed in the mesh instead of treating them as sawtooth shape, the model uses a cutting cell method. The main purpose of this technique is to use an orthogonal structured mesh in the simulations to save computational cost.

IH2VOF includes a complete set of wave generation boundary conditions, which cover most water depth ranges. These include a Dirichlet boundary condition and a moving boundary method, which are linked with an active wave absorption system to avoid an increase of the mean water level and the agitation. An internal source function can be also used to generate waves, but it has to be linked with a dissipation zone.

The RANS equations (clear fluid region) are redefined as follows:

$$\frac{\partial(\theta u_i)}{\partial x_i} = 0 \qquad (8.38)$$

$$\frac{\partial(\theta u_i)}{\partial t} + \theta u_j \frac{\partial(\theta u_i)}{\partial x_i} = -\frac{\theta}{\rho}\frac{\partial p}{\partial x_i} + \rho g_i + \frac{\theta}{\rho}\frac{\partial(\tau_{ij})}{\partial x_j} + f_b \quad (8.39)$$

Generally, IH2VOF application is within a detailed incident-wave and structure interaction (rubble-mound breakwaters, vertical structures and beaches), taking into account
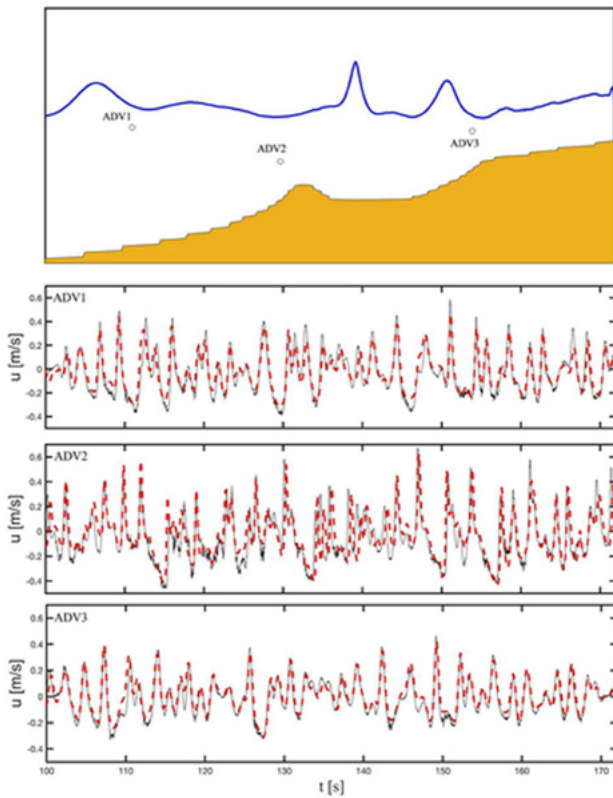
Figure 8.24. Irregular wave propagation towards a real profile beach. Free surface snapshot and wave velocity validation against field measurements (source: National University of Mexico).

a realistic wave breaking and porous media interaction (see Figure 8.24).

The general VARANS equations include conservation of mass (8.39), conservation of momentum (8.40), and the VOF function advection equation (8.41) as follows:

$$\frac{\partial}{\partial x_i}\frac{u_i}{n} = 0 \tag{8.40}$$

$$\frac{\partial}{\partial t}u_i + u_j\frac{\partial}{\partial X_i}\frac{u_i}{n} = -\frac{n}{\rho}\frac{\partial}{\partial x_i}p$$
$$+ ng_i + n\frac{\partial}{\partial x_i}\left(\nu\frac{\partial}{\partial x_i}\frac{u_i}{n}\right) - au_i - bu_i \mid u_i \mid -c\frac{\partial}{\partial t}u_i \tag{8.41}$$

$$\frac{\alpha_1}{\partial t} + \frac{\partial}{\partial x_i}\frac{u_i}{n}\alpha_1 = u_i \tag{8.42}$$

where u is the extended averaged Darcy velocity; n is the porosity (volume of voids over the total volume); ρ is the density; p is the pressure; g is the acceleration of gravity; ν is the kinematic viscosity, and α_1 is the VOF function indicator (quantity of water per unit of volume at each cell).

The OpenFOAM (Higuera et al., 2014a and 2014b) is an extensive software package that has been widely used in industrial and academic applications. It is freely distributed 🔗[7] as an open source CFD Toolbox, and it includes a broad range of features. IHFOAM 2.0 is an extension of the original software for coastal applications, newly developed with a three-dimensional numerical two-phase flow solver, specially designed to simulate coastal, offshore, and hydraulic engineering processes. It contains an advanced multiphysics model, widely used in the industry. A wide collection of boundary conditions, which handle wave generation and active absorption at the boundaries with a high practical application to coastal and harbour engineering (Figure 8.25), makes IHFOAM 2.0 different from the rest of solvers. Maza et
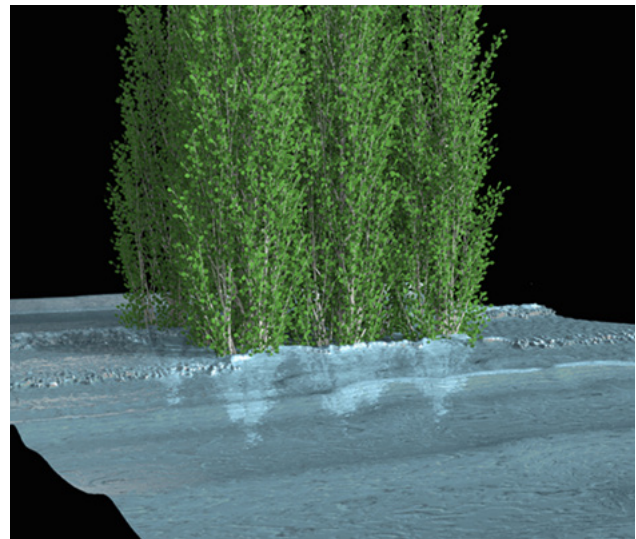
Figure 8.25. Free surface snapshot of irregular wave interacting with a natural-based protection (a tree patch) calculated with IHFOAM 2.0 (source: University of Cantabria).

al. (2016) have studied and proposed natural-based solutions for coastal protections using IHFOAM.

8.4.2. Discretization methods

Various discretization methods are used in water wave solving problems, a brief description for each of them is presented below (for additional references see Sections 5.4.2.4 and 7.2.3.5):

- FDM. Maybe the most used and simplest ways to solve numerically partial differential equations (PDEs). The method establishes the value of the flow variable at a given point based on the number of neighbour

7. https://www.openfoam.com/

Figure 8.26. Finite Element Metod (FEM) based on irregular sized triangles applied to Galicia (Spain) for SWAN model (source: University of Cantabria).

points. The numerical domain forms a grid. The governing equations of the fluid are considered in their differential form at each point in the domain, so that the solution is solved by replacing the partial derivatives with approximations by means of the nodal values of the functions. This method is recommended for structured grids and low-order equation schemes.

• FEM for the solution of PDEs employs variational methods to minimise the error of the approximated solution, similarly to the Galerkin method. FEM was used in structural mechanics but this technique developed for computational fluid dynamics applications being introduced to common wave propagation and agitations models. FEM technique, similarly to the FDM, is based on the concept of subdividing a continuum computational domain into elements, forming a grid of triangular or quadrilateral un-

structured elements or curved cells (Figure 8.26). Therefore, the method can handle problems with great geometric complexity, such as harbour perimeter definition, concentration of nodes at relevant parts of the domain, etc.

FEM used variational methods, which in practice means that the solution is assumed to have a prescribed form and to belong to a function space. The function space is built by varying functions, such as linear and quadratic. The varying functions connect the nodal points, which can be the vertices, mid-side points, mid-element points, etc., of the elements. As a result, the geometric representation of the domain plays a crucial role in the outcome of the numerical simulation. The original PDEs are not solved by the FEM. Instead, the solution is approximated locally by an integral form of the PDEs. The integral of the inner product of the residual and the weight functions are constructed. The integral is set to zero and trial functions are used to minimise the residual. The most general integral form is obtained from a weighted residual formulation. The process eliminates all the spatial derivatives from the PDEs and, therefore, differential type boundary conditions for transient problems and algebraic type boundary conditions for steady state problems can be considered, hence the differential equations become algebraic. Only one equation is solved per grid node, which has one variable as unknown. The same variable is also unknown at the neighbouring cells.

• FVM solves PDEs by transforming them to algebraic equations around a control volume (subdivisions of the computational domain). The variables are calculated at the centre of each control volume. General interpolation methods are used to derive the values of the variables at the surfaces of the control volume considering the neighbour control volumes as well. The FVM has two major advantages: i) it is able to accommodate any type of grid, making it applicable for domains of high complexity; and ii) it is conservative by definition, since the control volumes that share a boundary have the same surface integrals, describing the convective and diffusive fluxes. FVMs are very popular in the numerical wave propagation community, succeeding in free surface flow simulations, especially when highly nonlinear processes are involved, such as wave breaking.

8.5.
Data assimilation systems

In a wave forecasting system, data assimilation plays a key role in order to provide the best description of sea state, and also to correct uncertainties related to wind forcing from the atmospheric systems. Since the beginning of the 1990s, with the arrival of altimeter missions such the pioneer one Topex-Poseidon, the assimilation schemes have been implemented to use significant wave height in the WAM model (Janssen et al., 1989; Bauer et al., 1992; Lionello et al., 1992). Basically, the scheme uses an optimal interpolation through a weighted correction of the first SWH guess with that one from altimeters. The correlation model to spread the correction from altimeter SWH to other grid points is essentially a Gaussian function, depending on the distance between the observation and model locations, and a correlation length, which can vary with the wave regime (Greenslade and Young, 2004). The assimilation of SWH corrects the two-dimensional spectrum by introducing appropriate rescaling factors to the energy and frequency scales of the wind sea and swell components of the spectrum, and also updates the local forcing wind speed. The rescaling factors are computed for two classes of spectra: i) wind sea spectra, for which the rescaling factors are derived from fetch and duration growth relations; and ii) swell spectra, for which it is assumed that the wave steepness is conserved. Currently, there is abundant information on SWH (see Figure 8.27), as it is provided by eight satellite missions (Jason-3, Saral/Altika, Cryosat-2, Sentinel-3A and 3B, CFOSAT, HY2B, Sentinel-6MF). This ensures an excellent coverage for open ocean and it is evolving to a good coverage for coastal areas.

A variational technique has been also used in regional wave forecasting (Saulter et al., 2020) to assimilate SWH from altimeters. This scheme is an adaptation of the assimilation code NEMOVAR to wave assimilation.
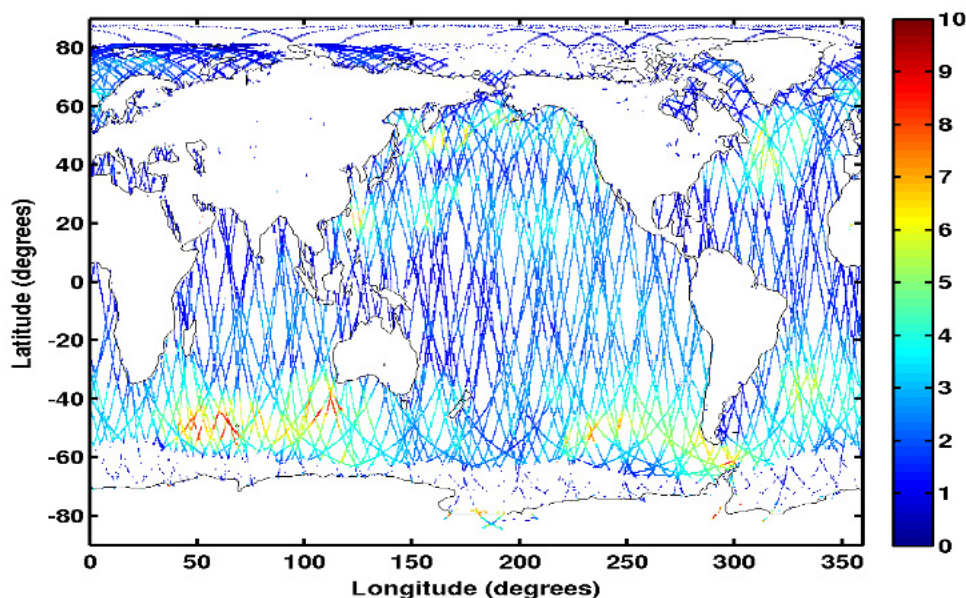
Figure 8.27. Significant wave height (in meters) observed by altimeter radars of six satellite missions (Jason-3, Saral/Altika, Cryosat-2, Sentinel-3A and 3B, CFOSAT) during the whole day of 11 October 2021 (source: Aouf et al., 2021).

Since the launch of the ERS-1 and 2 and ENVISAT (2002) satellites, the waves are observed with more detailed information (Hasselmann et al., 2013), characterised by the directional wave spectrum that can describe the different dominant wave trains (see Figure 8.28). The assimilation of such observations needs several steps and has been initiated at the end of 1990's. The method is based on the assimilation of wave systems as derived from a spectral partitioning scheme, which works on the principle of the inverted catchment area (Hasselmann et al., 1997; Voorrips et al., 1997; Breivik et al., 1998; Aouf et al., 2006). The different wave systems are characterised by their mean energy, frequency, and direction. The mean parameters are assimilated using an optimal interpo-

Figure 8.29. Difference of mean wave period (in seconds) from the model MFWAM with and without assimilation of wavenumber components of SAR partitions from ENVISAT during the period from September to December 2010; positive and negative values stand, respectively, for overestimation and underestimation of the model, (source: Aouf et al., 2021).

lation (OI) scheme, following a cross-assignment procedure that correlates the observed and modelled wave systems. The analysed spectra are reconstructed by resizing and reshaping the model spectra based on the mean parameters obtained from the OI scheme.

The SAR, from the ERS, ENVISAT and Sentinel-1 satellites, provides directional wave spectra with a limitation in azimuth direction of detecting waves with wavelength greater than 150 m. Such wave spectra are very useful to describe several wave trains in energy and wave numbers components. MFWAM started to assimilate wave partition parameters, such wavenumber components, by using optimal interpolation. This has provided a significant improvement of long swell propagation, and an assimilation impact which remains efficient at least 3 days in the period of forecast. Figure 8.29

Figure 8.28. Directional wave spectra observed by Synthetic Aperture Radar of Sentinel-1 (source: Derkani et al., 2021).
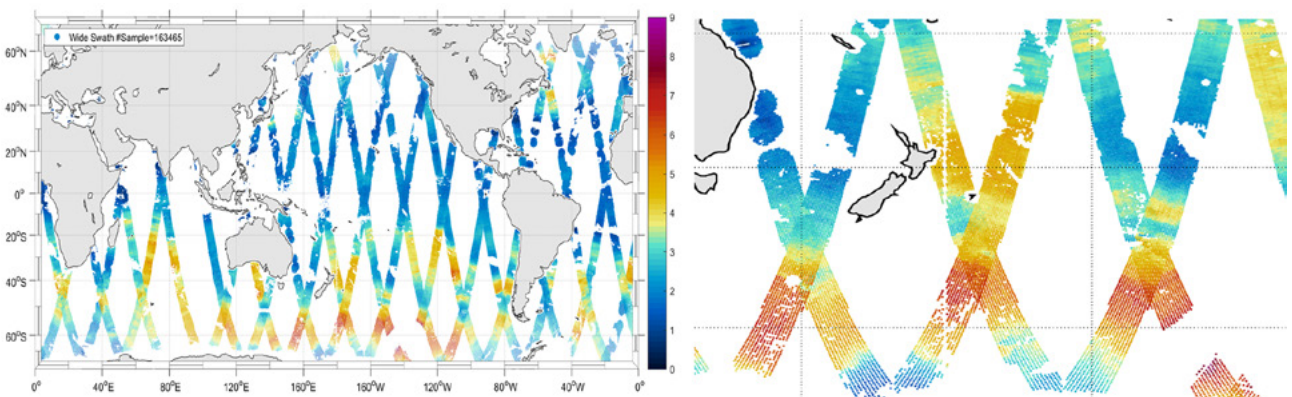
Figure 8.30. Wide swath significant wave height from the CFOSAT mission. Left: global view. Right: zoom focused on high SWH in Southwest Pacific Ocean (source: Wang et al., 2021).

shows the impact of the assimilation of wavenumber components of partitions from ENVISAT on the mean wave period. The different anomalies are strongly correlated with swell track propagation from the Southern Ocean.

Future wave forecasting systems will be able to assimilate both the wave heights and the directional components represented by the partitions. The impact of these assimilation systems ensures reliable integrated wave parameters in the 3-day forecast. The processing of satellite wave data is evolving rapidly; in a recent study by Wang et al. (2021), it is shown the retrieval of significant wave height on a scatterometer swath by using a deep learning technique. With this type of

wave data, the amount of data to be assimilated is significantly increased, which keeps consistent the correction of the model over a swath distance of 200 km. An example of a wide swath SWH obtained from the CFOSAT mission is shown in Figure 8.30. The assimilation of wide swaths of significant wave heights improves the initial conditions of the sea state generated by storms, for instance in the Southern Ocean, and also enhances the impact in coastal regions. Furthermore, with the trend of improved spatial resolution of the wave model, altimeters are providing better sampled wave heights, e.g. 5 hz (~1km), with the ability to correctly describe small scale variations such wave-current interactions.

8.6.
Ensemble modelling

Forecasts are subject to uncertainty by their nature. Some of the uncertainty is due to errors in model parameterizations of real-world processes, while some others can be attributed to observation errors. However, a significant amount of uncertainty is also introduced as a result of small differentials between the analysis and the state of environmental conditions at forecast initiation. These differences can lead to much wider discrepancies between the forecast and actual state at longer lead times, depending on the stability of the background meteorological conditions. One approach to forecasting is attempting to quantify the uncertainties, and view the forecast as sampling from a probability distribution of likely conditions rather than as a single "deterministic" outcome. Continuing increases in computing resources have enabled modelling centres to adopt a probabilistic forecasting approach based on running wave EPSs.

The aim of an EPS is to provide forecasters with a measure of model and climatic uncertainty associated with a given forecast. The ensemble will indicate lower forecast uncertainty in well- specified and stable weather conditions than in unstable conditions, where the present weather state might be poorly analysed and weather system development is more dynamic. As a forced-dissipative system, wave-forecast uncertainty is mostly determined by variations in the driving atmospheric data. Thus, the requirement for a complex EPS based on data assimilation, using perturbed initial conditions to generate starting conditions for ensemble members as in ensemble weather prediction, is limited. Pioneering applications have been developed for global medium-range

forecasts (1-4 weeks ahead) at centres such as the ECMWF (Molteni et al., 1996; Saetra and Bidlot, 2004), NCEP (Chen, 2006), and FNMOC (Alves et al., 2013). Research into short-range regional ensemble systems, which have a stronger requirement for uncertainty to be well specified at forecast initialization, is ongoing at the UKMO (Bunney and Saulter, 2015), the Italian Meteorological Service (Pezzutto et al., 2016), and the Australian Bureau of Meteorology (Zieger et al., 2018).

The data provided by an ensemble (see Figures 8.31 and 8.32) allow more than one approach to be adopted when interpreting and issuing a forecast. For example: i) individual members can be identified and used to describe alternative forecast scenarios deterministically; ii) dynamic changes in ensemble spread can be used to estimate the uncertainty associated with a deterministic product derived from the ensemble; or iii) probability information about a given outcome (for instance, the probability of wave height exceeding a certain operating threshold) can be used directly. The choice of approach requires an understanding of the end-user requirements and of the ensemble's performance.

However, a well-specified ensemble should show a good reliability relationship. Similarly, a good ensemble will show a strong correlation between spread in the EPS forecast and error in the ensemble control/mean forecast and observations. All these behaviours are fundamentally reliant on the quality of the underlying model. In the example in Figure 8.33, reliability is shown to be significantly affected for a short-range ensemble forecast when
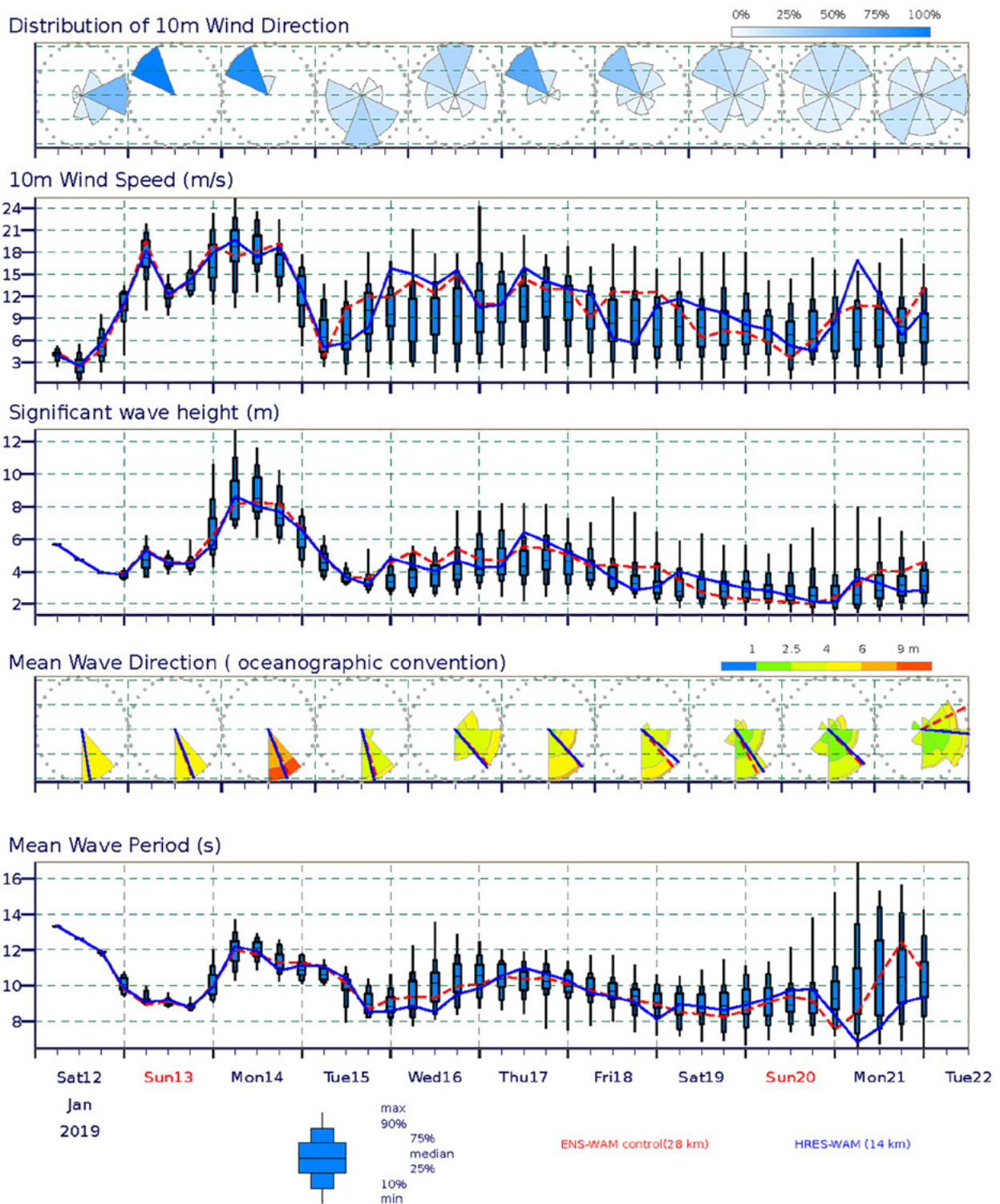
Figure 8.31.   Point time-series ensemble wave forecast product by ECMWF. Top two panels: direction variability and wind speed. Lower three panels: forecast of total wave parameters. In this instance, a high-resolution deterministic model and the ensemble control are overlaid using the blue and red lines, respectively (source: WMO, 2020).
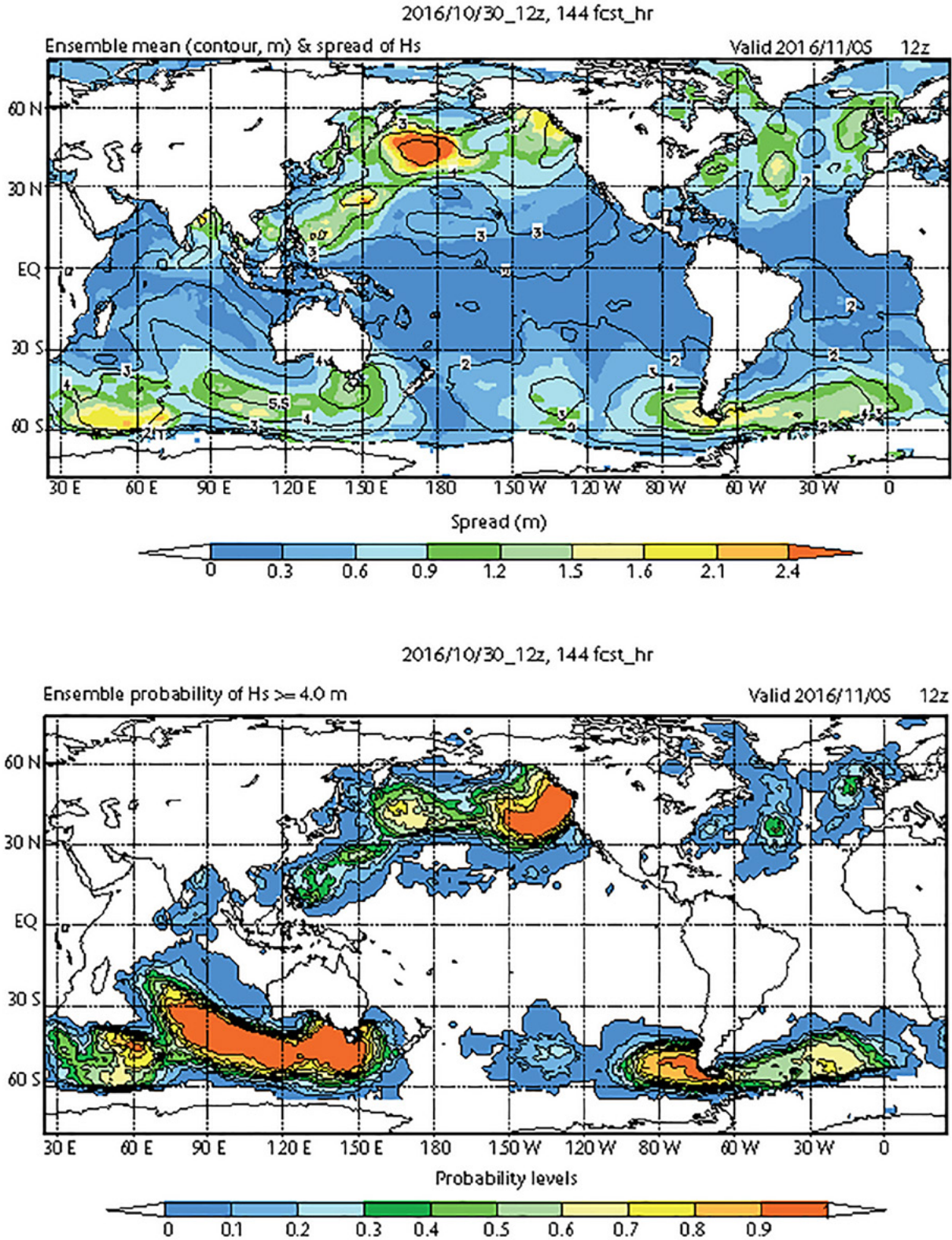
Figure 8.32. Ensemble forecast charts. Top: ensemble mean significant wave height (contours) and spread (shading). Bottom: probability of significant wave height exceeding 4 m (source: WMO, 2020).
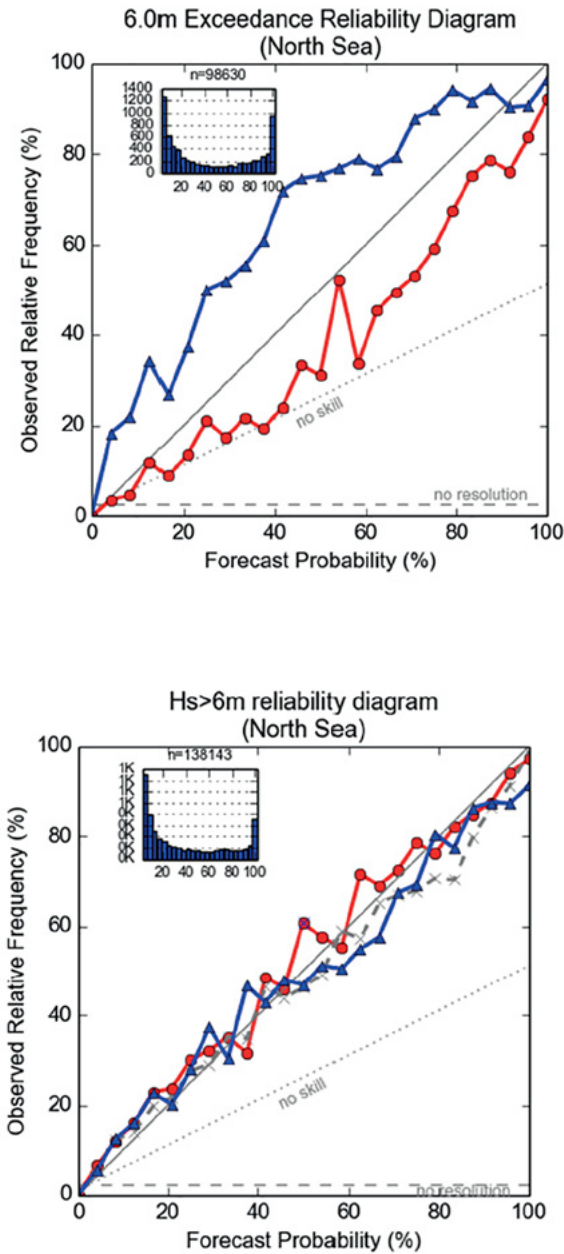
Figure 8.33. Reliability diagram for two wave EPS forecasts of significant wave height above 6 m at a forecast range of 2 d (blue: Atlantic regional model; red: regional model of the United Kingdom). The forecasts are considered reliable when the forecast probability and frequency of subsequent observations are similar (the data fall onto the 1:1 line). In this example, the effect of bias correcting the forecast is significant; in the bottom panel, the lines representing forecasts after bias correction are much closer to the 1:1 line than the raw forecasts in the top panel (source: WMO, 2020).

an underlying bias is corrected. A recommended practice when assessing probability of threshold exceedance is to evaluate the probability and also the quantity by which the threshold is exceeded. For example, a forecast where 90% of ensemble members exceeded a threshold by 1 m Hs should be given a stronger level of confidence than a forecast with a similar probability of 90%, but which threshold exceeds by only 10-20 cm.

One aspect of ensemble prediction that may have particular application is the identification of low-probability, high-impact occurrences of a "dangerous" sea state within the ensemble at long range (Petroliagis and Pinson, 2012). In extreme cases, the accuracy of the underlying model may be more questionable than everyday forecasting, but this can be mitigated using a background model climatology. Lalaurette (2003) described the ECMWF EFI methodology for wind, temperature, and precipitation parameters, in which forecast members were compared against a model climate. This EFI has also been extended to waves. Figure 8.34 shows an example in which the figure on the left is EFI (with range -1 to 1) for significant wave height, with values nearing 1 over the Norwegian Sea. The figure on the right is the corresponding 99th percentile of the wave-height distribution for that day. Therefore, EFI indicates that the model is predicting wave heights above 4 m and that this is not usual for that time of the year.

A computationally cheaper version of a full ensemble system is the so-called "poor man's ensemble" (Ebert, 2001), which combines some independent model forecasts from several operational centres. The availability of such a set of forecasts can also contribute to a "consensus forecast" in which the forecasts are weighted and bias corrected according to past performance to produce an "optimal consensus forecast", which typically outperforms any of the individual model forecasts (Durrant et al., 2009).

An example is given below for the interest of using a wave ensemble in the frame of emergency and wave submersion warning. Figure 8.34 right panel shows the high uncertainty between members on the location of the strong wave area generated by a storm event. The propagation of the storm is observed differently. Several members, including the deterministic forecast, estimate SWH of 10m on Brittany coasts at 102-hour forecast (06:00 UTC), as illustrated in Figure 8.35 left panel. In fact, the wave submersion warning in this case was triggered for the evening. It can be seen that about 20% of the members considered a probability of waves with SWH greater than 10m near the analysis. Uncertainty was also related to the location of the storm on the North-South axis.

Sat 12 Jan 2019 00UTC ©ECMWF t+48-72h VT:
Mon 14 Jan 2019 00UTC - Tue 15 Jan 2019 00UTC
Extreme forecast index and Shift of Tails
(black contours 0,1,2,5,8) for max significant wave height

Thu 10 Jan 2019 00UTC ©ECMWF VT:
Mon 14 Jan 2019 00UTC - Tue 15 Jan 2019 00UTC   48-72h
max significant wave height (in m) Model climate Q99
(one in 100 occasions realises more than value shown)
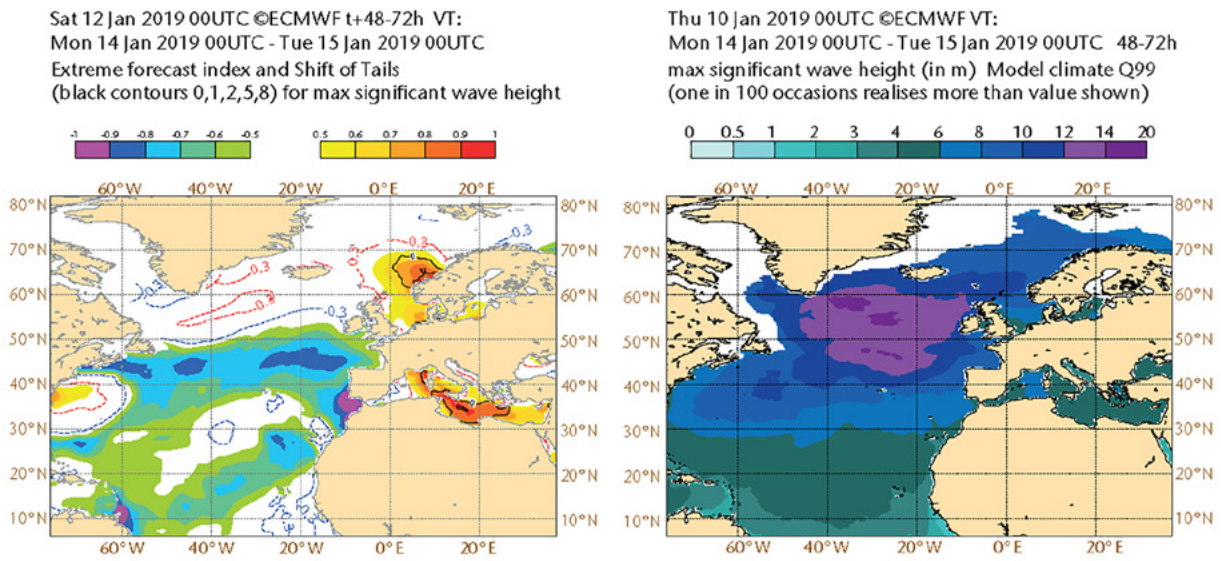
Figure 8.34.   Extreme Forecast Index (left) and associated 99th percentile of significant wave height derived from the model's long-term climate simulation (right panel) (source: WMO, 2020).
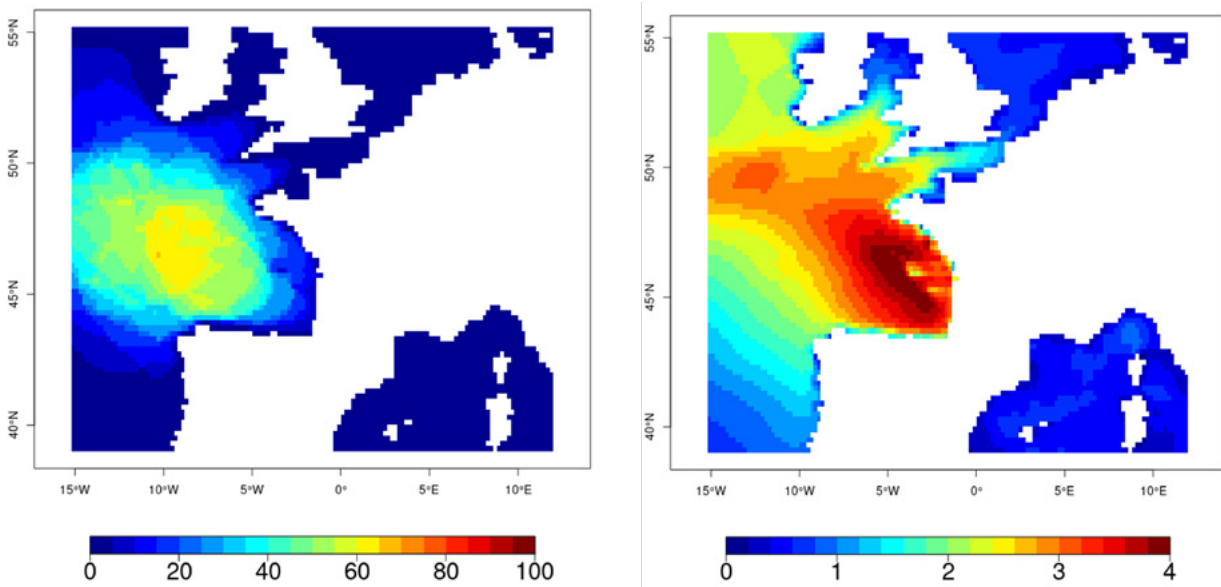
Figure 8.35.   Left: probability (in %) of SWH exceeding 10m at 102-hour forecast from the wave ensemble system. Right: standard deviation of SWH (in metre) between ensemble members, 30 January 2021 at 06:00 UTC (courtesy: A. Dalphinet, MeteoFrance).

8.7.
Validation and calibration strategies

For all operational ocean forecast systems, verification of wave models is dependent on the choice of metric, sampling strategy, and parameter(s) to be verified. Verification and measurement of model uncertainty include describing the difference between the model and observed conditions and their statistical properties; assessing the value of the model in accurately predicting specific ocean conditions for user decision making; providing a long term view of performance and measuring the impact of model changes; and/or investigating the model's ability to represent particular ocean processes or conditions. As with any statistical analysis, it is useful to frame the question or hypothesis that the verification should answer and ensure that the metrics provided are appropriate to the expertise of the audience.

For the verification, it is fundamental the sampling strategy applied to both model and observations. Sampling should consider spatial and temporal correlations with respect to data to be verified. These correlations will be dependent on the verification setting, for example in the open ocean wave fields may be well correlated over scales of hundreds of kilometres and several hours, whilst in coastal settings with a strong tidal component correlation in wave conditions, scales can diminish about tens of kilometres and periods of less than an hour (Saulter et al., 2020). The degree of correlation between data affects the sample size required to consider robust statistical verification. The verification can be affected if scales represented by models and observations are substantially different. In-situ observations tend to sample on scales equivalent to approximately 5-20 km depending on dominant wave periods, whilst a 1 Hz altimeter observation of significant wave height is derived over a spatial footprint that covers approximately 6-7 km in the along-track direction with a diameter 2-10 km increasing with the sea-state (since the backscatter increases as waves get bigger and wavelengths longer). Wave models can generally be considered to scale at a factor of 3-4 times of either the wave or forcing atmospheric model horizontal grid and integration time step (Janssen et al., 2007). It is recommended to define a benchmark representative scale for comparison with the data processed to that scale, as well as metadata describing this processing supplied alongside with metrics. It may also be important to communicate limitations in the data, for example in the case in which the available observations and processing methods cannot be extended to a full coverage of the model domain, such as coastal zones.

Existing standards for baseline performance metrics can be found via the WMO/LC-WFV established at ECMWF (Bidlot, 2016), and Product Quality Dashboard of the Copernicus Marine Service (🔗 [8]). Left panel in Figure 8.36 shows an example of scatter index of SWH monitoring provided by different operational
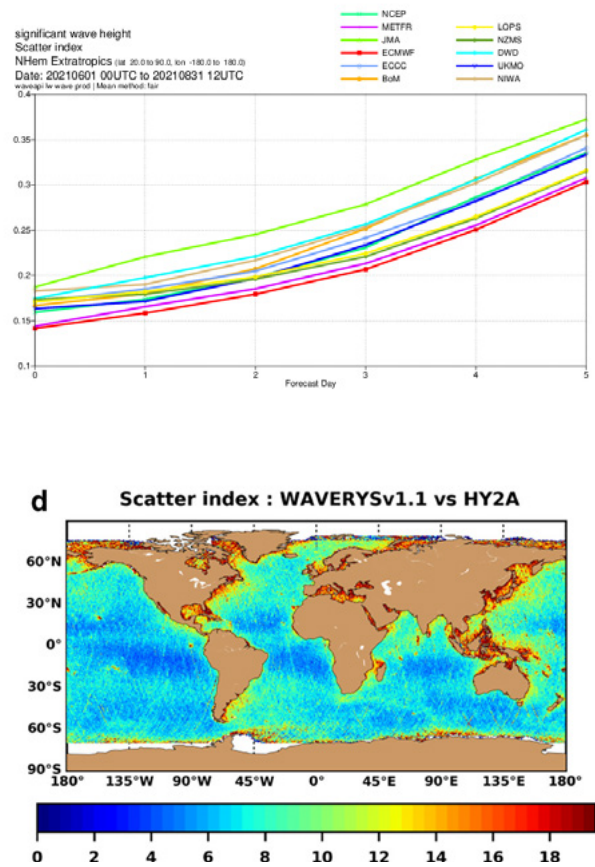
Figure 8.36. Top: variation of scatter index of SWH in a forecast compared to wave buoys from June to August 2021, colours stand for operational centres names (source: WMO/LC-WFV). Bottom: map of scatter index of SWH from Global Ocean Wave Reanalysis (WAVERYS) compared to altimeter HY2A during the 2013-2018 period (source: CMEMS-GLO-QUID-001-032 🔗 [9]).

8. https://pqd.mercator-ocean.fr

9. https://catalogue.marine.copernicus.eu/documents/QUID/CMEMS-GLO-QUID-001-028.pdf

centres in the framework of the WMO/LC-WFV. As illustrated by the Copernicus Marine Service global wave reanalysis (right panel in Figure 8.36), the altimeters have the advantage of covering all ocean basins, allowing the monitoring of the spatial variation of wave models errors.

Standards will continue to evolve with the increased use of ensemble forecast systems and reductions in horizontal scales of wave, atmosphere, and ocean models. However, model performance is better described by metrics that exploit the uncertainty in forecasts, either from the ensemble (Pezzutto et al., 2016) or using variability in spatial neighbourhoods surrounding an observation point (Ebert, 2008; Mittermaier and Csima, 2017). For long-term monitoring, an important ensemble prediction metric is the Cumulative Ranked Probability Score (Hersbach, 2000), which can be directly compared with Mean Absolute Error for deterministic predictions, therefore enabling the benefits of transition to high resolution or ensemble models from lower resolution or deterministic systems to be measured.

Wave observational data are dominated by SWH measurements available from in-situ sources and remote sensing via satellite missions and HF radar. SWH data are a primary health indicator for the wave model, describing the wave energy of the surface ocean as a response to momentum supplied by the atmosphere and redistributed through wave dispersion. SWH is often the main parameter of interest for users and decision makers about sea-state conditions (see also Chapter 4). However, to properly verify a wave model's performance at a process level, observations of further parameters describing the distribution of wave energy within

the two-dimensional frequency-direction spectrum should be also used. Full spectral coverage in the frequency (period) domain of ocean surface waves is currently obtained only by in-situ measurements. Attention is needed to understand the limitations imposed by a given platform's response to wave action, which determines a high frequency cut-off, and the distinction between directional spectra derived from the 'first five' approach used by in-situ data (Swail et al., 2010) versus the full frequency-direction distributions generated from models and remote sensing. Remote sensed data are strongly affected by frequency (wavelength) cut-off constraints as , for example, SAR will capture long period swells but not short wind-waves. From a verification perspective, it can be difficult obtaining a sufficient sample of data across the full directional wave spectrum to enable a robust statistical analysis over multiple frequencies and directions, and hence it is often preferable to compare wave heights, periods, and directions integrated over a reduced number of partitioned regions of the wave spectrum (Ardhuin et al., 2010). Since wave models are strongly influenced by the uncertainty inherited from the forcing atmosphere (Cavaleri et al., 2018), when evaluating wave models at the process level, it is recommended to verify wave parameters alongside contemporary measures of wind speed or stress.

A useful tool in the verification process is the wave rose analysis. Figure 8.37 shows a comparison between the directional wave properties by the Copernicus Marine Service WAVERYS and the buoy 51202 deployed by the NOAA NDBC at Oahu (Hawaii, USA).
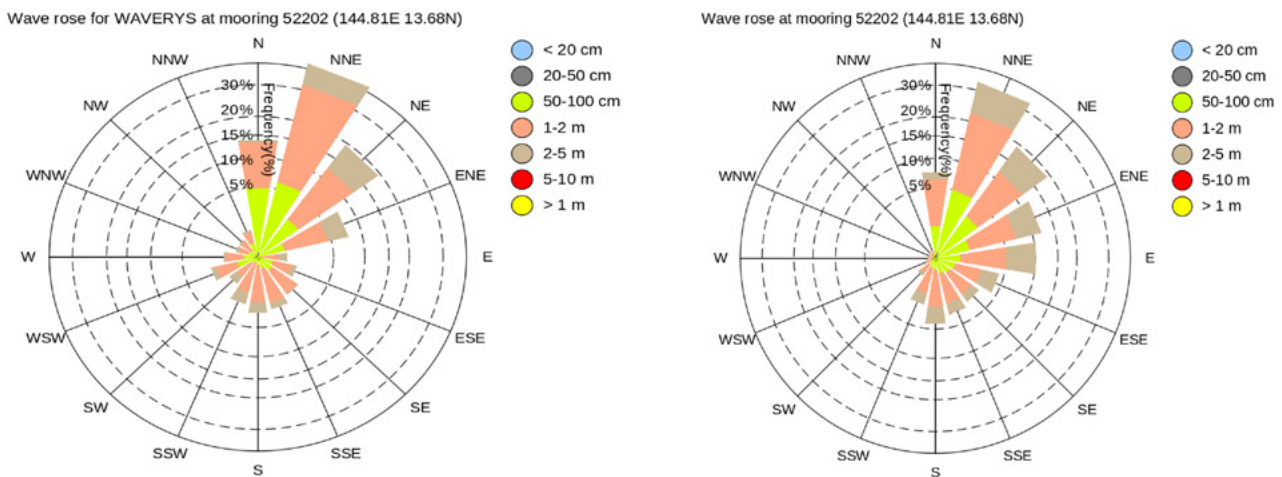
Figure 8.37.   Left: wave rose for Copernicus Marine Service WAVERYS. Right: wave rose at NDBC buoy 51202 (Hawaii, USA).

8.8.
Outputs and post processing

8.8.1. Post-processing of the wave model results for the final delivery

Wave models provide at each grid point two-dimensional wave spectrum $F(f, \theta)$, which describes how the wave energy is distributed as a function of frequency f and propagation direction θ. In general, the wave spectrum F is discretized in 30 frequencies and 24 directions. To simplify the study of wave conditions, integrated parameters are derived from weighted integrals of $F(f, \theta)$. The moment of order n, m_n is defined as the following integral:

$$m_n = \int \int f^n F(f, \theta) df f\theta \qquad (8.43)$$

The integrations are performed over all frequencies and directions or over a spectral subdomain when the spectrum is split between wind sea and swell or partitioned into main components. The wind sea wave component is subject to the wind forcing, and then wave phase speed is smaller than the wind speed at the ocean surface. The remaining part is considered swell. It is established in the WAM model for in-stance, the spectral energy is subject to wind forcing when the following approximation is satisfied:

$$1.2 \times 28 \left(\frac{u^*}{c} \right) \cos(\theta - \varphi) > 1 \qquad (8.44)$$

where u^* is the friction velocity, c is the phase speed as derived from the linear theory of waves and φ is the wind direction. The integrated parameters are therefore also computed for wind waves and swell by only integrating over the respective components of $F(f, \theta)$ that satisfies 8.43 or not.

Significant wave height

The wave energy is the 0th order of the moment m_0 and significant wave height (Hs) is defined as follows (Hs snapshot shown in Figure 8.38):

$$Hs = 4\sqrt{m_0} \qquad (8.45)$$

Sea surface wave significant height [m]

0   2   4   6   8   10

2022 Feb 04, 00:00 UTC
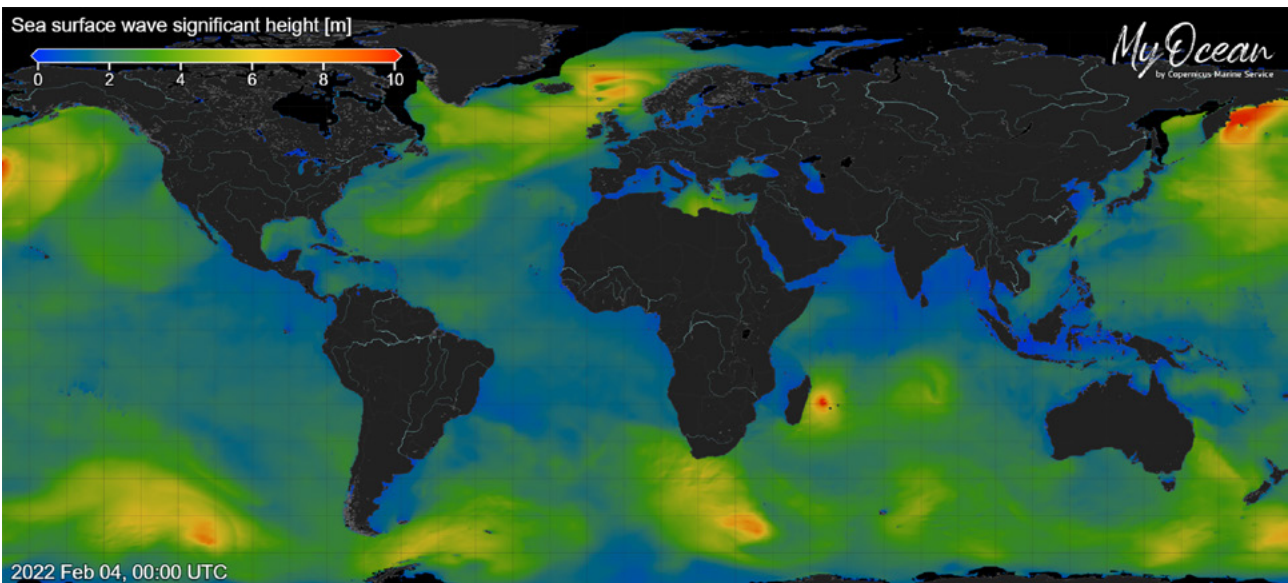
Figure 8.38.   Snapshot of Hs (in meters) from Copernicus Marine Service global wave system (3 February 2022 at 21 UTC).

Mean period

The mean period (snapshot in Figure 8.39) is expressed in several ways. The most used is Tm_{-1} which is based on the moment of order $_{-1}$, that is

$$Tm_{-1} = \frac{m_{-1}}{m_0} \qquad (8.46)$$

Tm_{-1} is also commonly known as the energy mean wave period. By considering Hs, it can be used to determine the wave energy flux per unit of wave-crest length in deep water, also indicated as the wave power per unit of wave-crest length P.

To analyse different aspects of the wave field, other moments can be used to define a mean period. Periods can be based on the first moment Tm_1 given by:

$$Tm_1 = \frac{m_0}{m_1} \qquad (8.47)$$

Tm_1 is essentially the reciprocal of the mean frequency. It can be used to estimate the magnitude of Stokes drift transport in deep water and periods based on the second moment Tm_2 given by:

$$Tm_2 = \frac{m_0}{m_2} \qquad (8.48)$$

Tm_2 is also known as the zero-crossing mean wave period, as it corresponds to the mean period that is determined from observations of the sea surface elevation using the zero-crossing method.

Peak period

The peak period is defined for total sea and can be expressed as the reciprocal peak frequency of the 1D wave spectrum $F(f)$ integrated over directions. There is a second way to compute the peak frequency and it is obtained from a parabolic fit around the discretized maximum of the two-dimensional wave spectrum $F(f,\theta)$.

Mean wave direction

The mean wave direction is defined by weighting the wave spectrum $F(f,\theta)$. It is expressed as follows:

$$< \theta > = \arctan \frac{S_1}{C_1} \qquad (8.49)$$

where S_1 is the integral of $sin(\theta)*F(f,\theta)$ over frequencies and directions, while C_1 is the integral of $cos(\theta)*F(f,\theta)$ over f and θ.

Directional spread

The wave directional spread gives the information on the directional distribution of the total sea, or it can be applied for different wave components. It is expressed as follows:

$$s_\theta = \sqrt{2(1 - M)} \qquad (8.50)$$

where M is I/m_0 and I is the integral of $cos(\theta - <\theta>)*F(f,\theta)$ over f and θ. $<\theta>$ is the mean direction. The directional spread can be computed for wind, sea, and swell components.
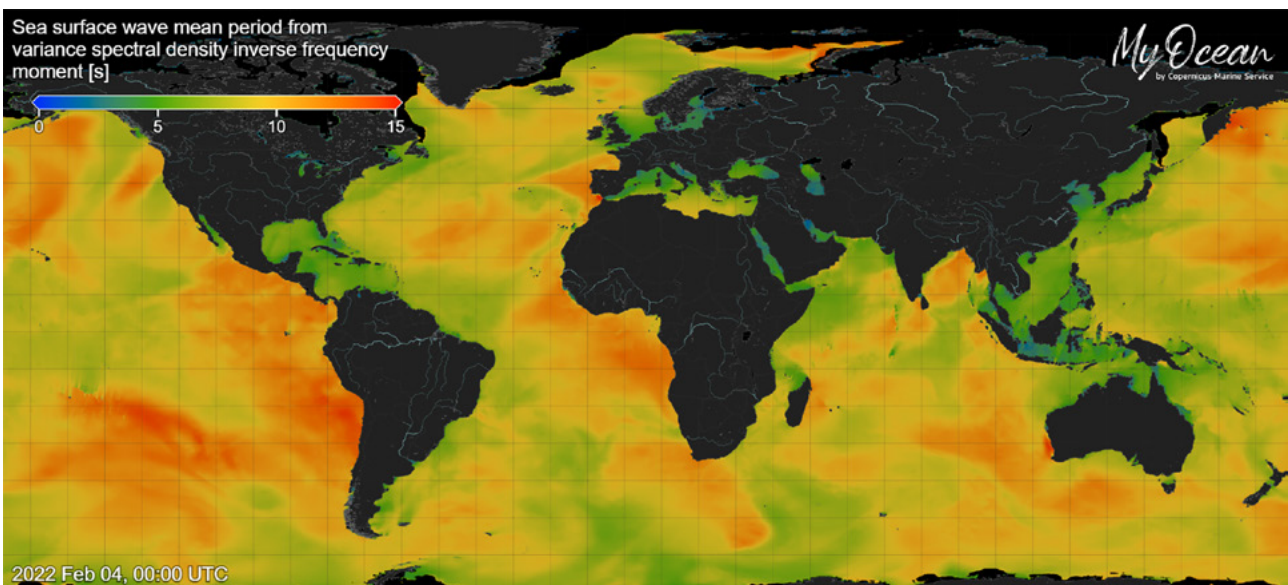
Figure 8.39. Snapshot of mean period Tm_{-1} (in seconds) from Copernicus Marine Service global wave system (3 February 2022 at 21 UTC).

Surface Stokes Drift

The Stokes drift impacts the turbulence in the upper ocean layers and contributes to the source of energy of the ocean circulation, particularly the Langmuir circulation. The surface Stokes drift Us is computed from the wave spectrum in deep water by the following relation:

$$U_s = \frac{16\pi^3}{g} \int \int f^3 \cdot k \cdot F(f,\theta)dfd\theta \qquad (8.51)$$

where the integration is over all frequencies and directions. k is the unit vector in the direction of the wave component. In the high frequency range, the Phillips spectral shape is used with accounting of spectral level of the last frequency bin. Figure 8.40 shows the ratio of Stokes drift magnitude to 10 m wind speed.

Partitioning wave spectrum

In general, wave forecasters firstly analyse the integrated parameters over the full wave spectrum describing the total sea. Then, they refine their analysis by examining the different dominant wave trains representing wind, sea, and swell. Most wave models include a partitioning procedure, which aims to separate the different wave systems represented by energy peaks in the wave spectrum. The most used partitioning procedure is adapted from Hanson and Phillips (2002) and is based on the watershed method inspired from image processing. After splitting the wind sea and swell wave spectrum, the method consists in identifying the energy peaks in

the wave spectrum and isolating a partition with decreasing energy from the peak to a limit corresponding to an increase in energy. Several partitions or wave systems can be detected in a wave spectrum, and they are classified by decreasing order of their wave height. An example of partitioning is shown in Figure 8.41, where three partitions are detected with two swells and one wind sea. The average height, period and direction can be calculated on each partition.

Wave energy flux

The wave energy flux per unit of wave-crest length in deep water can be computed by using the wave period Tm_{-1} and significant wave height H_s:

$$P = \frac{\rho_w \cdot g^2}{64\pi} Tm_{-1} H_s^2 \qquad (8.52)$$

where rw is the water density and g is the acceleration due to gravity.

The wave energy flux can be expressed by integrating the flux of each spectral component.

$$P = 2\pi g \int \int C_g \cdot F(f,\theta)dfd\theta \qquad (8.53)$$

where Cg is the group velocity in deep water.
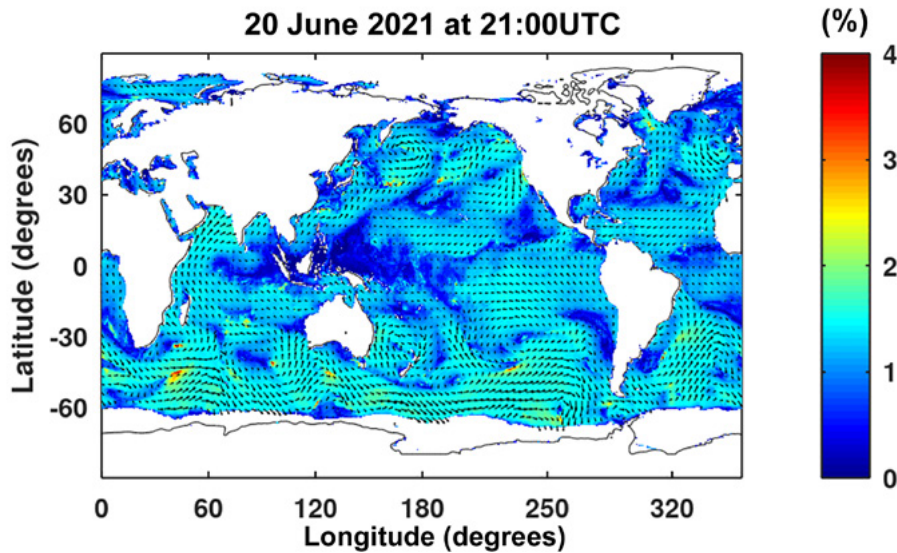
Figure 8.40. Ratio (in percentage) between surface Stokes drift and wind speed from Copernicus Marine Service global wave system on 20 June 2021 at 21 UTC. Arrows show the Stokes drift direction.
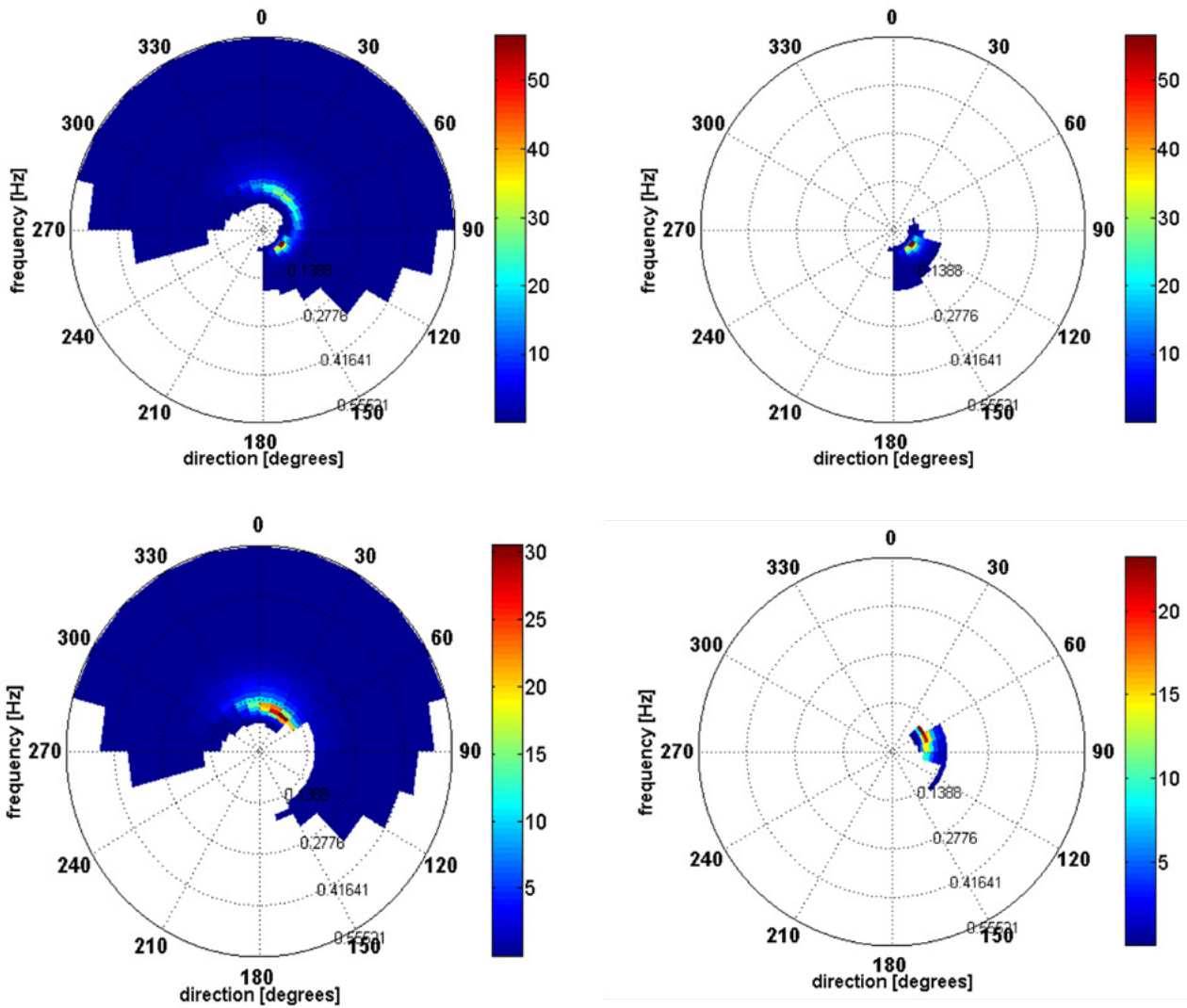
Figure 8.41.   Top left: full wave spectrum for the location of the Prestige ship accident (Trulsen et al., 2015). Top right: swell partition-1, the most energetic propagating to the South-East direction. Bottom left: long wind sea partition-2 propagating to the North-East direction. Bottom right: swell partition-3 propagating to the East-North-East direction (source: Copernicus Marine Service).

8.8.2. Common output variables

Numerical models for wave generation and propagation can provide different variables to be used in multi-year and predictive systems. Table 8.1 lists variables that are commonly provided by numerical and that may be of special relevance for users, as well as for developers who wish to set up future wave OOFS and multi-year systems.

Table 8.1. Common names of wave variables.

Common variable names *(usually provided by third-generation spectral wave model and/or a mild slope approximations)*	Symbol	Units
Significant wave height	Hs	m
Peak period	Tp	s
Mean wave period	Tm	s
Mean and Peak wave direction	Ɵ	ºN
Complete wave spectra matrix	S	m²/Hz/ºN
Mean parameters of wave partitions (Hs,Tm,Tp and Dir) for: 2 Swells and 1 wind sea	Hsi, Tpi, Diri	m, s, ºn
Maximum wave height	Hmax	m
Maximum wave period	Tmax	m
Meridional component of Stokes drift	Us	m/s
Zonal component of Stokes drift	Vs	m/s
Drag coefficient with waves	Cd	
Normalised stress to ocean	Tauoc	
Mean square slope	mss	

Advanced variable names *(usually provided by phase resolving models and CFD approaches)*	Symbol	Units
Free-surface time series at points and maps	η	m
Wave breaking-induced currents	U-V	m/s
Instantaneous wave run-up	Ru	m
Instantaneous wave overtopping volume	q	m^3/s per m
Infragravity wave oscillations	ηIG	m
Multi-directional wave spectra matrix (agitation)	S	$m^2/Hz/°N$
Instantaneous wave pressures over structures	P	N/m^2
Instantaneous forces over structures	F	N
Instantaneous wave currents	u-v	m/s

8.9.
Inventories

The purpose of this section is to provide an initial inventory of the operational ocean wave NearRealTime (NRT) and MultiYear (MY) operating at international level. Details about each specific system, resolution, implemented numerical tool, and data assimilation are provided in Tables 8.2 and 8.3 and, where existing, the website address to directly link to systems products and other relevant information.

8.9.1. Inventory of Near-real time wave forecasting systems

The present state-of-the-art operational ocean wave systems for NRT products from global to local scale is presented in Table 8.2.

Also, current contributors to the ocean wave forecast, either global or regional, are (among others): European Centre for Medium-Range Weather Forecasts, UK; Met Office, UK; Fleet Numerical Meteorology and Oceanography Centre, USA; Environment and Climate Change Canada, Canada; National Centres for Environmental Prediction, USA; Météo France, France; Deutscher Wetterdienst, Germany; Bureau of Meteorology, Australia; Service Hydrographique et Océanographique de la Marine, France; Japan Meteorological Agency, Japan; Korea Meteorological Administration, Republic of Korea; Puertos del Estado, Spain; Danmarks Meteorologiske Institut, Denmark; National Institute of Water and Atmospheric Research, New Zealand; Det Norske Meteorologiske Institutt, Norway; Servicio de Hidrografía Naval, Servicio Meteorológico, Argentina.

Table 8.2.   Initial inventory of global (G) and regional (R) Near-real time wave forecasting systems.

Type	System (Producer)	Area	Grid type and resolution	Wave model core	Data used for assimilation	Products	Website
G	Global Wave Forecasting System (MeteoFrance, France)	Global ocean	Regular grid, 0.083° - 0.083° - 9km; 1 level (surface)	MFWAM	SWH from satellite	3-hourly instantaneous for SWH MWT VMDR VSDXY WW, SW1 SW2	https://marine.copernicus.eu
R	Arctic Wave Forecasting System (The Norwegian Meteorological Institute, Norway)	Arctic region	3km; 1 level (surface)	WAM	NA	Hourly instantaneous for SWH MWT VMDR VSDXY WW, SW1 SW2	https://marine.copernicus.eu
R	Baltic Wave Forecasting System (FMI, Finland)	Baltic region	2km; 1 level (surface)	WAM	NA	Hourly instantaneous for SWH MWT VMDR VSDXY WW SW1 SW2	https://marine.copernicus.eu
R	European North West Shelf Seas Wave Forecasting System (UK MetOffice, United Kingdom)	European North-West shelf Seas	0.014° - 0.03°; 1 level (surface)	WW3	NA	Hourly instantaneous for SWH MWT VMDR VSDXY WW SW1 SW2	https://marine.copernicus.eu
R	Iberia Biscay Ireland Regional Seas Wave Forecasting System (Puertos del Estado, Spain)	Irish-Biscay-Iberian shelves	0.05° × 0.05°; 1 level (surface)	MFWAM	SWH from satellite	Hourly instantaneous for SWH MWT VMDR VSDXY WW SW1 SW2	https://marine.copernicus.eu
R	Mediterranean Wave Forecasting System (HCMR, Greece)	Mediterranean Sea	0.042° - 0.042° - 5km; 1 level (surface)	WAM	SWH from satellite	Hourly instantaneous for SWH MWT VMDR VSDXY WW SW1 SW2	https://marine.copernicus.eu
R	Black Sea Wave Forecasting System (HEREON, Germany)	Black Sea	0.025° - 0.025° - 3km; N/A level (surface)	WAM	NA	Hourly instantaneous for SWH MWT VMDR VSDXY WW SW1 SW2	https://marine.copernicus.eu

Type	System (Producer)	Area	Grid type and resolution	Wave model core	Data used for assimilation	Products	Website
R	High resolution wave and current forecast within Santander Bay entrance (Spain)	Santander, Spain	10 x 10 km; 10 m level (surface)	SWAN - Elliptic mild slope and tidal currents model (ROMS)	In situ measurements, buoys and radar	instantaneous data for waves SWH MWT VMDR VSDXY WW SW1 SW2 and currents	https://nowcastsdr.ih-cantabria.com/
R	Local Wave Forecasting System at the Harbour Authorities (SAPO)	Spain	Regular grid, 0.1° - 0.1°; 1 level (surface)	SAPO	In situ measurements, Coastal buoys	Hourly instantaneous for SWH MWT VMDR VSDXY WW SW1 SW2	https://portus.puertos.es/index.html?locale=en#/
R	Foras Na Mara / Marine Institute Wave Forecasts	Ireland	Regular grid. 0.025 degrees (approximately 1.5km)	SWAN	NA	Hourly instantaneous for SWH TP VMDR SW2	http://www.marine.ie/Home/site-area/data-services/marine-forecasts/wave-forecasts
R	Foras Na Mara / Marine Institute Wave Forecasts	Ireland	Regular grid. 0.025 degrees (approximately 1.5km)	SWAN	NA	Hourly instantaneous for SWH TP VMDR SW2	http://www.marine.ie/Home/site-area/data-services/marine-forecasts/wave-forecasts
R	Foras Na Mara / Marine Institute Wave Forecasts	Ireland	Regular grid. 0.025 degrees (approximately 1.5km)	SWAN	NA	Hourly instantaneous for SWH TP VMDR SW2	http://www.marine.ie/Home/site-area/data-services/marine-forecasts/wave-forecasts
R	AUSWAVE	Australia	AUSWAVE-G Global (78°S-78°N, 0°E-359°E) AWAVE-R Regional (60°S-12°N, 69°E-180°E)	WW3	NA	Hourly instantaneous for sig_wav_ht pk_wav_per pk_wav_dir mn_dir_wnd_sea (for SW1, SW2, SW3, and WND)	http://www.bom.gov.au/nwp/doc/auswave/data.shtml

Type	System (Producer)	Area	Grid type and resolution	Wave model core	Data used for assimilation	Products	Website
R	NOAA/NWS Marine Weather Forecasts	USA	Regional 0.1º aprox.	WW3	Offshore buoys	Marine, Tropical and Tsunami Services Branch	https://www.weather.gov/marine/
G	NOMADS NOAA Operational Model Archive and Distribution System	Global	Regular grid (global 0.251 to 0.5º and regional 11 km aprox.)	WW3	Offshore buoys	Hourly instantaneous for SWH MWT VMDR VSDXY WW SW1 SW2	https://nomads.ncep.noaa.gov/
R	CARICOOS Nearshore Wave Model	Puerto Rico and Virgin Islands	1 km grid to 200 m and 10 m grid	SWAN	NA	Hourly instantaneous for SWH MWT VMDR VSDXY WW SW1 SW2	https://www.caricoos.org/waves/forecast/SWAN/PRVI/hsig

8.9.2. Inventory of Multi-year wave systems (reanalysis, hindcast)

Table 8.3.   Initial inventory of global (G) and regional (R) Near-real time wave forecasting systems.

Type	System (Producer)	Area	Grid type and resolution	Wave model core	Data used for assimilation	Available timeseries	Products	Website
G	Global Ocean Waves Reanalysis (MOi, France)	Global Ocean	0.2° × 0.2°	MFWAM	Sea Wave Height (SWH)	1993-2021	3-hourly instantaneous for SWH MWT VMDR VSDXY WW, SW1 SW2	https://marine.copernicus.eu
R	Arctic Ocean Wave Hindcast (MetNo, Norway)	Arctic Sea	3km × 3km	WAM	NA		Hourly instantaneous for SWH MWT VMDR VSDXY WW SW1 SW2	https://marine.copernicus.eu
R	Baltic Sea Wave Hindcast (FMI, Finland)	Baltic Sea	2km × 2km	WAM	NA	1993/01/01 - 2020/12/31	Hourly instantaneous for SWH MWT VMDR VSDXY WW SW1 SW2	https://marine.copernicus.eu

Type	System (Producer)	Area	Grid type and resolution	Wave model core	Data used for assimilation	Available timeseries	Products	Website
R	Baltic Sea Wave Hindcast (FMI, Finland)	Baltic Sea	2km × 2km	WAM	NA	1993/01/01 - 2020/12/31	Hourly instantaneous for SWH MWT VMDR VSDXY WW SW1 SW2	https://marine.copernicus.eu
R	Mediterranean Sea Waves Reanalysis (HCMR, Greece)	Mediterranean Sea	0.042° × 0.042°	WAM	Sea Wave Height (SWH)	1993/01/01 - present	Hourly instantaneous for SWH MWT VMDR VSDXY WW SW1 SW2	https://marine.copernicus.eu
R	Atlantic -Iberian Biscay Irish-Ocean Wave Reanalysis (Puertos del Estado, Spain)	Irish-Biscay-Iberian shelves	0.05° × 0.05°	MFWAM	Sea Wave Height (SWH)	1993/01/01 - 2020/12/31	Hourly instantaneous for SWH MWT VMDR VSDXY WW SW1 SW2	https://marine.copernicus.eu
R	Atlantic- European North West Shelf-Wave Physics Reanalysis	European North-West shelf Seas	0.017° × 0.017°	WW3	NA	1980/01/01 - present	3-hourly instantaneous for SWH MWT VMDR VSDXY WW, SW1 SW2	https://marine.copernicus.eu
R	Black Sea Waves Reanalysis (HEREON, Germany)	Black Sea	0.037° × 0.028°	WAM	Sea Wave Height (SWH)	1979/01/01 - present	Hourly instantaneous for SWH MWT VMDR VSDXY WW SW1 SW2	https://marine.copernicus.eu
G	Global ocean wave reanalysis from Climate data service copernicus ERA5	Global	0.5°x0.5°	ECWAM	SWH	1980 - present	Hourly	https://climate.copernicus.eu/climate-reanalysis
G	Global wave reanalysis CFSR	Global	0.5°x0.5°	WW3	NA	1979 - 2017		https://polar.ncep.noaa.gov/waves/hindcasts/
G	Global wave reanalysis CAWCR (CSIRO)	Global	0.4°x0.4°	WW3	NA	1979 - 2010		https://data.csiro.au/collection/csiro:39819

8.10.
References

Álvarez-Fanjul, E., García-Sotillo, M., Pérez Gómez, B., García Valdecasas, J. M., Pérez Rubio, S., Rodríguez Dapena, A., et al. (2018). Operational oceanography at the service of the ports. In: "New Frontiers in Operational Oceanography", Editors: E. Chassignet, A. Pascual, J. Tintoré, and J. Verron (Cambridge: GODAE OceanView), 729-736, https://doi.org/10.17125/gov2018.ch27

Alves, J.-H.G.M., Wittmann, P., Sestak, M., Schauer, J., Stripling, S., Bernier, N.B., Mclean, J., Chao, Y., Chawla, A., Tolman, H., Nelson, G., and Klotz, S. (2013). The NCEP–FNMOC combined wave ensemble product: expanding benefits of inter-agency probabilistic forecasts to the oceanic environment. *Bulletin of the American Meteorological Society,* 94(12), 1893-1905, https://doi.org/10.1175/BAMS-D-12-00032.1

Aouf, L., Hauser, D., Law-Chune, S., Chapron, B., Dalphinet, A., and Tourain, C. (2021). New directional wave observations from CFOSAT: impact on ocean/wave coupling in the Southern Ocean. EGU General Assembly 2021, online, 19-30 Apr 2021, EGU21-7412, https://doi.org/10.5194/egusphere-egu21-7412

Aouf, L., Lefèvre, J., and Hauser, D. (2006). Assimilation of Directional Wave Spectra in the Wave Model WAM: An Impact Study from Synthetic Observations in Preparation for the SWIMSAT Satellite Mission. *Journal of Atmospheric and Oceanic Technology,* 23(3), 448-463, https://doi.org/10.1175/JTECH1861.1

Aouf, L., Danièle, H., Céline, T., Bertrand, C. (2018). On the Assimilation of Multi-Source of Directional Wave Spectra from Sentinel-1A and 1B, and CFOSAT in the Wave Model MFWAM: Toward an Operational Use in CMEMS-MFC. IGARSS 2018 - 2018 IEEE International Geoscience and Remote Sensing Symposium, 2018, pp. 5663-5666, doi: 10.1109/IGARSS.2018.8517731

Ardhuin, F., Otero, M., Merrifield, S., Grouazel, A., and Terril, E. (2020). Ice breakup controls dissipation of wind waves across Southern Ocean sea ice. *Geophysical Research Letters,* 47, e2020GL087699. https://doi.org/10.1029/2020GL087699

Ardhuin, F., Rogers, E., Babanin, A., Filipot, J.-F., Magne, R., Roland, A., van der Westhuysen, A., Queffeulou, P., Lefevre, J.-M., Aouf, L., Collard, F. (2010). Semi-empirical dissipation source functions for ocean waves. Part I: definitions, calibration and validations. *Journal of Physical Oceanography,* 40, 1917-1941, https://doi.org/10.1175/2010JPO4324.1

Babanin, A.V. (2011). Breaking and Dissipation of Ocean Surface Waves. Cambridge University Press, 480 p.

Babanin, A.V. (2018). Change of regime of air-sea dynamics in extreme Metocean conditions. Proceedings of the ASME 2018 37th International Conference on Ocean, Offshore and Arctic Engineering OMAE2018, June 17-22, 2018, Madrid, Spain, paper 77484, 6 p.

Babanin, A.V., Onorato, M., and Qiao, F. (2012). Surface waves and wave-coupled effects in lower atmosphere and upper ocean. *Journal of Geophysical Research: Ocean,* 117(C11), https://doi.org/10.1029/2012JC007932

Babanin, A.V., van der Westhuysen, A., Chalikov, D., and Rogers, W.E. (2017). Advanced wave modelling including wave-current interaction. In "The Sea: The Science of Ocean Prediction", Eds. Nadia Pinardi, Pierre F. J. Lermusiaux, Kenneth H. Brink and Ruth Preller, *Journal of Marine Research,* 75, 239-262.

Barstow, S., Mørk, G., Lønseth, L., and Schjølberg, P.. (2004). Use of satellite wave data in the world waves project. Gayana (Concepción), 68(2, Supl.TIProc), 40-47, http://dx.doi.org/10.4067/S0717-65382004000200007

Battjes, J.A., and Janssen, P.A.E..M. (1978). Energy Loss and Setup Due to Breaking in Random Waves. Proceedings of 16th Coastal Engineering Conference, Hamburg, Germany, 569-587.

Bauer, E., Hasselmann, S., Hasselmann, K. and Graber, H. C. (1992). Validation and assimilation of Seasat altimeter wave heights using the WAM wave model. *Journal of Geophysical Research: Ocean,* C97, 12671-12682, https://doi.org/10.1029/92JC01056

Berkhoff, J. C. (1972). Computation of combined refraction-diffraction. 13th International Conference on Coastal Engineering, (pp. 471-490). ASCE.

Beven J. (2019). Hurricane Pablo tropical cyclone report, NHC-NOAA.

Bidlot J. R. (2016). Twenty-one years of wave forecast verification. ECMWF Newsletter, 150, 2016.

Booij, N., Ris, R., and Holthuijsen, Leo. (1999). A third-generation wave model for coastal regions, Part I, Model description and validation. *Journal of Geophysical Research: Ocean,* 104. 7649-7656, https://doi.org/10.1029/98JC02622

Breivik, L-A., Reistad, M., Schyberg, H., Sunde, J., Krogstad, H. E., and Johnsen, H. (1998). Assimilation of ERS SAR wave spectra in an operational wave model. *Journal of Geophysical Research: Ocean,* 103, 7887-7900, https://doi.org/10.1029/97JC02728

Breivik, Ø., Gusdal, Y., Furevik, B.R., Aarnes, O.J., Reistand, M. (2009). Nearshore wave forecasting and hindcasting by dynamical and statistical downscaling. *Journal of Marine Systems,* 78, S235-S243, https://doi.org/10.1016/j.jmarsys.2009.01.025

Breivik, Ø., Mogensen, K., Bidlot, J.-R., Balmaseda, M. A., and Janssen, P. A. E. M. (2015), Surface wave effects in the NEMO ocean model: Forced and coupled experiments. *Journal of Geophysical Research: Ocean,* 120, 2973-2992, https://doi.org/10.1002/2014JC010565

Brocchini, M. (2013). A reasoned overview on Boussinesq-type models: the interplay between physics, mathematics and numerics. *Proceedings of the Royal Society A Mathematical, Physics and Engineering Science,* 469, https://doi.org/10.1098/rspa.2013.0496

Browne, M., Castelle, B., Strauss, D., Tomlinson, R., Blumenstein, M., Lane, C. (2007). Near-shore swell estimation from a global wind–wave model: spectral process, linear and artificial neural network models. *Coastal Engineering,* 54, 445-460, https://doi.org/10.1016/j.coastaleng.2006.11.007

Bunney, C., and Saulter, A. (2015). An ensemble forecast system for prediction of Atlantic-UK wind waves. *Ocean Modelling,* 96(1), 103-116, doi: 10.1016/j.ocemod.2015.07.005

Dean, R. G., Dalrymple, R. A. (1991). Water wave mechanics for engineers and scientists (Advanced series on ocean engineering - Volume 2), Singapore World Scientific Publishing.

Camus, P., Mendez, F., Medina, R. (2011). A hybrid efficient method to downscale wave climate to coastal areas. *Coastal Engineering,* 58(9), 851-862, https://doi.org/10.1016/j.coastaleng.2011.05.007

Camus, P., Mendez, F.J., Medina, R., Tomas, A., Izaguirre, C. (2013). High resolution downscaled ocean waves (DOW) reanalysis in coastal areas. *Coastal Engineering,* 72, 56-68, https://doi.org/10.1016/j.coastaleng.2012.09.002

Cavaleri, L., Alves, J.-H.G.M., Ardhuin, F., Babanin, A., Banner, M., Belibassakis, K., Benoit, M., Donelan, M., Groeneweg, J., Herbers, T.H.C., Hwang, P., Janssen, P.A.E.M., Janssen, T., Lavrenov, I.V., Magne, R., Monbaliu, J., Onorato, M., Polnikov, V., Resio, D., Rogers, W.E., Sheremet, A., McKee Smith, J., Tolman, H.L., van Vledder, G., Wolf, J., Young, I. (2007). Wave modeling - the state of the art. *Progress in Oceanography,* 75(4), 603-674, https://doi.org/10.1016/j.pocean.2007.05.005

Cavaleri, L., Abdalla, S., Benetazzo, A., Bertotti, L., Bidlot, J.-R., Breivik, Ø., Carniel, S., Jensen, R.E., Portilla-Yandun, J., Rogers, W.E., Roland, A., Sanchez-Arcilla, A., Smith, J.M., Staneva, J., Toledo, Y., van Vledder, G.Ph., and van der Westhuysen, A.J. (2018). Wave modelling in coastal and inner seas. *Progress in Oceanography,* 167, 164-233, https://doi.org/10.1016/j.pocean.2018.03.010

CERC, (1984). Shore Protection Manual. Department of the Army US. Army Corps of Engineers, Washington DC.

Chalikov, D. (2016). Numerical Modeling of Sea Waves. Springer, 330 p.

Chelton, D. B., and McCabe, P. J. (1985). A review of satellite altimeter measurement of sea surface wind speed: with a proposed new algorithm. *Journal of Geophysical Research: Oceans,* 90(3), 4707-4720, https://doi.org/10.1029/JC090iC03p04707

Chen, H.S. (2006). Ensemble Prediction of Ocean Waves at NCEP. Proceedings of 28th Ocean Engineering Conference, Taiwan.

Climate Change Initiative Coastal Sea Level Team (The). (2020). Coastal sea level anomalies and associated trends from Jason satellite altimetry over 2002-2018. *Scientific Data,* 7, 357, https://doi.org/10.1038/s41597-020-00694-w

Dean, R. G., and Dalrymple, R. A. (1991). Water wave mechanics for engineers and scientists. In: "Advanced Series on Ocean Engineering: Volume 2" by R.G. Dean and R.A. Dalrymple, World Scientific Publishing Co Pte Ltd, https://doi.org/10.1142/1232

Derkani, M. H., Alberello, A., Nelli, F., Bennetts, L.G., Hessner, K. G., MacHutchon, K., Reichert, L., Aouf, L., Khan, S., Toffoli, A. (2021). Wind, waves, and surface currents in the Southern Ocean: observations from the Antarctic Circumnavigation Expedition. *Earth System Science Data,* 13, 1189-1209, https://doi.org/10.5194/essd-13-1189-2021

Dingemanns, M. (1997). Waterwave propagation over uneven bottoms. *Advanced Series on Ocean Engineering,* 13(2), 967.

Donelan, M., Haus, B.K., Reul, N., Plant, W., Stiassnie, M., Graber, H.C., Brown, O., Saltzman, E. (2004). On the limiting aerodynamic roughness of the ocean in very strong winds. Geophysical Research Letters, 31(18), https://doi.org/10.1029/2004GL019460

Durrant, T.H., Woodcock F., and Greenslade, D.J.M. (2009). Consensus forecasts of modelled wave parameters. *Weather and Forecasting,* 24, 492-503, https://doi.org/10.1175/2008WAF2222143.1

Ebert, E. (2001). Ability of a poor man's ensemble to predict the probability and distribution of precipitation. *Monthly Weather Review,* 129(10), 2461–2480, https://doi.org/10.1175/1520-0493(2001)129<2461:AOAPMS>2.0.CO;2

Ebert, E.E. (2008). Fuzzy verification of high resolution gridded forecasts: A review and proposed framework. *Meteorological Applications,* 15, 51-64, https://doi.org/10.1002/met.25

Eckart, C. (1952). The propagation of gravity waves from deep to shallow water. *Circular 20, National Bureau of Standards,* 165-173.

Edson, J.B., Jampana, V., Weller, R.A., Bigorre, S.P., Plueddemann, A.J., Fairall, C.W., Miller, S.D., Mahrt, L., Vickers, D., and Hersbach, H. (2013). On the exchange of momentum over the open ocean. *Journal of Physical Oceanography,* 43(8), 1589-1610, https://doi.org/10.1175/JPO-D-12-0173.1

Fengyan, S., Kirby, J. T., Tehranirad, B., Harris, J. C., and Grilli, S. (2012). FUNWAVE-TVD: Fully Nonlinear Boussinesq Wave Model with TVD Solver. Documentation and User's Manual (Version 2.0). Center for Applied Coastal Research, University of Delaware, Newark, DE. Available at: https://www1.udel.edu/kirby/papers/shi-etal-cacr-11-04-version2.0.pdf

Gaslikova, L., Weisse, R. (2006). Estimating near-shore wave statistics from regional hindcasts using downscaling techniques. *Ocean Dynamics,* 56, 26-35, https://doi.org/10.1007/s10236-005-0041-2

Greenslade, D.J.M. and Young, I.R. (2004). Background errors in a global wave model determined from altimeter data. *Journal of Geophysical Research: Oceans,* 109(C9), https://doi.org/10.1029/2004JC002324

González-Marco, D., Sierra, J. P., Ybarra, O. F., Sánchez-Arcilla, A. (2008). Implications of long waves in harbour management: The Gijón port case study. *Ocean & Coastal Management,* 51(2), 180-201, https://doi.org/10.1016/j.ocecoaman.2007.04.001

Groeneweg, J., Ledden, M., Zijlema, M. (2007). Wave transformation in front of the Dutch Coast. Proceedings of the Coastal Engineering Conference, 552-564, https://doi.org/10.1142/9789812709554_0048

Gulev, S. K., Grigorieva, V., Sterl, A., and Woolf, D. (2003). Assessment of the reliability of wave observations from voluntary observing ships: Insights from the validation of a global wind wave climatology based on voluntary observing ship data. *Journal of Geophysical Research: Oceans,* 108(C7), https://doi.org/10.1029/2002JC001437

Hanley, K.E., Belcher, S.E., and Sullivan, P.P. (2010). A global climatology of wind-wave interaction. *Journal of Physical Oceanography,* 40, 1263-1282, https://doi.org/10.1175/2010JPO4377.1

Hanson, J. L., Phillips, O. M. (2001). Automated Analysis of Ocean Surface Directional Wave Spectra. *Journal of Atmospheric and Oceanic Technology,* 18(2), 277-293, https://doi.org/10.1175/1520-0426(2001)018<0277:AAOOSD>2.0.CO;2

Hansom, J. et al. (2015). Extreme Waves: Causes, Characteristics and Impact on Coastal Environments and Society January 2015. In: "Coastal and Marine Hazards, Risks, and Disasters", Edition: Hazards and Disasters Series, Elsevier Major Reference Works, Chapter 11: Extreme Waves: Causes, Characteristics and Impact on Coastal Environments and Society. Publisher: Elsevier; Editors: Ellis, J and Sherman, D. J.

Hasselmann, K. (1962). On the non-linear energy transfer in a gravity-wave spectrum part 1. General theory. *Journal of Fluid Mechanics,* 12 (4), 481-500.

Hasselmann, K., Barnett, T. P., Bouws, E., Carlson, H., Cartwright, D. E., Enke, K., Ewing, J. A.,Gienapp, H., Hasselmann, D. E., Kruseman, P., Meerburg, A., Müller, P., Olbers, D. J., Richter, K., Sell, W. and Walden, H. (1973). Measurements of wind-wave growth and swell decay during the Joint North Sea Wave Project (JONSWAP). *Hydraulic Engineering Reports,*. Available at: https://repository.tudelft.nl/islandora/object/uuid%3Af204e188-13b9-49d8-a6dc-4fb7c20562fc

Hasselmann, K., Hasselmann, K., Bauer, E., Janssen, P., Komen, G., Bertotti, L., Lionello, P., Guillaume, A., Cardone, V., Greenwood, J., Reistad, M., Zambresky, L., Ewing, J. (1988). The WAM model - a third generation ocean wave prediction model. *Journal of Physical Oceanography,* 18, 1775-1810.

Hasselmann, S., Hasselmann, K., Allender, J. H., and Barnett, T. P. (1985). Computations and parameterizations of the nonlinear energy transfer in a gravity wave spectrum, II, Parameterizations of the nonlinear energy transfer for application in wave models. *Journal of Physical Oceanography,* 15, 1378-1391.

Hasselmann, K. (1997). Multi-pattern fingerprint method for detection and attribution of climate change. *Climate Dynamics,* 13, 601-611, https://doi.org/10.1007/s003820050185

Hasselmann, K., Chapron, B., Aouf, L., Ardhuin, F., Collard, F., Engen, G., Hasselmann, S., Heimbach, P., Janssen, P., Johnsen, H., et al. (2013). The ERS SAR wave mode: A breakthrough in global ocean wave observations. In: "ERS Missions: 20 Years of Observing Earth", 1st ed.; Fletcher, K., Ed.; European Space Agency: Noordwijk, The Netherlands, 2013; pp. 165-198.

Herman, A., Kaiser, R., Niemeyer, H.D. (2009). Wind-wave variability in shallow tidal sea - spectral modelling combined with neural network methods. *Coastal Engineering,* 56(7), 759-772, https://doi.org/10.1016/j.coastaleng.2009.02.007

Hersbach H. (2000). Decomposition of the continuous ranked probability score for ensemble prediction systems. *Weather and Forecasting,* 5(15), 1697-1709, https://doi.org/10.1175/WAF-D-16-0164.1

Hewitt, J. E, Cummings, V. J., Elis, J. I., Funnell, G., Norkko, A., Talley, T.S., Thrush, S.F. (2003). The role of waves in the colonisation of terrestrial sediments deposited in the marine environment. *Journal of Experimental Marine Biology and Ecology,* 290, 19-47, https://doi.org/10.1016/S0022-0981(03)00051-0

Higuera, P., Lara, L. J., Losada, I.J. (2014a). Three-dimensional interaction of waves and porous coastal structures using OpenFOAM®. Part I: Formulation and validation. *Coastal Engineering,* 83, 243-258, https://doi.org/10.1016/j.coastaleng.2013.08.010

Higuera, P., Lara, L. J., Losada, I.J. (2014b). Three-dimensional interaction of waves and porous coastal structures using OpenFOAM®. Part II: Application. *Coastal Engineering,* 83, 259-270, https://doi.org/10.1016/j.coastaleng.2013.09.002

Holthuijsen, L.H. (2007). Waves in Oceanic and Coastal Waters. Cambridge University Press, https://doi.org/10.1017/CBO9780511618536

Iafrati, A., Babanin, A.V., Onorato, M. (2013). Modulational instability, wave breaking and formation of large scale dipoles. *Physical Review Letters,* 110, 184504, :https://doi.org/10.1103/PhysRevLett.110.184504

Janssen, P.A.E.M (1989). Wave-induced stress and the drag of air flow over sea waves. *Journal of Physical Oceanography,* 19(6), 745-754, https://doi.org/10.1175/1520-0485(1989)019<0745:WISATD>2.0.CO;2

Janssen, P.A.E.M (1991). Quasi-linear theory of wind wave generation applied to wave forecasting. *Journal of Physical Oceanography,* 21, 1631-1642.

Janssen, P.A.E.M. (2004). The Interaction of Ocean Waves and Wind. Cambridge University Press, 308 p.

Janssen, P.A.E.M. (2012). Ocean wave effects on the daily cycle in SST. J*ournal of Geophysical Research: Oceans,* 117, C00J32, https://doi.org/10.1029/2012JC007943

Janssen, P.A.E.M., Lionello, P., Reistad, M. and Hollingsworth, A. (1989). Hindcasts and data assimilation studies with the WAM model during the Seasat period. *Journal of Geophysical Research: Oceans,* C94, 973-993.

Janssen, P.A.E.M., Abdalla, S., Hersbach, H., Bidlot, J.R. (2007). Error estimation of buoy, satellite, and model wave height data. Journal of Atmospheric and Oceanic Technology, 24:1665-1677, https://doi.org/10.1175/JTECH2069.1

Kalra, R., Deo, M.C., Kumar, R., Agarwal, V.K. (2005). Artificial neural network to translate offshore satellite waves to data to coastal locations. *Ocean Engineering,* 32, 1917-1932, https://doi.org/10.1016/j.oceaneng.2005.01.007

Kirby, J., Dalrymple, R. (1983). Propagation of weakly nonlinear surface waves in the presence of varying depth and current. In: Proceedings of the 20th Congress, Int. Assoc. Hydraul. Res.(IAHR), Moscow, 1983, Paper S.1.5.3, pp. 198-202.

Komen, G.J., Hasselmann, K., and Hasselmann, S. (1984). On the existence of a fully developed windsea spectrum. *Journal of Physical Oceanography,* 14, 1271-1285.

Koutitas, C. G. (1990). Mathematical models in coastal engineering. *Applied Ocean Research,* 12(1), 52, https://doi.org/10.1016/S0141-1187(05)80022-7

Kudryavtsev, V.N., Makin, V.K., and Meirink, J.F. (2001). Simplified model of air flow above the waves. *Boundary Layer Meteorology,* 100, 63-90, https://doi.org/10.1023/A:1018914113697

Lalaurette, F. (2003). Early detection of abnormal weather conditions using a probabilistic extreme forecast index. *Quarterly Journal of the Royal Meteorological Society,* 129, 3037-3057, https://doi.org/10.1256/qj.02.152

Lara, J.L., Garcia, N., Losada, I.J. (2006). RANS modelling applied to random wave interaction with submerged permeable structures. *Coastal Engineering,* 53(5-6), 395-417, https://doi.org/10.1016/j.coastaleng.2005.11.003

Law Chune, S., Aouf, L. (2018). Wave effects in global ocean modeling: parametrizations vs. forcing from a wave model. *Ocean Dynamics,* 68, 1739-1758, https://doi.org/10.1007/s10236-018-1220-2

Le Traon, P.Y., Reppucci, A., Alvarez Fanjul, E., Aouf, L., Behrens, A., Belmonte, M., Bentamy, A., Bertino, L., Brando, V.E., Kreiner, M.B., Benkiran, M., Carval, T., Ciliberti, S.A., Claustre, H., Clementi, E., Coppini, G., Cossarini, G., De Alfonso Alonso-Muñoyerro, M., Delamarche, A., Dibarboure, G., Dinessen, F., Drevillon, M., Drillet, Y., Faugere, Y., Fernández, V., Fleming, A., Garcia-Hermosa, M.I., Sotillo, M.G., Garric, G., Gasparin, F., Giordan, C., Gehlen, M., Gregoire, M.L., Guinehut, S., Hamon, M., Harris, C., Hernandez, F., Hinkler, J.B., Hoyer, J., Karvonen, J., Kay, S., King, R., Lavergne, T., Lemieux-Dudon, B., Lima, L., Mao, C., Martin, M.J., Masina, S., Melet, A., Buongiorno Nardelli, B., Nolan, G., Pascual, A., Pistoia, J., Palazov, A., Piolle, J.F., Pujol, M.I., Pequignet, A.C., Peneva, E., Pérez Gómez, B., Petit de la Villeon, L., Pinardi, N., Pisano, A., Pouliquen, S., Reid, R., Remy, E., Santoleri, R., Siddorn, J., She, J., Staneva, J., Stoffelen, A., Tonani, M., Vandenbulcke, L., von Schuckmann, K., Volpe, G., Wettre, C.. and Zacharioudaki, A. (2019). From Observation to Information and Users: The Copernicus Marine Service Perspective. Frontiers in Marine Science, 6, 23, https://doi.org/10.3389/fmars.2019.00234

Lin, P. (2008). Numerical modeling of water waves (1st ed.). New York: Taylor and Francis.

Lionello, P., Gunther, H., and Janssen, P.A.E M. (1992). Assimilation of altimeter data in a global third generation wave model. *Journal of Geophysical Research: Oceans,* C97, 14453-14474, https://doi.org/10.1029/92JC01055

Madsen, P. A., and Larsen, J. (1987). An efficient finite-difference approach to the mild-slope equation. Coastal Engineering, 11, 329-351, https://doi.org/10.1016/0378-3839(87)90032-9

Marti F., Cazenave, A., Birol, F., Passaro, M., Léger, F., Niño, F., Almar, R., Benveniste, J., Legeais, J.F. (2021). Altimetry-based sea level trends along the coasts of Western Africa. *Advances in Space Research,* 68(2), 504-522, https://doi.org/10.1016/j.asr.2019.05.033

Maza, M., Lara, J. L., Losada, I. J. (2016). Solitary wave attenuation by vegetation patches. *Advances in Water Resources,* 98, 159-172, https://doi.org/10.1016/j.advwatres.2016.10.021

McCowan, J. (1894). On the Highest Waves of a Permanent Type. *Philosophical Magazine,* Edinburgh 38, 351-358.

Losada, I.J., Lara, J.L., Guanche, R., Gonzalez-Ondina, J.M. (2008). Numerical analysis of wave over-topping of rubble mound breakwaters. Coastal Engineering, 55, 47-62, https://doi.org/10.1016/j.coastaleng.2007.06.003

Mitsuyasu, H. (1970). On the growth of the spectrum of wind-generated waves. *Coastal Engineering in Japan,* 13(1), 1-14, https://doi.org/10.1080/05785634.1970.11924105

Mittermaier M. P., Csima, G. (2017). Ensemble versus deterministic Performance at kilometric scale. *Weather and Forecasting,* 32(5), https://doi.org/10.1175/WAF-D-16-0164.1

Molteni, F., Buizza, R., Palmer, T.N., Petroliagis, T. (1996). The ECMWF ensemble prediction system: methodology and validation. *Quarterly Journal of the Royal Meteorological Society,* 122(529), 73-119, https://doi.org/10.1002/qj.49712252905

Munk, W. H. (1950). Origin and generation of waves. *Coastal Engineering Proceedings,* 1, https://doi.org/10.9753/icce.v1.1

National Centers for Environmental Prediction (2012). Output fields from the NOAA WAVEWATCH III® wave model monthly hindcasts. NOAA National Centers for Environmental Information. Dataset.

Parkinson, C. L., and Cavalieri, D. J. (2012). Antarctic Sea ice variability and trends, 1979-2010. *The Cryosphere,* 6, 881–889, https://doi.org/10.5194/tc-6-881-2012

Pérez, B., Álvarez Fanjul, E., Pérez, S., de Alfonso, M., Vela, J. (2013). Use of tide gauge data in operational oceanography and sea level hazard warning systems, *Journal of Operational Oceanography,* 6(2), 1-18, https://doi.org/10.1080/1755876X.2013.11020147

Perez, J., Menendez, M., and Losada, I. J. (2017). GOW2: A global wave hindcast for coastal applications. *Coastal Engineering,* 124, 1-11, https://doi.org/10.1016/j.coastaleng.2017.03.005

Petroliagis, T.I., and Pinson, P. (2012). Early warnings of extreme winds using the ECMWF Extreme Forecast Index. *Meteorological Applications,* 21(2), 171-185, https://doi.org/10.1002/met.1339

Pezzutto P., Saulter A., Cavaleri L., Bunney, C., Marcucci, F., Sebastianelli, S. (2016). Performance comparison of meso-scale ensemble wave forecasting systems for Mediterranean Sea states. *Ocean Modelling,* 104, 171-186, https://doi.org/10.1016/j.ocemod.2016.06.002

Rascle N., Ardhuin, F., Queffeulou, P., Croizé-Fillon, D. (2008). A global wave parameter database for geophysical applications. Part 1: Wave-current–turbulence interaction parameters for the open ocean based on traditional parameterizations. *Ocean Modelling,* 25(3-4), 154-171, doi:10.1016/j.ocemod.2008.07.006

Reguero, B.G., Menéndez, M., Méndez, F.J., Mínguez, R., Losada, I.J. (2012). A global Ocean Wave (GOW) calibrated reanalysis from 1948 onwards. *Coastal Engineering,* 65, 38-55, https://doi.org/10.1016/j.coastaleng.2012.03.003

Ribal, A., Young, I.R. (2019). 33 years of globally calibrated wave height and wind speed data based on altimeter observations. *Scientific Data,* 6, 77, https://doi.org/10.1038/s41597-019-0083-9

Rusu, L., Pilar, P., Guedes Soares, C. (2008). Hindcast of the wave conditions along the west Iberian coast. *Coastal Engineering,* 55(11), 906-919, https://doi.org/10.1016/j.coastaleng.2008.02.029

Saetra, O., and Bidlot, J.-R. (2004). Potential benefit of using probabilistic forecasts for waves and marine winds based on the ECMWF ensemble prediction system. *Weather and Forecasting,* 19(4), 673-689, https://doi.org/10.1175/1520-0434(2004)019<0673:PBOUPF>2.0.CO;2

Saha, S., Moorthi, S., Pan, H.-L., Wu, X., Wang, J., Nadiga, S., … Goldberg, M. (2010). The NCEP Climate Forecast System Reanalysis. *Bulletin of the American Meteorological Society,* 91(8), 1015-1057, https://doi.org/10.1175/2010BAMS3001.1

Saulter A. N., Bunney, C., King, R., Water, J. (2020). An Application of NEMOVAR for Regional Wave Model Data Assimilation, Frontiers in Marine Science, 7, 579834, https://doi.org/10.3389/fmars.2020.579834

Shapiro, R. (1970). Smoothing filtering and boundary effects. *Reviews of Geophysics,* 8(2), 359-387, https://doi.org/10.1029/RG008i002p00359

State of the Global Climate 2020 (WMO-No. 1264).

Staneva, J., Alari, V., Breivik, Ø. et al. (2017). Effects of wave-induced forcing on a circulation model of the North Sea. *Ocean Dynamics,* 67, 81-101, https://doi.org/10.1007/s10236-016-1009-0

Staneva, J., Grayek, S., Behrens, A., and Günther, H. (2021). GCOAST: skill assessments of coupling wave and circulation models (NEMO-WAM). Journal of Physics: Conference Series, 1730, 012071. doi:10.1088/1742-6596/1730/1/012071

Stansby, P., Zhou, J., Kuang, C., Walkden, M., Hall, J., Dickson, M. (2007). Long-term prediction of nearshore wave climate with an application to cliff erosion. In: McKee Smith, Jane (Ed.), Proc. of International Conference Coastal Engineering, ASCE, pp. 616-627.

Stopa, J.E. (2018). Wind forcing calibration and wave hindcast comparison using multiple reanalysis and merged satellite wind datasets. *Ocean Modelling,* 127, 55-69, https://doi.org/10.1016/j.ocemod.2018.04.008

Swail, V., Jensen, R., Lee, B., Turton, J., Thomas, J., Gulev, S., Yelland, M., Etala, P., Meldrum, D., Birkemeier, W., Burnett, W., Warren, G. (2010). Wave Measurements, Needs and Developments for the Next Decade. Proceedings of OceanObs'09: Sustained Ocean Observations and Information for Society Conference (Volume 2), Venice, Italy, 21-25 September 2009 (J. Hall, D.E. Harrison and D. Stammer, eds.). ESA Publication WPP-306.

Thomson, J., Ackley, S., Girard-Ardhuin, F., Ardhuin, F., Babanin, A.V., Boutin, G., Brozena, J., Cheng, S., Collins, C., Doble, M., Fairall, C., Guest, P., Gebhardt, C., Gemmrich, J., Graber, H.C., Holt, B., Lehner, S., Lund, B., Meylan, M.H., Maksym, T., Montiel, F., Perrie, W., Persson, O., Rainville, L., Rogers, W.E., Shen, H., Shen, H., Squire, V., Stammerjohn, S., Stopa, J., Smith, M.M., Sutherland, P., Wadhams, P. (2018). Overview of the Arctic Sea State and Boundary Layer Physics Program. *Journal of Geophysical Research: Oceans,* 123(12), 8674-8687, https://doi.org/10.1002/2018JC013766

Tolman, H. L. (1989). The numerical model WAVEWATCH: a third generation model for the hindcasting of wind waves on tides in shelf seas. *Communications on Hydraulic and Geotechnical Engineering,* Delft Univ. of Techn., ISSN 0169-6548, Rep. no. 89-2, 72 pp.

Tolman, H.L. (2010). WAVEWATCH III development best practices. Camp Springs.

Tolman H.L., and the WAVEWATCH III® Development Group (2014). User Manual and System Documentation of WAVEWATCH III® version 4.18. Technical Note 316, NOAA/NWS/NCEP/MMAB. Available at: https://polar.ncep.noaa.gov/waves/wavewatch/manual.v4.18.pdf

Thomas, A., Mendez, F. J., and Losada, I. J. (2008). A method for spatial calibration of wave hindcast data bases. *Continental Shelf Research,* 28(3), 391-398, https://doi.org/10.1016/j.csr.2007.09.009

Trulsen, K. C., Nieto Borge, J., Gramstad, O., Aouf, L., and Lefèvre, J.-M. (2015). Crossing sea state and rogue wave probability during the Prestige accident. *Journal of Geophysical Research: Oceans,* 120, 7113-7136, https://doi.org/10.1002/2015JC011161

.Tsagareli, K.N., Babanin, A.V., Walker, D.J., and Young, I.R. (2010). Numerical investigation of spectral evolution of wind waves. Part 1. Wind input source function. *Journal of Physical Oceanography,* 40(4), 656-666, https://doi.org/10.1175/2009JPO4370.1

Tsay, T. K., Zhu, W., and Liu, P. L.-F. (1989) A finite element model for wave refraction, diffraction, reflection and dissipation. *Applied Ocean Research,* 11, 33-38, https://doi.org/10.1016/0141-1187(89)90005-9

Van der Meer, J., Allsop, W., Bruce, T., Rouck, J., Kortenhaus, A., Pullen, T., Schüttrumpf, H., Troch, P., Zanuttigh, B. (2016). EurOtop: Manual on wave overtopping of sea defences and related structures - An overtopping manual largely based on European research, but for worldwide application, 2nd edition.

Van der Ven, P., Reijmerink, B., Van der Hout, A., De Jong, M. (2018). Comparison of Validation Studies of Wave - Penetration Models using Open Benchmark Datasets of Deltares, PIANC World Congress 2018, At Panama City, Panama.

Veron, F. (2015). Ocean spray. Annual Review of Fluid Mechanics, 47, 507-538, https://doi.org/10.1146/annurev-fluid-010814-014651

Visbeck, M. (2018). Ocean science research is key for a sustainable future. *Nature Communication,* 9, 690, https://doi.org/10.1038/s41467-018-03158-3

Voorrips, A. C., Makin V. K., and Hasselmann S. (1997). Assimilation of wave spectra from pitch-and-roll buoys in a North Sea wave model. *Journal of Geophysical Research: Oceans,* 102, 5829-5849, https://doi.org/10.1029/96JC03242

WAMDI group (The) (1988). The WAM Model - A Third Generation Ocean Wave Prediction Model. *Journal of Physical Oceanography,* 18, 1775-1810, https://doi.org/10.1175/1520-0485(1988)018<1775:TWMTGO>2.0.CO;2

Wang, J. K., Aouf, L., Dalphinet, A., Zhang, Y. G., Xu, Y., Hauser, D., Liu, J. Q. (2021). The Wide Swath Significant Wave Height: An Innovative Reconstruction of Significant Wave Heights From CFOSAT's SWIM and Scatterometer Using Deep Learning. *Geophysical Research Lettera,* 48(6), https://doi.org/10.1029/2020GL091276

Wilby, R. and Dessai, S. (2010). Robust adaptation to climate change. *Weather,* 65, 180-185, https://doi.org/10.1002/wea.543

Young, I.R. (1999). Wind Generated Ocean Waves, Elsevier, Amsterdam, 288 p.

Zakharov, V.E. (1968). Stability of periodic waves of finite amplitude on the surface of a deep fluid. *Journal of Applied Mechanics and Technical Physics,* 9(2), 190-194

Zieger, S., Greenslade, D.J.M., and Kepert, J.D. (2018). Wave ensemble forecast system for tropical cyclones in the Australian region. *Ocean Dynamics,* 68(4-5):603-625, https://doi.org/10.1007/s10236-018-1145-9

Zijlema, M. (2009). Parallel, unstructured mesh implementation for SWAN. Proceedings of the Coastal Engineering Conference. 470-482, https://doi.org/10.1142/9789814277426_0040

Zijlema, M., Stelling, G., and Smit, P. (2011). SWASH: An operational public domain code for simulating wave fields and rapidly varied flows in coastal waters. *Coastal Engineering,* 58, 992-1012, https://doi.org/10.1016/j.coastaleng.2011.05.015

9.
Biogeochemical modelling

CHAPTER COORDINATOR

Elodie Gutknecht

CHAPTER AUTHORS *(in alphabetical order)*

Laurent Bertino, Pierre Brasseur, Stefano Ciavatta, Gianpiero Cossarini, Katja Fennel, David Ford,

Marilaure Grégoire, Diane Lavoie, and Patrick Lehodey

9. Biogeochemical modelling
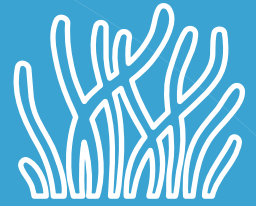
9.1. General introduction to Biogeochemical models

9.1.1. Objective, applications and beneficiaries

9.1.2. Fundamental theoretical background

9.1.2.1. Biogeochemical modelling

9.1.2.2. Model calibration

9.1.2.3. Physical-Biogeochemical coupling

9.1.2.4. From open ocean to coastal ecosystems

9.1.2.5. Potential predictability of ocean biogeochemistry

9.2. Biogeochemical forecast and multi-year systems

9.2.1. Architecture singularities

9.2.1.1. Physical, optical, and biogeochemical components

9.2.1.2. Propagation of uncertainties

9.2.1.3. BGC Data singularities

9.2.2. Input data: available sources and data handling

9.2.2.1. Physical conditions

9.2.2.2. Observational data

9.2.2.3. Climatologies, databases, and atlases

9.2.2.4. Atmospheric surface forcing

9.2.2.5. External inputs

9.2.2.6. Units

9.2.3. Modelling component

9.2.3.1. Numerical and discretisation choices

9.2.3.2. The different biogeochemical models

9.2.3.3. Connections Ocean-Earth systems

9.2.4. Ensemble modelling

9.2.5. Data assimilation systems

9.2.5.1. Biogeochemical state and parameter estimation

9.2.5.2. Assimilated observational products

9.2.5.3. Biogeochemical data assimilation methods

9.2.5.4. Current challenges and opportunities

Summary

Marine biogeochemistry is the study of essential chemical elements in the ocean (such as carbon, nitrogen, oxygen, and phosphorus), and of their interactions with marine organisms. Biogeochemical cycles are driven by physical transport, chemical reactions, absorption, and transformation by plankton and other organisms, which form the basis of the oceanic food web.

In the last decades, the interest for this cross-disciplinary science has greatly increased due to the occurrence of significant changes in the marine environment closely linked to the alteration of the biogeochemical cycles in the ocean. These alterations include phenomena such as acidification, coral bleaching, eutrophication, deoxygenation, harmful algal blooms, regime shifts in plankton, invasive species, and other processes deteriorating water quality and impacting the whole marine ecosystem.

Monitoring and forecasting the biogeochemical and ecosystem components of the ocean, also referred to as "Green Ocean", are essential for a better understanding of the current status and changes in ocean health and ecosystem functioning. Such operational systems provide indicators useful to scientists, industry (e.g. fisheries and aquaculture), policy makers and environmental agencies for the prediction of events, the management of living marine resources, and can support the decision-making process to respond to environmental changes.

This chapter gives an overview of the Green Ocean component of OOFS. The first section addresses the objectives, applications and beneficiaries of the Green Ocean and introduces the fundamental theoretical knowledge of marine biogeochemical modelling. The second section details and discusses each component of a biogeochemical OOFS to guide new forecasters in biogeochemistry. Modelling of higher trophic levels is introduced. Finally, several operational systems are mentioned as examples.

9.1.
General introduction to Biogeochemical models

9.1.1. Objective, applications and beneficiaries

Human activities, primarily the combustion of fossil fuels, cement production, and the industrial production of nitrogen-based fertilisers, are leading to ocean warming, acidification, deoxygenation, and coastal eutrophication, thus putting ever-increasing and compounding pressures on marine ecosystems (Figure 9.1).

At the same time, the ocean is serving as a major sink of carbon dioxide (CO_2), the most important anthropogenic greenhouse gas. This contributes to mitigating global warming, but the magnitude of this sink is likely to diminish. Our ability to quantify these phenomena and project their future course hinges on a mechanistic understanding of the biogeochemical cycles of carbon, oxygen, and nutrients in the ocean and how they are changing.

The Marine BGC, the study of elemental cycles and their interactions with the environment and living organisms, is a multidisciplinary science at the crossroads between ocean physics, chemistry, and biology, and intersects with atmospheric and terrestrial sciences as well as social science and environmental policy. As an example, Figure 9.2 illustrates the complex carbon cycle in the ocean and the interactions between biological, chemical, and physical processes.

Figure 9.1.   Threats on marine ecosystems. Changes and alterations in the marine environment observed in recent decades include acidification, coral bleaching, eutrophication, deoxygenation, harmful algal blooms, changes in planktonic regimes, invasive species, etc.
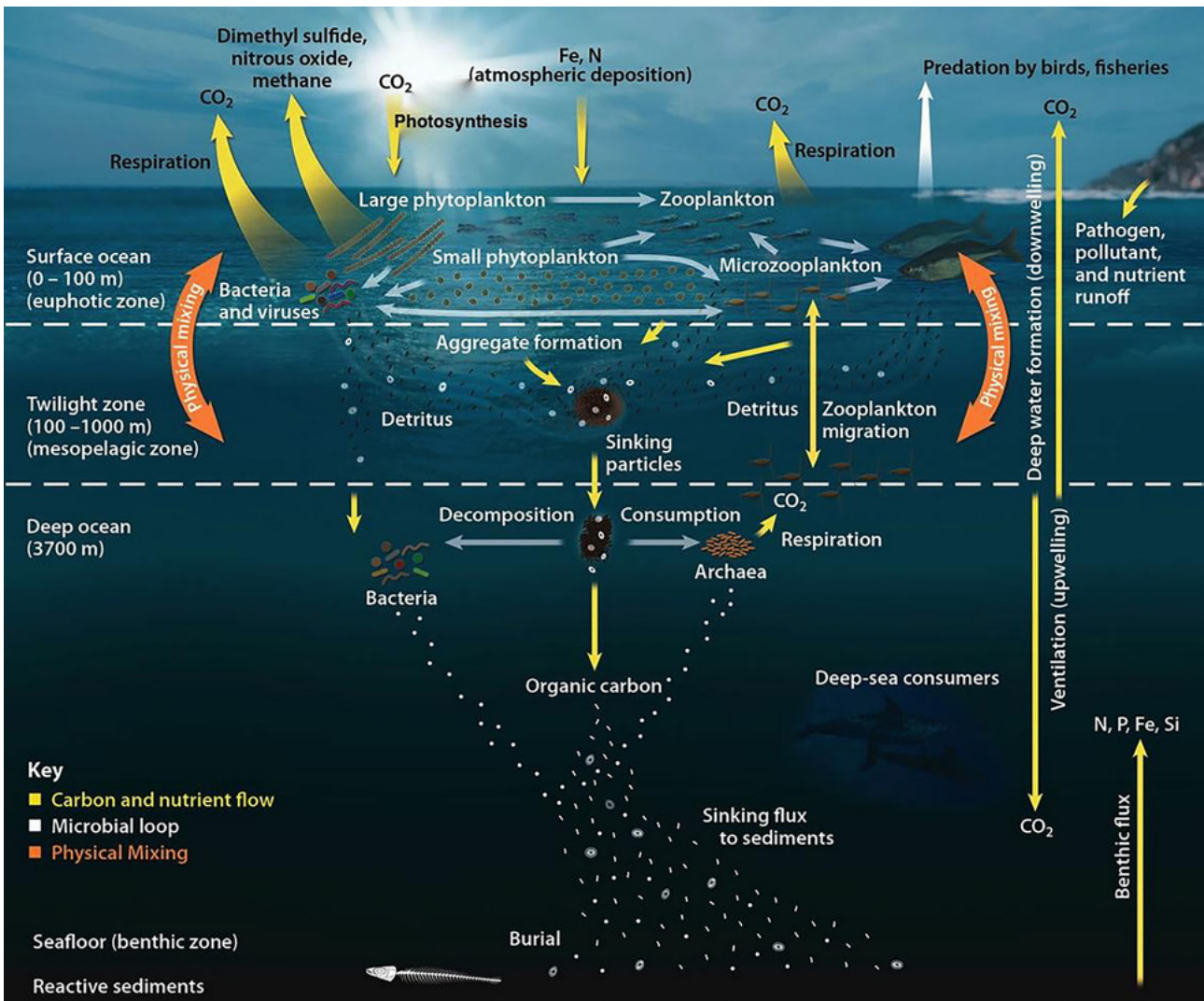
Figure 9.2. Cycling of carbon in the marine food chain. Phytoplankton assimilate CO2 via photosynthesis in the euphotic zone and are consumed by zooplankton. Zooplankton are the initial prey for many small and large aquatic organisms. Carbon is thus transferred further up the food web to higher-level predators. Different mechanisms contribute to the export and storage of carbon into the deep ocean. The carbon cycle in the ocean is complex and influenced by biological, chemical, and physical processes (credit: Oak Ridge National Laboratory at 🔗[1]).

Ocean BGC models describe the base of the marine food chain from bacteria to mesozooplankton and couple the cycles of carbon (C), nitrogen (N), oxygen (O2), phosphorus (P) and silicon (Si). They mostly focus on plankton, classifying the plankton diversity in accordance with their functional characteristics, the so-called Plankton Functional Types (PFTs). Species at higher trophic levels, such as fish and marine mammals play a lesser role in elemental cycling, they are thus generally not explicitly represented in BGC models, but they are very important for ecosystem models that focus on the ecology/biology of marine organisms. BGC and ecosystem models are sometimes referred to indistinctly because they can overlap in their representation of the lower trophic levels. Specific modelling approaches, like Lagrangian modelling, habitat modelling, or food web models, are used to connect BGC with the high trophic levels (e.g. fish).

The implementation of accurate OOFSs requires sustained, systematic, and NRT observation from (sub)mesoscale to large scale to initialise, parameterize, and validate ocean models. NRT information in operational oceanography means a description of the present situation with a delay of a few minutes to a few days.

1. https://www.ornl.gov/

The forecast of ocean physics has considerably improved in the last decades, reaching a high level of predictability (Chapter 5). The evolving equations governing the physical dynamics are based on physical laws, the model parameterizations are quite well-established, and the abundance of observations for temperature, salinity, and sea level height offers a way to improve model predictions through data assimilation. Forecasting of the Green Ocean has been developed more recently and it has not yet reached the same level of maturity, in most cases being incorporated into already existing physical OOFS. The formulation of ecosystem models is still empirical and the scarcity of in-situ biological and BGC data critically limits the capabilities to constrain their parameterization and to improve their performances through a robust data-model comparison exercise and data assimilation. The scarcity of data is even more critical in NRT, limiting data assimilation to surface chlorophyll-a (Chla) derived from satellite reflectance (Fennel et al., 2019).

The advent of in-situ robotic platforms combined with high resolution satellite products for the Green Ocean have the potential to palliate this deficiency. For instance, the advent of hyperspectral satellites is promising in terms of delivery of surface information on PFTs, detection of harmful algal blooms, and benthic habitat mapping, while the boost in robotic platforms will offer huge opportunities to map the (deep) seafloor with an unprecedented level of details. The combination of marine robotics, image analysis, machine learning, new sensor development, and the coordination of robotic platforms and satellite sensors will constitute a significant breakthrough in our knowledge of marine ecosystems. All this information would need to be integrated in models for forecasting and producing high quality reanalysis of the Green Ocean to support the production of added value products and innovative services. Coordination of Ocean OSSEs can help to design the new observing biological and biogeochemical systems with maximal impact to users, yet their development is still insufficient and should be encouraged (Le Traon et al., 2019).

Ultimately, BGC OOFS systems serve major environmental and societal issues, including the Ocean's role in the global carbon cycle and the impacts of natural changes and anthropogenic stressors in the physical-chemical marine environment on ecosystems and human activities. Applications range from multi-decadal retrospective simulations (namely, "reanalyses"), operational analysis of the current conditions ("nowcasts"), short-term and seasonal predictions ("forecasts"), scenario simulations, and climate change projections. These integrated systems are essential not only for a better understanding of the current status of key biogeochemical and ecosystem processes in the ocean and how they are changing, but also to provide stakeholders, policy makers and environmental agencies with indicators of ocean health in order to take appropriate mitigation, adaptation, conservation, and protection measures for living marine organisms and their habitats but also for human health.

"A predicted ocean whereby society has the capacity to understand current and future ocean conditions, forecast change and impact on human wellbeing and livelihoods" is an expected outcome of the United Nations Decade of Ocean Science for Sustainable Development, 2021-2030 (Ryabinin et al., 2019), supported also by the Sustainable Development Goals 14 (Life below water), 8 (Decent work and economic growth), and 9 (Industry, innovation and infrastructure).

9.1.2. Fundamental theoretical background

9.1.2.1. Biogeochemical modelling

Plankton (including phytoplankton and zooplankton) are organisms which are carried by tides and currents, or do not swim well enough to move against them. They form the base of the marine ecosystem and are a central component of the BGC models that simulate the cycling of elements through seawater and plankton.

Most models take an "NPZD" approach, simulating:

- Nutrients: substances which organisms require for growth.
- Phytoplankton: microscopic algae which obtain energy from sunlight through photosynthesis.
- Zooplankton: planktonic animals which obtain energy by eating other organisms.
- Detritus: dead and excreted organic matter.

Each of these is represented by one or more state variables, depending on the complexity of the model. Rather than considering individual organisms, state variables represent concentrations of elements such as nitrogen or carbon. They are often called tracers because they are transported and diffused by ocean dynamics.

As with physical models, BGC models are discretized on a grid covering the region of interest and require suitable initial and boundary conditions for each state variable. At each grid point, the evolution of a state variable C is given by the equation:

$$\frac{\partial C}{\partial t} = -\nabla \cdot (CU) + D^C + SMS(C) \qquad (9.1)$$

where $\nabla \cdot (CU)$ and D^C are the advection and diffusion terms equivalent to those used for temperature and salinity in physical models (please refer to Chapter 5). ∇ is the generalised derivative vector operator, t is the time, U the vector velocity, and D^C is the parameterization of small-scale physics for the tracer. The $SMS(C)$ stands for source-minus-sink terms for the tracer C and represents the BGC processes simulated by the model. Each 1D water column is normally treated independently, with lateral interactions limited to advection and diffusion. Most BGC models are formulated to conserve mass.
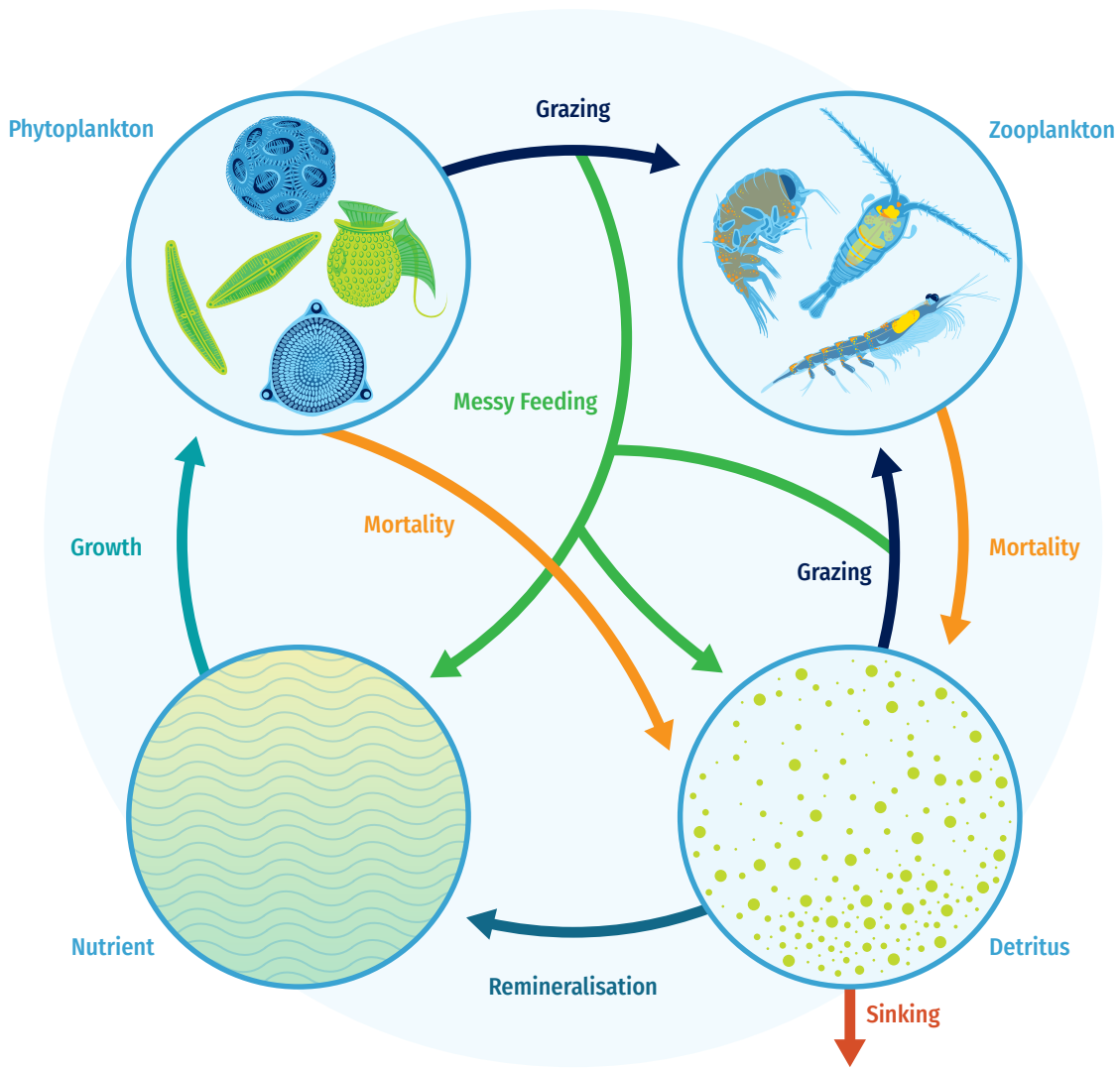
Figure 9.3.   Schematic of a basic NPZD model considering four state variables, one for each compartment.

Unlike the Navier-Stokes equations for physical models (Chapter 5), there is no known set of laws defining biological behaviour. Instead, empirical relationships are used to describe observed processes such as growth and mortality.

The basic source-minus-sink terms usually modelled in a NPZD model (Figure 9.3) are:

  • **Phytoplankton growth or Primary production**: the creation of organic matter through photosynthesis. It is a function of phytoplankton concentration, nutrient availability, and light availability. It can also be regulated by temperature.
  • **Grazing**: zooplankton eating phytoplankton and detritus.
  • **Mortality**: death through natural causes, e.g. viruses, predation by higher trophic levels (fish and marine mammals), etc.

  • **Messy feeding**: zooplankton graze inefficiently, and a proportion of organic matter enters the nutrient or detritus pool rather than being ingested by zooplankton.
  • **Remineralisation**: bacteria break down the organic matter in detritus, which is converted back to nutrients.
  • **Sinking**: detritus sinks through the water column due to gravity.

In this case, the differential equations for phytoplankton (P), zooplankton (Z), detritus (D), and nutrients (N) are as follows:

$$\frac{\partial P}{\partial t} = \mu_P P - G_P Z - m_P P \qquad (9.2)$$

where phytoplankton evolution depends on primary production, grazing and mortality;

$$\frac{\partial Z}{\partial t} = (\alpha_D + \alpha_N)(G_P + G_D)Z - m_Z Z \qquad (9.3)$$

where zooplankton evolution depends on grazing and mortality;

$$\frac{\partial D}{\partial t} = m_P P + m_Z Z - G_D Z$$
$$+ (1 - \alpha_D)(G_P + G_D)Z - rem_D D - w_D D$$

(9.4)

where detritus evolution depends on mortality, grazing, messy feeding, remineralisation and sinking;

$$\frac{\partial N}{\partial t} = \mu_P P + (1 - \alpha_N)(G_P + G_D)Z + rem_D D$$ (9.5)

where nutrients evolution depends on primary production, messy feeding, and remineralisation.

μ_P is the growth rate of phytoplankton due to photosynthesis; m_P and m_z are the mortality rates of phytoplankton and zooplankton; G_P and G_D are the grazing rates of zooplankton on phytoplankton and detritus; α_D and α_N represent the efficiency of the grazing; (1-α_D) and (1-α_N) the non-assimilated fractions of grazing by zooplankton that return to detritus and nutrients; rem_D is the remineralisation rate of detritus and w_D is the sinking speed of detritus.

The exact equations used differ between models, the ones given above are common examples. Other processes are often considered as well, notably respiration, excretion, and egestion, which cause loss of organic matter. Of course, additional processes may be included in more complex models.

The processes can be modelled using different mathematical forms, often with parameter values which are uncertain and can be tuned. While sinking and mortality rates are usually single parameters (linear functions), phytoplankton growth rate requires multiple parameters. μ_P is usually a function of nutrients, light and temperature:

$$\mu_P = \mu_P^{max} f(T) f(I) f(N)$$ (9.6)

μ_P^{max} is the maximum growth rate, $f(T)$ is the temperature effect, $f(I)$ and $f(N)$ are the limitation terms due to light and nutrients. Different formulations exist for each of these terms, but usually NPZD-type models characterise nutrient limitation of phytoplankton growth rate using Michaelis-Menten kinetics:

$$f(N) = \frac{N}{K + N}$$ (9.7)

K is known as the half-saturation constant for nutrient uptake, and N is the nutrient concentration. If nutrient is plentifully available, then $N/(K+N) \approx 1$ and phytoplankton growth is not limited by the nutrient.

The state variables of NPZD models represent concentrations of a given chemical element, often nitrogen, with other elements such as carbon derived using constant stoichiometry

between carbon, nitrogen and phosphorus, i.e. the Redfield ratio of 106:16:1 (Redfield, 1934).

More complex models include additional variables for each compartment. Phytoplankton can be split into PFTs, grouping together species which perform a similar function within the ecosystem (Le Quéré et al., 2005). PFTs are often based on organism size. It is also common to separate out diatoms, which form silicate shells and play an important role in the sinking of carbon. In models, PFTs are distinguished by differing parameters for traits such as maximum phytoplankton growth rates, grazing, and nutrient affinity. Zooplankton can also be split into functional types, again often based on size, with different feeding preferences. Note that the current paradigm neglects the fact that many plankton are mixotrophs: they both photosynthesize and eat other organisms (Flynn et al., 2013; Glibert et al., 2019).

Variable stoichiometry (elemental ratios) can also be introduced. Each PFT is then described by separate state variables for each element, such as nitrogen, carbon, and phosphorus.

Chla is often included into BGC models as it is the main photosynthetic pigment found in phytoplankton, and measurement of its concentration in water is used as an indicator of the phytoplankton biomass. Chla can be represented as a constant ratio to the carbon biomass, or a variable ratio depending on nutrient, light levels, and temperature (Geider et al., 1997).

Most models incorporate dissolved inorganic nitrogen as a nutrient, which includes nitrate and ammonium. Phosphate and iron may be modelled too, and silicate if diatoms are a PFT. Nutrient inputs from rivers and the atmosphere can also be specified. Detritus may be split into different sizes, with different sinking rates, and into different elements. Some models explicitly simulate bacteria and viruses, rather than just parameterising their effects.

Besides NPZD variables, models can also include other related processes, such as the oxygen and carbon cycles. The carbon cycle is usually represented by the state variables DIC and total alkalinity, the latter being the capacity of seawater to neutralise an acid. From these and other variables, quantities such as pH and air-sea CO_2 flux can be calculated (Zeebe and Wolf-Gladrow, 2001).

BGC models are closely related to higher trophic level models or ecosystem models. The latter require the underlying biogeochemistry, and BGC models require at least some parameterisation of the ecosystem, i.e. the explicit representation of part of the living component of the ocean (e.g. phytoplankton, zooplankton) with zooplankton mortality as a closure term, parameterising the predation of zooplankton by higher trophic levels such as fish and top predators (see Section 9.2.8).

Adding complexity to BGC models means that less important processes are neglected or amalgamated, but also increases the uncertainties associated with approximated formulations. There is no consensus on optimal structure and complexity, which will vary depending on the purpose (Fulton et al., 2003). Adding extra variables also increases computational cost, split between the computation of transport (advection and diffusion) for each state variable and the computation of the non-linear functions relating the state variables of the BGC model. In an operational context, the balance between model complexity and computational costs is critical and must be carefully evaluated. BGC models should be as simple as possible and as complex as necessary to answer specific questions.

9.1.2.2. Model calibration

As already mentioned, biogeochemical models are based on empirical relationships to describe the dynamics of biological processes. Observational data are then essential for tuning, adjusting or revising the formulations, i.e. making the model results match the observed distributions and fluxes of inorganic and organic quantities. Model calibration can be performed "by hand", i.e. by adjusting certain parameters of the biogeochemical models until the models show a "good" fit to the observed tracer fields, or by using objective optimi-

sation methods (Kriest et al., 2020). The resulting set of biogeochemical parameters is often closely linked to the ocean circulation, mixing, and ventilation derived from the physical model used, with its specificities and defaults.

9.1.2.3. Physical-Biogeochemical coupling

Ocean physics advects and diffuses BGC model variables, thus redistributing inorganic and organic amounts. In addition, some BGC processes depend on physical conditions such as temperature or salinity, particularly crucial for the carbon cycle. Thus, there is a very strong link between the physical conditions and the BGC, which makes the BGC models closely dependent on the physical models.

Vertical motions are particularly critical to bring nutrients from nutrient-rich deep waters into the uppermost layer that receives the sunlight needed for photosynthesis and marine life. Two critical layers together regulate phytoplankton production:

- The mixed layer is the upper layer of the ocean that interacts with the atmosphere. It is assumed to be mixed and homogeneous through convective/turbulent processes, generated by winds, surface heat fluxes, or processes modifying salinity. The deeper it is, the deeper
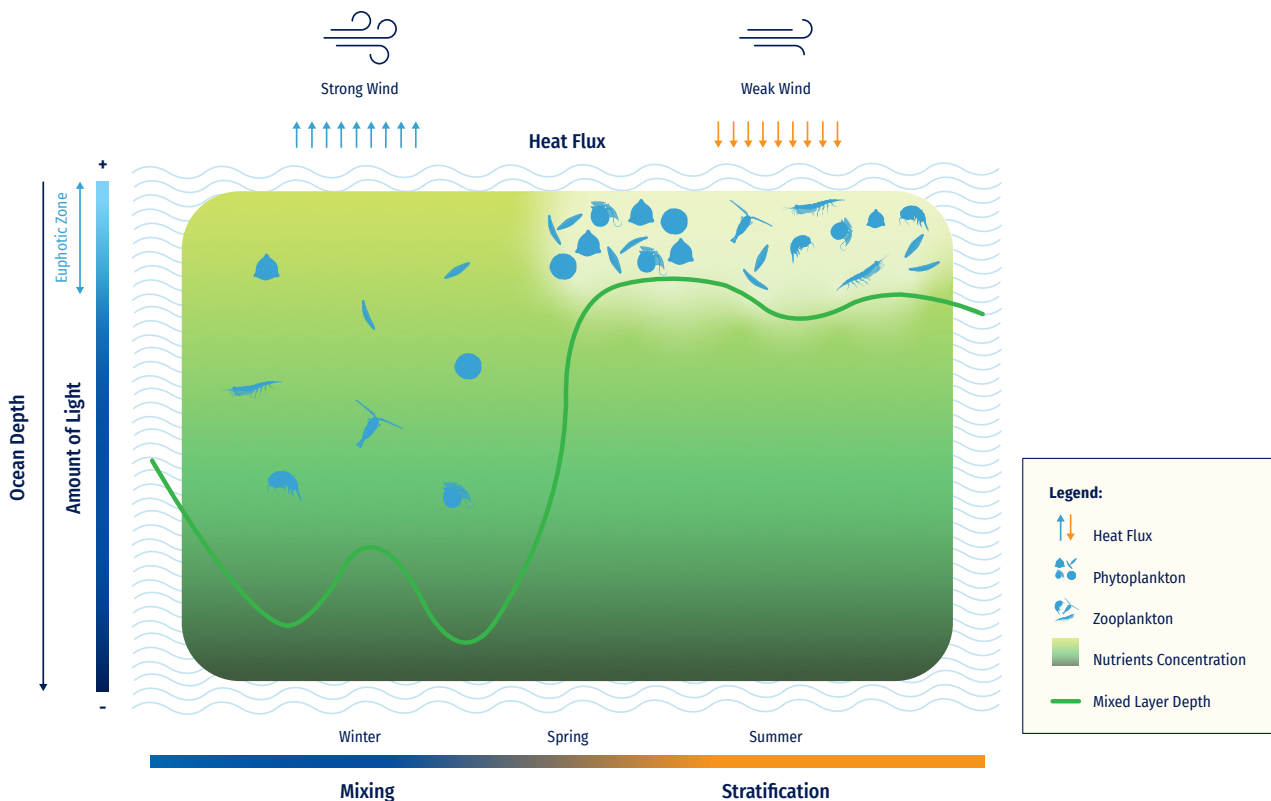
Figure 9.4. Schematic representation of the interplay between mixed layer depth (yellow line) and upper-ocean euphotic zone (light blue area) on the initiation of phytoplankton bloom (modified from Dall'Olmo et al., 2016).

phytoplankton are mixed, which will take them away from the light required for photosynthesis. Deep mixing also replenishes near-surface nutrient stocks.

• The euphotic zone is the layer from the surface down to the depth at which irradiance is 1% of the surface irradiance. The deeper the euphotic depth, the deeper the layer in which photosynthesis and phytoplankton production can occur. It extends from a few metres in turbid estuaries to approximately two hundred metres in the open ocean.

The mixed layer may develop within the euphotic layer (in stratified situations), or over a greater thickness of up to several hundred metres (in well-mixed situations). The interplay between these two critical layers controls the plankton exposure to sunlight and the coincident exposure to nutrients, thus regulating phytoplankton production (Figure 9.4). Exact mechanisms are still debated. Please refer to Ford et al. (2018) for more details.

In turn, phytoplankton abundance may feed back to physics, by absorbing radiation in the surface layers and therefore affecting heat penetration into the water column (Lengaigne et al., 2007).

9.1.2.4. From open ocean to coastal ecosystems

Different considerations are generally needed for open ocean and coastal ecosystems. In the open ocean, the seasonal cycle is quite well defined and recurring (Figure 9.5). Seasonal increases in temperature and solar radiation drive the phytoplankton spring bloom. The peak persists for a few weeks to months until nutrient limitation and grazing cause the bloom to collapse. A secondary biomass peak can develop in late summer or autumn.
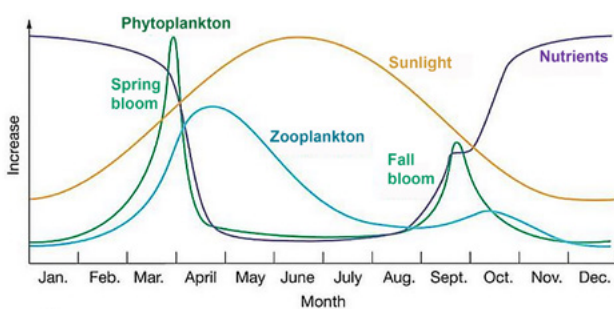
Figure 9.5.   Seasonal cycle of phytoplankton relative to variations in sunlight, nutrients, and zooplankton (Copyright: 2004 Pearson Prentice Hall, Inc).

In contrast, coastal ecosystems can be very complex, subject to a succession of blooms having different origins, thus requiring additional model complexity. Correct specification of river inputs also becomes more critical. Furthermore, the equations in Section 9.1.2.1 are for the pelagic (water column) ecosystem. In shallow waters, such as shelf seas, it becomes important to include the benthic (seafloor) ecosystem into the BGC models. This requires the addition of extra variables, though they do not need to be advected or diffused. Finally, coastal waters are often turbid, and the effect of sediments and coloured dissolved organic matter on light and therefore primary production should be included. Dedicated optical models are sometimes used for this purpose (Gregg and Rousseaux, 2016).

9.1.2.5. Potential predictability of ocean biogeochemistry

The potential predictability of ocean biogeochemistry varies considerably depending on the scales and quantities of interest. A lot of variability is driven by physics, with changes in mixing and stratification affecting light and nutrients and therefore primary production. When these physics changes can be predicted, e.g. changes in stratification with a warming climate and interannual variability related to phenomena such as the El Niño Southern Oscillation, associated large-scale changes to ocean biogeochemistry can also be predicted. Similarly, changes to the ocean carbon cycle and acidification with increasing atmospheric CO_2 concentrations can be predicted. When considering local regions and/or shorter time scales, both physics and biogeochemistry become harder to be accurately predicted.

Furthermore, various biogeochemical quantities change at very different rates. Phytoplankton react quickly to changes in light and nutrient availability and can double in concentration over a day (Laws, 2013). Zooplankton will exhibit a slightly more lagged response to these changes. Meanwhile, nutrient concentrations will typically change more slowly, and the carbon cycle even more slowly, although surface concentrations (of nutrients and carbon) can change rapidly, for example during a storm. These different rates of change have implications for the scales of predictability.

For accurate predictions, it is important to initialise models using data assimilation (see Section 9.2.5). At seasonal-to-decadal time scales, predictability is dominated by physics, and this must be accurately initialised and simulated. Physics remains important at shorter time scales, but is essential to initialise nutrient concentrations correctly, as this will help to determine the primary productivity. For short-range predictions, phytoplankton concentrations should be initialised, though the memory of the phytoplankton variables may be as short as a few days, given that they react to changes in nutrients and mixing. Accurate model formulations and parameterisations are also required, otherwise the model will react incorrectly to the data assimilation.

9.2.
Biogeochemical forecast and multi-year systems

Green Ocean modelling for operational oceanography is built in the same way as its Blue equivalent. The operational suite follows almost the same architecture (see Figure 4.1) and information flows from marine observation data up to end-user products enhancing the initial information. Each component includes a research stage, a development stage, and an operational stage. This Chapter mainly focuses on the last stage, in which the system is in operation.

The modelling component includes the BGC model, data assimilation, and ensemble modelling, executed for analysis and to forecast BGC conditions. The data include upstream data such as physical conditions, atmospheric forcing, external inputs of chemical compounds provided at interfaces (atmosphere, land, and seafloor), observational data from satellites, and in-situ measurements integrated into the systems via data assimilation methods. The data are also used for validation tasks: the near-real time evaluation of the forecast accuracy and the delay mode evaluation of the model system. Finally, the model outputs and end-user products are prepared by respecting certain standards of format, units, names, etc. for delivery to users and archiving.

9.2.1. Architecture singularities

In this section, we present the main architecture singularities of OOFS dedicated to the production of ocean biogeo-chemistry and marine ecosystems information. As most systems describing the "Green Ocean" in operation today are less advanced than their "Blue Ocean" equivalent, the "ideal" design proposed here includes some features that are still at the stage of research or development. Yet, they should be kept in mind for the construction of future systems.

9.2.1.1. Physical, optical, and biogeochemical components

As introduced in Section 9.1.2, the space-time evolution of the BGC quantities is driven by physical fields through horizontal and vertical advection, lateral diffusion, and vertical mixing. Vertical motions are particularly important as they supply nutrients to the lighted upper ocean, allowing photosynthesis to occur.

The limitation of photosynthesis by light thus requires a fine representation of the penetration of spectral irradiance in the upper ocean, as it is absorbed and scattered within the water column. Light penetration used to be managed by very simple optical schemes, but it is now increasingly managed by advanced bio-optical modules embedded into the physical-biogeochemical model systems, to both compute photosynthetic activity and to make the link with key observations such as spectral irradiances from ocean colour missions. The evolution of ecosystem variables in the trophic chain is driven by physics, optics, and biogeochemistry through primary production, which underpins the whole marine ecosystem (see Section 9.2.8).
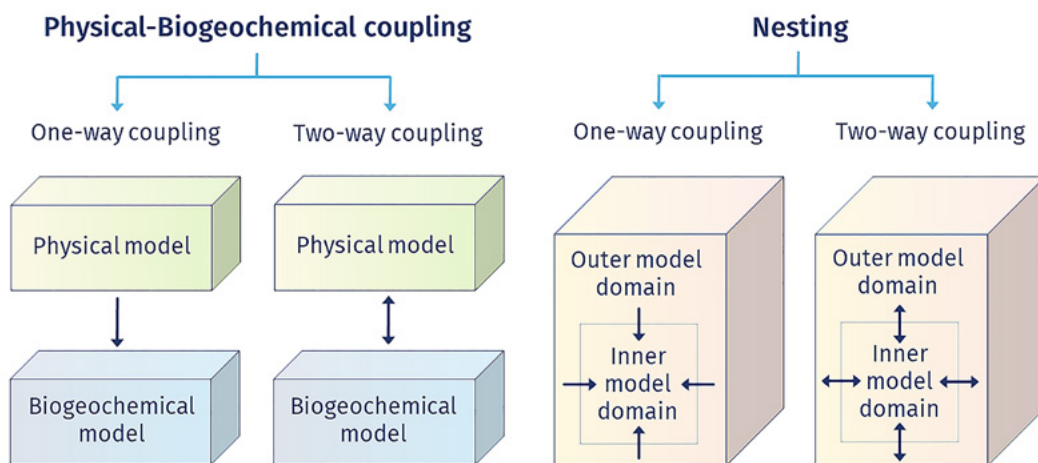
Figure 9.6.   Schematic of a physical-biogeochemical coupling (left) and nesting (right).

The physical fields can come from simulations of the ocean dynamics (reanalyses, nowcasts or forecasts) produced independently by the BGC modelling suite. Nevertheless, the physical fields must reflect the essential dynamical properties for the biogeochemistry, such as the right mixing rate, the right vertical velocity statistics, and the right phasing with mesoscale structures and frontal positions (Berline et al., 2007).

Although some feedback from biology to physics may exist, such as self-shading (Hernandez et al., 2017) or phytoplankton heat release, their effects are generally limited to moderate modifications of the upper-ocean heat budget and associated vertical structure of the thermocline. Therefore, the physical and BGC modelling components are usually linked by "one-way" coupling, resulting in successive model operations (Figure 9.6). As a result of the "one-way" approximation, the coupling can be implemented in "online" mode, i.e. the physical and biogeochemical models run simultaneously at each time step: the temporal update of the physical model is performed first, before being used for the update of the biogeochemical component. Alternatively, the coupling can be implemented in "offline" mode where the physics is computed beforehand and stored at lower frequency (e.g. each day/week) and then used as inputs for the biological model (Ford et al., 2018).

Such systems are usually less expensive in terms of computational resources. However, the practicality of the "offline" coupling approach can be questioned with respect to vertical viscosity and diffusivity coefficients, which typically vary with short time scales (~hours) compared to the storage rate of "offline" physical fields (typically a few days). This can be an issue in an integrated perspective that includes data assimilation. Burning questions underlying the coupling strategy for assimilative systems are still the subject of long-lasting research efforts by the community (Fennel et al., 2019).

Regional models with lateral open boundaries also require values of the model state variables at boundaries. A convenient way is nudging to fixed or climatological data from global reanalysis or datasets, but a more robust approach is to nest high-resolution regional ocean models into larger-domain (and usually lower-resolution) models (see Figure 9.6).
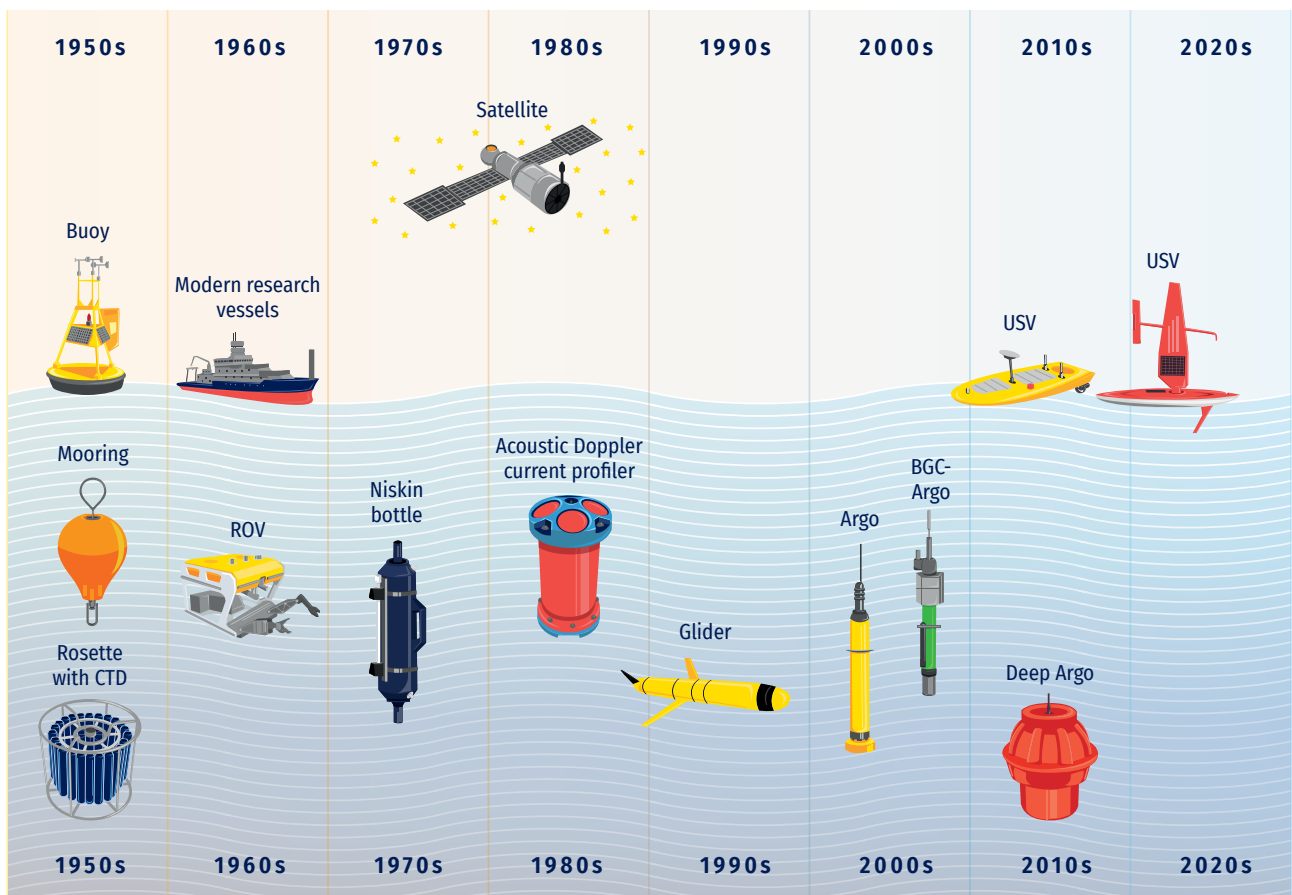
Figure 9.7. Chronology of oceanographic observation platforms to measure marine biogeochemistry (adapted from Chai et al., 2020).

As for the coupling between physics and biogeochemistry, the coupling between configurations nested in space can be "one-way", with the inner model having no influence on the outer model, or "two-way", in which the inner model provides information to the outer model. "One-way" coupling is mainly used in BGC operational systems for different reasons, as it offers the possibility to run the BGC model either in "online" or "offline" mode with the physics, while the "two-way" nesting requires by nature an "online" coupling between the physics and the BGC, making the operation of such coupled systems more complex and time-consuming.

For a sound representation of the biology, a specific design of the vertical discretization in the upper ocean is needed. The strong vertical gradients of the physical and biological variables typically require vertical spacing between horizontal levels ~ 1 metre. Regarding the horizontal grid, it is not always required to use the same numerical grid for physics and for biology. A coarsening approach that preserves the essential features of the resolved dynamics has been implemented in some systems to feed the biological equations at lower resolution, while saving numerical resources (Berthet et al., 2019; Bricaud et al., 2020).

9.2.1.2. Propagation of uncertainties

The forward integration of the discretized equations involved in the different modelling steps leads to results that are fundamentally uncertain. It is necessary to quantify this uncertainty, both to provide the user with useful information for decision making and for merging the forecast with future observations, which are also intrinsically uncertain.

The main possible sources of uncertainty in biogeochemical/ecosystem models are the following:

- initial conditions of the state variables;
- external data involved in the forcings, such as downward radiation, cloud cover, etc.;
- input physical data used to constrain the evolution equation of the biogeochemical/ ecosystem variables, such as currents, temperature, vertical eddy viscosity, etc.
- parameters involved in the representation of optical, BGC and ecosystem processes;
- numerical schemes and numerical approximations (such as coarsening or offline integration);
- unresolved, sub-grid scale processes that may induce bulk effects as a result of non-linearities.

These uncertainties can be quantified heuristically or can be explicitly considered by introducing stochastic parameterizations in the model equations, as proposed by Garnier et al. (2016). Multiple forward integrations can then be produced to generate ensembles that provide an approximation of the spread of the plausible solutions. A sample of the pri-

or probability distribution of the forecast is then generated by the different ensemble members (Santana-Falcon et al., 2020). As a result, the forward integration module (referred as Step 2 "Forecast" in Figure 4.1) should be designed in such a way that it can be called n times (with n = a few tens to hundreds) in parallel or in sequence. Please refer to Section 9.2.4 for more details on Ensemble modelling.

9.2.1.3. BGC Data singularities

Biogeochemical variables very often have non-Gaussian statistical properties. This can be explained by the nature of these variables (generally concentrations that repeatedly take values close to 0 or biomasses that can vary by several orders of magnitude), which is related to the non-linearities of the processes involved. Non-Gaussian behaviour requires special attention at the time of validation when comparing model variables to observations, using metrics calculated on log-transformed data or non-parametric metrics (please refer to Section 9.2.6 for more details).
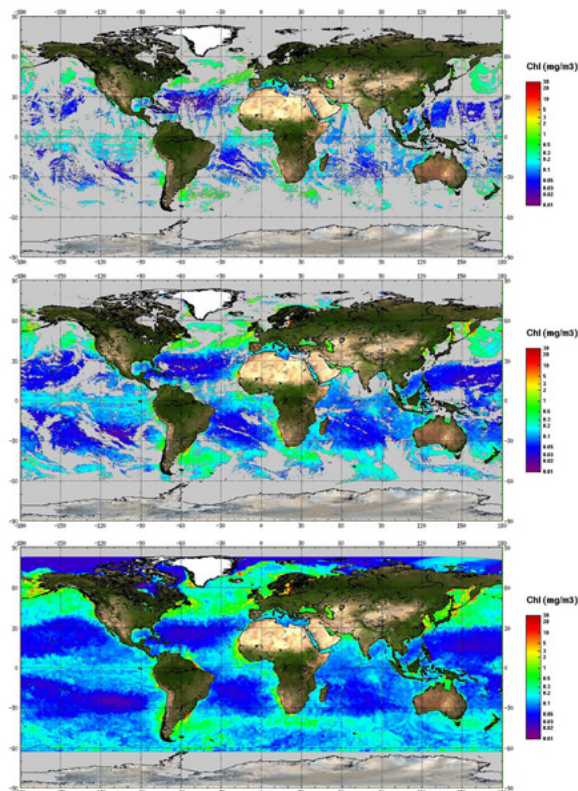
Figure 9.8. Examples of Chla ocean colour global multi sensor products available on the Copernicus Marine Service. They are daily products for 1st May 2019: a) OC-CCI product; b) Copernicus-GlobColour level 3 product; and c) Copernicus-GlobColour "Cloud Free" (interpolated) product (from Garnesson et al., 2021).
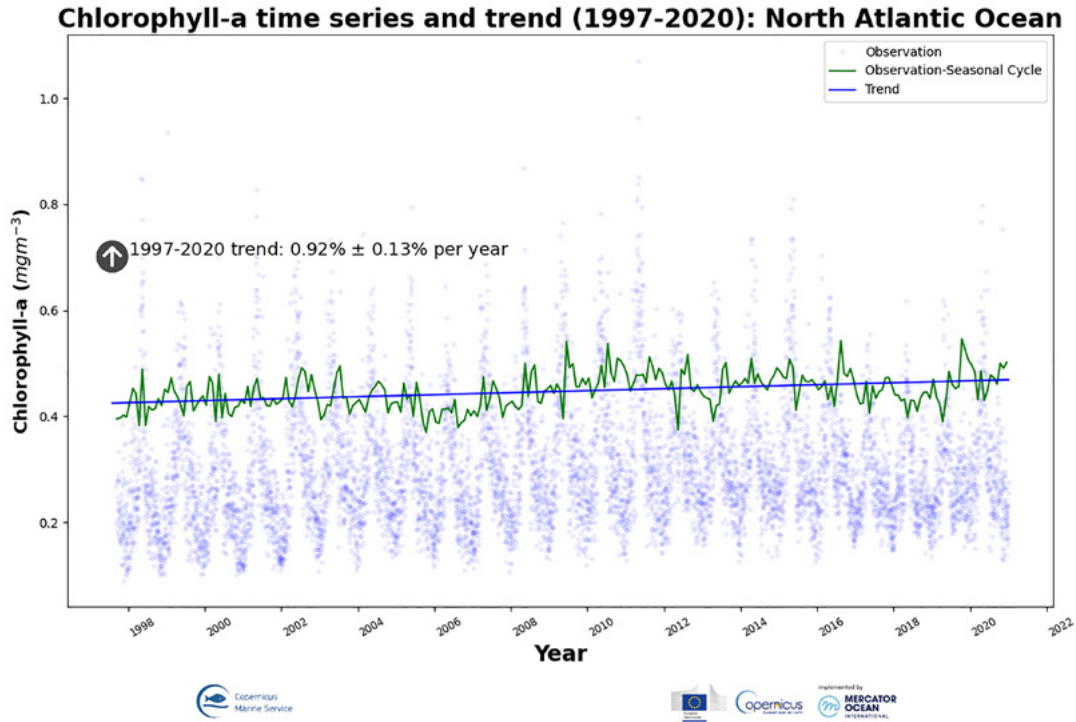
Figure 9.9. North Atlantic Ocean time series and trend (1997-2019) of satellite chlorophyll. Blue dots: daily regional average time series; green line: deseasonalized time series; blue line: linear trend (source: Copernicus Marine Service at 🔗²).

In addition, the assimilation methods applicable to large systems, e.g. Ensemble Kalman Filters, are typically adapted to Gaussian distributions: as a result, it is necessary to insert a so-called anamorphic transformation – a function matching the quantiles of the variable distribution to those of a standard Gaussian – between the outputs of the ensemble forward integration and the observational update step. This can be done in different ways: by prescribing a priori a given transformation (e.g. log-normal or truncated Gaussian), or by constructing the transformation from the ensemble information as proposed by Simon and Bertino (2009 and 2012) and Brankart et al. (2012). At the end of the analysis step, the inverse transformation must be applied to complete the assimilation cycle and prepare a new initialization.

Another issue comes from the highly heterogeneous distribution of the biogeochemical data in space and time, most of which coming from satellites (ocean colour) and fairly dispersed BGC-Argo profilers. The spatial scales captured by these observational data are therefore very different, requiring special care within biogeochemical data assimilation systems for localization at the analysis stage. The transformation in the Fourier space can then prove beneficial to carry out this step, as proposed by Tissier et al. (2019). The architecture of an operational chain dedicated to biogeochemis-try should therefore include a step to perform the observational update in a transformed space.

9.2.2. Input data: available sources and data handling

This Section provides a general description and technical information on the data used to both drive and validate a biogeochemical forecasting system. Observational data are required at different stages of an OOFS:

- Data is first used to set-up the model configuration: initial and lateral conditions, physical forcing, atmospheric surface forcing, and external inputs.
- Data is essential for calibrating the formulations of the BGC processes, i.e. making the model results to match the observed distributions and fluxes.
- Then data is used to evaluate the model product quality.
- Finally, observational information is incorporated into the numerical models using data assimilation methods with the objective to improve predicted model states.

2. https://marine.copernicus.eu/access-data/ocean-monitoring-indicators/north-atlantic-ocean-chlorophyll-time-series-and-trend
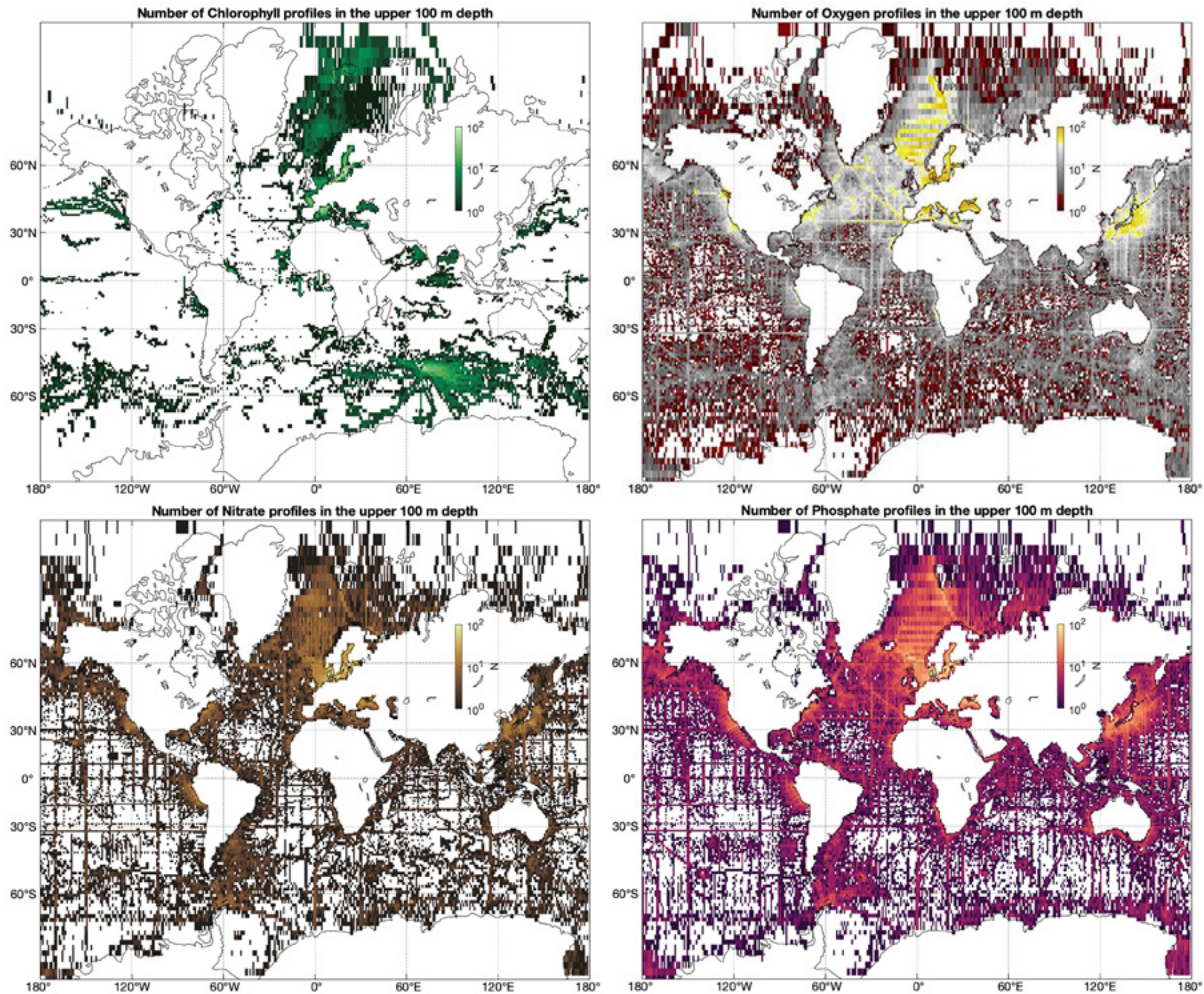
Figure 9.10. Spatial coverage of chlorophyll (top left), oxygen (top right), nitrate (bottom left) and phosphate (bottom right), shown as the number (N) of profiles in the upper 100 m water depth in 1°x1° cells, from 1990 to 2020. To show gaps more clearly, colour shading is from dark (low sampling) to light (high sampling), white colour indicates no sampling (from Jaccard et al., 2021).

9.2.2.1. Physical conditions

Required fields are currents, temperature, salinity, vertical diffusivity coefficient (Kz), and MLD. They are provided by a physical model to the BGC model with which it is coupled in either "online" or "offline" mode (see Section 9.2.1 for details). Advection and diffusion routines are usually shared with the physical model. A list of physical-BGC coupled systems is available in Section 9.2.9.

9.2.2.2. Observational data

Ocean-observing platforms to measure marine BGC encompass ship, mooring, and remote sensing observations. A good overview of the evolution and diversification of platforms over the past century is given by Chai et al. (2020) from which

is taken Figure 9.7. Among the traditional observing systems, satellites represented a revolution, providing a continuous spatiotemporal coverage of sea surface variables. More recently, autonomous mobile platforms measure ocean variables through the water column. They cover a wide range of spatial and temporal scales, filling the observational gaps.

9.2.2.2.1. Remote sensing observations

Remote sensing-derived Chla data have a good spatial coverage of the entire ocean in near-real time and reprocessed time series for global and regional mapped products. They are available through operational services, such as the Copernicus Marine Service (🔗 3; Le Traon et al., 2017). Figure 9.8

3. https://marine.copernicus.eu/

presents some Chla products and their spatial coverage. Figure 9.9 illustrates the long time series available. Remote sensing derived PFTs and optical properties are also starting to be distributed on the same portal.

9.2.2.2.2. In-situ observations

The Copernicus Marine Service collects and distributes in-situ observations from a variety of platforms, including manual CTD-O2 measurements, BGC-Argo profiling floats, ferrybox systems, gliders and moored buoys, gathered by global systems such as the EuroGOOS, SeaDataNet, NODCs, and the JCOMM. Two types of products are provided: 1) NRT products automatically quality controlled within 24 hours from acquisition for forecasting activities and 2) the reprocessed (or multi-year) products for reanalysis activities. The main biogeochemical variables available are dissolved oxygen concentration, nutrients (nitrate, silicate and phosphate), Chla, fluorescence, and pH. The spatial distribution of all chlorophyll, oxygen, nitrate and phosphate samples of the reprocessed product (from 1990 to 2020) are shown in. Figure 9.10.
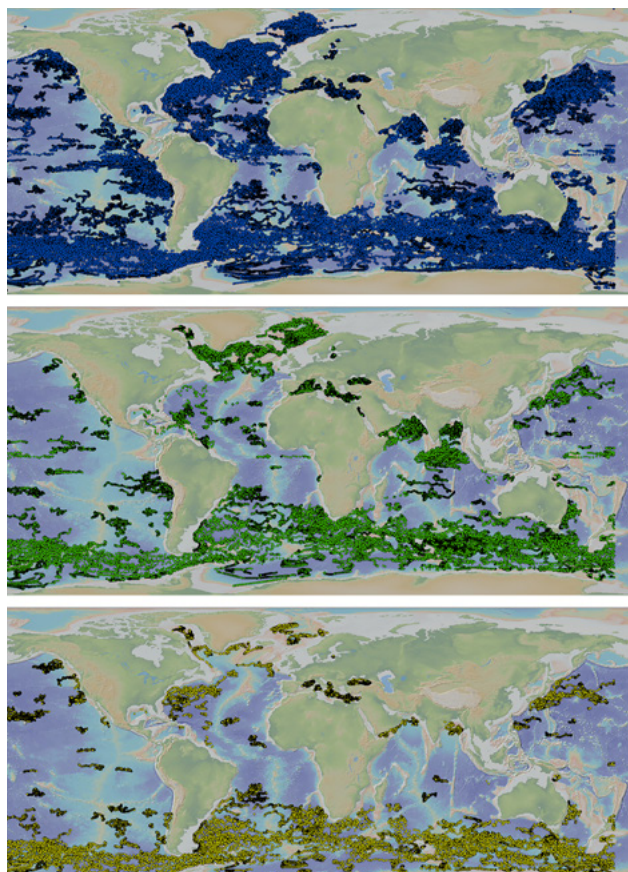
Special attention should be paid to autonomous robotic underwater vehicles. Argo profiling floats drift freely with the currents and measure ocean variables through the water column, reaching up to 2000 m, while gliders can be programmed to sample along a predetermined path, making the former more suited to the open ocean and the latter more suitable for observation at various depths in coastal and shallow oceans. After cycling vertically, both floats and gliders transmit their data to orbiting satellites once they have reached the surface, providing continuous monitoring and real-time data to operational centres.

The International Biogeochemical-Argo (BGC-Argo) program is revolutionising marine biogeochemistry by establishing a global, full-depth, and multidisciplinary ocean observation network, acquiring profiles in regions of the global ocean that previously were observationally sparse (Russell et al., 2014). They measure oxygen, Chla, nitrate, pH, suspended particles, and downwelling irradiance. Since their deployment in 2012, 1623 floats have acquired about 250000 profiles (Figure 9.11), the major part being oxygen. The aim is to have 1000 active profiling floats measuring simultaneously the six essential variables mentioned above (Biogeochemical-Argo Planning Group, 2016; Chai et al., 2020). At the time being, 410 floats are operational around the world (Figure 9.12). An example of time series is presented in Figure 9.13. BGC-Argo data are publically available in near real-time after an automated quality control, and in scientifically quality controlled form, delayed mode data, within six months of collection, via two Global Data Assembly Centers (Coriolis in France and US-GODAE in USA) (Argo, 2022; 🔗 [4]). They are also available through the Copernicus Marine Service (🔗 [5]).

Figure 9.11.   Spatial coverage of oxygen (top), Chla (middle), and nitrate (bottom) from the start of the BGC-Argo program. 230,202 profiles of oxygen, 94,947 profiles of Chla, and 49,939 profiles of nitrate have been acquired by October 2021 (source: T. Carval, personal communication using data from the Copernicus Marine Service).

4. https://www.seanoe.org/data/00311/42182/

5. https://marine.copernicus.eu/
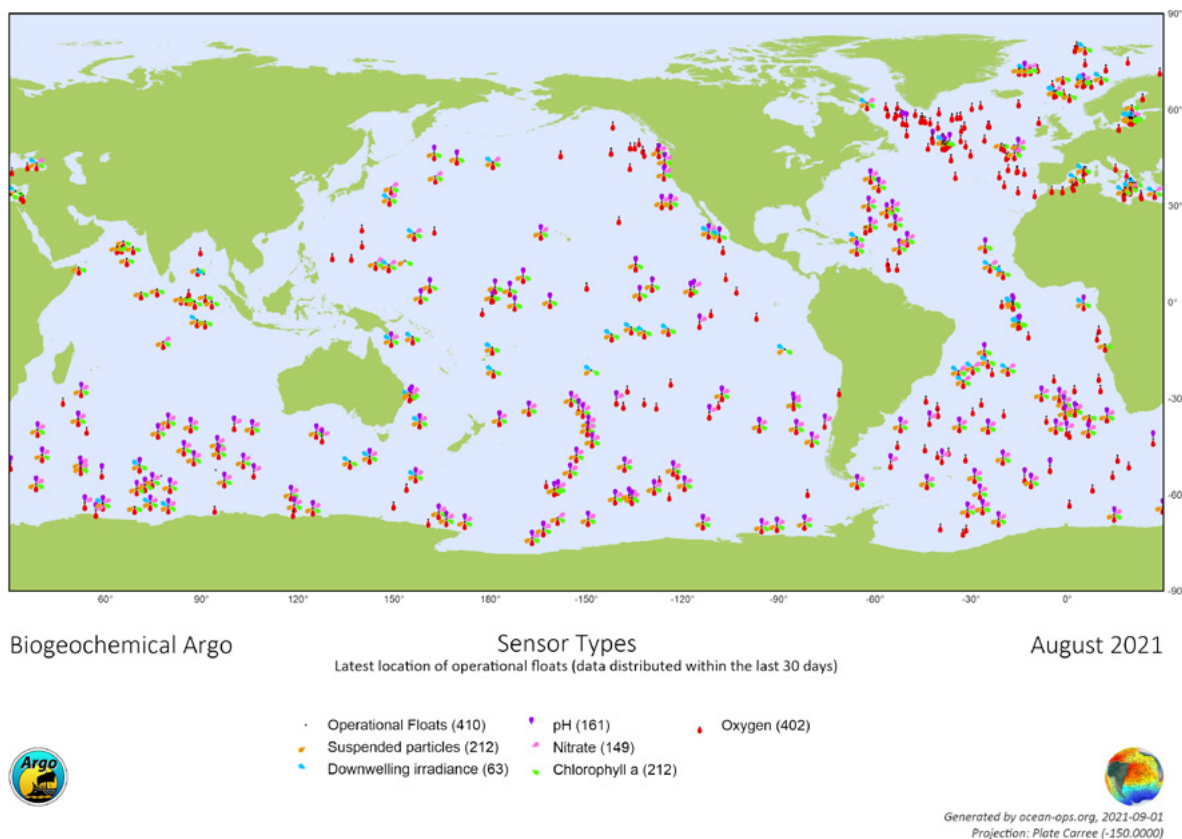
Figure 9.12. Location of operational BGC-Argo floats in August 2021 (🔗 6).
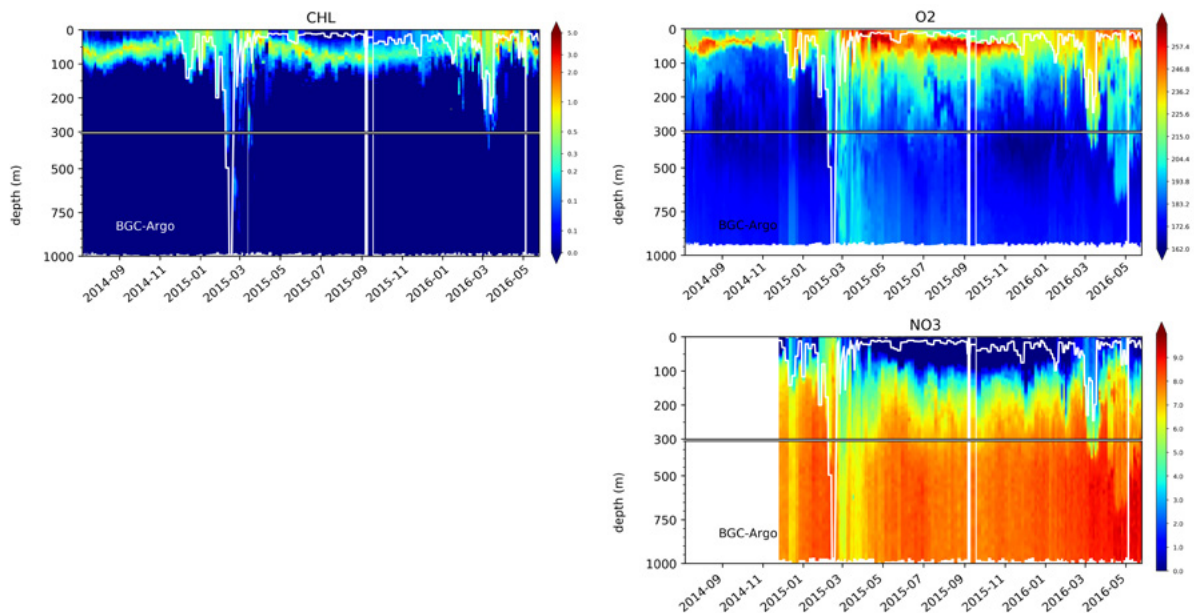
Figure 9.13. Time evolution of Chla (top left), oxygen (top right) and nitrate (bottom) along a BGC-Argo float trajectory in the North-East Atlantic.

6. www.ocean-ops.org

9.2.2.3. Climatologies, databases, and atlases

Databases and atlases are collections of uniformly formatted, quality controlled, and publicly available ocean surface or vertical profile data. Climatologies are mapped data products, produced from databases and atlases, representing the mean annual, seasonal, or monthly large-scale characteristics of the distribution of a quantity. They can be used to create initial and/or boundary conditions for ocean BGC models, evaluate numerical simulations, and corroborate satellite data.

The GLODAP provides a climatology (GLODAPv2.2020) of ocean biogeochemical variables of oxygen, phosphate, nitrate, silicate, dissolved inorganic carbon, total alkalinity, and pH on a uniform 1° longitude/latitude grid. The product is described in Olsen et al. (2020) and is publicly available at 🔗 [7].

The latest version of the WOA delivered in 2018 provides an annual, seasonal, and monthly climatology of oxygen and macronutrients (phosphate, silicate, and nitrate) on a 1° longitude/latitude grid (Figure 9.14).

It is described in Garcia et al. (2018ab) and is publicly available at 🔗 [8]. It is based on the latest major release of the WOD described in Boyer et al. (2018).

The SOCAT provides surface ocean fCO_2 (fugacity of carbon dioxide) observations, 🔗 [9]. The latest SOCAT (version 2020) has 28.2 million observations from 1957 to 2020 for the global oceans and coastal seas.

The EMODnet portal provides access to temporal and spatial distribution of marine chemistry data in European seas, 🔗 [10].

9.2.2.4. Atmospheric surface forcing

Atmospheric surface conditions drive biogeochemical quantities and processes, such as photosynthesis and air-sea exchanges of gas elements (oxygen, carbon). Typical surface data inputs include wind, solar radiation, and the evaporation-precipitation flux. They can be obtained from an operational weather prediction system, via the Copernicus Climate Change Service (🔗 [11]).
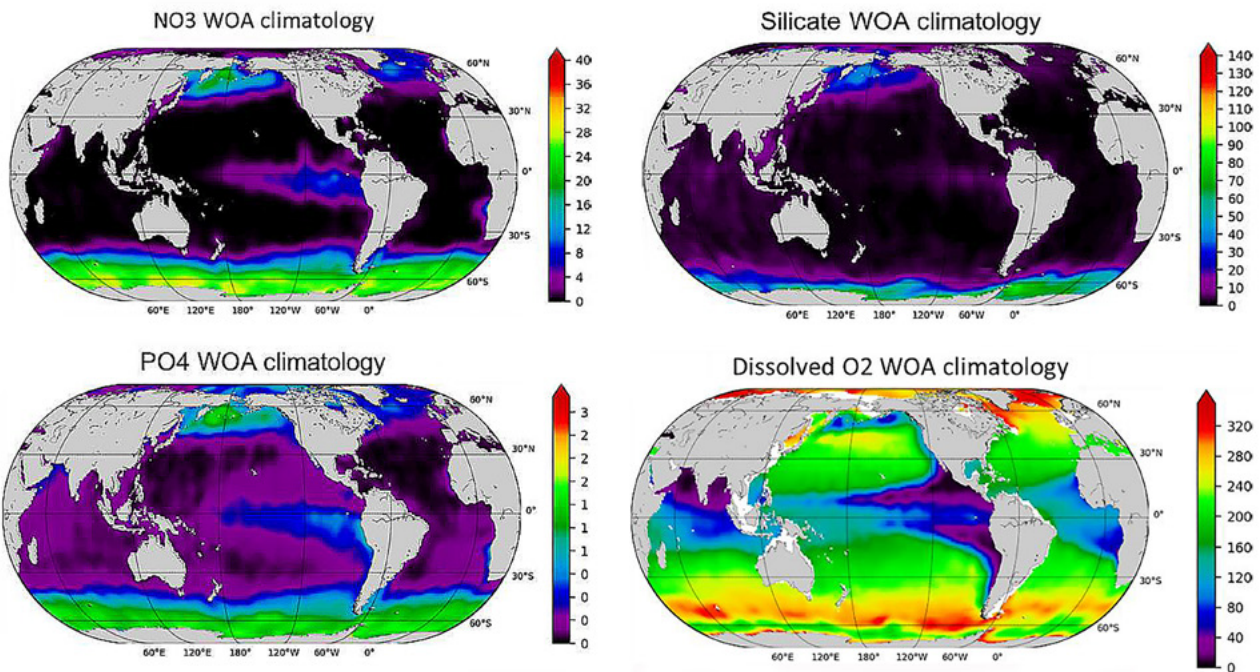
Figure 9.14.   Nitrate, phosphate, and silicate concentrations at sea surface and dissolved oxygen concentration at 200 m depth, all in mmol m^{-3} (from WOA climatology).

---

7. https://www.glodap.info

8. https://www.ncei.noaa.gov/products/world-ocean-atlas

9. https://www.socat.info/

10. https://emodnet.eu/en/chemistry

11. https://climate.copernicus.eu/

9.2.2.5. External inputs

External inputs of carbon and nutrients are provided to marine biogeochemical systems from observations or models. Although these inputs are currently simplified in current systems (from climatologies), the optimal solution would be to connect ocean operational systems with atmospheric and land operational systems. The link between the Copernicus Marine Service and the Copernicus Atmosphere and Land Services (respectively, 🔗 [12] and 🔗 [13]) is currently discussed.

9.2.2.6. Units

Special attention should be paid to the units of the BGC quantities because there is no standardisation among the different scientific communities. Model data are usually archived in the units specified by the SI Units but instruments frequently do not measure data in SI Units, making conversion necessary. For example, dissolved oxygen concentration in the seawater can be found in many different units (e.g. mg l^{-1}, ml l^{-1}, µmol l^{-1}, µmol kg^{-1}, mmol m^{-3}, µM), with the SI Units being mole per cubic metre (symbol mol m^{-3}).

It is worth noting the equivalences:

$$\mu mol \ l^{-1} = mmol \ m^{-3} = \mu M$$

$$1 \ l = 10^{-3} \ m^3 \approx 1.025 \ kg$$

and the conversions:

$$\mu g \ l^{-1} = \mu mol \ l^{-1} \times MW$$

$$\mu l \ l^{-1} = \mu mol \ l^{-1} \times MV$$

$$g \ l^{-1} \approx g \ kg^{-1} \times 1.025$$

To convert a quantity in sea water from mole concentration (in mol) to mass (in grams), multiply by Molar weight (MW in g mol^{-1}); from mole concentration (in mol) to volume fraction (in litre), multiply by Molar volume (MV in l mol^{-1}); expressed per unit mass (in gram) to volume (in litre), multiply by density (in kg l^{-1}). 1.025 is an approximate but general value for the density of seawater.

9.2.3. Modelling component

9.2.3.1. Numerical and discretisation choices

Marine biogeochemical models describe the cycling of essential elements (e.g. C, N, O2, P, and Si) through the lower trophic levels, usually from bacteria up to mesozooplankton.

Their complexity (i.e. number of state variables and processes) differs depending on the scientific question under interest, the information available for their parameterization and implementation, and the investigated time and space scales. BGC models consist of a set of evolution equations (e.g. differential equations) expressing the mass balance of each model component (e.g. state variable). These mass balance equations include local sources and sinks associated with biogeochemical processes (e.g. photosynthesis, respiration, and nitrification), trophic interactions (e.g. predation), the transport by physical processes in the three directions of space by advection (e.g. transport by the main current), and diffusion (i.e. unresolved processes that are parameterized on the model of the Fick's law of diffusion). As for physical models, biogeochemical models cannot be solved analytically and require a numerical model for their integration. A numerical grid has to be defined and the size of the grid cells will define the spatial scales that can be solved (it is usually assumed that the length scale of the solved processes equals twice the size of the grid). Given that the vertical scales of variations are much smaller than the horizontal ones due to the rapid extinction of the light field, the size of the vertical mesh is usually of the order of metres in the upper layer. The numerical scheme for time steps and time integration has to be carefully chosen in order to avoid generating negative concentrations. The choices may be identical to the physical model to which it is coupled, or different. Numerical and discretization techniques are described in Chapter 5 and biogeochemical singularities are discussed in Section 9.2.1.

Whether the processes can be resolved or not in models will depend on the grid resolution used to solve the numeric. Figure 9.15 shows the spatial and temporal scale of specific biogeochemical processes.

Regional and global scale models are able to capture the mesoscale signals with temporal scales of the order of a month and spatial scales of the order of 50-100 km. Coastal models have to solve the high frequency signal at daily and (sub)-mesoscale, but at this stage they are able to solve the dynamics of the system at weekly to monthly scales.

9.2.3.2. The different biogeochemical models

In marine biogeochemistry, the specificity lies mainly in the diversity of environments, ecosystems, and processes. The choice of a BGC model will thus depend on the study area and the topic of interest.

Models of marine biogeochemistry and of the lower trophic levels in the marine food web are usually of the NPZD type (see Section 9.1.2 for more details), which resolve community structure by the explicit representation of a few plankton groups, in accordance with their function in the ecosystem. Another approach is to let the community structure emerge from a wide

---

12. https://atmosphere.copernicus.eu/
13. https://land.copernicus.eu/

Source: modified from Dickey, 1991.
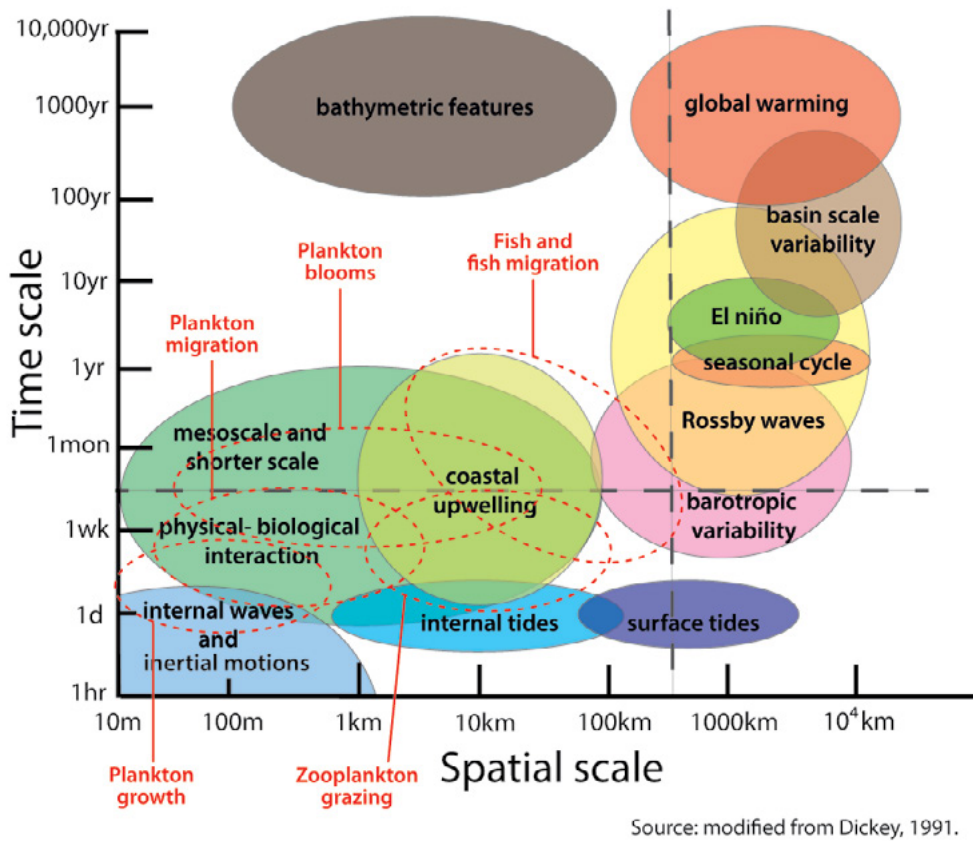
Figure 9.15. Time and space overlapping scales of major ocean processes. Main processes modelled by biogeochemical models are outlined in red (adapted from Dickey, 1991).

range of possibilities. For example, the DARWIN model (Follows et al., 2007) includes a large number (tens or hundreds) of PFTs whose physiological characteristics are stochastically determined (the parameters are prescribed randomly), allowing the fittest to emerge in the resulting ecosystem.

Some of the most used models in OOFS are summarised below:

- HadOCC (Palmer and Totterdell, 2001).
- MEDUSA (Yool et al., 2013).
- PISCES (Aumont et al., 2015). Its development is led by the Pisces Community gathering eight international research institutes/laboratories. The model can be downloaded from the NEMO and CROCO modelling systems into which it is embedded (🔗 [14] and 🔗 [15]).
- ERSEM (Baretta et al., 1995; Butenschön et al., 2016). Its development is led by the Plymouth Marine Laboratory and the code is available at 🔗 [16].
- BFM (Vichi et al., 2015). Its development is led by a con-

sortium of five members and the code is available at 🔗 [17].
- NORWECOM (Skogen, 1993; Skogen and Søiland, 1998). NORWECOM is the result of the cooperation between several Norwegian institutions, for more information see http://www.ii.uib.no/~morten/norwecom.html.
- ECOSMO (Daewel and Schrum, 2013) is developed by Hereon with contributions from the Nansen Centre and other collaborators, see 🔗 [18].
- ERGOM (Neumann, 2000). It was developed at IOW, Germany.
- BAMHBI (Grégoire et al., 2008; Grégoire and Soetaert, 2010; Capet et al., 2016).
- SCOBI, described in Eilola et al. (2009) and Almroth-Rosell et al. (2015).

Usually, these models are the result of the collaboration between different national and international research/academic institutes and laboratories, organised in formal or informal consortia. They are shared by several operators. In most cases, the code is available under open-source licences.

14. http://www.nemo-ocean.eu
15. https://www.croco-ocean.org
16. https://www.pml.ac.uk/Modelling/Home

17. https://bfm-community.github.io/www.bfm-community.eu/
18. https://www.hereon.de/institutes/coastal_systems_analysis_modeling/matter_transport_ecosystem_dynamics/models/index.php.en

Models have been developed to be applied to regional, shelf-sea, basin, or global ocean scale. The level of complexity differs depending on the application (biogeochemical cycling or ecological application). The models mainly differ in the biogeochemical cycles of major elements, the number of nutrients, the number of autotrophic and heterotrophic PFTs, the complexity in process formulation, as well as in the consideration of the benthic component. See refer to Gehlen et al. (2015) for a detailed description of these models.

The practical ability to switch between different physical and biogeochemical models is desirable to compare models and upgrade them smoothly. This ability is offered by the FABM (🔗[19]) and it has been used in NEMO and HYCOM, among other ocean/lake models programmed in Fortran.

9.2.3.3. Connections Ocean-Earth systems

Several kinds of models are used for a range of environments, but different considerations are needed for open ocean, regional, and coastal ocean. Moving from the open to the coastal ocean is often accompanied by an increase in the spatial resolution and complexity of the model.

Regional models of coastal ecosystems can be very complex. Their dynamics is essentially driven by the boundary conditions with the open sea and at the air-sediment-land interface.

For the ocean, atmosphere, rivers, and sediments are significant sources of carbon and bioactive nutrients, such as nitrogen, phosphorus, iron, and silicate. Model performances can be hampered by the quality of these boundary conditions. Coastline and topography are also important to trigger high-frequency physical processes.

Connections with the surrounding systems (Figure 9.16) that need to be carefully considered include:

- Connection with land. Rivers exchange freshwater as well as inorganic and organic material with the ocean. Coastal marine ecosystems have been subject to considerable modification in recent decades. The considerable nutrient load in river discharges is due to human activities on the land (e.g. agriculture, deforestation, waste discharge, etc.). Such inputs are critical for coastal ecosystem studies.

- Connection with the atmosphere. Atmospheric transport and deposition are a source of chemical compounds (e.g. carbon dioxide, nitrogen, oxygen, iron, and phosphorus) to the ocean, affecting marine biogeochemistry (e.g. source of nutrients, influence on pH, etc.) (Krishnamurthy et al., 2010).
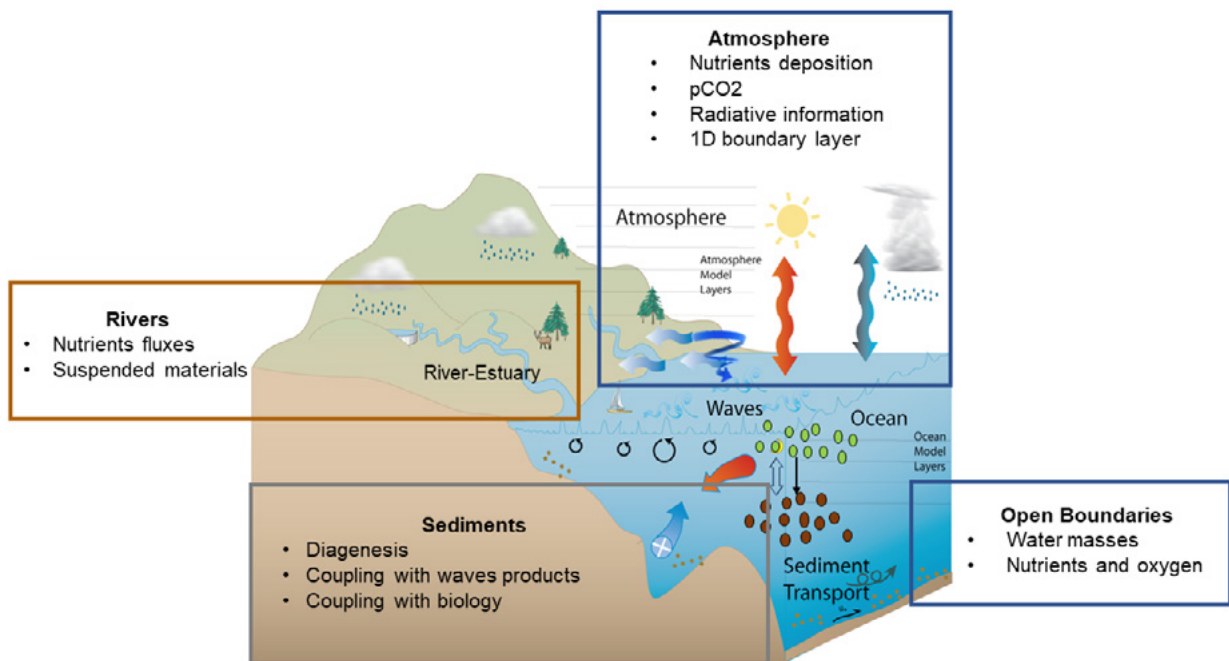
Figure 9.16.   Connections with interfaces (modified from Warner et al., 2010).

19. https://bolding-bruggeman.com/portfolio/fabm/

• Connection with the seafloor. Exchanges between the sediments and the ocean can be represented in a very basic way: they consist of the deposition of non-living organic material, resuspension, and release of inorganic nutrients from the sediments. But for a more robust approach it should be used an additional module representing (semi-) explicitly the diagenesis, benthic ecosystem, as well as bioturbation, diffusion, bio-irrigation effects into the upper sediments and sediment transport. A coupling with the waves is sometimes realised, e.g. using climatology.

• Connection with the open ocean. Open ocean and coastal ecosystems are intimately linked as they exchange mass, fluxes, and materials with each other. The best possible knowledge of open boundary conditions is essential for coastal modelling.

• The sea ice algae contribute between 4 and 26% of the primary production in the sea ice covered regions of the Arctic Ocean (Spindler, 1994; Gradinger, 2009; Dupont, 2012).

Connections listed above are not always optimally implemented in current OOFS. Rivers, atmosphere, and sediment exchanges are often introduced in a simplified way using climatologies or simplified exchanges. More refined interactions, including additional numerical modules or interannual observational data, are currently developing, and connections with surrounding systems should be considered for the construction of future systems.

9.2.4. Ensemble modelling

A forecasting system is literally designed to give an expectation of future conditions, having some knowledge of present conditions. The expectation is also a judiciously named statistic defined by the mean of all possible outcomes; for example, the expected primary production at a given location next week (time t_1) can be expressed as the mean of all possible values at the same time and location $\langle x(t_1) \rangle = \int x(t_1) dx$. If we make next week's primary production a function of today's primary production $x_1 = f(x_0)$, the function $f()$ implicitly includes all the other variables than primary production at present time such as nutrients, solar activity, currents, etc. We obtain a new expression for the expected forecast value (using the notation $\langle . \rangle$ for the expected value) $\langle x(t_1) \rangle = \int f(x(t_0)) dx$. The function $f()$ is unfortunately not a linear function because it represents the Michaelis-Menten equations (see Section 9.1.2.1), which after time integration become exponentials: if the concentration of plankton doubles today, you may expect a lot more than twice the plankton next week in a period of multiplicative growth. This means that one cannot swap the above integral and the $f()$ function, even if $x_1 = f(x_0)$ is true, $\langle x_1 \rangle = f(\langle x_0 \rangle)$ is generally false and will ineluctably generate a biased expectation: too high or too low depending on the convexity of the $f()$ function.

One general workaround for this problem is the use of an ensemble of simulations. Assuming that only a finite number of N possible outcomes is available, $\langle x(t_1) \rangle$ becomes an arithmetic average instead of an integral: $\langle x(t_1) \rangle \cong 1/N \Sigma(XN(T_1))$, with xn being a member of the ensemble: of the N possible outcomes, which are assumed independent from each other and identically distributed) If samples are like this, the arithmetic average will converge to the integral as N tends to infinity.

But why should one consider different possible outcomes when there is only one reality? The point is to manage uncertainties, which have more diverse origins in biogeochemical modelling than in physical or wave models, in particular the dependence on ocean physics is strong. Among the input data sources listed in Section 9.2.2, the following bear uncertainties that have an impact on biogeochemical model results:

• The seasonal restratification is critical. A too shallow mixed layer will confine the organisms near the surface and expose them to stronger lights than they should and exaggerate the bloom dynamics. A too shallow mixed layer will warm up too much and make the growth conditions artificially favourable. A late shoaling of the mixed layer in spring would lead to a delayed bloom in the simulation, leading to strong errors in surface Chla when comparing with observations.

• A good representation of winter mixing is also a desirable feature of the physical model, as it brings deep nutrients closer to the surface and makes them available for primary production.

• The ocean temperature influences the growth of microorganisms, so the simulated temperature should be accurate.

• The transport of nutrients from the rivers to the open ocean by ocean currents, or of any biological material from one oceanic region to another, requires accurate current simulations.

• The availability of light is fundamental for the ocean ecosystem. The amount of light reaching the surface of the ocean (i.e. how much light has been attenuated by the atmosphere, the clouds, the water, or sea ice) is uncertain.

• The initial conditions of the biogeochemical model are often based on very scarce climatologies of nutrients, some erroneous values may remain in the model during very long simulations.

• Nutrient inputs from rivers and atmospheric deposition are highly uncertain as well.

All the above are extrinsic source of errors, which can be accounted for by randomly perturbing various inputs of the biogeochemical model: perturbations of the downwelling shortwave radiations would account for uncertainties in light conditions, an ensemble of physical model outputs would account as well for the errors in the physical variables if the model is coupled offline. In the case of "online" coupling, the mixed layer depths can also be changed by adding perturbations to the surface winds and surface heat fluxes. There are various ways of generating random perturbations in 2 or 3 dimensions: a spectral method has been used in Natvik and Evensen (2003) and following works, but one could alternatively use an atmospheric ensemble prediction system or an empirical mode decomposition of atmospheric reanalysis data. The goal is to generate an ensemble of simulations, whose members differ slightly from each other because of the random perturbations they have received as input.

Intrinsic sources of errors have also been mentioned in Section 9.2.1. Among them, the BGC model parameters cannot be known with much certainty and can also be randomised. To do this, one needs to imagine their probability distribution, including their minimum and maximum admitted values. The random parameters may be fixed global values or values varying continuously in space (Simon et al., 2015) or discretely, according to designated provinces (the Longhurst provinces in Doron et al., 2011). Time-varying parameters also make sense since they may reflect neglected processes like population shifts. To this effect, an auto-regressive process is recommended in Garnier et al. (2016).

Other intrinsic sources of errors can be difficult to control, for example the noise caused by numerical advection schemes of the model or other model biases. If these are not too severe, it is desirable to emulate these uncontrollable errors by exaggerating the amplitude of other errors that can be controlled,
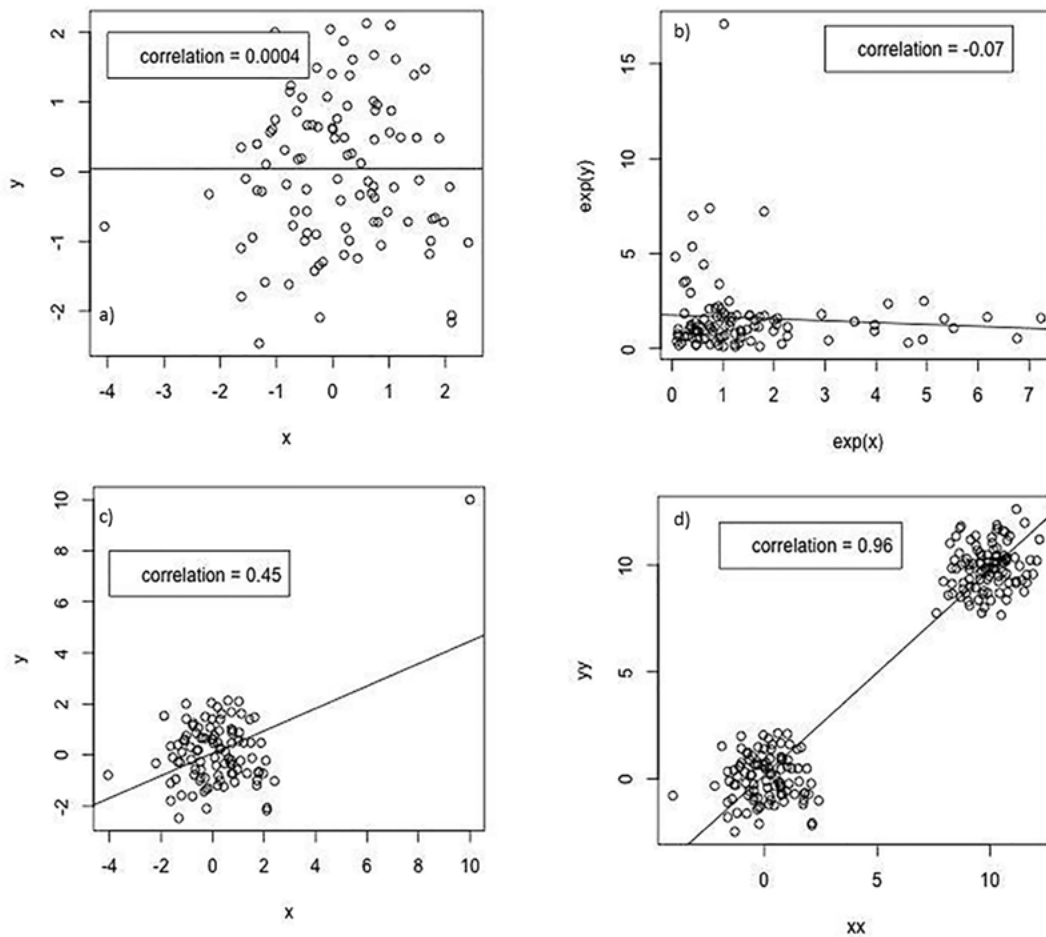
Figure 9.17.   Scatter plots illustrating second-order statistics from various types of ensembles of size 100. a) two independent random Gaussian vectors x and y. b) their exponentials. c) same as (a) but adding one outlier at (10,10). d) mixture of independent Gaussian vectors, with an offset of 10. The correlations between the two variables are indicated in the legend.

e.g. increasing the level of noise in the wind forcing (extrinsic error) to compensate for a bias in the model mixing scheme (intrinsic). The preferred action, however, should be to correct the biases at their origin, if this is possible.

It is interesting to keep track of the perturbations applied, so that the differences between ensemble members can be explained by the sensitivity to the input parameters. A contrario, Garnier et al. (2016) also directly perturb the concentrations of biogeochemical tracers, in which case the differences between ensemble members can no longer be attributed to input parameters alone.

An ensemble of simulations is thus a way to obtain unbiased expectations, defined as a first-order statistical moment, but it also provides other higher order statistics as well. One statistic that is critical for data assimilation is the variance-covariance matrix, a second-order statistic. In particular, the statistics based on an ensemble can provide all empirical cross-covariances between observations and unobserved model variables, which are an essential ingredient of all data assimilation methods (Carrassi et al., 2018).

However, the variance and covariance estimated from ensembles are sensitive to outliers and may be wrongly estimated in case of ill-behaved ensembles. This is illustrated on Figure 9.17 with a synthetic example. Figure 9.17a shows the scatterplot of two independent Gaussian variables, x and y, that display a low correlation, as expected. The exponential of these values in Figure 9.17b shows a negative relationship due to the exponential stretching of randomly high values, which is not desirable neither for interpretation nor for assimilation. Figure 9.17c illustrates that the correlation can be very sensitive to the introduction of a single outlier. Figure 9.17d shows that a clustered ensemble can make the correlation artificially high, essentially making two hundred members equivalent to a two-members ensemble only.

9.2.5. Data assimilation systems

The assimilation of biogeochemical data into marine models aims at estimating the "true" value of biogeochemical quantities in real ocean ecosystems. These quantities are either key "states" of the ocean (e.g. the phytoplankton biomass) or "parameters" characterising the functioning of the ecosystem (e.g. the maximum phytoplankton growth rate). They are estimated by merging model guesses with field observations (e.g. model predictions and satellite observations of the phytoplankton biomass). Such merging weights the errors of both the model and the observation, looking for the "true" value that (ideally) lies in their proximity. Operational oceanography aims at estimating these "true" biogeochemical quantities to evaluate trends of ocean biogeochemistry in the past (in ocean biogeochemistry reanalysis), or to set initial values for biogeochemical model prediction in future forecasts.

The theory and methods behind data assimilation are described thoroughly in Chapter 4, while the biogeochemical model components have been described in the previous sections of this chapter. The following section provides a synthesis on how these ingredients can be combined in modern operational biogeochemical systems. Comprehensive reviews of the subject were published recently by Fennel et al. (2019) and Ford et al. (2018).

9.2.5.1. Biogeochemical state and parameter estimation

Most of the modern BGC OOFS apply DA to improve model simulations of biogeochemical state variables rather than biogeochemical parameters (Fennel et al, 2019). The main reason for this bias is the straighter link between model state variables and ecosystem indicators that interest end-users in the policy, management, and blue growth sectors. For example, the MFCs of the Copernicus Marine Service provide assimilative reanalysis and forecasts of nutrients, phytoplankton biomass and oxygen concentrations (linked to coastal productivity and eutrophication), and water acidity (pH, linked to ocean acidification and climate change). All these state variables are linked to the Sustainable Development Goal 14 (Life below water) and are targets of marine policy (e.g. the European Union Marine Strategy Framework Directive).

However, the variables targeted by BGC DA systems are not necessarily assimilated into the model. In fact, most of the above-mentioned centres assimilate ocean colour chlorophyll only, as a proxy of phytoplankton biomass, and none of them assimilates pH. It is assumed that a non-assimilated variable can be corrected towards its true value since it is linked to the assimilated variable, e.g. pH is improved through its relation to the phytoplankton biomass via photosynthesis/respiration that modify dissolved inorganic carbon (DIC) concentration and alkalinity in the water column, and thus pCO_2 and pH. These corrections of non-assimilated variables can happen directly in the assimilative analysis step when using multivariate assimilation methods (Ciavatta et al., 2011). They can also happen indirectly during the model simulation of the ecosystem processes: in principle, an improved estimation of the phytoplankton biomass should quantify better the air-sea CO_2 fluxes and hence their impact on pH. However, the improvement of non-assimilated variables is a strong assumption that needs to be thoroughly verified via comparison with independent datasets (see Section 9.2.6).

Some operational centres use BGC DA to estimate biogeochemical model parameters, on their own or concurrently with the model state variables (e.g. in a multivariate analysis configuration). For example, the Arctic MFC estimates rates of phytoplankton growth and mortality, and this improves the simulation of the phytoplankton biomass that is a target variable of the operational system (Simon et al., 2015). The parameters can be estimated as variables in time and space, to somehow represent the variability of the real system

which cannot be formulated in the mechanistic equations of the model. For example, the variability of the phytoplankton species that are represented in biogeochemical models are often forced into few functional groups. In practice, the spatial-temporal variability of a given biogeochemical parameter is often represented as a random variable, with predefined statistical distribution. Its fluctuations are computed through the minimization of a cost-function between model prediction and field observations of a state variable, which is linked to the parameter and assimilated into the model. BGC DA for parameter estimation has an enormous potential to improve our understanding of marine ecosystems, their model representation, and the operational prediction of target variables. However, it is also challenging, mainly due to the scarcity of data to define realistic statistical distributions for the parameter variability and assess the reliability of the estimated parameter fluctuations. Schartau et al. (2017) provided an excellent review of these opportunities and challenges.

9.2.5.2. Assimilated observational products

Most of the modern BGC OOFS assimilate ocean colour Chla into their model systems (Fennel et al., 2019). That is because this satellite product: i) quantifies the biomass of a central component of biogeochemical models (phytoplankton); ii) provides data that are generally synoptic (~100 km), high resolution (~100 m), and frequent (~daily); and iii) has a timely and free access (e.g. through the Copernicus Marine Service; 🔗[20]). A thorough discussion on the use of ocean colour in biogeochemical modelling and assimilation is provided in the report of the IOCCG (IOCCG, 2020). Here it is worth mentioning that, after the seminal assimilation of ocean colour by Ishizaka (1990), biogeochemical reanalyses were produced by assimilating ocean-colour total Chla in the global ocean (Nerger and Gregg, 2008), in an ocean basin (Fontana et al., 2013), and in coastal and shelf-seas ecosystems (Ciavatta et al., 2016). More recent contributions include the decadal global ocean ecosystem reanalyses by Ford and Barciela (2017), obtained by assimilating different ocean colour products for 1997 to 2012, and the one by Gregg and Rousseaux (2019), who estimated global trends of primary production by assimilating ocean colour for 1998-2015. Besides the well-established assimilation of total Chla from ocean-colour (e.g. Hu et al., 2012), innovative applications have assimilated surface ocean colour products for: spectral diffuse attenuation coefficients (Ciavatta et al., 2014), size-fractionated Chla and POC (Xiao and Friedrichs, 2014), remote sensing reflectance (Jones et al., 2016) and both phytoplankton functional type Chla and spectral absorption (Ciavatta et al., 2018 and 2019; Skakala et al., 2018 and 2020; Pradhan et al., 2020). Surface data of partial pressure of CO2 (pCO2) from ships of opportunity were used in the reanalysis of air-sea CO2 fluxes in the global ocean (While et al., 2012).

20. https://marine.copernicus.eu/

Biogeochemical data are sparse for the ocean interior, but they can be useful to constrain vertical gradients that are extremely important in the functioning of marine ecosystems. For example, biogeochemical simulations were improved by assimilating vertical observations of nutrients, oxygen, and pCO2 data at fixed stations (Allen et al., 2003; Torres et al., 2006; Gharamti et al., 2017). The increasing number of autonomous underwater vehicles and floats observing biogeochemistry in the global ocean is an opportunity for the development of operational oceanography (see also Section 9.2.2). The assimilation of such data in the water column can complement the assimilation of ocean colour at the surface of the ocean. For example, glider data of Chla and POC were assimilated by Kaufman (2017), while Skakala et al. (2021a) assimilated glider Chla and oxygen data along with ocean colour data in an operational model of the European North West Shelf Seas. Recently, the assimilation of BGC-Argo float data led to improvements in the simulation of subsurface biogeochemistry in regional seas (Verdy and Mazloff, 2017; Wang et al., 2020), as well as in the global ocean (Carroll et al., 2020). OSSE analyses have shown the potential of improving the ocean biogeochemical simulations by combining the assimilation of the planned 1000 BGC-Argo fleet with ocean colour assimilation, with both variational data assimilation methods (Ford, 2021) and stochastic ensemble approaches (Germineaud et al., 2019). The Mediterranean MFC pioneered the assimilation of the BGC-Argo float for operational oceanography (Cossarini et al., 2019). This application is demonstrating remarkable advantages for the prediction of the subsurface phytoplankton dynamics and biogeochemistry, with respect to the assimilation of ocean colour alone. It also pointed out the current main challenges in using the BGC-Argo float data operationally: i) the availability of quality-controlled data in near-real time; ii) the relatively low number of floats available currently, which implies that the impact of their assimilation is spatially constrained; and iii) potential biases between the assimilated float and satellite data (e.g. the Chla concentrations derived for remote sensitive reflectance and in-situ fluorescence).

9.2.5.3. Biogeochemical data assimilation methods

The general theory and application of data assimilation methods were presented in Chapter 5. For the assimilation of biogeochemical data, current operational systems are using two methods (Fennel et al., 2019; Moore et al., 2019):

a. Ensemble methods, which use an ensemble of ocean model simulations or states to represent the evolution of the physical and biogeochemical state variables and their uncertainty.

b. Variational methods, which correct the model simulation towards the observation by minimising the differences between the observation and the model estimate of the variable.

Hybrid ensemble/variational assimilation methods have been applied successfully with physical ocean models (e.g., Storto et al., 2018) and are currently being developed for the assimilation of biogeochemical data in operational systems of the Copernicus Marine Service (EU H2020 SEAMLESS project: 🔗 [21]).

There is no "best" method for the assimilation of biogeochemical data. The choice depends mainly on: i) the target variable (or parameter) of the assimilative simulation; ii) the data being assimilated; and iii) the computational resources, which can become a major issue when using biogeochemical models with a large number of variables. For example, an ensemble method might be preferable if the target variable (e.g. nitrate) is different from the assimilated variable (e.g. ocean colour Chla) because one can exploit multivariate analyses that take the dynamical model error covariances into account. If the number of CPUs is a concern, efficient variational methods might be the best choice, if adequate information about the model error covariances is available.

As far as ensemble methods are concerned, since the introduction of the original EnKF (Evensen, 1994), different flavours of the filter have been developed (Vetra-Carvalho et al., 2018) and applied with operational biogeochemical systems (Fennel et al., 2019). For example, both the reanalysis system of the Arctic Ocean (Simon et al., 2015) and the operational system of the Great Barrier Reef (Jones et al., 2016) use the DEnKF (Sakov and Oke, 2008). In the Baltic MFC, work is in progress to apply the local ESTKF (Nerger et al., 2012), while the Global MFC is based on the SEEK (Pham et al., 1998). However, the propagation of an ensemble of model states implies a high computational cost. To ensure that the EnKFs perform adequately with affordable ensemble sizes (i.e. between 10 and 200), practical adaptations like "localization" have been adopted (Houtekamer and Mitchell, 1998). Localization approaches correct the model simulation towards the observation just around the point where the observation was taken. "How much around" (i.e. the localization scale) depends also on the spatial variability of the variable that is observed.

Examples of variational methods for biogeochemistry used by some operational centres include: the 3D-Variational assimilative system for the European North West Shelf Seas (Skakala et al., 2018) using NEMOVar (Mogensen et al., 2009; Waters et al., 2015) and for the Mediterranean Sea using 3DVarBio (Teruzzi et al., 2014 and 2019); the 4D-Variational system of the CCS (Song et al., 2016). In all the above cases, the assimilated variable is ocean colour Chla concentrations, but a limited number of other model variables are also updated by means of functional links such as background Chla-to-nutrients ratios of the phytoplankton cells.

A particular issue for biogeochemical data assimilation methods is the non-Gaussianity of the distributions of the biogeochemical variables (Campbell, 1995), which is related to the non-linearity of the ecosystem processes. In fact, most of the traditional methods assume that these distributions are Gaussian. The use of logarithm of the concentrations, in particular for Chla assimilation (Nerger and Gregg, 2007) and Gaussian anamorphosis (Bertino et al., 2003), has been demonstrated to handle the issue by bringing distributions closer to Gaussian before the assimilation of the data. This approach is currently exploited in operational systems of the Copernicus Marine Service, e.g. in the centres for the European North West Shelf Seas, Arctic and Global oceans (Simon et al., 2015; Skakala et al., 2018; Lamouroux et al., in prep.).

9.2.5.4. Current challenges and opportunities

State-of-the-art operational centres are using BGC DA to provide better model output products to their users. It is expected that this use will expand further in the future thanks to current research and developments that are addressing the BGC DA challenges and opportunities described below (see also Fennel et al., 2019, and the EU H2020 SEAMLESS project (🔗 [22]) specifically dedicated to the advancement of operational biogeochemical data assimilation systems).

Before applying any BGC DA method, the physical-biogeochemical models at hands need to be improved as much as possible, e.g. through implementation of the most relevant processes, improved parameterizations, corroboration of equations, and simulation by using laboratory and field data. In fact, biogeochemical data assimilation cannot fix (and actually might deteriorate) any systematic flaw of the applied ecosystem models (Ciavatta et al., 2011).

It is expected that the integrated assimilation of data from the expanding fleets of in-situ autonomous observing systems (e.g. BGC-Argo floats in the open ocean and gliders in shelf-seas and coastal areas), along with the traditional surface ocean colour data, will make possible to constrain better a larger number of model variables and parameters of operational models (Cossarini et al., 2019; Skakala et al., 2021a).

In current applications, the assimilation of physical data into ecosystem models can cause the deterioration of the biogeochemical simulations due to the breaking of physical balances and of their consistency with the biogeochemical fields (Anderson et al., 2000). In models of the equatorial ocean, the assimilation of temperature and salinity profiles, or sea surface height, can perturb the balance between pressure gradients and the wind stress, generating unobserved currents and spurious vertical velocities (Waters et al., 2017; Park et al., 2018). In turn, this can result in unrealistic upwell-

---

21. https://seamlessproject.org/

22. www.seamlessproject.org

ing of nutrients and excessive recreation of the water column, deteriorating biogeochemical model products (e.g. oxygen and primary production). The combined assimilation of physical and biogeochemical data is a promising approach to address the above issue, and preserve the consistency between the physical and biogeochemical simulations (Anderson et al., 2000; Ourmières et al., 2009; Song et al., 2016; Yu et al., 2018). Using bio-optical modules, which provide feedback from biology to ocean physics in "two-way" coupling interactions, models are expected to preserve even better such consistency, in both simulation and assimilation steps of operational systems (Skakala et al., 2021b). The opportunity for the combined assimilation of physical and biogeochemical data is increasing along with the growing number of BGC-Argo floats and gliders mounting multivariate sensors in the ocean (Skakala et al., 2020).

The steady expansion of computing capability will facilitate the use of ensemble methods (including hybrid ensemble-variational methods) to better represent the dynamics of the biogeochemical model errors. Nevertheless, this evolution should be accompanied by the use of new stochastic ensemble generation methods that can represent the actual model uncertainty (Santana-Falcon et al., 2020), and the careful consideration of potential non-linearity/non-Gaussianity issues that can weaken the applicability of traditional data assimilation methods. To address these issues, new DA methods such as particle filters (van Leeuwen, 2010) have been applied to coupled physical-biogeochemical models (Mattern et al., 2013) and might be used in operational systems in the future.

Finally, Artificial Intelligence/Machine Learning methods have supported data assimilation with geophysical models and will likely become relevant components of future operational biogeochemical data assimilation systems (Mattern et al., 2012).

9.2.6. Validation strategies

The validation methodology is built upon four classes of metrics that have been defined by the GODAE/OceanPredict community (Figure 4.30) to monitor the quality of ocean analyses and forecasts in physics (Section 5.7) and are used and supported by the broader biogeochemical community. These metrics gather a complete range of statistics and comparisons in space and time to properly assess the consistency, representativeness, accuracy, performance, and robustness of ocean model outputs. They are classified as follows (for a more detailed description see Hernandez et al., 2009 and Chapter 4):

- **Class 1:** metrics aim to provide a general overview, they are typically spatial maps or vertical profiles.
- **Class 2:** metrics correspond to virtual moorings or sections of the model domain.

- **Class 3:** metrics are derived quantities, such as integrated quantities.
- **Class 4:** metrics are model-observation match-ups products.

Based on this methodology, the validation strategy of biogeochemical operational systems consists of two phases: i) the near-real time evaluation of the forecast accuracy; and ii) the delay mode evaluation of the model system.

9.2.6.1. Near-real time evaluation

The NRT validation aims to provide information about the quality of the forecasts and relies on the availability of NRT observations (e.g. data from satellite and from autonomous underwater sensors such as BGC-Argo floats, BGC-gliders, and moorings equipped with biogeochemical sensors). A validation is defined as semi-independent (independent) when the observations are (not) assimilated in a sequence of analysis and forecast cycles. In fact, an observation from a continuously recording sensor, even if not yet assimilated, shares some level of correlation with already assimilated observations from the same sensor.

The forecast validation is commonly based on temporal and spatial match-ups of forecast model outputs and observations (i.e. GODAE Class 4 metrics), and on the computation of statistical skill metrics such as average difference (also referred to as average misfit or bias), average absolute difference, RMS Difference (RMSD), correlation index, and model efficiency (Stow et al., 2009). Skillfulness of forecasts can be compared in terms of persistence (i.e. comparison with previous day forecast) or with skill performance against a reference climatology. Skill statistics are often reported for various forecast lengths (i.e. number of days in the future).

Two examples are presented in the following figures. Figure 9.18 shows model analysis, six days of forecast and compare surface Chla model estimates to satellite observations for the European North West Shelf Seas system. Successive daily forecast values quickly diverge from the satellite product during spring and summer months, highlighting the strong effect of data assimilation during the production period. During winter, the satellite coverage decreases and the ocean colour error increases, inducing a negative forecast bias.

Figure 9.19 shows statistics for 1st and 6th forecast day in the Arctic Ocean. The onset of the spring bloom in the model is significantly delayed, but from the middle of May onwards, the model results are close to the observations. The quality barely changes as the length of the forecast period increases, except during the spring bloom (the first weeks of the time series) in which the bias is significantly smaller for a forecast range of one day, suggesting that, at this stage, the model is unable to support increased concentrations after the assimilation events.
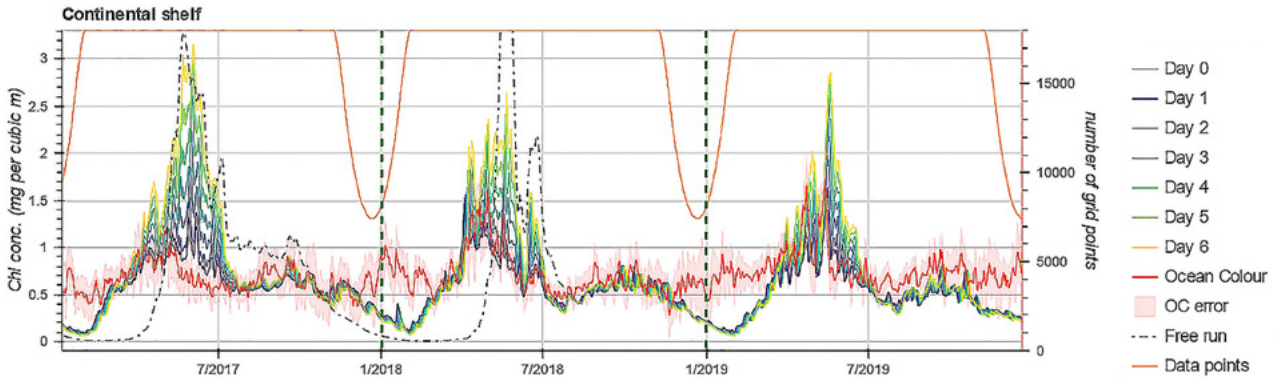
Figure 9.18.   Time series of surface Chla concentration for European North West Shelf Seas average. Day 0 is the analysis day, with assimilation of satellite Chla, and days 1-6 are forecast days. Satellite ocean colour values are shown in red for comparison and error in the pink shaded area. The number of grid point matchups is shown in orange (from McEwan et al., 2021).
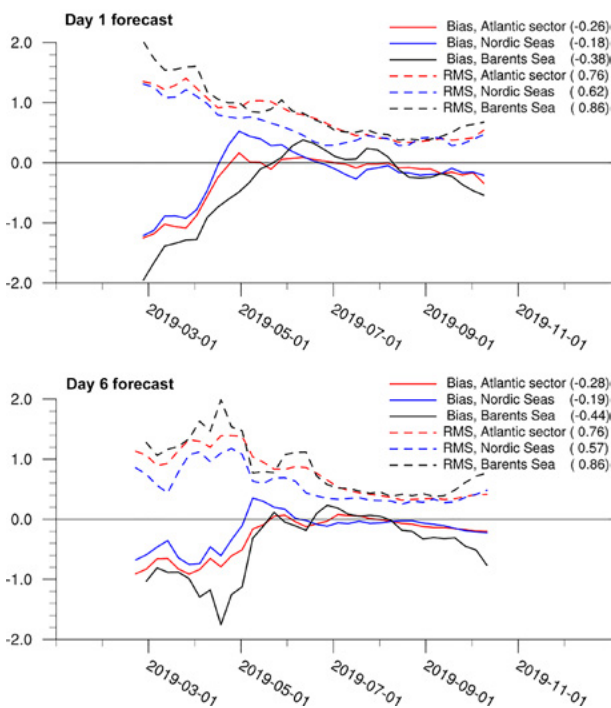
Figure 9.19.   Time series for bias and root mean square (RMS) differences between the Arctic Ocean model system and ocean colour satellite for 1st (top) and 6th (bottom) forecast day. Statistics are given for the various regions, log10 transformation has been applied (from Melsom and Yumruktepe, 2021).

A different class of metrics can be used to evaluate the capacity of the forecast system to reproduce specific events, such as algal blooms. In this case, the skill metrics are based on a binary discriminator test with a threshold (i.e. greater or lower than a given value of Chla concentration) and a yes/no decision. For example, the ROC (Brown and Davis, 2006) compares two independent information sets (i.e. forecast and observation) with respect to a threshold value. For each couple of yes/no decisions there are four possible outcomes, either correctly positive or correctly negative, and two model failures for incorrectly positive and incorrectly negative. Results of such metrics are plotted in contingent tables (Stow et al., 2009).

An example of the use of the ROC to characterise Chla in terms of events is presented in Figure 9.20, using the Mediterranean Sea system. The threshold is defined as the 75th percentile of surface concentration and identifies surface bloom occurrence.

Since biogeochemical variables are often not Gaussian distributed (e.g. surface Chla distribution resembles a log-normal density distribution), forecast skill performance metrics can be computed on log-transformed data or using non-parametric statistics, for example median of the misfit (i.e. model minus observation) instead of bias, interquartile range of the misfits instead of RMSD, and Spearman correlation instead of Pearson one. However, while data transformation (such as the log-transformation) preserves the statistical robustness of metrics, it results in metric values that may be difficult to understand by users, thus reducing the benefit of the validation information (Hernandez et al., 2009).
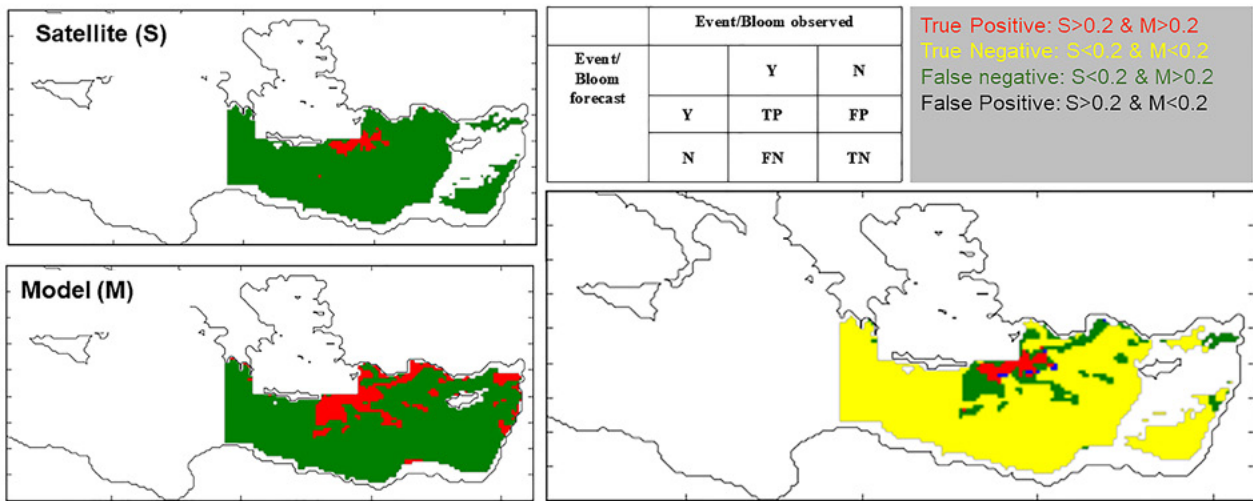
Figure 9.20. Time series of surface Chla concentration for European North West Shelf Seas average. Day 0 is the analysis day, with assimilation of satellite Chla, and days 1-6 are forecast days. Satellite ocean colour values are shown in red for comparison and error in the pink shaded area. The number of grid point matchups is shown in orange (from McEwan et al., 2021).

Real time skill statistics are reported in web pages which are continuously updated (e.g. the validation dashboard of the Copernicus Marine Service: 🔗 [23]). Indeed, time series of the validation metrics monitor the quality of the operational biogeochemical system and alert for quality degradation of the model outputs. Possible deviation from the nominal quality of the forecast products, which is specified in the delay mode validation, might be due to model failure to capture specific events, degradation of upstream input data (e.g. assimilated observations), model internal biases, but also to the day-to-day fluctuation in the number of available observations.

9.2.6.2. Delay mode evaluation

The DM validation conveys a more comprehensive and detailed evaluation of the model capability to reproduce the spatial and temporal scales of variability of marine biogeochemistry. DM validation assesses the reliability of the model results considering the user needs and requirements, measures the strengths and weaknesses of the model system for future developments, and defines the nominal quality level to which the forecast skill performance can be compared (Hernandez et al., 2018).

9.2.6.2.1. Common graphical representations

Results of the model performances assessment are generally provided in a variety of graphical representations that can be complementary each other, most common representations are:

23. https://pqd.mercator-ocean.fr/

- Spatial maps represent the spatial distribution of a given variable and highlight the model's ability to reproduce global patterns, spatial gradients, and basin inter-difference. The bias and RMSD maps between predicted and observed values identify the regions of high and low model uncertainty.

- Scatter plots compare the predicted values with the observed values in the form of a collection of pair-values (i.e. points in a model vs observation graph). If the points are coloured, one additional information can be displayed. Scatterplots are useful to identify relationships between the predicted and observed values.

- Vertical profiles compare the vertical structure of the predicted values with the observed values: surface values, vertical gradient, and deep content. The shape of the profiles gives indications of the physical and biogeochemical dynamics at work.

- Time series graphs represent the evolution of predicted values with the observed values as a function of time. Such representation allows analysis if temporal dynamics (such as seasonal variability, interannual variability or trends) are captured by the model.

- Hovmöller diagrams are latitude/longitude/depth versus time diagrams displaying the evolution of a variable. They are more powerful than the time series graphs because they offer an additional dimension, allowing to study how models reproduce spatial or vertical dynamics over time.

• Taylor diagrams display simultaneously information on model-observations skill for three metrics (Taylor, 2001): 1) the Pearson correlation coefficient, 2) the RMSD, and 3) the SD. RMSD and SD are usually normalised (RMSD and the model SD are divided by the SD of the observations) to represent all metrics with different units into a single diagram (normalised Taylor diagram). The Pearson correlation coefficient between the model and the observations is given by the azimuthal position. The normalised SD is proportional to the radial distance from the origin. The normalised RMSD is proportional to the distance from the reference point. The observational reference is indicated along the x-axis and corresponds to the normalised SD and correlation equal to 1. Such diagrams are used to compare different model versions or to summarise the model performance for different variables in a single and compact diagram (Jolliff et al., 2009).

9.2.6.2.2. Evaluation of different system versions

In the frame of the continuous improvement principle, any upgraded and novel version of an operational biogeochemical system should show advancements with respect to the previous one in terms of model characteristics (e.g. addition of new modelled variables and processes) and quality of the results. Updates of model formulations and upstream input data contribute to reduce the system uncertainty with respect to a standard skill performance framework allowing versioning comparison. Figures 9.21 and 9.22 show how metrics can be used to compare different versions of a system.

Figure 9.21 compares daily surface Chla for two model versions of the European North West Shelf Seas system using regionally-averaged time series (GODAE Class 4 metrics). The new product (V11 in Figure 9.21) is constrained by data assimilation while the previous product (V10 in Figure 9.21) was not. The new version shows a better match with satellites during the growing season, with lower summer peak and earlier spring bloom, although there are differences among regions.

In Figure 9.22, the Taylor diagram summarises the quality improvement for different system versions of the Irish-Biscay-Iberia MFC. Chla, nutrients, oxygen, and carbon variables are compared to ocean colour, WOA and GLODAP (GODAE Class 4 metrics). The evolution of the system shows an improvement in almost all variables, and particularly in carbon-related variables. This improvement is due to more realistic initial and boundary conditions in the latest version of the system.
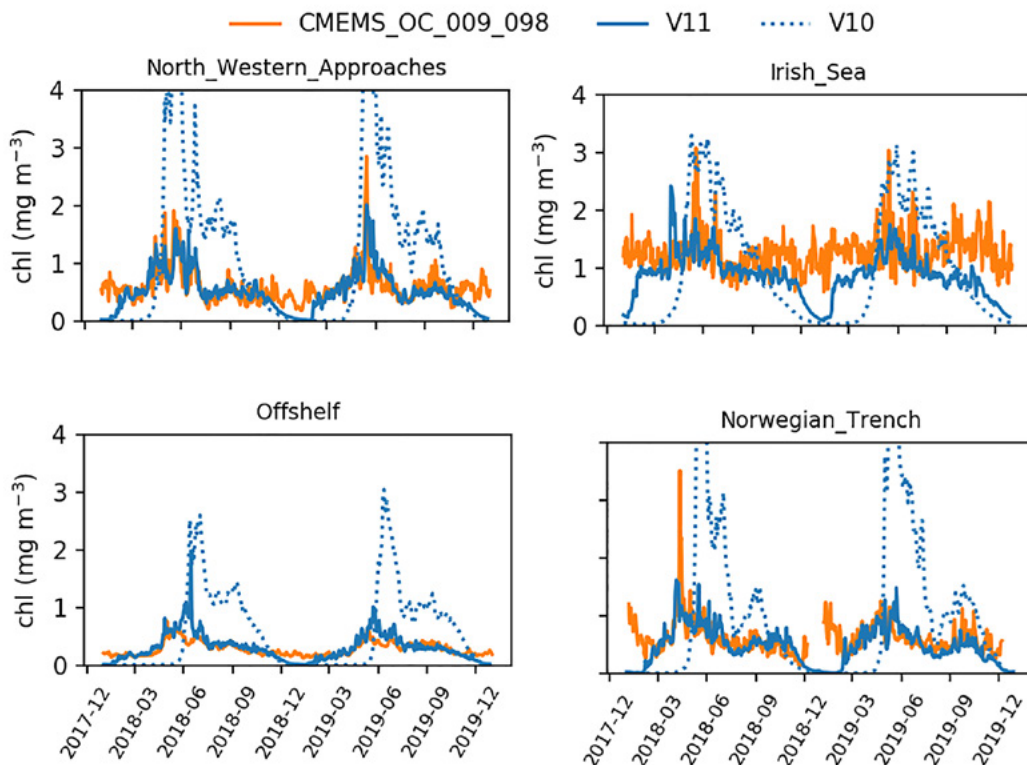
Figure 9.21. Time series of daily surface Chla for regions of the European North West Shelf Seas, from the new product (V11), the previous version (V10), and ocean colour satellite (from McEwan et al., 2021).
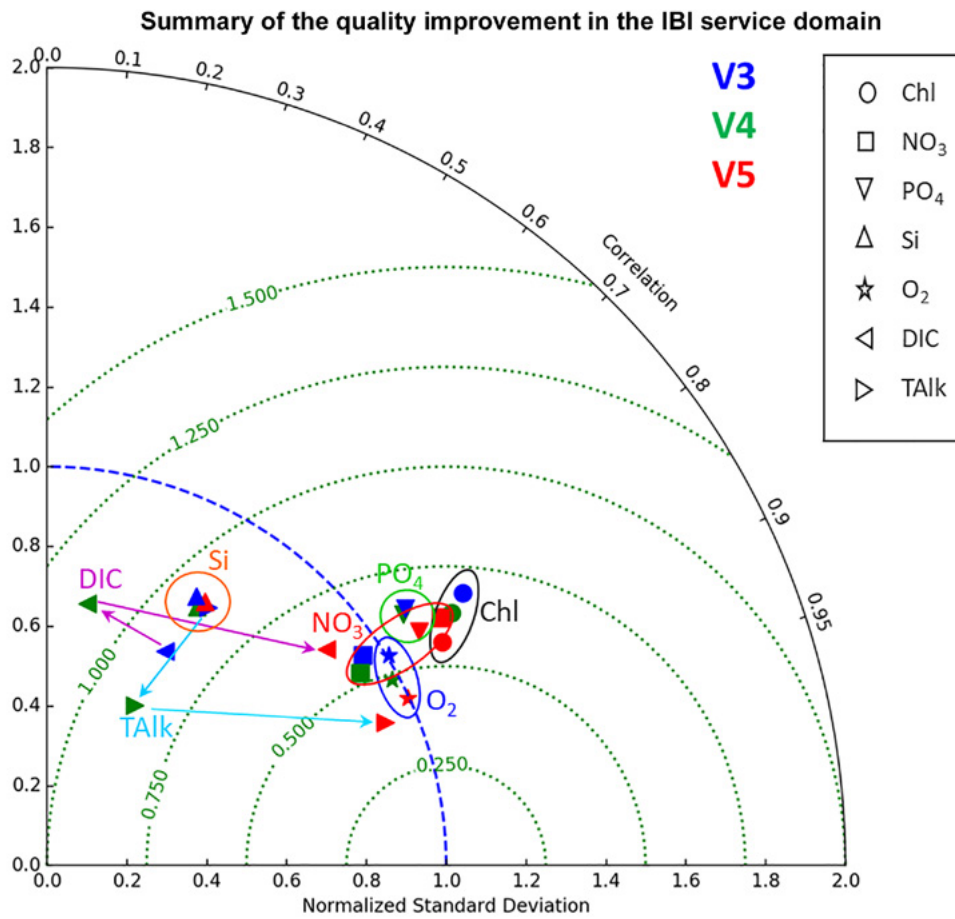
Figure 9.22.   Taylor diagram summarising the quality improvement of the operational system of the Irish-Biscay-Iberia MFC (part of the Copernicus Marine Service).

9.2.6.2.3. Spatial and temporal evaluation

The DM validation is commonly built to test the pre-operational system for a medium/long simulation using higher quality observation datasets. They can include the same observation data of the NRT validation but characterised by a higher quality check (e.g. reprocessed ocean colour product) and an additional number of historical in-situ data collections (e.g, World Ocean Database, SOCAT, EMODnet data collection) that, because of the delay mode quality check, become available a certain time after their acquisition time.

Chla derived from remote sensing is a major dataset for BGC OOFS. It is extensively used in DM validation to validate the spatial and temporal structures. Figure 9.23 shows the annual average distribution of Chla from the model and satellite observations (i.e. GODAE Class 1 metrics). The large-scale structures present a good agreement, i.e. the main biogeographic provinces of Longhurst (1998) including oligotrophic gyres (low levels of chlorophyll in the centre of the basins), Antarctic Circumpolar Current, tropical band, Eastern Bound-

ary Upwellings, are well reproduced. Differences at the regional spatial scale are found along the equatorial band, in the southern high latitudes, and in coastal regions as highlighted by the scatterplot (Figure 9.24). The distribution of points shows good estimations in the open sea (for depths higher than 1000 m) and underestimations in shallow waters (when bathymetry is lower than 1000 m).

Seasonal cycle and interannual variability can be analysed using Hovmöller diagrams. Figure 9.25 shows the seasonal cycle of Chla in the North Atlantic, from the Global Ocean system of the Copernicus Marine Service. The main features reproduced are: i) a bloom in spring when the mixed layer, rich in nutrients, shoals (light limitation); ii) a decrease of Chla concentration in summer due to a thin mixed layer very poor in nutrients (nutrient limitation); iii) a secondary bloom in autumn when the mixed layer is deepening and nutrients are transported in the euphotic layer; iv) a period of weak production (light limitation) in winter; and v) a marked seasonal cycle in the extension of the subtropical gyre (retraction in winter and extension in summer). The interannual variabili-
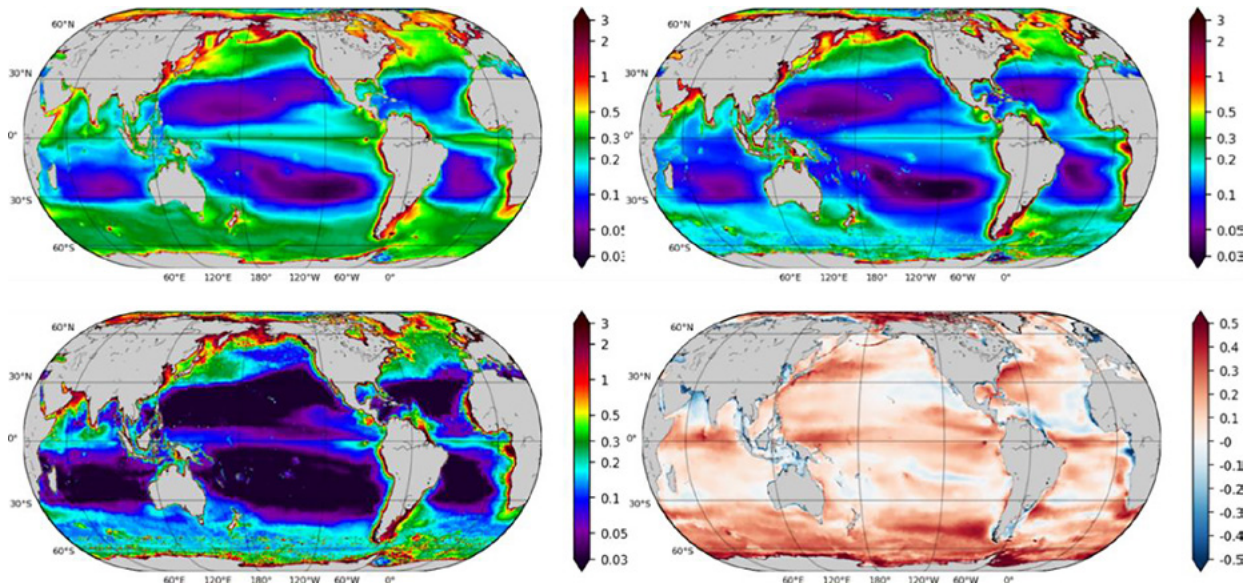
Figure 9.23. Annual mean of surface Chla averaged over the period 2009-2018 (mg Chl m⁻³). Top left: model. Top right: satellite L4 observations. Bottom left: RMSD between model and satellite observations. Bottom right: log bias (i.e. mean difference of log) between model and observations (from Lamouroux et al., 2019).

ty of the south boundary of the oligotrophic gyre (i.e. the area between 30°N to 40°N) is also well reproduced by the model.

Long-term oceanographic monitoring stations are invaluable platforms to investigate temporal and spatial scales of BGC variability and assess BGC and ecosystem models. An example is the BATS in the Sargasso Sea, situated in the North Atlantic subtropical gyre. Figure 9.26 compares the Chla modelled and measured at this station. The model predicts reasonably well the subsurface Chla maximum, with concentrations slightly higher than in BATS data. The model catches the seasonal cycle, with a bloom during the deepening of the mixed layer in winter. In summer, the production in the mixed layer is more limited and is mainly due to the local remineralization of organic matter (regenerated production).

Observations for a large number of variables are also available in historical in-situ collections (e.g. nutrients like nitrate, phosphate, ammonium, silicate, iron; and carbonate system variables like dissolved inorganic carbon, alkalinity, pH, pCO2, biomass for phytoplankton and optical quantities) contributing to enrich the state validation framework embracing multiple features of the biogeochemical model.

Figure 9.27 presents a multivariate GODAE Class 1 quantitative comparison between model average vertical profiles and the reference EMODnet climatological profiles in the North West Mediterranean sub-basin. The model reproduces the average values and shape of the profiles; modelled profiles are within the range of variability of the climatological profiles.
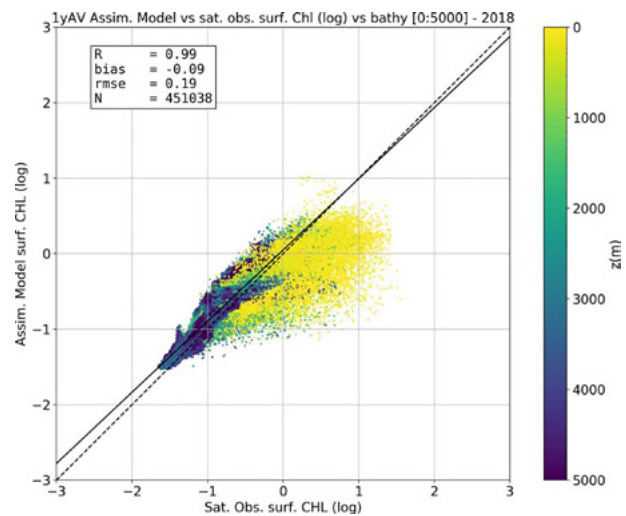
Figure 9.24. Scatterplot comparison of 2018 annual averaged surface Chla concentration for the model vs satellite observations. The colorbar represents the bathymetry (m), from shallow (yellow) to deep water columns (dark blue). The dashed line is the line 1:1, the plain line is the least square regression fit within the data. The correlation coefficient R, the bias, the RMSD (referred to as rmse) and the number of points N are computed on the log10-transformed space (from Lamouroux et al., 2019).
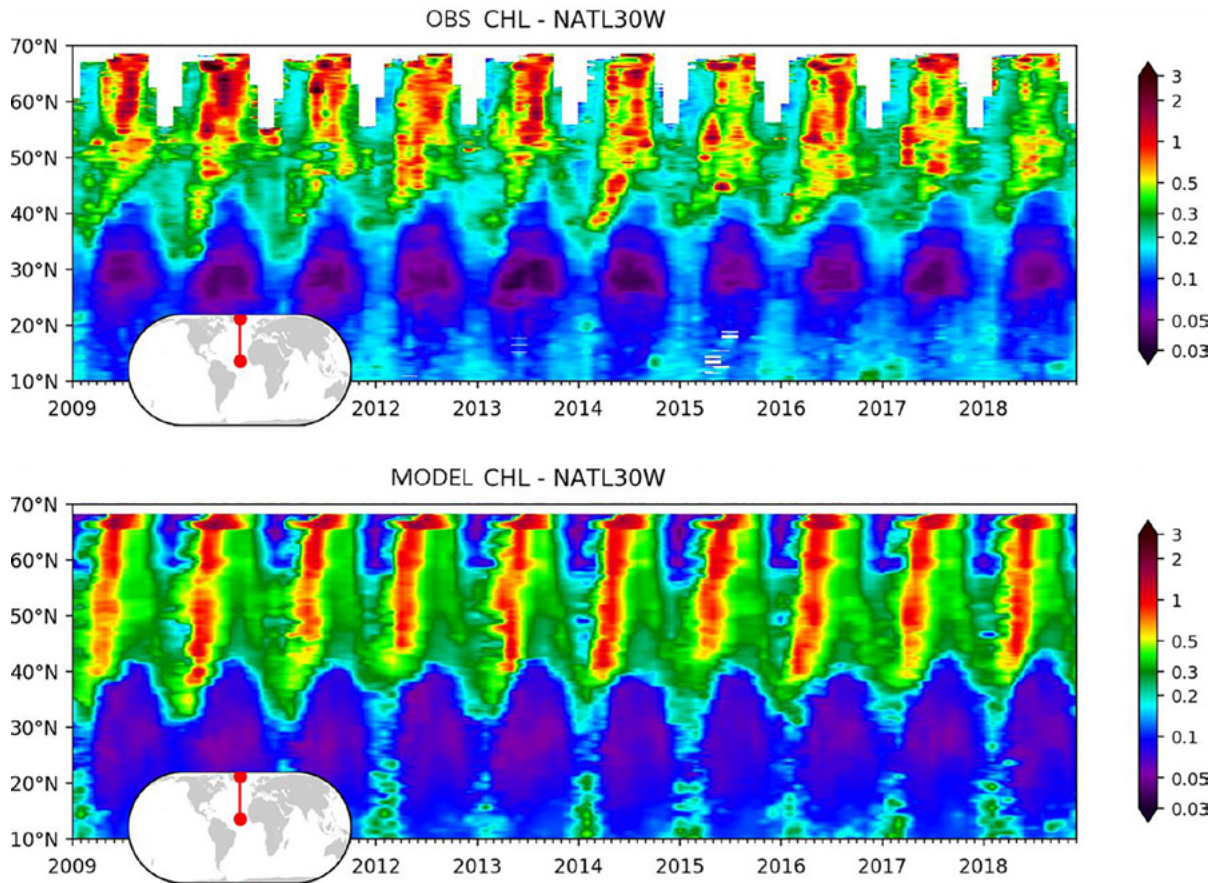
Figure 9.25. Hovmöller diagram (latitude versus time) of surface Chla concentration on 2009-2018 period computed with monthly mean fields. Top: model. Bottom: satellite observations (from Lamouroux et al., 2019).
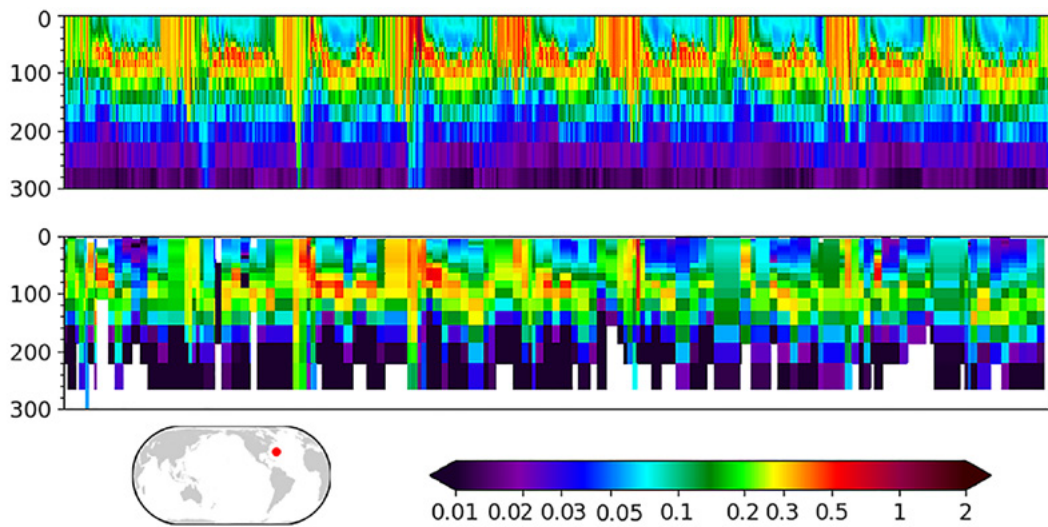
Figure 9.26. Hovmöller diagram (depth versus time) of Chla concentration (mg Chl .m-3) in the layer 0-300 m at BATS station, over the period 2008-2017. Top: model. Bottom: bottle data at BATS station (from Lamouroux et al., 2019).
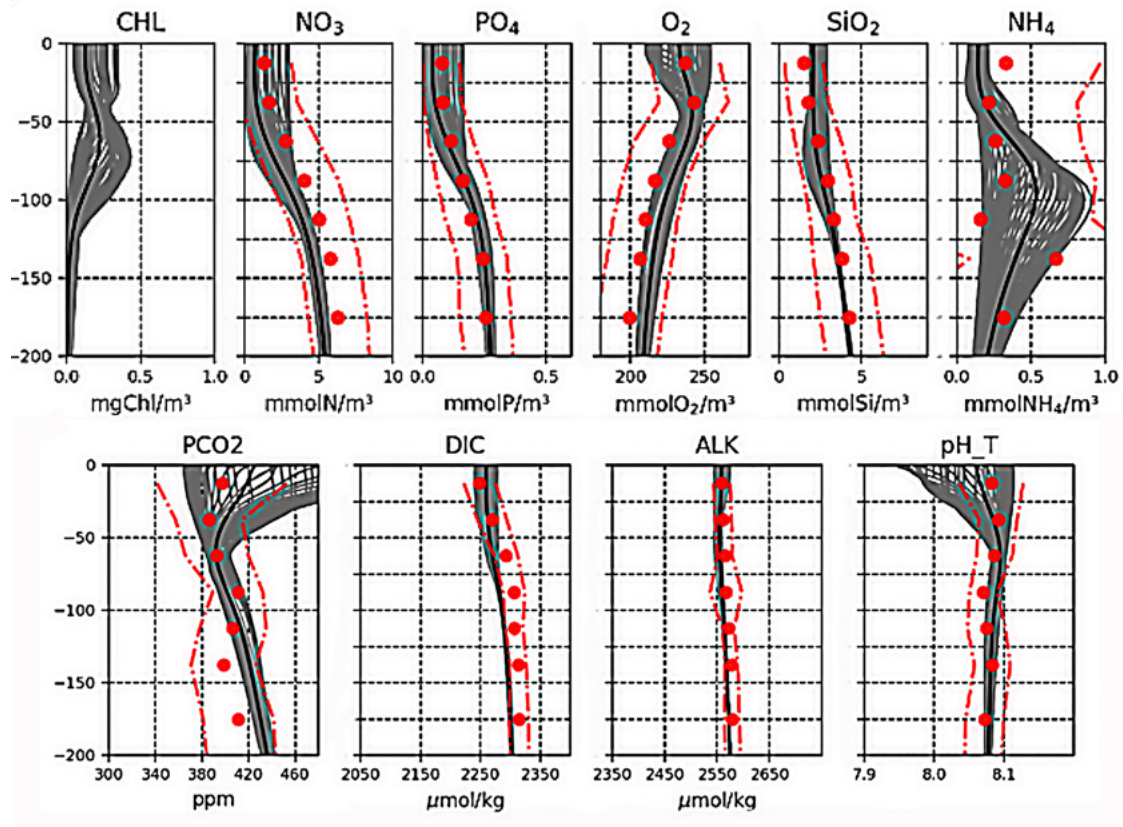
Figure 9.27.   Comparison between weekly (grey lines) and annual (black lines) vertical profiles from the model run for North West Mediterranean sub-basin in 2019 (part of the Copernicus Marine Service) and climatological profiles of nutrients, dissolved oxygen, and carbon variables retrieved or derived from EmodNET dataset (red dots for means and dashed lines for standard deviations) (from Salon et al., 2019; Feudale et al., 2021).

9.2.6.2.4. Process-oriented evaluation

Besides the already mentioned direct skill error calculation (e.g. bias, RMSD) and pattern assessments (e.g. spatial correlation between model and observational maps), DM validation is enriched by process-oriented metrics (i.e. quantities derived from state variables that describe the results of particular processes) and theoretical derived quantities, such as stoichiometric indicators N:P, DOC:POC, Chla:POC, which contribute to assess the fit-for-purpose of the model functioning. Among process-oriented metrics, it is worth mentioning those deriving from the use of the continuously growing amount of available BGC-Argo floats and glider profiles. Metrics are based on the depth, slope, and amplitude of several particular biogeochemical features, such as the deep Chla maximum, nitracline, and oxygen minimum zones. They are associated with the biological carbon pump, the air-sea CO_2 flux, oceanic pH, oxygen levels, and provide an innovative framework that evaluates the model capability to reproduce the interaction of physical (e.g. vertical mixing) and biogeochemical (e.g. phytoplankton growth and uptake) processes that shape variable vertical profiles (Salon et al., 2019; Mignot et al., 2021).

These metrics are currently used for DM validation but could also be easily implemented for NRT validation by routinely comparing the forecast skill with pre-operationally defined seasonal benchmarks and thus highlighting possible anomalies. For example, Salon et al. (2019) used such metrics to evaluate the system of the Mediterranean Sea (Figure 9.28), while Mignot et al. (2021) applied them to evaluate the system of the Global Ocean (Figure 9.29 and 9.30), both part of the Copernicus Marine Service.

Figure 9.28 shows how the time evolution of the vertical profiles matches up with the observations as well as several quantitative metrics along the corresponding float trajectory in the Mediterranean Sea. Temporal succession of the winter vertically mixed blooms, the onset, the time evolution, and the depth of the DCM, which typically establishes during the
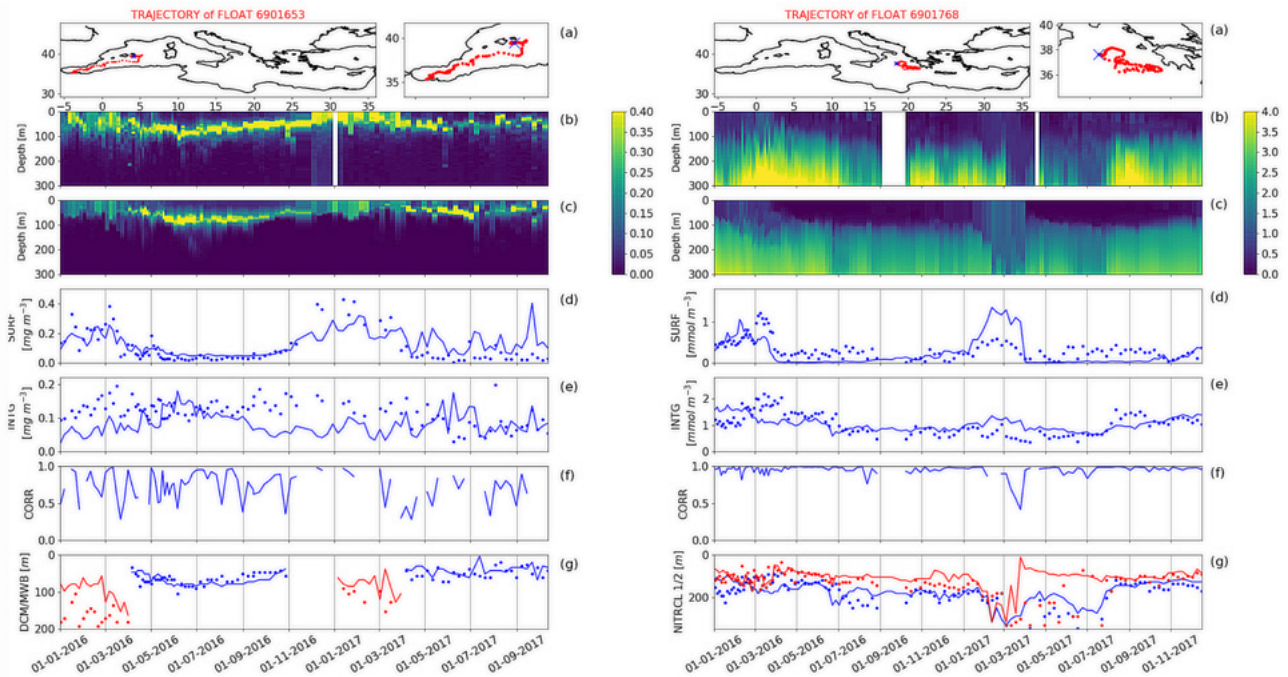
Figure 9.28. Time evolution of two BGC-Argo floats in Mediterranean Sea for Chla (left) and nitrate (right). a): trajectory of the BGC-Argo float; b): Hovmöller diagrams (depth versus time) of Chla and nitrate concentration from float data; c): model outputs matched-up with float position. Metrics for model (solid line) and float data (dots): d): surface concentration; e): 0–200 m vertically averaged concentration; f): correlation between vertical profiles; g): depth of the deep chlorophyll maximum (blue) and depth of the mixed layer bloom in winter (red) to the left, and depth of the nitracline (2 calculation methods) to the right (from Salon et al., 2019).

stratified season, are consistent in the Western Mediterranean Sea (Figure 9.28, left). The analysis is completed by Chla profiles, nitrate content, and nitrate-based metrics (Figure 9.28, right) that allow to evaluate the key coupled physical–biogeochemical processes (i.e. water column nutrient content, nitracline, and effect of winter mixing and summer stratification on the shape of nitrate profile). The shape of the nitrate profile (i.e. correlation values), the temporal evolution of the 0-200 m averaged values and of the nitracline depth are consistent for the selected float in the Eastern Mediterranean Sea.

Figure 9.29 compares the seasonal time series of MLD, surface Chla, NO3, Si and PO4 in the North Atlantic during the "spring bloom", derived from the BGC-Argo floats observations and from the Global Ocean system of the Copernicus Marine Service. The percent bias and percent RMSD are also represented for each metric. The model reproduces the seasonal cycle of surface Chla and nutrients, i.e. the timings of minima, maxima, and the onset of the bloom, the winter Chla minimum and winter nutrients maxima. However, the skill metrics deteriorate in summer with the model underestimating Chla maximum and overestimating NO3 and PO4 minima.

The Global system skill for 22 metrics (Mignot et al., 2021) is summarised in the Taylor diagram (Figure 9.30), which allows for a rapid evaluation of strengths and weaknesses of a model simulation. For instance, the global model is skilled at reproducing oxygen levels, cycling of nutrients, and DIC, but the representation of Chla, POC, spCO2 and spH needs to be improved.

Finally, DM validation can be enriched by additional levels of process and system validation (Hipsey et al., 2020). These aim to assess the model performance, to simulate fluxes and rates of transformation, which drive changes in model state variables, and to verify emergent properties that are not directly predictable by the choices made to build the model structure and formulations. Measuring time and space variability of in-situ fluxes is difficult and highly resource consuming, thus the list of metrics remains restricted to few fluxes, such as rate of primary production, nutrient uptake, grazing rates, and sinking of organic particles. Nevertheless, the general confidence and fit-for-purpose in the underlying function of biogeochemical operational models can be increased by informing users about the uncertainty of a wider range of processes featured in the model formulation.
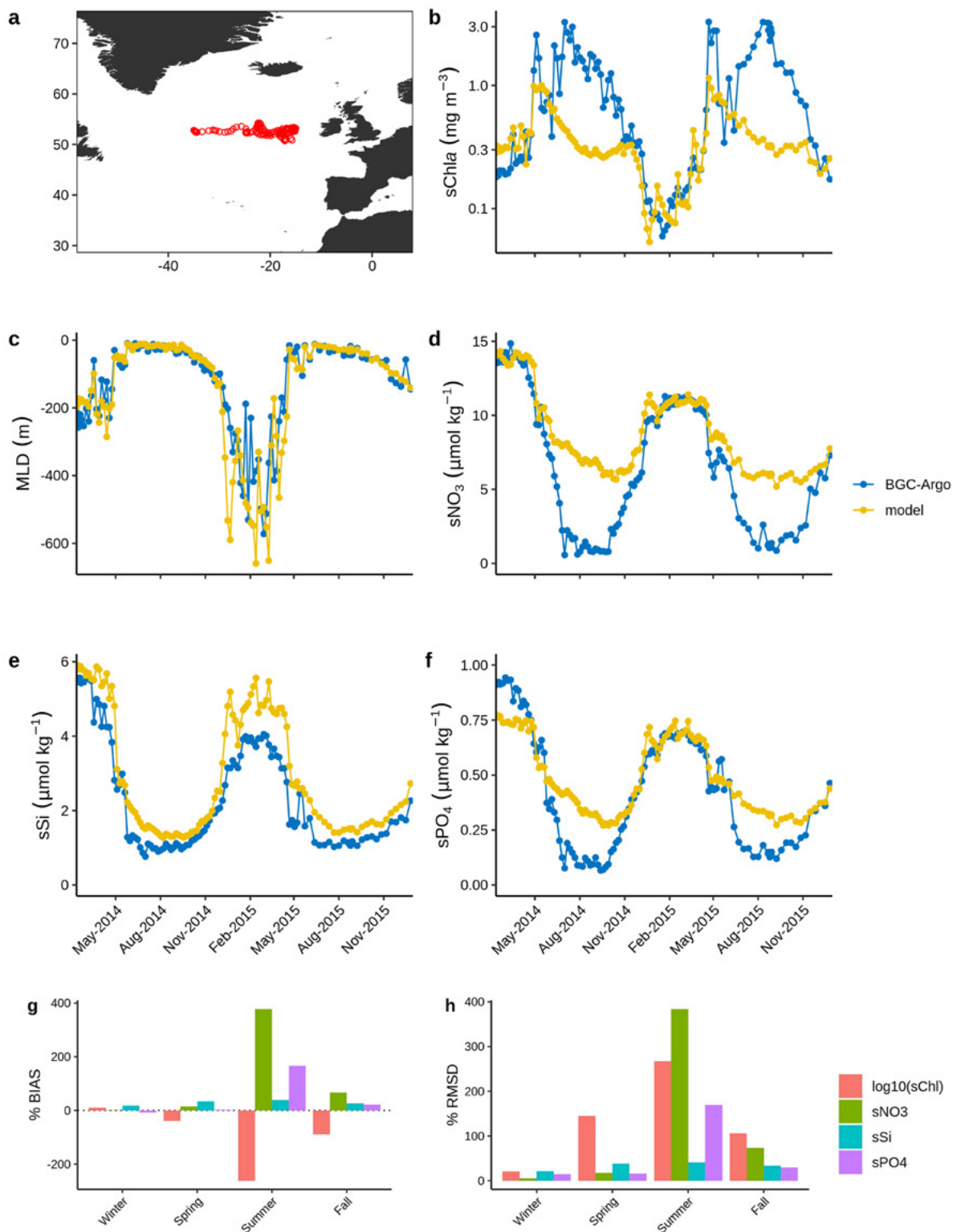
Figure 9.29.   a): trajectory of a BGC-Argo float located in the North Atlantic. Time series derived from the BGC-Argo (blue) and the model simulation (yellow): b): mixed layer depth; c): surface Chla; d): NO_3; e): Si; f): PO_4. For each metric: g): seasonal percent bias; h): percent RMSD (from Mignot et al., 2021).
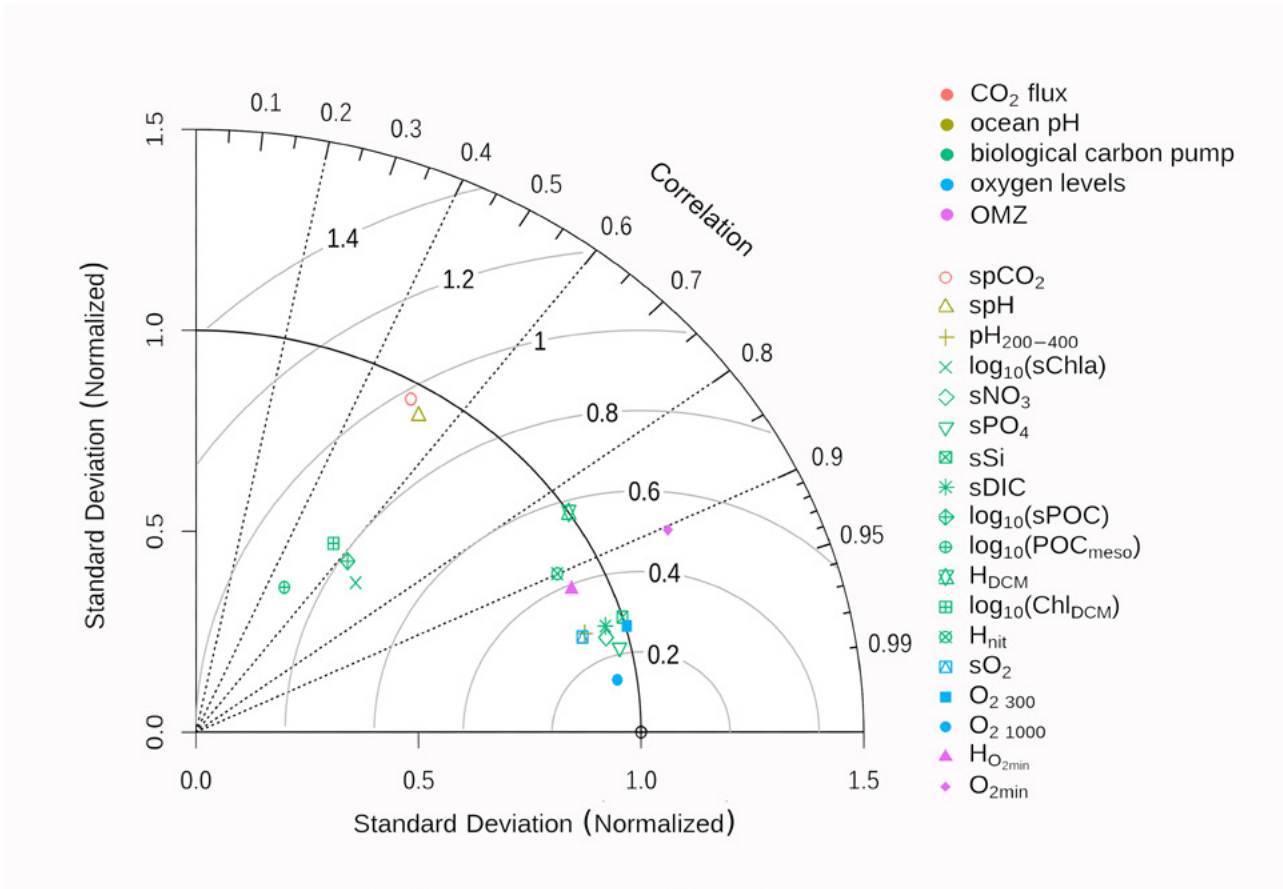
Figure 9.30. Comparison of BGC-Argo float observations and model values for 22 metrics using a Taylor diagram. The symbols correspond to the metrics and the colours represent the BGC processes with which they are associated (from Mignot et al., 2021).

9.2.7. Output

The purpose of this section is to provide recommendations and guidelines about the dissemination of products and the delivery of services based on BGC OOFS. These recommendations stem from the experience gained by some operational oceanography service centres, which deliver numerical products and have collected users' needs through the Service Desk, a structure dedicated to answer and manage any user request. Products and services, such as the production, preparation, and delivery of operational ocean forecasts to users in forms that meet their needs, are the final goal of an OOFS.

9.2.7.1. Data formats

Following the community of physical oceanographers, the biogeochemical community has widely adopted the NetCDF format (🔗 24) and the CF metadata conventions (🔗 25) for standard names and units. These standards are adopted by most operational oceanography actors (e.g. within GODAE OceanView), including the groups that operate numerical ocean prediction systems, and also by most of those delivering services based on oceanic observations.

24. https://www.unidata.ucar.edu/software/netcdf/
25. https://cfconventions.org/

9.2.7.2. Standard products

A BGC OOFS should offer users a reliable and easy access to valuable ocean information (past, present, and forecast). Each system operator should work to ensure that the following common variables (with their acronym or formula in brackets) are produced in delayed-mode and real time bases:

- nitrate concentration [NO_3]
- phosphate concentration [PO_4]
- dissolved oxygen concentration [O_2]
- chlorophyll-a concentration [Chla]
- phytoplankton concentration (expressed as carbon) [PHYC]
- net primary production of biomass (expressed as carbon) [NPP]

In addition to the above standard products, operators should also make available the following products, if they are represented in the model:

- silicate concentration [Si]
- iron concentration [Fe]
- ammonium concentration [NH_4]
- zooplankton concentration (expressed as carbon, mass, or mole) [ZOOC]
- PFTs chlorophyll-a concentration [PFTs]
- dissolved inorganic carbon concentration [DIC]
- total alkalinity [TALK]
- pH [pH]
- surface pCO_2 [$spCO_2$]
- air-sea CO_2 flux [fCO_2]
- light attenuation coefficient [Kd]
- photosynthetic photon flux [PAR]
- euphotic layer depth [ZEU]
- secchi_depth_of_sea_water [ZSD]

Model data are usually archived in the units specified by the International System of Units (SI Units), being mole per cubic metre (symbol mol m^{-3}) for concentration in seawater.

9.2.7.3. Data storage

The 2D or 3D concentrations of the modelled prognostics and diagnostics variables are saved and stored instantaneously, or averaged over specific time periods (daily, weekly, monthly, etc.). It has to be underlined that to store outputs requires substantial computer disk space, especially for biogeochemical models which can generate a lot of variables or derived quantities. This should be considered before the operational system is set up.

9.2.7.4. Other end-user products

Other data and information, called "end-user products", can be derived from or in addition to the standard products, with the purpose of building indicators of the marine environment for water quality monitoring, pollution control (eutrophication phenomena), food web indicators, etc.

9.2.7.5. Applications

The scientific community has identified key variables and indicators to evaluate current state and likely future conditions of the ocean, such as the EOV (from the GOOS Expert Panels) or the OMI (from the Copernicus Marine Service). Oxygen, chlorophyll-a, primary production, nutrients, pH, and CO2 air-sea flux are monitored to keep track of ocean health and changes, also to advise the policy makers. These indicators provide important information also for ecosystem-based fish management, sustainable aquaculture, and fisheries research. The number of users of BGC model products has been steadily increasing during the last years (Figure 9.31), highlighting the growing interest for BGC.

9.2.8. Higher trophic levels modelling

Researches by marine biologists, ecologists, and fishery scientists very often use a set of environmental variables to explain available observations for one species of interest and make predictions. Examples of frequently collected information include geo-referenced fishery catch data or acoustic-derived abundance of a fish species, scientific sampling of eggs, larvae or juveniles, satellite tracking of individuals of large fish, seabirds, turtles or marine mammals, or simply visual observations (whales). These studies are based on the correlation between
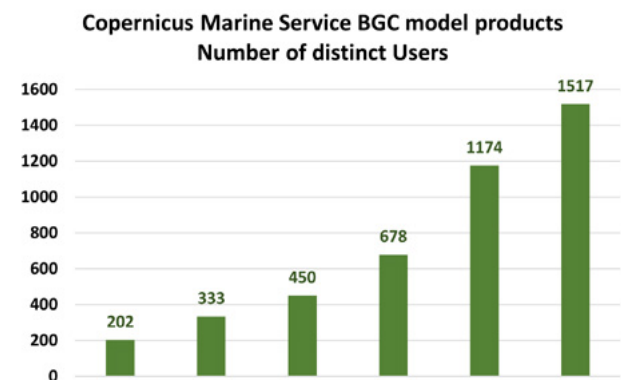
Figure 9.31. Number of distinct users of BGC model products of the Copernicus Marine Service during the last years (courtesy of the Service Desk).

outputs of the statistical or mechanistic model developed using the environmental variables and the observed variables, i.e. the presence or abundance of the studied species at a given stage of development. Since the relationships are defined using observations collected in a very dynamic environment with multiple sources of variability in time and space, it is essential to use environmental variables co-located with the observations. However, due to limitation in observations, marine scientists most often have to aggregate their data sets to crude resolutions, e.g. by season or year in large geographical boxes, or they restrain their analyses to satellite-derived oceanic variables, such as SST (available since early 1980s), SSH (since 1992), and sea surface Chla concentration (since 1998). The provision of these satellite-derived variables has generated large progress in the understanding of ecology and population dynamics of marine species. However, there are still some gaps in the use of these variables given that: i) satellites measure only the surface of the ocean; and ii) surface Chla is a proxy of primary production, which is not necessarily closely related to the upper trophic level animals that feed on zooplankton or larger organisms (e.g. micronekton). Furthermore, in the development phase of these organisms (lasting from days to months), the spatial and temporal correlation between primary production and these animals may be lost.

Modelling tools have the potential to fill these gaps, by simulating the marine food web with primary production, zooplankton, and micronekton as essential variables to support HTL. As explained in Section 9.1.1, BGC and HTL models are often separate models as they focus on different processes but BGC models can provide input for HTL models, and there are examples of BGC-HTL coupled models (e.g., Libralato and Solidoro, 2009; Rose et al., 2015; Aumont et al., 2018; Diaz et al., 2019). However, presently the link (online/offline coupling) is neither straightforward nor fully investigated. Thus, HTL models currently must rely also on other sources of input, such as satellite and in-situ data collection.

Connections, challenges, and expectations in bridging BGC and HTL modelling are discussed in the next subsections.

9.2.8.1. Essential variables

Primary production, zooplankton, and micronekton are essential ecosystem variables for the development of applications directed to management and conservation of marine resources and its biodiversity. Primary production is the source of energy to low and mid-trophic level functional groups. Zooplankton are a crucial link between the primary producers (mainly phytoplankton) and the micronekton at the mid-trophic level of the marine food web, as well as many mid-size pelagic species and some specialised large predators (e.g. baleen whales). Micronekton is defined by a size range between 1 and 10 cm, and include many species of

fish, crustaceans and cephalopods, as well as the early life stages of many larger fish species. The micronekton that inhabit permanently the lower mesopelagic depths (~ below 300-400m) feed on the organic matter sinking in the water column. All micronekton organisms, including the species temporarily occupying this trophic level and size range, are the forage of larger marine species that have developed various skills to detect and feed on them.

Primary production, zooplankton, and micronekton are thus key inputs to investigate the mechanisms driving fish recruitment, as well as movement and migration of oceanic predators.

9.2.8.2. Satellite-derived and in-situ observations

9.2.8.2.1. Primary production

To establish which mechanisms control the distribution, recruitment, and abundance of large oceanic exploited or protected species, marine scientists require a three-dimensional representation of the environment and not only surface observations as those provided by satellites. The existence of a deep Chla maximum (e.g. in tropical waters and the Arctic) is a good illustration of the lack of adequation between surface and subsurface. One possible solution for this problem is to extrapolate the satellite observations over the water column according to some empirical models developed to estimate vertically integrated primary production, or NPP, based on surface Chla and key variables (SST and solar radiation). This product provides an essential foundation to monitor ocean productivity. However, various flaws remain, there are caveats for shallow waters and the Arctic, as well as difficulties in resolving persistently cloudy regions. However, primary production can also be provided by BGC models, offering the better three-dimensional vision as opposed to the satellite-based estimates, but this solution is still little used although the improvements in BGC models (in particular thanks to the use of data assimilation) are promising.

9.2.8.2.2. Zooplankton

Zooplankton is certainly the variable on which have been developed the most advanced applications on larval recruitment, fish habitat, dynamics of small and mid-size pelagic species as well as baleen whales. Despite decades of sampling efforts at sea, zooplankton observations remain limited to a few valuable long-term time series from oceanographic stations and a partial global climatology from the compilation of all available data collected, which represents a huge effort of data standardisation (Moriarty and O'Brien, 2013). Therefore, only numerical models can provide the synoptic maps of zooplankton distributions needed by ecologists and fishery scientists.

9.2.8.2.3. Micronekton

Micronekton species, including a huge biomass of mesopelagic organisms, are among the largest unknowns in the functioning of the global ocean ecosystem. This is a critical gap to understand the ecology of their predators for which there is a lot of interest in terms of resource management and conservation. In recent years, climate change, carbon storage in the deep ocean, and the role of diel vertical migration of mesopelagic (and zooplankton) have become major scientific issues.

But, even more than for zooplankton, the sparsity of observations on a global scale and over time poses a real problem for modellers of higher trophic levels. The traditional approach for sampling micronekton is net trawling. Many studies are simply qualitative descriptions of species, quite often used in combination with acoustic sampling to support the extrapolation of acoustic signal to biomass estimates. However, biomass based on acoustic sampling, especially with one single frequency, can be easily biased by one or two order of magnitudes due to the very strong resonance (backscatter) of some organisms, e.g. gelatinous organisms containing gas bubbles (Proud et al., 2018) or conversely very weak resonance despite large biomass, e.g. fish without swim bladder (Dornan et al. 2019; Escobar-Flores et al. 2019). In the absence of sufficient data coverage, relatively simple modelling approaches are used to simulate these functional groups in a food web model, relying on allometric scale relationships, first macro-ecological principles, or fluxes between trophic boxes.

9.2.8.3. Models of zooplankton and mid-trophic levels

9.2.8.3.1. Complexified BGC models

Improving resolution of primary production in BGC models helps to get better zooplankton predictions, although the relationship is not so straightforward. The reason is that in models the zooplankton component is used as the closure term of the biogeochemical cycles. To compensate for the lack in biogeochemical models of zooplankton predation by higher trophic levels, a mortality function with a mortality rate increasing rapidly (quadratic term) is used to avoid numerical instability at high levels of biomass. A high mortality rate is realistic in warm tropical waters but less for cold waters in which the lifespan of zooplankton is much longer, leading to high biomass persisting during fall. Underestimated zooplankton biomass can then have a cascading effect on the phytoplankton mortality. To address this issue in biogeochemical models, it may help the addition of a trophic level feeding on zooplankton, e.g. the micronekton at the intermediate trophic level, or a simplified representation of the entire upper food web with a size spectrum approach (Zhou et al 2010). Gelatinous organisms are also increasingly recognised

as a key group in marine biogeochemical cycles as they need to be included to account for zooplankton mortality. A recent development consisted in the introduction of a jellyfish functional group in the biogeochemical model PLANKTOM (Wright et al., 2021), suggesting that it can have a large direct influence on the zooplankton as well as on the other groups through trophic cascades. However, parameterisation of physiological rates and validation of micronekton and jellyfish carbon biomass are limited by the deficit of data on these species. Moreover, adding mid-trophic level compartments would still increase complexity of BGC models, which are already complicated as including dozens of variables.

9.2.8.3.2. Spatially explicit models with transport

Models with less complexity and easier to parameterize can be used in the meantime. They are useful approaches complementary to more complex BGC models, allowing faster testing studies, e.g. for processes and new functional groups, with outputs providing useful intermediate benchmarks. These models do not include all the detailed biogeochemical cycles but focus on food web functional groups, size spectrum, or target species. The link with the lower trophic level can be as simple as an energy transfer coefficient between primary production and each functional group. A key advantage of reduced complexity is the greater facility to implement quantitative methods to estimate parameters using available observations, whether at global or regional level. Nevertheless, such models still simulate the transport by oceanic currents, either based on advection-diffusion equations like the ocean circulation and BGC models (Maury et al., 2007; Lehodey et al., 2010), or with mean transfers between adjacent grid cells and geographical boxes (Audzijonyte et al., 2019). Transport can be also simulated using Lagrangian IBM approaches that keep track of individuals or meta-individuals characterised by individual state variables (weight, length, energy storage, life stage, etc) and behavioural rules. However, due to computational cost, this approach is still usually limited to regional domains or single species (DeAngelis and Gross, 1992; Carlotti and Wolf, 1998; Miller et al., 1998; Huse et al., 2018).

9.2.8.3.3. Ecosystem food web and size spectrum models

Other modelling approaches are oriented towards a representation of the ecosystem food web to explore the interactions between fisheries and exploited, by-catch, or protected species (Christensen and Walters, 2004). Zooplankton and mid-trophic levels are often defined by a small number of functional groups in the food web interactions. The difficulty comes from the rapid increase in the number of parameters as functional groups and species are added in the food web model. The increasing complexity in the network of connections between the numerous groups, species and sometimes life stages of species, is developed at expense of the spatial description. A few approaches combine such complexity with

a semi-spatially explicit representation, i.e. through bulk-transfer between geographical regions or cells from various sizes (e.g. Audzijonyte et al., 2019). The size spectrum is an approach that strongly simplifies the view of a marine ecosystem.

The size-based ecosystem modelling is a classical approach that is used to predict biomass distribution and size-structure of marine consumers (see review in Blanchard et al., 2017). Jennings and Collingridge (2015) have developed this approach at global scale. The model predicts rates and magnitudes of energy flux from primary producers to consumers that depend on primary production, transfer efficiency, predator and prey body mass, and temperature. Biomass is estimated in the water column without considering the horizontal transport nor the vertical structure, and mesopelagic communities are not explicitly modelled. Maury et al. (2007) have developed a similar size-spectrum approach but that also accounts for the influence of spatial dynamics and vertical diel migration. Aumont et al. (2018) have fully coupled this latter model to a physical-biogeochemical model allowing to explore two-way interactions between lower and higher trophic levels of the pelagic ecosystem. Petrik et al. (2019 and 2020) have proposed another approach that discretizes the size spectrum into a few stage-structured functional groups as in De Roos et al. (2008). Their demographic system at each spatial grid cell is forced offline by vertically integrated temperature, vertically integrated zooplankton biomass concentrations and mortality losses, bottom temperature, and detrital fluxes, but there is no transport or fish movement.

There is no simple solution to model end-to-end ocean ecosystems (Fulton, 2010) but various approaches that reflect the different scientific questions that are investigated. The demand for greater details in taxonomic representation and population dynamics (including transport, recruitment, and migrations) of target species, creates major problems in calculation, estimation of parameters, and analysis of uncertainties, which may be a critical issue if the model has to support management and policy decisions. For these reasons, to formulate management advice for quotas of catches and/or effort and conservation measures, RFMOs mostly rely on standard stock assessment modelling approaches, fitted to key target species and fisheries. These models have been used since the 1960s and can integrate multiple sources of information to estimate the key parameters of population dynamics and fisheries for a single species (Maunder and Punt, 2013). However, they treat the environmental variability as noise that is removed from fishing data using standardisation methods or integrated as a random signal in the predicted recruitment process, and thus they cannot be used to project mid- to long-term changes (e.g. climate change effects on fisheries).

9.2.8.4. Contribution from operational oceanography

Improved BGC models with assimilation of in-situ and satellite data is an approach with promising results and rapid progress. Thanks to data assimilation, the physical and biogeochemical models used in operational oceanography to predict and forecast ocean physics and primary production are becoming more and more accurate. Consequently, they are used by an increasing number of marine biologists, ecologists, and fishery scientists. The outputs of biogeochemical models are also essential to explore the historical period before the satellite era, which started in the late 1970s (see Figure 9.7). The information generated by BGC models is also needed to develop seasonal forecasting of ocean ecosystems, population dynamics of marine animals, and to explore the impact of climate change with long-term projections, once forced by Earth System Models. Many BGC models also provide dissolved oxygen concentration and pH, which are useful variables for modelling habitats of fishes. Finally, the recent progress achieved in operational oceanography contributes to an overall improvement of all types of zooplankton, micronekton and ecosystem models.

A global zooplankton and micronekton model-based product (Lehodey et al., 2010 and 2015) is delivered in the Copernicus Marine Service. With only 11 parameters, the model simulates one functional group of zooplankton and six functional groups of micronekton in the global ocean, with a vertical structure simplified into three layers in the water column (epipelagic, and upper- and lower-mesopelagic) allowing to consider vertically migrant and non-migrant mesopelagic behaviours. The functional groups are driven by primary production, euphotic depth, temperature, and horizontal currents with time of development and mortality rate linked to water temperature. The limited number of parameters allows implementing quantitative methods to estimate their optimal values by searching for the best fit between observations and predictions (Lehodey et al., 2015). However, the sparsity of direct biomass observations and the difficulty to convert the signal of acoustic echo-sounders into biomass is still an issue that requires further developments. In particular, there is the need to progress on acoustic models (Jech et al., 2015).

9.2.8.5. Applications

Zooplankton and micronekton outputs produced by the Copernicus Marine Service have proved to be useful variables along with physical and biogeochemical variables to model feeding habitats, feeding behaviour, and migrations of large oceanic protected species such as marine mammals and turtles (e.g., Abecassis et al., 2013; Lambert et al., 2014; Chambault et al., 2016; Roberts et al., 2016; Green et al., 2020; Pérez-Jorge et al., 2020; Romagosa et al., 2020 and 2021). These applications contribute to the scientific advice needed to propose marine spatial management measures (e.g., Ma-

rine Protected Areas and Migratory Corridors), the planning of activities at seas (e.g., offshore energy, military exercises and tests, and navigation routes), and real-time operational tools to limit the interaction of fisheries with protected species (Howell et al., 2008; Hobday et al., 2010; Hazen et al. 2018). The combination of zooplankton and micronekton variables has been used in a mechanistic model of Antarctic krill population, including food conditions that adults need to successfully produce eggs and the density of predators feeding on spawned eggs (Green et al. 2021).

Finally, spatially explicit population dynamics of target species can be driven by these variables to study recruitment, natural mortality, and movements linked to feeding behaviour and spawning migrations of fish (Lehodey et al., 2008; Dueri et al., 2012; Hernandez et al., 2014; Scutt Phillips et al., 2018; Senina et al., 2019). These models, combined with quantitative methods integrating various sources of georeferenced data (i.e. catch, size frequencies of catch, tagging data, density of larvae, and acoustic biomass abundance), provide new tools to assess the status of exploited stocks (Senina et al., 2008 and 2020; Dragon et al., 2018), to test spatial management scenarios (Sibert et al., 2012), to develop real time monitoring applications (Lehodey et al., 2017), and forecast seasonal to long-term changes along with IPCC climate scenarios (Lehodey et al., 2013; Dueri et al., 2014; Bell et al., 2013 and 2021).

9.2.9. Inventories

The first Green Ocean applications of operational oceanography, coupling biogeochemical models, and assimilation components from the existing GODAE systems, were discussed in

Brasseur et al. (2009). Some years later, Gehlen et al. (2015) and Fennel et al. (2019) discussed the current state and future prospects of analysis and prediction tools for ocean biogeochemistry and ecosystems, and presented representative examples of global and regional physical–biogeochemical systems implemented in pre-operational or operational mode. Currently, a few forecasting systems are fully operational, i.e. maintained by an operational centre with strict commitment to routinely provide forecasts.

Tables 9.1 and 9.2 provide initial inventories of the operational forecasting and multi-year systems, based on the literature mentioned above and completed in collaboration with the MEAP-TT working group that is one of the OceanPredict Task Teams. General information is given for each system, along with type (from global to coastal scale), producer, resolution, implemented model, data assimilation method, and product catalogue, as well as the web address that the reader can consult for further details.

Table 9.1.   Initial inventory of BGC Global (G) to Regional (R) to Coastal (C) operational forecasting systems.

Type	System	Covered Area	Resolution	PHY-BGC models	BGC Data Assimilation (method and data)	Products	Website
G	Global Ocean BGC system (MOI, France)	Global ocean	1/4°	PISCES coupled offline with NEMO (1/12° degraded to 1/4°) at daily frequency	SEEK method, using total Chla from OC satellite data	Chla, NO3, PO4, Si, Fe, O2, PHYC, NPP, spCO2, pH, 10-days forecast, updated weekly	https://marine.copernicus.eu

Type	System	Covered Area	Resolution	PHY-BGC models	BGC Data Assimilation (method and data)	Products	Website
R	Northwest European Shelf Seas BGC system (UK Metoffice, UK)	European North-West shelf Seas	~7 km	ERSEM coupled online with NEMO	3D-Var NEMOVAR method, using total Chla from OC satellite data	Chla, NO3, PO4, O2, PHYC, NPP, spCO2, pH, Kd, 6-day forecast, updated daily	https://marine.copernicus.eu
R	TOPAZ5-ECOSMO Arctic Ocean system (Norwegian Meteorological Institute, Norway; Nansen Environmental and Remote Sensing Center, Norway)	Arctic Region	6 km	ECOSMO biological model coupled online to the HYCOM ocean physical model	Assimilates Chla from OC satellite data using a nudging approach, and surface observations are projected downward in the water column applying an algorithm described by Uitz et al. (2006).	Chla, NO3, PO4, Si, O2, PHYC, ZOOC, NPP, spCO2, DIC, pH, Kd, 10-day forecast, updated daily	https://marine.copernicus.eu
R	Baltic Sea system (Swedish Meteorological and Hydrological Institute, Sweden)	Baltic Sea	1 nautical mile	ERGOM coupled online with NEMO	_	Chla, NO3, PO4, NH4, O2, spCO2, pH, NPP, ZSD, 6-day forecast, updated twice daily	https://marine.copernicus.eu
R	Iberia-Biscay-Irish system (MOI, France + consortium)	Iberian-Biscay-Irish shelves	1/36°	NEMO-PISCES online coupled model; nested into PHY and BGC solutions from the Global MFC	No assimilation	Chla, NO3, NH4, PO4, Si, Fe, O2, PHYC, NPP, spCO2, DIC, pH, ZEU, 10-days forecast updated on a weekly basis	https://marine.copernicus.eu
R	MedBFM3 model system (Euro Mediterranean Center on Climate Change - CMCC, Italy; OGS, Italy)	Mediterranean Sea	1/24°	BFM v5 model, off-line coupled with NEMO	3DVAR-BIO method, using Chla from satellite and vertical profiles of Chla and nitrate from BGC-Argo	Chla, PHYC, ZOOC, NO3, NH4, PO4, Si, O2, spCO2, pH, fCO2, ALK, DIC, NPP, 10-day forecast updated daily	https://marine.copernicus.eu

Type	System	Covered Area	Resolution	PHY-BGC models	BGC Data Assimilation (method and data)	Products	Website
R	Black Sea system (University of Liege, Belgium)	Black Sea	~3km	BAMHBI, online coupled with NEMO	"Ocean Assimilation Kit" (OAK; Vandenbulcke and Barth, 2015) for assimilation of surface Chla from satellite	Chla, PHYC, NO3, PO4, Si, NH4, O2, spCO2, pH, fCO2, ALK, DIC, NPP, Kd, PAR, 10-day forecast produced daily	https://marine.copernicus.eu
R	POSEIDON system (HCMR, Greece)	Mediterranean Sea	1/10°	ERSEM-II model, on-line coupled with POM	No assimilation	Chla, PHYC, ZOOC, BACC, NO3, NH4, PO4, 4-day forecast updated daily	https://www.poseidon.hcmr.gr
C	J-SCOPE forecast system (JISAO's Seasonal Coastal Ocean Prediction of the Ecosystem, funded by NOAA, US)	California Current System	1/10°	ROMS ocean model coupled with a BGC model	_	Seasonal forecasts of sea surface temperature (SST) and BGC variables	http://www.nanoos.org/products/j-scope/home.php
C	Harmful Algal Bloom Monitoring System (National Centers for Coastal Ocean Science, formed by the NOAA, US)	Coastal and lake regions of the US	_	_	_	Daily forecast	https://coastalscience.noaa.gov/research/stressor-impacts-mitigation/hab-monitoring-system/
C	Great Barrier Reef (Bureau of Meteorology et al.)	Great Barrier Reef	_	CSIRO eReefs modeling suite	_	A few days forecast	https://ereefs.org.au/ereefs
C	Chesapeake Bay	Chesapeake Bay	600m	ChesROMS-ECB	_	Nowcasts and a few days forecasts of physical and BGC variables (focusing on O2, acidification metrics, T, S)	www.vims.edu/hypoxia; https://oceansmap.maracoos.org/chesapeake-bay/

Table 9.2. Inventory of BGC Global (G) to Regional (R) to Coastal (C) multi-year systems.

Type	System	Covered Area	Resolution	PHY-BGC models	BGC Data Assimilation (method and data)	Products	Website
G	Global Ocean BGC system (MOI, France)	Global ocean	1/4°	PISCES, coupled offline with NEMO at daily frequency	No assimilation	Chla, NO3, PO4, Si, Fe, O2, PHYC, NPP, spCO2, pH, 1993 onwards	https://marine.copernicus.eu
G	Global Ocean low and mid-trophic levels product (CLS, France)	Global ocean	1/12°	LMTL component of SEAPODYM dynamical population model, driven offline by NEMO, NPP from satellite and PISCES	No assimilation	2D fields of zooplankton biomass and six groups of micronekton biomass, 1998 onwards	https://www.cls.fr/
R	Northwest European Shelf Seas BGC system (UK Met Office, UK)	European North-West shelf Seas	~7 km	ERSEM, coupled online with NEMO	3D-Var NEMOVAR method, using surface PFT Chla from OC satellite data	Chla, PFTs, PHYC, NO3, PO4, O2, spCO2, pH, NPP, Kd, 1993 onwards	https://marine.copernicus.eu
R	TOPAZ-ECOSMO reanalysis system (Nansen Environmental and Remote Sensing Center, Norway)	Arctic Region	25 km	ECOSMO biological model coupled online to the HYCOM ocean physical model	Assimilates surface Chla a from OC satellite and in-situ nutrient profiles, using an Ensemble Kalman Smoother (EnKS) method, after a gaussian anamorphosis for all BGC data. EnKS is preferred to EnKF in delayed mode	Chla, NO3, PO4, O2, PHYC, ZOOC, Kd, 2007 onwards	https://marine.copernicus.eu
R	Baltic Sea system (Swedish Meteorological and Hydrological Institute, Sweden)	Baltic Sea	1 nautical mile	SCOBI coupled to NEMO	LSEIK data assimilation scheme, using oxygen and nutrients	Chla, NO3, NH4, PO4, O2, 1993 onwards	https://marine.copernicus.eu

Type	System	Covered Area	Resolution	PHY-BGC models	BGC Data Assimilation (method and data)	Products	Website
R	Iberia Biscay Irish system (MOI, France)	Irish-Biscay-Iberian shelves	1/12°	NEMO-PISCES online coupled model; nested into PHY and BGC solutions from the Global MFC	No assimilation	Chla, NO3, NH4, PO4, Si, Fe, O2, PHYC, NPP, spCO2, DIC, pH, ZEU, 1993 onwards	https://marine.copernicus.eu
R	Global Ocean low and mid-trophic levels product (CLS, France)	Global ocean	1/12°	LMTL component of SEAPODYM dynamical population model, driven offline by NEMO, NPP from satellite and PISCES	No assimilation	2D fields of zooplankton biomass and six groups of micronekton biomass, 1998 onwards	https://marine.copernicus.eu
R	MedBFM3 model system (OGS, Italy)	Mediterranean Sea	1/24°	BFM v5 model, off-line coupled with NEMO	3DVAR-BIO method, using surface Chla	Chla, PHYC, ZOOC, NO3, NH4, PO4, Si, O2, spCO2, pH, fCO2, ALK, DIC, NPP, 1999 onwards	https://marine.copernicus.eu
R	Black Sea system (University of Liege, Belgium)	Black Sea	~3km	BAMHBI model, online coupled with NEMO	No assimilation	Chla, PHYC, O2, NO3, PO4, spCO2, pH, fCO2, ALK, DIC, NPP, 1992 onwards	https://marine.copernicus.eu
R	China Sea Multi-Scale Ocean Modelling System (CMOMS)	China Seas	~3km	ROMS ocean model coupled with a BGC model	No assimilation	Chla, PHYC, ZOOC, NO3, NH4, PO4, O2, spCO2, pH, ALK, DIC, small detritus, large detritus, terrestrial POM, and terrestrial DOM; 1992 onwards	https://ocean.ust.hk:8443/SiteMapApi/new/index.jsp

9.3.
References

Abecassis, M., Senina, I., Lehodey, P., Gaspar, P., Parker, D., Balazs, G., Polovina, J. (2013). A Model of Loggerhead Sea Turtle (Caretta caretta) Habitat and Movement in the Oceanic North Pacific. *PLoS ONE*, 8(9), e73274, https://doi.org/10.1371/journal.pone.0073274

Allen, J. I., M. Eknes, and G. Evensen. (2003). An Ensemble Kalman Filter with a complex marine ecosystem model: hindcasting phytoplankton in the Cretan Sea. *Annales Geophysicae*, 21(1), 399-411, https://doi.org/10.5194/angeo-21-399-2003

Almroth-Rosell, E., Eilola, K., Kuznetsov, Hall, I.P.O.J., and Meier, H.E.M. (2015). A new approach to model oxygen dependent benthic phosphate fluxes in the Baltic Sea. *Journal of Marine Systems*, 144, 127-141, https://doi.org/10.1016/j.jmarsys.2014.11.007

Anderson, L.A., Robinson, A.R., Lozano, C.J. (2000). Physical and biological modeling in the Gulf Stream region: I. Data assimilation methodology. *Deep Sea Research Part I: Oceanographic Research Papers*, 47, 1787-1827, https://doi.org/10.1016/S0967-0637(00)00019-4

Audzijonyte, A., Pethybridge, H., Porobic, J., Gorton, R., Kaplan, I., Fulton, E.A. (2019). Atlantis: A spatially explicit end-to-end marine ecosystem model with dynamically integrated physics, ecology and socio-economic modules. *Methods in Ecology and Evolution*, 10, 1814-1819, https://doi.org/10.1111/2041-210X.13272

Aumont, O., Ethé, C., Tagliabue, A., Bopp, L., and Gehlen, M. (2015). PISCES-v2: an ocean biogeochemical model for carbon and ecosystem studies. *Geoscientific Model Development*, 8, 2465-2513, https://doi.org/10.5194/gmd-8-2465-2015

Aumont O., Maury O., Lefort S., Bopp L. (2018). Evaluating the Potential Impacts of the Diurnal Vertical Migration by Marine Organisms on Marine Biogeochemistry. *Global Biogeochemical cycles*, 32 (11), 1622-1643, https://doi.org/10.1029/2018GB005886

Baretta, J. W., Ebenhöh, W., and Ruardij, P. (1995). The European regional seas ecosystem model, a complex marine ecosystem model. *Netherlands Journal of Sea Research*, 33, 233-246, https://doi.org/10.1016/0077-7579(95)90047-0

Bell, J.D., Ganachaud, A., Gehrke, P.C., Griffiths, S.P., Hobday, A.J., Hoegh-Guldberg, O., Johnson, J.E., Le Borgne, R., Lehodey, P., Lough, J.M., Matear, R.J., Pickering, T.D., Pratchett, M.S., Sen Gupta, A., Senina, I. and Waycott, M. (2013). Mixed response of tropical Pacific fisheries and aquaculture will respond differently to climate change. Nature Climate Change, 3, 591-599, https://doi.org/10.1038/nclimate1838

Bell, J.D., Senina, I., Adams, T., Aumont, O., Calmettes, B., Clark, S., Dessert, M., Hampton, J., Hanich, Q., Harden-Davies, H., Gehlen, M., Gorgues, T., Holmes, G., Lehodey, P., Lengaigne, M., Mansfield, B., Menkes, C., Nicol, S., Pasisi, C., Pilling, G., Ota, Y., Reid, C., Ronneberg, E., Sen Gupta, A., Seto, K., Smith, N., Taei, S., Tsamenyi, M., Williams, P. (2021). Pathways to sustaining tuna-dependent Pacific Island economies during climate change. *Nature Sustainability*, 4, 900-910, https://doi.org/10.1038/s41893-021-00745-z

Berline, L., Brankart, J.M., Brasseur, P., Ourmières, Y., and Verron, J. (2007). Improving the physics of a coupled physical–biogeochemical model of the North Atlantic through data assimilation: Impact on the ecosystem. *Journal of Marine Systems*, 64(1-4), 153-172, https://doi.org/10.1016/j.jmarsys.2006.03.007

Berthet, S., Séférian, R., Bricaud, C.,Chevallier, M., Voldoire, A., and Ethé, C. (2019). Evaluation of an online grid-coarsening algorithm in a global eddy-admitting ocean biogeochemical model. *Journal of Advances in Modeling Earth Systems*, 11, 1759-1783, https://doi.org/10.1029/2019MS001644

Bertino, L., Evensen, G., and Wackernagel, H. (2003). Sequential data assimilation techniques in oceanography. *International Statistical Review*, 71(2), 223-241, https://doi.org/10.1111/j.1751-5823.2003.tb00194.x

Biogeochemical-Argo Planning Group (2016). The Scientific Rationale, Design andImplementation Plan for a Biogeochemical-Argo Float Array. https://doi.org/10.13155/46601

Blanchard, J.L., Heneghan, R.F., Everett, J.D., Trebilco, R., Richardson, A.J. (2017). From bacteria to whales: Using function size spectra to model marine ecosystems. *Trends in Ecology and Evolution*, 32(3), 174-186, https://doi.org/10.1016/j.tree.2016.12.003

Boyer, T.P., Baranova, O.K., Coleman, C., Garcia, H.E., Grodsky, A., Locarnini, R.A., Mishonov, A.V., Paver, C.R., Reagan, J.R., Seidov, D., Smolyar, I.V., Weathers, K., Zweng, M.M. (2018). World Ocean Database 2018. A.V. Mishonov, Technical Ed., NOAA Atlas NESDIS 87, https://www.ncei.noaa.gov/products/world-ocean-database

Brankart, J.-M., Testut, C.-E., Béal, D., Doron, M., Fontana, C., Meinvielle, M., and Brasseur, P. (2012). Towards an improved description of oceanographic uncertainties : effect of local anamorphic transformations on spatial correlations. *Ocean Science*, 8, 121-142, https://doi.org/10.5194/os-8-121-2012

Brasseur, P., Gruber, N., Barciela, R., Brander, K., Doron, M., El Moussaoui, A., Hobday, M. Huret, A.J., Kremeur, A.-S., Lehodey, P., and others. (2009). Integrating biogeochemistry and ecology into ocean data assimilation systems. *Oceanography*, 22(3), 206-215, https://doi.org/10.5670/oceanog.2009.80

Bricaud, C., Le Sommer, J., Madec, G., Calone, C., Deshayes, J., Éthé, C., Chanut, J., Lévy, M. (2020). Multigrid algorithm for passive tracer transport in the NEMO ocean circulation model: a case study with the NEMO OGCM (version 3.6). *Geoscientific Model Development*, 13(11), 5465-5483, https://doi.org/10.5194/gmd-13-5465-2020

Brown, C. D., and Davis, H. T. (2006). Receiver operating characteristics curves and related decision measures: A tutorial. *Chemometrics and Intelligent Laboratory Systems*, 80(1), 24-38 https://doi.org/10.1016/j.chemolab.2005.05.004

Butenschön, M., Clark, J., Aldridge, J. N., Allen, J. I., Artioli, Y., Blackford, J., Bruggeman, J., Cazenave, P., Ciavatta, S., Kay, S., Lessin, G., van Leeuwen, S., van der Molen, J., de Mora, L., Polimene, L., Sailley, S., Stephens, N., and Torres, R. (2016). ERSEM 15.06: a generic model for marine biogeochemistry and the ecosystem dynamics of the lower trophic levels. *Geoscientific Model Development*, 9, 1293-1339, https://doi.org/10.5194/gmd-9-1293-2016

Campbell, J. (1995). The lognormal distribution as a model for bio-optical variability in the sea. *Journal of Geophysical Research: Oceans*, 100, C7, 13237-13254, https://doi.org/10.1029/95JC00458

Capet, A., Meysman, F. J. R., Akoumianaki, I., Soetaert, K., and Grégoire, M. (2016). Integrating sediment biogeochemistry into 3-D oceanic models: A study of benthic-pelagic coupling in the Black *Sea. Ocean Modelling*, 101, 83-100, https://doi.org/10.1016/j.ocemod.2016.03.006

Carlotti, F., Wolf, K.U. (1998). A Lagrangian ensemble model of Calanus finmarchicus coupled with a 1-D ecosystem model. *Fisheries Oceanography*, 7, 191-204, https://doi.org/10.1046/j.1365-2419.1998.00085.x

Carrassi, A., Bocquet, M., Bertino, L., and Evensen, G. (2018). Data assimilation in the geosciences: An overview of methods, issues, and perspectives. *Wiley Interdisciplinary Reviews: Climate Change*, e535, https://doi.org/10.1002/wcc.535

Carroll, D., Menemenlis, D., Adkins, J.F., Bowman, K.W., Brix, H., Dutkiewicz, S., Fenty, I., Gierach, M.M., Hill, C., Jahn, O., and Landschützer, P. (2020). The ECCO-Darwin data-assimilative global ocean biogeochemistry model: Estimates of seasonal to multidecadal surface ocean pCO2 and air-sea CO2 flux. *Journal of Advances in Modeling Earth Systems*, 7(3-4), 191-204, https://doi.org/10.1029/2019MS001888

Chai, F., Johnson, K., Claustre, H., Xing, X., Wang, Y., Boss, E., Riser, S., Fennel, K., Schofield, O., Sutton, A. (2020). Monitoring ocean biogeochemistry with autonomous platforms. *Nature Reviews Earth & Environment*, 1, 315-326, https://doi.org/10.1038/s43017-020-0053-y

Chambault P., de Thoisy B., Heerah K., Conchon A., Barrioz S., Dos Reis V., Berzins R., Kelle L., Picard B., Roquet F., Le Maho Y., Chevallier D. (2016). The influence of oceanographic features on the foraging behavior of the olive ridley sea turtle Lepidochelys olivacea along the Guiana coast. *Progress in Oceanography*, 142: 58-71, https://doi.org/10.1016/j.pocean.2016.01.006

Christensen, V., and Walters, C. (2004). Ecopath With Ecosim: Methods, Capabilities and Limitations. *Ecological Modelling*, 172, 109-139, https://doi.org/10.1016/j.ecolmodel.2003.09.003

Ciavatta, S., Torres, R., Saux-Picart, S. and Allen, J.I. (2011). Can ocean color assimilation improve biogeochemical hindcasts in shelf seas? *Journal of Geophysical Research: Oceans*, 116(C12), https://doi.org/10.1029/2011JC007219

Ciavatta, S., Torres, R., Martinez-Vicente, V., Smyth, T., Dall'Olmo, G., Polimene, L., and Allen, J. I. (2014). Assimilation of remotely-sensed optical properties to improve marine biogeochemistry modelling. *Progress in Oceanography*, 127, 74-95, https://doi.org/10.1016/j.pocean.2014.06.002

Ciavatta, S., Kay, S., Saux-Picart, S., Butenschön, M. and Allen, J.I. (2016). Decadal reanalysis of biogeochemical indicators and fluxes in the North West European shelf-sea ecosystem. *Journal of Geophysical Research: Oceans*, 121(3), 1824-1845, https://doi.org/10.1002/2015JC011496

Ciavatta, S., Brewin, R. J. W., Skákala, J., Polimene, L., de Mora, L., Artioli, Y., and Allen, J. I. (2018). Assimilation of ocean-color plankton functional types to improve marine ecosystem simulations. *Journal of Geophysical Research: Oceans*, 123, 834-854, https://doi.org/10.1002/2017JC013490

Ciavatta, S., Kay, S., Brewin, R.J., Cox, R., Di Cicco, A., Nencioli, F., Polimene, L., Sammartino, M., Santoleri, R., Skakala, J. and Tsapakis, M. (2019). Ecoregions in the Mediterranean Sea through the reanalysis of phytoplankton functional types and carbon fluxes. *Journal of Geophysical Research: Oceans*, 124(10), 6737-6759, https://doi.org/10.1029/2019JC015128

Cossarini, G., Mariotti, L., Feudale, L., Mignot, A., Salon, S., Taillandier, V., Teruzzi, A., D'Ortenzio, F. (2019). Towards operational 3D-Var assimilation of chlorophyll Biogeochemical-Argo float data into a biogeochemical model of the Mediterranean Sea. *Ocean Modelling*, 133, 112-128, https://doi.org/10.1016/j.ocemod.2018.11.005

Daewel, U., and Schrum, C. (2013). Simulating long-term dynamics of the coupled North Sea and Baltic Sea ecosystem with ECOSMO II: Model description and validation. *Journal of Marine Systems*, 119-120, 30-49, https://doi.org/10.1016/j.jmarsys.2013.03.008

Dall'Olmo, G., Dingle, J., Polimene, L., Brewin, R.J.W., Claustre, H. (2016). Substantial energy input to the mesopelagic ecosystem from the seasonal mixed-layer pump. *Nature Geoscience*, 9, 820-823, https://doi.org/10.1038/ngeo2818

De Roos, A.M., Schellekens, T., Van Kooten, T., Van De Wolfshaar, K., Claessen, D., Persson, L. (2008). Simplifying a physiologically structured population model to a stage-structured biomass model. *Theoretical Population Biology*, 73, 47-62, https://doi.org/10.1016/j.tpb.2007.09.004

DeAngelis, D.L., Gross, L.J. (1992). Individual-based Models and Approaches in Ecology. Chapman & Hall, London.

Diaz, F., D Bănaru, P. Verley and Y.-J. Shin (2019). Implementation of an end-to-end model of the Gulf of Lions ecosystem (NW Mediterranean Sea). II. Investigating the effects of high trophic levels on nutrients and plankton dynamics and associated feedbacks. *Ecological Modelling*, 405, 51-68, https://doi.org/10.1016/j.ecolmodel.2019.05.004

Dickey, T.D. (1991). The emergence of concurrent high-resolution physical and bio-optical measurements in the upper ocean and their applications. *Reviews on Geophysics*, 29(3), 383- 413, https://doi.org/10.1029/91RG00578

Dornan, T., Fielding, S., Saunders, R.A., Genner, M.J. (2019). Swimbladder morphology masks Southern Ocean mesopelagic fish biomass. *Proceedings of the Royal Society B Biological Science*, 286(1903), http://dx.doi.org/10.1098/rspb.2019.0353

Doron, M., Brasseur, P., Brankart, J.M. (2011). Stochastic estimation of biogeochemical parameters of a 3d ocean coupled physical-biogeochemical model: twin experiments. *Journal of Marine Systems*, 87, 194-207, https://doi.org/10.1016/j.jmarsys.2013.02.007

Dragon A-C., Senina, Hintzen N.T., Lehodey P. (2018). Modelling South Pacific Jack Mackerel spatial population dynamics and fisheries. *Fisheries Oceanography*, 27(2), 97-113, https://doi.org/10.1111/fog.12234

Dueri S., Faugeras B., Maury O. (2012). Modelling the skipjack tuna dynamics in the Indian Ocean with APECOSM-E: Part 1. Model formulation. *Ecological Modelling*, 245, 41-54, https://doi.org/10.1016/j.ecolmodel.2012.02.008

Dueri, S., Bopp, L., Maury, O. (2014). Projecting the impacts of climate change on skipjack tuna abundance and spatial distribution. *Global Change Biology*, 20(3): 742-753, https://doi.org/10.1111/gcb.12460

Dupont, F. (2012). Impact of sea-ice biology on overall primary production in a biophysical model of the pan-Arctic Ocean. Journal of Geophysical Research: Oceans, 117(C8), https://doi.org/10.1029/2011JC006983

Eilola, K., Meier, H.E.M., Almroth, E. (2009). On the dynamics of oxygen, phosphorus and cyanobacteria in the baltic sea: A model study. *Journal of Marine Systems*, 75, 163-184, https://doi.org/10.1016/j.jmarsys.2008.08.009

Escobar-Flores, P.C., O'Driscoll, R.L., Montgomery, J.C. (2018). Spatial and temporal distribution patterns of acoustic backscatter in the New Zealand sector of the Southern Ocean. *Marine Ecology Progress Series*, 592, 19-35, https://doi.org/10.3354/meps12489

Evensen, G. (1994). Sequential data assimilation with a nonlinear quasi-geostrophic model using Monte Carlo methods to forecast error statistics. *Journal of Geophysical Research: Oceans*, 99(C5), 10143-10162, https://doi.org/10.1029/94JC00572

Fennel, K., Gehlen, M., Brasseur, P., Brown, C. W., Ciavatta, S., Cossarini, G., Crise, A., Edwards, C. A., Ford, D., Friedrichs, M. A. M., Grégoire, M., Jones, E., Kim, H.-C., Lamouroux, J., Murtugudde, R., Perruche, C. and the GODAE OceanView Marine Ecosystem Analysis and Prediction Task Team (2019). Advancing marine biogeochemical and ecosystem reanalyses and forecasts as tools for monitoring and managing ecosystem health. Frontiers in Marine Science, 6, 89, https://doi.org/10.3389/fmars.2019.00089

Feudale, L., Teruzzi, A., Salon, S., Bolzon, G., Lazzari, P., Coidessa, G., Di Biagio, V., Cossarini, G. (2021). Product Quality Document For the Mediterranean Sea Production Centre, MEDSEA_ANALYSISFORECAST_ BGC_006_014, https://doi.org/10.25423/cmcc/medsea_analysisforecast_bgc_006_014_medbfm3

Flynn, K. J., Stoecker, D. K., Mitra, A., Raven, J. A., Glibert, P. M. Hansen, P. J., Granéli, E., and Burkholder, J. M. (2013). Misuse of the phytoplankton-zooplankton dichotomy: the need to assign organisms as mixotrophs within plankton functional types. *Journal of Plankton Research*, 35, 3-11, https://doi.org/10.1093/plankt/fbs062

Follows, M. J., Dutkiewicz, S., Grant, S., and Chisholm, S. W. (2007). Emergent biogeography of microbial communities in a model ocean. *Science*, 315(5820), 1843-1846. https://doi.org/10.1126/science.1138544

Fontana, C., Brasseur, P., and Brankart, J. M. (2013). Toward a multivariate reanalysis of the North Atlantic Ocean biogeochemistry during 1998–2006 based on the assimilation of SeaWiFS chlorophyll data. *Ocean Science*, 9(1), 37-56, https://doi.org/10.5194/os-9-37-2013

Ford, D., and Barciela, R. (2017). Global marine biogeochemical reanalyses assimilating two different sets of merged ocean colour products. *Remote Sensing of Environment*, 203, 40-54, https://doi.org/10.1016/j.rse.2017.03.040

Ford, D., Key, S., McEwan, R., Totterdell, I. and Gehlen, M. (2018). Marine biogeochemical modelling and data assimilation for operational forecasting, reanalysis, and climate research. *New Frontiers in Operational Oceanography*, 625-652, https://doi.org/10.17125/gov2018.ch22

Ford, D. (2021). Assimilating synthetic Biogeochemical-Argo and ocean colour observations into a global ocean model to inform observing system design. *Biogeosciences*, 18(2), 509-534, https://doi.org/10.5194/bg-18-509-2021

Fulton, E.A. (2010). Approaches to end-to-end ecosystem models. *Journal of Marine Systems* 81, 171-183, https://doi.org/10.1016/j.jmarsys.2009.12.012

Fulton, E., Smith, A., Johnson, C. (2003). Effect of Complexity of Marine Ecosystem Models. *Marine Ecology Progress Series*, 253:1-16, doi:10.3354/meps253001

Garcia, H.E., Weathers, K., Paver, C.R., Smolyar, I., Boyer, T.P., Locarnini, R.A., Zweng, M.M, Mishonov, A.V., Baranova, O.K., Seidov, D., and Reagan, J.R. (2018a). World Ocean Atlas 2018, Volume 3: Dissolved Oxygen, Apparent Oxygen Utilization, and Oxygen Saturation. A. Mishonov Technical Ed.; NOAA Atlas NESDIS 83, 38pp.

Garcia, H.E., Weathers, K., Paver, C.R., Smolyar, I., Boyer, T.P., Locarnini, R.A., Zweng, M.M, Mishonov, A.V., Baranova, O.K., Seidov, D., and Reagan, J.R. (2018b). World Ocean Atlas 2018, Volume 4: Dissolved Inorganic Nutrients (phosphate, nitrate and nitrate+nitrite, silicate). A. Mishonov Technical Ed.; NOAA Atlas NESDIS 84, 35pp.

Garnesson, P., Mangin, A., and Bretagnon M. (2021). Quality Information Document, Ocean Colour Production Centre, Satellite Observation Copernicus-GlobColour Products, https://catalogue.marine.copernicus.eu/documents/QUID/CMEMS-OC-QUID-009-030-032-033-037-081-082-083-085-086-098.pdf

Garnier, F., Brankart, J. M., Brasseur, P. and Cosme, E. (2016). Stochastic parameterizations of biogeochemical uncertainties in a 1/4° NEMO/PISCES model for probabilistic comparisons with ocean color data. *Journal of Marine Systems*, 155, 59-72, https://doi.org/10.1016/j.jmarsys.2015.10.012

Gehlen, M., Barciela, R., Bertino, L., Brasseur, P., Butenschön, M., Chai, F., Crise, A., Drillet, Y., Ford, D., Lavoie, D., Lehodey, P., Perruche, C., Samuelsen, A., and Simon, E. (2015). Building the capacity for forecasting marine biogeochemistry and ecosystems: recent advances and future developments. *Journal of Operational Oceanography*, 8:sup1, s168-s187, https://doi.org/10.1080/1755876X.2015.1022350

Geider, R.J., MacIntyre, H.L., and Kana, T.M. (1997). Dynamic model of phytoplankton growth and acclimation: responses of the balanced growth rate and the chlorophyll a: carbon ratio to light, nutrient-limitation and temperature. *Marine Ecology Progress Series*, 148, 187-200, https://doi.org/10.3354/meps148187

Germineaud, C., Brankart, J.M., and Brasseur, P. (2019). An ensemble-based probabilistic score approach to compare observation scenarios: an application to biogeochemical-Argo deployments. *Journal of Atmospheric and Oceanic Technology*, 36(12), 2307-2326, https://doi.org/10.1175/JTECH-D-19-0002.1

Gharamti, M.E., Tjiputra, J., Bethke, I., Samuelsen, A., Skjelvan, I., Bentsen, M., Bertino, L. (2017). Ensemble data assimilation for ocean biogeochemical state and parameter estimation at different sites. *Ocean Modelling*, 112, 65-89, https://doi.org/10.1016/j.ocemod.2017.02.006

Glibert, P., Mitra, A., Flynn, K., Hansen, P., Jeong, H., and Stoecker, D. (2019). Plants Are Not Animals and Animals Are Not Plants, Right? Wrong! Tiny Creatures in the Ocean Can Be Both at Once! *Frontiers for Young Minds*, 7:48, https://doi.org/10.3389/frym.2019.00048

Gradinger, R. (2009). Sea-ice algae: Major contributors to primary production and algal biomass in the Chukchi and Beaufort Seas during May/June 2002. *Deep Sea Research Part II: Topical Studies in Oceanography*, 56, 1201-1212, https://doi.org/10.1016/j.dsr2.2008.10.016

Green, D.B., Bestley, S., Corney, S.P., Trebilco, R., Lehodey, P., and Hindell, M.A. (2021). Modeling Antarctic krill circumpolar spawning habitat quality to identify regions with potential to support high larval production. *Geophysical Research Letters*, 48, e2020GL091206, https://doi.org/10.1029/2020GL091206

Green, D.B., Bestley, S., Trebilco, R., Corney, S.P., Lehodey, P., McMahon, C.R., Guinet, C., and Hindell, M.A. (2020). Modelled mid-trophic pelagic prey fields improve understanding of marine predator foraging behaviour. *Ecography*, https://doi.org/10.1111/ecog.04939

Gregg, W.W., and Rousseaux, C.S. (2016). Directional and spectral irradiance in ocean models: effects on simulated global phytoplankton, nutrients, and primary production. *Frontiers in Marine Science*, 3, 240, http://dx.doi.org/10.1088/1748-9326/ab4667

Gregg, W.W., and Rousseaux, C.S. (2019). Global ocean primary production trends in the modern ocean color satellite record (1998-2015). *Environmental Research Letters*, 14(12), 124011, https://doi:10.1088/1748-9326/ab4667

Grégoire, M., Raick, C., and Soetaert, K. (2008). Numerical modelling of the central black sea ecosystem functioning during the eutrophication phase. *Progress in Oceanography*, 76, 286-333, https://doi.org/10.1016/j.pocean.2008.01.002

Grégoire, M., Soetaert, K. (2010). Carbon, nitrogen, oxygen and sulfide budgets in the Black Sea: a biogeochemical model of the whole water column coupling the oxic and anoxic parts. *Ecological Modelling*, 221(19), 2287-2301.

Hazen, E. L., Scales, K.L., Maxwell, S.M., Briscoe, D.K., Welch, H., Bograd, S.J., Bailey, H., Benson, S.R., Eguchi, T., Dewar, H., Kohin, S., Costa, D.P., Crowder, L.B., Lewison R.L. (2018). A dynamic ocean management tool to reduce bycatch and support sustainable fisheries.Science Advances, 4(5), DOI: 10.1126/sciadv.aar3001

Hernandez, F., Bertino, L., Brassington, G., Chassignet, E., Cummings, J., Davidson, F., Drevillon, M., Garric, G., Kamachi, M., Lellouche, J.M., Mahdon, R., Martin, M.J,, Ratsimandresy, A., and Regnier, C. (2009). Validation and Inter-comparison studies within GODAE. *Oceanography*, 22(3): 128-143, https://doi.org/10.5670/oceanog.2009.71

Hernandez, F., Smith, G., Baetens, K., Cossarini, G., Garcia-Hermosa, I., Drevillon, M., von Schuckman, K. (2018). Measuring performances, skill and accuracy in operational oceanography: New challenges and approaches. In: "New Frontiers in Operational Oceanography", E. Chassignet, A. Pascual, J. Tintoré, and J. Verron, Eds., GODAE OceanView, 759-796, DOI: 10.17125/gov2018.ch29

Hernandez, O., Lehodey, P., Senina, I., Echevin, V., Ayon, P., Bertrand, A., Gaspar, P. (2014). Understanding mechanisms that control fish spawning and larval recruitment: Parameter optimization of an Eulerian model (SEAPODYM-SP) with Peruvian anchovy and sardine eggs and larvae data. *Progress in Oceanography*, 123, 105-122, http://dx.doi.org/10.1016/j.pocean.2014.03.001

Hipsey, M.R., Gal, G., Arhonditsis, G.B., Carey, C.C., Elliott, J.A., Frassl, M. A., ... & Robson, B.J. (2020). A system of metrics for the assessment and improvement of aquatic ecosystem models. *Environmental Modelling & Software*, 128, 104697, https://doi.org/10.1016/j.envsoft.2020.104697

Hobday, A.J., Hartog, J.R., Timmiss, T., Fielding, J. (2010). Dynamic spatial zoning to manage southern bluefin tuna (Thunnus maccoyii) capture in a multi-species longline fishery. *Fisheries Oceanography*, 19(3), 243-253, https://doi.org/10.1111/j.1365-2419.2010.00540.x

Houtekamer, P. L., and Mitchell, H. L. (1998). Data Assimilation Using an Ensemble Kalman Filter Technique. *Monthly Weather Review*, 126(3), 796-811, https://doi.org/10.1175/1520-0493(1998)126<0796:DAUAEK>2.0.CO;2

Howell, E.A., Kobayashi, D.R., Parker, D.M., Balazs, G.H., Polovina, J.J. (2008). TurtleWatch: a tool to aid in the bycatch reduction of loggerhead turtles Caretta caretta in the Hawaii-based pelagic longline fishery. *Endangered Species Research*, 5:267-278, https://doi.org/10.3354/esr00096

Hu, J., Fennel, K., Mattern, J.P. and Wilkin, J. (2012). Data assimilation with a local Ensemble Kalman Filter applied to a three-dimensional biological model of the Middle Atlantic Bight. *Journal of Marine Systems*, 94, 145-156, https://doi.org/10.1016/j.jmarsys.2011.11.016

Huse, G., Melle, W., Skogen, M.D., Hjøllo, S.S., Svendsen, E., and Budgell, W.P. (2018). Modeling Emergent Life Histories of Copepods. Frontiers in Ecology and Evolution, 6(23), https://doi.org/10.3389/fevo.2018.00023

IOCCG. (2020). Synergy between Ocean Colour and Biogeochemical/Ecosystem Models. Dutkiewicz, S. (ed.), IOCCG Report Series, No. 19, International Ocean Colour Coordinating Group, Dartmouth, Canada, http://dx.doi.org/10.25607/OBP-711

Ishizaka, J. (1990). Coupling of coastal zone color scanner data to a physical-biological model of the southeastern US continental shelf ecosystem: 2. An Eulerian model. *Journal of Geophysical Research: Oceans*, 95(C11), 20183-20199, https://doi.org/10.1029/JC095iC11p20183

Jaccard, P., Hjermann, D. Ø., Ruohola, J., Marty, S., Kristiansen, T., Sørensen, K., Kaitala, S., Mangin, A., Pouliquen, S., et al. (2021). Quality Information Document For Global Ocean Reprocessed in-situ Observations of Biogeochemical Products INSITU_GLO_BGC_REP_OBSERVATIONS_013_046, http://doi.org/10.13155/54846, https://catalogue.marine.copernicus.eu/documents/QUID/CMEMS-INS-QUID-013-046.pdf

Jech, J.M., Horne, J.K., Chu, D., Demer, D.A., Francis, D.T.I., Gorska, N., Jones, B., Lavery, A.C., Stanton, T.K., Macaulay, G.J., Reeder, D.B., Sawada, K. (2015). Comparisons among ten models of acoustic backscattering used in aquatic ecosystems. *The Journal of the Acoustical Society of America*, 138: 3742, https://doi.org/10.1121/1.4937607

Jennings, S., and Collingridge, K. (2015). Predicting Consumer Biomass, Size-Structure, Production, Catch Potential, Responses to Fishing and Associated Uncertainties in the World's Marine Ecosystems. *PLoS ONE*, 10(7), e0133794. https://doi.org/10.1371/journal.pone.0133794

Jolliff, J.K., Kindle, J.C., Shulman, I., Penta, B., Friedrichs, M.A.M., Helber, R.W., and Arnone, R. (2009). Summary diagrams for coupled hydrodynamic-ecosystem model skill assessment. *Journal of Marine Systems*, 76, 64-82, https://doi.org/10.1016/j.jmarsys.2008.05.014

Jones, E.M., Baird, M.E., Mongin, M., Parslow, J., Skerratt, J., Lovell, J., Margvelashvili, N., Matear, R.J., Wild-Allen, K., Robson, B. and Rizwi, F. (2016). Use of remote-sensing reflectance to constrain a data assimilating marine biogeochemical model of the Great Barrier Reef. *Biogeosciences*, 13(23), 6441, https://doi.org/10.5194/bg-13-6441-2016

Kaufman, D.E. (2017). Using High-Resolution Glider Data and Biogeochemical Modeling to Investigate Phytoplankton Variability in the Ross Sea. Dissertations, Theses, and Masters Projects, William & Mary, Paper 1499449869, http://dx.doi.org/10.21220/M2BK8V

Kriest, I., Kähler, P., Koeve, W., Kvale, K., Sauerland, V., and Oschlies, A. (2020). One size fits all? Calibrating an ocean biogeochemistry model for different circulations. *Biogeosciences*, 17, 3057-3082, https://doi.org/10.5194/bg-17-3057-2020

Krishnamurthy, A., Moore, J. K., Mahowald, N., Luo, C., and Zender, C.S. (2010). Impacts of atmospheric nutrient inputs on marine biogeochemistry. *Journal of Geophysical Research: Biogeosciences*, 115(G1), https://doi.org/10.1029/2009JG001115

Lambert, C., Mannocci, L., Lehodey, P., Ridoux, V. (2014). Predicting Cetacean Habitats from Their Energetic Needs and the distribution of Their Prey in Two Contrasted Tropical Regions. PLoS ONE, 9(8), e105958, https://doi.org/10.1371/journal.pone.0105958

Lamouroux, J., Perruche, C., Mignot, A., Paul, J., Szczypta, C. (2019). Quality Information Document For Global Biogeochemical Analysis and Forecast Product, https://catalogue.marine.copernicus.eu/documents/QUID/CMEMS-GLO-QUID-001-028.pdf

Lamouroux, J., Perruche, C., Mignot, A., Gutknecht, E., Ruggiero, G., Evaluation of the CMEMS global biogeochemical simulation, with assimilation of satellite Chla concentrations, in prep.

Laws, E.A. (2013). Evaluation of In Situ Phytoplankton Growth Rates: A Synthesis of Data from Varied Approaches. *Annual Review of Marine Science*, 5(1), 247-268, https://doi.org/10.1146/annurev-marine-121211-172258

Le Quéré, C., Harrison, S. P., Prentice, I. C., Buitenhuis, E. T., Aumont, O., Bopp, L., Claustre, H., Cotrim Da Cunha, L., Geider, R., Giraud, X., Klaas, C., Kohfeld, K. E., Legendre, L., Manizza, M., Platt, T., Rivkin, R. B., Sathyendranath, S., Uitz, J., Watson, A. J., and Wolf Gladrow, D. (2005). Ecosystem dynamics based on plankton functional types for global ocean biogeochemistry models. *Global Change Biology*, 11, 2016-2040, https://doi.org/10.1111/j.1365-2486.2005.1004.x

Le Traon et al. (2017). The Copernicus marine environmental monitoring service: main scientific achievements and future prospects. Special Issue Mercator Océan International #56. Available at: https://marine.copernicus.eu/it/node/594

Le Traon, P. Y., Reppucci, A., Fanjul, E. A., Aouf, L., Behrens, A., Belmonte, M., Bentamy, A., Bertino, L., Brando, V. E., Kreiner, M. B., Benkiran, M., Carval, T., Ciliberti, S. A., Claustre, H., Clementi, E., Coppini, G., Cossarini, G., De Alfonso Alonso- Muñoyerro, M., Delamarche, A., Dibarboure, G., Dinessen, F., Drevillon, M., Drillet, Y., Faugere, Y., Fernández, V., Fleming, A., Garcia-Hermosa, M. I., Sotillo, M. G., Garric, G., Gasparin, F., Giordan, C., Gehlen, M., Grégoire, M., Guinehut, S., Hamon, M., Harris, C., Hernandez, F., Hinkler, J. B., Hoyer, J., Karvonen, J., Kay, S., King, R., Lavergne, T., Lemieux-Dudon, B., Lima, L., Mao, C., Martin, M. J., Masina, S., Melet, A., Nardelli, B. B., Nolan, G., Pascual, A., Pistoia, J., Palazov, A., Piolle, J. F., Pujol, M. I., Pequignet, A. C., Peneva, E., Gómez, B. P., de la Villeon, L. P., Pinardi, N., Pisano, A., Pouliquen, S., Reid, R., Remy, E., Santoleri, R., Siddorn, J., She, J., Staneva, J., Stoffelen, A., Tonani, M., Vandenbulcke, L., von Schuckmann, K., Volpe, G., Wettre, C., and Zacharioudaki, A. (2019). From observation to information and users: The Copernicus Marine Service Perspective. *Frontiers in Marine Science*, https://doi.org/10.3389/fmars.2019.00234

Lehodey, P., Senina, I., Murtugudde, R. (2008). A Spatial Ecosystem And Populations Dynamics Model (SEAPODYM) - Modelling of tuna and tuna-like populations. *Progress in Oceanography*, 78, 304-318, https://doi.org/10.1016/j.pocean.2008.06.004

Lehodey, P., Senina, I., Wibawa, T.A., Titaud, O., Calmettes, B., Tranchant, B., and Gaspar, P. (2017). Operational modelling of bigeye tuna (Thunnus obesus) spatial dynamics in the Indonesian region. *Marine Pollution Bulletin*, 131, 19-32, https://doi.org/10.1016/j.marpolbul.2017.08.020

Lehodey, P., Conchon, A., Senina, I., Domokos, R., Calmettes, B., Jouanno, J., Hernandez, O., and Kloser, R. (2015). Optimization of a micronekton model with acoustic data. I*CES Journal of Marine Science*, 72(5), 1399-1412, https://doi.org/10.1093/icesjms/fsu233

Lehodey, P., Murtugudde, R., and Senina, I. (2010). Bridging the gap from ocean models to population dynamics of large marine predators: A model of mid-trophic functional groups. Progress in Oceanography, 84, 69-84.

Lehodey, P., Senina, I., Calmettes, B, Hampton, J, Nicol S. (2013). Modelling the impact of climate change on Pacific skipjack tuna population and fisheries. Climatic Change, 119 (1): 95-109, DOI 10.1007/s10584-012-0595-1

Lengaigne, M., Menkes, C., Aumont, O., Gorgues, T., Bopp, L., André, J. M., and Madec, G. (2007). Influence of the oceanic biology on the tropical Pacific climate in a coupled general circulation model. *Climate Dynamics*, 28(5), 503-516. https://doi.org/10.1007/s00382-006-0200-2

Libralato, S., and Solidoro, C. (2009). Bridging biogeochemical and food web models for an End-to-End representation of marine ecosystem dynamics: The Venice lagoon case study. *Ecological Modelling*, 220(21), 2960-2971, https://doi.org/10.1016/j.ecolmodel.2009.08.017

Longhurst, A. (1998). Ecological geography in the sea. Academic Press.

Mattern, J. P., Fennel, K., and Dowd, M. (2012). Estimating time-dependent parameters for a biological ocean model using an emulator approach. *Journal of Marine Systems*, 96, 32-47, https://doi.org/10.1016/j.jmarsys.2012.01.015

Mattern, J.P., Dowd, M. and Fennel, K. (2013). Particle filter-based data assimilation for a three-dimensional biological ocean model and satellite observations. *Journal of Geophysical Research: Oceans*, 118(5), 2746-2760, https://doi.org/10.1002/jgrc.20213

Maunder, M.N., Punt, A.E. (2013). A review of integrated analysis in fisheries stock assessment. *Fisheries Research*, 142, 61-74, https://doi.org/10.1016/j.fishres.2012.07.025

Maury, O., Faugeras, B., Shin, Y.-J., Poggiale, J.-C., Ben Ari, T., and Marsac, F. (2007). Modeling environmental effects on the size-structured energy flow through marine ecosystems. Part 1: The model. *Progress in Oceanography*, 74(4), 479-499, https://doi.org/10.1016/j.pocean.2007.05.002

McEwan, R., S. Kay, D. Ford (2021). Quality Information Document For the Atlantic - European North West Shelf Production Centre, https://catalogue.marine.copernicus.eu/documents/QUID/CMEMS-NWS-QUID-004-002.pdf, https://doi.org/10.48670/moi-00056

Melsom, A. and Ç. Yumruktepe (2021), Quality Information Document For the Arctic Production Centre, https://catalogue.marine.copernicus.eu/documents/QUID/CMEMS-ARC-QUID-002-004.pdf, https://doi.org/10.48670/moi-00003

Mignot, A., Claustre, H., Cossarini, G., D'Ortenzio, F., Gutknecht, E., Lamouroux, J., Lazzari, P., Perruche, C., Salon, S., Sauzède, R., Taillandier, V., Teruzzi, A. (2021). Defining BGC-Argo-based metrics of ocean health and biogeochemical functioning for the evaluation of global ocean models. *Biogeosciences*, https://doi.org/10.5194/bg-2021-2

Miller, C.B., Lynch, D.R., Carlotti, F., Gentleman, W., Lewis, C.V.W. (1998). Coupling of an individual-based population dynamic model of Calanus finmarchicus to a circulation model for the Georges Bank region. *Fisheries Oceanography*, 7(3-4), 219-234, https://doi.org/10.1046/j.1365-2419.1998.00072.x

Mogensen, K.S., Balmaseda, M.A., Weaver, A., Martin, M.J., Vidard, A. (2009). NEMOVAR: A variational data assimilation system for the NEMO ocean model. ECMWF Newsl., 120, 17-21.

Moore, A. M., Martin, M. J., Akella, S., Arango, H. G., Balmaseda, M., Bertino, L., ... and Weaver, A. T. (2019). Synthesis of ocean observations using data assimilation for operational, real-time and re-analysis systems: A more complete picture of the state of the ocean. Frontiers in Marine Science, 6:90, https://doi.org/10.3389/fmars.2019.00090

Moriarty, R., and O'Brien, T. (2013). Distribution of mesozooplankton biomass in the global ocean. *Earth System Science Data*, 5(1), 45-55, https://doi.org/10.5194/essd-5-45-2013

Natvik, L., and Evensen, G. (2003). Assimilation of ocean colour data into a biochemical model of the North Atlantic. Part 1: Data assimilation experiments. *Journal of Marine Systems*, 41, 127-153, https://doi.org/10.1016/S0924-7963(03)00016-2

Nerger, L. and Gregg, W.W. (2007). Assimilation of SeaWiFS data into a global ocean-biogeochemical model using a local SEIK filter. *Journal of Marine Systems*, 68, 237-254, https://doi.org/10.1016/j.jmarsys.2006.11.009

Nerger, L., and Gregg, W.W. (2008). Improving assimilation of SeaWiFS data by the application of bias correction with a local SEIK filter. *Journal of Marine Systems*, 73, 87-102, https://doi.org/10.1016/j.jmarsys.2007.09.007

Nerger, L., Janjić, T., Schröter, J., and Hiller, W. (2012). A Unification of Ensemble Square Root Kalman Filters. *Monthly Weather Review*, 140(7), 2335-2345, https://doi.org/10.1175/MWR-D-11-00102.1

Neumann, T. (2000). Towards a 3D-ecosystem model of the Baltic Sea. *Journal of Marine Systems*, 25(3), 405-419, https://doi.org/10.1016/S0924-7963(00)00030-0

Olsen, A., Lange, N., Key, R. M., Tanhua, T., Bittig, H. C., Kozyr, A., Àlvarez, M., Azetsu-Scott, K., Becker, S., Brown, P. J., Carter, B. R., Cotrim da Cunha, L., Feely, R. A., van Heuven, S., Hoppema, M., Ishii, M., Jeansson, E., Jutterström, S., Landa, C. S., Lauvset, S. K., Michaelis, P., Murata, A., Pérez, F. F., Pfeil, B., Schirnick, C., Steinfeldt, R., Suzuki, T., Tilbrook, B., Velo, A., Wanninkhof, R. and Woosley, R. J. (2020). GLODAPv2.2020 - the second update of GLODAPv2. *Earth System Science Data*, https://doi.org/10.5194/essd-12-3653-2020

Ourmières, Y., Brasseur, P., Lévy, M., Brankart, J.M. and Verron, J. (2009). On the key role of nutrient data to constrain a coupled physical-biogeochemical assimilative model of the North Atlantic Ocean. *Journal of Marine Systems*, 75(1-2), 100-115, https://doi.org/10.1016/j.jmarsys.2008.08.003

Palmer, J. R., and Totterdell, I. J. (2001). Production and export in a global ocean ecosystem model. *Deep Sea Research Part I: Oceanographic Research Papers*, 48(5), 1169-1198, https://doi.org/10.1016/S0967-0637(00)00080-7

Park, J.-Y., Stock, C. A., Yang, X., Dunne, J. P., Rosati, A., John, J., et al. (2018). Modeling global ocean biogeochemistry with physical data assimilation: A pragmatic solution to the equatorial instability. *Journal of Advances in Modeling Earth Systems*, 10, 891- 906, https://doi.org/10.1002/2017MS001223

Pérez-Jorge, S., Tobeña, M., Prieto, R., Vandeperre, F., Calmettes, B., Lehodey, P., Silva, M.A. (2020). Environmental drivers of large-scale movements of baleen whales in the mid-North Atlantic Ocean. *Diversity and Distributions*, 26(6), 683-698, https://doi.org/10.1111/ddi.13038

Petrik, C.M., Stock, C.A., Andersen, K.H., van Denderen, P.D., and Watson, J.R. (2019). Bottom-up drivers of global patterns of demersal, forage, and pelagic fishes. *Progress in Oceanography*, 176:102124, https://doi.org/10.1016/j.pocean.2019.102124

Petrik, C.M., Stock, C.A., Andersen, K.H., van Denderen, P.D., and Watson, J.R. (2020). Large pelagic fish are most sensitive to climate change despite pelagification of ocean foodwebs. *Frontiers in Marine Science*, 7, 588482, https://doi.org/10.3389/fmars.2020.588482

Pham, D.T., Verron, J., Roubaud, M.C. (1998). A singular evolutive extended Kalman filter for data assimilation in oceanography. *Journal of Marine Systems*, 16(3-4): 323-340, https://doi.org/10.1016/S0924-7963(97)00109-7

Pradhan, H.K., Völker, C., Losa, S.N., Bracher, A., and Nerger, L. (2020). Global assimilation of ocean-color data of phytoplankton functional types: Impact of different data sets. *Journal of Geophysical Research: Oceans*, 125, e2019JC015586, https://doi.org/10.1029/2019JC015586

Proud, R., Handegard, N. O., Kloser, R. J., Cox, M. J., and Brierley, A. S. (2018). From siphonophores to deep scattering layers:Uncertainty ranges for the estimation of global mesopelagic fish biomass. *ICES Journal of Marine Science*, 76, 718-733, https://doi.org/10.1093/icesjms/fsy037

Redfield, A.C. (1934). On the proportions of organic derivatives in sea water and their relation to the composition of plankton. James Johnson Memorial Volume, R. J. Daniel, Ed., University Press of Liverpool, 177-192.

Roberts, J. J., Best, B. D., Mannocci, L., Fujioka, E., Halpin, P. N., Palka, D. L., … Lockhart, G. G. (2016). Habitat-based cetacean density models for the U.S. Atlantic and Gulf of Mexico. *Nature Scientific Reports*, 6, 22615, https://doi.org/10.1038/srep22615

Romagosa M., Lucas C., Pérez-Jorge S., Tobeña M., Lehodey P., Reis J., Cascão I., Lammers M. O., Caldeira R. M. A., Silva M. A. (2020). Differences in regional oceanography and prey biomass influence the presence of foraging odontocetes at two Atlantic seamounts. *Marine Mammal Science*, 36: 158-179, https://doi.org/10.1111/mms.12626

Romagosa, M., Pérez-Jorge, S., Cascão, I., Mouriño, H., Lehodey, P., Marques, T.A, Silva, M.A. (2021). Food talk: 40-Hz fin whale calls are associated with prey availability. *Proceedings of the Royal Society B Biological Sciences*, 288(1954), https://doi.org/10.1098/rspb.2021.1156

Rose, K.A., Fiechter, J., Curchitser, E.N., Hedstrom, K., Bernal, M., Creekmore, S., Haynie, A.C., Ito, S., Lluch-Cota, S.E., Megrey, B.A., Edwards, C.A., Checkley, D.M., Koslow, T., Mcclatchie, S., Werner, F.E., Maccall, A.D., and Agostini, V.N. (2015). Demonstration of a fully-coupled end-to-end model for small pelagic fish using sardine and anchovy in the California Current. *Progress in Oceanography*, 138, 348-380, https://doi.org/10.1016/j.pocean.2015.01.012

Russell, J., Sarmiento, J., Cullen, H., Hotinski, R., Johnson, K.S., Riser, S.C., et al. (2014). The Southern Ocean Carbon and Climate Observations and Modeling Program (SOCCOM). Ocean Carbon Biogeochem. News. Available at https://web.whoi.edu/ocb/wp-content/uploads/sites/43/2016/12/OCB_NEWS_FALL14.pdf

Ryabinin, V., Barbière, J., Haugan, P., Kullenberg, G., Smith, N., McLean, C., Troisi, A., Fischer, A., Aricò, S., Aarup, T., Pissierssens, P., Visbeck, M., Enevoldsen, H.O., Rigaud, J. (2019). The UN Decade of Ocean Science for Sustainable Development, *Frontiers in Marine Science*, 6,470, https://doi.org/10.3389/fmars.2019.00470

Sakov, P., and Oke, P.R. (2008). A deterministic formulation of the ensemble Kalman filter: an alternative to ensemble square root filters. *Tellus* A, 60, 361-371, https://doi.org/10.1111/j.1600-0870.2007.00299.x

Salon, S., Cossarini, G., Bolzon, G., Feudale, L., Lazzari, P., Teruzzi, A., Solidoro, C., Crise, A. (2019). Novel metrics based on Biogeochemical Argo data to improve the model uncertainty evaluation of the CMEMS Mediterranean marine ecosystem forecasts. *Ocean Science*, 15, 997-1022, https://doi.org/10.5194/os-15-997-2019

Santana-Falcon, Y., Brasseur, P., Brankart, J.M., and Garnier, F. (2020). Assimilation of chlorophyll data into a stochastic ensemble simulation for the North Atlantic ocean, *Ocean Science*, 16, 1297-1315, https://doi.org/10.5194/os-16-1297-2020

Schartau, M., Wallhead, P., Hemmings, J., Löptien, U., Kriest, I., Krishna, S., Ward, B. A., Slawig, T., and Oschlies, A. (2017). Reviews and syntheses: parameter identification in marine planktonic ecosystem modelling. *Biogeosciences*, 14, 1647-1701, https://doi.org/10.5194/bg-14-1647-2017

Scutt Phillips, J., Sen Gupta, A., Senina, I., van Sebille, E., Lange, M., Lehodey, P., Hampton, J., Nicol, S. (2018). An individual-based model of skipjack tuna (Katsuwonus pelamis) movement in the tropical Pacific Ocean. *Progress in Oceanography*, 164, 63-74, https://doi.org/10.1016/j.pocean.2018.04.007

Senina, I., Lehodey, P., Hampton, J., Sibert, J. (2019). Quantitative modelling of the spatial dynamics of South Pacific and Atlantic albacore tuna populations. *Deep Sea Research Part II: Topical Studies in Oceanography*, 175, 104667, https://doi.org/10.1016/j.dsr2.2019.104667

Senina, I., Lehodey, P., Sibert, J., Hampton, J. (2020). Improving predictions of a spatially explicit fish population dynamics model using tagging data. *Canadian Journal of Aquatic and Fisheries Sciences*, 77(3), 576-593, https://doi.org/10.1139/cjfas-2018-0470

Senina, I., Sibert, J., and Lehodey, P. (2008). Parameter estimation for basin-scale ecosystem-linked population models of large pelagic predators: Application to skipjack tuna. *Progress in Oceanography*, 78, 319-335, https://doi.org/10.1016/j.pocean.2008.06.003

Sibert, J., Senina, I., Lehodey, P., Hampton, J. (2012). Shifting from marine reserves to maritime zoning for conservation of Pacific bigeye tuna (Thunnus obesus). *Proceedings of the National Academy of Sciences*, 109(44): 18221-18225.

Simon, E. and Bertino, L. (2009). Application of the Gaussian anamorphosis to assimilation in a 3-D coupled physical-ecosystem model of the North Atlantic with the EnKF: a twin experiment. *Ocean Science*, 5(4), 495-510, https://doi.org/10.5194/os-5-495-2009

Simon, E. Bertino, L. (2012). Gaussian anamorphosis extension of the DEnKF for combined state parameter estimation: Application to a 1D ocean ecosystem model. *Journal of Marine Systems*, 89(1), 1-18, https://doi.org/10.1016/j.jmarsys.2011.07.007

Simon, E., Samuelsen, A., Bertino, L. and Mouysset, S. (2015). Experiences in multiyear combined state-parameter estimation with an ecosystem model of the North Atlantic and Arctic Oceans using the Ensemble Kalman Filter. *Journal of Marine Systems*, 152, 1–17, https://doi.org/10.1016/j.jmarsys.2015.07.004

Skákala, J., Ford, D., Brewin, R. J. W., McEwan, R., Kay, S., Taylor, B., Mora, L., and Ciavatta, S. (2018). The assimilation of phytoplankton functional types for operational forecasting in the northwest European shelf. *Journal of Geophysical Research: Oceans*, 123, 5230-5247, https://doi.org/10.1029/2018JC014153

Skakala, J., Bruggeman, J., Brewin, R.J., Ford, D.A. and Ciavatta, S. (2020). Improved representation of underwater light field and its impact on ecosystem dynamics: A study in the North Sea. *Journal of Geophysical Research: Oceans*, 125(7), e2020JC016122, https://doi.org/10.1029/2020JC016122

Skákala, J., Ford, D., Bruggeman, J., Hull, T., Kaiser, J., King, R.R., Loveday, B., Palmer, M.R., Smyth, T., Williams, C.A. and Ciavatta, S. (2021a). Towards a multi-platform assimilative system for North Sea biogeochemistry. *Journal of Geophysical Research: Oceans*, 126(4), e2020JC016649, https://doi.org/10.1029/2020JC016649

Skakala, J., Bruggeman, J., Ford, D.A., Wakelin, S.L., Akpınar, A., Hull, T., Kaiser, J., Loveday, B.R., Williams, C.A.J. and Ciavatta, S. (2021b). Improved consistency between the modelling of ocean optics, biogeochemistry and physics, and its impact on the North-West European Shelf seas. *Earth and Space Science Open Archive ESSOAr*, https://doi.org/10.1002/essoar.10506737.2

Skogen, M.D. (1993). A User's guide to NORWECOM (the NORWegian ECOlogical Model system). Technical report 6, Inst.of Marine Research, Division of Marine Env., Pb 1870, N-5024 Bergen, Norway.

Skogen, M.D. and Søiland, H. (1998). A User's guide to NORWECOM v2.0 (the NORWegian ECOlogical Model system). Tech.rep. Fisken og Havet 18, Inst. of Marine Research, Pb.1870, N-5024 Bergen. Norway.

Song, H., Edwards, C.A., Moore, A.M., and Fiechter, J. (2016). Data assimilation in a coupled physical-biogeochemical model of the California current system using an incremental lognormal 4-dimensional variational approach: part 3 - Assimilation in a realistic context using satellite and in situ observations. Ocean Modelling, 106, 1531-145, https://doi.org/10.1016/j.ocemod.2016.04.001

Spindler, M. (1994). Notes on the biology of sea ice in the Arctic and Antarctic. *Polar Biology*, 14, 319-324, https://doi.org/10.1007/BF00238447

Storto, A., Oddo, P., Cipollone, A., Mirouze, I. and Lemieux-Dudon, B. (2018). Extending an oceanographic variational scheme to allow for affordable hybrid and four-dimensional data assimilation. *Ocean Modelling*, 128,.67-86, https://doi.org/10.1016/j.ocemod.2018.06.005

Stow, C. A., Jolliff, J., McGillicuddy Jr, D. J., Doney, S. C., Allen, J. I., Friedrichs, M. A., Wallhead, P., 2009. Skill assessment for coupled biological/physical models of marine systems. *Journal of Marine Systems*, 76(1-2), 4-15, https://doi.org/10.1016/j.jmarsys.2008.03.011

Taylor, K.E. (2001). Summarizing multiple aspects of model performance in a single diagram. *Journal of Geophysical Research: Atmospheres*, 106(D7), 7183-7192, https://doi.org/10.1029/2000JD900719

Teruzzi, A, Di Cerbo, P, Cossarini, G, Pascolo, E, Salon, S. (2019). Parallel implementation of a data assimilation scheme for operational oceanography: The case of the MedBFM model system. *Computers & Geosciences*, 124, 103-114, https://doi.org/10.1016/j.cageo.2019.01.003

Teruzzi, A., Dobricic, S., Solidoro, C., and Cossarini, G. (2014). A 3-D variational assimilation scheme in coupled transport-biogeochemical models: Forecast of Mediterranean biogeochemical properties. *Journal of Geophysical Research: Oceans*, 119, 200-217, https://doi.org/10.1002/2013JC009277

Tissier, A.-S., Brankart, J.M., Testut, C.E., Ruggiero, G., Cosme, E., and Brasseur, P. (2019). A multiscale ocean data assimilation approach combining spatial and spectral localization. *Ocean Science*, 15, 443-457, https://doi.org/10.5194/os-15-443-2019

Torres, R., Allen, J.I. and Figueiras, F.G. (2006). Sequential data assimilation in an upwelling influenced estuary. *Journal of Marine Systems*, 60(3-4), 317-329, https://doi.org/10.1016/j.jmarsys.2006.02.001

Uitz, J., Claustre, H., Morel, A., and Hooker, S. B. (2006). Vertical distribution of phytoplankton communities in open ocean: An assessment based on surface chlorophyll. *Journal of Geophysical Research: Oceans*, 111(C8), https://doi.org/10.1029/2005JC003207

van Leeuwen, P.J. (2010). Nonlinear data assimilation in geosciences: an extremely efficient particle filter. *Quarterly Journal of the Royal Meteorological Society*, 136(653), 1991-1999, https://doi.org/10.1002/qj.699

Vandenbulcke, L., and Barth, A. (2015). A stochastic operational system of the Black Sea: Tech. and validation. *Ocean Modelling*, 93, 7-21.

Verdy, A., and Mazloff, M.R. (2017). A data assimilating model for estimating Southern Ocean biogeochemistry. *Journal of Geophysical Research: Oceans*, 122(9), 6968-6988, https://doi.org/10.1016/j.ocemod.2015.07.010

Vetra-Carvalho, S., Van Leeuwen, P.J., Nerger, L., Barth, A., Altaf, M.U., Brasseur, P., Kirchgessner, P. and Beckers, J.M. (2018). State-of-the-art stochastic data assimilation methods for high-dimensional non-Gaussian problems. *Tellus A: Dynamic Meteorology and Oceanography*, 70(1), 1-43, https://doi.org/10.1080/16000870.2018.1445364

Vichi, M., Cossarini, G., Gutierrez Mlot, E., Lazzari, P., Lovato, T., Mattia, G., Masina, S., McKiver, W., Pinardi, N., Solidoro, C., Zavatarelli, M. (2015). The Biogeochemical Flux Model (BFM): Equation Description and User Manual. BFM version 5.1. BFM Report series N.1, March 2015, Bologna, Italy, pp. 89.

Wang, B., Fennel, K., Yu, L. and Gordon, C. (2020). Assessing the value of biogeochemical Argo profiles versus ocean color observations for biogeochemical model optimization in the Gulf of Mexico. *Biogeosciences*, 17(15), 4059-4074, https://doi.org/10.5194/bg-17-4059-2020

Warner, J.C., Armstrong, B., He, R., Zambon, J.B. (2010). Development of a Coupled Ocean–Atmosphere–Wave–Sediment Transport (COAWST) Modeling System. *Ocean Modelling*, 35(3), 230-244, https://doi.org/10.1016/j.ocemod.2010.07.010

Waters, J., Lea, D.J., Martin, M.J., Mirouze, I., Weaver, A. and While, J. (2015). Implementing a variational data assimilation system in an operational 1/4 degree global ocean model. *Quarterly Journal of the Royal Meteorological Society*, 141(687), 333-349, https://doi.org/10.1002/qj.2388

Waters, J., Bell, M. J., Martin, M. J., and Lea, D. J. (2017). Reducing ocean model imbalances in the equatorial region caused by data assimilation. *Quarterly Journal of the Royal Meteorological Society, 143(702), 195-208.*

While, J., Totterdell, I. and Martin, M. (2012). Assimilation of pCO2 data into a global coupled physical-biogeochemical ocean model. *Journal of Geophysical Research: Oceans*, 117(C3), https://doi.org/10.1029/2010JC006815

Wright, R.M., Le Quéré, C., Buitenhui, E., Pitois, S., Gibbons, M. (2021). Role of jellyfish in the plankton ecosystem revealed using a global ocean biogeochemical model. *Biogeosciences*, 18, 1291-1320, https://doi.org/10.5194/bg-18-1291-2021

Xiao, Y., and M.A.M. Friedrichs (2014). Using biogeochemical data assimilation to assess the relative skill of multiple ecosystem models: effects of increasing the complexity of the planktonic food web. *Biogeosciences*, 11(11), 3015-3030, https://doi.org/10.5194/bg-11-3015-2014

Yool, A., Popova, E. E., and Anderson, T. R. (2013). MEDUSA-2.0: an intermediate complexity biogeochemical model of the marine carbon cycle for climate change and ocean acidification studies. *Geoscientific Model Development*, 6, 1767-1811, https://doi.org/10.5194/gmd-6-1767-2013

Yu, L., Fennel, K., Bertino, L., El Gharamti, M., and Thompson, K. R. (2018). Insights on multivariate updates of physical and biogeochemical ocean variables using an Ensemble Kalman Filter and an idealized model of upwelling. *Ocean Modelling*, 126, 13-28, doi:10.1016/j.ocemod.2018.04.005

Zeebe, R., and Wolf-Gladrow, D. (2001). CO2 in Seawater: Equilibrium, Kinetics, Isotopes. Elsevier Oceanography Book Series, 65, 346 pp, Amsterdam.

Zhou M., Carlotti F., Zhu Y. (2010). A size-spectrum zooplankton closure model for ecosystem modelling. *Journal of Plankton Research*, 32(8), 1147-1165, https://doi.org/10.1093/plankt/fbq054

10.
Coupled Prediction: Integrating Atmosphere-Wave-Ocean forecasting

CHAPTER COORDINATOR

John Siddorn

CGAPTER AUTHORS (*in alphabetical order*)

Natacha B. Bernier, Øyvind Breivik, Kai H. Christensen, Stephen G. Penny, and Keguang Wang

10. Coupled Prediction: Integrating Atmosphere-Wave-Ocean forecasting

10.1.
Introduction to coupled prediction

In the early days of numerical modelling of the various components of the Earth system, each component was treated individually. Figure 10.1 shows a representation of two systems, ocean and atmosphere, that run independently: the output of one system is used to "force" the other. The interface between the ocean and the atmosphere was considered a phenomenon that had to be modelled independently of the two media.
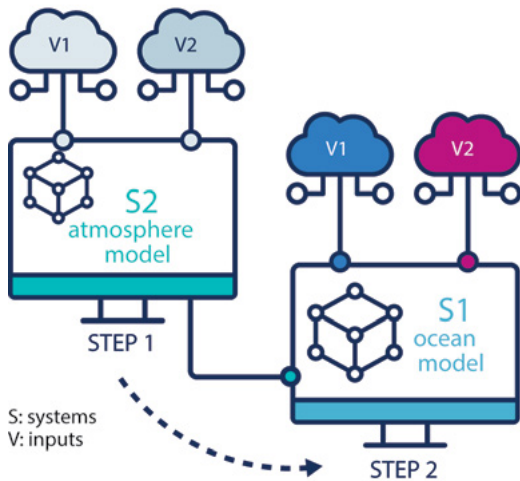
Figure 10.1.   Traditional modelling platform characterised by Systems (S), like ocean model and atmosphere model, and inputs to each System (V).

This representation of the Earth system interactions is in some sense arbitrary. As the complexity of models grew, attempts were made to integrate the components more tightly, particularly in the field of climate modelling. Weather forecasting has a time scale of days to a couple of weeks (Lorenz, 1967) and, as new forecasts would be initialised regularly (typically every day), excessive diffusivity was never considered a problem. Making the early numerical weather prediction models *conservative* was therefore not a priority. The problem of conserving quantities such as heat, moisture, or momentum to avoid *model drift*, began to manifest itself only with the advent of long integrations of climate models. It became clear that long climate integrations of the atmosphere needed to also consider the impact of a (slowly) changing ocean, not least because the various climate components interact in nonlinear ways. This produces feedback loops that can fundamentally alter the state of each climate component. Numerical weather prediction models also need-

ed to close the energy budget at the top of the atmosphere (or in the case of climate change, get that imbalance right). This led to the first attempts at coupling ocean and atmosphere models. The ice floating on the ocean and the soil in the ground were also separate from the ocean and the atmosphere. The latter was the first to be incorporated into more complex models, leading to the first coupled models.

Figure 10.2 shows a conceptual representation of systems that can interact through a "mechanism" called coupler. Figure 10.3 shows a more detailed and realistic representation of this coupling process.

Theoretical challenges to producing skilful weather forecasts were noted early in the history of NWP. For example, Lorenz (1963) pointed to the phenomenon of sensitive dependence on initial conditions. This means that small changes in our current best guess of the atmosphere or ocean could lead to very large changes in the forecasts. As a consequence, skillful weather prediction is limited to a finite time horizon of around 1-2 weeks. However, this perspective tends to focus on synoptic scale atmospheric dynamics. When a numerical model of the atmosphere is coupled to numerical models of the ocean and other Earth system components, new timescales are introduced into the system. In such multiscale systems,
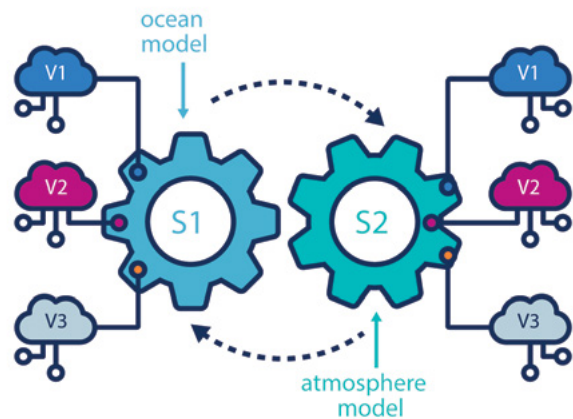
Figure 10.2.   Coupling modelling platform where Systems (S) communicate with each other through an interface code called "coupler".
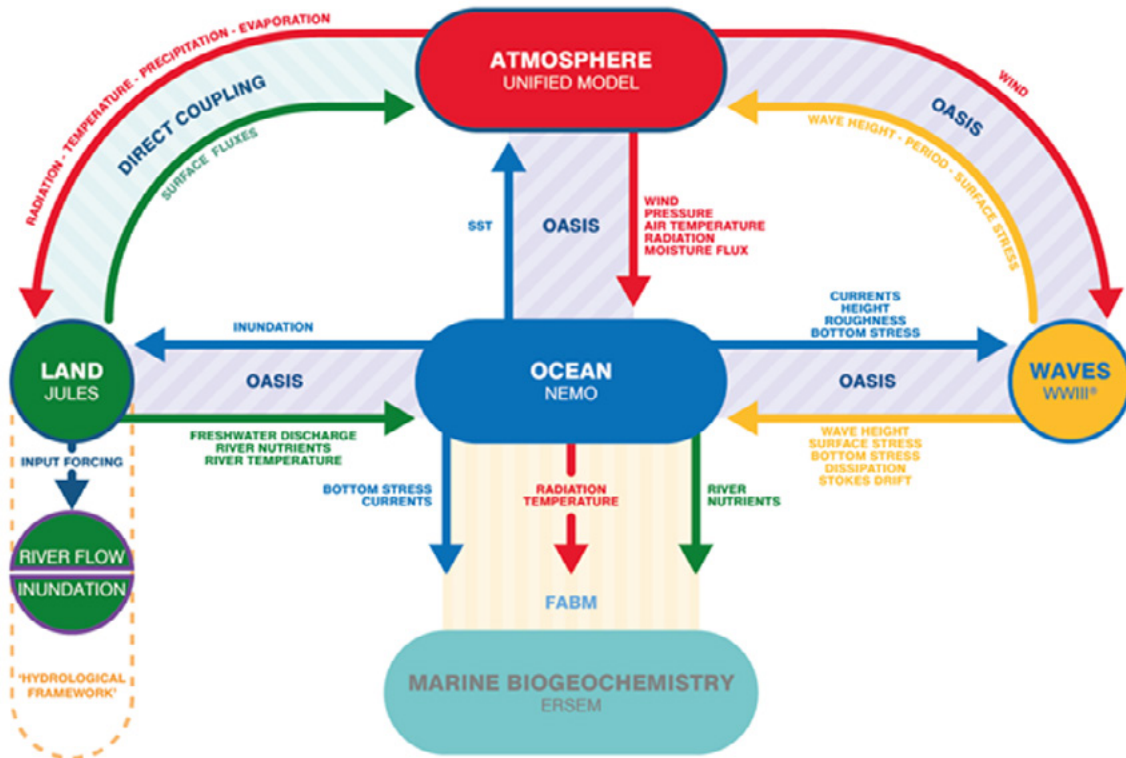
Figure 10.3. A schematic of the components (ocean, waves, etc.), the models (NEMO, WWIII, etc.), and the coupling exchanges between them, based on the system described in Lewis et al. (2019). Note the use of the coupler OASIS, the use of input forcing between Jules and the river flow model, direct coupling between Jules and the UM and direct forcing between the NEMO and ERSEM systems. A relatively simple coupled system (no ice) that includes 6 different models and 4 different approaches to coupling between them.

fast growing errors tend to be associated with processes that evolve quickly but saturate at smaller scales (Harlim et al., 2005), while slower growing or decaying errors tend to be associated with larger scale oscillations (Penland and Sardeshmukh, 1995; Penland and Matrosova, 1998; Vannitsem and Duan, 2020).

DA is the process of integrating information from numerical models with observations derived from real world measurements. At operational centres, DA systems have typically been built for each Earth system component independently. Early efforts to produce coupled forecasts maintained this separation of components when applying DA to provide initial conditions (Saha et al., 2006, 2010, and 2014; Zhang et al., 2007), an approach that is now called WCDA. More recently, there have been efforts to treat the entire coupled Earth system as one state and update accordingly. This more integrated approach allows observations to have immediate influence across domain boundaries (e.g. the air-sea interface), and as such is called SCDA. There are also approaches that fall on the spectrum between these extremes, such as the CERA system at the ECMWF that applies different DA systems to the

atmosphere and ocean but still allows influence across the air-sea interface via an iterative cycling over a moving 6-12 hour time window (Laloyaux et al., 2018).

Beyond these theoretical considerations, there are many technical complications involved in transitioning to coupled prediction. Many centres have developed monitoring and prediction tools independently for individual Earth components (e.g. atmosphere, ocean, land, waves, etc.). This is natural based on the historical context of their development and limitations on computing capabilities, but it has created an infrastructure within and across institutions that adds complexity to the task of unifying prediction systems. The major prediction centres are making progress towards an integrated approach by unifying software infrastructure for models and data assimilation capabilities, as well as providing opportunities to increase interactions among the development teams of each system component. Data formats for model output and observational data sets have not been fully standardised across the various Earth system domains, and so this adds further steps before seamless integration.

A very important practical limitation that has most certainly curtailed research and development in coupled prediction is the extreme demands it places on computational resources. The best performing applications for atmospheric prediction and ocean prediction have already been pushed to their limits of resource consumption. Acknowledging the fact that coupled systems can perform very differently at low resolutions versus high resolutions, there remain very few organisations with the resources needed to explore unanswered questions in coupled prediction at relevant resolutions for operational prediction. For this reason, there are efforts underway to identify methods to reduce the computational demands at bottlenecks within the cycled data assimilation and forecast systems.

10.2.
Coupling processes

10.2.1. Waves and their role in air-sea exchange

Waves have been called the gearbox of the climate system (Semedo et al., 2011). The analogy highlights the mediating role of the wave field between the atmosphere and the ocean interior. It may seem surprising that the sea surface demands its own class of numerical model. The other components (atmosphere, ocean, sea ice, land surface) have real substance, i.e. they each represent a three-dimensional chunk of the Earth system. In contrast, the wave model is a representation of a *surface* between two media, namely the air and the sea (Figure 10.4). There are, however, good practical reasons for this split. If we had access to unlimited computing power, we could model the ocean and the atmosphere with a grid resolution approaching Kolmogorov's microscale. That would mean that the Navier Stokes equations could be solved in the approximative limit known as DNS (Moin and Mahesh, 1998). In this case, the (liquid) ocean would presumably interact with the (gaseous) atmosphere and on their interface would form a wavy surface that, given a sufficiently strong momentum flux (mostly from the atmosphere to the ocean), would form droplets and bubbles as the waves start to break. The computational reality is far from this. At present, we can model the ocean and the atmosphere with models that have grid cells of tens of metres in the horizontal if we limit ourselves to small domains, whereas the waves that form under the influence of the wind have wavelengths of the order of some metres to hundreds of metres and so cannot be explicitly resolved together with the bulk ocean properties.

The behaviour of these waves determines the mass and momentum fluxes between the ocean and the atmosphere. As waves grow under the influence of the wind, they become steeper. In this phase they are also choppier than they will
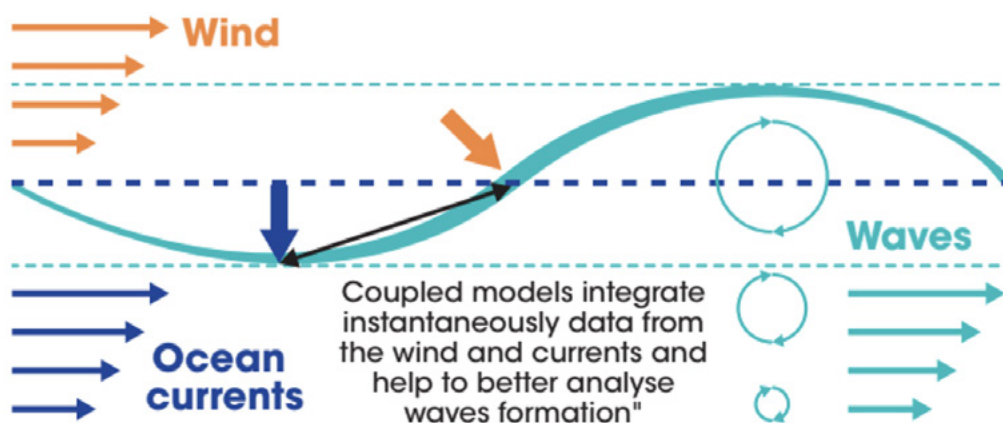
Figure 10.4. Representation of AWO coupled models.

be later on. All this means that the momentum flux between the atmosphere and the ocean is affected by the presence of waves (Janssen et al., 2004; Breivik et al., 2015). There is also very important feedback between the waves and the atmosphere. As waves grow, the sea surface becomes rougher, slowing the near-surface winds and increasing the momentum flux from the atmosphere to the wave field. This has the effect of stemming the deepening of low-pressure systems. This is important in the formation and growth of extratropical lows (Janssen, 1991 and 2004), but also in the evolution of tropical cyclones (discussed further below).

A secondary effect of waves on the air-sea interaction is through their ability to impart momentum and turbulent kinetic energy to the ocean interior (Figure 10.4). As waves grow, they absorb momentum that would otherwise go directly to the formation of ocean currents. As waves break, they part with this momentum, and also inject turbulent kinetic energy into the ocean (Janssen et al., 2004; Rascle et al., 2006; Ardhuin et al., 2008 and 2009). This leads to a redistribution of momentum and kinetic energy in time and space (Ardhuin and Jenkins, 2006; Breivik et al., 2015; Staneva et al., 2017; Wu et al., 2019), and has a profound effect on near-shore processes (Uchiyama et al., 2010; Kumar et al., 2012) where waves interact strongly with the currents. It is also clear that in open ocean conditions the mixed-layer depth is a function of the wave activity, in part sustained by the Langmuir turbulence (McWilliams et al., 1997; Fan and Griffies, 2014; Li et al., 2016 and 2017; Li and Fox-Kemper, 2017; Ali et al., 2019). The enhanced mixing due to waves is thus important for the sea surface temperature, which helps to determine the air-sea heat flux and thus constitutes an important feedback mechanism between the atmosphere and the ocean.

10.2.2. Land/sea exchanges

Land-sea interactions take place on a wide range of spatial and temporal scales. The presence of land modifies the weather in the coastal zone, e.g. the daily variations in wind speed and direction due to the sea breeze, and hence the atmosphere provides an indirect link between the land and the ocean. Another example of this indirect coupling is the way large-scale weather systems can influence the transport pathways of river water (Osadchiev et al., 2020).

The physical couplings between land, ocean, and atmosphere are not necessarily equal in strength and importance, and we often observed a lagged response. The runoff from rivers is dependent on the precipitation over a potentially very large catchment area, with significant lag between specific precipitation events and the freshwater discharge to the coastal ocean. This lag is particularly pronounced in temperate and polar regions where the precipitation accumulates as snow during parts of the year. This is reflected by the

state-of-the-art of coupled modelling, as very few systems couple the ocean to the land, but rather use the atmosphere as a mediator.

10.2.3. Air-sea exchanges across sea ice

At high latitudes, air-sea exchange is modified by the presence of sea ice. Varying in thickness up to a couple of metres, sea ice is sensitive to forcing from both air and sea and the air, sea, and sea ice are strongly coupled. Geophysical scale sea ice is essentially a mixture of ice floes of varying size and thickness, with the added complexity of being rafted and ridged. Describing accurately the sea ice mechanical behaviour is extremely challenging, although modelling sea ice as plastic materials at the large scale has long been a successful approach (Coon et al., 1974; Hibler, 1979; Hunke and Dukwicz, 1997; Girard et al., 2011). In medium to high model resolutions (≤ 10km), such models can generate small-scale features such as the ice leads (Hutchings et al., 2005; Wang and Wang, 2009; Girard et al., 2011; Spreen et al., 2017). This thin ice cover has a very small heat content and easily melts away during summer, resulting in large seasonal variations of sea ice extent.

In much of the pack ice region, the thermodynamic and dynamic interactions between air and sea are greatly suppressed. During wintertime, the air-sea heat flux through leads is two orders of magnitude larger than that through thick ice (Maykut, 1978). Dynamically, pack ice behaves as a low-pass filter, the air and sea surface stresses act on the ice cover thus driving the advection and deformation of sea ice, while ocean waves are generally suppressed. The MIZ is a highly complex region consisting of ice floes of varying dimensions and shapes. Wave energy propagating into the MIZ can lead to rapid breakup. The damping of waves in sea ice is directly related to the amount of energy imparted on the sea ice. This is a field of active research, and it is presently not fully clear how the MIZ attenuates wave energy (Doble and Bidlot, 2013; Williams et al., 2013; Kohout et al., 2014; Sutherland and Rabault, 2016; Ardhuin et al., 2016; Rabault et al., 2020).

Landfast ice is a special region where the air-sea interaction nearly ceases. It generally appears in winter seasons and often occurs in shallow waters where ridged ice grounds on the seabed (Mahoney et al., 2014), or occurs where islands are close to each other (Divine et al., 2003). Modelling studies have shown that adding base stress due to grounding ridges and increasing ice tensile strength improve the simulation of landfast ice evolution (Lemieux et al., 2016), although in some Arctic shelf seas the time duration needs to be further improved.

In coupled modelling, a key consideration is whether to couple the sea ice directly to the atmosphere or only through the ocean model. In some recent coupled models, particularly

for high-resolution short-term atmosphere, ocean, and sea ice forecasts, the timestep for coupling has decreased to one hour or less, e.g. the coupled ocean-ice model METROMS at the Norwegian Meteorological Institute (Naughten et al., 2018), or the atmosphere-ice coupled model at UKMO (Ridley et al., 2018). In these cases, the difference between using the atmosphere timestep or ocean timestep is generally negligible.

10.2.4. The importance of air-sea exchanges during storms and other extreme events

Air-sea exchange really comes to the fore in the development of tropical cyclones. The sea surface temperature must as a general rule exceed 26.5°C to sustain the growth of the cyclone (Emanuel, 1986). However, the depth to which the ocean's temperature must be above this critical threshold is also important. As the cyclone moves across the sea surface, the Ekman transport will lead to divergence, and vertical Ekman pumping will eventually lead cooler water to the surface. If the cyclone is moving sufficiently slowly, this will eventually kill the cyclone (Mogensen et al, 2017). Thus, it is essential to include an ocean model component that responds to the atmospheric forcing.

Polar lows are of a decidedly less extreme nature than tropical cyclones, but they share the same dependence on sea surface temperature (Rasmussen and Turner, 2003). As winds blow off the sea ice, the air is rapidly warmed by the (relatively) warm ocean surface. Under the appropriate atmospheric conditions (Kolstad, 2015), this can lead to the formation of polar lows. These are small-scale, intense cyclones, typically with gale-force winds. If the cyclone is rather stationary, a shallow layer of warmer water can mix with cooler waters through Ekman pumping. As the ocean temperature is key to sustaining a cyclone, the water mixing can sometimes be enough to inhibit further growth of the polar low.

Examples of instantaneous coupling between land, ocean, and atmosphere also include coastal inundation during landfall of tropical cyclones (Lee et al., 2019). In these cases, heavy precipitation leads to a swelling of local rivers, which is often coincidental with a large storm surge. The result is a rapid sea-level rise that may cause extensive damage to coastal infrastructure, especially when combined with large surface waves and strong winds.

10.3.
Benefits expected from coupling

The importance of coupled ocean-atmosphere prediction systems in providing seasonal predictability is well-known (Kim et al., 2012, and references therein). Sources of predictability in seasonal forecasting systems tend to be, by their very nature, coupled systems driven by teleconnections that are functions of climate modes, such as the North Atlantic Oscillation and the El Niño–Southern Oscillation that have geographically far-reaching consequences. However, as timescales shorten and the dominance of these coupled climate modes become less fundamental to predictability of the atmosphere-ocean system, it becomes less obvious whether the benefits of fully coupled systems justify the computational cost or the technical and scientific complexity required. The coupling between atmospheric and wind wave models was first introduced operationally in 1998 at ECMWF. The method based on the theoretical work of Janssen (1991) contributed to an improvement of both atmospheric and surface wave forecasts at the medium range on the global scale. The usual approach of forcing the ocean with atmospheric conditions (Takano et al., 1973), and referred to in this section as "forced") using bulk parameterisations of

the fluxes (Large and Yeager, 2009) is computationally and structurally far easier and cheaper than coupling approaches. However, the key boundary layer processes (see Section 9.1 for details) are not taken into account and thus the feedback between the atmospheric boundary layer and the upper ocean is not represented. It is necessary to understand how important these processes might be, bearing in mind that coupled models can suffer from systematic errors as a result of positive feedback leading to drifts in the forecast (Hyder et al., 2018).

Ocean forecasting systems have become increasingly high-resolution, resolving coastlines, bathymetry, and eddy-scale processes. The effect of coupling on model predictions becomes more important with increasing grid resolution (Janssen et al., 2004), and so the question of the benefits of coupling to ocean forecasting is perhaps more relevant now than ever. A small but growing body of literature demonstrates the benefits to ocean prediction of coupling at shorter time-ranges (Brassington et al, 2015; Allard et al., 2010; Lewis et al., 2018 and 2019).

Understanding the advantages of coupled over uncoupled predictions in short-range ocean forecasting is in its infancy. Although the future of advanced systems is clearly coupling, as several processes are better represented, predictive modelling without coupling is however possible thanks to parameterizations and should never be discarded as an option. At a recent science meeting of OceanPredict (Vinayachandran et al., 2020), the need for a careful evaluation of how ocean and atmosphere components interact and impact each other was highlighted. At monthly or shorter timescales, the benefits of running coupled systems need to be evaluated, balancing scientific and service benefits against complexity and computing costs. Intermediate complexity coupling may also be an appropriate approach if full coupling is not viable and the service is not reliant on the atmosphere and ocean information. Lemarié et al. (2021) provided an example of an atmospheric boundary layer approach that gives some of the benefits of coupling whilst being significantly simpler and computationally cheaper.

The potential benefits of using a coupled framework is reinforced by the move towards a multi-hazard approach to predictions. Natural hazards from multiple sources may combine or occur concurrently (Lewis et al., 2015). Large waves, storm surges, high-wind speeds, and extreme precipitation are all hazards that are likely to co-occur, and influence each other through coupled feedbacks that can compound one another (for example through over-topping). Coupled systems that predict these coupled feedbacks may enable an improvement in the range and consistency of actionable information to be provided through hazard warnings and guidance.

When considering providing services in multi-hazards frameworks, the opportunities that coupling provides should be considered alongside the scientific benefits. A coupled system combining the full water-cycle – including consistent precipitation, river runoff, wave, currents, and surge forecasts - can give users mutually consistent products in a joint probability framework. This can be important in coastal flooding, where the impacts for coastal communities or industries can come from high river flows and local heavy precipitation events, alongside overtopping waves and extreme surges. From a service perspective, it is attractive to provide probabilistic frameworks in which the timings and intensities of events are consistently incorporated and interact appropriately; these services increasingly rely on probabilistic information for decision making. An area that has had limited attention but seems likely to prove significant is the impact of feedback among Earth-system components upon ensemble spread, and hence the quality of the probabilistic information.

Ocean phenomena are usefully classified depending on their nature, which determines the timescale for oceanic predictive skill and whether a coupled ocean-atmosphere model would be advantageous. Some phenomena have strong de-

pendence, and a rapid response, to the atmosphere forcing and can be thought of as forced-dissipative systems. This category includes, surface waves, responses to surface heating and wind in the ocean boundary layer, and storm surges. These systems largely depend upon skill in the atmosphere model, and so the benefits of coupling to the atmosphere can be a leading-order driver of the ocean system skill. The advantage of coupling and its impact upon predictability often focus on the benefits to the atmosphere (Brunet et al., 2010; Belcher et al., 2015). The impact of ocean coupling on tropical meteorology is well documented with tropical cyclones (Bender and Ginis 2000; Mogensen et al., 2017; Smith et al., 2018; Neetu et al., 2019), monsoons (Fu, 2007), and the Madden–Julian Oscillation (Bernie et al., 2008; Shelly et al., 2014; Seo et al., 2014), which predictability improved in coupled systems. There is also an increasing body of evidence that the oceans have a significant local (important for short-range forecasts) and non-local (increasingly significant at longer lead-times) influence on the extra tropics (Minobe et al., 2008).

In the literature, there is limited quantification of the impact of the coupled improvement in atmospheric parameters on ocean services but it is an increasing area of study. Guiavarc'h et al. (2019) explored the impact of a coupled (atmosphere-ocean) system on short-range ocean forecast skill and showed that there are benefits in SST predictability at the short-range, but with mixed results for other parameters. Given that the research system they used is at a relatively early stage in development, and the resolution of the atmosphere is significantly lower than in comparable forced systems, these results are encouraging.

Although the importance of coupling the wave-ocean interface for improving forecasts of surge and waves is well documented (Wolf, 2008; Lewis et al., 2018), most storm surge and wave prediction systems remain largely independent. As well as the atmospheric forcing, ocean currents have a significant role in modifying ocean wave properties. The presence of eddies, fronts, and filaments with length scales of tens to hundreds km and ubiquitous in the world's oceans, can be the main source of variability in significant wave heights at these scales. Ardhuin et al. (2017) made a compelling case for the importance of coupling the ocean surface currents to a wave model allowing adequate representation of wave height variability in the world's open oceans. Wave predictions in shelf seas environments are shown to be improved as a result of coupling to an ocean model (Allard et al., 2012; Wahle et al., 2017; Lewis et al., 2018). as well as the predictions of ocean current and other ocean parameters, including upwelling due to stokes drift effects, were enhanced (Wu et al, 2019). Fan et al. (2009) showed that time and spatial variations in the surface wave field, as a result of coupling to winds, are particularly strong in hurricanes, with significant additional feedback from ocean currents and near-surface temperatures.

The ocean eddy kinetic energy is damped when taking into account the feedbacks between ocean surface current and winds (Oerder et al., 2018; Jullien et al., 2020). As ocean models increasingly resolve the mesoscale explicitly, they are likely to have the tendency to over-predict the eddy activity. In uncoupled systems, there is an option to calculate the wind stress using relative wind speeds (taking into account the eddies and other ocean current interactions). However, in these systems there is no imprint of ocean eddies on the atmospheric wind stress curl (due to the lack of ocean eddies in the uncoupled atmospheric modelling system), and so the feedback onto the wind stress results in over-damping of the eddies. A fully coupled system will correctly allocate the feedback between the winds and currents, allowing the eddy and wind fields to co-evolve correctly. This coupling between the winds and currents can also lead to upscaling to the large scale, e.g. Renault et al. (2016) showed that current/wind feedback, through its eddy killing effect, resolves long-lasting biases in Gulf Stream path.

Marine heatwaves have recently been recognised for their importance (Holbrook et al., 2019). They are high impact events that can be induced by anomalous heating at the ocean surface; their predictability is dependent upon air-sea coupled phenomena (Jacox, 2019). At the other end of the temperature scale, Pellerin et al. (2004) showed that

coupling can also have strong impacts in ice-infested seas even down to sub-daily time scales, due to rapid changes in coastal sea ice cover (i.e. the formation of coastal polynyas). The sea ice acts as a barrier between a relatively warm–wet ocean and cold–dry atmosphere, and changes in the sea ice cover can have dramatic effects on heat and moisture fluxes. The importance of coupling has also been recognized in polar regions (Jung and Vitart, 2006).

Coastal regions are particularly impacted by coupled processes, both between the ocean and atmosphere and coupling with river and estuaries. The impact of freshwater discharges on the ocean circulation is highlighted by Røed and Albretsen (2007) and, more broadly on the coastal marine environment, by Dzwonkowski et al., 2017. The inputs from the land surface, mediated through estuaries and lagoons, are generally poorly represented in ocean forecasting systems due to their scale (time and space) and their complexity. It is extremely difficult to accurately model nutrient inputs, which are mediated strongly by land use and societal factors, and the associated plankton response is therefore compounded. Although this problem is not fundamentally a coupling problem, there is still scope for improving the inputs to the coastal environment through specifying better the river-estuary-ocean interface.

10.4.
Ocean Information Services based on Coupled Frameworks

Over the past decades, operational oceanography underwent a rapid transition and gradually became part of core systems of operational centres previously largely focusing on weather. Sufficient observations are now available to improve the estimation of the ocean state, including mesoscale variability, ice cover, or wave spectra for wave systems. The development of weakly coupled data assimilation techniques, the exploration of strongly coupled data assimilation using cross-domain error covariance (Sluka et al., 2016), the ability to assimilate an ever-growing source of observations, the improvements in physics and dynamics of the various components of the Earth system, and rapidly increasing computing capacities, keep pushing forward the quality of forecasts and reanalyses that can be produced. As a result, information available for products and services is continuously expanding and including a rapid increase in the quality and quantity of ocean and marine services. It is now well established that marine services are essential to any nation with coastal assets.

In the late 90s and early 2000s, operational marine services were limited to a few marine weather variables such as waves, tides, and surges. With coupled systems now in place in many operational centres and the continuous push for increased resolution to better reflect local conditions, a wide variety of new services has and continues to emerge. It is now common for service providers to be overwhelmed with information drawn from many prediction systems, and for users to be submerged with products. In the next subsections are discussed the few steps that should be followed to sort through the very large number of products that can be generated numerically, so that services are centred on needs in a fit for purpose and accessible approach. A few simple examples are used to demonstrate ways of tying together all this numerical knowledge and provide forecasts and services that are informative and tailored to various groups of users.

10.4.1. Establishing service needs

The first step when evaluating services' needs, including whether to use or not a coupled or forced system, is to clearly define the service gap and how current capacity can be leveraged to address it. The second step is to identify enough resources required to bring the project to completion. Numerous capacities are required to sustain timely and accurate services: i) reliable and sufficient computing resources including telecommunications, bandwidth, and storage, along with staff to operate and maintain the IT infrastructure; ii) physical scientist to install; optimise; run; validate, and verify numerical systems; iii) physical scientists to produce forecasts; iv) forecasters able to disseminate and explain forecasts; v) the ability to sustain such services through extreme conditions (e.g. during a powerful cyclone); and vi) the capacity to overcome throughout the years the changes in IT infrastructure, complexification of systems, increasing volumes of data, etc. However, it should never be forgotten that, whatever is the capacity and the complexity of a state-of-the-art forecast, it only has value if it reaches the users in the due time.

For those countries that choose to operate regional systems driven with data provided by major operational centres, the capacity to download the required data quickly enough to run regional systems and issue timely regional forecasts is also key. It should be also ensured that sufficient local expertise is available to monitor, , and fix any issue with the regional system.

When launching new or improved forecast services, another important step is to identify user groups (e.g. marine engineers, marine transportation industries, search and rescue operations, fisheries and aquaculture, coastal communities) and understand their needs. It should be also kept in mind that within each group there can be considerable modulation of needs and that needs can evolve with time and hence they should be reviewed periodically. See section 4.8 for more details on user requirements.

10.4.2. Identifying the required information

Search and rescue and coastal flooding cases are used to illustrate how to select the modelling tools that are required to best address the problem. They are also used to demonstrate how a fit for purpose approach may identify the numerical systems best suited to deliver services.

A search and rescue incident that requires drift predictions is an example of a service to illustrate the choices needed. Forecasts of the trajectory of the drifting object requires knowledge of tides, eddies, inertial oscillations, winds, and waves. Such incidents often occur during high winds and large waves conditions and, as discussed in 9.1, it is under such conditions that interactions between tides, waves, ocean, and atmosphere are most important. This suggests that coupled predictions could add value (Davidson et al., 2009) to the use of independent ocean, wave, and atmosphere forecasting systems. As already discussed, ensembles are essential to sampling uncertainty in various components of a system. In their comprehensive review of the Deepwater Horizon oil spill event, Barker et al. (2020) made a case for the importance of coupled atmosphere-wave-ocean systems for effective oil spill response. All these considerations point to the use of ensemble coupled ocean-wave-atmosphere systems that are post-processed though tracking systems capable of considering the characteristics of various objects, such as a person in the water or a vessel at drift. However, the simulation overhead (in time and computer resources) of the coupled system needs to be balanced with the need to quickly run ensemble simulations to provide probabilities of the search zone to help optimise search patterns. A case similar to that of search and rescue is the response to oil spill or tracking of nuclear debris, which also requires models to predict particulate dispersion but also need to consider other chemically induced processes, such as fate and behaviour.

Coastal flooding is the other example used here to illustrate how to select the best modelling tools. Local communities typically have precise questions such as: "How much water will there be and for how long?" "Will the water reach my street and my house?" "Will it damage my property?" "Will it erode my land or the cliff my house is perched on?" Local authorities and disaster management agencies might have further considerations such as: "What are the most likely and the worst-case scenarios?" "When should we consider evacuations and through what route?" "What critical infrastructures might be at risk?" However, the nature of the service will depend on local conditions. Consider for example a community living at high latitudes. In the event of a polar low (discussed in 9.1), ice can recede rapidly to expose long stretches of ocean leaving the coastline exposed to large swells. In these areas, wave-ice interactions can lead to rapid changes and coupled ice-ocean-wave-atmosphere systems should be preferred to provide accurate forecasts of the low's evolution, rapidly changing marine conditions, and to warn the coastal communities. On the other hand, locations exposed to tropical cyclones will need a system more focused on predicting ocean-atmosphere interactions in support of track and intensity prediction. However, the concept of a forecast based on total water level at the coast remains, although the fit for purpose numerical guidance to be used might have some differences. It is then particularly important to consider user orientated questions. User groups rarely care about technical issues, such as if the models are coupled or if the surge component is barotropic or baroclinic. They care that scientists put forward the combination that best addresses their concerns. They want to receive a fit for purpose service. Simulations of tide, surge, wave, erosion,

hydrodynamic, and atmospheric may all be required, but to decide whether they should be coupled or not it is necessary to understand if this improves the specific predictions identified by the user questions outlined above.

Advanced knowledge of the risk of an upcoming event is useful to put in place mitigation measures. An outlook for several days to several weeks is of particular interest, as well as the early identification of upcoming risk for which ensemble systems are relevant. At early stages, the focus should be on identifying risk and uncertainties, and communicating them in a clear manner. As the high impact event nears (e.g. next couple days), ensembles can be replaced with resolution increases, so that the risk forecast is changed into an impact-based forecast (i.e. damage to housing, risk of cars being swept away, risk of cutting off of an evacuation route, etc.). This should make the scientists understand that for the users the waves, surges, tides, and other phenomena are relevant only as much as they affect flooding in their areas of interest. This further highlights the importance of metrics used to evaluate models and forecasts. When it comes to flooding, having a slightly better RMSD and thus a better representation of the mean state is useless if the total water level peaks are missed. Thus, relying on an overly complicated ocean system that results in little to no added skill in total water level forecasts is useless. Similarly, if a complicated system cannot be operated with sufficient resolution over long enough periods, or with enough ensemble members to sample uncertainties, it is not fit for purpose. In addition, coupling should be considered also in the context of the resources (always limited) of operational centres.

Finally, whether numerical systems are run locally or remotely and whether all systems required to produce such forecasts are coupled or not, the path forward should be one in which the forecasters are experts at providing added value taking into account the perspective of the public (e.g. placing in the context a particular expected extreme, comparing it to previous ones, explaining the subtle differences to be expected with the forecast risk, etc.). As such, the forecasters are the ultimate downscalers bringing added value based on local knowledge and history.

⚙

10.5.
References

Ali, A., Christensen, K., Breivik, O., Malila, M., Raj, R., Bertino, L., Chassignet, E., Bakhoday-Paskyabi M. (2019). A comparison of Langmuir turbulence parameterizations and key wave effects in a numerical model of the North Atlantic and Arctic Oceans. *Ocean Modelling,* 137, pp 76-97, https://doi.org/10.1016/j.ocemod.2019.02.005

Allard, R. A., Campbell, T. J. , Smith, T. A., Jensen, T. G., Chen, S., Cummings, J. A., Chen, S., Doyle, J., Xiaodong, H., Small, R.J., Carrol, S.N. (2010). Validation Test Report for the Coupled Ocean Atmosphere Mesoscale Prediction System (COAMPS) Version 5.0 NRL/MR/7322–10-9283. Stennis Space Center, MS: Oceanography Division, Naval Research Laboratory, 172 pp.

Allard, R. A., Travis, A. S., Jensen, T. G., Chu, P. Y., Rogers, E., and Campell, T. J. (2012). Validation Test Report for the Coupled Ocean / Atmosphere Mesoscale Prediction System (COAMPS) Version 5.0: Ocean / Wave Component Validation. Naval Research Lab Tech Report, (NRL/MR/7320--12-9423).

Ardhuin, F., Rascle, N., Belibassakis, K. (2008). Explicit wave-averaged primitive equations using a generalized Lagrangian mean. *Ocean Modelling*, 20(1), 35-60, https://doi.org/10.1016/j.ocemod.2007.07.001

Ardhuin, F., Marie, L., Rascle, N., Forget, P., Roland, A. (2009). Observation and estimation of Lagrangian, Stokes and Eulerian currents induced by wind and waves at the sea surface. *Journal of Physical Oceanography*, 39, 2820-2838, https://doi.org/10.1175/2009JPO4169.1

Ardhuin, F., and Jenkins A., (2006). On the Interaction of Surface Waves and Upper Ocean Turbulence. *Journal of Physical Oceanography*, 36, 551-557, https://doi.org/10.1175/JPO2862.1

Ardhuin, F., Sutherland, P., Doble, M., Wadhams, P. (2016). Ocean waves across the Arctic: Attenuation

due to dissipation dominates over scattering for periods longer than 19 s. *Geophysical Research Letters*, 43(11), 5775-5783, https://doi.org/10.1002/2016GL068204

Ardhuin, F., Gille, S. T., Menemenlis, D., Rocha, C. B., Rascle, N., Chapron, B., Gula, J., Molemaker, J. (2017). Small-scale open ocean currents have large effects on wind wave heights. *Journal of Geophysical Research: Oceans*, 122(6), 4500–4517. https://doi.org/10.1002/2016JC012413

Barker, C. H., Kourafalou, V. H., Beegle-Krause, C. J., Boufadel, M., Bourassa, M. A., Buschang, S. G., Androulidakis, Y., Chassignet, E.P., Dagestad, K.-F., Danmeier, D.G., Dissanayake, A.L., Galt, J.A., Jacobs, G., Marcotte, G., Özgökmen, T., Pinardi, N., Schiller, R.V., Socolofsky, S.A., Thrift-Viveros, D., D., Zhang, A., Zheng, Y. (2020). Progress in operational modeling in support of oil spill response. *Journal of Marine Science and Engineering*, 8(9), 1-55, https://doi.org/10.3390/jmse8090668

Belcher, S.E., Hewitt, H.T., Beljaars, A., Brun, E., Fox-Kemper, B., Lemieux, J.F., Smith, G., and Valcke, S. (2015). Ocean-Waves-Sea Ice- Atmosphere Interactions. In: Brunet, G., Jones, S. and Ruti, P. (eds.) "Seamless prediction of the Earth system: from minutes to months", WMO, 1156. World Meteorological Organisation, Geneva, pp. 155-170.

Bender, M. A., and Ginis, I. (2000). Real-Case Simulations of Hurricane–Ocean Interaction Using A High-Resolution Coupled Model: Effects on Hurricane Intensity. *Monthly Weather Review*, 128(4), 917-946, https://doi.org/10.1175/1520-0493(2000)128<0917:RCSOHO>2.0.CO;2

Bernie, D. J., Guilyardi, E., Madec, G., Slingo, J. M., Woolnough, S. J., and Cole, J. (2008). Impact of resolving the diurnal cycle in an ocean-atmosphere GCM. Part 2: A diurnally coupled CGCM. *Climate Dynamics*, 31(7-8), 909-925, https://doi.org/10.1007/s00382-008-0429-z

Brassington, G. B., Martin, M. J., Tolman, H. L., Akella, S., Balmeseda, M., Chambers, C. R. S., Chassignet, T., Cummings, J.A., Drillet, Y., Jansen, P.A.E.M., Laloyaux, P., Lea, D., Mehra, A., Mirouze, I., Ritchie, H., Samson, G., Sandery, P.A., Smith, G.C., Suarez, M., and Todling, R. (2015). Progress and challenges in short- to medium-range coupled prediction. *Journal of Operational Oceanography*, 8, s239-s258, https://doi.org/10.1080/1755876x.2015.1049875

Breivik, Ø., Mogensen, K., Bidlot, J.-R., Balmaseda, M.A., Janssen, P.A. (2015). Surface Wave Effects in the NEMO Ocean Model: Forced and Coupled Experiments. *Journal of Geophysical Research: Oceans*, 120, 2973-2992, https://doi.org/10.1002/2014JC010565

Brunet, G., Keenan, T., Onvlee, J., Béland, M., Parsons, D., and Mailhot, J. (2010). The next generation of regional prediction systems for weather, water and environmental applications. CAS XV Vision paper (Agenda item 8.2).

Coon, M. D., Maykut, G. A., Pritchard, R. S., Rothrock, D. A., and Thorndike A. S. (1974). Modeling the pack ice as an elastic-plastic material. AIDJEX Bull. 24, pp. 1-106, Univ. of Wash., Seattle, Washington.

Davidson, F.J.M., Allen, A., Brassington, G.B., Breivik, Ø., Daniel, P., Kamachi, M., Sato, S., King, B., Lefevre, F., Sutton, M., and Kaneko, H. (2009). Applications of GODAE ocean current forecasts to search and rescue and ship routing. *Oceanography*, 22(3), 176-181, https://doi.org/10.5670/oceanog.2009.76

Divine, D., Korsnes, R., and Makshtas, A. P. (2003). Variability and climate sensitivity of fast ice extent in the north-eastern Kara Sea. *Polar Research*, 22, 27-34, https://doi.org/10.3402/polar.v22i1.6440

Doble, M. J., and Bidlot, J.-R. (2013). Wave buoy measurements at the Antarctic sea ice edge compared with an enhanced ECMWF WAM: Progress towards global waves-in-ice modelling. *Ocean Modelling*, 70, 166-173, https://doi.org/10.1016/j.ocemod.2013.05.012

Dzwonkowski, B., Greer, A.T., Briseno-Avena, C., Krause, J.W., Soto, I.M., Hernandez, F.J., Deary, A.L., Wiggert, J.D., Joung, D., Fitzpatrick, P.J., O'Brien, S.J., Dykstra, S.L., Lau, Y., Cambazoglu, M.K., Lockridge, G., Howden, S.D.,

Shiller, A.M., Graham, W.M. (2017). Estuarine influence on biogeochemical properties of the Alabama shelf during the fall season. *Continental Shelf Research*, 140, 96-109, https://doi.org/10.1016/j.csr.2017.05.001

Emanuel, K.A. (1986). An Air-Sea Interaction Theory for Tropical Cyclones. Part I: Steady-State Maintenance. *Journal of the Atmospheric Sciences*, 43(6), 585-605, https://doi.org/10.1175/1520-0469(1986)043<0585:AASITF>2.0.CO;2

Fan, Y., Ginis, I., and Hara, T. (2009). The effect of wind-wave-current interaction on air-sea momentum fluxes and ocean response in tropical cyclones. *Journal of Physical Oceanography*, 39(4), 1019-1034, https://doi.org/10.1175/2008JPO4066.1

Fan, Y., and Griffies, S.M. (2014). Impacts of parameterized Langmuir turbulence and non-breaking wave mixing in global climate simulations. *Journal of Climate*, 27, 4752-4775, https://doi.org/10.1175/JCLI-D-13-00583.1

Fu, L.L. (2007). Intraseasonal variability of the equatorial Indian ocean observed from sea surface height, wind, and temperature data. *Journal of Physical Oceanography*, 37(2), 188-202, https://doi.org/10.1175/JPO3006.1

Girard, L., Bouillon, S., Weiss, J., Amitrano, D., Fichefet, T., and Legat, V. (2011). A new modeling framework for sea-ice mechanics based on elasto-brittle rheology. *Annals of Glaciology*, 52(57), 123-132, https://doi.org/10.3189/172756411795931499

Guiavarc'h, C., Roberts-Jones, J., Harris, C., Lea, D. J., Ryan, A., and Ascione, I. (2019). Assessment of ocean analysis and forecast from an atmosphere–ocean coupled data assimilation operational system. *Ocean Science*, 15(5), 1307-1326, https://doi.org/10.5194/os-15-1307-2019

Harlim, J., Oczkowski, M., Yorke, J. A., Kalnay, E., and Hunt, B.R. (2005). Convex Error Growth Patterns in a Global Weather Model. *Physical Review Letters*, 94, 228501, https://doi.org/10.1103/PhysRevLett.94.228501

Hibler, W. D. III (1979). A dynamic thermodynamic sea ice model. *Journal of Physical Oceanography*, 9, 815-846, https://doi.org/10.1175/1520-0485(1979)009<0815:ADTSIM>2.0.CO;2

Holbrook, N. J., Scannell, H. A., Sen Gupta, A., Benthuysen, J. A., Feng, M., Oliver, E. C. J., Alexander, L.V., Burrows, M.T., Donat, M.G., Hobday, A.J., Moore, P.J., Perkins-Kirkpatrick, S.E., Smale, D.A., Straub, S.C., Wernberg, T. (2019). A global assessment of marine heatwaves and their drivers. *Nature Communications*, 10(1), 1-13, https://doi.org/10.1038/s41467-019-10206-z

Hunke, E. C., and Dukowicz, J. K. (1997). An elastic-viscous-plastic model for sea ice dynamics. *Journal of Physical Oceanography*, 27(9), 1849-1867, https://doi.org/10.1175/1520-0485(1997)027<1849:AEVPMF>2.0.CO;2

Hutchings, J. K., Heil, P., and Hibler, W. D. III (2005). Modeling linear kinematic features in sea ice. *Monthly Weather Review*, 133, 3481-3497, https://doi.org/10.1175/MWR3045.1

Hyder, P., Edwards, J.M., Allan, R., Hewitt, H.T., Bracegirdle, T.J., Gregory, J.M., Wood, R.A., Meijers, A.J.S., Mulcahy, J., Field, P., Furtado, K., Bodas-Salcedo, A., Williams, K.D., Copsey, D., Josey, S.A., Liu, C., Roberts, C.D., Sanchez, C., Ridley, J., Thorpe, L., Hardiman, S.C., Mayer, M., Berry, D.I., Belcher, S.E. (2018). Critical Southern Ocean climate model biases traced to atmospheric model cloud errors. *Nature Communications*, 9, 3625, https://doi.org/10.1038/s41467-018-05634-2

Jacox, M. G. (2019). Marine heatwaves in a changing climate. *Nature*, 571, 485-487. https://doi.org/10.1038/d41586-019-02196-1

Janssen, P.A.E.M. (1991). Quasi-linear theory of wind wave generation applied to wave forecasting. *Journal of Physical Oceanography*, 21, 1631-1642.

Janssen, P. (2004). The interaction of ocean waves and wind. Cambridge University Press, Cambridge, UK.

Janssen, P., Saetra, O., Wettre, C., Hersbach, H., Bidlot, J. (2004). Impact of the sea state on the atmosphere and ocean. *Annales Hydrographiques 6e série*, 772, 3-23.

Jullien, S., Masson, S., Oerder, V., Samson, G., Colas, F., and Renault, L. (2020). Impact of ocean-atmosphere current feedback on ocean mesoscale activity: Regional variations and sensitivity to model resolution. *Journal of Climate*, 33(7), 2585-2602, https://doi.org/10.1175/JCLI-D-19-0484.1

Jung, T., and Vitart, F. (2006). Short-Range and Medium-Range Weather Forecasting in the Extratropics during Wintertime with and without an Interactive Ocean. *Monthly Weather Review,* 134(7), 1972-1986, https://doi.org/10.1175/MWR3206.1

Kim, H. M., Webster, P. J., and Curry, J. A. (2012). Seasonal prediction skill of ECMWF System 4 and NCEP CFSv2 retrospective forecast for the Northern Hemisphere Winter. *Climate Dynamics*, 39(12), 2957-2973, https://doi.org/10.1007/s00382-012-1364-6

Kohout, A., Williams, M.J.M., Dean, S.M., Meylan, M.H. (2014). Storm-induced sea-ice breakup and the implications for ice extent. *Nature*, 509(7502), 604-607, https://doi.org/10.1038/nature13262

Kolstad, E. (2015). Extreme small-scale wind episodes over the Barents Sea: When, where and why? *Climate Dynamics*, 1-14, https://doi.org/10.1007/s00382-014-2462-4

Kumar, N., Voulgaris, G., Warner, J.C., Olabarrieta, M. (2012). Implementation of the vortex force formalism in the coupled ocean-atmosphere-wave-sediment transport (COAWST) modeling system for inner shelf and surf zone applications. *Ocean Modelling*, 47, 65-95, https://doi.org/10.1016/j.ocemod.2012.01.003

Laloyaux, P., de Boisseson, E., Balmaseda, M., Bidlot, J. R., Broennimann, S., Buizza, R., Dalhgren, P., Dee, D., Haimberger, L., Hersbach, H., Kosaka, Y., Martin, M., Poli, P., Rayner, N., Rustemeier, E., Schepers, D. (2018). CERA-20C: A Coupled Reanalysis of the Twentieth Century. *Journal of Advances in Modeling Earth Systems*, 10(5), 1172-1195. https://doi.org/10.1029/2018MS001273

Large, W. G., and Yeager, S. G. (2009). The global climatology of an interannually varying air - Sea flux data set. *Climate Dynamics*, 33(2-3), 341-364, https://doi.org/10.1007/s00382-008-0441-3

Lee, C., Hwang, S., Do, K., and Son, S. (2019). Increasing flood risk due to river runoff in the estuarine area during a storm landfall. *Estuarine, Coastal and Shelf Science*, 221, 104-118, https://doi.org/10.1016/j.ecss.2019.03.021

Lemarié, F., Samson, G., Redelsperger, J.-L., Giordani, H., Brivoal, T., and Madec, G. (2021). A simplified atmospheric boundary layer model for an improved representation of air-sea interactions in eddying oceanic models: implementation and first evaluation in NEMO(4.0). *Geoscientific Model Development*, 14, 543-572, https://doi.org/10.5194/gmd-14-543-2021

Lemieux, J.-F., Dupont, F., Blain, P., Roy, F., Smith, G. C., and Flato, G. M. (2016). Improving the simulation of landfast ice by combining tensile strength and a parameterization for grounded ridges. *Journal of Geophysical Research: Oceans*, 121, 7354-7368, https://doi.org/10.1002/2016JC012006

Lewis, H., Mittermaier, M., Mylne, K., Norman, K., Scaife, A., Neal, R., ... Pilling, C. (2015). From months to minutes - exploring the value of high-resolution rainfall observation and prediction during the UK winter storms of 2013/2014. *Meteorological Applications*, 22(1), 90-104, https://doi.org/10.1002/met.1493

Lewis, H. W., Castillo Sanchez, J. M., Siddorn, J., King, R. R., Tonani, M., Saulter, A., Sykes, P., Pequignet, A.C., Weedon, G.P., Palmer, T., Staneva, J., Bricheno, L. (2018). Can wave coupling improve operational regional ocean forecasts for the North-West European Shelf? *Ocean Science*, 15, 669-690, https://doi.org/10.5194/os-15-669-2019

Lewis, H. W., Castillo Sanchez, J. M., Arnold, A., Fallmann, J., Saulter, A., Graham, J., Bush, M., Siddorn, J., Tamzin, P., Adrian, L., Edwards, J., Bricheno, L., Martinez-de la Torre, A., Clark, J. (2019). The UKC3 regional coupled environmental

prediction system. *Geoscientific Model Development*, 12(6), 2357-2400, https://doi.org/10.5194/gmd-12-2357-2019

Li, Q., Webb, A., Fox-Kemper, B., Craig, A., Danabasoglu, G., Large, W.G., Vertenstein, M. (2016). Langmuir mixing effects on global climate: WAVEWATCH III in CESM. *Ocean Modeling*, 103, 145-160, https://doi.org/10.1016/j.ocemod.2015.07.020

Li, Q., and Fox-Kemper, B. (2017). Assessing the Effects of Langmuir Turbulence on the Entrainment Buoyancy Flux in the Ocean Surface Boundary Layer. *Journal of Physical Oceanography*, 47(12), 2863-2886, https://doi.org/10.1175/JPO-D-17-0085.1

Li, Q., Fox-Kemper, B., Breivik, O., Webb, A. (2017). Statistical Models of Global Langmuir Mixing. *Ocean Modelling*, 113, 95-114, https://doi.org/10.1016/j.ocemod.2017.03.016

Lorenz, E.N. (1963). Deterministic nonperiodic flow. *Journal of the Atmospheric Sciences*, 20, 130-141

Lorenz, E.N. (1967). The nature and theory of the general circulation of the atmosphere. *World Meteorological Organization*, 218. Available at; https://library.wmo.int/doc_num.php?explnum_id=10889

Mahoney, A. R., Eicken, H., Gaylord, A.G., and Gens, R. (2014). Landfast sea ice extent in the Chukchi and Beaufort Seas: The annual cycle and decadal variability. *Cold Regions Science and Technology*, 103, 41-56, https://doi.org/10.1016/j.coldregions.2014.03.003

Maykut, G. A. (1978). Energy exchange over young sea ice in the central Arctic. *Journal of Geophysical Research: Oceans*, 83(C7), 3646-3658, https://doi.org/10.1029/JC083iC07p03646

McWilliams, J.C., Sullivan, P.P., and Moeng, C.-H. (1997). Langmuir turbulence in the ocean. *Journal of Fluid Mechanics*, 334, 1-30, https://doi.org/10.1017/S0022112096004375

Minobe, S., Kuwano-Yoshida, A., Komori, N., Xie, S. P., and Small, R. J. (2008). Influence of the Gulf Stream on the troposphere. *Nature*, 452(7184), 206-209, https://doi.org/10.1038/nature06690

Mogensen, K. S., Magnusson, L., Bidlot, J-R. (2017). Tropical cyclone sensitivity to ocean coupling in the ECMWF coupled model. *Journal of Geophysical Research: Oceans*, 122(5), 4392-4412, https://doi.org/10.1002/2017JC012753

Moin, P. and Mahesh, K. (1998). Direct numerical simulation: A Tool in Turbulence Research. Annual Review of Fluid Mechanics, 30(1), 539-578, https://doi.org/10.1146/annurev.fluid.30.1.539

Naughten, K. A., Meissner, K. J., Galton-Fenzi, B. K., England, M. H., Timmermann, R., Hellmer, H. H., Hattermann, T., and Debernard, J. B. (2018). Intercomparison of Antarctic ice-shelf, ocean, and sea-ice interactions simulated by MetROMS-iceshelf and FESOM 1.4. *Geoscientific Model Development*, 11(4), 1257-1292, https://doi.org/10.5194/GMD-11-1257-2018

Neetu, S., Lengaigne, M., Vialard, J., Samson, G., Masson, S., Krishnamohan, K. S., and Suresh, I. (2019). Premonsoon/Postmonsoon Bay of Bengal Tropical Cyclones Intensity: Role of Air-Sea Coupling and Large-Scale Background State. *Geophysical Research Letters*, 2019, 46(4), 2149-2157.

Oerder, V., Colas, F., Echevin, V., Masson, S., and Lemarié, F. (2018). Impacts of the Mesoscale Ocean-Atmosphere Coupling on the Peru-Chile Ocean Dynamics: The Current-Induced Wind Stress Modulation. *Journal of Geophysical Research: Oceans*, 123(2), 812-833, https://doi.org/10.1002/2017JC013294

Osadchiev, A. A., Pisareva, M. N., Spivak, E. A., Shchuka, S. A., and Semiletov, I. P. (2020). Freshwater transport between the Kara, Laptev, and East-Siberian seas. Scientific Reports, 10(1), 1-14, https://doi.org/10.1038/s41598-020-70096-w

Pellerin, P., Ritchie, H., Saucier, F. J., Roy, F., Desjardins, S., Valin, M., and Lee, V. (2004). Impact of a two-way coupling between an atmospheric and an ocean-ice model over the Gulf of St. Lawrence. *Monthly*

Weather Review, 132, 1379-1398, https://doi.org/10.1175/1520-0493(2004)132<1379:IOATCB>2.0.CO;2

Penland, C., and Matrosova, L. (1998). Prediction of tropical Atlantic sea surface temperatures using Linear Inverse Modeling. *Journal of Climate*, 11, 483-496, https://doi.org/10.1175/1520-0442(1998)011<0483:POTASS>2.0.CO;2

Penland, C., and Sardeshmukh, P. D. (1995). The optimal growth of tropical sea surface temperature anomalies. *Journal of Climate*, 8, 1999-2024.

Rabault, J., Sutherland, G., Gundersen, O., Jensen, A., Marchenko, A., Breivik, O. (2020). An Open Source, Versatile, Affordable Waves in Ice Instrument for Scientific Measurements in the Polar Regions. *Cold Regions Science and Technology*, 170, 11, https://doi.org/10.1016/j.coldregions.2019.102955

Rascle, N., Ardhuin, F., Terray, E. (2006). Drift and mixing under the ocean surface: A coherent one-dimensional description with application to unstratified conditions. *Journal of Geophysical Research*, 111(C3), 16, https://doi.org/10.1029/2005JC003004

Rasmussen, E.A., Turner (2003). Polar lows: mesoscale weather systems in the polar regions, Cambridge University Press.

Renault, L., Molemaker, M. J., Gula, J., Masson, S., and McWilliams, J. C. (2016) Control and Stabilization of the Gulf Stream by Oceanic Current Interaction with the Atmosphere. *Journal of Physical Oceanography*, 46, 3439-3453, https://doi.org/10.1175/JPO-D-16-0115.1

Ridley, J. K., Blockley, E.W., Keen, A.B., Rae, J.G.L., West, A.E., and Schroeder, D. (2018). The sea ice model component of HadGEM3-GC3.1. *Geoscientific Model Development*, 11(2), 713-723, https://doi.org/10.5194/gmd-11-713-2018

Røed, L.P., and Albretsen, J. (2007). The impact of freshwater discharges on the ocean circulation in the Skagerrak/northern North Sea area Part I: Model validation. *Ocean Dynamics*, 57(4-5), 269-285, https://doi.org/10.1007/s10236-007-0122-5

Saha, S., Nadiga, S., Thiaw, C., Wang, J., Zhang, Q., Van den Dool, H.M., Pan, H.-L., Moorthi, S., Behringer, D., Stokes, D., Peña, M., Lord, S., White, G., Ebisuzaki, W., Peng, P., Xie, P. (2006). The NCEP Climate Forecast System. *Journal of Climate*, 19, 3483-3517, https://doi.org/10.1175/JCLI3812.1

Saha, S., Moorthi, S., Pan, H.-L., Wu, X., Wang, J., Nadiga, S., Tripp, P., Kistler, R., Woollen, J., Behringer, D., Liu, H., Stokes, D., Grumbine, R., Gayno, G., Wang, J., Hou, Y.-T., Chuang, H., Juang, H.-M.H., Sela, J., Iredell, M., Treadon, R., Kleist, D., Delst, P.V., Keyser, D., Derber, J., Ek, M., Meng, J., Wei, H., Yang, R., Lord, S., van den Dool, H., Kumar, A., Wang, W., Long, C., Chelliah, M., Xue, Y., Huang, B., Schemm, J.-K., Ebisuzaki, W., Lin, R., Xie, P., Chen, Y., Han, Y., Cucurull, L., Reynolds, R.W., Rutledge, G., Goldberg, M. (2010). The NCEP Climate Forecast System Reanalysis. *Bulletin of the American Meteorological Society*, 91, 1015-1057, https://doi.org/10.1175/2010BAMS3001.1

Saha, S., Moorthi, S., Wu, X., Wang, J., Nadiga, S., Tripp, P., Behringer, D., Hou, Y.-T., Chuang, H., Iredell, M., Ek, M., Meng, J., Yang, R., Peña Mendez, M., van den Dool, H., Zhang, Q., Wang, W., Chen, M., and Becker, E. (2014). The NCEP Climate Forecast System Version 2. *Journal of Climate*, 27, 2185-2208, https://doi.org/10.1175/JCLI-D-12-00823.1

Semedo, A., Suvselj, K., Rutgersson, A., Sterl, A. (2011). A global view on the wind sea and swell climate and variability from ERA-40. *Journal of Climate*, 24(5), 1461-1479, https://doi.org/10.1175/2010JCLI3718.1

Seo, H., Subramanian, A. C., Miller, A. J., and Cavanaugh, N. R. (2014). Coupled impacts of the diurnal cycle of sea surface temperature on the Madden-Julian oscillation. *Journal of Climate*, 27(22), 8422-8443, https://doi.org/10.1175/JCLI-D-14-00141.1

Shelly, A., Xavier, P., Copsey, D., Johns, T., Rodriguez, J.M., Milton, S., and Klingaman, N. (2014). Coupled versus uncoupled hindcast simulations of the Madden-Julian Oscillation in the Year of Tropical Convection. *Geophysical Research Letters*, 41, 5670-5677, https://doi.org/10.1002/2013GL059062

Sluka, T., Penny, S.G., Kalnay, E. and Miyoshi, T. (2016). Assimilating atmospheric observations into the ocean using strongly coupled ensemble data assimilation. *Geophysical Research Letters*, 43(2), 752-759, https://doi.org/10.1002/2015GL067238

Smith, G. C., Bélanger, J. M., Roy, F., Pellerin, P., Ritchie, H., Onu, K., Roch, M., Zadra, A., Surcel Colan, D., Winter, B., Fontecilla, J.S., Deacu, D. (2018). Impact of coupling with an ice-ocean model on global medium-range NWP forecast skill. *Monthly Weather Review*, 146(4), 1157-1180, https://doi.org/10.1175/MWR-D-17-0157.1

Spreen, G., Kwok, R., Menemenlis, D., and Nguyen, A. T. (2017). Sea-ice deformation in a coupled ocean-sea-ice model and in satellite remote sensing data. *The Cryosphere*, 11, 1553-1573, https://doi.org/10.5194/tc-11-1553-2017

Staneva, J., Alari, V., Breivik, O., Bidlot, J.-R., Mogensen, K. (2017). Effects of wave-induced forcing on a circulation model of the North Sea. *Ocean Dynamics*, 67, 81-101, https://doi.org/10.1007/s10236-016-1009-0

Sutherland, G., and Rabault, J. (2016). Observations of wave dispersion and attenuation in landfast ice. *Journal of Geophysical Research: Oceans*, 121(3), 1984-1997, https://doi.org/10.1002/2015JC011446

Takano, K., Mintz, Y., Han, Y.-J. (1973). Numerical simulation of the world ocean circulation. Paper presented at the 2nd Conference on Numerical Prediction. Am. Meteorol. Soc. (1973), Monterey, CA (unpublished).

Uchiyama, Y., McWilliams, J. C., Shchepetkin, A. F. (2010). Wave-current interaction in an oceanic circulation model with a vortex-force formalism: Application to the surf zone. *Ocean Modelling*, 34(1), 16-35, https://doi.org/10.1016/j.ocemod.2010.04.002

Vannitsem, S., and Duan, W. (2020). On the use of near-neutral Backward Lyapunov Vectors to get reliable ensemble forecasts in coupled ocean–atmosphere systems. *Climate Dynamics*, 55, 1125-1139, https://doi.org/10.1007/s00382-020-05313-3

Vinayachandran, P. N., Davidson, F., and Chassignet, E. P. (2020). Toward Joint Assessments, Modern Capabilities, and New Links for Ocean Prediction Systems. *Bulletin of the American Meteorological Society*, 101(4), E485-E487, https://doi.org/10.1175/bams-d-19-0276.1

Wahle, K., Staneva, J., Koch, W., Fenoglio-Marc, L., Ho-Hagemann, H. T. M., and Stanev, E. V. (2017). An atmosphere-wave regional coupled model: Improving predictions of wave heights and surface winds in the southern North Sea. *Ocean Science*, 13(2), 289-301, https://doi.org/10.5194/os-13-289-2017

Wang, K., and Wang, C. (2009). Modeling linear kinematic features in pack ice. *Journal of Geophysical Research: Oceans*, 114(C12), https://doi.org/10.1029/2008JC005217

Williams, T.D., Bennetts, L.G., Squire, V.A., Dumont, D., Bertino, L. (2013). Wave-ice interactions in the marginal ice zone. Part 1: Theoretical foundations. *Ocean Modelling*, 71, 81-91, https://doi.org/10.1016/j.ocemod.2013.05.010

Wolf, J. (2008). Coupled wave and surge modelling and implications for coastal flooding. *Advances in Geosciences*, 17, 19-22, https://doi.org/10.5194/adgeo-17-19-2008

Wu, L., Rutgersson, A., Breivik, O. (2019). Ocean-wave-atmosphere interaction processes in a fully coupled modelling system. *Journal of Advances in Modeling Earth Systems*, 11, 3852-3874, https://doi.org/10.1029/2019MS001761

Wu, L., Staneva, J., Breivik, Ø., Rutgersson, A., Nurser, A. J. G., Clementi, E., and Madec, G. (2019). Wave effects on coastal upwelling and water level. *Ocean Modelling*, 101405, https://doi.org/10.1016/J.OCEMOD.2019.101405

Zhang, S., Harrison, M. J., Rosati, A., and Wittenberg, A. T. (2007). System Design and Evaluation of Coupled Ensemble Data Assimilation for Global Oceanic Climate Studies. *Monthly Weather Review*, 135(10), https://doi.org/10.1175/MWR3466.1

11.
Downstream applications: From data to products

CHAPTER COORDINATOR

Giovani Coppini

CHAPTER AUTHORS *(in alphabetical order)*

Enrique Alvarez Fanjul, Laurence Crosnier, Tomasz Dabrowski, Pierre Daniel, José Chambel Leitão,

Svitlana Liubartseva, Gianandrea Mannarini, and Glen Nolan

11. Downstream applications: From data to products

11.1. The need of downstream products

11.1.1. Blue Economy

11.1.2. Applications and services

11.2. Examples of advanced downstream systems

11.2.1. Sea Situational Awareness
(web pages and other dissemination mechanisms)

11.2.1.1. The Copernicus Marine Service MyOcean Viewer

11.2.1.2. SeaConditions

11.2.1.3. Marine-Analyst

11.2.1.4. NOAA Sea Level Rise viewer

11.2.2. Oil spill forecasting

11.2.2.1. MOTHY

11.2.2.2. WITOIL

11.2.3. Ports

11.2.3.1. SAMOA service for Spanish ports

11.2.3.2. AQUASAFE

11.2.4. Voyage planning

11.2.4.1. VISIR

11.2.5. Fisheries and aquaculture

11.2.5.1. Bluefin tuna

11.2.5.2. Harmful algal bloom warning system

11.2.5.3. Weather window tool

11.2.5.4. Aquaculture site selection

11.3. References

11.1.
The need of downstream products

11.1.1. Blue Economy

The importance of the ocean for global society and economy is represented in the context and framework of the Blue Economy and is also very relevant for the Sustainable Development Goal 14 (SDG14): Life Below Water 🔗[1]. The ocean is the single largest natural asset on the planet, contains 97% of all the water on Earth and about 99% of the habitable space on this planet, and delivers numerous benefits to humanity. The ocean is responsible for the oxygen in every other breath we take. It supplies 15% of humanity's protein needs. It helps to slow climate change by absorbing 30% of carbon dioxide emissions and 90% of the excess heat trapped by greenhouse gases. It serves as the highway for some 90% of internationally traded goods, via the shipping sector. If the ocean were a country, with several trillion dollars per year of economic activity it would rank 7th on the list of largest nations by GDP. The ocean is also the source of hundreds of millions of jobs, in sectors such as fisheries, aquaculture, shipping, tourism, energy production, etc. It is also the source of about 30% of the world's oil and gas resources but this percentage will change if the necessary transition to a low carbon development pathway will succeed. Millions of the world's poorest people depend heavily on the ocean and coastal resources for their subsistence and livelihoods. Small-scale fisheries catch about half of the world's seafood but engage 44 times as many jobs per ton of fish as industrial fisheries do.

According to the Water and Ocean Governance Programme of UNDP 🔗[2], the Blue Economy is a sustainable ocean economic paradigm and is the natural next step in the overall conceptualization and realisation of sustainable human development. On the other hand, there is the important aspect related to the impact that the Blue Economy might have on the ocean. The European Commission stated 🔗[3] that all blue economy sectors, including fisheries, aquaculture, coastal tourism, maritime transport, port activities and shipbuilding, will have to reduce their environmental and climate impact. Tackling the climate and biodiversity crises requires healthy seas and a sustainable use of their

resources, as well as creating alternatives to fossil fuels and traditional food production.

Transitioning to a sustainable Blue Economy requires investing in innovative technologies. Wave and tidal energy, algae production, fisheries management, restoration of marine ecosystems, etc., will create new green jobs and businesses in the Blue Economy.

Downstream services provided by the operational oceanography community should be able to facilitate and support this transition towards a more sustainable Blue Economy worldwide.

11.1.2. Applications and services

Operational oceanography is available nowadays to many users through solutions (services and products) dealing with several SDGs, and societal and scientific challenges. Oceanographic products from global to regional scale are produced by national and international forecasting centres. They are then downscaled to sub-regional scales, transformed, and provided to users, private companies, public users, stakeholders, and citizens through an ocean products value chain that includes development of specific solutions, advanced visualisation, usage of multi-channel technological platforms, specific models, and algorithms. Figure 2.1 in Chapter 2 shows a representation of ocean value chain: forecasting centres manages Marine Core Service, which produces Information (e.g. forecast products) that are delivered to Intermediate Users through ad hoc Interfaces managed by the Central Information System. Then, such information is elaborated by Developers and transformed for Multiple Downstream Services that use customised end user information to deliver new information to End Users.

Important steps forwards have been carried out in order to facilitate the dialogue among service providers and users to identify requirements and needs, and to co-develop and test the applications and solutions. Collaborative frameworks like the Copernicus Users Uptake programme, the international initiative Geo Blue Planet, the GOOS Regional Alliances downstream effort, the IOC and WMO working groups, etc., are in support of the Blue Economy's growth.

The private sector has been playing an important role in the development of operational systems, providing operational services in areas that in the past were covered only by public institutions. Some businesses are impacted every day by oceanographic conditions, and sometimes disrupted by extreme events. Accurate and reliable oceanographic and me-

---

1. https://sdgs.un.org/goals/goal14

2. https://www.undp.org/blog/blue-economy-sustainable-ocean-economic-paradigm?utm_source=EN&utm_medium=GSR&utm_content=US_UNDP_PaidSearch_Brand_English&utm_campaign=CENTRAL&c_src=CENTRAL&c_src2=GSR&gclid=Cj0KCQiAweaNBhDEARIsAJ5hwbdEFafpkIcJuzISsldLg4UzxIkqOhAo6MClAjSwEBvBA_ZHi10o_8IaAn_0EALw_wcB

3. https://ec.europa.eu/commission/presscorner/detail/en/ip_21_2341

teorological predictions may increase business productivity, if appropriate standards of safety are adopted.

The public sector mostly focuses on protecting lives and property. Often this is not enough to protect economic operations at sea, in which monitoring and forecast information is needed on a regular basis and representing local scale processes. Downstream applications play a key role addressing (and adjusting to) end users' needs, while simultaneously justifying global scale modelling and monitoring investments done by the public sector in the past.

Most of the developments in downstream applications have been driven by international grants and individual countries. In some areas, end users' willingness to pay for such applications is very low. There is a need to improve the applications but also to promote and disseminate information on existing applications. The main reason is that a reasonable cost/benefit relationship for businesses must be achieved to have a market driven demand for downstream operational services.

It is therefore of paramount importance to show how research and technological development in the different application fields (e.g. advanced visualisation, usage of multi-channels technological platforms, and development of specific models and algorithms) have advanced in recent years, and that more accurate and user friendly applications are available for users.

International standards have been developed and should be further consolidated to support interoperability and a common formatting of ocean application products and services, as well as quality assessment. Downstream applications are an essential component contributing to ocean literacy through the dissemination to the public of operational oceanography knowledge. Economic sustainability and mar-

ket exploitation of downstream application is a key aspect to fill the gap towards a fully sustainable development of operational oceanography added value services and products.

It is also of fundamental importance to improve the dialogue among producers and users to identify requirements, as well as co-developing and testing the applications. Engaging end users in the analysis and evaluation process is critical in order to tailor downstream products in the best way.

An effort for gathering and promoting applications by worldwide producers should include different sectors, such as: a) Fishery and aquaculture; b) Tourism and sports activities; c) ICZM and MSP; d) Transport and harbour services; e) Marine digital services; f) Technologies for maritime safety; g) Climate change and anthropogenic impacts on marine environment; and h) Energy from the sea.

To achieve this goal, producers are asked to manage and promote the adoption of an international standard to support interoperability and a common formatting of ocean application products and services, as well as quality assessment. It is fundamental to promote market development of downstream applications as well as liaise with and gather input from the other international and national initiatives (e.g., EuroGOOS, Geo Blue Planet, IOC, WMO).

With a view to the Ocean Decade implementation, in this chapter will be discussed key challenges, best practices, relevant examples of applications, as well as the present advanced capabilities and future challenges in the following applications fields: 1) Sea Situational Awareness (web pages and other dissemination mechanisms); 2) Oil spill observing and forecasting; 3) Ports; 4) Voyage planning; and 5) Fisheries and aquaculture.

11.2.
Examples of advanced downstream systems
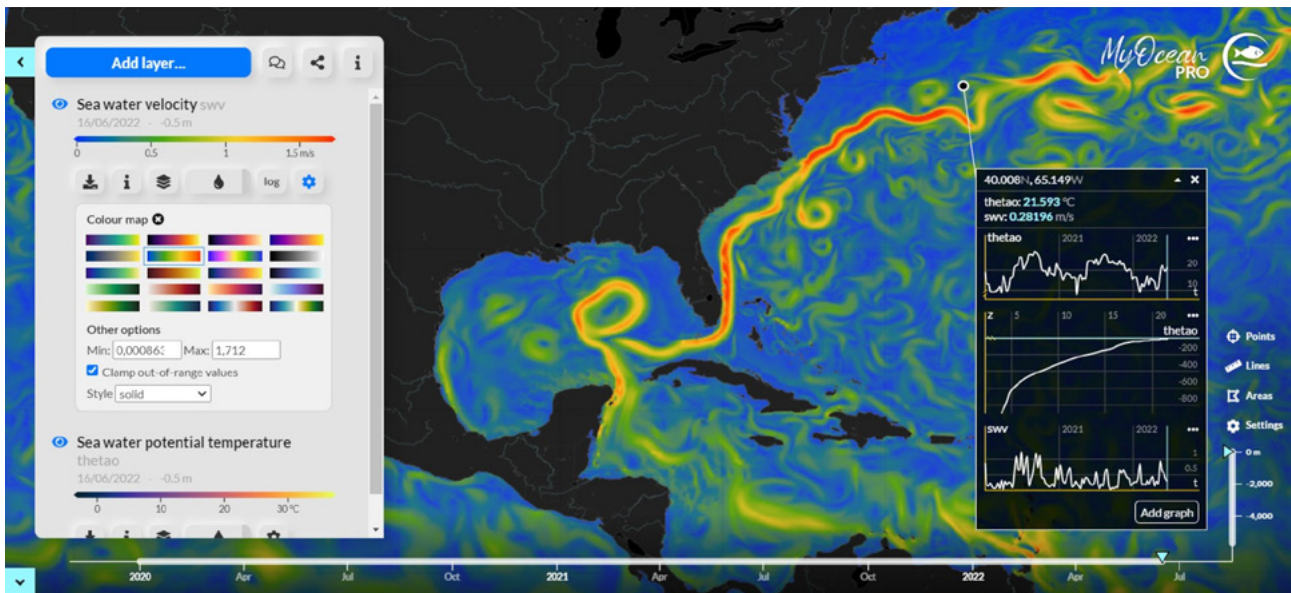
Figure 11.1. Examples of screenshots from MyOcean Viewer web application, including visualisation of sea-water velocity for the Global Ocean and time series/time-depth plots in a specific location (source: 🔗 4).

11.2.1. Sea Situational Awareness (web pages and other dissemination mechanisms)

Dissemination services provide users with databases on relevant environmental information and set up their formatting to support marine and maritime activities. These services include the collection and validation of existing information and the production of new geo-localised information to users. Mechanisms for data sharing among databases are offered to intermediate and final users, so that the integration with existing services is facilitated.

The mechanisms of access to databases from private and public users is a matter of concern for the dissemination services as it could limit the accessibility of the services. Users should be able to access information in the applications through the Internet, using either desktop or mobile phone.

These issues are quite critical since information on marine and coastal areas is currently dispersed in heterogeneous, not connected, poorly known and not accessible systems. Consequently, it is important to develop systems that widen

availability, improve information sharing, and facilitate access to the data. Public and private users are supported by mechanisms of open and free access, including massive (e.g. FTP, THREDDS, P2P) and system communication services (e.g. web services, tiling services).

11.2.1.1. The Copernicus Marine Service MyOcean Viewer

The Copernicus Marine Service MyOcean Viewer (🔗 5) allows exploration of most of the online catalogue with multi-projection maps, graphs vs. time, and elevation and/or distance. Using information from both satellite and in-situ observations, the CMEMS provides state-of-the-art analyses and forecasts daily, which offer the capability to observe, understand, and predict the marine environment state (Figure 11.1). The Copernicus Marine Service MyOcean Viewer has been developed by Lobelia Earth. The Basemap layer contains information from the GSHHG dataset provided by the University of Hawaii and the US NOAA.

4, 5. https://myocean.marine.copernicus.eu/
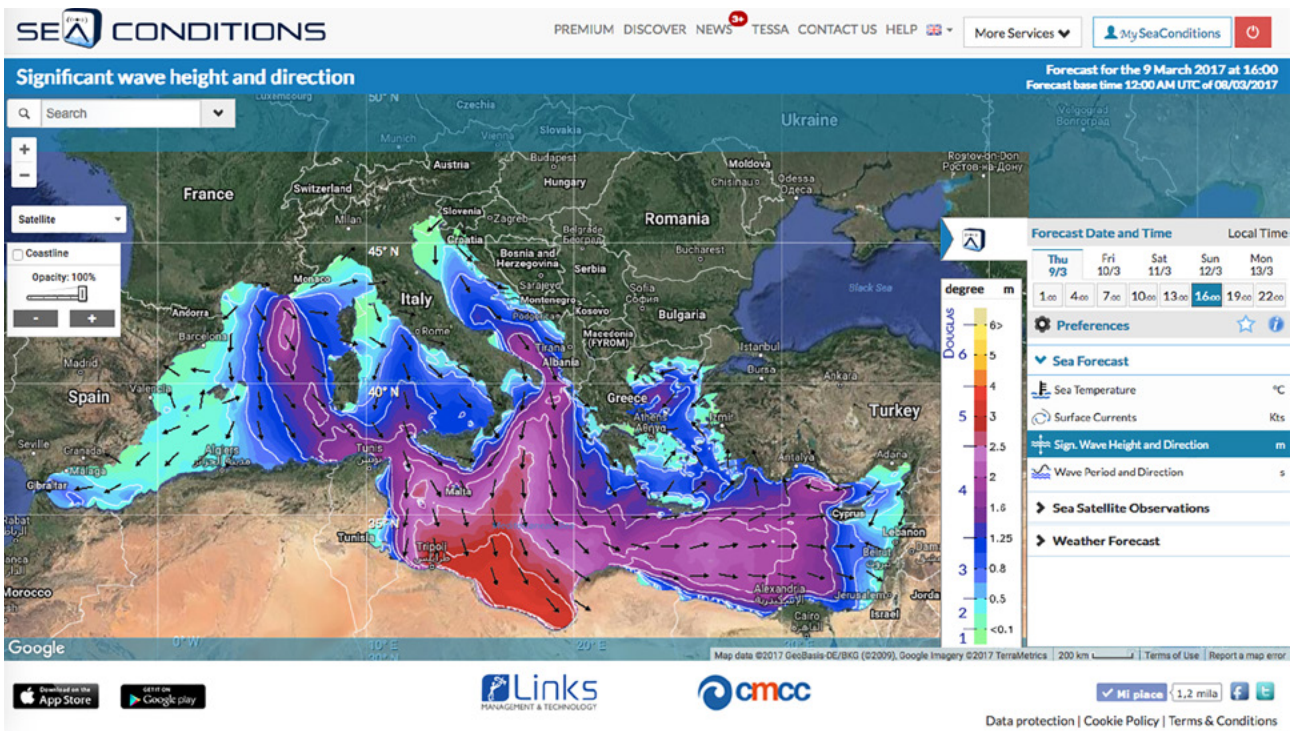
Figure 11.2. SeaConditions web service for the Mediterranean Sea.

11.2.1.2. SeaConditions

An example of web service for sea situational awareness is SeaConditions (🔗 6). It is a service providing weather forecasts, including oceanographic and sea state forecasts (sea surface temperature, surface currents, significant wave height and direction, wave period, sea level), meteorological forecasts (air temperature, mean sea level pressure, precipitation, cloud cover, and 10 metre winds), bathymetry and satellite observations of chlorophyll-a, and water transparency. Forecasts are referred to a time period of 5 days and are based on state-of- the-art meteorological, oceanographic, and wave modelling that allow obtaining high quality data (Figure 11.2). SeaConditions includes data from Copernicus Marine Service (including satellite data) and the ECMWF.

SeaConditions covers the Mediterranean Sea: it has commercial and free versions available on the web and downloadable for mobile (Google Play and Apple Store). Its users are more than 100000.

11.2.1.3. Marine-Analyst

The Marine-Analyst (🔗 7) is a platform for searching, viewing, processing, transferring, advertising, and disseminating marine spatial data from numerous data sources (Figure 11.3).
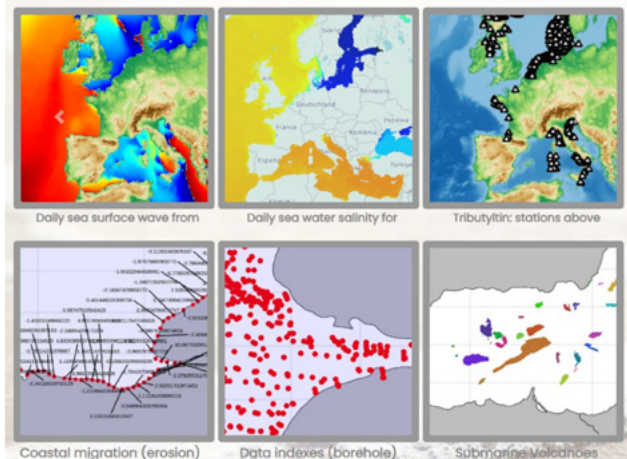
Figure 11.3. Example of data accessible from Marine-Analyst.eu application.

Launched in October 2020, it is powered by WEkEO (🔗 8), the Copernicus DIAS. The Marine-Analyst.eu enables users to access data and key analyses for the location of their choice in Europe. It offers a personal dashboard where each user can collate the reports created for the chosen datasets. Generating on-demand data analyses for any location, the platform is able to address multidisciplinary challenges, for example:

6. https://www.sea-conditions.com

7. http://marine-analyst.eu/

8. https://www.wekeo.eu/
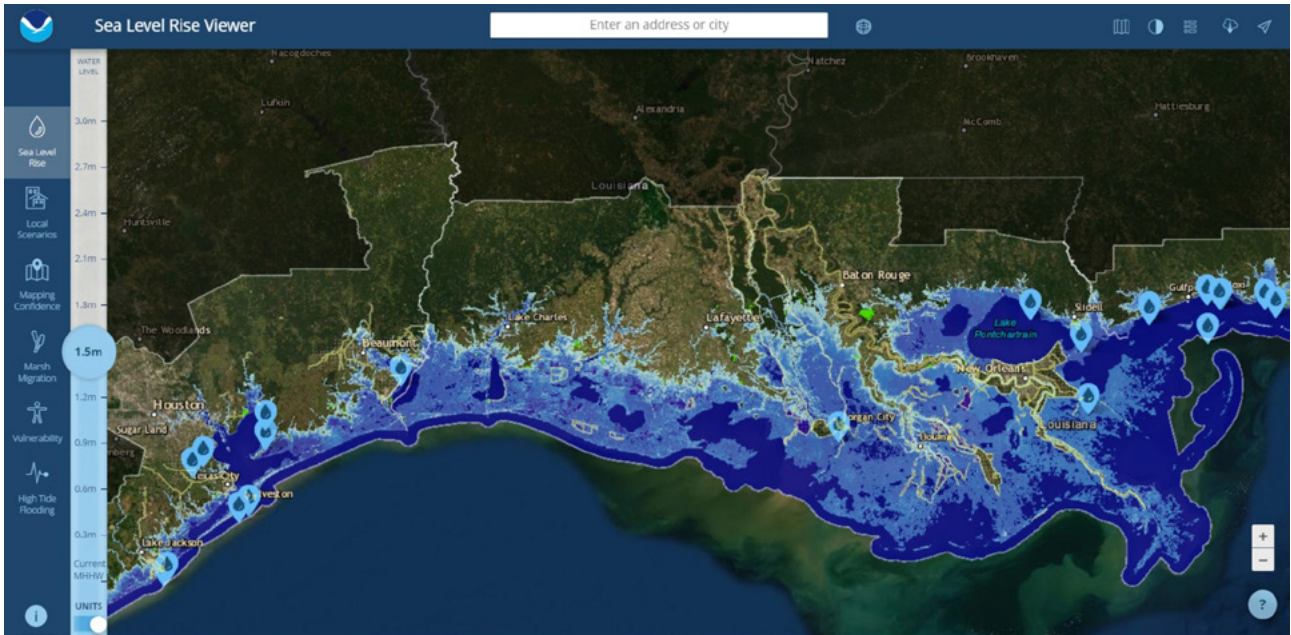
Figure 11.4. Example of NOAA Viewer.

- **Maritime spatial planning:** it represents a solution for coordinating decision-making on identified areas and specific activities, by considering a basin as a whole or partitioning it, including its ecological functioning and the activities it supports, e.g. zonation based on essential biophysical ocean parameters (such as chlorophyll Chla and light attenuation Kd) (from Copernicus Marine Service), human activities inventory (from EMODnet), etc. ("MSP challenge" at the Ocean Hackathon Brest 2020);

- **Climate change:** addressing climate change not only requires better science, but it is also crucial to inform journalists, interested citizens, and the wider public. The Marine-Analyst facilitates access to information and transparent analyses, e.g. sea surface temperature trends and anomalies (from Copernicus Marine Copernicus), coastal erosion (from EMODnet) ("Climate change at my Beach challenge" at the Hack the Ocean Hackathon 2019).

- **Marine protected areas:** park managers benefit from simplified access to various information comprising key information for the management of their MPA, e.g. MPA bulletins (from Copernicus Marine Service, forecast products), vessel density hierarchical clustering and statistical analysis (from EMODnet) (Environmental impact of Shipping traffic at the Blue Innovation Hackathon 2021).

11.2.1.4. NOAA Sea Level Rise viewer

NOAA provides map viewer and applications for marine data such as the Sea Level Rise - Map Viewer (🔗 [9]), which gives users a way to visualise community-level impacts from coastal flooding or sea level rise (up to 10 feet above average high tides). Photo simulations of how future flooding might impact local landmarks are also provided, as well as data related to water depth, connectivity, flood frequency, socio-economic vulnerability, wetland loss and migration, and mapping confidence. The viewer shows areas along the contiguous United States coast, except for the Great Lakes. The maps are produced using detailed elevation maps with local and regional tidal variability. By using real photos at some specific locations, the viewer is able to show the impact of a certain sea level rise in the "real world" (Figure 11.4).

11.2.2. Oil spill forecasting

In the past decade, much effort has been made to support operational oil spill modelling as a crucial component of the response. The most advanced systems are fully operational 24/7, meet the robustness and accuracy criteria, as well as the real-time requirements in terms of performance and dynamic service delivery. Examples of these systems are: OS-CAR (Aamo et al., 1997), GNOME (Zelenke et al., 2012), OilMap

9. https://www.climate.gov/maps-data/dataset/sea-level-rise-map-viewer

(Spaulding et al., 1992), MOTHY (Daniel, 1996), MEDSLIK-II (De Dominicis et al., 2013), COSMoS (Marcotte et al., 2016), and OpenDrift (Dagestad et al., 2018). Oil spill models' capabilities range from prediction of sea surface and upper layer transport to fully 3D oil and associated gas movement, including intrusion formation and high-pressure physics effects.

Incorporated oil spill models are coupled to up-to-date meteo-ocean monitoring and forecasting systems that provide the fields of ocean circulation, wind, and waves on a regular basis. The Copernicus Marine Service provides such data to most European systems. This information not only allows computing the oil drift, but it also helps to simulate the oil transformation processes and interaction with sediments, both coastal and seabed. The results are typically represented by oil mass balance time series delineating what fraction of the original spilled oil is expected to be kept afloat, evaporated, dispersed in the water column, beached or sedimented.

During the oil spill accidents, tight coordination between the oil spill detection/monitoring unit and operational modelling is vital for starting the spill forecasts, ground-truthing, and fast decision making. Real oil spills provided unique opportunities to examine the predictive skills of operational oil spill models, using observations carried out during oil spill accidents. Such combined studies have been conducted on spills in many geographic regions: the Prestige disaster in the Atlantic Spanish coast in 2002 (Castanedo et al., 2006; Daniel, 2010), the Fu Shan Hai wreck in the Baltic Sea in 2003 (De Carolis et al., 2013), the Lebanon crisis in 2006 (Coppini et al., 2011), the Kerch Strait oil spill in 2007 (Ivanov, 2010), the Deepwater Horizon oil spill in the Gulf of Mexico in 2010 (Liu et al., 2013), the Agia Zoni II oil spill in the Aegean Sea in 2017 (Coppini et al., 2018), the Sanchi spill disaster in the East China Sea in 2018 (Qiao et al., 2019), the Ulysse-Virginia oil spill in the Ligurian Sea in 2018 (Liubartseva et al., 2020a; Daniel et al., 2021), and in the Grande America accident in the Bay of Biscay in 2019 (Daniel et al., 2020).

Since oil transport is mainly controlled by ocean currents, the accuracy of oil spill simulations crucially depends on the resolution of the hydrodynamic models used. To resolve coastal scale processes, downscaling techniques that switch from high-resolution hydrodynamics to ultra-fine scales, with a resolution of around 100 m, are being developed. As an example, an operational decision supporting system for oil spill emergencies addressed to the Italian Coast Guard was developed by Sorgente et al. (2020) in the Western and Central Mediterranean Sea. Progress in downscaling led to operational oil spill modelling in harbour and port areas, such as the Port of Taranto in south Italy (Liubartseva et al., 2020b) and the Port of Tarragona in Spain (Morell Villalonga et al., 2020). In these three examples, the MEDSLIK-II oil spill model was applied in

various configurations. Two examples of oil spill forecasting applications are described in the following subsections.

11.2.2.1. MOTHY

MOTHY is a dual system consisting of an ocean model, developed to best represent the surface current, and a slick or object model (Figure 11.5). It operates worldwide, and can be implemented immediately, 24 hours a day, by the marine forecasting service of the National Forecasting Centre of Météo-France (🔗 [10]), located in Toulouse. This Centre provides met-ocean support and drift forecasts to assist authorities in charge of accidental marine pollution and search and rescue operations. The oil spill forecasting system was developed by combining the Cedre's (🔗 [11]) expertise in oil chemistry with the Météo-France's expertise in weather and ocean forecasting and modelling to provide a robust operational service maintained by Météo-France. The system is operated at Cedre's request in support of oil spill response operations and at the request of the Maritime Rescue Coordination Centres in support of search and rescue operations.

MOTHY has been operational since 1994 and was widely used during the Erika 🔗 [12] (December 1999), Prestige 🔗 [13] (November 2002), and Grande America 🔗 [14] (March 2019) crises. The system is activated about 20 times a week for actual spills or search and rescue operations. The search for objects or people constitutes almost three quarters of the applications.

The model is regularly updated and improved. MOTHY includes a Lagrangian model with the possibility of backtracking. The 3D version takes into account vertical buoyancy- and turbulence driven movement. There are 3 components:

- oil or any substance that drifts like a slick, including vegetable oil or a few chemicals;
- cargo containers;
- search and rescue targets.

Drift predictions depend primarily on reliable and timely access to observed and predicted environmental data. From this point of view, Météo-France is equipped with the best atmospheric models:

- The AROME limited area model covers the entire French coastline, with a 1.3 km resolution around France and 2.5 km around the French overseas territories;

---

10. https://meteofrance.com/
11. http://wwz.cedre.fr/en
12. http://wwz.cedre.fr/en/Resources/Spills/Spills/Erika
13. http://wwz.cedre.fr/en/Resources/Spills/Spills/Prestige
14. http://wwz.cedre.fr/en/Resources/Spills/Spills/Grande-America
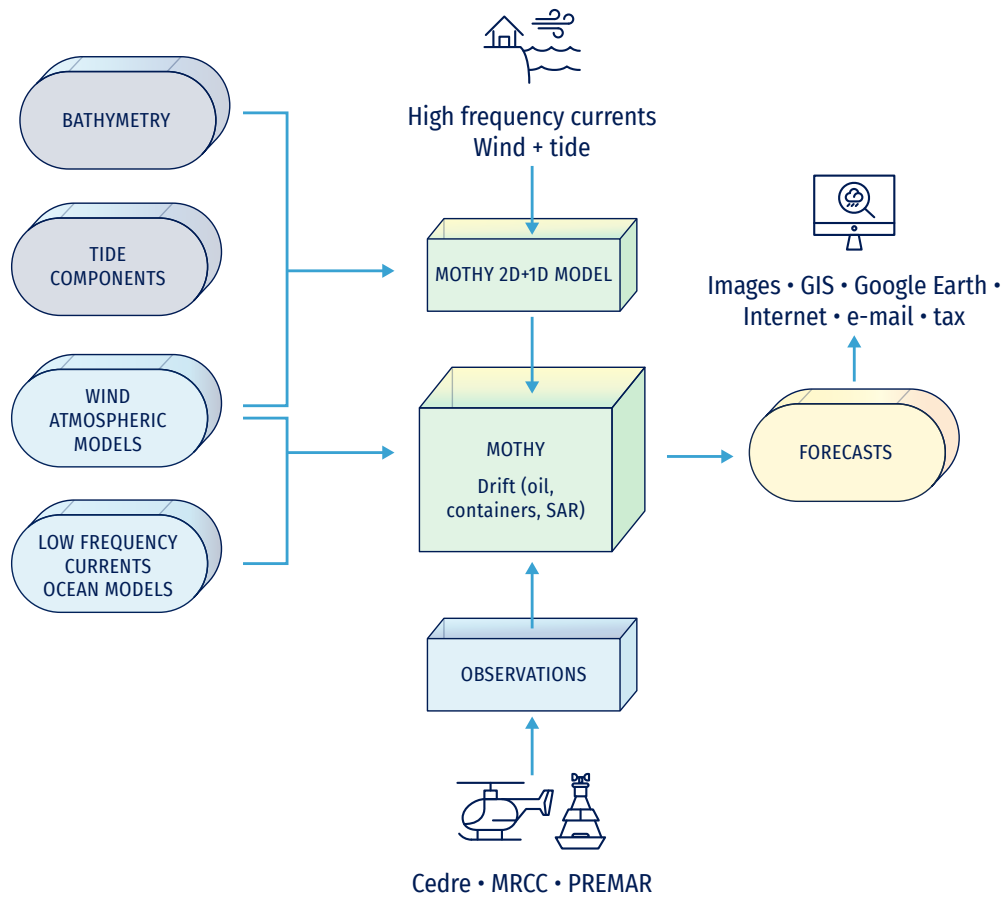
Figure 11.5. General diagram of the MOTHY system. Blue: static data. Green: data sets stored in the Météo-France database; includes all Météo-France/ECMWF atmospheric models and Copernicus Marine ocean models.

• The ARPEGE 🔗[15] global model with variable mesh (1/10 ° or 1/2 ° depending on the area), centred on France, for forecasts over the European seas and near Atlantic;
• The IFS 🔗[16] global model of the ECMWF has a resolution of 1/8° and GFS at 1/4 ° in R&D mode.

and ocean models:

• Global ocean system by Mercator Ocean International 🔗[17] with a resolution of 1/12°;
• Regional systems (IBI at 0.028°×0.028° resolution, MedFS at 0.042°×0.042° resolution, Atlantic-European NWS at 0.014°×0.03° resolution);
• SCHISM in New Caledonia (1/200° resolution).

The MOTHY model, which calculates the three-dimensional drift of surface and subsurface oil, is a "superparticles" mod-el. Superparticles are seeded at each time step, according to the specified location, duration, and rate of release.

Being operated by Météo-France's Marine Forecasting service, MOTHY is free for the French authorities and certain foreign weather services as a part of their public service mission. After requesting an account, users can freely perform modelling in the Channel - North Sea on the Noos-Drift online platform: 🔗[18].

11.2.2.2. WITOIL

WITOIL (Where Is The Oil) is a multi-model oil spill forecasting service providing predictions on transport and transformation of actual or hypothetical oil spills for the global ocean, the regional European Seas, and selected coastal areas (Figure 11.6). Being an interactive system, WITOIL requires the input of data about atmospheric winds, sea surface temperatures, and sea currents.

15. http://www.umr-cnrm.fr/gmap/nwp/nwpreport.pdf
16. https://www.ecmwf.int/
17. https://www.mercator-ocean.eu/

18. https://odnature.naturalsciences.be/noosdrift/api/home/
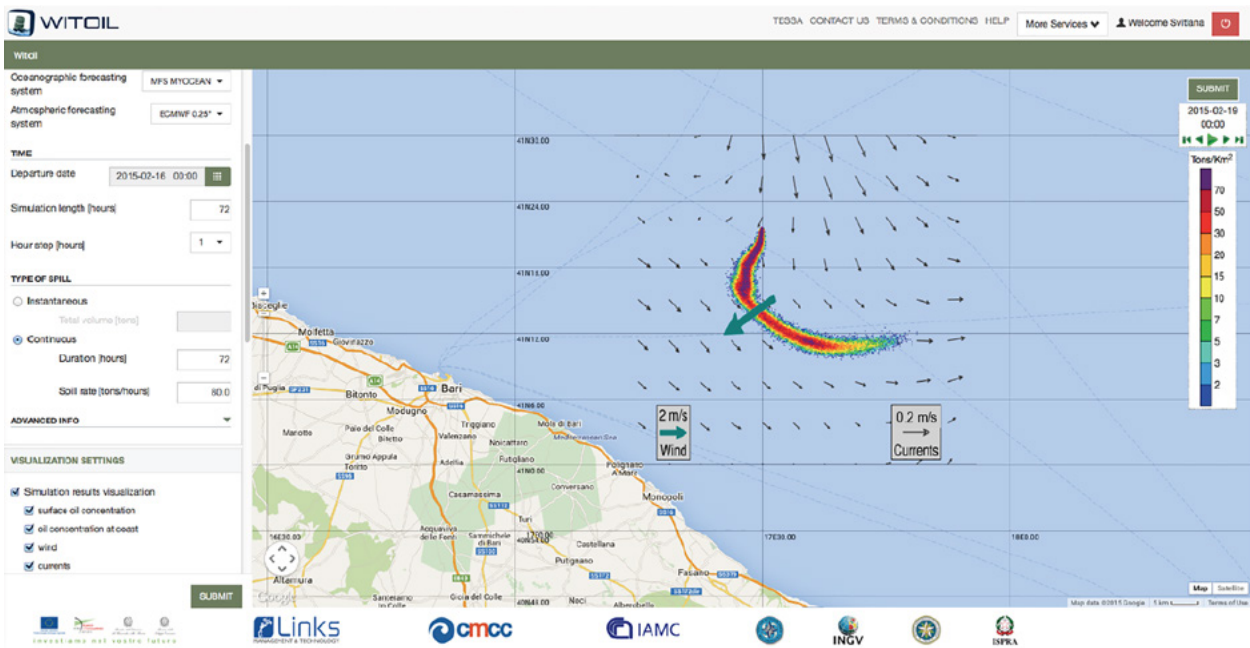
Figure 11.6. Example of the user interface and results of the WITOIL oil spill forecasting application.

WITOIL provides users with spatial-temporal distributions of oil concentration at the sea surface and on the coastline. WITOIL output consists of graphics and animations available through web browser and downloadable products (both ocean and atmospheric fields and oil slick simulation outputs). Moreover, WITOIL provides an interoperable service that can be accessed from and integrated in any GIS system.

Data used in the WITOIL application are: i) the atmospheric wind data from ECMWF provided by Italian Aeronautica Militare at a resolution of 1/10°: 6-hourly analysis, 1 hour for the first 3 days of forecast, 3 hours for the following 3 days of forecast, and 6 hours for the last 4 days of forecast; and ii) the ocean current and SST data are provided by the Copernicus Marine Service.

In particular, the following domains and ocean products are used in WITOIL:

1. The Global Ocean at 1/12° (from Copernicus Marine Service) and 1/16° (Global Ocean Forecasting System by CMCC);
2. Mediterranean Sea using the MedFS products at 1/24° horizontal resolution from Copernicus Marine Service;
3. Black Sea using the BSFS products at 1/40° horizontal resolution from Copernicus Marine Service;
4. Baltic Sea using the Baltic Sea Forecasting System at 0.028°×0.017° horizontal resolution from Copernicus Marine Service;
5. Southern Adriatic and Northern Ionian Sea coastal areas using the CMCC SANIFS (🔗 [19]), based on the SHYFEM

unstructured grid ocean model, reaching a horizontal resolution of 10-100 m in the coastal areas;
6. Several areas in the Persian Gulf using the CMCC ocean forecasting systems based on SHYFEM, reaching a horizontal resolution of 10-100 m in the coastal areas.

Free-access WITOIL version, a web-based application at 🔗 [20], is available for the Mediterranean Sea in English, Italian, French, Spanish, Arab, Greek, and Russian. Advanced multi-model WITOIL version is available upon request: 🔗 [21].

Various systems collaborated to provide information support for a recent oil spill. On 25th July 2020, the MV Wakashio hit a reef and ran aground off Pointe d'Esny on the southeast coast of Mauritius, in the Indian Ocean (Figure 11.7). In the morning of 6th August, oil leaked out of a fuel tank and oil pumping operations were carried out. They were completed on 12th August. On 16th August, the ship broke in two. On 19th August, the front part of the ship was towed about 20 kilometres from the coast. It sank on 24th August.

Following a request from the Mauritian authorities for assistance from France, the Prefect of the Reunion Island, activated a crisis cell. Meteo-France was then involved to forecast the oil drift (Daniel and Virasami, 2021). Also CMCC and MOI produced oil spill simulations and forecasts with WITOIL and sent them to relevant authorities.

19. http://sanifs.cmcc.it

20. http://www.witoil.com/
21. witoil@cmcc.it

Figure 11.7. A recent oil spill emergency: the August 2020 incident in Mauritius.

11.2.3. Ports

Ports and activities linked to maritime transport, for both commercial and tourism purposes, have a significant economic value for coastal countries. Ports may be affected by very serious environmental issues that have consequences on the safety of port activities, as well as be a vehicle for concentration and dispersal of alien species through ballast waters.

11.2.3.1. SAMOA service for Spanish ports

Approximately 85% of imports and 60% of Spanish exports are channelled through ports, and such figures highlight the vital role they play in the national economy. The ports suffer the extreme events of the main physical variables, in particular wind, waves, and sea level. These phenomena affect the installations throughout all phases of the port life, from design to operation. To respond to these complex needs, the Spanish Puertos del Estado and Port Authorities co-financed the SAMOA initiative.

SAMOA fully integrates a comprehensive set of products in a specific visualisation tool that is managed by administrators in the harbours. It also includes an alert system via e-mail and SMS, fully configurable by the port community users. In addition, an extended set of applications, such as oil spill models and air pollution monitoring tools, have been fully integrated into the system.

The main functions of the system are: 1) provision of information for knowledge-based operation of infrastructures (e.g. forecast of port closure due to extreme events); 2) aid for pilot operations; 3) safer and more efficient port operations (e.g. crane operations affected by winds and planning of Ro-Ro operations); 4) fight against oil spills in the interior of the harbours; and 5) control of water and air quality.

SAMOA is heavily relying on previously existing Puertos del Estado monitoring networks (25 buoys, 8 HF radars and 40 tide gauges) and it has been used to detect and fill gaps, improving the coverage of meteorological stations on the ports, and the control of the tide gauges by means of continuous GNSS.

The SAMOA wave component has been designed to provide a three-day forecast of agitation (significant wave height in the interior of the port) inside 10 Spanish ports of special interest: Almería (two ports), Gijón, Las Palmas (three ports), Málaga, and Santa Cruz de Tenerife (three ports). Prior to SAMOA, Puertos del Estado was running an operational wave
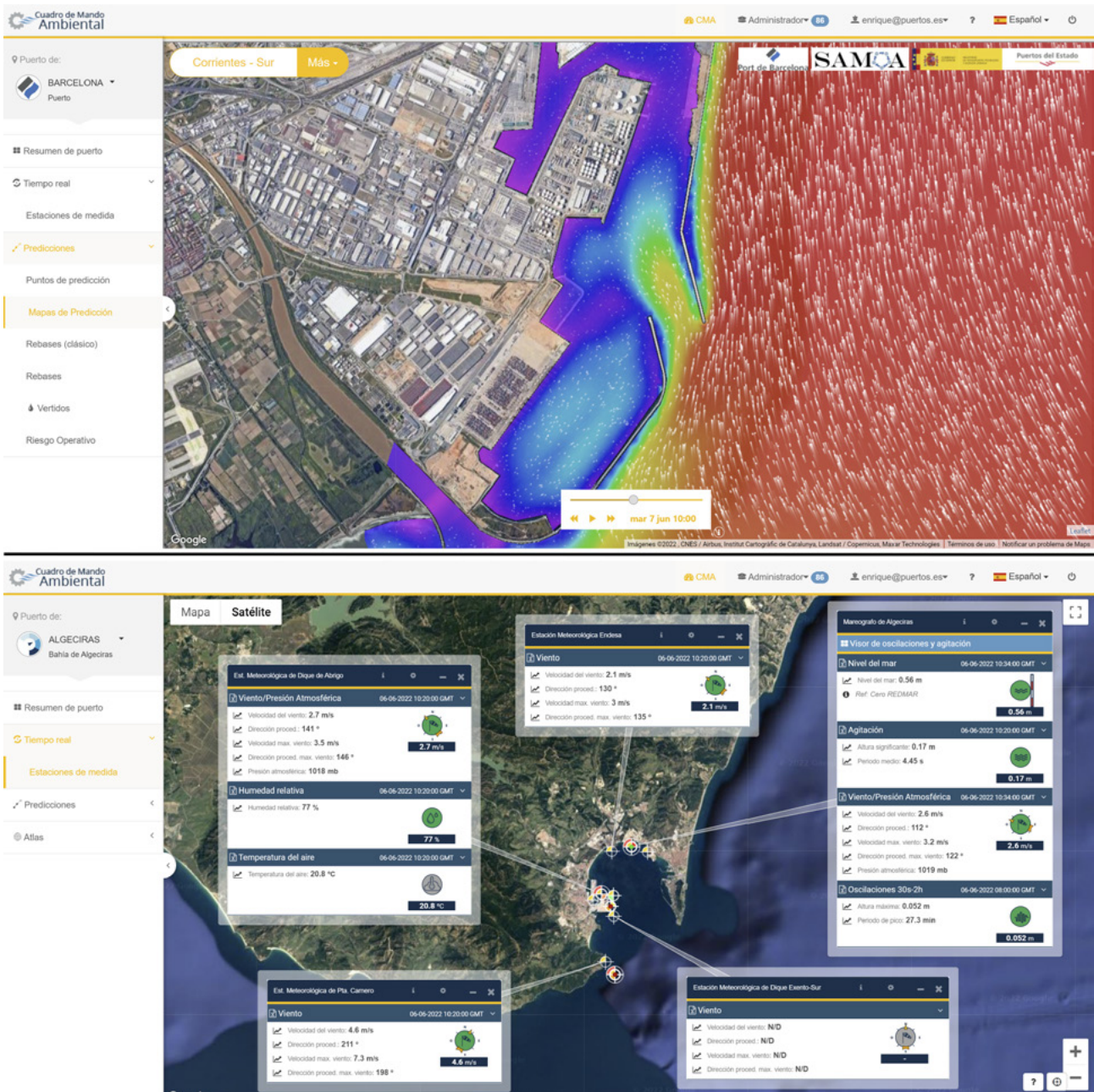
Figure 11.8. The SAMOA visualisation tool, showing the circulation at Barcelona Port (upper panel) and the real-time measurements at Algeciras Harbour (lower panel).

forecast able to provide, using the SWAN model, wave forecasts at the harbours mouth. Thanks to the development of SAMOA, this forecast has now been downscaled to the interior of the ports at extremely high resolution (2 m).

The SAMOA circulation component produces daily a short-term (three-day) forecast of three-dimensional currents and other oceanographic variables, such as temperature, salinity, and sea level for nine Spanish ports in the Mediterranean (Barcelona, Tarragona, Almería), the Iberian Atlantic (Bil-

bao, Ferrol), and the Canary Islands (Las Palmas, Tenerife, La Gomera, and Santa Cruz de la Palma). The three-dimensional hydrodynamic model used in the SAMOA circulation component is the ROMS (Shchepetkin and McWilliams, 2005).

The SAMOA model outputs are freely accessible through the Puertos del Estado's THREDDS catalogue (the THREDDS is a web server that provides access to data and metadata for scientific purposes using a variety of remote data access protocols). Likewise, free access to some products is grant-

ed via a web interface ($\mathscr{O}$ 22). Additionally, a specific tool for port authorities - the CMA shown in Figure 11.8) - has been developed to properly exploit all SAMOA products and so far has been implemented in 46 ports. The CMA, developed by Nologin Ocean Weather Systems ($\mathscr{O}$ 23), is based on a web interface ($\mathscr{O}$ 24) and provides easy access to all information generated by the SAMOA systems, both in real time and in forecast mode. Users can define thresholds for all spatial points inside the application (model points and measuring stations) that are employed to trigger alerts. The CMA is also capable of creating custom PDF reports for each forecast point. Furthermore, a user-friendly oil spill model and an atmospheric dispersion model have been developed and incorporated into the CMA. Port managers granted access to the tool can define the level of permission allowed to users. For example, some users can get permission for visualisation, but might not have access to the oil spill model. The CMA is also used to configure personalised alert systems, defining the points and the alerts to be triggered, as well as the reception method (e-mail or SMS). The alerts can be defined as a combination of parameters, conditions, and/or thresholds as complex as desired by the user. A very good example of how the CMA tool should be used is the Algeciras harbour, in which it is utilised by a community of 500 users, including the companies located at the facilities.

Building on the success of SAMOA, a SAMOA 2 project is now on its final stage of implementation. This second phase will include new components, such as a wave overtopping forecast and extremely high-resolution wind prediction (2 m). In 2022, once SAMOA 2 is completed, the system will have the following components: 44 CMA implementations in different ports (of a total of 46 ports in the national system), 20 1-km resolution atmospheric forecasts, 21 agitation systems, 31 circulation systems, 19 new meteorological stations, eight GNSS, 15 very high wind forecast systems, plus other additional modules. Work is ongoing on how to use the new models to explore, for example, the wave current interactions.

With the new system in place, the most important challenge for the Spanish port system will be to implement the methodologies necessary to make proper use of all the new available tools. While some ports are very active and are already making good use of the new information, others are still not able to fully exploit it. Several initiatives will be launched to reduce this gap. Making operational oceanography a core part of the port management business is probably the most significant result of SAMOA.
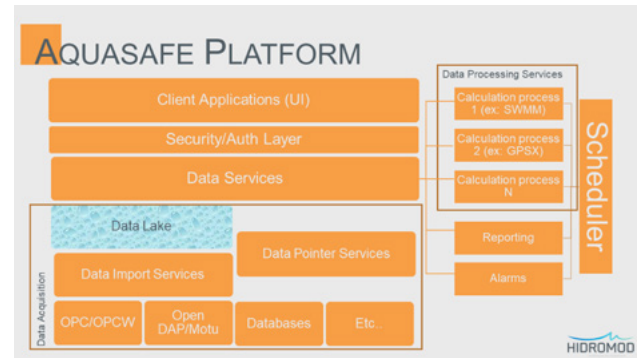
Figure 11.9. Architecture of the AQUASAFE platform.

11.2.3.2. AQUASAFE

The AQUASAFE platform ($\mathscr{O}$ 25) aims to increase efficiency in management of maritime operations, providing real time information and its integration with forecast and diagnostics tools. This platform is operational for all Portuguese Ports and in the Port of Santos (Brazil). It is also used to support aquacultures, inland navigation, irrigation, and water utilities.

Measured data (sensors, remote detection, etc.) and modelled data (meteorology, hydrodynamics, waves, etc.) are integrated in a platform which synchronises all of them in time, space and dimensional units to provide easy and robust access to real time and forecast information. The global architecture of the Platform is presented in Figure 11.9.

AQUASAFE has a micro-service, cloud native architecture. Each one of the platform's components (data download, data formatting, model execution, etc.) is implemented in a completely isolated way, facilitating both its maintenance and scalability. It also uses Container technology (from Docker) so that each component is portable and consistent and can be quickly instantiated.

The Client Applications (User Interfaces) connect to Data services via a state-of-the-art authentication layer. A Data services layer is managing the Data acquisition (ingestion of data from external systems to the platform, and storage) and the Processing Services (which performs computational loads that generate new data). It also manages Reporting and Alarms. Data Processing Services, Reporting and Alarms are processed through a common Scheduler.

Using this system, port operations have better efficiency and safety as it improves the match between tight schedules of container ships, or tight security of liquefied natural

22. https://portus.puertos.es/index.html?locale=en#/
23. https://www.nologin.es/en/nowsystems
24. https://cma.puertos.es

25. https://hidromod.com/?s=aquasafe
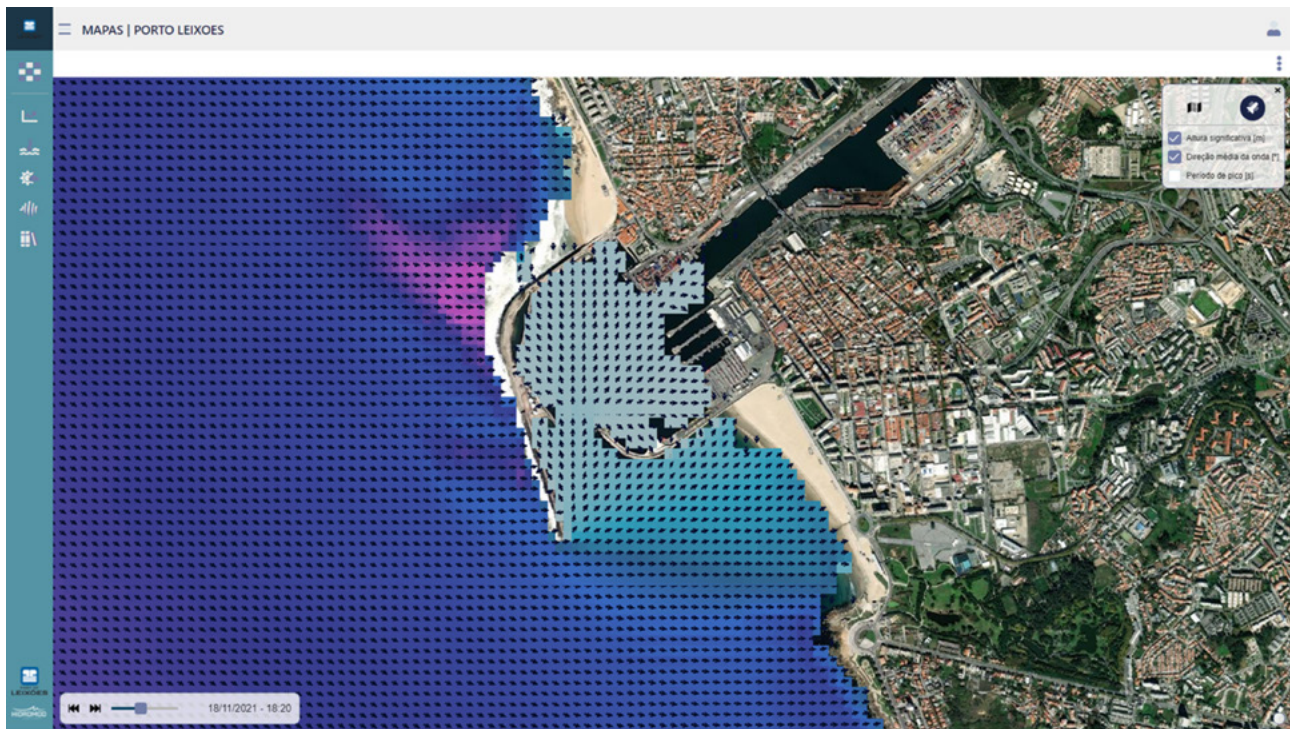
Figure 11.10.AQUASAFE platform: wave model at the Port of Leixões (Portugal).

gas (LNG) carriers, and the operational weather limits of each Terminal. Thus, the impact in the logistic chain including ports is extremely positive.

In this context, PIANC's Maritime Navigation Commission Working Group 54 produced a set of recommendations "on the use of hydro/meteo information for navigational channel and port basin operations, including the determination of operational limits" (PIANC, 2012). The AQUASAFE platform was developed along those recommendations.

Hydrodynamics and wave propagation modelling methodology used in the operational systems implemented with AQUASAFE is based on downscaling global models to local scale, to correctly forecast parameters like sea level, currents, or waves (Figure 11.10). Meteorological forecasting also has a similar approach, but institutes or companies specialised in meteorology are usually used as data suppliers (e.g. MeteoGalicia).

This downscaling methodology is also embedded in the concepts behind some modelling systems like WRF (atmospheric model) or SWAN (waves nearshore).

11.2.4. Voyage planning

Shipping moves the global commerce as, according to UNCTAD, around 80% of the volume of international trade in

goods is carried by sea [26]. This tremendous effort comes with a significant environmental footprint. According to the Fourth GHG study of the IMO, shipping accounted in 2018 for nearly 3% of global anthropogenic CO_2 emissions. Container ships, bulk carriers, and oil tankers are the greatest emitters of the world fleet. When it comes to per-ship emissions, cruise ships also distinguish themselves for their carbon footprint.

Various measures are presently discussed both at IMO [27] and at the European Union level [28] for reducing the GHG emission from shipping. In the short term (i.e. the current decade), more efficient operations for both old and newbuild ships would be possible via a blend of design and operational measures. Among the operational ones, both speed limitation and voyage planning could be considered. Speed limitation leads to reduction in emission at the cost of longer voyage durations, and could be viable for delivering non-perishable goods. However, for all ship types, the environmental benefits of speed limitation could be enhanced through voyage planning or weather routing. This wording may refer to quite

26. https://unctad.org/topic/transport-and-trade-logistics/review-of-maritime-transport

27. https://www.imo.org/en/MediaCentre/MeetingSummaries/Pages/MEPC76meetingsummary.aspx

28. https://eur-lex.europa.eu/legal-content/EN/TXT/?uri=CELEX%3A52021DC0550

different systems supporting the definition of the route to be sailed. It is possible to distinguish among:

- Strategic/Tactical planning. The former refers to optimally deploy the fleet of a given shipowner to pursue some benefit, while the latter to the shape of a specific route between given ports of call;

- Global/Local optimization. The former refers to optimise some figure of merit integrated along a voyage (such as total voyage GHG emissions), while the latter to locally constrain the vessel behaviour (wind, waves, or ship motions below a given threshold);

- Single/Multiple Objectives. In the former case, the optimization objective (such as emissions, duration, cost, and comfort) is one at time, while in the latter multiple, conflicting objectives can be addressed (usually making use of some mathematical compromise);

- Deterministic/Stochastic. In the former case, an algorithm is used to deliver exactly the same solution for given boundary conditions (usually a proof of optimality is available), while in the latter stochastic approaches (such as genetic ones) are used for speeding up computations at the cost of losing full optimality and reproducibility.

In most items of the above taxonomy, voyage planning is related to weather and ocean state, both observed and predicted, to be used for either constraining the navigational options or defining the route's optimization objectives. A recent joint IMO-WMO symposium 🔗[29], highlighted that routing optimization may help ships to increase their operational efficiency and simultaneously reduce emissions, while it is especially relevant for safety of navigation in extreme marine conditions. Voyage planning tools are developed by several research organisations in various countries, such as (non-exhaustive list): Sweden (Li et al., 2021), Portugal (Vettor and Guedes Soares, 2016), Poland (Krata and Szlapczynska, 2018), Italy (Mannarini et al., 2016a), South-Korea (Lee et al., 2018). An attempt to classify ship routing models can be found in (Zis et al., 2020).

Finally, for its contribution to GHG emission reduction, voyage planning embeds a potential to contribute to several targets of the UN Sustainable Development Goals (🔗[30]), notably to 12.2, 12.4, and 13.

11.2.4.1. VISIR

The VISIR is a voyage planning model developed since 2012 by the CMCC and the University of Bologna. It can be defined as a tactical, global-optimization, single-objective, deterministic model system for ship route planning. It is based on an exact graph-search method (Dijkstra's algorithm) modified for dealing with dynamic environmental fields. It is coastline- and sea-bottom-aware, thanks to a masking procedure in preparing the graph. It was used for both motor and sailboat routing in the Mediterranean Sea (Mannarini et al., 2016) and in the Atlantic Ocean (Mannarini and Carelli, 2019). So far, VISIR has been used in conjunction with both analysis and forecast wave and current fields from Copernicus Marine Service, and with wind fields from ECMWF or COSMO-ME (Mannarini et al., 2015).

In its first version, VISIR computed only least-distance and least-time routes. However, starting from version 2, also a least-CO2 route algorithm was embedded into VISIR. VISIR-1 used polar plots for representing sailboat speeds through water (STW) in dependence of wind magnitude and direction (Mannarini et al., 2015), while wave fields were used for motorboat routing (Mannarini et al., 2016). VISIR-1-b made use of sea surface currents for correcting STW for sea current drag and drift (Mannarini and Carelli, 2019). Starting from VISIR-1b, the angular resolution of the routes was enhanced thanks to a higher degree of connectivity of the underlying graph. While all VISIR-1 versions are based on a parametrization of calm water and wave added resistance for motorboats, VISIR-2 can alternatively make use of a ferry response model derived from a ship simulator. This allows for inclusion of wind-wave angle of attack, a more accurate representation of involuntary speed loss in waves, as well as of fuel consumption and CO2 emissions (Mannarini et al., 2021).

The validation of the path planning component of VISIR was performed via both analytical benchmarks (Mannarini and Carelli, 2019) and model inter-comparison (Mannarini et al., 2019).

VISIR is an open-source model and its updates are usually released upon documentation on peer-reviewed publications. In Table 11.1 is provided an overview of VISIR features across its versions (🔗[31]). So far, only version 1.a and 1.b have been released, which were coded in Matlab. However, the model version currently being developed is coded in python. VISIR-2 powers an operational service for ferries in the Adriatic Sea, available at 🔗[32].

In Figure 11.11 an example of optimal routes from the most recent version of VISIR is displayed.

---

29. https://library.wmo.int/doc_num.php?explnum_id=10305
30. https://sdgs.un.org/goals
31. http://www.visir-model.net/
32. https://gutta-visir.eu

Table 11.1. Overview of features in VISIR model versions.

Version	Released	Language	Ship model	Fields	Angular resolution	Objectives
1.a	2016	matlab	Semiempirical parametrization of resistances	Waves (height, period)	26.6°	distance, time
1.b	2019	matlab	Semiempirical parametrization of resistances	Waves (height, period) & currents	7.1° or better	distance, time
2.a	>2021	python	Semiempirical parametrization of resistances or fitted ship simulator response	Waves (height, direction) & currents	14.0° or better	distance, time, CO2

a)

b)
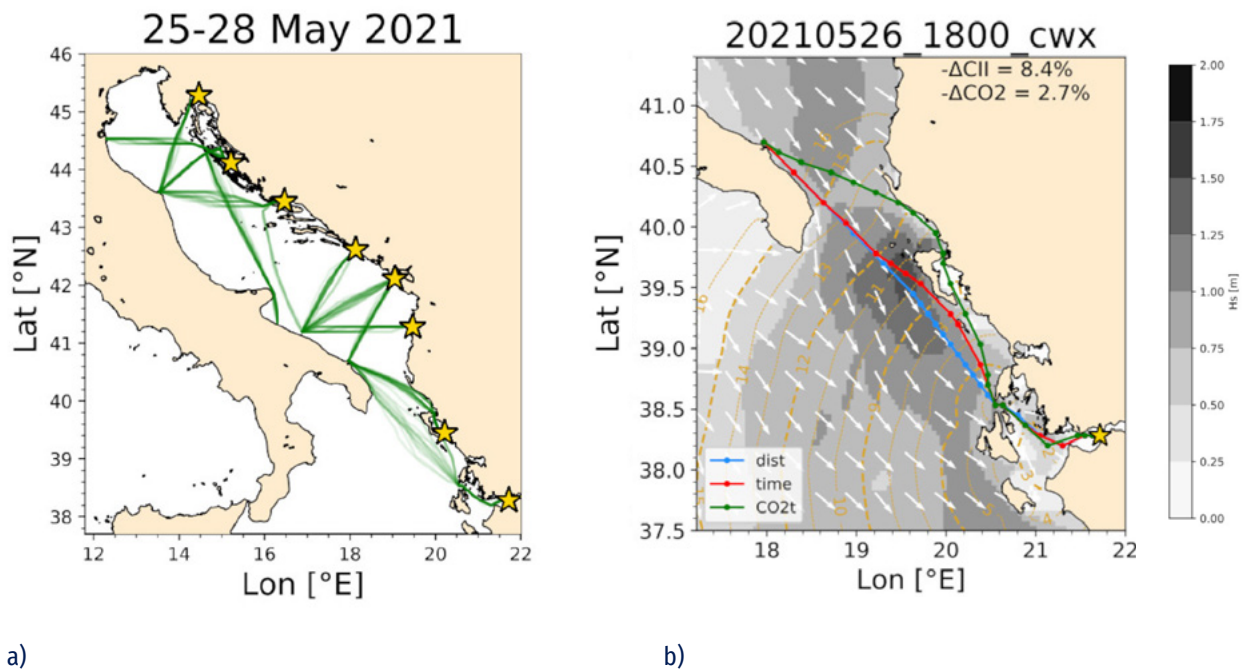
Figure 11.11. Optimal routes for a ferry of 125 m, computed via VISIR-2. Left panel: bundles of East-bound CO2-optimal routes for 25 departure times any 3 hour and three engine load values (70, 85, or 100% of maximum engine power). Right panel: least-distance (cyan), least-time (red), and least-CO2 (green) route from Patras (Greece) to Brindisi (Italy) for departure date and time as in the title and engine load at 70%. Relative CO2 and CII savings with respect to the shortest route are also indicated.

11.2.5. Fisheries and aquaculture

New technologies are developing for management and monitoring of fisheries, valorisation and protection of fish species, enhancing environmental standards for sustainable aquaculture, reducing wastes and improving safety, developing commercial platforms for direct selling of fish products, and tracing products in innovative ways. Another aspect to take into consideration is the characterization of fisheries and aquaculture products, with the purpose of diversifying products and innovating traditional practices. Information technologies can assist in the development of important systems to support the economic sustainability of the fishing industry, which may help fishers to guarantee the quality of products, as well as get information on sea conditions and on fishing models. In the following subsection are presented three examples on the use of operational oceanographic products for stock assessment, and management of fisheries and aquaculture.

Figure 11.12. The Weather window tool
(source: 🔗[33]).

11.2.5.1. Bluefin tuna

The SOCIB and the IEO have developed a habitat model for predicting spawning distribution of Atlantic bluefin tuna (Thunnus thynnus) in the Western Mediterranean. Observed data for larvae location are incorporated in a predictive system of the habitat model, forced by operational oceanographic products from the Copernicus Marine Service, such as satellite altimetry and chlorophyll, as well as sea surface temperature and salinity from hydrodynamic models for forecasting the Bluefin tuna habitats (Alvarez-Berastegui, 2016; Ingram, 2018). Analysis, satellite data, and forecast by the MedFS, in situ data for OC, SST, and Total Allowable Catch set by ICCAT are used in the application. Description of the application is available at 🔗[34].

11.2.5.2. Harmful algal bloom warning system

The Harmful algal bloom warning system provides near real-time forecast information for the aquaculture industry along Europe's Atlantic coast, it is of vital importance for mitigating the effects of HABs. It was originally developed in the FP7 Asimuth project (Cusack et al., 2016), subsequently further developed in H2020 AtlantOS (Cusack et al., 2018) and Interreg Atlantic Area PRIMROSE (🔗[35]). The warning system has been operational at the Irish Marine Institute since 2013 and subsequently deployed in Spain by IEO and in Norway by the NIVA. HAB information is disseminated in the form of a weekly bulletin to a wide audience with plots easy to interpret and explanatory text. The EOVs are used to develop data products for the weekly HAB bulletin and include: phytoplankton biomass and diversity, sea surface temperature, ocean colour, ocean surface stress, sea surface height, subsurface temperature, surface currents, subsurface currents, sea surface salinity, subsurface salinity, and ocean surface heat flux. Other EOVs required to produce the HAB bulletin are the biotoxins and/or phycotoxins produced by some phytoplankton species that can accumulate in shellfish. Numerical models, satellites and in-situ data are integrated and undergo expert interpretation before finding their way to the weekly bulletin.

11.2.5.3. Weather window tool

The Weather window tool provides a user-friendly interface to short-term wave forecasts. It was developed by the Marine Institute, Ireland, in the framework of AtlantOS (Dale et al., 2018) and is currently developed further in MyCOAST (Interreg Atlantic Area) to include more locations along the European Atlantic coasts. Availability of "coordinated" coastal observatories and forecasting models is the prerequisite for the transferability

---

33. https://www.digitalocean.ie

34. http://www.socib.es/index.php?seccion=detalle_noticia&id_noticia=191

35. https://www.shellfish-safety.eu/

PHYSICS	BIOGEOCHEMISTRY	BIOLOGY & ECOSYSTEMS
● Sea State*	● Oxygen	● Phytoplankton Biomass & Diversity
Ocean Surface Stress	Nutrients	Zooplankton Biomass & Diversity
● Sea Ice	Inorganic carbon	● Fish Abundance & Distribution
Sea Surface Height	Transient Tracers	● Marine turtles, birds, mammals abundance & Distribution
● Sea Surface Temperature	Suspended Particulates	● Live Coral
Subsurface Temperature	Nitrous Oxide	● Sea Grass Cover
● Surface Currents	Carbon Isotope (°C)	Mangrove Cover
Subsurface Currents	Dissolved Organic Carbon	● Macroalgal Canopy
● Sea Surface Salinity	● Ocean Colour	
Subsurface Salinity		
Ocean surface heat flux		

*Wave height is essential for site selection

Mature	Pilot	Concept	● Useful for site selection

Table 11.2. List of physical variables for building the aquaculture site selection (source: Dale et al., 2017).

of this tool to other locations. To this aim, MyCOAST project developed a guideline to the standardisation of data from the observing and forecasting systems based on the NcML 🔗 [36]. The user of the tool selects a location from a dropdown menu, inputs a cut-off wave height that is deemed by the user as safe for specific field activity at the site, and selects the time period up to a week (limited by the duration of wave forecast). Two graphs are then displayed: i) significant wave height time series with the cut-off height marked and safe dates and times coloured green; and ii) wave period and direction as a supplementary information. A snapshot of the tool is presented in Figure 11.12.

11.2.5.4. Aquaculture site selection

Aquaculture site selection is a key factor in aquaculture operation, including offshore aquaculture, and proper site selection is a prerequisite for the economic sustainability of the operation, for animal welfare, and for product quality. It is possible to base the identification of suitable sites for offshore aquaculture on observational and modelling systems. In response to the industry requirement, a relevant demonstration of this service was performed in the framework of AtlantOS (Dale et al., 2017). GIS approach has been used as it offers a means to organise, process, and analyse different data types and data models, as well as to perform a spatial multi-criteria evaluation. A set of criteria needs to be fulfilled for a site to be suitable for offshore aquaculture. These criteria, presented in Table 11.2, are related to physical factors like temperature, waves, and currents, as well as legal or administrative factors such as distance to ship routes, marine protected areas, offshore windmills, etc. A conceptual model of the aquaculture site selection approach using GIS is presented in Figure 11.13.

Figure 11.13. A conceptual model of aquaculture site selection approach using GIS (source: Dale et al. 2017).

36. https://www.unidata.ucar.edu/software/netcdf-java/v4.6/ncml/Tutorial.html

11.3.
References

Aamo, O.E., Reed, M., Lewis, A. (1997). Regional contingency planning using the OSCAR Oil Spill Contingency and Response Model. In Proceedings of the 20th Arctic and Marine Oil Spill Program (AMOP) Technical Seminar, Vancouver, BC, Canada, 11-13 June 1997.

Alvarez-Berastegui, D., Hidalgo, M., Tugores, M.P., Reglero, P., Aparicio-González, A., Ciannelli, L., Juza, M., Mourre, B., Pascual, A., Lopez-Jurado, J.L., García, A., Rodríguez, J.M., Tintoré, J., Alemany, F. (2016). Pelagic seascape ecology for operational fisheries oceanography: modelling and predicting spawning distribution of Atlantic bluefin tuna in Western Mediterranean. *ICES Journal of Marine Science,* 73(7), 1851-1862, https://doi.org/10.1093/icesjms/fsw041

Castanedo, S., Medina, R., Losada, I.J., Vidal, C., Mèndes, F.J., Osario, A., Juanes, J.A., Puente, A. (2006). The Prestige oil spill in Cantabria (Bay of Biscay). Part I: operational forecasting system for quick response, risk assessment and protection of natural resources. *Journal of Coastal Research,* 22, 1474-1489, https://doi.org/10.2112/04-0364.1

Coppini, G., De Dominicis, M., Zodiatis, G., Lardner, R., Pinardi, N., Santoleri, R., Colella, S., Bignami, F., Hayes, D.R., Soloviev, D., Georgiou, G., Kallos, G. (2011). Hindcast of oil spill pollution during the Lebanon Crisis, July-August 2006. *Marine Pollution Bulletin,* 62, 140-153, https://doi.org/10.1016/j.marpolbul.2010.08.021

Coppini, G., Gonzalez, G., Perivoliotis, L., Smaoui, M., Liubartseva, S., Bourma, E., Lecci, R., Cretì, S. (2018). MONGOOS-REMPEC operational experience during Agia Zoni II oil spill, September 2017. EGU General Assembly 2018, 8-13 April 2018, EGU2018-6745-1.

Cusack, C., Dabrowski, T., Lyons, K., Berry, A., Westbrook, G., Nolan, G., Silke, J. (2016). Harmful Algal Bloom warning system for SW Ireland. Part II: ASIMUTH-tailored model products, observations. *Harmful Algae,* 53, 86-101, https://doi.org/10.1016/j.hal.2015.11.013

Cusack, C., Silke, J., Ruiz-Villarreal, M., Eikrem, W., Dale, T., Moejes, F., Maguire, J., Chamberlain, T., Dabrowski, T., Gerritsen, H., Hynes, P., Leadbetter, A., Lyons, K., O'Rourke, E., Smyth, D., Miguez, B. M., Marty, S., McFadden, Y. and O'Toole, D. (2018). Harmful Algal Bloom Bulletins. *AtlantOS Deliverable,* D8.6, AtlantOS, 36 pp., doi:10.3289/AtlantOS_D8.6

Dagestad, K.F., Röhrs, J., Breivik, Ø., Ådlandsvik, B. (2018). OpenDrift v1.0: a generic framework for trajectory modelling. *Geoscientific Model Development,* 11, 1405-1420, https://doi.org/10.5194/gmd-11-1405-2018

Dale, T., Cusack, C. and Ruiz, M. (2017) Aquaculture site selection Report. AtlantOS Deliverable, D8.2, AtlantOS, 39 pp., doi:10.3289/AtlantOS_D8.2

Dale, T., Cusack, C., Ruiz Villarreal, M., Leadbetter, A., Lyons, K., Burke, N., Smyth, D., Dabrowski, T., O'Rourke, E. and Gonzalez-Nuevo, G. (2018). Aquaculture operation Bulletin: Weather window nowcast/forecast Bulletin tool for offshore aquaculture operators. AtlantOS Deliverable, D8.8, AtlantOS, 18 pp., doi:10.3289/AtlantOS_D8.8

Daniel, P. (1996). Operational forecasting of oil spill drift at Météo-France. *Spill Science & Technology Bulletin,* 3, 53-64, https://doi.org/10.1016/S1353-2561(96)00030-8

Daniel P. (2010). Drift forecasts for the Erika and Prestige oil spills. Practical Applications in Engineering, 27(4), https://doi.org/10.1002/9781118557792.ch27

Daniel, P., Drevillon, M., Levier, B., Gouriou, V. (2020). Relevant CMEMS products to predict oil slick drift in the Grande America accident. EGU General Assembly 2020, Online, 4-8 May 2020, EGU2020-13905.

Daniel, P., and Virasami, R. (2021). Oil spill management and salvage in the Indian Ocean. WMO Bulletin, 70(1), 109-110. More information available at: https://public.wmo.int/en/resources/bulletin/Products_and_services/Oil_spill_Indian_Ocean

Daniel P., Paradis, D., Gouriou, V., Le Roux, A., Garreau, P., Le Roux, J.-F., and Louazel, S. (2021). Forecast of oil slick drift from Ulysse/CSL Virginia and Grande America accidents. International Oil Spill Conference Proceedings 2021, 1, 1141410. Available at: https://archimer.ifremer.fr/doc/00742/85421/

De Carolis, G., Adamo, M., Pasquariello, G., De Padova, D., Mossa, M. (2013). Quantitative characterization of marine oil slick by satellite near-infrared imagery and oil drift modelling: the Fun Shai Hai case study. *International Journal of Remote Sensing,* 34, 1838-1854, https://doi.org/10.1080/01431161.2012.727494

De Dominicis, M., Pinardi, N., Zodiatis, G., Lardner, R. (2013). MEDSLIK-II, a Lagrangian marine surface oil spill model for short-term forecasting - Part 1: Theory. *Geoscientific Model Development,* 6, 1851-1869, https://doi.org/10.5194/gmd-6-1851-2013

Ingram, G.W. Jr. (2018). Annual Indices of Bluefin Tuna (Thunnus Thynnus) Spawning Biomass in the Gulf of Mexico (1977-2016). *Collective Volumes of Scientific Papers ICCAT,* 74(6), 2571-2771.

Ivanov, A.Y. (2010). The oil spill from a shipwreck in Kerch Strait: radar monitoring and numerical modelling. *International Journal of Remote Sensing,* 31, 4853-4868, https://doi.org/10.1080/01431161.2010.485215

Krata, P., and Szlapczynska, J. (2017). Ship weather routing optimization with dynamic constraints based on reliable synchronous roll prediction. *Ocean Engineering,* 150, 124-137, https://doi.org/10.1016/j.oceaneng.2017.12.049

Lee, S.-M., Roh, M.-I., Kim, K.-S., Jung, H., and Park, J.J. (2018). Method for a simultaneous determination of the path and the speed for ship route planning problems. *Ocean Engineering,* 157, 301-312, https://doi.org/10.1016/j.oceaneng.2018.03.068

Li, Z., Ryan, C., Huang, L., Ding, L., Ringsberg, J.W., and Giles, T. (2021). A comparison of two ship performance models against full-scale measurements on a cargo ship on the Northern Sea Route. *Ships and Offshore Structures,* 16, 237-244, https://doi.org/10.1080/17445302.2021.1926146

Liu, Y., MacFadyen, A., Zhen-Gang, J., Weisberg, R. H. (2013). Monitoring and Modeling the Deepwater Horizon Oil Spill: A Record Breaking Enterprise. American Geophysical Union, 271 pp., ISBN: 978-1-118-66675-3

Liubartseva, S., Smaoui, M., Coppini, G., Gonzalez, G., Lecci, R., Creti, S., Federico, I. (2020a). Model-based reconstruction of the Ulysse-Virginia oil spill October-November 2018. *Marine Pollution Bulletin,* 154, 111002, https://doi.org/10.1016/j.marpolbul.2020.111002

Liubartseva, S., Federico, I., Coppini, G., Lecci, R. (2020b). Oil spill modeling for the Port of Taranto (SE Italy). EGU General Assembly 2020, Online, 4-8 May 2020, EGU2020-2946.

Mannarini, G., Lecci, R., and Coppini, G. (2015). Introducing sailboats into ship routing system visir. In "2015 6th International Conference on Information, Intelligence, Systems and Applications (IISA)", IEEE, 15723531, 1-6, https://doi.org/10.1109/IISA.2015.7387962

Mannarini, G., Pinardi, N., Coppini, G., Oddo, P., and Iafrati, A. (2016). VISIR-I: small vessels - least-time nautical routes using wave forecasts. *Geoscientific Model Development,* 9(4), 1597-1625, https://doi.org/10.5194/gmd-9-1597-2016

Mannarini, G., and Carelli, L. (2019). VISIR-1.b: ocean surface gravity waves and currents for energy-efficient navigation. *Geoscientific Model Development,* 12(8), 3449-3480, https://doi.org/10.5194/gmd-12-3449-2019

Mannarini, G., Subramani, D., Lermusiaux, P., and Pinardi, N. (2019). Graph-Search and Differential Equations for Time-Optimal Vessel Route Planning in Dynamic Ocean Waves. *IEEE Transactions on Intelligent Transportation Systems,* 21(8), 3581-3593, https://ieeexplore.ieee.org/document/8815853

Mannarini, G., Carelli, L., Orović, J., Martinkus, C.P., and Coppini, G. (2021). Towards Least-CO2 Ferry Routes in the Adriatic Sea. Journal of Marine Science and Engineering, 9(2), doi:10.1109/TITS.2019.2935614

Marcotte, G., Bourgouin, P., Mercier, G., Gauthier, J.-P., Pellerin, P., Smith, G., Onu, K., Brown, C.E. (2016). Canadian Oil Spill Modelling Suite: An overview. In "Proceedings of the 39th Arctic and Marine Oil Spill Program (AMOP) Technical Seminar", Halifax, NS, Canada, 7-9 June 2016.

Micallef, L., Deidun, A., Cutajar, D., Gauci, A. (2014). The development of the MED-JELLY smartphone application in the Maltese islands. MED-JELLYRISK Conference and Training Seminar: Addressing Jellyfish Blooms to Safeguard Coastal Economic Activities Research, Innovation, Management and Education, St. Julian's. 29.

Morell Villalonga, M., Espino Infantes, M., Grifoll Colls, M., Mestres Ridge, M. (2020). Environmental management system for the analysis of oil spill risk using probabilistic simulations. Application at Tarragona Monobuoy. *Journal of Marine Science and Engineering,* 8(4), 277, https://doi.org/10.3390/jmse8040277

PIANC. (2012). PIANC-CODEPEC VIII. Proceedings of the Eighth International Conference on Coastal and Port Engineering in Developing Countries. IIT Madras, Chennai, India, 20-24 February 2012, https://www.pianc.org/uploads/publications/Proceedings-Congresses/proceedings-copedec/PIANC-COPE-DEC-VIII-2012.pdf

Qiao, F., Wang, G., Yin, L., Zeng, K., Zhang, Y., Zhang, M., Xiao, B., Jiang, S., Chen, H., Chen, G. (2019). Modelling oil trajectories and potentially contaminated areas from the Sanchi oil spill. *Science of The Total Environment,* 685, 856-866, https://doi.org/10.1016/j.scitotenv.2019.06.255

Shchepetkin, A.F., and McWilliams, J.C. (2005). The regional oceanic modeling system (ROMS): a split-explicit, free-surface, topography-following-coordinate oceanic model. *Ocean Modelling,* 9(4), 347-404, https://doi.org/10.1016/j.ocemod.2004.08.002

Sorgente, R., La Guardia, D., Ribotti, A., Arrigo, M., Signa, A., Pessini, F., Oliva, G., Pes, A., Perilli, A., Di Maio, A. (2020). An operational supporting system for oil spill emergencies addressed to the Italian Coast Guard. *Journal of Marine Science and Engineering,* 8, 1035, https://doi.org/10.3390/jmse8121035

Spaulding, M.L., Howlett, E., Anderson, E., Jayko, K. (1992). OILMAP: A global approach to spill modeling (EC/EPS–93-01710), Canada.

Vettor, R., and Guedes Soares, C. (2016). Development of a ship weather routing system. *Ocean Engineering,* 123, 1-14, https://doi.org/10.1016/j.oceaneng.2016.06.035

Zelenke, B., O'Connor, C., Barker, C., Beegle-Krause, C.J., Eclipse, L. (2012). General NOAA Operational Modeling Environment (GNOME) Technical Documentation. U.S. Dept. of Commerce: Washington, DC, USA, NOAA Technical Memorandum OR&R; Emergency Response Division; NOAA: Seattle, WA, USA.

Zis, T.P., Psaraftis, H.N., and Ding, L. (2020). Ship weather routing: A taxonomy and survey. *Ocean Engineering,* 213, 107697, https://doi.org/10.1016/j.oceaneng.2020.107697

12.
Challenges and future perspectives in ocean prediction

CHAPTER COORDINATOR

Fraser Davidson

ChAPTER AUTHORS *(in alphabetical order)*

Enrique Alvarez Fanjul, Alain Arnaud, Stefania Ciliberti, Marie Drevillon, Ronan Fablet, Yosuke Fujii, Isabel Garcia-Hermosa, Stéphanie Guinehut, Emma Heslop, Villy Kourafalou, Julien Le Sommer, Matt Martin, Andrew M. Moore, Nadia Pinardi, Elizabeth Remy, Paul Sandery, Jun She, Marcos G. Sotillo, and Joaquin Tintorè.

12. Challenges and future perspectives in ocean prediction

12.1. Introduction

12.2. Observing system evolution with ocean prediction engagement

12.2.1. Challenges for the current ocean observing systems

12.2.2. Observing System Evaluation

12.2.3. Argo evolution plans

12.2.4. Next phase for satellite missions

12.3. Numerical models planned evolutions, including adaptation to new HPC systems

12.4. Future evolutions in ocean data assimilation for operational ocean forecasting

12.5. Future of ensemble prediction systems

12.6. Opportunities of artificial intelligence for ocean forecasting systems

12.6.1. Expected contributions of machine learning to ocean forecasting pipelines

12.6.2. Designing fully trainable ocean forecasting systems core engines

12.6.3. Towards user-centric, ocean digital twins leveraging lightweight emulators

12.7. Seamless prediction

12.7.1. Optimal use of modelling workforce and model consolidation

12.7.2. Development of seamless UOM for multiple temporal scales

12.7.3. Geographic configurations and seamless UOM in space and in a marine system of systems

12.7.4. Evolution in short-, mid- and long-term perspectives

12.1.
Introduction

The growth of ocean prediction research, capability, applicability, availability, maturity, and user uptake from an initial idea 25 years ago, while gradual, has been unrelenting. Today's capacity and maturity in ocean prediction goes beyond what was initially conceived and provides a strong basis for advancement of societal benefits. Over the next 10 years, ocean prediction systems will continue to gradually rival weather prediction systems in the sense of ubiquitous use, protecting lives, economic impact, and supporting custodianship of the environment. Building a framework with standards and best practices for the full operational oceanography value chain will enable further harnessing of prediction systems in supporting a healthy ocean at the same time of a blue economic growth for all countries. This will further awareness and accessibility of the marine environment through digital platforms underpinning increases in ocean prediction literacy, capacity building, applications, and services (Figure 4.1).

Herein we outline the expected advances of ocean prediction and other supporting components of operational oceanography over the next decade. An underlying theme is the integration of ocean prediction systems within the larger context of operational oceanography, seamless environmental prediction, and the blue economy. This requires a transparent framework approach of standards and best practices, enabling all countries, particularly those with the least resources, to engage and benefit.

This chapter introduces the key drivers for the next generation of OOFS, spanning from global to coastal scale observing systems (Section 12.2) to numerical models evolution (Section 12.3), data assimilation (Section 12.4) and ensemble systems for prediction (Section 12.5), from the growing AI techniques for understanding physical processes (Section 12.6) to seamless approach (Section 12.7) and DTO (Section 12.8), including as well the evolution in quality assessment (Section 12.9). The last sections focus on planned evolution for state-of-the-art services like the Copernicus Marine Service (Section 12.10) and international initiatives promoted by the UN Decade of the Ocean (Section 12.11).

12.2.
Observing system evolution with ocean prediction engagement

The quality of the ocean analysis and forecasts highly relies on observations assimilated for constraining the ocean circulation in ocean forecasting systems. The evolution of the forecasting systems towards increased realism to represent a larger spectrum of ocean processes and scales will be underpinned by the 'adapted' in situ and satellite observations that efficiently constrain the different scales of the ocean variability. Close collaboration between ocean forecasting centres and the observation providers is crucial to promote such evolution. Communication ensures the best use of information from the present to the future observation systems. It allows forecasting centres to inform on the observation use and to report on their impacts on analysis and forecasts. In the longer term, it also increases opportunities for the ocean forecasting centres to contribute to evolve ocean observing system designs to optimally meet requirements and enable capabilities of future operational systems. Inclusion of forecasting centres in designing and evaluating the future impact of the GOOS [1] component has started to be recognized as a best practice in the observation and prediction community.

In such a context, OOFS strictly depends on the availability of near-real time observations for assimilation and validation purposes. Accuracy of forecast products is largely impacted by the quality of assimilated observations, so that the effort of the community is to support the forecasters with high quality data in space and time sampling. Le Traon et al. (2019) provides the Copernicus Marine Service strategy for observational network evolutions and the requirements for OOFS to support maritime safety, marine resources, marine and coastal environments, weather, seasonal forecasting, and climate. According to this document, the main priorities are:

---

1. https://www.goosocean.org/

- For satellite data:

  - Guaranteeing continuity of the present operational missions' capacity of Sentinel for downstream coastal applications, and of Cryosat mission for monitoring of sea ice thickness and sea level in polar regions;
  - Developing new capacity for wide swath altimetry for the future OOFS and services;
  - Developing microwave mission for the improvement of spatial coverage of sea surface temperature, sea ice drift, sea ice thickness, and sea surface salinity;
  - Enforcing R&D for observing sea surface salinity and ocean currents from space.

- For in-situ data:

  - At global scale, the main future challenges are: a) to improve the coverage of biogeochemical measurement, b) the measurement of deep temperature and salinity, and c) measurement of in-situ velocity observations, sea ice observations, and open-ocean wave measurements;
  - At a regional scale, the main priority is to fill gaps for a wide range of variables in the shelf-coastal observational networking, in order to improve monitoring and forecasting capacities.

Copernicus Marine Service provides specific strategic documents 🔗² for both satellite and in-situ observations to support monitoring and forecasting activities. The GOOS defines the following strategic objectives for observing systems at global level towards 2030:

- to deepen engagement and impact by enforcing the connection with forecasting centres;
- to deliver an integrated fit-for-purposes observing system able to support and expand the implementation of observing systems and ensuring data management according to the FAIR principles;
- to build future observational networks by supporting innovation in observing technologies and extending systematic observations to understand impacts on the ocean.

12.2.1. Challenges for the current ocean observing systems

Major challenges for the current ocean observing systems include: i) most of the ocean observations made by non-operational oceanography communities (e.g. environment, fishery, research, and industrial sectors) have not been used for operational forecasting; the ocean observations are made by

various sectors with different monitoring and data collection standards, and little efforts have been made to harmonise observations from the different sectors; and ii) technologic bottlenecks and significant data gaps in sub-surface, sea bottom, geological and biological observations.

For developing an integrated and unified ocean observing system to support the seamless information service, three pillars are recommended, , as shown in Fig. 12.1. The first pillar is to maximise the value of existing observations by breaking the institutional and sectorial barrier (She et al., 2019) and fit for the purposes of multi-sectors. This can be implemented by performing multidimensional integration of operational and non-operational ocean observing communities, including operational monitoring, environment monitoring, fishery monitoring, research monitoring, crowd (citizens and NGOs) monitoring and other sectoral monitoring (industrial and socioeconomic). The observations should be "collected once and used for many times" (Martín Míguez et al., 2019). Due to the existing mandate of monitoring entities, either public or private, current ocean observing practices are designed separately to fit for the purpose of individual sectorial service, and observations are hardly shared from different monitoring communities. When designing multidimensional integration on a national and regional scale, unified standards should be applied. The operational and autonomous platform is an efficient framework for the integrated and unified ocean observing, which is highly recommended.

The second pillar is to develop, deploy, and utilise large networks of autonomous, cost-effective, innovative sensors to fill the observation gaps in subsurface and emerging observations, e.g. marine litter, biological variables, and underwater noise. A combination of breakthroughs in underwater communication technology, underwater robotics, and ML/AI may significantly improve the capacity of underwater monitoring, especially for pollutants, biogeochemical and biological variables. Adaptable observations are also needed for characterising key processes underpinning predictability in the marine earth system.

The third pillar is to design and optimise existing ocean observing to fill gaps in the characterizations of processes and sensitive regions that are crucial to the predictability and fit for the purposes in multi-sectors. It is essential that the monitoring capacity is based on an integrated system of in-situ, remote sensing, models, assimilation, and ML/AI tools. Sampling schemes of such a system can then be designed to optimise the integrated monitoring capacity, so that observations would most effectively be used to reduce the earth system prediction uncertainties. It should be noted that dedicated observations should be identified and included to address specific predictability in the UOM (She et al., 2016).

---

2. https://marine.copernicus.eu/about/observation-requirements
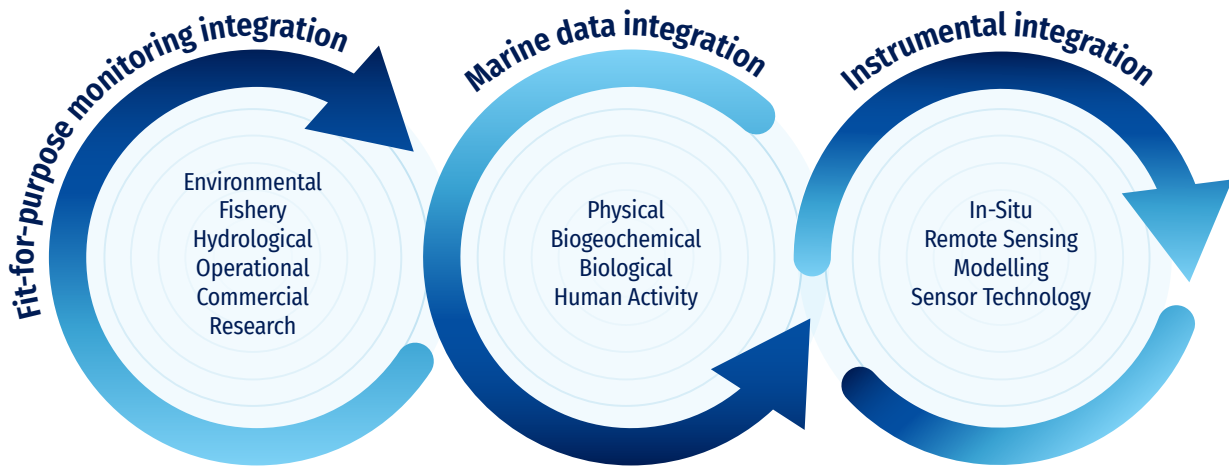
Figure 12.1. Integrated observing. Unlocking the value of ocean observing by integrating observations in three dimensions: fit for purpose, parameter, and instrumental (source: She et al., 2019).

12.2.2. Observing System Evaluation

At present, OS-Eval, based on ocean forecasting systems, are not often conducted in a coordinated manner. The most used techniques of OS-Eval are data denial experiments with real or simulated observations (e.g., OSE and OSSE). Although only observation platforms which are already existing with real observations can be evaluated, simulated observations allow us to evaluate the impact of future platforms or evolution of the observation network. Impact assessment methods will evolve in the future with more sophisticated techniques based on ensemble and adjoint methods, and potentially also AI. Considering that BGC applications and the earth system predictions, including the ocean component, are progressively becoming more important, the development of suitable evaluation methods for those applications is also indispensable. Improving analysis/forecast accuracy and developing methods assimilating new types of observation data will increase the ability to make fair assessments for various platforms. Multi-system evaluation and regular re-assessment of the observation impact to follow the system evolutions are required to improve the robustness of the results by moderating system-dependency.

Enhanced communication and coordination between modelling/data assimilation experts and observation/network experts will be essential for a proper design and interpretation of OS-Eval, especially to extract compelling messages on the ability of the ocean observing system to control processes having different temporal and spatial scales. The provision of regular reports on ocean observation impacts in ocean prediction systems is expected to enhance such communication. It should also be noted that OS-Eval activities require dedicated infrastructures and resources. Cooperation with internation-

al partners (e.g. OceanPredict, GOOS/ROOS, WMO, IOC, etc.) is hence essential to establish a substantial value chain between ocean observation networks and ocean prediction systems.

OS-Eval activities require dedicated infrastructures and resources. It is essential to strengthen the capabilities of operational and climate centres to assess the impact of present and future observations to guide observing system agencies but also to improve the use of observations in models.

An observation network cannot be considered by its own but should be evaluated in complementarity with other in-situ and satellite networks. The synergy from a combination of observation platforms' data with the other existing and planned in-situ and satellite observations should be evaluated. This will be necessary since the model forecasts need to be constrained on a large spectrum of scales, as individual platforms cannot provide it. Optimally leveraging satellite and in-situ observations to improve the ocean predictability is an important research topic with strategic importance. Understanding and being able to showcase and demonstrate the impact of both present and future observing systems in improving ocean prediction (and environmental prediction in general) is important to justify and maintain long term investments for the observation system. Feedback from such efforts enables observation groups to know where to invest their efforts, both technologically and in terms of geographic coverage in density and scope.

To best showcase evaluations of the observing system, prediction impact metrics should be generated in terms of value for: (1) user and application needs; and (2) observing system needs. On the user and application side, elements like the WMO RRR can be used, in which the impact of an observa-

tion on the forecast system is framed in terms of impact on a user or application. This can entail further post processing of prediction output, to translate forecasting impact into information that the end user will use directly. For example, for Search and Rescue at sea it may be necessary to know the impact of an observing system on drift prediction, and quantifying how much it would decrease the search area at sea while still ensuring high probability of detection. There is also a need to show the impact of an observing system on a variety of applications, as well as to provide insight into the impact of decreasing or augmenting the number of observations. Additionally, when developing metrics to support observing system needs, the multi-purposeless of the observations (climate, ocean services and health) needs to be covered.

Real-time impact assessment methods should also be developed to monitor and report on the use and impact of the different assimilated observation networks by operational ocean forecasting centres. This will help to detect impacts of changes in the observation network, and take countermeasures against them.

In the next subsections are presented the evolution plans for the observatory component, i.e. ARGO and satellite observations, which will drive the next generation of OOFS.

12.2.3. Argo evolution plans

The international programme Argo (🔗 3) is currently the major global initiative for the collection of "information from inside the ocean using a fleet of robotic instruments that drift with the ocean currents and move up and down between the surface and a mid-water level". In Chapter 4 can be found an overview on the current ARGO operational capabilities for OOFS. Argo design after 2020 is available at 🔗 4, including the following major targets:

• Improved observational capacity in the polar sea-ice regions and marginal seas;
• Increased resolution in key areas like the Western Boundary Currents in which mesoscale noise is high, and the Equatorial region for which high temporal resolution is needed;
• Launch of new missions for biogeochemical and deep region variables.

Next generation Argo programme is also oriented towards validation and deployment of new sensors for measuring ocean turbulence and small-scale mixing, which is fundamental for improving OOFS, numerical models, data assimilation schemes, and validation of forecast products.

Expansion of the observing network requires maintenance and advancements of data management systems among providers and forecasting centers to ensure interoperability and open access to growing data inflow (Roemmich et al., 2019)

12.2.4. Next phase for satellite missions

Satellite observations, together with those in-situ, are the key element for the global ocean observing system. In Chapter 4, it has already been provided a general overview of the type of data used for building OOFS. Next generation of forecasting systems will also exploit the new technological advancements in the observational network, and satellite measurements will play an important role in monitoring the cryosphere, coastal zones, and inland waters to improve the quality of marine services. The International Altimetry Team has recently published a contribution about the future 25 years of progress in altimetry measurements (International Altimetry Team, 2021); according to this work, the main requirements by altimetry for scientific and operational advances of operational oceanography, and more in general for Earth system science, are:

• Increasing the coverage of satellite measurements to support ocean dynamics understanding, from smaller mesoscale to sub-mesoscale, by means of multi-platform in-situ measurements, multi-satellite and SAR, and SAR-interferometry altimetry;
• The design of ad-hoc experiments for in-situ data collection guided by remote data;
• The evaluation of vertical circulation by means for in-situ and high resolution sea surface height measurements;
• Guaranteeing the continuity of the current operational measurements;
• Estimating uncertainties on regional sea level trends by comparing tide gauges with GNSS positioning with altimetry;
• Improving sea level record at coastal scale by using high resolution SAR altimetry, tide gauges with GNSS positioning, and developing GNSS reflectometry (the last is very promising for providing sea level change measurements);
• Increasing the spatial resolution of altimetry products with advanced techniques like SARIn-based "swath mode" processing and fully focused SAR over polar oceans;
• Increasing not only spatial but also temporal resolution by means of higher resolving altimeter such as SWOT, accompanied by larger altimetry constellation that includes swath and conventional altimetry, doppler wave and current scatterometer, and integrated altimeter.

---

3. https://argo.ucsd.edu/
4. https://argo.ucsd.edu/argo-beyond-2020/

To support operational oceanography and marine applications, Copernicus Marine Service has drawn up a document ✑ 5 that describes the main requirements for the evolution of the Copernicus Satellite Components. It focuses on the need of a multi-sensor and multi-mission approach for collecting SST, SSS, ocean colour, currents, wind, and wave measurements. This would constrain future high resolution open ocean, coastal models, and coupled ocean/wave models. The document also recognizes the need of improving space/time resolution, to better monitor and forecast the physical and biogeochemical state of the ocean at fine scale, and to improve the monitoring of coastal zones and of rapidly changing polar regions.

12.3.
Numerical models planned evolutions, including adaptation to new HPC systems

Ocean models are one of the pillars for OOFS. Chapter 4 provides information on current modelling capacities while Chapters from 5 to 10 deepen the theoretical aspects, but still remain a main question to be answered: *What is expected by ocean models for the future OOFS*? Fox-Kemper et al. (2019) provided an extensive review on challenges and perspectives in ocean models, touching many scientific open questions and issues to solve. In particular, evolving the core models to address adequate scales in space and time, accurately representing physical processes, and running fastly is the baseline for improving predictability, as well as past reconstruction of the blue, green and white ocean. These are the challenges that have to be tackled for the improvement of future OOFS.

Le Sommer et al. (2018) showed that the evolution in ocean modelling for operational oceanography is strictly connected to resolve physical processes down to the submesoscale (Chassignet and Xu, 2021) and to describe internal wave and internal tides at a global scale thanks to increase in computer power and improved physical parameterization (Shriver et al., 2012). Increasing resolution in space and time is not the only way to address high quality operational products: modularity of modern geoscientific models is key for addressing modelling complexity (Le Sommer et al., 2018).

Modelling complexity and modularity for the next generation of OOFS have a computational cost that needs to be accounted for once we consider evolutions in numerics. Evolutions in High Performance Computing is then another pillar on which establishing OOFS; scientific questions to be solved require also to face technological challenges. Le Sommer et al. (2018) highlighted how the main current limitations in the modelling framework capacity is not due to computational speed of the processors, but on access to memory and latency in input/output. Such limits require a deep revision on the way developments are carried on, but sustained collaboration between ocean modellers and computer scientists is also key.

The usage of graphics processing units (GPU) is progressively accelerating the Earth system modelling the atmosphere and the ocean. This transition to modern massive supercomputers requires re-design numerical codes and HPC optimization/parallelization strategies. In the oceanographic community, codes have been progressively ported on hybrid CPU/GPU architectures: for example, Xu et al. (2015) provided a first example of porting of the POM on GPU architecture, focusing on adopted strategy for memory access optimization, new design of communications, boundary optimization overlapping approach, and I/O optimization, achieving over 400x speedup against a single CPU core, reducing energy consumption by about seven times. Liu et al. (2019) provided a description of the first parallel implementation and optimization of the ROMS on a *many-processor* system, the Sunway sw26010: the result showed that the speedup of optimised hotspot program can be up to 3.69x with respect to original ROMS one. Such examples demonstrate how future complex computing architectures can be exploited for accelerating ocean models execution, benefiting operational systems, and opening new frontiers in numerical modelling.

Growing application requirements push from petascale to exascale: in the near future larger datasets, more parameters, much more computing, more need for parallelism, and large power consumption will be available. These improvements are strictly connected to evolutions in climate and ocean modelling that aim to represent real-world systems characterised by multi-physics and multi-scale interaction in space and time, opening to predictive science.

5. https://marine.copernicus.eu/sites/default/files/media/pdf/2020-10/CMEMS-requirements-satellites.pdf

Exascale computing is then the next frontier to build global climate systems at the optimal model resolution that requires a high level of performance capabilities but remaining within a specific power budget. Operational centres need to account for heterogeneous computing resources: heterogeneous computing aims to match the requirements of each application to the strengths of CPU/GPU architectures (Mittal and Vetter, 2015). The collaborative framework among different hardware components is an open research field that aims at:

- Port large-scale codes written in CPU or GPU-suited languages into heterogeneous computing systems minimising overhead and error-prone;
- Design new suitable data-access strategies to take full advantage of fused CPU-GPU systems;
- Reduce use of more classical programming languages like Fortran in favour of more modern computing languages such as Python;
- Increase data analytics capacities;
- Decrease energy consumption towards Green Computing.

12.4.
Future evolutions in ocean data assimilation for operational ocean forecasting

Emerging observing technologies provide impetus to the development of DA systems. Operational ocean DA systems are constantly evolving their application of improved data assimilation methods, their use with increased resolution models and models with increased complexity, their use of new and upcoming observing technology, and their use of new community DA software and computer hardware infrastructures. Below is a summary of some of the areas in which DA is expected to evolve in operational forecasting systems over the next 10 years.

In terms of the DA methodology, the most immediate development is the merging of ensemble and variational methods. Drawing on the strengths of both approaches, the "hybrid" approach is being developed in a number of forecasting centres. The static or parametrized version of the background error covariances used in variational methods and the flow-dependent estimates from an ensemble are combined. Experience from NWP suggests that the hybrid approach performs better than an either pure variational or pure ensemble method (Lorenc and Jardak, 2018); efforts are underway to implement similar capability in global and regional ocean forecasting systems. These are likely to reach some maturity over the coming few years. More sophisticated DA methods, which do not rely on the assumption that forecast errors have an unbiased Gaussian distribution (such as particle filters, van Leeuwen et al., 2015), are being actively pursued to deal with, for instance, biogeochemical variables. Another growing area of methodological development is the application of machine learning to the data assimilation problem (Bonavita et al., 2021), particularly in regard to model error estimation, model parameter estimation, and the estimation of forecast error covariance statistics.

Ocean model resolution is constantly being increased as more computer resources become available. DA systems need to evolve to make sure they can deal with the larger range of scales in the models. The complexity of models is also increasing in both the ocean models themselves and the different types of coupled models being used. Applying DA methods to ocean/sea-ice models, physical-biogeochemical models, acoustic-physical models, and more complete earth system models that include many different earth system components, is an active area of research (Penny et al., 2019). Models used for operational ocean, sea-ice, and atmosphere forecasting on short timescales are increasingly becoming coupled together and the data assimilation methods needed to effectively initialise these systems are being developed. Most operational coupled weather forecasting systems do not currently use strongly coupled data assimilation methods, whereby ocean observations can directly influence the atmospheric analysis and vice versa, but they are expected to be developed and implemented over the next decade.

The software infrastructure needed to apply the data assimilation is also under development by several new community DA software systems, including the DART (Anderson et al., 2009), the OOPS, the JEDI, EnKF-C (Sakov, 2014), and the PDAF (Nerger et al., 2020). The computer hardware used to run forecasting systems is also evolving with different architectures such as GPUs, which will become a strong computational candidate for operational forecasting systems in a 10-year timeframe along with the evolution of numerical codes. The community software systems provide the opportunity for more collaboration between operational forecasting groups, and between operational and research groups.

12.5.
Future of ensemble prediction systems

Numerical ocean, weather, seasonal and climate forecasting systems across the world are tending towards becoming coupled ensemble data assimilation prediction systems (Brassington et al., 2015; Barton, 2021; Buizza, 2021; Frolov, 2021; Fujii et al., 2021; Komaromi, 2021), including a better coverage of the inter-relationships among the geophysical domains of the ocean, atmosphere, sea ice, land, and biogeochemistry (Sandery et al., 2020; O'Kane et al., 2021). Forecasting systems are also increasingly applied to finer spatiotemporal scales.

The need to quantify the probability distribution of forecast error in coupled and downscaled models, as well as the reliability and accuracy of forecasts, will be served well by ensemble prediction systems, such as those using the EnKF (e.g., Sandery et al., 2020; O'Kane et al., 2021; Sun et al., 2020; Minamide and Posselt, 2022).

Ensemble prediction systems enable synthesis of models and observations leading to data that can be used to provide best estimates of geophysical variables and quantify the dynamics of their uncertainty (Sandery et al., 2019) (Figure 12.2). Uncertainty quantification will become as important in forecasts as the forecasts themselves, providing guidance on reliability and insight into fast growing disturbances in the geophysical environment. As described in other sections of this chapter, advances in ensemble prediction will also be coupled to improvements in models, observations, data assimilation, computer resources and technology.

There is an associated loss of predictability towards finer scales (Jacobs et al., 2021). Prediction systems using coupled data assimilation and finer spatial resolution will require larger ensembles, more frequent, representative and accurate observations, and improved data assimilation practices. Extending the range of predictability will be facilitated by advances to ensemble prediction systems. Operational ensemble systems will incorporate improved methods for data assimilation in the presence of model error and strong non-linearities, such as the iterative EnKF (Sakov et al., 2017), hybrid covariance methods (Kotsuki and Bishop, 2022), and assimilation of non-linear observations such as water vapour, cloud, precipitation, sea-ice, and phytoplankton concentration (Bishop, 2016; Posselt and Bishop, 2018).

Combining ensemble prediction with machine learning and artificial intelligence will also play an increasing role in forecasting (Brajard et al., 2021; Weyn et al., 2021). In some instances, forward models with reduced order low dimensional and data-driven differentiable emulators (Maulik et al., 2021) will be able to replace full non-linear models to reduce computational cost and assist in searches for initial conditions, patterns, parameterisations and ensemble perturbations appropriate for particular forecasts. Ensemble prediction systems will be used to identify initial states, forcing and dynamics that contribute to regime transitions (O'Kane et al 2019; Quinn et al., 2020) and in the forecasting of extreme events (Hawcroft et al., 2021).

Forecast model parameters will continue to be poorly known, subject to uncertainty, dependent on grid resolution, and a source of model bias requiring joint state and parameter estimation (Kitsios et al., 2021). With this approach, predictability of certain geophysical processes may be improved (Zhang et al., 2017). Future ensemble prediction systems will be optimised with model parameters that minimise bias in the ensemble mean but that adequately represent the parameter's error probability distribution in the ensemble (Gao et al., 2021). Coupled model forecasts will be able to be optimised in state and parameter space. Model error minimization will be multi-variate and simultaneous across the geophysical realms with respect to the global network of observations (Sandery et al., 2020).

Ensemble prediction systems will play an increasing role in the future design of observation systems (Sandery et al., 2019 and 2020). Coupled ensemble prediction provides insight into unobserved variables through cross domain covariances. Future applications of coupled ensemble prediction systems will provide improved reanalysis products with tighter constraints on carbon, sea-ice volume, air-sea fluxes, ocean heat storage and transport, using optimally designed observing systems.
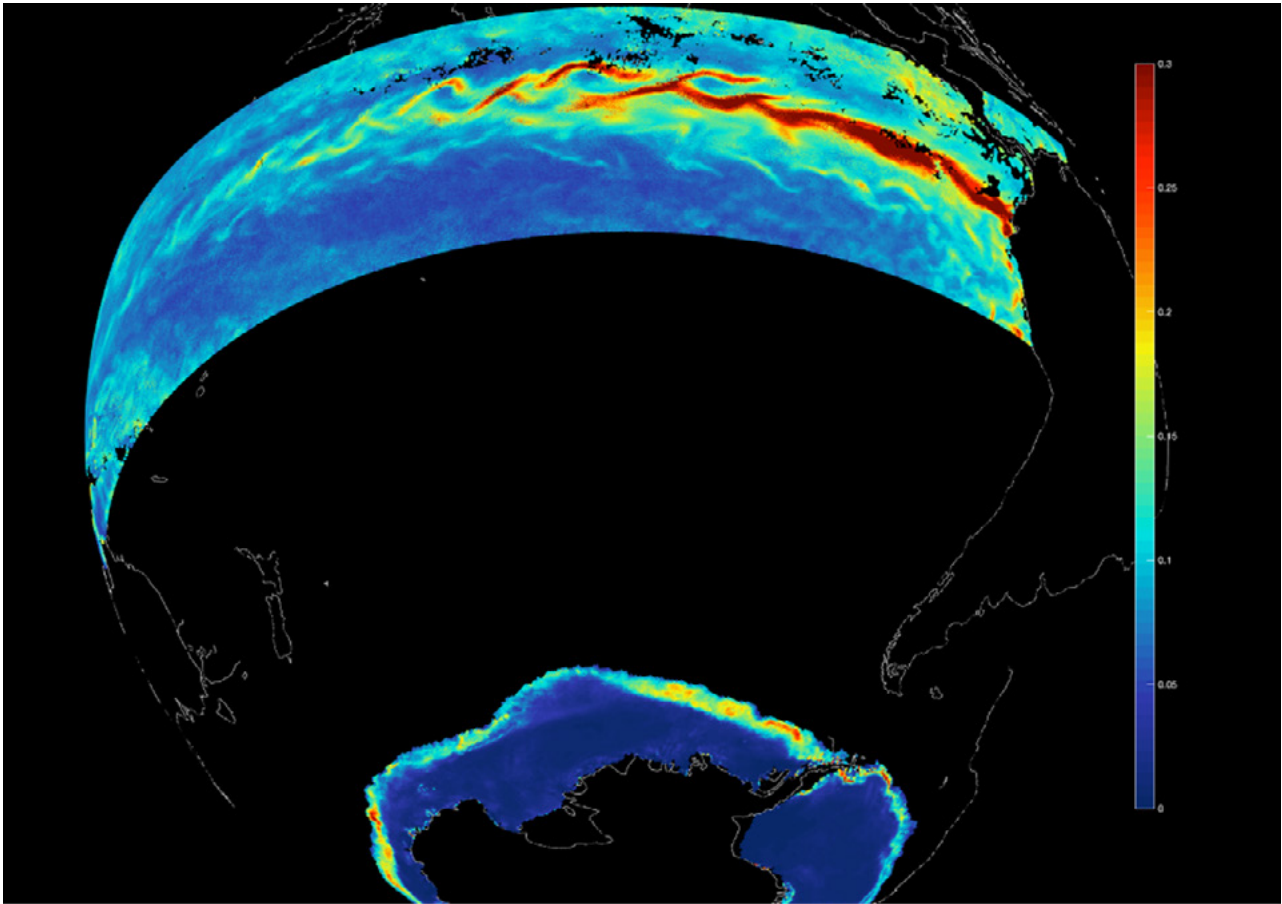
Figure 12.2. Quantifying the dynamics of system uncertainty. This image shows forecast ensemble spread in sea surface temperature (K) and sea ice concentration on 28th September 2017 (in observation space) from a 96 member, 0.1o horizontal resolution coupled ocean-sea-ice EnKF prediction system, known as ACCESS-OM2-EnKF-C (Sakov, 2014; Kiss et al., 2020). SST spread is related to uncertainty: the forecast dynamical state of Tropical Instability Waves and sea ice spread shows that forecast uncertainty at this time of year is greatest in certain areas.

Unstructured mesh models that enhance resolution towards the coastline for detailed hydrodynamic and biogeochemical forecasting of coastal and river, lake and estuarine circulation processes (Herzfeld et al., 2020) will be run as ensemble prediction systems. Meshes that adapt resolution according to areas of most rapidly growing geophysical instabilities, such as in tropical cyclone, tsunami, and flood forecasting (Beisiegel et al., 2021) will also be run as ensemble prediction systems.

As systems continue to be developed, improving the accuracy of forecast error covariance estimates will deliver coupled downscaled analyses and forecasts with greater skill. With advances to observation systems, relatively higher resolution monitoring and ensemble prediction of sea-ice, waves, currents, sea-levels, temperatures, biogeochemistry, and the tracing of river plumes containing sediments, contaminants, and pollutants may be made possible using ensemble prediction systems. Access to future higher resolution ocean in-situ and satellite data may enable prediction of the

ocean sub-mesoscale circulation and near-field currents for search and rescue, ship-routing, safety, and recreation. As science, technology, networking, and connectivity improves, real-time assimilation of user-supplied observations into ensemble prediction systems to augment local predictability may become possible.

12.6.
Opportunities of artificial intelligence for ocean forecasting systems

Recent developments in AI open many interesting opportunities in the context of operational oceanography and ocean forecasting systems. Operational forecasting systems are indeed not only based on observational data but also on algorithms. These algorithms gather and encode our understanding of physical systems and their dynamics, as well as of observation networks and associated uncertainties. They also reflect our collective knowledge on the relevant criteria for evaluating ocean data products. As in many activities relying on algorithms, the emergence of artificial intelligence, and especially of deep learning, opens a number of new possibilities, and is therefore the subject of growing interest in our community.

The ML generally refers to all the methods used to build algorithms whose components and parameters are not defined a priori but are trained according to a given objective. This field encompasses a large number of different methods, algorithms, and training strategies. It is a wide and fast-moving research field that includes, but is not restricted to, deep learning. ML is also intimately linked to a technological landscape and a software ecosystem in constant evolution. These technologies allow researchers and engineers to assemble complex algorithms from elementary building blocks in a very versatile and modular way, with interesting performances compared to state-of-the-art methods in many disciplines.

Applications of artificial intelligence are currently in vogue but, beyond the hype, artificial intelligence and machine learning can help us to overcome some of the current limitations of ocean forecasting systems. Ocean models and data assimilation methods, which are the scientific underpinning of current ocean forecasting systems, are indeed facing important challenges. Performing large ensemble simulations with full ocean models at increasingly fine spatial resolution is becoming more and more difficult computationally. We still do not know how to fully exploit hybrid computing architectures in our systems. We do not have a robust and plug-and-play framework to adapt their complexity to new custom applications. Although they are constantly being improved, our systems are also becoming increasingly difficult to modify and maintain. As developed in the following subsections, AI and ML may well help us to overcome these limitations and may even deeply impact on the structure of our operational systems.

12.6.1. Expected contributions of machine learning to ocean forecasting pipelines

Machine learning has long been used in ocean sciences and operational oceanography. However, these applications have so far mostly been limited to data retrieval algorithms upstream of forecasting systems (remote sensing, quality control), or to data processing and analysis in downstream applications (data mining, data fusion). In this context, ML algorithms have been essentially seen as black boxes without much physical basis. This perception is fundamentally renewed with the emergence of physics based machine learning and differentiable programming, which now allow to bridge physical sciences, scientific computing, uncertainty quantification, and machine learning (Carleo et al., 2019).

If we adopt a data-centric viewpoint, ocean forecasting systems can indeed be described as a succession of independent data processing steps in sequential pipelines (see Figure 4.1). These pipelines include the collection of past observational data, data-assimilation to reconstruct the current state of the ocean, forecasting with a physics-based model, and eventually the post-processing and dissemination to users. Data is being processed with algorithms at each step of the pipelines. It is now obvious that modern machine learning has the potential to impact each step of the data-processing pipelines of operational oceanography and ocean forecasting systems.

As mentioned above, many applications can be identified upstream or downstream of the core engines of ocean forecasting systems. Typical applications of ML upstream of core engines include, for instance, algorithms for alleviating observational noise, for retrieving parameters (Malmgren-Hansen, 2021), or for data quality control (Castelão, 2021). ML can thus be used for detecting outliers in Argo profiles (Maze et al., 2017). The range of possible downstream uses of core forecasting engines is even wider. ML is here expected to help design tailored services addressing key challenges (Persello et al., 2022), such as improving the prediction of Lagrangian drift or detecting anomalous extreme events.

However, what is probably more difficult to perceive is how machine learning may soon affect the core engine of ocean forecasting systems, and eventually all the services to users. Machine learning and differentiable programming are indeed opening many opportunities in computational fluid dy-

namics (Vinuesa and Brunton, 2021), while deeply renewing inverse methods in many areas (Cranmer et al., 2020). These recent advances could be leveraged for improving ocean models, e.g. for better accounting for unresolved processes (Brunton et al., 2020; Zanna and Bolton, 2021). They could also help improve data assimilation schemes (Bonavita and Laloyaux, 2020), or even possibly replace full inversion pipelines (Fablet et al., 2021).

These recent advances open the possibility to design and train our core forecasting engines in such a way that their complexity and performance could be optimised for specific applications, ultimately improving our ability to meet the diversity of user needs.

12.6.2. Designing fully trainable ocean forecasting systems core engines

The core engines of current ocean forecasting systems are based on two types of objects that are still quite independent, namely ocean circulation models and data assimilation methods. Ocean models, data assimilation methods, and their implementation in forecasting systems are being continuously improved. But our core forecasting engines are still rather static in their design and structure, due to technological, organisational and historical reasons. For instance, ocean models are generally developed without taking into account how they will be implemented with data assimilation. As such, there is no guarantee of the optimality of the overall design of our systems and its fit for purpose in specific contexts.

Recent developments at the interface of machine learning and scientific computing could open the possibility of optimising the design of our core prediction engines according to predefined objectives. Indeed, beyond the improvements of specific components of ocean models or data assimilation schemes, the real benefit to be expected from machine learning in forecasting systems is the ability to optimise entire pipelines with end-to-end strategies. The term end-to-end here refers to the ability to optimise components of processing pipelines based on metrics measuring the performance of the entire pipeline. End-to-end strategies may eventually allow the design of fit for purpose and user-centric processing chains and products.

There are obviously technological conditions to realise this potential. Integrating trainable components in core forecasting engines is indeed greatly facilitated if these engines are already composed of independent modules with robust and stable interfaces. It is therefore necessary a gradual evolution to make the system more modular and composable. Moreover, if we want to take advantage of end-to-end strategies, the core engines should be fully differentiable. This would allow to back-propagate a misfit in the prediction into

an increment in the parameters of the engine. This is only possible if the core engine is written in a high-level differentiable language or programming framework.

Such prerequisites may at first appear daunting, but a gradual evolution towards modular, composable, and differentiable core engines would also have important side benefits. First, this effort to redesign our core engines, may actually provide a viable strategy for exploiting upcoming computing architectures, starting from GPUs (Kochkov et al., 2021). It may also simplify the maintenance of our engines, as for instance the development of adjoint models (Hatfield et al., 2021), therefore speeding up the transfer from research to operation (R2O). Another benefit is also the built-in treatment of uncertainties, thanks to recent advances in probabilistic programming (van de Meent et al., 2021) and Bayesian Machine Learning 🔗[6].

12.6.3. Towards user-centric, ocean digital twins leveraging lightweight emulators

Looking further ahead, it can be guessed what future digital twins of the ocean will eventually look like. The integration of AI components may indeed gradually change the underlying paradigm of ocean forecasting systems. While current systems essentially implement "single-core engines" with a predefined level of complexity, future systems may be based on collections of core engines, tailored to the specific needs of particular users. These tailored core engines would instantiate core methods and building blocks in a versatile and user-centric way, providing fit for purpose tools and products to users.

Whatever form digital twins will eventually take, a key methodology will be the ability to train emulators of existing systems at reduced costs and with controlled complexity. As described above, a gradual evolution of our core forecasting engines will be needed for leveraging the full potential of AI and ML. This transition may in particular leverage DDEs. They provide approximations of pre-existing algorithms (Kasim et al., 2021) and can be integrated in data assimilation schemes (Nonnenmacher and Greenberg, 2021). As such, DDEs offer a good solution for building upon existing expertise and tools, while benefiting from the pace of scientific and technological advances in AI.

---

6. https://jorisbaan.nl/2021/03/02/introduction-to-bayesian-deep-learning.html

In conclusion, it appears that we are at the beginning of an exciting phase in the evolution of ocean forecasting systems, which could deeply transform the entire service offered to users. The integration of AI in ocean forecasting systems will require a gradual but profound change of the algorithms that constitute their underpinnings. This transition will take advantage of the wealth of expertise on ocean physics, observing networks, and user needs available in ocean forecasting centres. It will also require developing and nurturing new collaborations with the broader AI technological and scientific community, and benefit from the adoption of open science practices.

12.7.
Seamless prediction

Palmer et al. (2008) used "seamless" to refer to predictions across the range of weather and climate time scales, e.g. ranging from forecast in days to projections in decades. The WMO, in its document "Seamless prediction of the Earth system: from minutes to months" (WMO, 2015), further developed this concept, with a main focus on the weather component but also starting to consider its importance for the ocean. Then, within EuroGOOS this concept has been expanded to promote next generation of ocean services able to seamlessly span spatially from global ocean to coastal areas and estuaries as a continuum with high resolution information (She et al., 2021). To achieve the objectives of the seamless approach, numerical ocean models need to evolve (Chassignet and Xu, 2021; Fox-Kemper et al., 2019) towards:

• Use of nested and regional downscaling simulations, by means of high-resolution spatial grid spacing or using variable-resolution and multi-scale modelling;
• New parameterizations and improvement of the existing ones (e.g. air-sea parameterization, turbulence and mixing, internal tides, vertical convection, coastal estuaries interface with open ocean);
• More direct simulation of sea level changes and tides.

Seamless is also connected to coupling as global coupled ocean-atmosphere-land-ice modelling systems are used to perform climate change projections and studies, from decadal to seasonal timescales (Hewitt et al., 2017). The overall advancements of numerics in ocean dynamics, biogeochemistry, weather modelling, and hydrology open new opportunities for coupled systems to address predictions on short-range timescales from regional to coastal scales.

In order to establish a seamless marine information service, integrated and unified ocean observing systems and seamless unified modelling and forecasting systems should be developed. Integrated ocean observing implies that ocean observations made by multiple sectors for all subsystems with multiple means - remote sensing, robotics, and in-situ - are integrated, while monitoring schemes and data management are designed in an unified way, so that the observations, after being integrated with the seamless models, will be able to fit users' purposes. Furthermore, ocean observing should be cost effective and sustainable.

The seamless models can be based on mathematical equations or statistical and AI algorithms, which simulate or emulate marine physical-chemical-geological-biological systems. There are still significant gaps in current forecasting capacity to reach seamless predictability. The development of a seamless modelling capacity will be discussed in the next subsections from three aspects: space, time, and system of systems. The seamless ocean earth system prediction models should be based on UOMs and including atmospheric models. Development of UOMs has been identified as one of the four EuroGOOS research priorities (She et al., 2016).

12.7.1. Optimal use of modelling workforce and model consolidation

A seamless UOM modelling framework should be developed to leverage global efforts to enable joint code development. One notable feature of the ocean modelling community is the great diversity of the models but the very limited research workforce for each model. An incomplete survey of ocean circulation modelling by EuroGOOS (🔗[7]) showed that EU countries use 32 ocean models for operational and/or ocean climate modelling, among which 24 were developed in the EU and 8 from the US. Twenty ocean circulation models have been used in Europe for operational forecasting (Capet et al., 2020). In the US, at least ten ocean models are currently used for operational forecasts. If this count would be extended to ocean circulation models developed and used in other countries (i.e. Australia, Canada, China, and Japan) the number of ocean models in use could be huge. It is well-known that a significant workforce is needed to keep an ocean model at the state-of-the-art.

---

7. https://eurogoos.eu/models/

However, each ocean modelling group has only a very limited workforce for ocean model development. Even though joint or community model development has improved the situation for a small number of models, the number of ocean model developers is still far from sufficient for most of the models. Therefore, it is necessary to optimise the use of ocean modelling workforces focusing only on a limited number of models. The future UOMs can be made so that one model would have options with multiple coordinates and parameterizations, hence emulating different model behaviours.

Optimal use of modelling workforce should be coordinated in national, regional (such as the GRAs), and global scales so that the UOMs in different scales can be well addressed and consolidated with a critical mass of model developers. However, it is not always possible to have a critical mass of model developers at the national level, as only countries with strong national investment in ocean science have such a capacity. It is easier to reach a critical mass at the regional or global levels. In fact, most of the effective modelling co-operation is carried out at regional level. The global co-development of models is probably less active due to both administrative and political barriers. It is highly recommended to strengthen global collaboration on UOM development.

12.7.2. Development of seamless UOM for multiple temporal scales

Predictability in an ocean earth system has a multi-scale feature, relating to the spatiotemporal scales of its subsystems as well as their interactions, which can be divided into forcing-based predictability, self-constrained subsystem predictability, and coupled system predictability. For atmospheric systems, according to the high-resolution global forecast model experiments, the upper limit of the self-constrained predictability for deterministic prediction is two weeks. Longer-scale predictability is related to blocking events with time scales ranging from weeks to years, e.g. MJO, PNA, NAO, AO, ENSO, QBO, which relies on interaction between atmosphere and ocean-ice systems and solar radiation. It is well-known that the surface ocean is mainly dominated by forcing-based predictability, i.e. variability of waves, ice and sea level in synoptic scale are largely determined by weather conditions. Subsurface ocean and sea ice can store forcing signals and release them to affect the atmosphere at a "slower" pace. This generates longer predictability in the coupled ocean-ice-atmospheric system. MJO, PNA, NAO, AO, and ENSO are all phenomena generated in such a coupled system. As stated by Brian Hoskins in the WMO Lecture 2011[8]: "The background provided by the longer time-scales and by external conditions, and the phenomena that occur on each range of time-scales in the seamless weather-climate prediction problem, give the promise of some predictive power on all time-scales".

---

8. https://public.wmo.int/en/bulletin/predictability-beyond-deterministic-limit

Most of these long-scale processes can still not be predicted successfully by current coupled-system models. UOM development is a key to improve the earth system predictability in the current stage as it will provide insight knowledge, as well as simulate the processes that the ocean-ice system filters, absorbs, and transfers the atmospheric signals into a slow-motion signal and then feeds back to the atmosphere.

To reach breakthroughs in longer-scale predictability, it is important to consider that: i) ocean earth system forecast is a probability prediction problem; ii) multi-model ensemble has shown expanded atmospheric forecasting skills than the deterministic prediction; iii) shorter-scale phenomena, although constrained by longer-scale ones, are also a statistical forcing to the longer-scale, thus should not be treated only as noise; and iv) solar radiation, volcano eruption, and changes of pollutants in both ocean and atmosphere can affect the intrinsic signals in the system and then should be included. UOM development should address these issues.

12.7.3. Geographic configurations and seamless UOM in space and in a marine system of systems

For a coordinated UOM development, proper geographic scales should be defined as well, so that both scientific requirements and collaboration needs are met. Three types of forecast UOMs can be expected: i) global-scale coupled UOMs aiming at longer-scale prediction of the earth system, which is not necessarily high resolution but should be able to use short-scale as a statistical forcing; ii) global and regional scale coupled models aiming at produce refined forecast within a "foreseeable" time, e.g. a month, for which high resolution will be important; and iii) for "touchable" spatiotemporal scale, i.e. inland water-estuary-coastal-regional sea in space and a few days in time. It should also be noted that the smaller-scale UOMs can be easily applied to long-term forecast applications when forecasts at boundaries are well defined.

The coupled UOMs will mainly be developed for global and regional scale to address longer scales from months to seasons. For the regional scale coupled UOMs, geographic coverage should be sufficiently large to reflect impacts of the atmosphere-ocean coupling. The resolution of the coupled UOMs can be a few kilometres (mesoscale resolving) for global scale and hundreds to thousands metres for regional scale to resolve sub-mesoscale eddies and narrow straits connecting sea basins. Therefore for regional scale coupled UOMs, flexible grid and high-performance computing are two basic requirements. For one regional scale there might be more than one coupled UOM.

High resolution is required to provide a seamless prediction in space. For example, narrow straits connecting two large water bodies and archipelago water areas may need a res-

olution of 100-1000 m; inland waters-estuary-coastal-open sea continuum, essential for pollutant transport modelling, nutrient cycle, and carbon cycle modelling, needs also a similar model resolution. An even higher resolution (10-100 m) may be required when dealing with river inputs to the sea, impact of flooding, hydropower, barriers to pollutant transport, coastal inundation, compound flooding-surge events, and port management. Hence, a spatial seamless UOM should have flexible grids, either unstructured grid or dynamic two-way nested grid.

12.7.4. Evolution in short-, mid- and long-term perspectives

In short- to mid-term (3-5 years) perspectives, the objective would be to develop a UOM framework and continuous improvement of prediction skills of the marine earth system models with a forecast range of 10 days to 1 month. The research should focus on: (i) establishing UOM global cooperation framework to harmonise, coordinate, and further evolve existing UOM development work; (ii) designing the UOM concept, framework, and multiple configurations for different scales, considering international cooperation and sharing of best practices, optimal use of workforce, critical mass for

UOM development, code portability, relocatability, scalability, flexibility, resolvability, and reducing the redundancy of models; (iii) improving model process description, so that each UOM sub-model can effectively model major features in the subsystem; (iv) investigate possibility for establishing forecasting capacity in emerging modelling areas, such as SPM, marine litter, underwater noise, and fisheries, and also develop prototype pre-operational models in these areas; v) improving high-performance computing through code modernization; (vi) improving the UOM subsystem coupling; and (vii) develop high-resolution models with flexible grids and interfaces with basin and global scale models, as well as resolving coastal processes for downstream applications

In the long-term (10 years), the objective is to improve prediction skills in time scales from months to seasons for climate, physical, and biogeochemical systems, establish and improve forecasting capacity in emerging areas such as SPM, marine litter, underwater noise, and fisheries. For the ESP in seasonal and longer scales, coupled UOMs including atmosphere-ocean-wave-ice coupling and ocean-optics-SPM-biogeochemical coupling will be developed for ensemble prediction. UOM code will also be optimised for efficient hybrid parallel computing.

12.8.
Operational forecasting and scenarios in a digital ocean

A Digital Twin of the Ocean (DTO) is a highly accurate model of the ocean to monitor and predict environmental change, human impact, and vulnerability, with the support of an openly accessible and interoperable dataspace that can function as a central hub for informed decision making (Figure 12.3) (see for example 🔗 [9]). Such an information system consists of one or more digital replicas of the state and temporal evolution of the oceanic system constrained by the available observations and the laws of physics, making imperative to integrate a set of models or software that pairs the digital world with physical assets, and to feed this set with information from sensors.

A DTO aims to deliver a holistic and cost-effective solution for the integration of all information sources related to seas and oceans, like in situ-data and satellite information combined with IoT techniques, Citizen science, state-of-the-art

ocean modelling together with AI and HPC resources into a digital, consistent, high-resolution, multi-dimensional, and near real-time representation of the ocean. This will result in a shared capacity to access, manipulate, analyse, and visualise marine information. The knowledge generated by the DTO platform will empower scientists, citizens, governments, and industries to collectively share the responsibility to monitor, preserve and enhance marine and coastal habitats, while promoting action and sustainable measures in the framework of the blue economy (tourism, fishing, aquaculture, transport, renewable energy, etc.), contributing to a healthy and productive ocean.

9. https://digitaltwinocean.mercator-ocean.eu/

Figure 12.3. Schematic representation of Digital Twin of the Ocean concept.

12.8.1. Construction of an open DTO service platform

To properly address the construction of a digital twin, break-throughs are needed in various aspects of the digital twin information system, including information completeness and quality, information access and intervention, as well as the underlying supporting infrastructure, tools, and services. The operational pilot of DTO, under development at Europe-an level, will encompass the production of a new quality of information, incorporating human systems in the prediction problem and leveraging advances in information theory and digital technologies. Ensembles of simulations combining models from different disciplines, informed by spatial cor-relations determined from high-resolution observations and by data-driven learning of unknown processes and missing constraints, will enable the DTO to reduce uncertainty in esti-mation and forecasting of ocean states, changes, and impacts.

Enhancing information quality requires a step change in computational complexity. This means adequate infrastruc-ture including support of very high computing throughputs, concurrency, and extreme-scale hardware. However, it is im-portant to conceal this complexity so that users can run and configure involved workflows and access the information but without requiring expert intervention. In addition, the underlying models and data need to be scientifically sound.

This will require a multi-layered software framework where tasks like simulations, observational data ingestion, and post-processing are treated as objects that are executed on federated computing infrastructures, feed data into virtual data repositories with standardised metadata, and from which a heavily machine-learning-based toolkit extracts information that can be manipulated in any possible way. The result should be the provision of on-demand, conveniently accessible mod-elling and simulation products, data and processes or MSaaS.
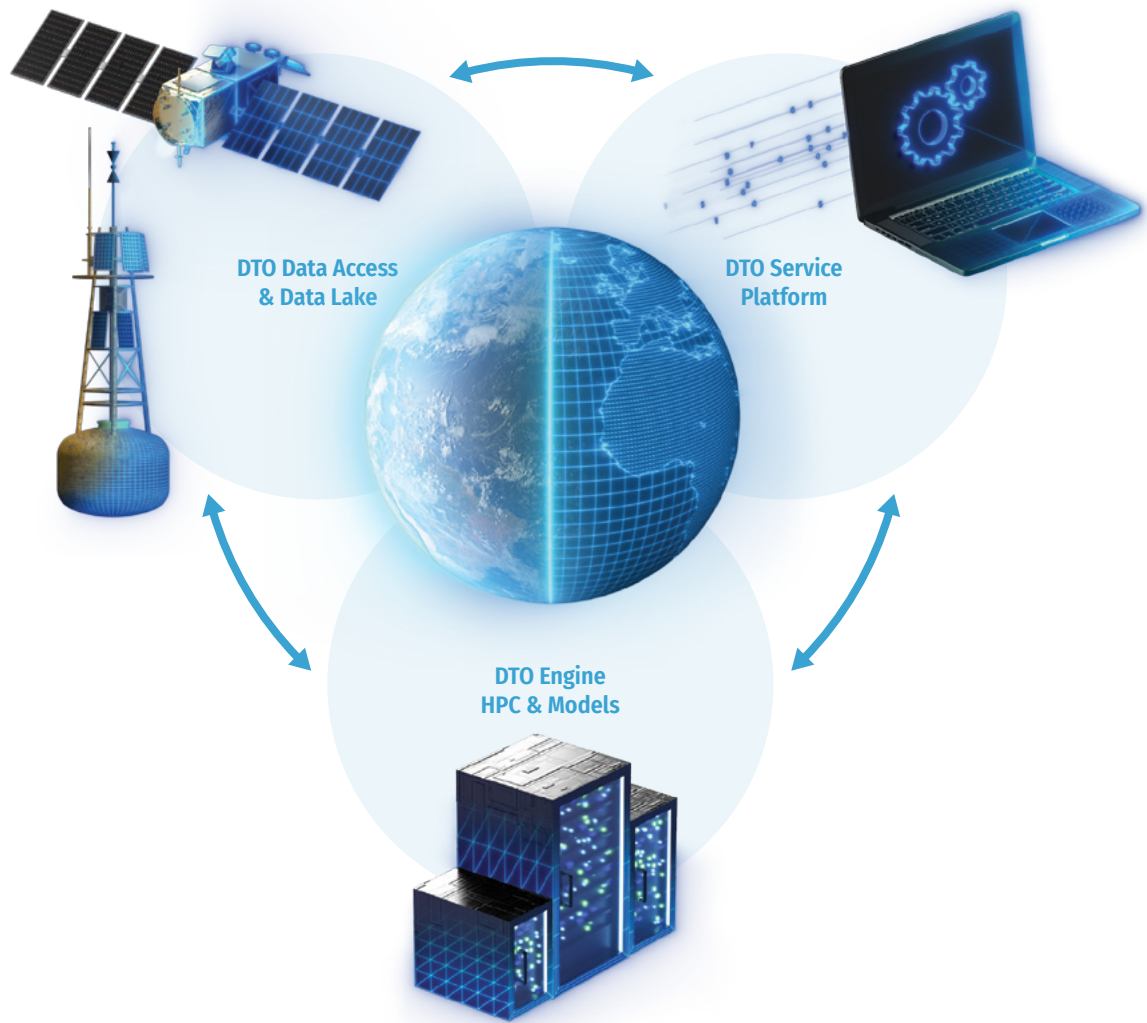
Figure 12.4. DTO Architecture.

12.8.2. Underlying architecture

The multi-layered framework enabling this digital twin ocean pilot operational service comprises 3 major interrelated structural elements (Figure 12.4):

• A DTO data access layer that mixes results and tools from ongoing projects and existing infrastructures with new developments targeting data ingestion, and data harmonising into a Data lake for subsequent use in the DTO engine;

• A DTO engine comprising a set of modelling capabilities, including on-demand modelling and what-if scenario modelling that fill the observational gaps in space and time in a physically consistent way, and observation-driven learning of unknown processes and missing

constraints, which will enable to reduce uncertainty in estimation and forecasting;

• A DTO interactive service layer supplying tools, libraries, and interfaces to simplify running and configuration of workflows, as well as access to information, including its analysis and visualisation.

12.9.
Quality assessment for intermediate and end users

As described in Chapter 4, PQ assessment is an essential service component for any operational oceanographic centre. In the case of climate and short-term forecasting services, validation of ocean models (physical and biogeochemical) is a crucial issue. Despite the continuous progress of the services towards providing regularly updated quality information, there are still gaps and deficiencies in the operational capacity to assess model solutions. It is still challenging to properly quantify the uncertainties in real time and in a way that is directly understandable and useful to the users. Capet et al. (2020), in their review of the operational modelling capacity in European Seas, pointed out that only 20% of operational coastal model services provide a dynamic uncertainty together with the forecast products. This deficit in terms of operational model validation processes may be mainly linked to the lack of real-time access to a local ocean observation network.

This limitation seems to be partially alleviated within core services that have a regional or global focus. In these services, the PQ processes seems to be favoured by: 1) a wider scope (services dealing not only with forecast models but also with the monitoring component and observational data products); 2) a more integrated data use (for instance through data assimilation in ocean analysis and reanalysis products); and 3) wider spatial coverages (allowing the use of a higher number of observational data sources to validate model predictions). The Copernicus Marine Service is one of these core comprehensive services and in recent years has built some standards for model assessments and delivery of PQ information to end-users. This service, and its evolution roadmap in terms of PQ processes, can illustrate the main expectations for the future evolution of validation and quality information on operational oceanography products.

As described in Sotillo et al. (2021), the Copernicus Marine Service ensures:

- Standardised processes to assess each product's scientific quality against appropriate metrics;
- Product quality information regularly updated and available from a central website, called the "PQ-Dashboard" (https://pqd.mercator-ocean.fr/);
- Specific PQ documentation delivered with each Copernicus Marine Service product, completed by regularly updated quality summaries, including fit for purpose information, and evolving towards peer reviewed technical reports.

From this baseline, the Copernicus Marine Service Product Quality Strategic Plan 🔗 [10], identified a list of developments, challenges and opportunities foreseen for the next Copernicus-2 service phase period (2022-2028). The availability of an increasing number of ocean observations should enable and support new developments, and eventually improve the information quality associated with oceanographic products. The three main working lines along which the plan will unfold are discussed in the following subsections and shown in Figure 12.5: future observations, future developments in OO centres, and future quality information. These lines are the way forward for the future development of model validation and quality assessment techniques.

12.9.1. New observations for improved quality assessment

The use of new satellite products (e.g. from next Sentinel missions or wide swath altimetry) will enable a significant increase of data coverage towards higher resolution, allowing not only a quality increase but also more validation opportunities for a wide range of operational oceanography products. The continuation of the BGC-Argo and Deep Argo missions and networks are crucial for providing quality information in areas and on variables that are still highly undersampled. The potential extension of Argo coverage towards coastal areas may also be essential for its important socio-economic impact and the benefit for coastal model assessments. In that sense, there are some on-going initiatives in the framework of R&D Projects (such as the Euro-Argo RISE H2020 one) to test Argo on shelf extensions, targeting shallower waters in European marginal seas.

Additionally, operational oceanography centres should improve the effective use of existing observing products and networks through:

- Upgrade of PQ processes to properly assess high frequency datasets: PQ metrics are generally computed daily. However, currently, and to a greater extent in the future, some near real-time (NRT) model product datasets that are delivered with higher frequency (i.e. every 15 minutes) would need a dedicated assessment.

10. https://marine.copernicus.eu/about/service-evolution-strategy
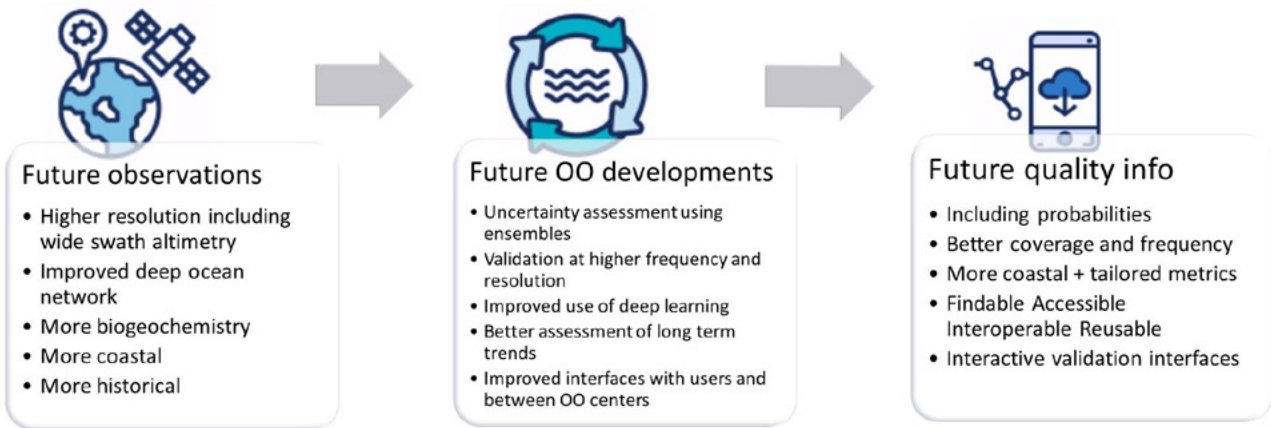
Figure 12.5. New observations enable new developments in operational oceanography centres, which will also benefit from growing computational resources and advanced AI and big data techniques. This will allow significant improvements of the quality information, improving its relevance and its frequency.

• Enhancement of water mass assessment at synoptic scales: at present, sampled only partially. To improve their characterisation in the upper ocean, it is necessary to extend the use of available observational platforms (i.e. more ship of opportunity measurements, thermosalinograph/ferry box data, new glider opportunities, sea mammals). Below 2000m, water mass distributions are still poorly understood, and historical data do not guarantee the reliability of existing climatologies. Deep floats and deep ocean observations also need to be considered to support global prediction assessment.

• Promote the use of data from specific multi-platform campaigns (specially in hot spots): regular and periodic campaigns in the same waters are necessary for climate monitoring and periodic model assessments (i.e. glider periodic missions along straits); current measurements are also much needed (both Lagrangian and Eulerian observations), not only for temperature and salinity.

• Ensure easy access to historic observations: there are large amounts of data from research surveys that are either not available or available only in operational catalogues. These independent data (in the sense of not assimilated) can be crucial for assessing model performance. A progressive integration of this kind of data will be advantageous for forecasters, and its "discovery" is foreseen to increase. Access to these sources should be automated, data loss reduced, and the investment on data collection will be recovered. In the context of Copernicus Marine Service, EMODNET, EuroGOOS alliances or other networks, it is crucial for OO centres and data providers to connect initiatives and efforts to better in-

tegrate the existing ocean observing systems, as well as the new expected instruments/observations.

12.9.2. Expected development of quality assessment techniques

The use of ensemble data assimilation methods and the expected increase in the use of prediction systems based on model ensembles should significantly improve the quantification of model product uncertainty using probabilistic scores, the evaluation of error propagation, and of model systematic errors and attractors. An increasing number of high-resolution observations will be used to characterise model skill at all observed scales, while advanced statistical techniques (such as deep learning) should contribute to improve cross-validation capabilities between different types of observations, and between observations and models.

Errors in the ocean circulation models, in particular on vertical transport and mixing, strongly impact the coupled biogeochemical model solutions. Thus, monitoring errors in key parameters of the physical forcing should characterise errors (their causes) and subsequent impacts in biogeochemical solutions. The mixed layer depth variable is a typical example of this due to its impact on biogeochemistry processes.

Quality assessment of model downscaling should be eased in the future by advances in integrated systems (following on the idea of monitoring uncertainties "propagating" along the value chain). The added value of downscaling (higher resolution with better representation of the ocean processes) needs to be assessed through a more systematic comparison of global vs. regional and coastal models. To this aim, alternative/innovative validation metrics are needed for

model assessment that avoid double penalty when comparing different resolution models (Ebert, 2009). More relevant skill scores are needed for forecasting, implementing new approaches to validate and inter-compare new physical, and biogeochemical model products at very high-resolution.

Finally, there is a growing need to identify and understand long-term trends in ocean parameters and their impact at regional to coastal scale. The validation of such signals is challenging for physical and even more for biogeochemical parameters, such as carbon, oxygen, and ocean acidification, which are of great interest on both regional and global scales. It is crucial to improve the validation methodology and to increase the number of reference observations as much as possible.

12.9.3. Quality information communication improvements

There is an increasing demand for regional fit for purpose assessments, especially in coastal areas. The quality information content must evolve following users' needs. The current OceanPredict product quality metric monitoring has to be complemented with process- (and user-) oriented metrics, and better quantification of uncertainties. Probabilistic scores and robustness assessments with multi-product

(model and observed) intercomparisons should help answer many user requirements. The use of application-oriented metrics, such as Lagrangian drift metrics or "event oriented" metrics (e.g. categorical scores based on thresholds) should also be generalised.

The collaboration among forecasting services to agree on international validation standards must continue. Collaboration between forecast services and users should result in the introduction of new user-oriented metrics to be considered as local case studies and validation "benchmarks".

Operational oceanography centres will have to develop both high-level summarised quality information and high-resolution uncertainty estimates to be delivered alongside the products following FAIR guidelines, as initiated by Peng et al. (2021a, 2021b).

High-level quality summaries, such as product "maturity matrices", will guide users to choose the most appropriate product for a given use, while the uncertainty information delivered alongside the product will enable the access to tailored product quality information, as a valuable addition to many oceanographic applications.

12.10.
Expected future evolution of Copernicus Marine Service products and services

The first operational phase 2014-2021 of the Copernicus Marine Service has successfully implemented a service chain devoted to ocean information, involving committed producers throughout Europe, and serving expert users worldwide. The Copernicus Marine Service will develop an ambitious 7-year plan (Copernicus 2, 2021-2027) with staged implementation that answers to increasing user and policy (e.g. EU Green Deal) needs. The objective is to fully embrace the capabilities of new digital services and implement the next generation of ocean monitoring and forecasting for the Blue/White/Green ocean.

Copernicus Marine Service products and services are delivered by means of state-of-the-art, user-oriented, scientific and technical methodologies, which induces openness to newly developing ideas and associated capacities. Apart from guaranteeing service continuity, the Copernicus Marine Service is continuously evolving to ensure that its services and products remain state-of-the-art and meet a wide range

of existing and emerging user and policy needs related to all marine and maritime sectors: maritime safety, coastal environment monitoring, trade and marine navigation, fishery, aquaculture, marine renewable energy, marine conservation and biodiversity, ocean health, climate and climate adaptation, recreation, education, science and innovation.

The following major improvements of current products, as well as new products benefiting from science and technology advances, are already planned to ensure an enhanced continuity of the service, keeping the service at the state-of-art and at internationally competitive and fit for purpose standards, considering the European policies' priorities (Green Deal, Common Fisheries Policy, Marine Strategy Framework Directive, and Convention on Biological Diversity):

- High resolution monitoring, modelling, and forecasting of the blue ocean with an increase of the horizontal

resolutions of the current systems by a factor of at least 3 (e.g. global 1/36°, regional 1/108°). Coupling and interaction with waves, sea ice, atmosphere, biogeochemistry, and rivers will also be implemented for improved ocean forecasts. New high-resolution sea level observations from the SWOT wide swath altimeter mission, new ocean topography, sea surface temperature, salinity from the Sentinel, HPMC, CRISTAL, and CIMR missions will be included as observational products. These improvements will impact the different Copernicus Marine Service areas and their key applications: maritime security and safety, maritime transport, pollution monitoring and offshore operations, and coastal zone monitoring and forecasting.

• Probabilistic forecasting and extended (1-month) forecasts based on model ensembles, allowing a better characterization of model uncertainties in analyses and forecast. Data assimilation techniques will evolve toward more multivariate schemes to constrain in a more extended and coherent way the different inanimate components of the marine environment (physics, sea ice, and biogeochemistry). Coupled ocean/atmosphere data assimilation will also be implemented. Probabilistic forecasts will be instrumental for early warning systems, and to support decision-making based on operational products by better characterising the confidence level associated with the provided information.

• Reanalyses of the 20th century physical and biogeochemical data for the global ocean and the European regional seas, assimilating historical in-situ observations (e.g. sea surface temperature and tige gauges mainly for the first half of the century and temperature and salinity profiles from 1950 onwards). The purpose of these reanalyses is to better assess the past evolution of the ocean in response to climate change and to better monitor Essential Ocean Variables and Essential Climate Variables related to the ocean.

• Step changes in Arctic Ocean monitoring, modelling, and forecasting through upgrade in sea-ice models, improved coupling with the atmosphere and hydrology (river discharge and nutrient loads), higher-resolution, extended forecasting ranges from a week to a month, and ensemble forecasting for an improved characterization of forecasting uncertainties. Provision of icebergs' forecasts will complement the information produced for ice services. Improved satellite products on sea-ice detection and a pan-Arctic ice chart will complete the offer. These evolutions will address user needs regarding maritime transport (e.g. ship routine) and marine safety in sea-ice and iceberg infested regions, marine resources (fisheries and conservation) and climate change impact in the Arctic.

• Air/sea fluxes of CO_2 monitoring and modelling, including advanced modelling/data assimilation systems at global and regional scales as well as including error estimations. Foreseen developments also include processing and quality control of novel in-situ observations from the BGC Argo array and improvement of observation-based products derived from Neural Network methods. These evolutions are required by the Copernicus anthropogenic CO_2 service as well as for blue carbon monitoring.

• Coastal zone monitoring and forecasting with improved capacities to link and co-production between coastal systems with Copernicus Marine Service upstream systems. Consistency and river-ocean continuity will be ensured by using standardised methods to couple hydrological models (for river run-offs) with global, regional, and coastal ocean models. Time-series (past, present, forecasts) of standardised modelled river discharges of freshwater, nutrients, particulate, and dissolved matter will be provided. Coastal zone monitoring will also be enhanced through satellite observations – based on Sentinel (especially S1, S2, S3, and S6) and other missions - for nearshore bathymetry and shoreline position and their evolution, high-resolution winds, spectral wave information, detection of plastic debris, monitoring of marine litter, ecosystems, water quality, and sea surface temperature. Given the huge social, economic, and biological value of coastal zones, these improvements will contribute to a wide range of applications (coastal zone management, climate adaptation, coastal modelling, aquaculture and fisheries, navigation and shipping, marine renewable energy, oil spill management and search and rescue), supporting various policies and resilience to climate change.

• Marine biology monitoring and forecasting with major improvement in numerical models to represent processes (e.g. benthic/pelagic coupling, riverine inputs) increasing accuracy, advanced data assimilation techniques (e.g. combining state and parameter estimation), and new modules linking optical properties in the near-surface ocean to biomass to better couple ocean colour and subsurface data from in-situ such as BGC Argo. End-to-end ecosystem modelling will also be included to link along the food web low trophic levels (e.g. plankton) to mid-trophic levels (e.g. micronekton), and to high-trophic levels (e.g. predator fishes and marine mammals). Marine biology monitoring will also be enhanced through the improvement of gathering, processing, quality control, and characterization of biogeochemical and marine biology in-situ (e.g. optical and acoustic sensors) and satellite (e.g. S2, S3 and hyperspectral) observations in open and coastal oceans. These products will support international and European

Union objectives in terms of biodiversity, development of sustainable food resources, water quality, assessment of blue carbon in the overall carbon stake accounting.

• Long-term projections of the marine environment (both physics, biogeochemistry, and marine ecosystems) under climate change from global to regional scales (downscaling of climate scenarios), and associated consequences for main stocks of exploited fishes. These products will support climate assessments for decision-making on adaptation and mitigation of climate risks (e.g. coastal floods, surges, etc.).

• Enhanced digital services with online cloud processing capabilities for manipulating and processing data with advanced analytics and scientific computing software (e.g.

artificial intelligence toolboxes), access to Sentinel Level 1&2 data, marine data (e.g. from EMODnet, SAF, etc.), and connection to HPC computing nodes. This will consolidate the Copernicus Marine Service as a one-stop shop for operational and digital ocean services.

A document 🔗 [11] presenting the Copernicus Marine Service Evolution Strategy for R&D priorities has been prepared by its STAC 🔗 [12] and reviewed by MOI. This document details the expected future products and services by Copernicus Marine Service and the required developments. It is a living document, as it is updated periodically according to feedback from users and policy needs, the status of scientific developments achieved within and outside the Copernicus Marine Service community, and to the high-level Copernicus Marine Service evolution strategy.

12.11. The United Nations Decade of Ocean Science for Sustainable Development

At the beginning of the third millennium, ocean science was largely competent for diagnosing problems. However, its ability to offer solutions of direct relevance to sustainable development requires a massive upgrade.

The world needed a large-scale and adequately resourced campaign to transform ocean science empowering and engaging stakeholders across disciplines, geographies, generations, and genders, and of sufficiently long duration to deliver the lasting change that is required. In 2016, the IOC of UNESCO (🔗 [13]) initiated a concept for this campaign. In December 2017, this work culminated in the proclamation by the 72nd Session of the UNGA of the UN Decade of Ocean Science for Sustainable Development 2021-2030 (referred to as 'the Ocean Decade'). UNGA called on the IOC to prepare an Implementation Plan for the Ocean Decade in consultation with Member States, United Nations partners, and diverse stakeholder groups.

In 2021, the United Nations launched the Ocean Decade (2021-2030) (🔗 [14]) whose aim is to '*support efforts to reverse the*

cycle of decline in ocean health and gather ocean stakeholders worldwide behind a common framework that will ensure ocean science can fully support countries in creating improved conditions for sustainable development of the Ocean'. In this framework, the IOC plays an important role: it coordinates the Decade's design and preparation, identifies programmatic contributions, and implements the Decade.

The vision of the Ocean Decade is '*the science we need for the ocean we want*'. The mission is '*to catalyse transformative ocean science solutions for sustainable development, connecting people and our ocean*'.

Seven outcomes describe what should be the 'ocean we want' at the end of the Ocean Decade:

1. A clean ocean where sources of pollution are identified and reduced or removed.
2. A healthy and resilient ocean where marine ecosystems are understood, protected, restored and managed.
3. A productive ocean supporting sustainable food supply and a sustainable ocean economy.
4. A predicted ocean where society understands and can respond to changing ocean conditions.
5. A safe ocean where life and livelihoods are protected from ocean-related hazards.
6. An accessible ocean with open and equitable access to data, information and technology and innovation.

11.   https://marine.copernicus.eu/sites/default/files/media/pdf/2021-09/CMEMS%20Service_evolution_strategy_RD_priorities_v5-June-2021.pdf

12.   http://marine.copernicus.eu/science-learning/service-evolution/about-stac

13.   https://ioc.unesco.org/

14.   https://www.oceandecade.org

7. An inspiring and engaging ocean where society understands and values the ocean in relation to human wellbeing and sustainable development.

The decade will be implemented via "Actions", which are the tangible initiatives that will be carried out across the globe over the next ten years to fulfil the Ocean Decade vision. They will be implemented by a wide range of proponents, including research institutes and universities, governments, UN agencies, intergovernmental organisations, other international and regional organisations, business and industry, philanthropic and corporate foundations, NGOs, educators, community groups or individuals. Actions can be implemented by promoting Activities, Contributions, specific Programs or Projects.

The Ocean Decade will involve a large number of partners and actors around the world, and hence it cannot be rigidly governed. A simple, robust coordination structure will manage day-to-day implementation. The DCU, to be located at the IOC Secretariat, will be the central hub for the coordination of Ocean Decade activities. Governments or partners will host a number of Decade Coordination Offices and DCCs – referred to as decentralised coordination structures – that will be located in different regions around the world. These structures will help to coordinate efforts between national, regional, and global initiatives, share knowledge and tools developed through the Ocean Decade, create links between potential Decade partners, and monitor and report on the impact of the Decade. One DCC will be devoted to Ocean Prediction 🔗 [15].

The following subsections describe some examples of Actions and Collaborative Centres that will be linked to OOFS.

12.11.1. The Decade Collaborative Centre for Ocean Prediction

DCCs serve as the main interface between Decade Actions and the DCU at the IOC-UNESCO Secretariat. MOI has been selected to host the DCC for Ocean Prediction. It will provide:

• A communication and collaboration hub bringing together Decade programmes with ocean prediction activities, institutes, and organisations outside of the Decade;

• A global technical and organisational structure to establish a pilot for a Global Ocean Data Processing, Modelling, and Forecasting System, building on the innovations generated by the Decade programmes and other national, regional, and international partners.

The DCC for Ocean Prediction will ensure that the efforts of multiple Decade programmes combine to meet Decade objectives and that innovations are integrated into operational ocean forecasting systems through a harmonised global network with shared information and services.

12.11.2. CoastPredict Program

The University of Bologna (Italy) was selected for another thematic DCC which will focus on coastal resilience in a changing climate. The same University is also leading the CoastPredict Programme that was endorsed as a Decade Programme of Ocean Science in June 2021.

CoastPredict is one of the 3 Programmes co-designed with GOOS, and it has the purpose of revolutionising the global coastal ocean observing and forecasting sector (🔗 [16]). The high-level objectives of CoastPredict are:

1. A predicted global coastal ocean;
2. The upgrade to a fit for purpose oceanographic information infrastructure;
3. Co-design and implementation of an integrated coastal ocean observing and forecasting system adhering to best practices and standards, designed as a global framework, and implemented locally.

The Global Coastal Ocean is a concept central to the transformative science pursued by CoastPredict. CoastPredict will re-define the concept of the Global Coastal Ocean that was firstly described as follows by Robinson and Brink (2006; concept developed in volumes 10 to 14 of "The Sea" series): '*the coastal ocean – that area, extending inshore from the estuarine mouths to river catchments affected by salt waters and offshore from the surf zone to the continental shelf and slope where waters of continental origins meet open ocean currents.*'

According to this concept, all coastal ocean regions are an interface area where atmosphere, land, ice, hydrology, coastal ecosystems, open ocean, and humans interact on a multiplicity of space and time scales that need to be resolved with a proper observing and downscaling methodology, including the consideration of uncertainties.

The legacy of CoastPredict will be new science for the observing systems, and new methods for the development of reliable predictions extending as far as possible into the future to solve problems co-defined with stakeholders. Additionally, it will enhance the capacity to formulate R2O practices, a new set of coastal observing and modelling standards for all. This will go hand-in-hand with the organisation and upgrade of the basic global ocean information infrastructure for open

---

15.   https://www.oceandecade.org/news/decade-collaborative-centres-to-provide-focused-regional-and-thematic-support-for-decade-actions/

16.   https://www.coastpredict.org/

and free access to coastal information using standards and best practices.

CoastPredict will capitalise on three previous major international initiatives:

1. GOOS Coastal observation panels (i.e. COOP and succeeding PICO). COOP started in 2000 to define a strategy for integrated observing and forecasting in the coastal areas. One of the main outcomes was the recommendation that a global network of observations, data communications, data management, and data analysis/forecasting should be secured providing economies of scale. Another important COOP/PICO outcome was the initial definition of common variables to be monitored and forecasted in the coastal areas. However, PICO's work did not continue because the international ocean observing network was not adequately organised and technology was not yet ready for data collection on biogeochemistry, biodiversity, and other marine environmental variables. Furthermore, the satellite observing system for coastal areas was still under development (except for coastal ocean colour).

2. OceanPredict and its COSS-TT. OceanPredict organised the global ocean observation uptake for the development of global and regional forecasting systems. In addition, OceanPredict/COSS-TT defined the international quality control standards for ocean analyses, reanalyses, and forecasts in the coastal ocean and shelf seas. COSS-TT promoted the use of OceanPredict large scale products for seamless integration of ocean to coastal forecasting, defined the state-of-the-art methodology for downscaling, data assimilation, array design in the coastal/shelf areas. COSS-TT focuses on advancing science in support of coastal forecasting and is one of the backbones of CoastPredict.

3. The JCOMM. From 2000 to 2019, JCOMM has coordinated ocean observing networks, in particular the GLOSS network for tide gauges and the HF radar network. Furthermore, it started to develop coastal services for wave and storm surges by meteorological offices in developing countries. Moreover, it has coordinated the development of marine environmental emergency services. However, such developments led by JCOMM were not fully integrated and connected with the growing oceanographic research communities of OceanPredict and COSS-TT. While the observing systems and the large-scale ocean forecasting systems are now coordinated in GOOS, the coastal downscaling and forecasting research developments are not currently connected to coastal services.

All these activities have been partly disconnected and have not produced a global international network bringing together the fragmented scientific communities for advancing the research on the global coastal ocean. New advances that make a science-focused programme such as CoastPredict urgent and achievable are: a) operational oceanography is now implemented from the global to the regional scales, making available open and free data for coastal downscaling; and b) major technology advancements have taken place in observing, from satellites to in-situ robotics to the use of Artificial Intelligence, which makes the monitoring of the coastal ocean practical and feasible. CoastPredict will capitalise on this game-changing operational oceanography framework and extend to coastal predictive capabilities, including the land-water cycle (rivers, underground and transitional waters) and, for the first time, integrating the coastal ocean, through estuaries and rivers, with the "urban ocean" (waters within and around coastal cities).

CoastPredict will be implemented through several projects focusing on 6 areas:

- **Focus Area 1** - Integrated Observing and Modelling for short term coastal forecasting and early warnings. This area will contribute to Ocean Decade Challenge 6 'Increase community resilience to ocean hazards': enhance multi-hazard early warning services for all geophysical, ecological, biological, weather, climate and anthropogenic related ocean and coastal hazards, and mainstream community preparedness and resilience (🔗 [17]).

- **Focus Area 2** - Future Coastal Ocean climates: Earth system observing and modelling. This area will contribute to Challenge 5 'Unlock ocean-based solutions to climate change': enhance understanding of the ocean-climate nexus and generate knowledge and solutions to mitigate, adapt and build resilience to the effects of climate change across all geographies and at all scales, and to improve services including predictions for the ocean, climate and weather.

- **Focus Area 3** - Solutions for Integrated Coastal Management. This area will contribute to Challenge 8 'Create a digital representation of the Ocean': through multi-stakeholder collaboration, develop a comprehensive digital representation of the ocean, including a dynamic ocean map, which provides free and open access for exploring, discovering, and visualising past, current, and future ocean conditions in a manner relevant to diverse stakeholders.

- **Focus area 4** - Coastal Ocean and Human Health. This area does not match with a specific Decade Challenge but it is cross-cutting to all the 10 Challenges.

---

17. https://www.oceandecade.org/challenges/

• **Focus Area 5** - Coastal Information integrated in the open and free exchange international infrastructure. This area will contribute to Challenge 7 'Expand the Global Ocean Observing System': ensure a sustainable ocean observing system across all ocean basins that delivers accessible, timely, and actionable data and information to all users.

• **Focus Area 6** - Equitable coastal ocean capacity. This area will contribute to Challenge 9 'Skills, knowledge and technology for all': ensure comprehensive capacity development and equitable access to data, information, knowledge and technology across all aspects of ocean science and for all stakeholders.

12.11.3. ForeSea Program

ForeSea is hosted by OceanPredict (🔗[18]), a science programme for the coordination and improvement of global and regional ocean analysis and forecasting systems. ForeSea aims to build the next generation of ocean predictions pursuing a strong coordination of the scientific community and institutes at the international level (🔗[19]). Its main goals are:

• To improve the science, efficiency, use, and impact of ocean prediction systems;

• To build a seamless ocean information value chain, from observations to end users, able to support the economy and society.

ForeSea 🔗[20] focuses on 2 main themes:

1. Catalysing transformative ocean prediction science solutions for sustainable development, connecting people and ocean prediction;
2. Increasing impact and relevance: improving science and science capacity for the ocean we want.

Such themes are developed through a number of items. In theme 1 they span from integrating forecasts of ocean hazards with socioeconomic forecasts for supporting policy and management to maximisation of the impact and value of observations, from capacity building and training to contribution to a digital ocean. In theme 2, they cover from usage of advanced ocean prediction technologies in weather and climate predictions to coupled systems (in partnership with CoastPredict), from usage of Earth system models (ESM) to development of limited ESM areas with coupled components to improve model predictability (in collaboration with CoastPredict).

Expected outcomes[21] are considerable as ForeSea should contribute to:

• An operational oceanography information value-chain where verified/certified information and knowledge are exchanged freely enabling all operational oceanographic components, integrated from the open ocean to the coastal areas, to effectively synergize;
• A continuously optimised ocean observing system integrated from the open ocean to the coastal areas that provides maximum information benefit with manageable cost;An ocean information delivery system that provides the right information at the right time for facilitating marine decisions in support of human safety and environmental safety, and an efficient and sustainable blue economy;
• Improved extended range forecasting capabilities for ocean prediction systems;
• Better assessment and prediction of the ocean state (including reliable uncertainty estimates) and ocean impact on forecasts of other earth system components (e.g. atmosphere, ice, waves, marine ecosystems, estuaries, etc.);
• An informed ocean literate society and global economy;
• Coordinated capacity building across all elements of the operational oceanography value chain to sustain production and delivery of ocean prediction;
• Demonstrated impact and value of predictions for coastal communities;
• Effective use of ocean prediction technologies for weather and climate predictions.

To facilitate realisation of the expected outcomes, ForeSea established through OceanPredict connections with GOOS, WMO, IOC, JCOMM, Argo, GHRSST, GEO, and GEO BluePlanet.

---

18. https://oceanpredict.org/
19. https://oceanpredict.org/foresea/
20. https://oceanpredict.org/foresea/foresea-planned-activities/

21. https://oceanpredict.org/foresea/foresea-expected-outcomes/

12.12.
References

Anderson, J., Hoar, T. J., Raeder, K., Liu, H., Collins, N., Torn, R., et al. (2009). The data assimilation research test bed: a community facility. *Bulletin of the American Meteorological Society*, 90, 1283-1296, https://doi.org/10.1175/2009BAMS2618.1

Barton, N., Metzger, E.J., Reynolds, C.A., Ruston, B., Rowley, C., Smedstad, O.M., Ridout, J.A., Wallcraft, A., Frolov, S., Hogan, P. and Janiga, M.A. (2021). The Navy's Earth System Prediction Capability: A new global coupled atmosphere-ocean-sea ice prediction system designed for daily to subseasonal forecasting. *Earth and Space Science*, 8(4), e2020EA001199, https://doi.org/10.1029/2020EA001199

Beisiegel, N., Castro, C.E., and Behrens, J. (2021). Metrics for Performance Quantification of Adaptive Mesh Refinement. *Journal of Scientific Computing*, 87(1), 1-24, https://doi.org/10.1007/s10915-021-01423-0

Bishop, C.H. (2016). The GIGG-EnKF: ensemble Kalman filtering for highly skewed non-negative uncertainty distributions. *Quarterly Journal of the Royal Meteorological Society*, 142(696), 1395-1412, https://doi.org/10.1002/qj.2742

Bonavita, M., and Laloyaux, P. (2020). Machine learning for model error inference and correction. *Journal of Advances in Modeling Earth Systems*, 12(12), e2020MS002232, https://doi.org/10.1029/2020MS002232

Bonavita, M., Arcucci, R., Carrassi, A., Dueben, P., Geer, A. J., Le Saux, B., Longépé, N., Mathieu, P., and Raynaud, L. (2021). Machine Learning for Earth System Observation and Prediction. *Bulletin of the American Meteorological Society*, 102(4), E710-E716, https://doi.org/10.1175/BAMS-D-20-0307.1

Brajard, J., Carrassi, A., Bocquet, M. and Bertino, L. (2021). Combining data assimilation and machine learning to infer unresolved scale parametrization. *Philosophical Transactions of the Royal Society A*, 379(2194), https://doi.org/10.1098/rsta.2020.0086

Brassington, G.B., Martin, M.J., Tolman, H.L., Akella, S., Balmeseda, M., Chambers, C.R.S., Chassignet, E., Cummings, J.A., Drillet, Y., Jansen, P.A.E.M. and Laloyaux, P. (2015). Progress and challenges in short-to medium-range coupled prediction. *Journal of Operational Oceanography*, 8(sup2), s239-s258, https://doi.org/10.1080/1755876X.2015.1049875

Brunton, S. L., Noack, B. R., and Koumoutsakos, P. (2020). Machine learning for fluid mechanics. *Annual Review of Fluid Mechanics*, 52(1), 477-508 https://doi.org/10.1146/annurev-fluid-010719-060214

Buizza, R. (2021). Probabilistic view of numerical weather prediction and ensemble prediction. In "Uncertainties in Numerical Weather Prediction", Editors: H. Ólafsson and J.-W. Bao, Elsevier, https://doi.org/10.1016/C2017-0-03301-3

Carleo, G., Cirac, I., Cranmer, K., Daudet, L., Schuld, M., Tishby, N., Vogt-Maranto, L., and Zdeborová, L. (2019). Machine learning and the physical sciences. *Reviews of Modern Physics*, 91(4), 045002, https://doi.org/10.1103/RevModPhys.91.045002

Capet, A., Fernández, V., She, J., Dabrowski, T., Umgiesser, G., Staneva, J., Mészáros, L., Campuzano, F., Ursella, L., Nolan, G., El Serafy, G. (2020). Operational Modeling Capacity in European Seas - An EuroGOOS Perspective and Recommendations for Improvement. *Frontiers in Marine Science*, 7,129, https://doi.org/10.3389/fmars.2020.00129

Castelão, G. P. (2021). A machine learning approach to quality control oceanographic data. *Computers & Geosciences*, 155, 104803, https://doi.org/10.1016/j.cageo.2021.104803

Chassignet, E.P., and Xu, X. (2021). On the Importance of High-Resolution in Large-Scale Ocean Models. *Advances in Atmospheric Sciences*, 38, 1621-1634, https://doi.org/10.1007/s00376-021-0385-7

Cranmer, K., Brehmer, J., and Louppe, G. (2020). The frontier of simulation-based inference. *Proceedings of the National Academy of Sciences*, 117(48), 30055-30062 https://doi.org/10.1073/pnas.1912789117

Ebert, E.E. (2009). Neighborhood verification - a strategy for rewarding close forecasts. Weather and Forecasting 24(6), 1498-1510, https://doi.org/10.1175/2009WAF2222251.1

Fablet, R., Chapron, B., Drumetz, L., Mémin, E., Pannekoucke, O., and Rousseau, F. (2021). Learning variational data assimilation models and solvers. *Journal of Advances in Modeling Earth Systems*, 13(10), e2021MS002572, https://doi.org/10.1029/2021MS002572

Fox-Kemper, B., Adcroft, A., Böning, C.W., Chassignet, E.P., Curchitser, E., Danabasoglu, G., Eden, C., England, M.H., Gerdes, R., Greatbatch, R.J., Griffies, S.M., Hallberg, R.W., Hanert, E., Heimbach, P., Hewitt, E.T., Hill, C.N., Komuro, Y., Legg, S., Le Sommer, J., Masina, S., Marsland, S.J., Penny, S.G., Qiao, F., Ringler, T.D., Treguier, A.M., Tsujino, H., Uotila, P., Yeager, S.G. (2019). Challenges and Prospects in Ocean Circulation Models. *Frontiers in Marine Science*, 6, https://doi.org/10.3389/fmars.2019.00065

Frolov, S., Reynolds, C.A., Alexander, M., Flatau, M., Barton, N.P., Hogan, P. and Rowley, C. (2021). Coupled Ocean-Atmosphere Covariances in Global Ensemble Simulations: Impact of an Eddy-Resolving Ocean. *Monthly Weather Review*, 149(5), 1193-1209, https://doi.org/10.1175/MWR-D-20-0352.1

Fujii, Y., Ishibashi, T., Yasuda, T., Takaya, Y., Kobayashi, C. and Ishikawa, I. (2021). Improvements in tropical precipitation and sea surface air temperature fields in a coupled atmosphere–ocean data assimilation system. *Quarterly Journal of the Royal Meteorological Society*, 147(735), 1317-1343, https://doi.org/10.1002/qj.3973

Gao, Y., Tang, Y., Song, X. and Shen, Z. (2021). Parameter Estimation Based on a Local Ensemble Transform Kalman Filter Applied to El Niño-Southern Oscillation Ensemble Prediction. *Remote Sensing*, 13(19), 3923, https://doi.org/10.3390/rs13193923

Hatfield, S., Chantry, M., Dueben, P., Lopez, P., Geer, A., and Palmer, T. (2021). Building Tangent-Linear and Adjoint Models for Data Assimilation With Neural Networks. *Journal of Advances in Modeling Earth Systems*, 13(9), https://doi.org/10.1029/2021MS002521

Hawcroft, M., Lavender, S., Copsey, D., Milton, S., Rodríguez, J., Tennant, W., Webster, S. and Cowan, T. (2021). The benefits of ensemble prediction for forecasting an extreme event: The Queensland Floods of February 2019. *Monthly Weather Review*, 149(7), 2391-2408, https://doi.org/10.1175/MWR-D-20-0330.1

Herzfeld, M., Engwirda, D., and Rizwi, F. (2020). A coastal unstructured model using Voronoi meshes and C-grid staggering. *Ocean Modelling*, 148, 101599, https://doi.org/10.1016/j.ocemod.2020.101599

Hewitt, C. D., Garrett, N., Newton, P. (2017). Climateurope - Coordinating and supporting Europe's knowledge base to enable better management of climate-related risks. *Climate Services*, 6, 77-79, https://doi.org/10.1016/j.cliser.2017.07.004

International Altimetry Team (2021). Altimetry for the future: Building on 25 years of progress. *Advances in Space Research*, 68, 319-363, https://doi.org/10.1016/j.asr.2021.01.022

Jacobs, G., D'Addezio, J.M., Ngodock, H. and Souopgui, I. (2021). Observation and model resolution implications to ocean prediction. *Ocean Modelling*, 159, 101760, https://doi.org/10.1016/j.ocemod.2021.101760

Kasim, M. F., Watson-Parris, D., Deaconu, L., Oliver, S., Hatfield, P., Froula, D. H., Gregori, G., Jarvis, M., Khatiwala, S., Korenaga, J., Topp-Mugglestone, J., Viezzer, E., and Vinko, S. M. (2021). Building high accuracy emulators for scientific simulations with deep neural architecture search. *Machine Learning: Science and Technology*, 3(1), 015013, https://doi.org/10.1088/2632-2153/ac3ffa

Kiss, A.E., Hogg, A.M., Hannah, N., Boeira Dias, F., Brassington, G.B., Chamberlain, M.A., Chapman, C., Dobrohotoff, P., Domingues, C.M., Duran, E.R. and England, M.H. (2020). ACCESS-OM2 v1.0: A global ocean-sea ice model at three resolutions. Geosci. Model Dev., 13, 401–442, 2020, https://doi.org/10.5194/gmd-13-401-2020

Kitsios, V., Sandery, P., O'Kane, T.J. and Fiedler, R. (2021). Ensemble Kalman filter parameter estimation of ocean optical properties for reduced biases in a coupled general circulation model. *Journal of Advances in Modeling Earth Systems*, 13(2), https://doi.org/10.1029/2020MS002252

Kochkov, D., Smith, J. A., Alieva, A., Wang, Q., Brenner, M. P., and Hoyer, S. (2021). Machine learning–accelerated computational fluid dynamics. *Proceedings of the National Academy of Sciences*, 118(21), e2101784118, https://doi.org/10.1073/pnas.2101784118

Komaromi, W.A., Reinecke, P.A., Doyle, J.D., and Moskaitis, J.R. (2021). The Naval Research Laboratory's Coupled Ocean–Atmosphere Mesoscale Prediction System-Tropical Cyclone Ensemble (COAMPS-TC Ensemble). *Weather and Forecasting*, 36(2), 499-517, https://doi.org/10.1175/WAF-D-20-0038.1

Kotsuki, S., and Bishop, C.H. (2022). Implementing Hybrid Background Error Covariance into the LETKF with Attenuation-based Localization: Experiments with a Simplified AGCM. *Monthly Weather Review*, 150(1), 283-302, https://doi.org/10.1175/MWR-D-21-0174.1

Le Sommer, J., Chassignet, E.P. Wallcraft, A.J. (2018). Ocean circulation modeling for operational oceanography: Current status and future challenges. In "New Frontiers in Operational Oceanography", E. Chassignet, A. Pascual, J. Tintoré, and J. Verron, Eds., GODAE OceanView, 289-306, https://doi.org/10.17125/gov2018.ch12

Le Traon, P.Y., Reppucci, A., Alvarez Fanjul, E., Aouf, L., Behrens, A., Belmonte, M., Bentamy, A., Bertino, L., Brando, V.E., Kreiner, M.B., Benkiran, M., Carval, T., Ciliberti, S.A., Claustre, H., Clementi, E., Coppini, G., Cossarini, G., De Alfonso Alonso-Munoyerro, M., Delamarche, A., Dibarboure, G., Dinessen, F., Drevillon, M., Drillet, Y., Faugere, Y., Fernandez, V., Fleming, A., Garcia-Hermosa M.I., Sotillo, M.G., Garric, G., Gasparin, F., Giordan, C., Gehlen, M., Grégoire, M.L., Guinehut, S., Hamon, M., Harris, C., Hernandez, F., Hinkler, J.B., Hoyer, J., Karvonen, J., Kay, S., King, R., Lavergne, T., Lemieux-Dudon, B., Lima, L., Mao, C., Martin, M.J., Masina, S., Melet, A., Buongiorno Nardelli, B., Nolan, G., Pascual, A., Pistoia, J., Palazov, A., Piolle, J.F., Pujol, M.I., Pequignet, A.C., Peneva, E., Perez Gomez, B., Petit de la Villeon, L., Pinardi, N., Pisano, A., Pouliquen, S., Reid, R., Remy, E., Santoleri, R., Siddorn, J., She, J., Staneva, J., Stoffelen, A., Tonani, M., Vandenbulcke, L., von Schuckmann, K., Volpe, G., Wettre, C., Zacharioudaki, A. (2019) From Observation to Information and Users: The Copernicus Marine Service Perspective. *Frontiers in Marine Science*, 6, 234, https://doi.org/10.3389/fmars.2019.00234

Liu, T., Zhuang, Y., Tian, M., Pan, J., Zeng, T., Guo, Y., Yang, M. (2019). Parallel Implementation and Optimization of Regional Ocean Modeling System (ROMS) Based on Sunway SW26010 Many-core Processor. *IEEE Access*, 7, 146170-146182, doi:10.1109/ACCESS.2019.2944922

Lorenc, A., and Jardak, M. (2018). A comparison of hybrid variational data assimilation methods for global NWP. *Quarterly Journal of the Royal Meteorological Society*, 144(717), 2748-2760, https://doi.org/10.1002/qj.3401

Malmgren-Hansen, D. (2021). Deep learning for high-dimensional parameter retrieval. In: "Deep Learning for the Earth Sciences", G. Camps-Valls, D. Tuia, X. X. Zhu, and M. Reichstein Eds., Wiley, https://doi.org/10.1002/9781119646181.ch16

Martín Míguez, B., Novellino, A., Vinci, M., Claus, S., Calewaert, J.-B., Vallius, H. et al. (2019). The European Marine Observation and Data Network (EMODnet): Visions and Roles of the Gateway to Marine Data in Europe. Frontiers in Marine Science, 6, 313, https://doi.org/10.3389/fmars.2019.00313

Maulik, R., Rao, V., Wang, J., Mengaldo, G., Constantinescu, E., Lusch, B., Balaprakash, P., Foster, I. and Kotamarthi, R. (2021). Efficient high-dimensional variational data assimilation with machine-learned reduced-order models. Geoscientific Model Development, https://doi.org/10.5194/gmd-2021-415

Maze, G., Mercier, H., Fablet, R., Tandeo, P., Lopez Radcenco, M., Lenca, P., Feucher, C., and Le Goff, C. (2017). Coherent heat patterns revealed by unsupervised classification of Argo temperature profiles in the North Atlantic Ocean. *Progress in Oceanography*, 151, 275-292, https://doi.org/10.1016/j.pocean.2016.12.008

Minamide, M., and Posselt, D.J. (2022). Using Ensemble Data Assimilation to Explore the Environmental Controls on the Initiation and Predictability of Moist Convection. *Journal of the Atmospheric Sciences*, 79(4), 1151-1169, https://doi.org/10.1175/JAS-D-21-0140.1

Mittal, S., Vetter, J.S. (2015). A Survey of CPU-GPU Heterogeneous Computing Techniques. *ACM Computing Surveys*, 47(4), 1-35, https://doi.org/10.1145/2788396

Nerger, L., Tang, Q., and Mu, L. (2020). Efficient ensemble data assimilation for coupled models with the Parallel Data Assimilation Framework: example of AWI-CM (AWI-CM-PDAF 1.0). *Geoscientific Model Development*, 13, 4305-4321, https://doi.org/10.5194/gmd-13-4305-2020

Nonnenmacher, M., and Greenberg, D. S. (2021). Deep emulators for differentiation, forecasting, and parametrization in Earth science simulators. *Journal of Advances in Modeling Earth Systems*, 13, e2021MS002554, https://doi.org/10.1029/2021MS002554

O'Kane, T.J., Sandery, P.A., Kitsios, V., Sakov, P., Chamberlain, M.A., Squire, D.T., Collier, M.A., Chapman, C.C., Fiedler, R., Harries, D. and Moore, T.S. (2021). CAFE60v1: A 60-year large ensemble climate reanalysis. Part II: Evaluation. *Journal of Climate*, 34(13), 5171-5194, https://doi.org/10.1175/JCLI-D-20-0518.1

O'Kane, T.J., Sandery, P.A., Monselesan, D.P., Sakov, P., Chamberlain, M.A., Matear, R.J., Collier, M.A., Squire, D.T. and Stevens, L. (2019). Coupled data assimilation and ensemble initialisation with application to multi-year ENSO prediction. *Journal of Climate*, 32(4), 997-1024, https://doi.org/10.1175/JCLI-D-18-0189.1

Palmer, T. N., Doblas-Reyes, F. J., Weisheimer, A., Rodwell, M. J. (2008). Toward Seamless Prediction: Calibration of Climate Change Projections Using Seasonal Forecasts. *Bulletin of the American Meteorological Society*, 89(4), 459-470, https://doi.org/10.1175/BAMS-89-4-459

Peng, G., Downs, R.R., Lacagnina, C., Ramapriyan, H., Ivánová, I., Moroni, D., Wei, Y., Larnicol, G., Wyborn, L., Goldberg, M., Schulz, J., Bastrakova, I., Ganske, A., Bastin, L., Khalsa, S.J.S., Wu, M., Shie, C.-L., Ritchey, N., Jones, D., Habermann, T., Lief, C., Maggio, I., Albani, M., Stall, S., Zhou, L., Drévillon, M., Champion, S., Hou, C.S., Doblas-Reyes, F., Lehnert, K., Robinson, E. and Bugbee, K., (2021a). Call to Action for Global Access to and Harmonization of Quality Information of Individual Earth Science Datasets. *Data Science Journal*, 20(1), 19, http://doi.org/10.5334/dsj-2021-019

Peng, G., Lacagnina, C., Ivánová, I., Downs, R.R., Ramapriyan, H., Ganske, A., Jones, D. et al. (2021b). International Community Guidelines for Sharing and Reusing Quality Information of Individual Earth Science Datasets. AGU Fall Meeting, 1-17 December 2020, https://doi.org/10.1002/essoar.10508481.1

Persello, C., Wegner, J. D., Hänsch, R., Tuia, D., Ghamisi, P., Koeva, M., and Camps-Valls, G. (2022). Deep learning and earth observation to support the sustainable development goals. *IEEE Geoscience and Remote Sensing Magazine*, 2-30, https://doi.org/10.48550/arXiv.2112.11367

Posselt, D.J., Bishop, C.H. (2018). Nonlinear Data Assimilation for Clouds and Precipitation using a Gamma-Inverse Gamma Ensemble Filter. *Quarterly Journal of the Royal Meteorological Society*, 144(716), 2331-2349, https://doi.org/10.1002/qj.3374

Quinn, C., O'Kane, T.J., Kitsios, V. (2020). Application of a local attractor dimension to reduced space strongly coupled data assimilation for chaotic multiscale systems. *Nonlinear Processes in Geophysics*, 27 (1), 51-74, https://doi.org/10.5194/npg-27-51-2020

Robinson A. R., and K. Brink (Eds.). 2006. The Sea. Vols. 10 to 14. Harvard University Press.

Roemmich, D., Alford, M.J., Hervé, C., Johnson, K., King, B., Moum, J., Oke, P., Owens, W.B., Pouliquen, S., Purkey, S., Scanderbeg, M., Suga, T., Wijffels, S., Zilberman, N., Bakker, D., Baringer, M., Belbeoch, M., Bittig, H.C., Boss, E., Calil, P., Carse, F., Carval, T., Chai, F., Conchubhair, D.Ó., d'Ortenzio, F., Dall'Olmo, G., Desbruyeres, D., Fennel, K., Fer, I., Ferrari, R., Forget, G., Freeland, H., Fujiki, T., Gehlen, M., Greenan, B., Hallberg, R., Hibiya, T., Hosoda, S., Jayne, S., Jochum, M., Johnson, G.C., Kang, K., Kolodziejczyk, N., Körtzinger, A., Le Traon, P.-Y., Lenn, Y.-D., Maze, G., Mork, K.A., Morris, T., Nagai T., Nash, J., Garabato, A.N., Olsen, A., Pattabhi, R.R., Prakash, S., Riser, S., Schmechtig, C., Schmid, C., Shroyer, E., Sterl, A., Sutton, P., Talley, L., Tanhua, T., Thierry, V., Thomalla, S., Toole, J., Troisi, A., Trull, T.W., Turton, J., Velez-Belchi, P. J., Walczowski, W., Wang, H., Wanninkhof, R., Waterhouse, A.F., Waterman, S., Watson, A., Wilson, C., Wong, A.P.S., Xu, J., Yasuda, I.(2019). On the Future of Argo: A Global, Full-Depth, Multi-Disciplinary Array. *Frontiers in Marine Science*, 6, https://doi.org/10.3389/fmars.2019.00439

Sakov, P. (2014). EnKF-C User Guide, https://doi.org/10.48550/arXiv.1410.1233

Sakov, P., Haussaire, J.-M., Bocquet, M. (2017). An iterative ensemble Kalman filter in presence of additive model error. *Quarterly Journal of the Royal Meteorological Society*, 144(713), https://doi.org/10.48550/arXiv.1711.06110

Sandery, P., Brassington, G., Colberg, F., Sakov, P., Herzfeld, M., Maes, C., Tuteja, N. (2019). An ocean reanalysis of the western Coral Sea and Great Barrier Reef. *Ocean Modelling*, 144, 101495, http://dx.doi.org/10.1016/j.ocemod.2019.101495

Sandery, P., O'Kane, T., Kitsios, V., and Sakov, P. (2020). Climate model state estimation using variants of EnKF coupled data assimilation. *Monthly Weather Review*, 148(6), 2411-2431, https://doi.org/10.1175/MWR-D-18-0443.1

She, J, Muñiz Piniella, Á, Benedetti-Cecchi, L, Boehme, L, Boero, F, Christensen, A, et al. (2019). An integrated approach to coastal and biological observations. *Frontiers in Marine Science*, 6, 314, https://doi.org/10.3389/fmars.2019.00314

She, J., Allen, I., Buch, E., Crise, A., Johannessen, J.A., Le Traon P.-Y. et al. (2016). Developing European operational oceanography for Blue Growth, climate change adaptation and mitigation, and ecosystem-based management. Ocean Science, 12, 953-976, https://doi.org/10.5194/os-12-953-2016

She, J., Bethers, U., Cardin, V., Christensen, K.H., Dabrowski, T., et al. (2021). Develop EuroGOOS marine climate service with a seamless earth system approach. 9th EuroGOOS International conference, Shom; Ifremer; EuroGOOS AISBL, May 2021, Brest (Virtual), France, 554-561.

Shriver, J. F., Arbic, B. K., Richman, J. G., Ray, R. D., Metzger, E. J., Wallcraft, A. J., Timko, P. G. (2012), An evaluation of the barotropic and internal tides in a high-resolution global ocean circulation model. Journal of Geophysical Research: Oceans, 117(C10), https://doi.org/10.1029/2012JC008170

Sotillo, M.G., Garcia-Hermosa, I., Drévillon, M., Régnier, C., Szczypta, C., Hernandez, F., Melet, A., Le Traon, P-Y. (2021). Communicating CMEMS Product Quality: evolution & achievements along Copernicus-1 (2015-2021). Included in "Special Issue: The Copernicus Marine Service from 2015 to 2021: six years of achievements", by LeTraon et al., *Mercator Océan Journal #57*, https://doi.org/10.48670/moi-cafr-n813

Sun, Y., Bao, W., Valk, K., Brauer, C. C., Sumihar, J., and Weerts, A. H. (2020). Improving forecast skill of low-land hydrological models using ensemble Kalman filter and unscented Kalman filter. *Water Resources Research*, 56, e2020WR027468, https://doi.org/10.1029/2020WR027468

van de Meent, J.-W., Paige, B., Yang, H., AND Wood, F. (2021). An introduction to probabilistic programming, https://doi.org/10.48550/arXiv.1809.10756

van Leeuwen, S., Tett, P., Mills, D., van der Molen, J. (2015). Stratified and non stratified areas in the North Sea: Long-term variability and biological and policy implications. *Journal of Geophysical Research: Oceans*, 120(7), 4670-4686, https://doi.org/10.1002/2014JC010485

Vinuesa, R., and Brunton, S. L. (2021). The potential of machine learning to enhance computational fluid dynamics, https://doi.org/10.48550/arXiv.2110.02085

Weyn, J.A., Durran, D.R., Caruana, R., Cresswell-Clay, N. (2021). Sub-Seasonal Forecasting With a Large Ensemble of Deep-Learning Weather Prediction Models. J*ournal of Advances in Modeling Earth Systems,* 13(7), e2021MS002502, https://doi.org/10.1029/2021MS002502

WMO (2015). Seamless prediction of the Earth system: from minutes to months. WMO-No. 1156, ISBN 978-92-63-11156-2.

Xu, S., Huang, X., Oey, L.-Y., Xu, F., Fu, H., Zhang, Y., Yang, G. (2015). POM.gpu-v1.0: a GPU-based Princeton Ocean Model. *Geoscientific Model Development*, 8, 2815-2827, https://doi.org/10.5194/gmd-8-2815-2015

Zanna, L., and Bolton, T. (2021). Deep learning of unresolved turbulent ocean processes in climate models. In: "Deep Learning for the Earth Sciences", G. Camps-Valls, D. Tuia, X. X. Zhu, and M. Reichstein (Eds.), Wiley https://doi.org/10.1002/9781119646181.ch20

Zhang, L., Delworth, T.L., Jia, L. (2017). Diagnosis of Decadal Predictability of Southern Ocean Sea Surface Temperature in the GFDL CM2.1 Model. *Journal of Climate*, 30(16), 6309-6328, https://doi.org/10.1175/JCLI-D-16-0537.1

Editors and Authors

Editors: Enrique Alvarez Fanjul[1], Stefania Ciliberti[2], Pierre Bahurel[3]

Editorial support: Romane Zufic[3]

Chapter 1	Author: Enrique Alvarez Fanjul[1]
Chapter 2	Authors: Pierre Bahurel[3] and Enrique Alvarez Fanjul[1]
Chapter 3	Coordinator: Enrique Alvarez Fanjul[1] Authors: Marcos Garcia Sotillo[4] and John Wilkin[5]
Chapter 4	Coordinator: Avichal Mehra[6] Authors: Roland Aznar[7], Stefania Ciliberti[2], Laurence Crosnier[3], Marie Drevillon[3], Yann Drillet[3], Begoña Pérez Gómez[8], Antonio Reppucci[3], Joseph Sudheer[9], Marcos Garcia Sotillo[4], Marina Tonani[1], P. N. Vinaychandranand[10], and Aihong Zhong[11]
Chapter 5	Coordinator: Stefania Ciliberti[2] Authors: Nadia Ayoub[12], Jérôme Chanut[3], Mauro Cirano[13], Anne Delamarche[3], Pierre De Mey-Frémaux[12], Marie Drevillon[3], Yann Drillet[3], Helene Hewitt[14], Simona Masina[15], Clemente Tanajura[13], Vassilios Vervatis[16], and Liying Wan[17]
Chapter 6	Coordinator: Laurent Bertino[18] Authors: Ed Blockley[14], Johnny A. Johannessen[18], and Einar Örn Ólason[18]
Chapter 7	Coordinator: Fujiang Yu[17] Authors: David Byrne[19], Jianxi Dong[17], Shichao Liu[17], and Begoña Pérez Gómez[8]
Chapter 8	Coordinators: Gabriel Diaz-Hernandez[20], Lotfi Aouf[21] Authors: Alexander Babanin[22], Jean Bidlot[23], Andy Saulter[14], and Joanna Staneva[24]
Chapter 9	Coordinator: Elodie Gutknecht[3] Authors: Laurent Bertino[18], Pierre Brasseur[25], Stefano Ciavatta[26], Gianpiero Cossarini[27], Katja Fennel[28], David Ford[14], Marilaure Gregoire[29], Diane Lavoie[30], and Patrick Lehodey[31]
Chapter 10	Coordinator: John Siddorn[19] Authors: Øyvind Breivik[32,33], Natacha B. Bernier[34], Kai H. Christensen[32,35], Stephen G. Penny[36,37], and Keguang Wang[32]
Chapter 11	Coordinator: Giovanni Coppini[2] Authors: Enrique Alvarez Fanjul[1], José Chambel Leitão[38], Laurence Crosnier[3], Pierre Daniel[21], Tomasz Dabrowski[39], Svitlana Liubartseva[2], Gianandrea Mannarini[2], and Glen Nolan[39]
Chapter 12	Coordinator: Fraser Davidson[40] Authors: Enrique Alvarez Fanjul[1], Alain Arnaud[3], Stefania Ciliberti[2], Marie Drevillon[3], Ronan Fablet[41], Yosuke Fujii[42], Isabel Garcia-Hermosa[3], Marcos Garcia Sotillo[4], Stéphanie Guinehut[3], Emma Heslop[43], Villy Kourafalou[44], Julien Le Sommer[45], Matt Martin[14], Andrew M. Moore[46], Nadia Pinardi[47], Elizabeth Remy[3], Paul Sandery[48], Jun She[49], and Joaquin Tintorè[50]

1) Mercator Ocean International, France - previously at Puertos del Estado, Spain
2) Ocean Predictions and Applications Division, Fondazione Centro Euro-Mediterraneo sui Cambia-menti Climatici, Lecce, Italy
3) Mercator Ocean International, France
4) Nologin Ocean Weather Systems, Spain - previously at Puertos del Estado, Spain
5) Rutgers University, USA
6) NWS/NOAA, USA
7) Nologin Ocean Weather Systems, Spain
8) Puertos del Estado, Spain
9) Indian National Centre for Ocean Information Services, India
10) Indian Institute of Science, India
11) Bureau of Meteorology, Canada
12) LEGOS, Université de Toulouse, CNRS, CNES, and IRD, France
13) Federal University of Rio de Janeiro, Brazil
14) Met Office, UK
15) Ocean modelling and Data Assimilation Division, Fondazione Centro Euro-Mediterraneo sui Cam-biamenti Climatici, Bologna, Italy
16) University of Athens, Department of Physics, Greece
17) National Marine Environmental Forecasting Center, China
18) Nansen Environmental and Remote Sensing Center, Norway
19) National Oceanography Centre, UK
20) IHCantabria - Instituto de Hidráulica Ambiental de la Universidad de Cantabria, Spain
21) MeteoFrance, France
22) University of Melbourne, Australia
23) ECMWF, UK
24) HEREON, Germany
25) Institute for Geosciences and Environmental research, France
26) Plymouth Marine Laboratory, UK
27) National Institute of Oceanography and Applied Geophysics, Italy
28) Dalhousie University, Canada
29) Liege University, Belgium
30) Fisheries and Oceans Canada, Canada
31) Collecte Localisation Satellites - CLS, France
32) Norwegian Meteorological Institute, Norway
33) University of Bergen, Norway
34) Environment and Climate Change, Canada
35) University of Oslo, Norway
36) NOAA Physical Sciences Laboratory (PSL), USA
37) Cooperative Institute for Research in Environmental Sciences (CIRES), University of Colorado, Boulder
38) Hidromod, Portugal
39) Marine Institute, Ireland
40) Dynamic Hydrographic Products with Fisheries and Oceans, Canada
41) IMT Atlantique, France
42) MRI/JMA, Japan
43) IOC/UNESCO, France
44) University of Miami, USA
45) CNRS, France
46) Ocean Sciences Department, Institute of Marine Sciences, USA
47) University of Bologna, Italy
48) CSIRO Australia's National Science Agency, Australia
49) Danish Meteorological Institute, Denmark
50) SOCIB, Spain

GOOS / ETOOFS Secretariat: Denis Chang Seng
Corresponding author: Enrique Alvarez Fanjul (ealvarez@mercator-ocean.fr)

ACNFS	Arctic Cap Nowcast/Forecast System
ADCIRC	ADvanced CIRCulation Model For Oceanic, Coastal And Estuarine Waters
ADCP	Acoustic doppler current profilers
AGRIF	Adaptive Grid Refinement in Fortran
AHI	Advanced Himawari Infrared
AI	Artificial Intelligence
AMR	Adaptive Mesh Refinement
AMSR-E	Advanced Microwave Scanning Radiometer for EOS
AMSR2	Advanced Microwave Scanning Radiometer 2
AO	Arctic Oscillation
AOGCM	Atmosphere-Ocean General Circulation Model
AUV	Autonomous Underwater Vehicle
AVHRR	Advanced Very High Resolution Radiometer
AWO	Atmosphere-Waves-Ocean
BAM	Bayesian Model Average
BAMHBI	Biogeochemical Model for Hypoxic and Benthic Influenced areas
BATS	Bermuda Atlantic Time-series Study
BBM	Brittle Bingham-Maxwell
BE	Boussinesq Equations
BFM	Biogeochemical Flux Model
BGC	Biogeochemistry
BSFS	Black Sea Forecasting System
BUFR	Binary Universal Form for the Representation
CCS	California Current System
CCSM	Community Climate System Model
CDOM	Coloured Dissolved Organic Matter
CERA	Coupled ECMWF ReAnalysis
CF	Climate and Forecast
CFD	Computational Fluid Dynamics
CFL	Courant-Friedrichs-Lewy
CFOSAT	Chinese-French Oceanography Satellite
CFSR	Climate Forecast System Reanalysis
CHL	Chlorophyll
CIMR	Copernicus Imaging Microwave Radiometer
CMA	Cuadro de Mando Ambiental
CMCC	Fondazione Centro Euro-Mediterraneo sui Cambiamenti Climatici
CMIP	Coupled Model Intercomparison Project
CO-OPS	Center for Operational Oceanographic Products and Services

COARDS	Cooperative Ocean/Atmosphere Research Data Service
COAWST	Coupled Ocean-Atmosphere-Wave-Sediment Transport system
COE	Coefficient of Efficiency
COOP	Coastal Ocean Observing Panel
CORA	Coriolis Ocean Dataset for Reanalysis
COSMoS	Canadian Oil Spill Modelling Suite
COSS-TT	Coastal and Shelf Seas Task Team
CPU	Central processing unit
CROCO	Coastal and Regional Ocean Community Model
CRPS	Continuous Rank Probability Score
CRPS	Continuous Rank Probability Score
CTD	Conductivity-Temperature Depth
DA	Data assimilation
DART	Data Assimilation Research Testbed
DAS	Data assimilation scheme
DBCP	Data Buoy Cooperation Panel
DCCs	Decade Collaborative Centres
DCM	Deep Chlorophyll Maximum
DCSM	Dutch Continental Shelf Model
DCU	Decade Coordination Unit
DDE	Deep Differentiable Emulator
DEM	Digital Elevation Model
DEnKF	Deterministic EnKF
DEOS	Delft Institute for Earth-Oriented Space Research
DIAS	Data and Information Access Service
DIC	Dissolved inorganic carbon
DM	Delayed mode
DMS	Data Management System
DMSP	Defense Meteorological Satellite Program
DNS	Direct Numerical Simulation
DTO	Digital Twins for the Ocean
DUACS	Data Unification and Altimeter Combination System
EAP	Elastic-Anisotropic-Plastic
ECMWF	European Centre for Medium-Range Weather Forecasts
ECOSMO	ECOSystem MOdel
ECV	Essential Climate Variable
EFAS	European Flood Awareness System
EFI	Extreme Forecast Index
EKF	Extended Kalman Filter

EMODnet	European Marine Observation and Data Network		**GEO**	Group on Earth Observations
EnKF	Ensemble Kalman Filter		**GFDL**	Geophysical Fluid Dynamics Laboratory
EnOI	Ensemble Optimal Interpolation		**GFLOPS**	giga FLOPS
ENSO	El Niño-Southern Oscillation		**GFS**	Global Forecasting System
ENSURF	ENsemble SURge Forecast		**GHFRN**	Global High Frequency Radar Network
EORC	Earth Observation Research Centre		**GHG**	Greenhouse Gas
EOV	Essential Ocean Variable		**GHRSST**	Group for High Resolution Sea Surface Temperature
EPS	Ensemble prediction systems		**GIS**	Geographic Information System
ERSEM	European Regional Seas Ecosystem Model		**GLO-PHY**	Global Ocean Forecasting System
ESA	European Space Agency		**GLODAP**	Global Ocean Data Analysis Project
ESM	Earth system model		**GLOFAS**	Global Flood Awareness System
ESMF	Earth System Modelling Framework		**GLOSS**	Global Sea Level Observing System
ESP	Earth System Prediction		**GNOME**	General NOAA Operational Modelling Environment
ESTKF	Error-Subspace Transform Kalman Filter		**GNSS**	Global Navigation Satellite System
ETOOFS	Expert Team on Operational Ocean Forecasting Systems		**GODAE**	Global Ocean Data Assimilation Experiment
EU	European Union		**GOOS**	Global Ocean Observing System
EUMETSAT	European Operational Satellite Agency		**GPU**	Graphics Processing Unit
EuroGOOS	European component of the Global Ocean Observing System		**GRDC**	Global Runoff Data Centre
EVP	Elastic-Viscous-Plastic		**GSHHG**	Global Self-consistent, Hierarchical, High-resolution Geography Database
FABM	Framework for Aquatic Biogeochemical Models		**GTS**	Global Telecommunication System
FAIR	Findability, accessibility, interoperability, and reusability		**HAB**	Harmful Algal Bloom
FAO	Food and Agriculture Organisation		**HadOCC**	Hadley Centre Ocean Carbon Cycle Model
FDM	Finite Difference Method		**HF**	High Frequency
FEM	Finite Element Method		**HPC**	High Performance Computing
FESOM	Finite-Element/volumE Sea ice-Ocean Model		**HTL**	Higher Trophic Level
FESOM	Finite Element Solution		**HYCOM**	Hybrid Coordinate Ocean Model
FNMOC	Fleet Numerical Meteorology and Oceanography Centre		**I/O**	Input/Output
FRAC	Full Resolution Area Coverage		**IABP**	International Arctic Buoy Program
FSS	Fraction of Skill Score		**IBI**	Iberian-Biscay-Irish
FVCOM	Finite Volume Community Ocean Model		**IBM**	Individual-Based Model
FVCOM	Finite-Volume Coastal Ocean Model		**ICCAT**	International Commission for the Conservation of Atlantic Tunas
FVM	Finite Volume Method		**ICESat**	Ice, Cloud, and land Elevation Satellite
FYI	First-year Ice		**ICZM**	Integrated Coastal Zone Management
GAC	Global Area Coverage		**IEO**	Instituto Español de Oceanografía
GBN	Global Buoy Network		**IFS**	Integrated Forecasting System
GCOS	Global Climate Observing System		**IHO**	International Hydrographic Organization
GDAC	Global Data Assembly Centre		**IIEE**	Integrated Ice Edge Error
GDP	Global Drifter Program		**IMO**	International Maritime Organization
GDP	Gross Domestic Product		**INCOIS**	Indian National Centre for Ocean Information Services
			INS	In-Situ

IOCCG	International Ocean Colour Coordinating Group
IOCCP	International Ocean Carbon Coordination Project
IOC	Intergovernmental Oceanographic Commission
IOOS	Integrated Ocean Observing System
IOP	Inherent Optical Property
IoT	Internet of Things
IPCC	Intergovernmental Panel on Climate Change
ITD	Ice Thickness Distribution
ITIC	International Tsunami Information Center
ITU	International Telecommunications Union
JAXA	Japan Aerospace Exploration Agency
JCOMM	Joint Technical Commission for Oceanography and Marine Meteorology
JEDI	Joint Effort for Data assimilation Integration
JMA	Japan Meteorological Agency
JPL	Jet Propulsion Laboratory
JPSS	Joint Polar Satellite System
KPI	Key performance indicators
LEO	Low Earth Orbit
LiDAR	Laser Imaging Detection and Ranging
LKF	Linear Kinematic Features
LOCEAN	Laboratoire d'Océanographie et du Climat: Expérimentation et Approches Numériques
MEAP-TT	Marine Ecosystem Analysis and Prediction Task Team
MedFS	Mediterranean Forecast System
MEDUSA	Model of Ecosystem Dynamics, nutrient Utilisation, Sequestration and Acidification
MEOP	Marine Mammals Exploring the Oceans Pole to Pole
MFC	Monitoring and Forecasting Centre
MFWAM	Météo-France WAve Model
MISST	Multi-sensor Improved Sea Surface Temperature
MITgcm	MIT general circulation model
MIZ	Marginal Ice Zone
MJO	Madden-Julian Oscillation
ML	Machine Learning
MLD	Mixed Layer Depth
MODIS	Moderate Resolution Imaging Spectroradiometer
MOI	Mercator Ocean International
MOM	Modular Ocean Model
MOTHY	Modèle Océanique de Transport d'HYdrocarbures

MPA	Marine Protected Area
MPAS	Model for Prediction Across Scales
MPQ	Model product quality
MSaaS	Modelling and Simulation as a Service
MSE	Mild-slope equation
MSP	Maritime Spatial Planning
MTCSWA	Multi-platform Tropical Cyclone Surface Winds Analysis
MY	Multi Year
MYI	Multiyear Ice
NAO	North Atlantic Oscillation
NAVOCEANO	US Naval Oceanographic Office
NcML	NetCDF Markup Language
NDBC	National Data Buoy Center
NEMO	Nucleus for European Modelling of the Ocean
NGO	Non-governmental organization
NIVA	Norwegian Institute for Water Research
NOAA	National Oceanic and Atmospheric Administration
NODC	National Oceanographic Data Centres
NORWECOM	Norwegian Ecological Model
NPP	Net Primary Production
NRT	Near-Real-Time
NSIDC DAAC	National Snow and Ice Data Center Distributed Active Archive Center
NSR	Northern Sea Route
NSWE	Non-linear Shallow Water Equations
NWP	Numerical weather prediction
NWS	North West Shelf
OBC	Open Boundary Condition
OC	Ocean Colour
OC	Ocean Colour
ODV	Ocean Data View
OGCM	Ocean general circulation model
OI	Optimal Interpolation
OMI	Ocean Monitoring Indicator
ONR	Office of Naval Research
OO	Operational Oceanography
OOFS	Operational Ocean Monitoring and Forecasting Systems
OOPC	Ocean Observations Physics and Climate
OOPS	Object-Oriented Prediction System
OpenFOAM	Open source Field Operation and Manipulation

OS-Eval	Observing System Evaluation
OSCAR	Oil Spill Contingency and Response
OSE	Observing System Experiment
OSI SAF	Ocean and Sea Ice Satellite Applications Facility
OSPO	Office of Satellite and Product Operations
OSR	Ocean State Report
OSSE	Observing System Simulation Experiment
PAR	Photosynthetically Available Radiation
PDAF	Parallel Data Assimilation Framework
PDF	Probability density function
PFT	Phytoplankton Functional Type
PICO	Panel for Integrated Coastal Observations
PISCES	Pelagic Interactions Scheme for Carbon and Ecosystem Studies
PMOST	Parallel Model Of Surge from Typhoon
PNA	Pacific-North American Pattern
PO.DAAC	Physical Oceanography Distributed Active Archive Centre
POC	Particulate Organic Carbon
POM	Princeton Ocean Model
PQ	Product Quality
PSMSL	Permanent Service for Mean Sea Level
PSS	Practical Salinity Scale
QBO	Quasi-Biennial Oscillation
QC	Quality Control
QUID	Quality Information Document
R/COFS	Regional/Coastal Ocean Forecasting Systems
R2O	Research to Operations
RADS	Radar Altimeter Database System
RANS	Reynolds-Averaged Navier–Stokes
RCP	Representative Concentration Pathways
RFMOs	Regional Fisheries Management Organisations
RHS	Right Hand Side
RIOPS	Regional Ice Ocean Prediction System
RMSD	Root Mean Square Difference
ROC	Receiver Operator Characteristic
ROMS	Regional Ocean Modeling System
ROSE-L	Copernicus Radar Observation System for Europe in L-band
RRR	Rolling Review of Requirements
Rrs	Remote Sensing Reflectance
SAMOA	System of Meteorological and Oceanographic Support for Port Authorities

SANGOMA	Stochastic Assimilation for the Next Generation Ocean Model Applications
SANIFS	Southern Adriatic - Northern Ionian Forecasting System
SARAL	Satellite with ARgos and ALtika
SAR	Synthetic Aperture Radar
SCDA	Strongly Coupled Data Assimilation
SCHISM	Semi-implicit Cross-scale Hydroscience Integrated System Model
SCOBI	Swedish Coastal and Ocean Biogeochemical Model
SCVTs	Spherical Centroidal Voronoi Tessellations
SD	Standard Deviation
SDGs	Sustainable Development Goals
SEEK	Singular Evolutive Extended Kalman filter
SHYFEM	Shallow water HYdrodynamic Finite Element Model
SI	Scatter Index
SI	International System of Units
SIDFEx	Sea Ice Drift Forecast Experiment
SIS	Sea Ice Simulator
SIT	System Information Table
SKEB	Stochastic Kinetic Energy Backscatter
SLA	Sea Level Anomaly
SLOSH	Sea, Lake, and Overland Surges from Hurricanes
SMAP	Soil Moisture Active Passive
SMMR	Scanning Multi-channel Microwave Radiometer
SMOS	Soil Moisture and Ocean Salinity mission
SOCAT	Surface Ocean CO_2 Atlas
SOCIB	Balearic Islands Coastal Observing and Forecasting System
SONEL	Système d'Observation du Niveau des Eaux Littorales
SOOP	Ship-of-opportunity
SPM	Suspended Particulate Matter
SPOT	Satellite pour l'Observation de la Terre
SPP	Stochastic Perturbed Parameters
SPPT	Stochastic Perturbed Parametrized Tendencies
SPUF	Stochastic Parameterization of Unresolved Fluctuations
SSES	Sensor Specific Error Statistics
SSH	Sea Surface Height
SSM/I	Special Sensor Microwave Imager
SSS	Sea surface salinity
SST	Sea surface temperature

STAC	Science and Technological Advisory Committee
SURF	Structured and Unstructured Relocatable Ocean Model for Forecasting
SWAN	Simulating WAves Nearshore
SWASH	Simulating WAves till SHore model
SWE	Shallow Water Equations
SWH, or Hs	Significant Wave Height
SWOT	Surface Water and Ocean Topography
TAC	Thematic Assembly Center
TGTT	Tide Gauge Task Team
TSG	Thermosalinographs
TVD	Total Variation Diminishing
UHSLC	University of Hawaii Sea Level Centre
UKMO	UK Met Office
UN	United Nations
UNCTAD	United Nations Conference on Trade and Development
UNDP	United Nations Development Programme
UNFCCC	United Nations Framework Convention on Climate Change
UNGA	United Nations General Assembly
UOM	Unified Ocean system Model
US	United States
USA	United States of America
USSR	Union of Soviet Socialist Republics
VARANS	Volume-Averaged Reynolds Averaged Navier–Stokes
VIIRS	Visible Infrared Imaging Radiometer Suite
VISIR	DiscoVerIng Safe and effIcient Routes
VOF	Volume-O-Fluid
VP	Viscous-plastic
WAM	Wave prediction Model
WAVERYS	Global Ocean Waves Reanalysis
WCDA	weakly coupled data assimilation
WCOFS	West Coast Operational Forecasting System
WMO	World Meteorological Organization
WMO/LC-WFV	World Meteorological Organisation Lead Centre for Wave Forecast Verification
WOA	World Ocean Atlas
WOD	World Ocean Database
WRF	Weather Research and Forecasting Model
XBT	Expendable bathythermograph

This guide hopes to be a guideline and inspiration to professionals all around the globe, stimulating the reader to research deeper knowledge on this vast field. If this objective is achieved, this publication is expected to foster the generation of valuable information that will be used in decision making processes and, therefore, to advocate a wiser and more sustainable relation with our always generous ocean.